frontiers | Research Topics

Strigolactone: Signaling and functions in plants

Edited by
Ruifeng Yao, Tadao Asami, Steven Michael Smith and Catherine Rameau

Published in
Frontiers in Plant Science

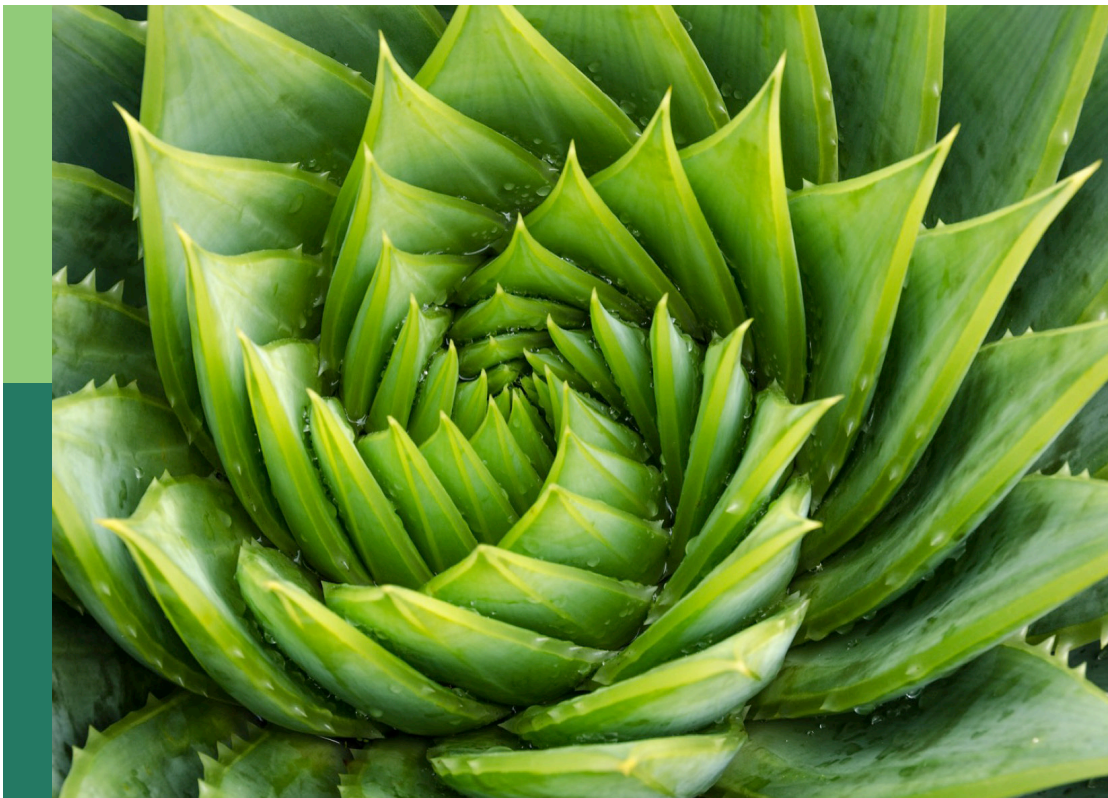

ISSN 1664-8714
ISBN 978-2-83252-015-4
DOI 10.3389/978-2-83252-015-4

About Frontiers

Frontiers is more than just an open access publisher of scholarly articles: it is a pioneering approach to the world of academia, radically improving the way scholarly research is managed. The grand vision of Frontiers is a world where all people have an equal opportunity to seek, share and generate knowledge. Frontiers provides immediate and permanent online open access to all its publications, but this alone is not enough to realize our grand goals.

Frontiers journal series

The Frontiers journal series is a multi-tier and interdisciplinary set of open-access, online journals, promising a paradigm shift from the current review, selection and dissemination processes in academic publishing. All Frontiers journals are driven by researchers for researchers; therefore, they constitute a service to the scholarly community. At the same time, the *Frontiers journal series* operates on a revolutionary invention, the tiered publishing system, initially addressing specific communities of scholars, and gradually climbing up to broader public understanding, thus serving the interests of the lay society, too.

Dedication to quality

Each Frontiers article is a landmark of the highest quality, thanks to genuinely collaborative interactions between authors and review editors, who include some of the world's best academicians. Research must be certified by peers before entering a stream of knowledge that may eventually reach the public - and shape society; therefore, Frontiers only applies the most rigorous and unbiased reviews. Frontiers revolutionizes research publishing by freely delivering the most outstanding research, evaluated with no bias from both the academic and social point of view. By applying the most advanced information technologies, Frontiers is catapulting scholarly publishing into a new generation.

What are Frontiers Research Topics?

Frontiers Research Topics are very popular trademarks of the *Frontiers journals series*: they are collections of at least ten articles, all centered on a particular subject. With their unique mix of varied contributions from Original Research to Review Articles, Frontiers Research Topics unify the most influential researchers, the latest key findings and historical advances in a hot research area.

Find out more on how to host your own Frontiers Research Topic or contribute to one as an author by contacting the Frontiers editorial office: frontiersin.org/about/contact

Strigolactone: Signaling and functions in plants

Topic editors

Ruifeng Yao — Hunan University, China

Tadao Asami — The University of Tokyo, Japan

Steven Michael Smith — University of Tasmania, Australia

Catherine Rameau — INRA UMR1318 Institut Jean Pierre Bourgin, France

Citation

Yao, R., Asami, T., Smith, S. M., Rameau, C., eds. (2023). *Strigolactone: Signaling and functions in plants*. Lausanne: Frontiers Media SA. doi: 10.3389/978-2-83252-015-4

Table of contents

frontiers in Plant Science

ORIGINAL RESEARCH
published: 17 September 2021
doi: 10.3389/fpls.2021.725949

Synthesis and Evaluation of New Halogenated GR24 Analogs as Germination Promotors for *Orobanche cumana*

Yuchao Chen[1,2,3†], Yi Kuang[4†], Liyang Shi[4†], Xing Wang[4], Haoyu Fu[4], Shengxiang Yang[4], Diego A. Sampietro[5]*, Luqi Huang[1,2]* and Yuan Yuan[2]**

[1]School of Pharmacy, Anhui University of Chinese Medicine, Hefei, China, [2]State Key Laboratory of Dao-di Herbs Breeding Base, National Resources Center for Chinese Materia Medica, China Academy of Chinese Medical Sciences, Beijing, China, [3]Agricultural Biotechnology Center, Ningxia Academy of Agriculture and Forestry Sciences, Yinchuan, China, [4]Zhejiang Provincial Collaborative Innovation Center for Bamboo Resources and High-Efficiency Utilization, Zhejiang A&F University, Lin'an, China, [5]LABIFITO, National University of Tucumán, Tucumán, Argentina

OPEN ACCESS

Edited by:
Ruifeng Yao,
Hunan University, China

Reviewed by:
Christopher McErlean,
The University of Sydney, Australia
Cristina Prandi,
University of Turin, Italy

***Correspondence:**
Yuan Yuan
y_yuan0732@163.com
Luqi Huang
huangluqi01@126.com
Diego A. Sampietro
dasampietro@hotmail.com
Shengxiang Yang
shengxiangyang2000@163.com

†These authors have contributed equally to this work

Specialty section:
This article was submitted to Plant Physiology, a section of the journal Frontiers in Plant Science

Received: 16 June 2021
Accepted: 12 August 2021
Published: 17 September 2021

Citation:
Chen Y, Kuang Y, Shi L, Wang X, Fu H, Yang S, Sampietro DA, Huang L and Yuan Y (2021) Synthesis and Evaluation of New Halogenated GR24 Analogs as Germination Promotors for Orobanche cumana. Front. Plant Sci. 12:725949. doi: 10.3389/fpls.2021.725949

Orobanche and *Striga* are parasitic weeds extremely well adapted to the life cycle of their host plants. They cannot be eliminated by conventional weed control methods. Suicidal germination induced by strigolactones (SLs) analogs is an option to control these weeds. Here, we reported two new halogenated (+)-GR24 analogs, named 7-bromo-GR24 (7BrGR24) and 7-fluoro-GR24 (7FGR24), which were synthesized using commercially available materials following simple steps. Both compounds strongly promoted seed germination of *Orobanche cumana*. Their EC_{50} values of $2.3 \pm 0.28 \times 10^{-8}$ M (7BrGR24) and $0.97 \pm 0.29 \times 10^{-8}$ M (7FGR24) were 3- and 5-fold lower, respectively, than those of (+)-GR24 and *rac*-GR24 ($EC_{50} = 5.1 \pm 1.32$–$5.3 \pm 1.44 \times 10^{-8}$; $p < 0.05$). The 7FGR24 was the strongest seed germination promoter tested, with a stimulation percentage of $62.0 \pm 9.1\%$ at 1.0×10^{-8} M and $90.9 \pm 3.8\%$ at 1.0×10^{-6} M. It showed higher binding affinity ($IC_{50} = 0.189 \pm 0.012$ μM) for the SL receptor ShHTL7 than (+)-GR24 ($IC_{50} = 0.248 \pm 0.032$ μM), *rac*-GR24 ($IC_{50} = 0.319 \pm 0.032$ μM), and 7BrGR24 ($IC_{50} = 0.521 \pm 0.087$ μM). Molecular docking experiments indicated that the binding affinity of both halogenated analogs to the strigolactone receptor OsD14 was similar to that of (+)-GR24. Our results indicate that 7FGR24 is a promising agent for the control of parasitic weeds.

Keywords: strigolactones, *Orobanche cumana*, parasitic weeds, GR24 analogs, suicidal germination

INTRODUCTION

The parasitic weeds *Orobanche* spp. (broomrapes) and *Striga* spp. (witchweeds) can feed through haustoria invading the roots of host plants (Musselman, 1980). They parasitize major crops, including maize (*Zea mays*), sorghum (*Sorghum bicolor*), rice (*Oryza sativa*), tomato (*Lycopersicon esculentum*), tobacco (*Nicotiana tabacum*), and sunflower (*Helianthus annuus*). *Orobanche* and *Striga* species infest more than 60 million hectares of farmland worldwide, resulting in the

loss of billions of dollars each year (Chesterfield et al., 2020). For instance, approximately 1.34 million hectares of rain-fed rice field in Africa are infested with *Striga*, resulting in crop losses of more than USD100 million. These weeds cause economic pressure on millions of smallholder farmers (Parker, 2012; Rodenburg et al., 2016). These parasitic weeds are expanding their geographical range. *Orobanche cumana* was first reported on sunflowers in central Russia at the end of the 19th century. It spread over east Europe in a few decades along with the successful expansion of sunflower harvests. It is currently found in most of the main sunflower-producing countries in Eurasia, from Spain to China and is regarded as the most important biotic constraint for sunflower production (Rubiales, 2020).

Orobanche and *Striga* weeds are not effectively controlled by conventional methods, such as breeding resistant varieties, rotation, and herbicides (Hearne, 2009). Their plants produce tens of thousands of tiny seeds that remain viable and dormant for over 10 years and lead to the formation of extensive seed stocks in the soil (Musselman, 1980). The seeds only germinate in response to specific germination signals, known as strigolactones (SLs), which are released in the rhizosphere by the host plants. Strigol was the first SL identified (Cook et al., 1967). Since then, more than 20 SLs have been isolated from host crop plants, including sorghum, maize, rice, and tobacco (Hauck et al., 1992; Siame et al., 1993; Xie et al., 2013). Molecules of these natural SLs are composed of a tricyclic lactone ring (ABC-ring) and a butenolide ring (D-ring) that are connected by an enol-ether linkage, where the bioactiphore for germination resides in the CD part (Zwanenburg et al., 2009; Zwanenburg and Blanco-Ania, 2018). *Orobanche* and *Striga* weeds need their plant hosts to survive. Hence, the application of SLs to soils infested with parasitic weeds is a promising alternative to stimulate suicidal seed germination before the crop is planted (Zwanenburg et al., 2016). However, natural SLs found in root exudates are available at picogram levels and have an unstable structure (Yoneyama et al., 2013). Therefore, synthetic analogs, such as GR24, GR7, GR5, Nijmegen-1, and T-010, were synthesized. They offer interesting prospects for eliminating parasitic weeds through suicidal germination (Zwanenburg and Blanco-Ania, 2018). However, most of the synthetic SL analogs promote less seed germination than natural SLs. Thus, modification of synthetic SL analogs for commercial application toward controlling parasitic weeds remains highly desirable. Here, we reported the synthesis of new SLs analogs and their effect on seed germination of parasitic weeds.

MATERIALS AND METHODS

General Experimental Procedure

All reactions requiring anhydrous or inert conditions were carried out under a positive atmosphere of argon in oven-dried glassware. Solutions or liquids were introduced into round-bottomed flasks using oven-dried syringes through rubber septa. All reactions were stirred magnetically using Teflon-coated stirring bars. If needed, reactions were warmed using an electrically heated silicon oil bath. Organic solutions obtained after aqueous workup were dried over $MgSO_4$. The removal of solvents was accomplished using a rotary evaporator at water aspirator pressure. GR24 stands for *rac*-GR24, which was purchased from Shanghai Yuanye Biotechnology (Shanghai, China). Chemicals for the syntheses were purchased from Sigma-Aldrich (Shanghai, China).

NMR spectra were recorded on Bruker ADVANCE III (400 MHz) spectrometers (Karlsruhe, Germany) for ^{1}H NMR and ^{13}C NMR. CD_3OD and $CDCl_3$ were used as solvents for the NMR analysis, with tetramethylsilane as the internal standard. Chemical shifts were reported upfield to TMS (0.00 ppm) for ^{1}H NMR and relative to $CDCl_3$ (77.3 ppm) for ^{13}C NMR. Optical rotation was determined using a Perkin Elmer 343 polarimeter. HPLC analysis was conducted on an Agilent 1260 series instrument (California, America). Column chromatography was performed using silica gel Merck 60 (230–400 mesh). All new products were further characterized by HRMS. A positive ion mass spectrum of the sample was acquired on a Thermo LTQ-FT mass spectrometer (MA, United States) with an electrospray ionization source.

Synthesis of (+)-GR24

Small portions of potassium tert-butoxide (0.85 g, 7.56 mmol) were added to a solution of compound D (1.1 g, 6.3 mmol) and methyl formate (0.82 ml, 9.45 mmol) in anhydrous THF (15 ml) at 0°C under nitrogen (**Figure 1**). The reaction mixture was stirred at 25°C until completion. THF was removed *in vacuo*. The resulting solid was solubilized in 20 ml anhydrous DMF under N_2. Bromobutenolide (1.67 g, 9.45 mmol) was added to this solution and the reaction mixture was stirred overnight. The reaction was quenched with saturated aqueous ammonium chloride (20 ml). The reaction mixture was diluted with ethyl acetate (50 ml) and washed with water (3 × 30 ml). The organic extract was then washed with brine, dried with Na_2SO_4, and the solvent removed under vacuum. The residue was finally purified by silica gel column chromatography (eluent: petroleum ether/ethyl acetate = 3:1, *v*/*v*) to give the(+)-GR24.

Synthesis of (–)-epi-GR24

The synthetic protocol described for (+)-GR24 was carried out starting with compound E (1.1 g, 6.3 mmol; **Figure 2**) to yield a residue. The residue was finally purified by silica gel column chromatography (eluent: petroleum ether/ethyl acetate = 3:1, *v*/*v*) to give the (−)-epi-GR24.

Synthesis of 7-bromo-GR24 and 7-fluoro-GR24

Compound A (10 mmol of a ketone) and 15 mmol of glyoxylic acid were added to a round bottomed flask (**Figure 3**). Then, the mixture was stirred at 95°C for 3 h. The reaction mixture was dissolved in acetic acid (15 ml) and water (5 ml). Zinc dust (15 ml) was added to the solution for 1 h and the mixture was stirred for an additional 3 h. The mixture was diluted with ethyl acetate and then filtered through celite. The filtrate

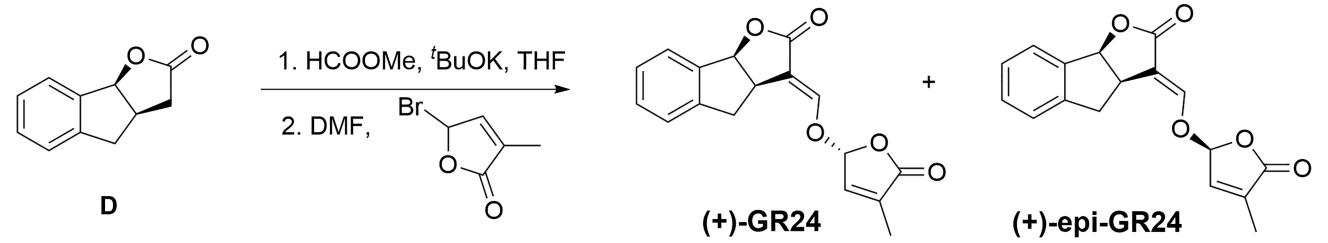

FIGURE 1 | Synthesis of (+)-GR24.

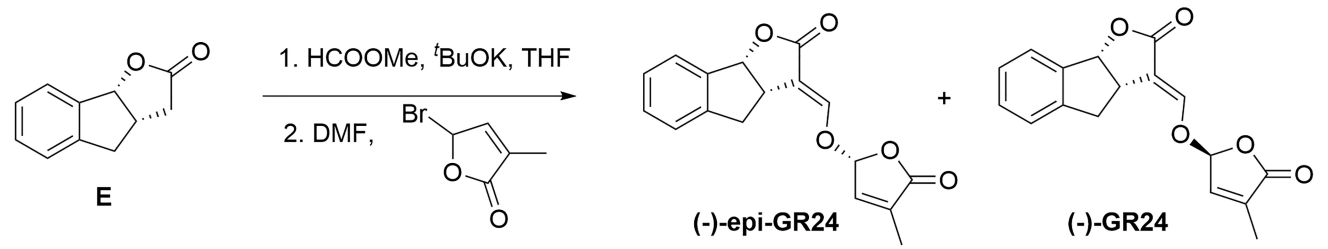

FIGURE 2 | Synthesis of (–)-epi-GR24.

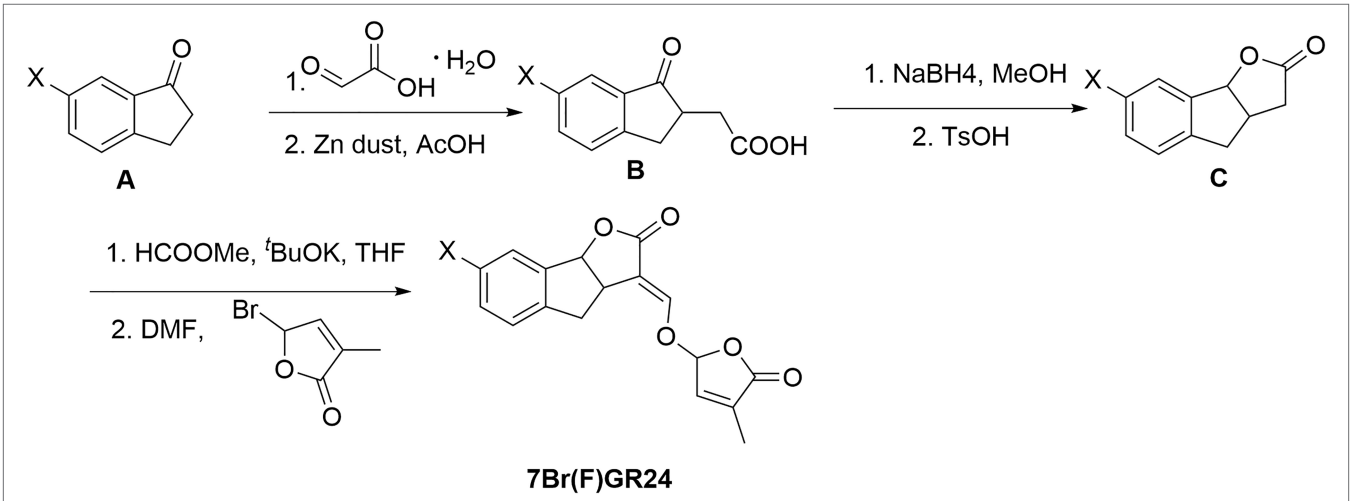

FIGURE 3 | Synthesis of 7-bromo-GR24 (7BrGR24) and 7-fluoro-GR24 (7FGR24), respectively.

was extracted with ethyl acetate, washed with brine, dried over Na_2SO_4, and concentrated under vacuum. The residue was purified by chromatography on silica gel using hexane:ethyl acetate (2:1, *v*/*v*) and 0.5% acetic acid as an eluent, resulting in 70% yield of compound B.

Compound B (5 mmol) was dissolved in 15 ml of anhydrous MeOH. Then, 15 mmol of $NaBH_4$ were added in small portions at 0°C under nitrogen. The reaction mixture was stirred at 25°C until the completion of the reaction. We carefully added 20 ml of distilled water to the mixture. The solution was extracted three times with ethyl acetate and the combined organic phase was dried over Na_2SO_4, filtered, and concentrated under vacuum. The resulting solid was solubilized in 20 ml anhydrous MeOH. TsOH (0.1 mmol) was added to this solution and the reaction mixture was stirred at 75°C for 6 h. MeOH was removed *in vacuo*. Then, 20 ml of distilled water was added. The solution was extracted with ethyl acetate three times and the combined organic phase was dried over Na_2SO_4, filtered, and concentrated under vacuum. The residue was purified by chromatography on silica gel using hexane:ethyl acetate (3:1, *v*/*v*) and 0.5% acetic acid as eluents. It yielded 95% of compound C.

The protocol described for (+)-GR24 was performed starting with compound C (1.1 g, 6.3 mmol) to finally obtain a residue that was subjected to column chromatography, generating pure 7-bromo-GR24 (7BrGR24) and 7-fluoro-GR24 (7FGR24).

Germination Assays

Seeds of *O. cumana* were kindly provided by professor Yongqing Ma (North-west Agriculture & Forest University, Yangling, China). The assay was carried out in petri dishes according to a method previously reported by Kang et al. (2020). Prior to use, the seeds were sterilized for 8 min in 1% sodium hypochlorite, soaked in 75% ethanol for another 1 min, rinsed five times with sterile distilled water, and finally left to air dry on a clean bench. A sterile filter paper disk of 6 mm in diameter was placed in each petri dish and wetted with 200 µl of sterile distilled water. Then, aqueous solutions of the tested compounds (100 µl per filter paper) were added. The sterile seeds were distributed on the paper disks at a density of approximately 65 seeds per dish. Finally, the sealed petri dishes were stored in the dark and incubated at 25°C for 14 days. After the incubation, the percentage of germination were calculated with the assistance of a stereomicroscope. Compounds 7BrGR24 and 7FGR24 were assayed at concentrations of 1.0×10^{-6}, 1.0×10^{-7}, 2.0×10^{-8}, 1.0×10^{-8}, and 1.0×10^{-9} M. Three petri dishes were used for each concentration, and assays were carried out three times. The compounds (+)-GR24, (-)-epi-GR24, and *rac*-GR24 were used as the positive control, and the filter paper disk added with 100 µl of sterile distilled water was used as the negative control. The EC_{50} values of the tested compounds were calculated with probit tests using SPSS 21.0 software.

Yoshimulactone Green Assay

The assay was carried out according to a method previously reported by Tsuchiya et al. (2015). The stock solutions of yoshimulactone green (YLG), *rac*-GR24, (+)-GR24, (-)-epi-GR24 and the new SL analogs dissolved in DMSO (1 ml, 1 mM). Then, stock solutions were diluted with sterile distilled water to final concentrations of 50 µM (YLG), and 20, 5, 2.5, 1, 0.5, and 0.1 µM [*rac*-GR24, (+)-GR24, (-)-epi-GR24, and the new SL analogs]. Protein coding sequences for ShHTL7 were inserted into KpnI and HindIII sites of the pET32a(+) vector (Invitrogen, CA, United States) and transformed into the *Escherichia coli* strain BL21(DE3; TransGen Biotech, Beijing, China). Briefly, a single colony on the plate was inoculated into a 25 ml sterilized LB medium containing 0.28 mM ampicillin for 12 h. Then, the cultures (1 ml) were inoculated into 200 ml of the same medium and the cells were grown at 37°C, shaken at 220 rpm until an OD (600 nm) of 0.6 is reached. We added 0.5 mM isopropyl β-D-1-thiogalactopyranoside (IPTG) into the culture to induce protein expression at 16°C for 16 h. The culture was centrifuged at 7,000 rpm at 4°C for 5 min to harvest bacteria. The pellet was suspended in 10 ml PBS buffer (6.7 mM PO_4, pH 7.0) containing 1 mM PMSF. The cells were lysed using sonication with 5 s intervals and centrifuged at 12,000 rpm at 4°C for 10 min. The supernatant was filtered with a 0.45 µm filter and the filtrate was added into a Ni-NTA column (TransGen Biotech, Beijing, China), which had been equilibrated with a PBS buffer. After the Ni-NTA column was washed three times with the PBS buffer, the column was eluted with a 15 ml gradient of 20, 50, 100, and 300 mM imidazole prepared in the PBS buffer. Fractions from 100 mM eluant were pooled for the YLG assay.

The volume of each reaction solution (200 µl) contained 5 µl of YLG (50 µM), 10 µl of a dilution of an SL analog, 15 µl of ShHTL7 protein (1.5 mg/ml), and 170 µl of PBS buffer. Reactions were carried out for 3 h in the dark in a water bath at 26°C. The blank control contained water (10 µl) instead of a dilution of the SL analog. Then, the reaction solutions were added to a 96-well black plate (Nest, Wuxi, China) and its fluorescent intensity was measured by SpectraMax i3 (Molecular Devices, CA, United States) at an excitation wavelength of 480 nm and emission wavelength of 520 nm. Relative fluorescence units (FU) were calculated as $(k–k')/k$, where k and k' are the fluorescence intensities of the blank control and a dilution of the SL analog, respectively. FU were used to calculate IC_{50} values with probit tests using SPSS 21.0 software.

Molecular Docking Experiment

The molecular modeling computational study was performed using Autodock vina 1.1.2 software. The crystal structure of rice DWARF14 (OsD14; PDB: 5DJ5) was used for the docking study. The grid box was set as a $20\times20\times20$ Å three cube and its center was set at the position of the original ligand GR24 ($x=-30.72$, $y=14.69$, and $z=-21.23$). The docking results were visualized by PyMol and Maestro12.7 (for 2D interaction).

Statistical Analysis

Data of seed germination and fluorescence-based competition assays were subjected to the ANOVA and differences among means were evaluated by the least significant difference test ($p<0.05$).

RESULTS AND DISCUSSION

Synthesis of SL Analogs

The main features of the synthesized compounds were as follow:

(+)-GR24: White solid, 0.65 g, 35% yield, $[\alpha]_D20=+449$ (c = 0.50, $CHCl_3$). ^{1}H NMR (400 MHz, $CDCl_3$) δ 7.51–7.49 (m, ^{2}H), 7.35 (m, ^{3}H), 7.00 (s, ^{1}H), 6.21 (s, ^{1}H), 5.95 (d, J = 7.9 Hz, ^{1}H), 3.97–3.92 (m, ^{1}H), 3.44 (dd, J = 16.9, 9.4 Hz, ^{1}H), 3.11 (dd, J = 16.9, 3.2 Hz, ^{1}H), 2.03 (t, J = 1.4 Hz, ^{3}H). ^{13}C NMR (100 MHz, $CDCl_3$) δ 171.44, 170.37, 151.27, 142.66, 141.16, 138.82, 135.83, 130.04, 127.49, 126.42, 125.18, 113.14, 100.71, 85.99, 38.85, 37.31, 10.73.

(-)-epi-GR24: White solid, 0.56 g, 30% yield, $[\alpha]_D20=-290$ (c = 0.50, $CHCl_3$). ^{1}H NMR (400 MHz, $CDCl_3$) δ 7.50–7.49 (m, ^{1}H), 7.35–7.23 (m, ^{1}H), 6.99 (s, ^{1}H), 6.21 (s, ^{1}H), 5.96 (d, J = 8.0 Hz, ^{1}H), 3.97–3.92 (m, ^{1}H), 3.42 (dd, J = 16.9, 9.3 Hz, ^{1}H), 3.10 (dd, J = 16.9, 3.1 Hz, ^{1}H), 2.03 (t, J = 1.4 Hz, ^{3}H). ^{13}C NMR (100 MHz, $CDCl_3$) δ 171.42, 170.40, 151.29, 142.69, 141.25, 138.76, 135.76, 130.05, 127.45, 126.34, 125.28, 113.26, 100.79, 86.00, 38.79, 37.42, 29.69, 10.74.

7BrGR24: White solid, mp 195–198°C, 0.83 g, 37% yield. ^{1}H NMR (400 MHz, $CDCl_3$) δ 7.66 (^{1}H, d, J = 1.2 Hz, H-8), 7.51 (^{1}H, d, J = 2.5 Hz, H-6'), 7.47 (^{1}H, dd, J = 8.0, 1.7 Hz, H-6), 7.13 (^{1}H d, J = 8.0 Hz, H-5), 6.97 (^{1}H, m, H-3'), 6.21 (^{1}H, m, H-2'), 5.93 (^{1}H, d, J = 8.0 Hz, H-8b), 3.97 (^{1}H, m, H-3a),

3.39 (^{1}H, dd, J = 17.1, 9.3 Hz, H-4β), 3.08 (^{1}H, dd, J = 17.0, 3.1 Hz, H-4α), 2.07 (^{3}H, s, H-7'). ^{13}C NMR(100 MHz, $CDCl_3$) δ 170.8 (C-2), 169.9 (C-5'), 151.1 (C-6'), 141.4 (C-8a), 141.1 (C-3'), 140.7 (C-4a), 136.0 (C-8), 134.4 (C-4'), 129.4 (C-5), 126.3 (C-7), 121.0 (C-6), 112.5 (C-3), 100.3 (C-2'), 85.2 (C-8b), 39.2 (C-4), 36.8 (C-3a), 10.8 (C-7'). HR-ESI-MS (m/z): calcd. For $C_{17}H_{13}BrNaO_5$ 398.9839; found 398.9835 $[M+Na]^+$.

7FGR24: White solid, mp 183–186°C, 0.69 g, 35% yield. ^{1}H NMR (400 MHz, $CDCl_3$) δ 7.49 (^{1}H, d, J = 2.0 Hz, H-8), 7.43 (^{1}H, dd, J = 8.4, 4.4 Hz, H-6'), 7.01 (^{1}H, m, H-5), 6.97 (^{1}H, m, H-6), 6.88 (^{1}H, m, H-3'), 6.22 (^{1}H, s, H-2'), 5.88 (^{1}H, d, J = 7.9 Hz, H-8b), 4.01 (^{1}H, m, H-3a), 3.40 (^{1}H, dd, J = 17.2, 9.3 Hz, H-4β), 3.07 (^{1}H, dd, J = 17.2, 3.1 Hz, H-4α), 2.01 (^{3}H, s, H-7'). ^{13}C NMR (100 MHz, $CDCl_3$) δ 171.2 (C-2), 170.4 (C-5'), 165.1 (C-7), 151.4 (C-6'), 145.3 (C-8a), 141.2 (C-3'), 135.8 (C-4a), 134.8 (C-4'), 127.9 (C-5), 115.1 (C-8), 112.8 (C-6), 111.9 (C-3), 100.7 (C-2'), 85.0 (C-8b), 39.4 (C-4), 37.3 (C-3a), 10.7 (C-7'). HR-ESI-MS (m/z): calcd. For $C_{17}H_{13}FNaO_5$ 339.0639; found 339.0642 $[M+Na]^+$.

Seed Germination Assay

Table 1 shows the impact of (+)-GR24, (-)-epi-GR24, *rac*-GR24, 7BrGR24, and 7FGR24 on the seed germination of *O. cumana*. (+)-GR24 and *rac*-GR24 showed a similar stimulatory effect (EC_{50} = 5.1 ± 1.32–5.3 ± 1.44 × 10^{-8} M), whereas (-)-epi-GR24 had no effect. These results suggested strong stereospecificity in the SL perception of *O. cumana*. (+)-GR24 and (-)-epi-GR24 were diasteroisomers with opposite stereochemistry in the C-ring that is β- and α-oriented, respectively, and had the same 2'-*R* configuration of the D-ring. Indeed, parasitic plant species also vary considerably in their germination responses to different SLs (Wang and Bouwmeester, 2018; Bouwmeester et al., 2021). In general, the 2'-*R* configuration of the D-ring has been confirmed essential for SLs germination activity, and stereochemistry in the C-ring is considered to be closely related to the activity (Thuring et al., 1997a,b; Xie et al., 2010). The use of (+)-GR24 and (-)-epi-GR24 in germination tests could provide profound clues about the general stereochemical adaptation of parasitic weeds for the perception of strigol-like (β-oriented C-ring) and orobanchol-like (α-oriented C-ring) SLs, respectively. These are the two families of natural canonical SLs currently known (Scaffidi et al., 2014; Ueno et al., 2014; Xie, 2016). Seed germination responsiveness reported for either (+)-GR24 or (-)-epi-GR24 exhibited strong variations among the parasitic weed species. For example, *Striga hermonthica* and *Orobanche crenata* germinated when exposed to (+)-GR24 or (-)-epi-GR24 at concentrations between 1 × 10^{-5} and 1 × 10^{-9} M (Thuring et al., 1997b; Ueno et al., 2011). However, *S. hermonthica* was generally more responsive to (+)-GR24 than *O. crenata* at low concentrations. (-)-epi-GR24 showed lower activity compared to (+)-GR24 on both weed species irrespective of the concentration tested (Thuring et al., 1997b). In contrast, *Orobanche minor* seed showed a higher germination rate when exposed to orobanchol (orobanchol-like SLs) compared with strigol (strigol-like SLs; Xie et al., 2010). Furthermore, *S. hermonthica* could respond to 36 stereoisomers of the naturally occurring SLs including both strigol-like and orobanchol-like SLs, while *Striga gesnerioides* only responded to three orobanchol-like SLs of them (Nomura et al., 2013). These facts comfirmed that some parasitic plant species possessed the strict structural requirements of SLs for induction of germination (Ueno et al., 2011). The differential responsiveness of the parasitic plant species to SLs could be an adaptation to avoid being triggered to germinate by non-host plants (Nomura et al., 2013). Hence, the specific stereochemistry recognition of SLs analogs observed for *O. cumana* in this work was likely due to its host specificity, which was restricted to a short number of plant species (Fernández-Aparicio et al., 2011).

The A-ring and B-ring in SLs can be modified through methylation, hydroxylation, epoxidation, or ketolation, giving rise to the structural plasticity of SLs that often results in changes in their biological activity (Thuring et al., 1997c; Boyer et al., 2012; Al-Babili and Bouwmeester, 2015). In the case of 7BrGR24 and 7FGR24, halogenation of the A-ring at the C-7 increased the germination of *O. cumana* 3- and 5-fold, respectively, compared to (+)-GR24 (p < 0.05). Hence, the 7FGR24 showed the highest promotive activity achieving germination of 62.0 ± 9.1% at 1.0 × 10^{-8} M and reaching 90.9 ± 3.8% at 1.0 × 10^{-6} M. Previous reports indicated that the incorporation of substitutions in the A-ring and varying sizes of the side groups modified the promotive activity of the (+)-GR24 molecule on the germination of parasitic seeds. For example, (+)-GR24 analogs monohydroxylated in the A-ring from C-8 to C-5 were reported less active than (+)-GR24 on *S. hermonthica*, with a stronger fall in activity, when the hydroxyl group was closer to the bioactiphore part of the molecule (Ueno et al., 2011). However, the introduction of a hydroxyl

TABLE 1 | Values of half-maximal effective concentration (EC_{50}) calculated for germination of *Orobanche cumana* seeds exposed to increasing concentrations of (+)-GR24, (–)-epi-GR24, *rac*-GR24, and the halogenated (+)-GR24 analogs.

Compounds	Concentration (M)					EC_{50} (10^{-8} M)
	1.0 × 10^{-9}	1.0 × 10^{-8}	2.0 × 10^{-8}	1.0 × 10^{-7}	1.0 × 10^{-6}	
(+)-GR24	7.3 ± 5.9%^{a}	21.5 ± 13.4%^{c}	41.1 ± 10.1%^{b}	66.6 ± 9.1%^{c}	81.5 ± 3.9%^{b}	5.1 ± 1.32
(–)-epi-GR24	0^b	0^d	0^c	0^d	0^d	–
7-bromo-GR24	16.9 ± 4.1%^{a}	39.6 ± 5.0%^{b}	49.1 ± 6.6%^{b}	69.6 ± 3.3%^{b}	83.8 ± 2.5%^{b}	2.3 ± 0.28
7-fluoro-GR24	11.2 ± 7.8%^{a}	62.0 ± 9.1%^{a}	63.8 ± 4.9%^{a}	84.2 ± 8.6%^{a}	90.9 ± 3.8%^{a}	0.97 ± 0.29
rac-GR24	15.3 ± 8.5%^{a}	27.2 ± 4.2%^{c}	47.1 ± 5.0%^{b}	58.5 ± 10.7%^{c}	75.2 ± 5.7%^{c}	5.3 ± 1.44

Different lowercase letters in the same column indicate significant differences between means, according to the least significant difference test (p < 0.05). Values represent means ± SD (n = 3).

group on the A-ring enhanced the germination-stimulating activity on *O. minor*, where a hydroxyl group is preferable at C-9 instead of at C-5 (Kim et al., 2010). Furthermore, the 6-methyl substituent on (+)-GR24 resulted in higher percentages of germinated *O. crenata* seeds (Wigchert and Zwanenburg, 1999). Moreover, bulky side groups joined to the A-ring also reduced the activity of SL analogs more than small groups (Cohen et al., 2013). Accordingly, the germination-stimulating activity of SLs depended on both the position and size of the substituent on A-ring. Although, a few of reports declared the introduction of substituent such as iodine atom to the A-ring at the C-7 reduced the activity of SL analogs on *O. crenata* and *Pisum sativum* (Thuring et al., 1997c; Boyer et al., 2012). In our results, 7FGR24 showed higher activity. It might be due to the fact that both the A-ring halogenation at the 7-C position, which was far from the GR24 bioactiphore and the small size of the fluorine atom likely favored a high affinity of 7FGR24 to the active site of SLs receptors of *O. cumana*.

YLG Assay

(+)-GR24 and its halogenated analogs showed binding affinity to ShHTL7, an SL receptor found in the parasitic plant *S. hermonthica*, with a high affinity to SLs (Tsuchiya et al., 2015). Binding affinity was tested by an *in vitro* fluorescence-based competition assay involving YLG. The YLG was a small probe that emits fluorescence only after the hydrolysis, which was catalyzed by ShHTL7. A decrease in FUs showed the competition for receptor binding between a fixed YLG concentration and increasing concentrations of the SL analog. The halogenated GR24 analogs 7BrGR24 and 7FGR24 tested at concentrations between 2.5 and 20 μM showed approximately 0.1 FU, which were similar to those recorded for (+)-GR24 and *rac*-GR24 (**Figure 4**). The FU of 7FGR24 were below 0.34 as in the case of (+)-GR24 and *rac*-GR24, even at a concentration range from 0.5 to 1.0 μM. Moreover, 7FGR24 tested at 0.1 μM was 0.72 FU, which was significantly lower than 0.81 and 0.92 FU recorded for *rac*-GR24 and (+)-GR24, respectively ($p < 0.05$). Probit analysis based on FUs indicated that 7FGR24 was the strongest competitor tested ($IC_{50} = 0.189 \pm 0.012$ μM), followed by (+)-GR24 ($IC_{50} = 0.248 \pm 0.032$ μM), whereas *rac*-GR24 and 7BrGR24 had a lower affinity for ShHTL7 with IC_{50} values of 0.319 ± 0.032 and 0.521 ± 0.087 μM, respectively. Consistent with this, the substituent at C-8 also showed higher affinity for ShHTL7 (Tsuchiya et al., 2015). Although, the 7BrGR24 posed lower affinity, as compared to (+)-GR24, which was inconsistent with seed germination activity. The discrepancy could be due to the fact that the that ShHTL7 protein was derived from a *Striga* ssp. not an *Orobanche* ssp., both of which could respond differently to 7BrGR24.

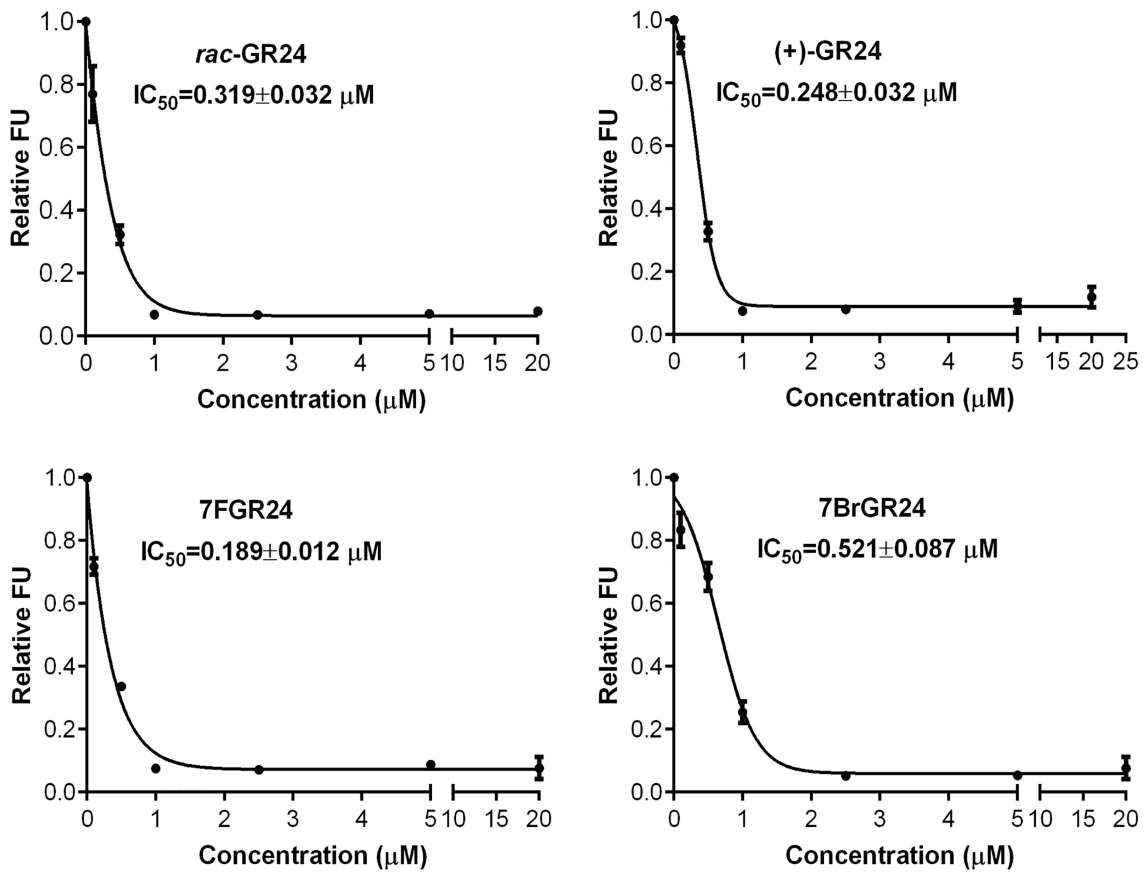

FIGURE 4 | Relative fluorescence unit (FU) values were recorded for *rac*-GR24, (+)-GR24, and the halogenated (+)-GR24 analogs when tested at several concentrations in the yoshimulactone green (YLG) assay. IC_{50} values for these strigolactone (SL) analogs were calculated. Values represent means ± SD ($n = 4$).

Molecular Docking Assays

Rice DWARF14 (OsD14) was selected for docking studies in order to understand how the SL analogs interacted with the SL receptor. SLs receptors were AtD14 paralogs forming part of the α, β-fold hydrolases family, which not only binded to the SL molecules but also cleaved them into their ABC-ring and the D-ring parts (Hamiaux et al., 2012). They were structurally similar and had a conserved catalytic pocket consisting of a triad of serine, histidine, and aspartate (Yao et al., 2016). The docking analyses indicated that (+)-GR24 and the halogenated (+)-GR24 analogs could smoothly enter the binding pocket of the OsD14 protein (**Figure 5**). Their D-rings acquire the same orientation predicted for (+)-GR24 during its interaction with the receptor (Trott and Olson, 2010; **Figure 5D**). As shown in **Figure 5B**, the carbonyl oxygen in the D-ring of 7FGR24 formed hydrogen bonding forces with Ser97 and Hip247, which were part of the OsD14 catalytic triad. The polar connection between the hydroxyl hydrogen atom in Ser97 and the carbonyl oxygen in the D-ring of SLs was a key step required for the successful hydrolysis of SLs (Kagiyama et al., 2013). Further predictions obtained for these two hydrogen bonds in the enzyme-catalyzed reactions revealed that their distances and positions were similar to those expected for the ligation of (+)-GR24 (**Figure 5C**). This should be responsible for the high biological activity observed in 7FGR24. It was worth noting that, the fluorine atom could modify physicochemical properties of the GR24 analog, such as pKa and lipophilicity, improving its permeability through cell membranes (Purser et al., 2008). Moreover, as shown in **Figure 5F**, the posture of the D ring in 7FGR24 was obviously more similar to the original ligand of the crystal structure-GR24, which meant that 7FGR24 could be more conducive to hydrolysis, compared to 7BrGR24. Furthermore, these different postures could be related to the distinct atomic radii and electronegativities of observed between atoms F and Br.

In addition, we also conducted docking experiments on (-)-epi-GR24, which was inactive on seed germination. The (-)-epi-GR24 had two main binding poses differing from each other in the location of the D-ring. One pose showed the D-ring into the active site, while the other revealed the ABC-ring positioned into the active pocket with its D-ring in an outer location (**Figure 5G**). In both cases, D-ring orientation was different from the expected during (+)-GR24-OsD14 interaction. Binding energies calculated for the poses of (-)-epi-GR24 were near to the binding energy predicted for (+)-GR24. Hence, both bindings of (-)-epi-GR24 were possible, although, the D-ring would be not properly oriented

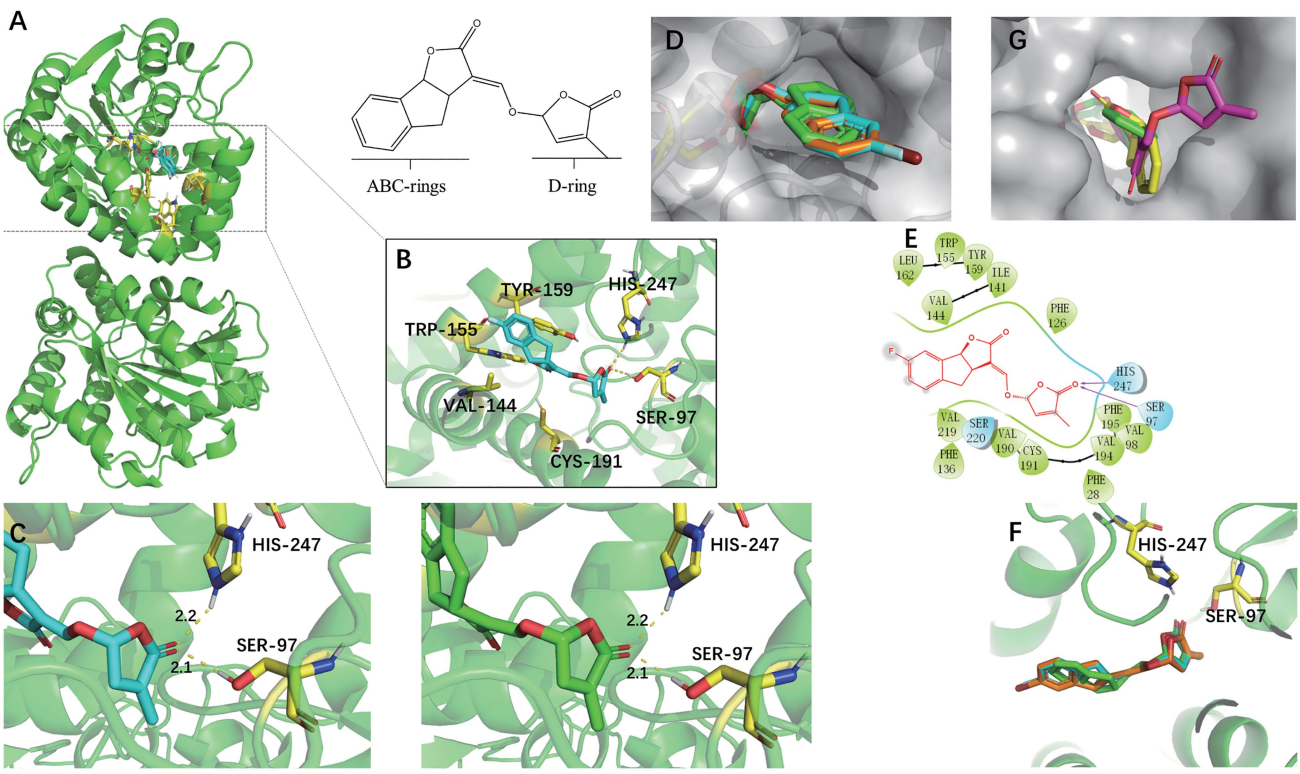

FIGURE 5 | Docking modes of (–)-epi-GR24 and the halogenated (+)-GR24 analogs with OsD14. **(A)** Pocket location of OsD14 when 7FGR24 combined on it. **(B)** Spatial position and interaction force between 7FGR24 and important amino acid residues in the active pocket. **(C)** The distance of the polar connection between the 7FGR24/(+)-GR24 and Ser 97 and His 247. **(D)** The halogenated (+)-GR24 analogs in the active pocket (the yellow sticks in the pocket are SER97). **(E)** 2D view of 7FGR24 in the catalytic site of OsD14. **(F)** Comparison of binding postures of 7FGR24, 7BrGR24, and (+)-GR24. **(G)** Two ways of connecting (–)-epi-GR24 to active pocket. The (–)-epi-GR24 is shown as yellow and purple sticks, 7BrGR24 as orange sticks, 7FGR24 as blue sticks, and the original ligand of OsD14 – (+)-GR24 as green sticks.

for the hydrolytic cleavage at the enol–ether bond catalyzed by OsD14. In addition, the docking analyses for (+)-GR24 and 7BrGR24 were similar to those obtained for 7FGR24.

CONCLUSION

Two halogenated (+)-GR24 analogs (7BrGR24 and 7FGR24) were synthesized through a relatively short number of synthetic steps and their promotive effect were tested on seed germination of *O. cumana*. Both stimulated its germination and showed a binding affinity for the SL receptor protein ShHTL7. However, 7FGR24 was the strongest germination promoter tested and had the highest binding affinity to ShHTL7. Molecular docking assays supported structural features of 7FGR24, which explained the higher activity compared to that of *rac*-GR24 and (+)-GR24. Our results indicate that 7FGR24 is a promising agent for the control of parasitic weeds.

DATA AVAILABILITY STATEMENT

The original contributions presented in the study are included in the article/**Supplementary Material**, further inquiries can be directed to the corresponding authors.

AUTHOR CONTRIBUTIONS

YY, LH, and SY conceived and designed the experiments. YK, LS, and XW designed and synthesized the analogs. YC, YK, LS, and XW assisted and performed the experiments. YC, YK, LS, XW, HF, SY, DS, LH, and YY wrote the manuscript and respective parts. YY and SY supervised the study. All authors contributed to the article and approved the submitted version.

FUNDING

This research was funded by the Ability Establishment of Sustainable Use for Valuable Chinese Medicine Resources (2060302), the National Science & Technology Fundamental Resources Investigation Program of China (2018FY100800), the Fundamental Research Funds for the Central Public Welfare Research Institutes (ZZ10-008), National Natural Science Foundation of China (81891013, 81891010, and 21702187), and Scientific and Technological Innovation Project of China Academy of Chinese Medical Sciences (CI2021A041).

ACKNOWLEDGMENTS

The authors would like to thank Yongqing Ma (Northwest Agriculture & Forest University, Xianyang, China) for kindly providing the seeds of *O. cumana*. and Dongliang Xie (Zhejiang Provincial Collaborative Innovation Center for Bamboo Resources and High-Efficiency Utilization, Zhejiang A&F University, Lin'an, China) for help with data processing.

SUPPLEMENTARY MATERIAL

The Supplementary Material for this article can be found online at: https://www.frontiersin.org/articles/10.3389/fpls.2021.725949/full#supplementary-material

Supplementary Figure S1 | ^{1}H NMR of 7BrGR24.

Supplementary Figure S2 | ^{13}C NMR of 7BrGR24.

Supplementary Figure S3 | ^{1}H NMR of 7FGR24.

Supplementary Figure S4 | ^{13}C NMR of 7FGR24.

REFERENCES

Al-Babili, S., and Bouwmeester, H. J. (2015). Strigolactones, a novel carotenoid-derived plant hormone. *Annu. Rev. Plant Biol.* 66, 161–186. doi: 10.1146/annurev-arplant-043014-114759

Bouwmeester, H., Li, C. S., Thiombiana, B., Rahimi, M., and Dong, L. M. (2021). Adaptation of the parasitic plant lifecycle: germination is controlled by essential host signaling molecules. *Plant Physiol.* 185, 1292–1308. doi: 10.1093/plphys/kiaa066

Boyer, F. D., de Saint Germain, A., Pillot, J. P., Pouvreau, J. B., Chen, V. X., Ramos, S., et al. (2012). Structure-activity relationship studies of strigolactone-related molecules for branching inhibition in garden pea: molecule design for shoot branching. *Plant Physiol.* 159, 1524–1544. doi: 10.1104/pp.112.195826

Chesterfield, R. J., Vickers, C. E., and Beveridge, C. A. (2020). Translation of strigolactones from plant hormone to agriculture: achievements, future perspectives, and challenges. *Trends Plant Sci.* 25, 1087–1106. doi: 10.1016/j.tplants.2020.06.005

Cohen, M., Prandi, C., Occhiato, E. G., Tabassco, S., Wininger, S., Resnick, N., et al. (2013). Structure-function relations of strigolactone analogs: activity as plant hormones and plant interactions. *Mol. Plant* 6, 141–152. doi: 10.1093/mp/sss134

Cook, C. E., Whichard, L. P., Turner, B., Wall, M. E., and Egley, G. H. (1967). Germination of witchweed (*Striga lutea* Lour.): isolation and properties of a potent stimulant. *Science* 154, 1189–1190. doi: 10.1126/science.154.3753.1189

Fernández-Aparicio, M., Yoneyama, K., and Rubiales, D. (2011). The role of strigolactones in host specificity of *Orobanche* and *Phelipanche* seed germination. *Seed Sci. Res.* 21, 55–61. doi: 10.1017/S0960258510000371

Hamiaux, C., Drummond, R. S. M., Janssen, B. J., Ledger, S. E., Cooney, J. M., Newcomb, R. D., et al. (2012). DAD2 is an alpha/beta hydrolase likely to be involved in the perception of the plant branching hormone, strigolactone. *Curr. Biol.* 22, 2032–2036. doi: 10.1016/j.cub.2012.08.007

Hauck, C., Müller, S., and Schildknecht, H. (1992). A germination stimulant for parasitic flowering plants from *Sorghum bicolor*, a genuine host plant. *J. Plant Physiol.* 139, 474–478. doi: 10.1016/S0176-1617(11)80497-9

Hearne, S. J. (2009). Control-the Striga conundrum. *Pest Manag. Sci.* 65, 603–614. doi: 10.1002/ps.1735

Kagiyama, M., Hirano, Y., Mori, T., Kim, S. Y., Kyozuka, J., Seto, Y., et al. (2013). Structures of D14 and D14L in the strigolactone and karrikin signaling pathways. *Genes Cells* 18, 147–160. doi: 10.1111/gtc.12025

Kang, Y. Y., Pang, Z. L., Xu, N. N., Chen, F. J., Jin, Z., and Xu, X. H. (2020). Strigolactone analogues derived from dihydroflavonoids as potent seed germinators for the broomrapes. *J. Agric. Food Chem.* 68, 11077–11087. doi: 10.1021/acs.jafc.9b08044

Kim, H. S., Chun, J. C., Yoneyama, K., Nomura, T., Takeuchi, Y., and Yoneyama, K. (2010). Structure-activity relationship of naturally occurring strigolactones in *Orobanche minor* seed germination stimulation. *J. Pestic. Sci.* 35, 344–347. doi: 10.1584/jpestics.G10-17

Musselman, L. J. (1980). The biology of *Striga*, *Orobanche*, and other root-parasitic weeds. *Annu. Rev. Phytopathol.* 18, 463–489. doi: 10.1146/annurev.py.18.090180.002335

Nomura, S., Nakashima, H., Mizutani, M., Takikawa, H., and Sugimota, Y. (2013). Structural requirements of strigolactones for germination induction and inhibition of *Striga gesnerioides* seeds. *Plant Cell Rep.* 32, 829–838. doi: 10.1007/s00299-013-1429-y

Parker, C. (2012). Parasitic weeds: a world challenge. *Weed Sci.* 60, 269–276. doi: 10.1614/WS-D-11-00068.1

Purser, S., Moore, P., and Gouverneur, V. R. (2008). Fluorine in medicinal chemistry. *Chem. Soc. Rev.* 37, 320–330. doi: 10.1039/B610213C

Rodenburg, J., Demont, M., Zwart, S. J., and Bastiaans, L. (2016). Parasitic weed incidence and related economic losses in rice in Africa. *Agric. Ecosyst. Environ.* 235, 306–317. doi: 10.1016/j.agee.2016.10.020

Rubiales, D. (2020). Broomrape threat to agriculture. *Outlooks Pest Manag.* 31, 141–145. doi: 10.1564/v31_jun_12

Scaffidi, A., Waters, M. T., Sun, Y. M., Skelton, B. W., Dixon, K., Ghisalberti, E. J., et al. (2014). Strigolactone hormones and their stereoisomers signal through two related receptor proteins to induce different physiological responses in *Arabidopsis*. *Plant Physiol.* 165, 1221–1232. doi: 10.1104/pp.114.240036

Siame, A. B., Weerasuriya, Y., Wood, K., Ejeta, G., and Bulter, L. G. (1993). Isolation of strigol, a germination stimulant for *Striga asiatica*, from host plants. *J. Agric. Food Chem.* 41, 1486–1491. doi: 10.1021/jf00033a025

Thuring, J. W. J. F., Heinsman, N. W. J. T., Jacobs, R. W. A. W. M., Nefkens, G. H. L., and Zwanenburg, B. (1997a). Asymmetric synthesis of all stereoisomers of demethylsorgolactone. Dependence of the stimulatory activity of *Striga hermonthica* and *Orobanche crenata* seed germination on the absolute configuration. *J. Agric. Food Chem.* 45, 507–513. doi: 10.1021/jf9605106

Thuring, J. W. J. F., Keltjens, R., Nefkens, G. H. L., and Zwanenburg, B. (1997c). Synthesis and biological evaluation of potential substrates for the isolation of the strigol receptor. *J. Chem. Soc. Perk. T.* 1, 759–765. doi: 10.1039/A604685A

Thuring, J. W. J. F., Nefkens, G. H. L., and Zwanenburg, B. (1997b). A symmetric synthesis of all stereoisomers of the strigol analogue GR24. Dependence of absolute configuration on stimulatory activity of *Striga hermonthica* and *Orobanche crenata* seed germination. *J. Agric. Food Chem.* 45, 2278–2283. doi: 10.1021/jf960466u

Trott, O., and Olson, A. J. (2010). AutoDock Vina: improving the speed and accuracy of docking with a new scoring function, efficient optimization and multithreading. *J. Comput. Chem.* 31, 455–461. doi: 10.1002/jcc.21334

Tsuchiya, Y., Yoshimura, M., Sato, Y., Keiko, K., Toh, S., Holbrook-Smith, D., et al. (2015). Probing strigolactone receptors in *Striga hermonthica* with fluorescence. *Science* 349, 864–868. doi: 10.1126/science.aab3831

Ueno, K., Fujiwara, M., Nomura, S., Mizutani, M., Sasaki, M., Takikawa, H., et al. (2011). Structural requirements of strigolactones for germination induction of *Striga gesnerioides* seeds. *J. Agric. Food Chem.* 59, 9226–9231. doi: 10.1021/jf202418a

Ueno, K., Sugimoto, Y., and Zwanenburg, B. (2014). The genuine structure of alectrol: end of a long controversy. *Phytochem. Rev.* 14, 835–847. doi: 10.1007/s11101-014-9380-2

Wang, Y. T., and Bouwmeester, H. (2018). Structural diversity in the strigolactones. *J. Exp. Bot.* 69, 2219–2230. doi: 10.1093/jxb/ery091

Wigchert, S. C. M., and Zwanenburg, B. (1999). An expeditious preparation of all enantiopure diastereoisomersof aromatic A-ring analogues of strigolactones, germination stimulants for seeds of the parasitic weeds *Striga* and *Orobanche*. *J. Chem. Soc. Perk. T.* 1, 2617–2623. doi: 10.1039/a904480i

Xie, X. N. (2016). Structural diversity of strigolactones and their distribution in the plant kingdom. *J. Pestic. Sci.* 41, 175–180. doi: 10.1584/jpestics.J16-02

Xie, X. N., Yoneyama, K., Kisugi, T., Uchida, K., Ito, S., Akiyama, K., et al. (2013). Confirming stereochemical structures of strigolactones produced by rice and tobacco. *Mol. Plant* 6, 153–163. doi: 10.1093/mp/sss139

Xie, X. N., Yoneyama, K., Nomura, T., and Yoneyama, K. (2010). Structure-activity relationship of naturally occurring strigolactones in *Orobanche minor* seed germination stimulation. *J. Pestic. Sci.* 35, 345–347. doi: 10.1584/jpestics.G10-17

Yao, R. F., Ming, Z. H., Yan, L. M., Li, S. H., Wang, F., Ma, S., et al. (2016). DWARF14 is a non-canonical hormone receptor for strigolactone. *Nature* 563, 469–473. doi: 10.1038/nature19073

Yoneyama, K., Xie, X. N., Kisugi, T., Nomura, T., and Yoneyama, K. (2013). Nitrogen and phosphorus fertilization negatively affects strigolactone production and exudation in *sorghum*. *Planta* 238, 885–894. doi: 10.1007/s00425-013-1943-8

Zwanenburg, B., and Blanco-Ania, D. (2018). Strigolactones: new plant hormones in the spotlight. *J. Exp. Bot.* 69, 2205–2218. doi: 10.1093/jxb/erx487

Zwanenburg, B., Mwakaboko, A. S., and Kannan, C. (2016). Suicidal germination for parasitic weed control. *Pest Manag. Sci.* 72, 2016–2025. doi: 10.1002/ps.4222

Zwanenburg, B., Mwakaboko, A. S., Reizelman, A., Anilkumar, G., and Sethumadhavan, D. (2009). Structure and function of natural and synthetic signalling molecules in parasitic weed germination. *Pest Manag. Sci.* 65, 478–491. doi: 10.1002/ps.1706

Conflict of Interest: The authors declare that the research was conducted in the absence of any commercial or financial relationships that could be construed as a potential conflict of interest.

Publisher's Note: All claims expressed in this article are solely those of the authors and do not necessarily represent those of their affiliated organizations, or those of the publisher, the editors and the reviewers. Any product that may be evaluated in this article, or claim that may be made by its manufacturer, is not guaranteed or endorsed by the publisher.

frontiers in Plant Science

ORIGINAL RESEARCH
published: 11 November 2021
doi: 10.3389/fpls.2021.747160

Identification of Conserved and Divergent Strigolactone Receptors in Sugarcane Reveals a Key Residue Crucial for Plant Branching Control

Anqi Hu[1†], Qiaoqiao Zhao[2†], Li Chen[1†], Jinping Zhao[1,3], Yuehua Wang[1], Kuiliang Feng[1], Ling Wu[1], Miao Xie[1], Xuemei Zhou[1], Langtao Xiao[3], Zhenhua Ming[2], Meng Zhang[1*] and Ruifeng Yao[1*]*

[1] State Key Laboratory of Chemo/Biosensing and Chemometrics, Hunan Provincial Key Laboratory of Plant Functional Genomics and Developmental Regulation, College of Biology, Hunan University, Changsha, China, [2] State Key Laboratory for Conservation and Utilization of Subtropical Agro-Bio Resources, Guangxi Key Laboratory for Sugarcane Biology, College of Life Science and Technology, Guangxi University, Nanning, China, [3] Hunan Province Key Laboratory of Phytohormones and Growth Development, Southern Regional Collaborative Innovation Center for Grain and Oil Crops in China, Hunan Agricultural University, Changsha, China

Strigolactones (SLs) are a class of important plant hormones mainly regulating plant architecture such as branching, which is crucial for crop yield. It is valuable to study SL signaling pathway and its physiological function in sugarcane, the most important sugar crop, for further molecular breeding. Here, two putative SL receptors SsD14a/b and the interacting F-box protein SsMAX2 were identified in *Saccharum spontaneum*. SL induced both SsD14a and SsD14b to interact with SsMAX2 in yeast. SsD14a, but not SsD14b, could bind with AtMAX2 and AtSMXL7/SsSMXL7. Overexpression of *SsD14a* or *SsMAX2* rescued the increased branching phenotypes of *Arabidopsis thaliana d14-1* or *max2-3* mutants, respectively. Moreover, the crystal structure of N-terminal truncated SsD14a was solved, with an overall structure identical to AtD14 and OsD14 in the open state, consistent with its conserved branching suppression capacity in *Arabidopsis*. In line with the biochemical observations, *SsD14b* could not completely complement in *d14-1* although these two SsD14 proteins have almost identical primary sequences except for very few residues. Complement with the combination of *SsD14b* and *SsMAX2* still failed to rescue the *d14-1 max2-3* double mutant multi-branching phenotype, indicating SsD14b–AtSMXL7 complex formation is required for regulating branching. Mutagenesis analyses revealed that residue R310 at α10 helix of SsD14a was crucial for the binding with SsSMXL7/AtSMXL7 but not SsMAX2. The site-equivalent single-residue P304R substitution enabled SsD14b to bind with AtMAX2 and AtSMXL7/SsSMXL7 and to rescue the phenotype of *d14-1 max2-3* together with SsMAX2. Moreover, this conserved Arg residue across species including rice and *Arabidopsis* determined the activity of SL receptors through maintaining their interaction with SMXL repressors. Taken together, our work identified conserved and divergent strigolactone receptors in sugarcane core SL signaling pathway and revealed a key residue crucial for plant branching control.

Keywords: sugarcane, strigolactone, receptor, D14, MAX2, SMXL

OPEN ACCESS

Edited by:
Junxian He,
The Chinese University of Hong Kong, China

Reviewed by:
Jian You Wang,
King Abdullah University of Science and Technology, Saudi Arabia
Hidemitsu Nakamura,
The University of Tokyo, Japan
Hong Yu,
Institute of Genetics and Developmental Biology, Chinese Academy of Sciences (CAS), China

***Correspondence:**
Zhenhua Ming
zhming@gxu.edu.cn
Meng Zhang
zhangmeng2019@hnu.edu.cn
Ruifeng Yao
ryao@hnu.edu.cn

[†] These authors have contributed equally to this work

Specialty section:
This article was submitted to Plant Physiology, a section of the journal Frontiers in Plant Science

Received: *25 July 2021*
Accepted: *12 October 2021*
Published: *11 November 2021*

Citation:
Hu A, Zhao Q, Chen L, Zhao J, Wang Y, Feng K, Wu L, Xie M, Zhou X, Xiao L, Ming Z, Zhang M and Yao R (2021) Identification of Conserved and Divergent Strigolactone Receptors in Sugarcane Reveals a Key Residue Crucial for Plant Branching Control. Front. Plant Sci. 12:747160. doi: 10.3389/fpls.2021.747160

INTRODUCTION

Strigolactones (SLs), which function as novel phytohormones in plant branching control (Gomez-Roldan et al., 2008; Umehara et al., 2008), promote the germination of root parasitic weeds (Cook et al., 1966) and regulate the symbiosis of arbuscular mycorrhizal fungi (Akiyama et al., 2005). SL biosynthesis and signaling pathway have become one of the most important and interesting research areas in recent years (Burger and Chory, 2020). Nowadays, enormous efforts have been made in studying SL signaling pathway. Several key components have been characterized, including receptor DWARF14 (D14), F-box protein MORE AXILLARY GROWTH2 (MAX2) and SUPPRESSOR OF MORE AXILLARY GROWTH2-LIKE-6 (SMXL6), SMXL7, and SMXL8 (Stirnberg et al., 2007; Umehara et al., 2008; Arite et al., 2009; Jiang et al., 2013; Stanga et al., 2013; Zhou et al., 2013). Different from other receptors, which could only sense hormone molecules, the receptor D14 have dual roles to sense and hydrolyze SL, demonstrating a brand-new function mode (Nakamura et al., 2013; Jia et al., 2014; de Saint Germain et al., 2016; Yao et al., 2016; Hu et al., 2017; Shabek et al., 2018; Marzec and Brewer, 2019; Seto et al., 2019; Lee et al., 2020). As a bifunctional receptor for SL, D14 is an α/β hydrolase with a complete catalytic triad, S97-H247-D218 (in *Arabidopsis*). The catalytic triad undergoes conformational change and hydrolyzes the four-ring complete SL molecules into two final products containing ABC-ring and D-ring, respectively (Kagiyama et al., 2013; Zhao et al., 2013; Yao et al., 2016; Hamiaux et al., 2018). During the hydrolysis of SL, D14 covalently binds to the D-ring at the catalytic center, then it associates with downstream protein MAX2/D3 to form D14–MAX2/D3 SCF E3 complex. This ubiquitin ligase complex will recruit the downstream transcription repressors SMXL6/7/8/D53, leading to the degradation of SMXLs/D53 through the 26S proteasome pathway (Hamiaux et al., 2012; Jiang et al., 2013; Yao et al., 2016; Wang et al., 2020). Thus, the downstream target genes, such as *Ideal Plant Architecture* 1 (IPA1) (Song et al., 2017) which inhibited by D53, would be released to regulate plant branching. Undoubtedly, the interaction with MAX2 and SMXLs by D14 is the core to turn the transduction system on (Jiang et al., 2013; Zhou et al., 2013; Soundappan et al., 2015; Wang et al., 2015; Yao et al., 2016; Khosla et al., 2020).

As the main sugar crop, sugarcane (*Saccharum* hybrid) has great economic value (Tuma, 1987; Zhang et al., 2012). Modern commercial sugarcane varieties are derived from hybrids between *Saccharum officinarum* L. and *Saccharum spontaneum* L. The yield of *Saccharum* is usually determined by the total number of effective stems and the average single stem weight. Thus, promoting tillering and improving effective tillers are key to increase production (Aitken et al., 2008; Tena et al., 2016; Glassop et al., 2021). As an important parent, *S. spontaneum* is a representative material for sugarcane research, providing the toughness, disease resistance, and regeneration of modern sugarcane, making *S. spontaneum* an important material for SL signaling study.

Here, we studied the function of core SL signaling components from *S. spontaneum*, identified two putative SL receptors with conserved and divergent capabilities to regulate plant branching, respectively, and revealed a key residue crucial for recruiting downstream signaling component and SL responses.

MATERIALS AND METHODS

Generation of Transgenic Plants

The modified vector pCAMBIA1300-cFlag (Yao et al., 2016) carrying the full coding sequence of *Arabidopsis thaliana D14* (*AtD14*), *S. spontaneum D14b* (*SsD14b*), N-terminal (amino acids 1–49) truncated *S. spontaneum D14a* (Ss*D14a*Δ*N*), N-terminal (amino acids 1–44) truncated *S. spontaneum D14b* (Ss*D14b*Δ*N*) and *S. spontaneum MAX2* (*SsMAX2*) under the control of the CaMV 35S promoter was introduced into the *Atd14-1* (Salk_057876) (Waters et al., 2012) or *Atmax2-3* (Salk_092836) (Jia et al., 2014) mutant by using the Agrobacterium-mediated floral dip method.

Similarly, we used GoldenBraid 2.0 system (Addgene[1]) (Sarrion-Perdigones et al., 2013) to construct binary plant expression vectors: 35S:SsD14b–35S:SsMAX2 (P35s:SsD14b:Tnos–P35s:SsMAX2:Tnos–Pnos:NptII:Tnos), 35S:SsD14bP304R–SsMAX2 (P35s:SsD14bP304R:Tnos–P35s:SsMAX2:Tnos–Pnos:NptII:Tnos), and 35S:AtD14–35S:AtMAX2 (P35s:AtD14:Tnos–P35s:AtMAX2:Tnos–Pnos:NptII:Tnos), which were introduced into the *Atd14-1 Atmax2-1 double* mutant, respectively, to generate transgenic plants. The primary rosette branching numbers were counted for 5-week-old plants, which were germinated on plates and grown in soil under a light/dark photoperiod of 16 h/8 h at 22°C.

Yeast Two-Hybrid Assays

To construct plasmids for yeast two-hybrid (Y2H) assays, the CDS of SsD14a/b and SsD14a/b truncations (SsD14aΔN49 and SsD14bΔN44) were cloned into yeast expression vector pGBKT7 to generate BD-SsD14a/b and BD-SsD14a/b-ΔN, and we also constructed the mutations BD-SsD14aR310P and BD-SsD14bP304R. Similarly, we obtained BD-OsD14 and BD-OsD14ΔN53. The CDS of SsMAX2, AtMAX2, and AtSMXL7 were cloned into pGADT7 to make Gal4 DNA activation domain (AD) constructs, respectively. Y2H assays were performed using the Yeastmaker Yeast Transformation System 2 (Clontech, United States). In brief, yeast strain AH109 cells were co-transformed with specific bait and prey constructs and coating on selective growth medium SD/-Leu/-Trp for 3 days at 30°C, pick the positive constructs into liquid-selective growth medium SD/-Leu/-Trp for 36 h at 30°C, 200 rpm. Washed yeast cells three times and diluted, make sure OD_{600} reached 2.5, then serial 10-fold dilutions of yeast cultures were spotted onto selective growth medium that was supplemented with 5 μM *rac*-GR24 or dimethyl sulfoxide (DMSO). All yeast transformants were grown on selective growth medium at 30°C, 4 days.

Expression and Purification of SsD14aΔN

The positive clones of *SsD14a*Δ*N* (residues 1–49) proved by DNA sequencing were transformed into *Escherichia coli* strain

[1]http://www.addgene.org/browse/article/10316/

BL21 (DE3) for protein expression. Kanamycin-resistant colonies were picked to grow in the Luria–Bertani (LB) medium (10 g/L tryptone, 10 g/L NaCl, and 5 g/L yeast extract) at 37°C until OD_{600} reached 0.6–1.0. Then 0.5 mM isopropyl-beta-D-thiogalactopyranoside (IPTG) was added to induce protein expression at 16°C for 18 h. The cell pellet was resuspended in phosphate-buffered saline (PBS) buffer containing 30 mM imidazole, and homogenized by using an ultrahigh pressure cell disrupter (JNBIO, Guangzhou, China). The lysate was centrifuged at 15,000 rpm for 1 h, and soluble proteins were loaded onto the Ni-NTA column. Target proteins were eluted by the PBS buffer containing 300 mM imidazole. The eluted SsD14aΔN (residues 1–49) was further purified by Superdex^{TM}75 (GE Healthcare, United States) at 16°C with the buffer containing 150 mM NaCl, 2 mM $MgCl_2$, 20 mM Tris pH 8.0, and 10% glycerol.

Crystallization, Data Collection, and Structure Determination

Purified SsD14aΔN (residues 1–49) (roughly 10 mg/ml) were dissolved in the buffer containing 150 mM NaCl, 2 mM $MgCl_2$, 20 mM Tris pH 8.0, and 10% glycerol. The crystals of SsD14aΔN (residues 1–49) were obtained using the hanging-drop method by mixing 1 μl protein with equal volume of reservoir solution containing 0.01 M magnesium chloride hexahydrate, 0.05 M Tris hydrochloride pH 7.5, 5% v/v 2-Propanol at 16°C for 1 week. The data of the SsD14aΔN (residues 1–49) crystal were collected on beamline BL17U1 at Shanghai Synchrotron Radiation Facility (SSRF) and processed by XDS (20124692). The structure of SsD14aΔN (residues 1–49) was determined by molecular replacement, using the structure of OsD14ΔN (residues 1–51) (PDB ID: 3VXK) as the initial searching template. Model building and structural refinement were performed by using COOT (20383002) and PHENIX (22505256), respectively. In the final model, more than 97% residues fall in the favored region in the Ramachandran plot, and the final R_{work}/R_{free} is 0.1914/0.2275. Data collection and refinement statistics are summarized in **Table 1**. The atomic coordinates and structure factors have been deposited in the Protein Data Bank.

TABLE 1 | Data collection and structure refinement statistics.

Parameters	SsD14aΔN
Data collection statistics	
Cell parameters	
a (Å)	48.81
b (Å)	88.29
c (Å)	118.52
α, β, and γ (°)	90, 90, and 90
Space group	$P2_12_12_1$
Wavelength used (Å)	0.9792
Resolution (Å)	70.81–1.65 (1.74–1.65)
No. of all reflections	356,698
No. of unique reflections	580,49
Completeness (%)	93.6 (99.5)
Average I/σ(I)	12.1 (2.6)
R_{merge}[a] (%)	11.5 (74.4)
Refinement statistics	
No. of reflections used [σ(F) > 0]	110,054
R_{work}[b] (%)	19.14
R_{free}[b] (%)	22.75
RMSD bond distance (Å)	0.008
RMSD bond angle (°)	0.909
Average *B*-value	
Average *B*-value for protein atoms	28.69
Average *B*-value for solvent atoms	28.61
No. of atoms	
No. of protein atoms	415,0
No. of solvent atoms	357
Ramachandran plot	
Res. in favored regions (%)	97.94
Res. in outlier regions (%)	0.0

RMSD, root-mean-square deviations.

[a] $R_{merge} = \Sigma_h \Sigma_i | I_{h,i} - I_h | / \Sigma_h \Sigma_i I_{h,i}$, *where,* I_h *is the mean intensity of the i observations of symmetry-related reflections of h.*

[b] $R_{work} = \Sigma(||F_p(obs)| - |F_p(calc)||)/\Sigma|F_p(obs)|$; R_{free} *is an R factor for a preselected subset (5%) of reflections that was not included in refinement.* F_p, *structure factor of protein.*

[c] *Numbers in parentheses are corresponding values for the highest resolution shell.*

RESULTS

Identification of D14 Orthologs in *Saccharum spontaneum*

The SL biosynthesis and core signaling pathways have been thoroughly studied in many plant species including *Arabidopsis thaliana* and *Oryza sativa* (**Figure 1A**), but remain to be investigated in sugarcane. To identify and investigate the SL receptor(s) D14 in *S. spontaneum* (SsD14), we searched Saccharum Genome Database (SGD)[2] (Zhang et al., 2018) using BLAST with *Arabidopsis thaliana* D14 (AtD14) and *Oryza sativa* D14 (OsD14) as queries to obtain the predicted sequences of D14 orthologs from *S. spontaneum*. Accordingly, we found two putative *D14* orthologous genes *SsD14a* (Sspon.001B0005800) and *SsD14b* (Sspon.001B0005830) in *S. spontaneum*.

[2]http://sugarcane.zhangjisenlab.cn

The phylogenetic analysis showed that SsD14s exhibit closer relationships with OsD14 from rice, which belongs to Gramineae too (**Figure 1B**). The similarity between SsD14a and OsD14 is 84.91% at the amino sequence, and the similarity between SsD14b and OsD14 is 85.94%. Sequence alignment and structural annotation showed that SsD14a/b, AtD14, and OsD14 exhibit both considerable identities at the primary amino acid sequence level and have the same catalytic triad Ser-His-Asp (**Figure 1C**). These information implies conserved physiological functions of SsD14 proteins.

SsD14a and SsD14b Have Different Binding Properties With MAX2 and SMXLs

Similarly, we searched SGD to obtain the predicted sequences of MAX2 and SMXL7 orthologs from *S. spontaneum*. Then, we found the putative orthologous genes *SsMAX2*

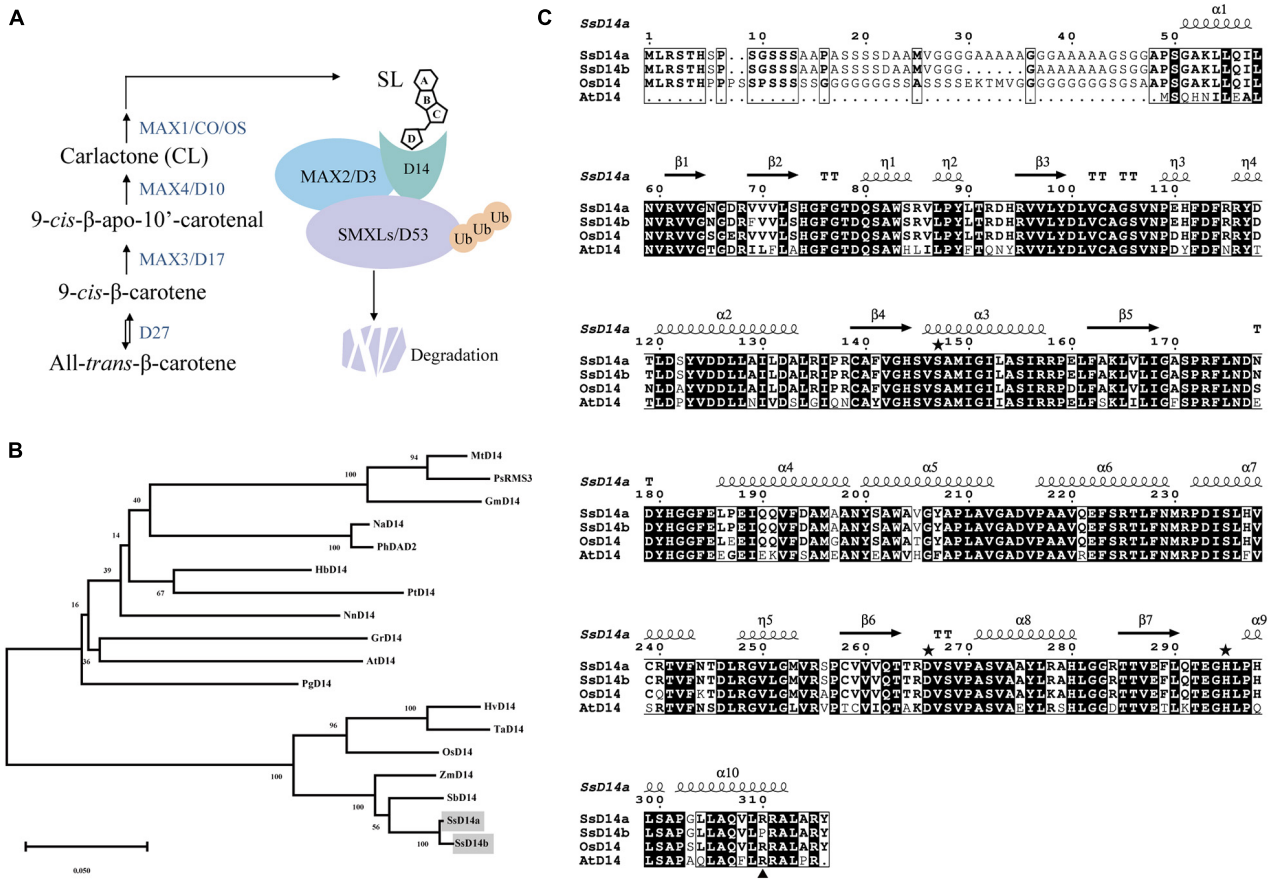

FIGURE 1 | Phylogenetic analysis and sequence alignment of D14 orthologs. **(A)** A simplified model for SL biosynthesis and core signaling pathway. **(B)** Phylogenetic analysis of D14 orthologs. The phylogenetic tree was generated with 18 full-length amino acid sequences of D14 orthologs using MEGA. The evolutionary history was inferred using the Neighbor-Joining method. The percentage of replicate trees in which the associated taxa clustered together in the bootstrap test (1,000 replicates) were shown next to the branches. The evolutionary distances were computed using the p-distance method. Sequence information in this work can be found in GenBank or the Saccharum Genome Database (http://sugarcane.zhangjisenlab.cn/) under the following accession numbers: *Medicago truncatula* D14 (XP_003589086), *Pisum sativum* RMS3 (AMB61024), *Glycine max* D14 (XP_003557012), *Nicotiana attenuata* D14 (XP_019258478), *Petunia hybrida* DAD2 (AFR68698), *Hevea brasiliensis* D14 (XP_021646820), *Populus trichocarpa* D14 (XP_002302409), *Nelumbo nucifera* D14 (XP_010248100), *Gossypium raimondii* D14 (XP_012451974), *Arabidopsis thaliana* D14 (NP_566220), *Punica granatum* D14 (OWM70752), *Hordeum vulgare* D14 (AJP07999), *Triticum aestivum* D14 (AK332360), *Oryza sativa* D14 (XP_015631400), *Zea mays* D14 (NP_001150635), *Sorghum bicolor* D14 (XP_002468316), *Ss5800* (Sspon.001B0005800), and *Ss5830* (Sspon.001B0005830). **(C)** Sequence alignment and structural annotation of D14 orthologs. ESPript was used to analyze the multiple sequence alignments generated by Clustal Omega (Sievers et al., 2011; Robert and Gouet, 2014) with the several D14 orthologs listed in **Figure 1A**. Secondary structure elements of *Saccharum spontaneum* D14 (GO:0005800) crystal structure (PDB code: 7F5W) are displayed on top of the alignments. Identical and conserved residues are highlighted by red and yellow grounds, respectively. The three catalytic residues, Ser, Asp, and His, are indicated by green stars. The amino acids marked with blue triangles are putative key amino acids for identifying downstream inhibitors.

(Sspon.008D0018870) and SsSMXL7 (Sspon.007A0023280). To determine the biochemical function of SsD14a and SsD14b, we used Y2H assays to examine the interaction of SsD14s proteins with SsMAX2, AtMAX2, SsSMXL7, and AtSMXL7. Surprisingly, there were significant binding ability differences between SsD14a and SsD14b. The results showed that SsD14a interacted with SsSMXL7 and AtSMXL7 and interacted with AtMAX2 slightly. However, SsD14b interacted with neither AtMAX2 nor AtSMXL7. Meanwhile, Y2H results showed a strong interaction of SsMAX2 with both SsD14a and SsD14b (**Figure 2**). In other words, although SsD14a and SsD14b share 97.47% similarity in amino acid sequence, they have different preferences in binding downstream signaling partners, which leading us to speculate that the differences in interactions are attributed to some of these different residues.

SsD14aΔN, but Not SsD14b and SsD14bΔN, Can Well Rescue the Branching Phenotype of *Arabidopsis d14-1* Mutant

Previous reports showed that many D14 of Gramineae species contain an extra N-terminal peptides when compared to AtD14 (Yao et al., 2018). Related studies have proved that both the full-length OsD14 and the N-terminally truncated OsD14 were able to complement the multi-branching mutant *Arabidopsis d14-5*,

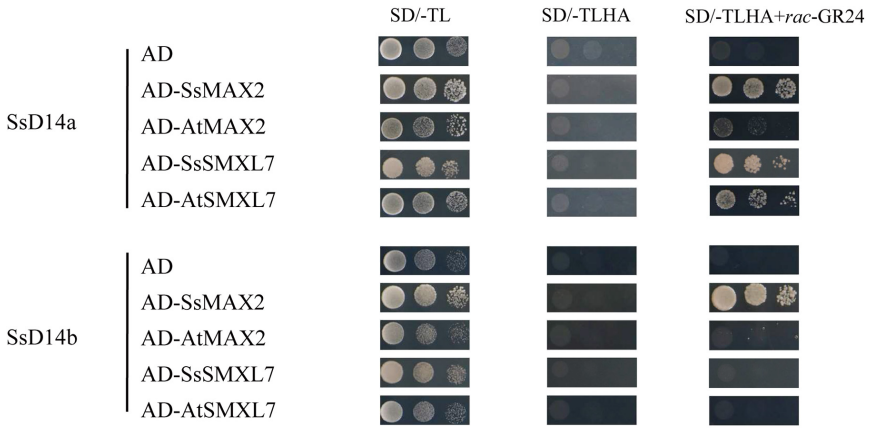

FIGURE 2 | Binding capacity of SsD14s with downstream signaling partners. Yeast two-hybrid (Y2H) assays for SsD14s and AtD14 interactions with SsMAX2/AtMAX2 and SsSMXL7/AtSMXL7. SsD14a, SsD14b, and AtD14 were fused to GAL4-BD. SsMAX2, AtMAX2, SsSMXL7, and AtSMXL7 were fused to GAL4-AD. Serial 10-fold dilutions of yeast cultures were spotted onto the control medium (SD/-Leu/-Trp) and selective medium (SD/-Leu/-Trp/-His/-Ala) in the absence or presence of 5 μM *rac*-GR24 or DMSO control. Images show growth after 4 days at 30°C.

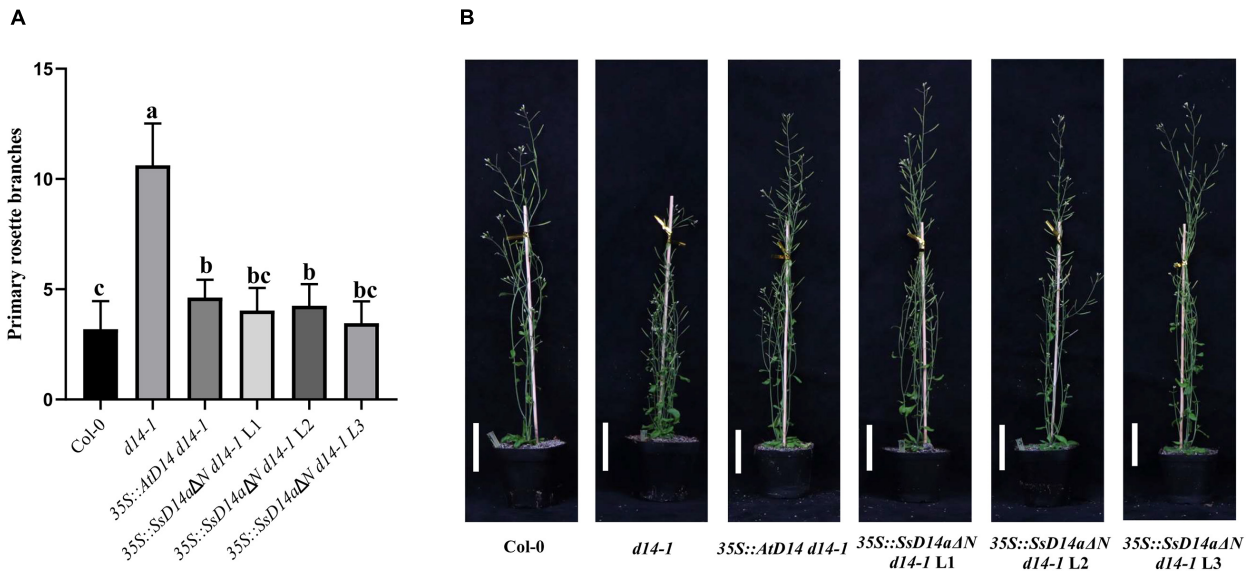

FIGURE 3 | SsD14aΔN can rescue the branching phenotype of *Arabidopsis d14-1* mutant. **(A)** Quantitative analysis on primary branch numbers of Col-0, *d14-1*, *AtD14 14-1*, and three lines for overexpression of *35S:SsD14aΔN*. Values are represented as mean ± SD ($n \geq 16$); $p < 0.05$ [one-way ANOVA and Tukey's honestly significant difference (HSD)]. The different letters indicated the different significance. **(B)** The representative branching phenotypes of 5-week-old Col-0 and the indicated mutants. Scale bar = 5 cm.

even the N-truncated D14 have more stronger interaction with AtMAX2 and complement *d14* mutant better than the full-length version (Yao et al., 2018). According to our results of Y2H assays, SsD14aΔN can interact with AtMAX2 and AtSMXL7 as the full-length SsD14a did (**Supplementary Figure 1**). SsD14aΔN was introduced to complement *Arabidopsis d14-1* mutants. We also generated the *35S:AtD14 d14-1* plants as positive control. The results showed no significant difference between the number of primary branches between *35S:SsD14aΔN d14-1* and *35S:AtD14 d14-1* (**Figures 3A,B**), which means that SsD14aΔN was able to rescue the multi-branching phenotypes. In addition, the leaf morphology (length/width ratio) was also recovered by *SsD14aΔN* (**Supplementary Figure 2A**). Therefore, SsD14a is functionally conserved when compared with AtD14.

However, the complementation results were quite different for SsD14b. According to the Y2H results, neither N-terminal truncated SsD14b nor full-length SsD14b could interact with AtMAX2 and AtSMXL7 (**Figure 2** and **Supplementary Figure 1**). We transferred the full-length *SsD14b* to the *Arabidopsis d14-1* mutant and obtained *35S:SsD14b d14-1* plants. We found that SsD14b cannot rescue the *d14-1* multi-branching phenotype (**Figure 4A**). But interestingly, we found that the height of

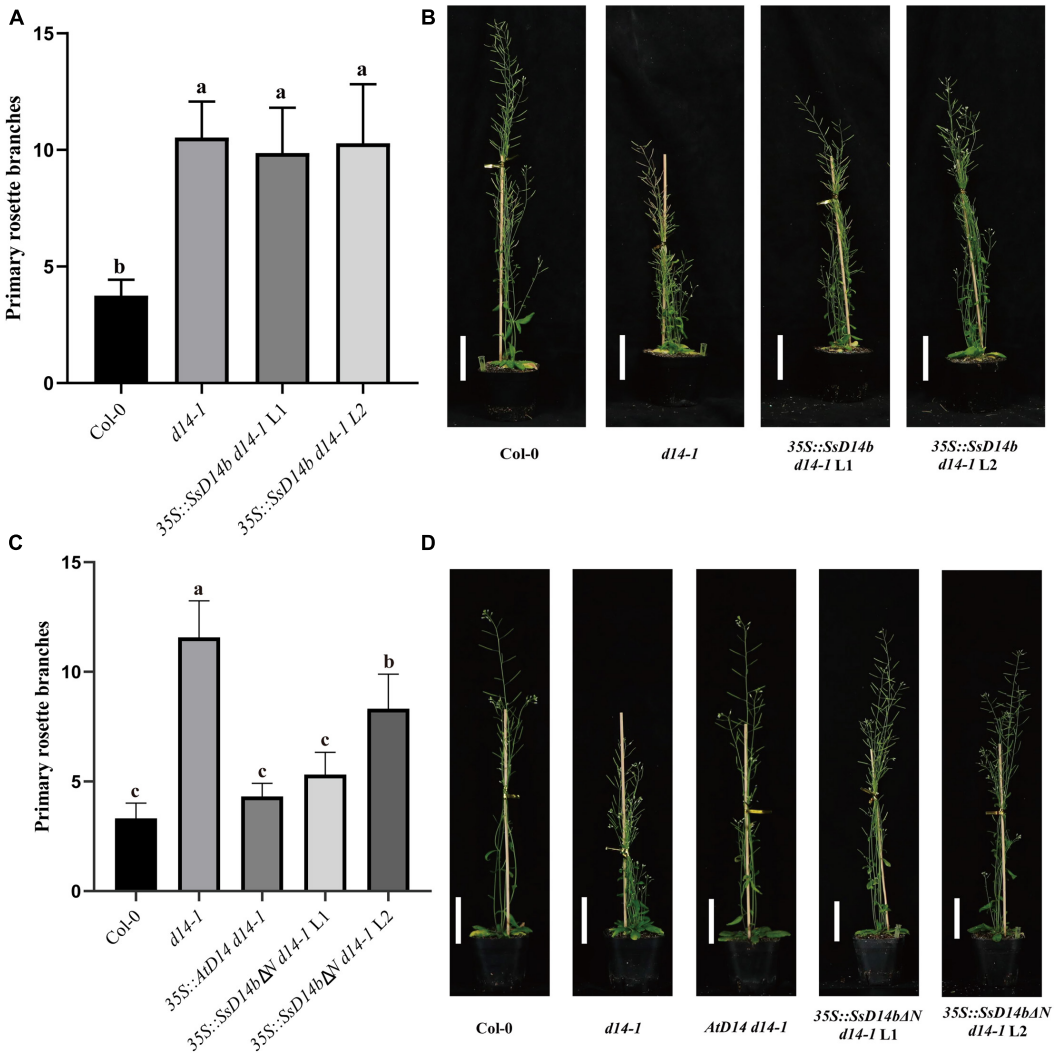

FIGURE 4 | SsD14b and SsD14bΔN failed to well rescue the branching phenotype of *Arabidopsis d14-1* mutant. **(A)** Quantitative analysis on primary branch numbers of Col-0, *d14-1,* and two lines for overexpression of *35S:SsD14b*. Values are represented as mean ± SD ($n \geq 16$); $p < 0.05$ [ANOVA and Tukey's honestly significant difference (HSD)]. The different letters indicated the different significance. **(B)** The representative branching phenotypes of 5-week-old Col-0 and the indicated mutants. Scale bar = 5 cm. **(C)** Quantitative analysis on primary branch numbers of Col-0, *d14-1*, *AtD14 14-1*, and two lines for overexpression of *35S:SsD14b*Δ*N49*. Values are represented as mean ± SD ($n \geq 16$); $p < 0.05$ [ANOVA and Tukey's honestly significant difference (HSD)]. The different letters indicated the different significance. **(D)** The representative branching phenotypes of 5-week-old Col-0 and the indicated mutants. Scale bar = 5 cm.

transgenic *35S:SsD14b d14-1* seemed to have a partial restoration (**Figure 4B**), which will be further investigated in the future project. We found that the multi-branched phenotype of one complemented line was only partially restored in *35S:SsD14b*Δ*N d14-1* transgenic lines and still differed from WT, indicating that *35S:SsD14b*Δ*N* cannot fully complement *Atd14-1*. The difference between *35S:SsD14b d14-1* and *35S:SsD14b*Δ*N d14-1* was that multi-branching and the leaf morphology of *35S:SsD14b*Δ*N d14-1* were rescued in different degrees but both not thoroughly (**Figure 4** and **Supplementary Figure 2B**). No obvious interactions of SsD14b/SsD14bΔN with AtSMXLs were detected in our work, which is probably because that the interactions were too weak to be detected in our current Y2H system. Consistent with this, the complementation effect of SsD14bΔN is significantly lower compared to SsD14a. Taken together, SsD14a and SsD14b may function as conserved and divergent SL receptors in sugarcane, respectively.

Crystal Structure of SsD14aΔN Possesses an Overall Architecture Identical to Other D14 Orthologs in the Open State

The crystal structure of SsD14aΔN was determined at a resolution of 1.65 Å (**Table 1**). SsD14a belongs to the α/β hydrolase superfamily, of which the structure consists of an α/β hydrolase core domain and a four-helix lid domain (αT1, αT2, αT3, and αT4) (**Figure 5**). The catalytic triad residues of S145,

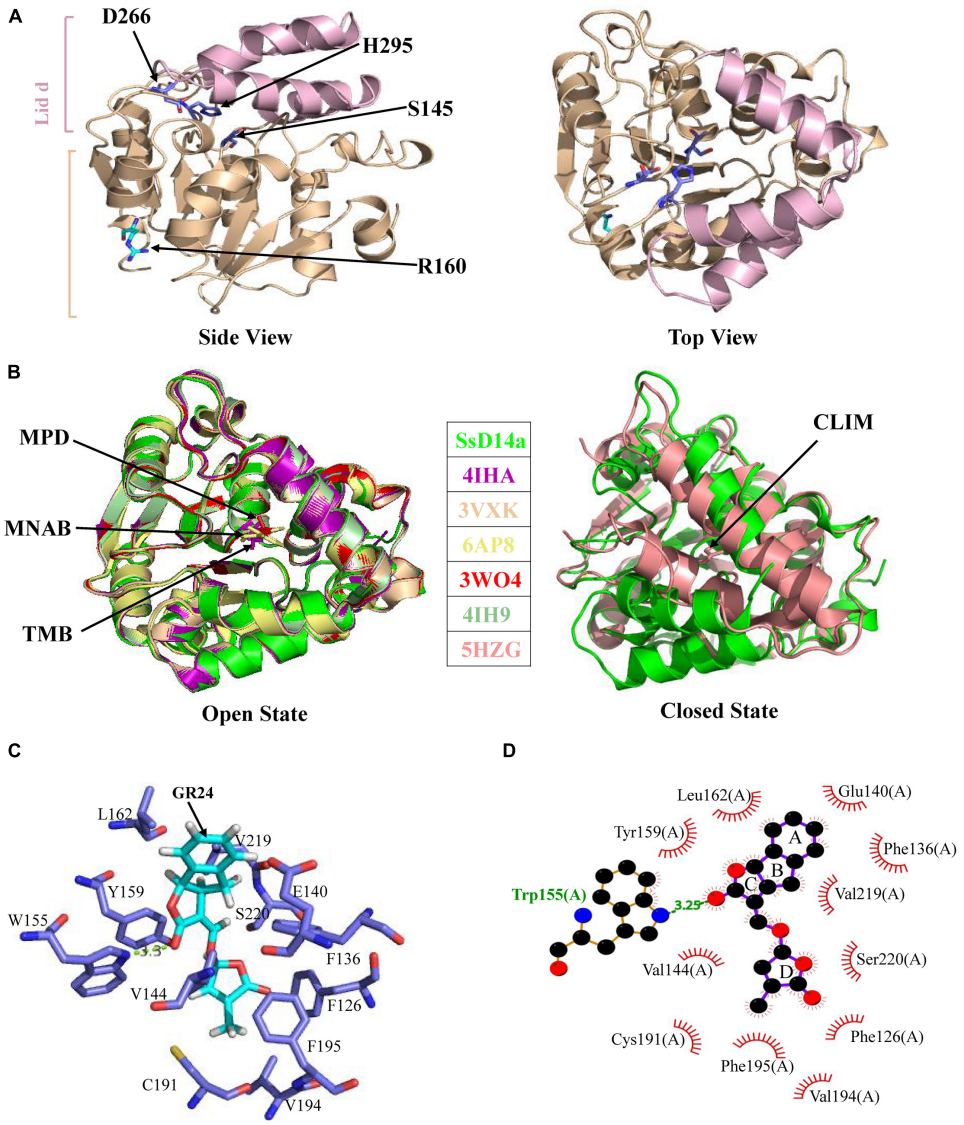

FIGURE 5 | Crystal structure of SsD14aΔN and structural comparisons with other D14 orthologs. **(A)** Crystal structure of SsD14a. Left panel is a side view of SsD14a. The overall structure is represented in cartoon, with the core domain colored in light wheat and the lid domain colored in pink. The three catalytic triad residues are indicated and shown in sticks. Right panel is a top view of SsD14a. **(B)** Structural comparisons reveal that SsD14a is in an open state. Left and right panels show structural comparison of SsD14a with the orthologous proteins of other species in the open and closed state, respectively. AtD14 and OsD14 structures are indicated by their respective PDB IDs, whereas, the structure of SsD14 is indicated by SsD14a. The bound ligands are highlighted and represented as sticks. MPD (in PDB ID 3W04), MNAB (in PDB ID 6AP8), TMB (in PDB ID 4IHA), and CLIM (in PDB ID 5HZG) are abbreviated for 2-methyl-pentanediol, 2-(2′-methyl-3′-nitroanilino) benzoic acid, (2R,3R)-2,4,4-trihydroxy-3-methylbutanal, and (2Z)-2-methylbut-2-ene-1,4-diol, respectively. **(C)** A model for GR24 binding in SsD14a. The SsD14a–GR24 complex is generated by the UCSF DOCK 6.0. Details of GR24 binding are illustrated in the catalytic pocket of SsD14a, which is shown in the light blue cartoon representation. The SL analog GR24, together with its key contacting residues from the binding pocket, are labeled as colored sticks. **(D)** The LigPlot of possible SsD14a–GR24 interactions, related to **(C)**. The red, blue and black atoms denote oxygen, nitrogen and carbon, respectively. Hydrogen bonds between SsD14a and GR24 are shown as green dashed lines. The van der Waals contacts are indicated as continuous red lines.

D266, and H295, distributed on the loops following the β4, β6, and β7 strands, are located at the bottom of the hydrophobic substrate-binding pocket. The rest of the core domain is made up of seven β strands (β1–β7) and six α helices (α1, α2, α3, α8, α9, and α10). R310 is located at the α10 helix of SsD14a.

To gain insights into the conformational state of SsD14a, we performed structural comparisons between SsD14a and other D14 orthologs from other plants. Structure comparisons revealed that the overall structure of SsD14a was identical to those from other plants in the open state (**Figure 5B**), with root-mean-square deviations (RMSD) ranging from 0.250 to 0.301 Å (**Figure 5B**). Notably, the overall structure of SsD14a in the open state was apparently larger than the closed state of AtD14-CLIM (covalently linked intermediate molecule, a hydrolysis

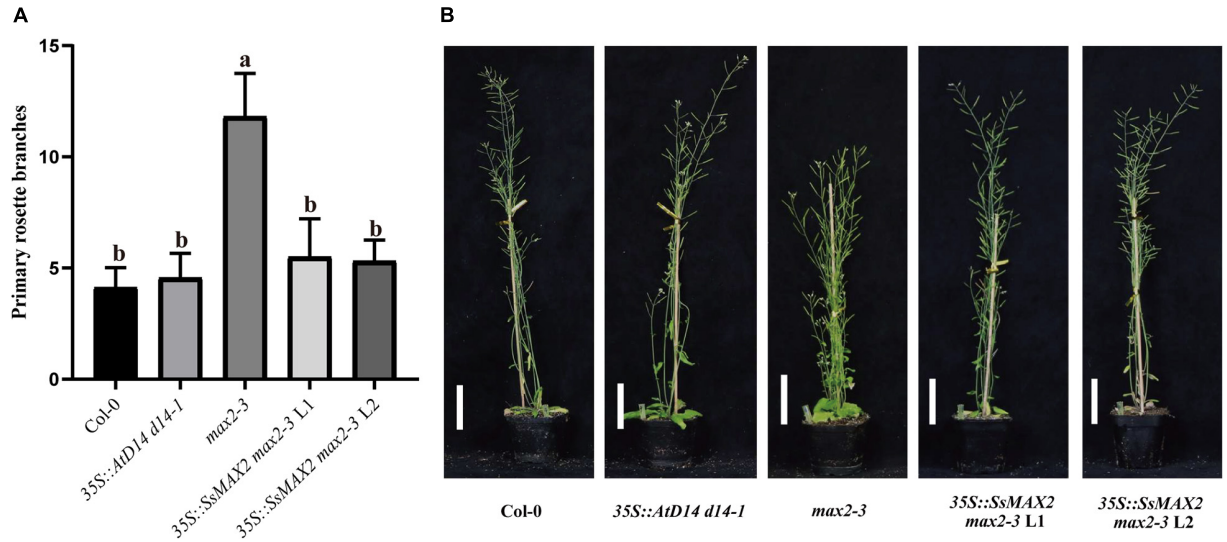

FIGURE 6 | SsMAX2 can rescue the phenotypes of *max2-3* mutant. **(A)** Quantitative analysis on primary branch numbers of Col-0, *max2-3*, *AtD14 d14-1* and two lines for overexpression of *35S*:SsMAX2. Values are represented as mean ± SD ($n \geq 16$); $p < 0.05$ [ANOVA and Tukey's honestly significant difference (HSD)]. The different letters indicated the different significance. **(B)** The representative branching phenotypes of 5-week-old Col-0 and the indicated mutants. Scale bar = 5 cm.

intermediate of SL molecule), thus these two structures cannot be well aligned, with an RMSD of 0.662 Å. Furthermore, results of docking approaches demonstrated extensive binding of GR24 by residues in the catalytic pocket of SsD14a (**Figures 5C,D**). In general, the structural characteristics of SsD14a are highly conserved and guarantee its branching inhibition function.

SsMAX2 Rescued the Branching Phenotype of *Arabidopsis max2-3* Mutant

To clarify the differences on SL transduction between the two SsD14 proteins, SsMAX2, another key SL signaling transduction component, was obtained and verified its function. SsMAX2 interacted with AtD14 in an SL-dependent manner with the intensity similar to AtMAX2 (**Figure 2**). We further investigated the physiological function of SsMAX2 proteins in *Arabidopsis*. We introduced full-length *S. spontaneum MAX2* into the *Arabidopsis max2-3* mutant under the control of a 35S promoter. As shown in **Figure 6** and **Supplementary Figure 2C**, *35S:SsMAX2 max2-3* rescued the branching and leaf phenotype of *max2-3* to a level comparable with the wild-type Col-0. These genetic data indicated that SsMAX2 could inhibit axillary branching of *Arabidopsis*. Our results demonstrated that SsMAX2 can resemble AtMAX2 to play a physiological role in *Arabidopsis*.

Single Residue Substitution of SsD14b Rescues the Binding Affinity With MAX2 and SMXLs

Further sequence comparison with AtD14 and OsD14 found that only SsD14b had a proline (P304) at the α10 helix, whereas, other D14 proteins contained an arginine (R) (**Figure 1B**). To further explore the mechanism underlying the differences in protein interactions, we made point mutations to SsD14a and SsD14b to obtain BD-SsD14aR310P and BD-SsD14bP304R, respectively. We were surprised to find that the point mutation SsD14aR310P no longer interacted with SsSMXL7 and AtSMXL7 (**Figure 7A**), but still interacted with SsMAX2. The point mutation SsD14bP304R turn out to obviously interact with AtSMXL7. Inferring from these results, for D14, residue R (like R310 of SsD14a) at the α10 helix might be the key residue contributing to the association with repressor factors SMXLs.

The R262P/R312P Point Mutation Disrupts the Function of AtD14/OsD14 to Bind With Downstream Signaling Partners

To further investigate the importance and the widespread of the amino acid site of R310 (in SsD14a), we performed point mutation validation in AtD14 and OsD14. We obtained BD-AtD14R262P and BD-OsD14ΔNR261P by site-directed mutagenesis PCR. Y2H results showed that AtD14R262P substitution largely affected the interaction with AtSMXL7 and also greatly weakened the interaction with AtMAX2 (**Figure 7B**). Similar observation was also found in BD-OsD14ΔNR261P (**Figure 7C**). Unlike AtD14, OsD14 showed hormone-dependent interaction with SsSMXL7. We speculate that this is a result of the higher sequence similarity between rice and sugarcane, which both belong to Gramineae. Interestingly, AtD14R262P and OsD14ΔNR261P, like wild-type proteins, still have strong hormone-dependent interactions with SsMAX2. The SsMAX2 protein can bind strongly with mutant proteins, which may have application in resolving the crystal structures of certain important D14 mutant proteins in complex with SsMAX2. In general, for AtD14 and OsD14, we further

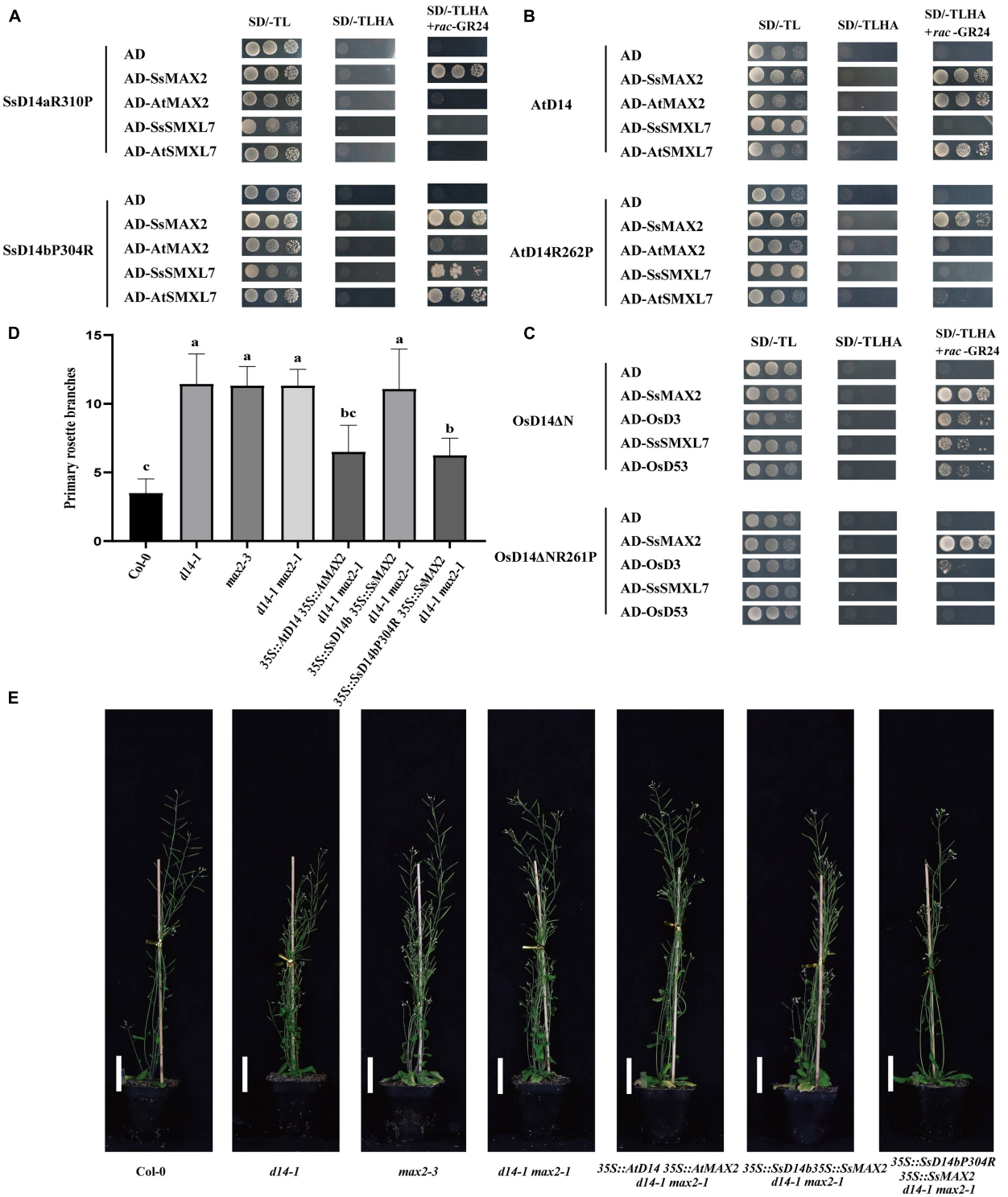

FIGURE 7 | Single residue substitution rescues the biochemical and physiological function of SsD14b. **(A)** Y2H analyses of the interaction between BD-SsD14aR310P and BD-SsD14bP304R for AD-SsMAX2, AD-AtMAX2, AD-SsSMXL7, and AD-AtSMXL7. Serial 10-fold dilutions of yeast cultures were spotted onto the control medium (SD/-Leu/-Trp) and selective medium (SD/-Leu/-Trp/-His/-Ala) in the absence or presence of 5 μM rac-GR24) or DMSO control. Images show growth after 4 days at 30°C. **(B)** Y2H analyses of the AtD14 and AtD14R262P binding with SsMAX2, AtMAX2, SsSMXL7, and AtSMXL7. **(C)** Y2H analyses of the OsD14ΔN and OsD14ΔNR261P binding with SsMAX2, OsD3, SsSMXL7, and OsD53. **(D)** Quantitative analysis on primary branch numbers of Col-0, *d14-1, max2-3*, *d14-1 max2-1*, and T1 lines for overexpression of *35S:D14 35S:MAX2 d14-1 max2-1*, *35S:SsD14b 35S:SsMAX2 d14-1 max2-1*, *35S:SsD14b-P304R 35S:SsMAX2 d14-1 max2-1*, and the indicated mutants. Values are represented as mean ± SD ($n \geq 16$); $p < 0.05$ [ANOVA and Tukey's honestly significant difference (HSD)]. The different letters indicated the different significance. **(E)** The representative branching phenotypes of five-week-old Col-0 and the indicated mutants. Bars = 5 cm.

verified the importance of this site for binding downstream signal components.

Single Residue Substitution Rescues the Physiological Function of SsD14b

In the SL signaling pathway, the D14 receptor senses SL before binding the F-box protein MAX2 to form the D14–MAX2 complex. Later, the complex would recruit and degrade the downstream repressor protein AtSMXLs through ubiquitination–proteasome pathway to regulate plant branching (Jiang et al., 2013; Zhou et al., 2013). To investigate whether SsD14bP304R has gained the capability in plant branching control, we generated and compared the transgenic *Arabidopsis 35S:SsD14b 35S:SsMAX2 d14-1 max2-1* and *35S:SsD14b-P304R 35S:SsMAX2 d14-1 max2-1* by introducing full-length *SsMAX2* together with *SsD14b* or *SsD14b-P304R* into the *d14-1 max2-1* double mutant. We also generated the *35:AtD14 35S:AtMAX2 d14-1 max2-1* plants as positive control. We found that *35S:SsD14b-P304R 35S:SsMAX2 d14-1 max2-1* showed similar primary branching and leaf morphology as *35S:AtD14 35S:AtMAX2 d14-1 max2-1* (**Figures 7D,E** and **Supplementary Figure 2D**). However, the complex of SsD14b–SsMAX2 was unable to inhibit the branching of *d14-1 max2-1* double mutant, consistent with the capability of SsD14b or SsD14b-P304R to bind AtSMXL7 (**Figures 2**, **7A**). These results demonstrated that P304R single-residue substitution endows SsD14b with the branching inhibition function, indicating the close correlation between SL responses and receptor–repressor interaction.

DISCUSSION

Sugarcane is a raw material for sucrose and can also be used as an energy substitute for refined ethanol, which has high economic value. The effective yield of sugarcane is closely related to the effective branching and robust plant architecture. As the ancestor of modern sugarcane and possessing a complete genome database, *S. spontaneum* is an important research material. To lay a foundation for further sugarcane SL pathway studies and related molecular breeding, we turned to identify and study core SL components in *S. spontaneum*.

The SL perception by the receptor D14 initiates the SL signaling transduction pathway. At present, the function of D14 has been studied in many species, such as *Oryza sativa* (D14), *Petunia hybrida* (DAD2), and *Pisum sativum* (RMS3), certificating that D14 is highly conserved in different species (Arite et al., 2009; Hamiaux et al., 2012; de Saint Germain et al., 2016; Yao et al., 2018). Here, two *D14* orthologous genes in *S. spontaneum*, *SsD14a* and *SsD14b*, were identified according to ortholog searching in *S. spontaneum* genome. SsD14a and SsD14b were extremely similar with only few residue exceptions. Additionally, evolutionary analysis showed that both SsD14s were closer to SbD14, ZmD14, and OsD14, all of which are Gramineae. However, Y2H experiments revealed that only SsD14a could interact with AtMAX2 and AtSMXL7/SsSMXL7, whereas, SsD14b could not. Interestingly, there was no difference in the binding affinity with SsMAX2 between SsD14b and SsD14a. Transgenic *Arabidopsis* plants showed that only SsD14a could well rescue the *d14-1* mutant. Furthermore, the structure of SsD14a is identical to AtD14 and OsD14 in the open state, with RMSD ranging from 0.250 to 0.301 Å. These results indicated SsD14a functioned the same as known D14 proteins, such as AtD14, suggesting that a similar SL transduction system exists in *S. spontaneum*.

In the current model, upon perception of SL, the receptor D14 recruits MAX2 and SMXLs to initiate SL signal transduction to regulate branching. However, SsD14b has problems in binding with AtSMXL7/SsSMXL7 and AtMAX2 and is unable to transduce SL signals to inhibit branching by forming such D14–MAX2–SMXL complex. It is interesting that SsD14b, with only very few residue differences from SsD14a, cannot rescue *d14-1* mutant. Meanwhile, through further sequence comparison with AtD14, OsD14, and other reported D14 orthologs, it was found that only SsD14b contains a Proline (P) at position 304, and the rest of the D14 proteins were all Arginine (R) (**Figure 1**). To verify the effects of this residue site, we obtained point mutations at equivalent sites to obtain SsD14aR310P and SsD14bP304R. After Y2H verification, the point mutation of the two proteins did not affect the interaction with SsMAX2. By contrast, SsD14aR310P no longer interacted with SsSMXL7 or AtSMXL7, but SsD14bP304R interacted with SsSMXL7 and AtSMXL7, suggesting that the R310/P304 site in SsD14s did affect the interaction with the downstream repressor protein SMXLs to form functional D14–MAX2–SMXL complex.

To further verify whether the failure of SsD14b to rescue *Arabidopsis d14-1* is attributed to the loss of SMXL binding ability, we introduced *SsMAX2* together with *SsD14b* or *SsD14b-P304R* into the *d14-1 max2-1* double mutant to express c D14–MAX2 complex. Our results confirmed the importance of SMXL binding by SL receptor and indicated that the assembly of complete D14–MAX2–SMXLs complex is essential for SL responses, although SsD14b–SsMAX2 complex might associate with other proteins but not SMXLs to exert certain function. Additionally, we found that SsMAX2 could bind with D14 proteins from various species much stronger than AtMAX2 and OsD3, suggesting that MAX2 proteins from different plant species may have diverse capabilities to transduce SL signal and would serve as valuable sources for structural studies on SL signaling.

Taken together, our findings shed new light on the study of strigolactone receptors and their interaction with downstream signaling partners, and may have potential application value in the molecular breeding of plant architecture.

ACCESSION NUMBER

The crystal structure of SsD14a has been deposited in the Protein Data Bank under the accession code 7F5W. *S. spontaneum* genes involved in this article can be found at the Saccharum Genome

Database (SGD: http://sugarcane.zhangjisenlab.cn) under the following accession numbers: *SsD14a* (Sspon.001B0005800), *SsD14b* (Sspon.001B0005830), *SsMAX2* (Sspon.008D0018870), and *SsSMXL7* (Sspon.007A0023280).

DATA AVAILABILITY STATEMENT

The datasets presented in this study can be found in online repositories. The names of the repository/repositories and accession number(s) can be found in the article/**Supplementary Material**.

AUTHOR CONTRIBUTIONS

RY, MZ, and LC conceived and designed the research. AH and MX constructed the vectors. AH performed the yeast two-hybrid assays. QZ and ZM performed the protein purification, crystallization, and structure analysis. AH, JZ, YW, KF, XZ, LW, and XZ conducted *Arabidopsis* transformation and phenotype observations. AH, QZ, LC, LX, MZ, ZM, and RY analyzed the data. AH, QZ, LC, MZ, ZM, and RY wrote the manuscript. All authors read and approved the manuscript.

FUNDING

We acknowledge the funding support by the National Natural Science Foundation of China (Nos. 32070321 and 32000226), State Key Laboratory for Conservation and Utilization of Subtropical Agro-Bio resources (Nos. SKLCUSA-b201807, SKLCUSA-b201906, and SKLCUSA-b201907), China Hunan Provincial Science and Technology Department (Nos. 2019RS2019 and 2020JJ3007), and the Guangxi Natural Science Foundation (No. 2020GXNSFFA297007).

ACKNOWLEDGMENTS

We thank David C. Nelson (University of California, Riverside, CA, United States) and Ke-xuan Tang (Shanghai Jiao Tong University) for providing *Arabidopsis* mutants or vectors.

SUPPLEMENTARY MATERIAL

The Supplementary Material for this article can be found online at: https://www.frontiersin.org/articles/10.3389/fpls.2021.747160/full#supplementary-material

REFERENCES

Aitken, K. S., Hermann, S., Karno, K., Bonnett, G. D., McIntyre, L. C., and Jackson, P. A. (2008). Genetic control of yield related stalk traits in sugarcane. *Theor. Appl. Genet.* 117, 1191–1203. doi: 10.1007/s00122-008-0856-6

Akiyama, K., Matsuzaki, K., and Hayashi, H. (2005). Plant sesquiterpenes induce hyphal branching in arbuscular mycorrhizal fungi. *Nature* 435, 824–827. doi: 10.1038/nature03608

Arite, T., Umehara, M., Ishikawa, S., Hanada, A., Maekawa, M., Yamaguchi, S., et al. (2009). d14, a strigolactone-insensitive mutant of rice, shows an accelerated outgrowth of tillers. *Plant Cell Physiol.* 50, 1416–1424. doi: 10.1093/pcp/pcp091

Burger, M., and Chory, J. (2020). The Many Models of Strigolactone Signaling. *Trends Plant Sci.* 25, 395–405. doi: 10.1016/j.tplants.2019.12.009

Cook, C. E., Whichard, L. P., Turner, B., Wall, M. E., and Egley, G. H. (1966). Germination of Witchweed (Striga lutea Lour.): isolation and Properties of a Potent Stimulant. *Science* 154, 1189–1190. doi: 10.1126/science.154.3753.1189

de Saint Germain, A., Clave, G., Badet-Denisot, M. A., Pillot, J. P., Cornu, D., Le Caer, J. P., et al. (2016). An histidine covalent receptor and butenolide complex mediates strigolactone perception. *Nat. Chem. Biol.* 12, 787–794. doi: 10.1038/nchembio.2147

Glassop, D., Perroux, J., and Rae, A. (2021). Differences in sugarcane stool branching within Saccharum spontaneum genotypes and compared to Saccharum officinarum and commercial varieties. *Euphytica* 217:50. doi: 10.1007/s10681-021-02789-w

Gomez-Roldan, V., Fermas, S., Brewer, P. B., Puech-Pages, V., Dun, E. A., Pillot, J. P., et al. (2008). Strigolactone inhibition of shoot branching. *Nature* 455, 189–194. doi: 10.1038/nature07271

Hamiaux, C., Drummond, R. S., Janssen, B. J., Ledger, S. E., Cooney, J. M., Newcomb, R. D., et al. (2012). DAD2 is an alpha/beta hydrolase likely to be involved in the perception of the plant branching hormone, strigolactone. *Curr. Biol.* 22, 2032–2036. doi: 10.1016/j.cub.2012.08.007

Hamiaux, C., Drummond, R. S. M., Luo, Z., Lee, H. W., Sharma, P., Janssen, B. J., et al. (2018). Inhibition of strigolactone receptors by N-phenylanthranilic acid derivatives: structural and functional insights. *J. Biol. Chem.* 293, 6530–6543. doi: 10.1074/jbc.RA117.001154

Hu, Q., He, Y., Wang, L., Liu, S., Meng, X., Liu, G., et al. (2017). DWARF14, A Receptor Covalently Linked with the Active Form of Strigolactones, Undergoes Strigolactone-Dependent Degradation in Rice. *Front. Plant Sci.* 8:1935. doi: 10.3389/fpls.2017.01935

Jia, K. P., Luo, Q., He, S. B., Lu, X. D., and Yang, H. Q. (2014). Strigolactone-regulated hypocotyl elongation is dependent on cryptochrome and phytochrome signaling pathways in Arabidopsis. *Mol. Plant* 7, 528–540. doi: 10.1093/mp/sst093

Jiang, L., Liu, X., Xiong, G., Liu, H., Chen, F., Wang, L., et al. (2013). DWARF 53 acts as a repressor of strigolactone signalling in rice. *Nature* 504, 401–405. doi: 10.1038/nature12870

Kagiyama, M., Hirano, Y., Mori, T., Kim, S. Y., Kyozuka, J., Seto, Y., et al. (2013). Structures of D14 and D14L in the strigolactone and karrikin signaling pathways. *Genes Cells* 18, 147–160. doi: 10.1111/gtc.12025

Khosla, A., Morffy, N., Li, Q., Faure, L., Chang, S. H., Yao, J., et al. (2020). Structure-Function Analysis of SMAX1 Reveals Domains That Mediate Its Karrikin-Induced Proteolysis and Interaction with the Receptor KAI2. *Plant Cell* 32, 2639–2659. doi: 10.1105/tpc.19.00752

Lee, H. W., Sharma, P., Janssen, B. J., Drummond, R. S. M., Luo, Z., Hamiaux, C., et al. (2020). Flexibility of the petunia strigolactone receptor DAD2 promotes its interaction with signaling partners. *J. Biol. Chem.* 295, 4181–4193. doi: 10.1074/jbc.RA119.011509

Marzec, M., and Brewer, P. (2019). Binding or Hydrolysis? How Does the Strigolactone Receptor Work?. *Trends Plant Sci.* 24, 571–574. doi: 10.1016/j.tplants.2019.05.001

Nakamura, H., Xue, Y. L., Miyakawa, T., Hou, F., Qin, H. M., Fukui, K., et al. (2013). Molecular mechanism of strigolactone perception by DWARF14. *Nat. Commun.* 4:2613. doi: 10.1038/ncomms3613

Robert, X., and Gouet, P. (2014). Deciphering key features in protein structures with the new ENDscript server. *Nucleic Acids Res.* 42, W320–W324. doi: 10.1093/nar/gku316

Sarrion-Perdigones, A., Vazquez-Vilar, M., Palací, J., Castelijns, B., Forment, J., Ziarsolo, P., et al. (2013). GoldenBraid 2.0: a comprehensive DNA assembly framework for plant synthetic biology. *Plant Physiol.* 162, 1618–1631. doi: 10.1104/pp.113.217661

Seto, Y., Yasui, R., Kameoka, H., Tamiru, M., Cao, M., Terauchi, R., et al. (2019). Strigolactone perception and deactivation by a hydrolase receptor DWARF14. *Nat. Commun.* 10:191. doi: 10.1038/s41467-018-08124-7

Shabek, N., Ticchiarelli, F., Mao, H., Hinds, T. R., Leyser, O., and Zheng, N. (2018). Structural plasticity of D3-D14 ubiquitin ligase in strigolactone signalling. *Nature* 563, 652–656. doi: 10.1038/s41586-018-0743-5

Sievers, F., Wilm, A., Dineen, D., Gibson, T. J., Karplus, K., Li, W., et al. (2011). Fast, scalable generation of high-quality protein multiple sequence alignments using Clustal Omega. *Mol. Syst. Biol.* 7:539. doi: 10.1038/msb.2011.75

Song, X., Lu, Z., Yu, H., Shao, G., Xiong, J., Meng, X., et al. (2017). IPA1 functions as a downstream transcription factor repressed by D53 in strigolactone signaling in rice. *Cell Res.* 27, 1128–1141. doi: 10.1038/cr.2017.102

Soundappan, I., Bennett, T., Morffy, N., Liang, Y., Stanga, J. P., Abbas, A., et al. (2015). SMAX1-LIKE/D53 Family Members Enable Distinct MAX2-Dependent Responses to Strigolactones and Karrikins in Arabidopsis. *Plant Cell* 27, 3143–3159. doi: 10.1105/tpc.15.00562

Stanga, J. P., Smith, S. M., Briggs, W. R., and Nelson, D. C. (2013). SUPPRESSOR OF MORE AXILLARY GROWTH2 1 controls seed germination and seedling development in Arabidopsis. *Plant Physiol.* 163, 318–330. doi: 10.1104/pp.113.221259

Stirnberg, P., Furner, I. J., and Ottoline Leyser, H. M. (2007). MAX2 participates in an SCF complex which acts locally at the node to suppress shoot branching. *Plant J.* 50, 80–94. doi: 10.1111/j.1365-313X.2007.03032.x

Tena, E., Mekbib, F., and Ayana, A. (2016). Correlation and Path Coefficient Analyses in Sugarcane Genotypes of Ethiopia. *Am. J. Plant Sci.* 07, 1490–1497. doi: 10.4236/ajps.2016.710141

Tuma, E. H. (1987). Agricultural Innovation in the Early Islamic World: the Diffusion of Crops and Farming Techniques, 700–1100. By Andrew M. Watson. Cambridge Studies in Islamic Civilization. New York: Cambridge University Press, 1983. 1983. Pp. x, 260. $39.50. *J. Econ. Hist.* 47, 543–544. doi: 10.1017/s0022050700048531

Umehara, M., Hanada, A., Yoshida, S., Akiyama, K., Arite, T., Takeda-Kamiya, N., et al. (2008). Inhibition of shoot branching by new terpenoid plant hormones. *Nature* 455, 195–200. doi: 10.1038/nature07272

Wang, L., Wang, B., Jiang, L., Liu, X., Li, X., Lu, Z., et al. (2015). Strigolactone Signaling in Arabidopsis Regulates Shoot Development by Targeting D53-Like SMXL Repressor Proteins for Ubiquitination and Degradation. *Plant Cell* 27, 3128–3142. doi: 10.1105/tpc.15.00605

Wang, L., Wang, B., Yu, H., Guo, H., Lin, T., Kou, L., et al. (2020). Transcriptional regulation of strigolactone signalling in Arabidopsis. *Nature* 583, 277–281. doi: 10.1038/s41586-020-2382-x

Waters, M. T., Nelson, D. C., Scaffidi, A., Flematti, G. R., Sun, Y. K., Dixon, K. W., et al. (2012). Specialisation within the DWARF14 protein family confers distinct responses to karrikins and strigolactones in Arabidopsis. *Development* 139, 1285–1295. doi: 10.1242/dev.074567

Yao, R., Ming, Z., Yan, L., Li, S., Wang, F., Ma, S., et al. (2016). DWARF14 is a non-canonical hormone receptor for strigolactone. *Nature* 536, 469–473. doi: 10.1038/nature19073

Yao, R., Wang, L., Li, Y., Chen, L., Li, S., Du, X., et al. (2018). Rice DWARF14 acts as an unconventional hormone receptor for strigolactone. *J. Exp. Bot.* 69, 2355–2365. doi: 10.1093/jxb/ery014

Zhang, J., Nagai, C., Yu, Q., Pan, Y.-B., Ayala-Silva, T., Schnell, R. J., et al. (2012). Genome size variation in three Saccharum species. *Euphytica* 185, 511–519. doi: 10.1007/s10681-012-0664-6

Zhang, J., Zhang, X., Tang, H., Zhang, Q., Hua, X., Ma, X., et al. (2018). Allele-defined genome of the autopolyploid sugarcane Saccharum spontaneum L. *Nat. Genet.* 50, 1565–1573. doi: 10.1038/s41588-018-0237-2

Zhao, L. H., Zhou, X. E., Wu, Z. S., Yi, W., Xu, Y., Li, S., et al. (2013). Crystal structures of two phytohormone signal-transducing alpha/beta hydrolases: karrikin-signaling KAI2 and strigolactone-signaling DWARF14. *Cell Res.* 23, 436–439. doi: 10.1038/cr.2013.19

Zhou, F., Lin, Q., Zhu, L., Ren, Y., Zhou, K., Shabek, N., et al. (2013). D14-SCF(D3)-dependent degradation of D53 regulates strigolactone signalling. *Nature* 504, 406–410. doi: 10.1038/nature12878

Conflict of Interest: The authors declare that the research was conducted in the absence of any commercial or financial relationships that could be construed as a potential conflict of interest.

Publisher's Note: All claims expressed in this article are solely those of the authors and do not necessarily represent those of their affiliated organizations, or those of the publisher, the editors and the reviewers. Any product that may be evaluated in this article, or claim that may be made by its manufacturer, is not guaranteed or endorsed by the publisher.

frontiers in Plant Science

MINI REVIEW
published: 09 February 2022
doi: 10.3389/fpls.2022.835160

Structure Elucidation and Biosynthesis of Orobanchol

Takatoshi Wakabayashi[1†], Kotomi Ueno[2†] and Yukihiro Sugimoto[1†]*

[1] Graduate School of Agricultural Science, Kobe University, Kobe, Japan, [2] Faculty of Agriculture, Tottori University, Tottori, Japan

Strigolactones (SLs), a class of phytohormones that regulate diverse developmental processes, were initially characterized as host-derived germination stimulants for seeds belonging to the genera *Striga*, *Orobanche*, and *Phelipanche*. Orobanchol (**1**), which is detected in the root exudates of several plants and recognized as a prevalent SL, was first isolated from the root exudates of red clover as a germination stimulant for *Orobanche minor* in 1998. However, the structure of this stimulant proposed at that time was disputable considering its predicted germination-inducing activity for *Striga gesnerioides*. The genuine structure of orobanchol was elucidated following a decade-long controversy, which ultimately facilitated the understanding of the importance of SL stereochemistry in *Striga* seed germination. Recently, studies focusing on clarifying the biosynthesis pathway of orobanchol are being conducted. Cytochrome P450 monooxygenases are involved in orobanchol biosynthesis downstream of carlactonoic acid (CLA) via two pathways: either through 4-deoxyorobanchol or direct conversion from CLA. Substantial progress in the identification of more SL structures and clarification of their biosynthetic mechanisms will further contribute in the comprehension of their structural diversity's functional importance and agricultural applications. Herein, we have reviewed the history leading to the discovery of the genuine structure of orobanchol and the current understanding of its biosynthetic mechanisms.

Keywords: cytochrome P450 monooxygenase, germination, root parasitic weeds, stereochemistry, strigolactone

OPEN ACCESS

Edited by:
Tadao Asami,
The University of Tokyo, Japan

Reviewed by:
Mikihisa Umehara,
Toyo University, Japan

****Correspondence:***
Yukihiro Sugimoto
yukihiro@kobe-u.ac.jp

†ORCID:
Takatoshi Wakabayashi
orcid.org/0000-0001-7065-6839
Kotomi Ueno
orcid.org/0000-0002-3227-2073
Yukihiro Sugimoto
orcid.org/0000-0002-8767-9671

Specialty section:
This article was submitted to Plant Physiology, a section of the journal Frontiers in Plant Science

Received: *14 December 2021*
Accepted: *18 January 2022*
Published: *09 February 2022*

Citation:
Wakabayashi T, Ueno K and Sugimoto Y (2022) Structure Elucidation and Biosynthesis of Orobanchol. Front. Plant Sci. 13:835160. doi: 10.3389/fpls.2022.835160

INTRODUCTION

Strigolactones (SLs) were initially characterized as germination stimulants for seeds belonging to the genera *Striga*, *Orobanche*, and *Phelipanche*, which are a renowned group of root parasitic weeds of global economic importance (Parker, 2009). Strigol (**2**), the first canonical SL structurally defined, was isolated from the root exudates of cotton (*Gossypium hirsutum*) (Cook et al., 1966, 1972). Following the isolation of strigol, the SLs sorgolactone (**3**) (Hauck et al., 1992), alectrol (**4**) (Müller et al., 1992), and orobanchol (**1**) (Yokota et al., 1998) were isolated from the root exudates of sorghum (*Sorghum bicolor*), cowpea (*Vigna unguiculata*), and red clover (*Trifolium pratense*), respectively. Consequent studies revealed that SLs not only promoted hyphal branching of arbuscular mycorrhizal fungi (Akiyama et al., 2005) but also represented a new class of

phytohormones that regulated plant architecture (Gomez-Roldan et al., 2008; Umehara et al., 2008). Structurally, canonical SLs consist of tricyclic lactone (ABC ring) and butenolide (D ring) connected with an enol ether bridge (**Figure 1**). The structures of strigol (**2**) and sorgolactone (**3**) were unambiguously determined by X-ray crystallographic analysis and organic synthesis (Brooks et al., 1985; Sugimoto et al., 1998), whereas the genuine structures of orobanchol (**1**) and alectrol (**4**) were eventually established in 2011 (Ueno et al., 2011b). Orobanchol has been detected in the root exudates of numerous plants, including Fabaceae, Solanaceae, a few Gymnosperm species, and rice (*Oryza sativa*) (Xie, 2016; Wang and Bouwmeester, 2018). Several derivatives of orobanchol, such as its acetate, orobanchyl acetate (alectrol), fabacol that contains an epoxide group, and solanacol that has an aromatic A-ring, have also been identified (Müller et al., 1992; Xie et al., 2007, 2009). The illustration of the genuine structure of orobanchol allowed canonical SLs to be divided into two subgroups that were categorized in terms of their C-ring configuration, the orobanchol- and strigol-types. The C-ring configuration was found to be essential in fulfilling the structural requirements of the canonical SLs for inducing germination in *Striga gesnerioides* seeds (Ueno et al., 2011a; Nomura et al., 2013). The classification of the canonical SLs into the two subgroups presented an avenue to study the enzymes involved in their biosynthesis from the common intermediate, carlactonoic acid (CLA) (Zhang et al., 2014; Wakabayashi et al., 2019, 2020; Mori et al., 2020).

This review outlines the course of determining the genuine structure of orobanchol, its biological importance as a seed germination stimulant for the genus *Striga*, and its biosynthesis pathway at biochemical and molecular levels. The components involved in the biosynthesis of orobanchol and its related canonical SLs that are yet to be clarified are also discussed.

STRUCTURE AND GERMINATION-INDUCING ACTIVITY

History Leading to the Determination of the Genuine Structure of Orobanchol

Orobanchol was isolated from the root exudates of red clover as the first germination stimulant for *Orobanche minor*, together with alectrol (Yokota et al., 1998). Alectrol had been previously isolated from the root exudates of cowpea as an isomer of strigol and a germination stimulant for *Alectra vogelii* and *S. gesnerioides*. A structure for alectrol was proposed based on a detailed comparison of its spectroscopic data with those of strigol (Müller et al., 1992). Since the isolated amount of orobanchol from red clover was constrained, it was considered to be a strigol-related compound and no specific structure for it was proposed. Following these reports, a series of strigol analogs, including the tentative structures of orobanchol and alectrol, were synthesized (Matsui et al., 1999a,b). The structure **5** was assigned to orobanchol by comparing its ^{1}H NMR spectra and chromatographic behavior in gas chromatography–mass spectrometry, in which the C-ring configuration was consistent with that of strigol (**2**) (**Figure 1**). Chiroptical data were not utilized in the structural determination process. After about a decade, alectrol was independently re-isolated from the root exudates of red clover and cowpea (Matsuura et al., 2008; Xie et al., 2008), and its structure was reported as an acetylated product of synthetic orobanchol (**6**). However, synthetic orobanchol (**5**) and its acetate (**6**) did not induce seed germination in *S. gesnerioides* (Ueno et al., 2011a), indicating that the assigned structures of these SLs were controversial. These results triggered the re-isolation of the germination stimulants of *S. gesnerioides* from the root exudates of cowpea and red clover (Ueno et al., 2011b). The details of the bioassay-guided re-isolation and unambiguous structural elucidation of these stimulants have been described in a previous review (Ueno et al., 2015). In brief, two stimulants were isolated from both cowpea and red clover root exudates. The ^{1}H NMR spectra of these stimulants suggested that they were canonical SLs having an oxygen functional group at C-4 in the B-ring. The chromatographic behavior of the stimulants in liquid chromatography–tandem mass spectrometry (LC-MS/MS) analysis was inconsistent with that of synthetic orobanchol (**5**) and its acetate (**6**) but consistent with their respective 2′-epimers. Additionally, the circular dichroism spectra of the stimulants were vertically inverted compared with the 2′-epimers of **5** and **6**. Therefore, the absolute structures of orobanchol and alectrol were determined to be **1** and **4**, respectively (**Figure 1**).

Figure 1 (**1**) illustrates the genuine structure of orobanchol, which has the (3a*R*, 8b*R*, 2′*R*)-configuration. Contrary to strigol (**2**), orobanchol (**1**) demonstrates an inverted BC-junction configuration. Dehydroxylated orobanchol and strigol, 4-deoxyorobanchol (4DO) (**7**) and 5-deoxystrigol (5DS) (**8**), respectively, have opposite C-ring configurations, and hence, 5DS is also known as *ent*-2′-*epi*-4DO. It was predictable that the absolute skeletal configuration of redefined orobanchol was the *ent*-2′-*epi*-form of the strigol skeleton. Before the structural revision, 2′-*epi*-5-deoxystrigol (*epi*-5DS) had been found in the hydroponic culture media of rice seedlings (cv. Shiokari) by LC-MS/MS analysis using a reversed-phase octadecyl silica (ODS) column (Umehara et al., 2008). The detected "*epi*-5DS" is presumed to be 4DO (*ent*-2′-*epi*-5DS, **7**), since an LC-MS/MS analysis with an ODS column only distinguishes between diastereomers. Subsequently, it was reported that rice produces orobanchol in addition to *epi*-5DS (Jamil et al., 2011). Moreover, the absolute configuration of fabacyl acetate isolated from pea (*Pisum sativum*) was the same as that of 4DO (Xie et al., 2009). Therefore, the correction of the absolute configuration of orobanchol was readily accepted by the community of SL researchers.

Importance of the Stereochemistry of Orobanchol in Inducing Seed Germination

The structure of both synthetic (**5**) and naturally occurring orobanchol (**1**) have the *R*-configuration at C-2′, which is an

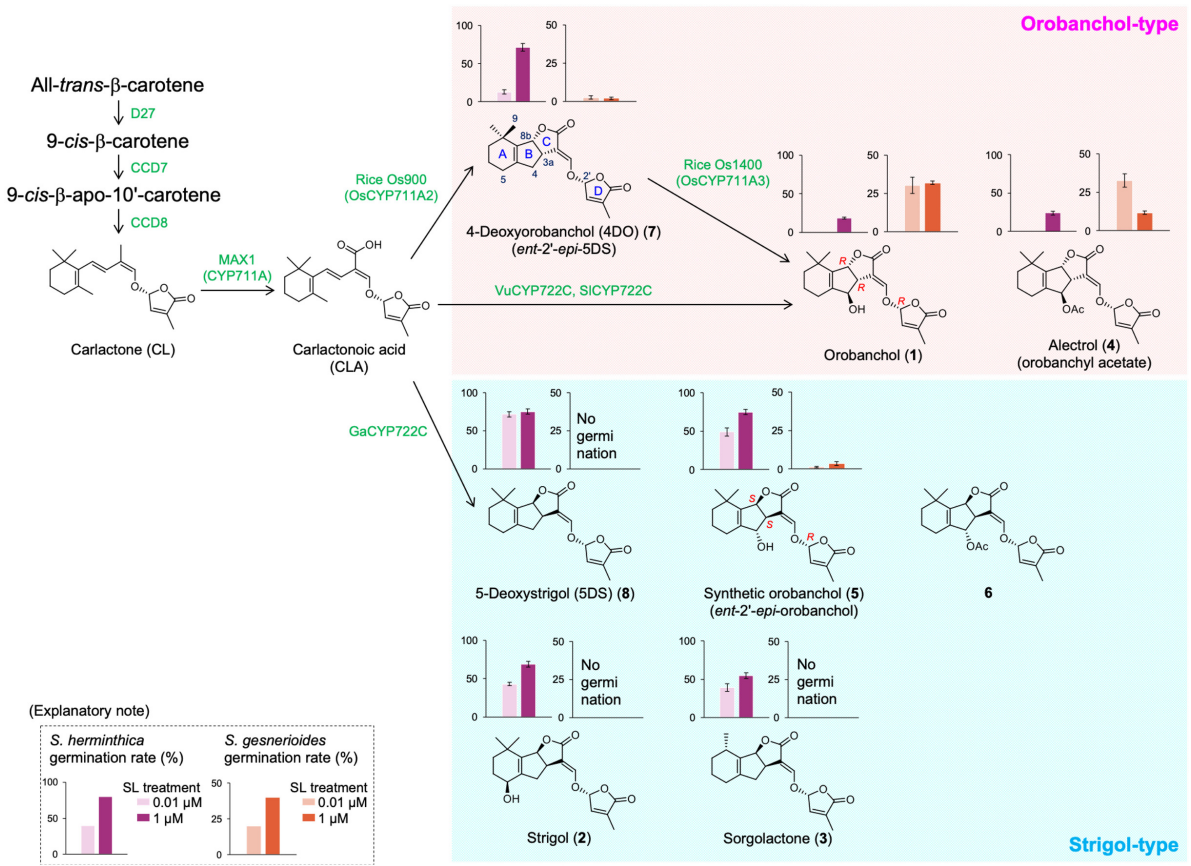

FIGURE 1 | Proposed strigolactone (SL) biosynthesis pathway from β-carotene and the seed germination induction of *Striga* by each SL. The sequential reactions catalyzed by D27, CCD7, and CCD8 enzymes produce carlactone (CL) from all-*trans*-β-carotene. CL is further converted to carlactonoic acid (CLA) by the CYP711A subfamily. Downstream of CLA, Os900/OsCYP711A2 in rice (*Oryza sativa*), VuCYP722C and SlCYP722C in cowpea (*Vigna unguiculata*) and tomato (*Solanum lycopersicum*), respectively, and GaCYP722C in cotton (*Gossypium arboreum*) can produce 4-deoxyorobanchol, orobanchol, and 5-deoxystrigol, respectively. The bar graphs at the top of each SL structure indicate the germination rates of *S. hermonthica* and *S. gesnerioides* induced by each SL as reported previously (Ueno et al., 2011b; Nomura et al., 2013).

important structural feature for shoot branching inhibitory activity. Synthetic (**5**) as well as naturally occurring orobanchol (**1**) has shown to inhibit shoot branching in rice (Umehara et al., 2015). In contrast, during the structural examination of orobanchol, the importance of its stereochemistry in inducing seed germination in *S. gesnerioides* was suggested (Ueno et al., 2011a; Nomura et al., 2013; **Figure 1**). Detailed structure–activity relationship studies on 36 SL stereoisomers, including naturally occurring and synthetic ones, exemplified the strict structural requirements of the canonical SLs for inducing germination in *S. gesnerioides* seeds. Only a limited number of compounds, including orobanchol, induced significant germination in *S. gesnerioides* seeds. The SLs with high germination-inducing activity for *S. gesnerioides* seeds have a consistent C-ring configuration with that of orobanchol (**1**) and a hydroxy group at C-4 with β-orientation or at C-9, the *trans* methyl group against the C-ring. Notably, these germination inducers of *S. gesnerioides* induced a lower germination rate in *S. hermonthica*, which had a more sensitive response to synthetic orobanchol (**5**) that has the same configuration as strigol (**1**). Sorghum, one of the host plants of *S. hermonthica*, exudes sorgomol, which also has the same configuration as strigol (**2**). Additionally, SLs with the same C-ring configuration as strigol suppressed the orobanchol-induced germination of *S. gesnerioides* seeds. Therefore, root parasitic weeds may have evolved to germinate closer to the roots of compatible host plants where they can parasitize by strictly recognizing the configuration of the SLs. These findings indicated that not only the total amount but also the composition of SLs exuded by the host plants influence the adverse effects caused by parasitic weeds. Studies focused on elucidating the biosynthesis pathway of orobanchol were consequently pursued.

BIOSYNTHESIS

Two Distinct Biosynthesis Pathways of Orobanchol

In SL biosynthesis, D27 isomerizes all-*trans*-β-carotene to 9-*cis*-β-carotene, followed by CCD7-induced cleavage to form 9-*cis*-apo-10′-carotenal, and further CCD8 catalyzed conversion to the

SL biosynthetic precursor, carlactone (CL) (Alder et al., 2012; Seto et al., 2014; **Figure 1**). Cytochrome P450 monooxygenase (CYP) AtCYP711A1 encoded by *MORE AXIALLY GROWTH 1* (*MAX1*) converts CL to CLA and is responsible for the branching phenotype observed in Arabidopsis and OsCYP711As, which belong to the same subfamily of rice, also catalyze this reaction (Abe et al., 2014; Zhang et al., 2014). Subsequently, the conversion of CL to CLA has been indicated to be a common function of the CYP711A subfamily in different plant species, suggesting that CLA is also a precursor in SL biosynthesis (Yoneyama et al., 2018). Based on the commonality of planar structure of the basic skeleton, it was assumed that the canonical SLs downstream of CLA first generated the tricyclic skeletons (5DS and 4DO), and then underwent hydroxylation and further modifications to generate strigol, orobanchol, and their acetates.

The pioneering study on canonical SL biosynthesis in japonica rice first elucidated the biosynthesis pathway of orobanchol through the conversion to 4DO (Zhang et al., 2014). The rice CYP711A subfamily shares the common functionality of CL to CLA conversion and is also involved in the conversion to orobanchol. In the rice CYP711A subfamily, OsCYP711A2/Os900 catalyzes the conversion of CL to 4DO via CLA, and OsCYP711A3/Os1400 catalyzes the hydroxylation of 4DO at C-4 to ultimately form orobanchol. Based on these results, it was assumed that the CYP711A subfamily in other plant species is also responsible for the conversion of CLA to the respective canonical SLs, including orobanchol; however, the catalyzing property of this subfamily that converts CL and CLA to canonical SLs in seed plants has been exclusively identified only in rice (Yoneyama et al., 2018). Alternatively, conventional feeding experiments observed that orobanchol producing plants (cowpea, red clover, pea, red bell pepper) that were exogenously administered with 4DO did not convert it to orobanchol, whereas CLA was converted to orobanchol (Iseki et al., 2018; Ueno et al., 2018). These results further suggested a direct biosynthesis pathway of orobanchol from CLA in addition to the indirect pathway through the conversion to 4DO, involving the OsCYP711A2/Os900 and OsCYP711A3/Os1400 of rice. The involvement of other enzymes besides the CYP711A subfamily in canonical SL biosynthesis has been suggested.

Direct Conversion of Carlactonoic Acid to Orobanchol by CYP722C in Orobanchol Producing Plants (Cowpea and Tomato)

Uniconazole-P, a CYP inhibitor, suppressed the conversion of CLA to orobanchol in cowpea, suggesting that CYP plays a role in this conversion. *VuCYP722C*, whose function was unknown, was highlighted as a candidate gene via gene co-expression analysis using RNA-seq data of cowpea roots grown under various conditions with different SL production levels. The results of the *in vitro* enzyme assay conducted with a crude enzyme of recombinant VuCYP722C demonstrated that the enzyme produced orobanchol and its diastereomer, *ent*-2'-*epi*-orobanchol (**5**), with an opposite configuration in the C-ring, in approximately equal amounts using CLA as a substrate. Additionally, presumed 18-hydroxy-CLA was detected in the enzyme-reaction mixtures. VuCYP722C did not catalyze the conversion of 4DO to orobanchol, which is consistent with the previous results of the feeding experiments (Wakabayashi et al., 2019).

The enzymatic function of SlCYP722C was analyzed in tomato (*Solanum lycopersicum*), another representative orobanchol producer. The changes in *SlCYP722C* gene expressions were similar to that of known SL biosynthetic genes; upregulated under phosphate-deficient conditions that promote SL production. The recombinant enzyme exhibited an activity that was comparable to that of cowpea VuCYP722C. These results further demonstrated the existence of an alternative orobanchol biosynthesis pathway involving CYP722C (Wakabayashi et al., 2019; **Figure 1**).

The Function of CYP722C in Tomato, a Model Orobanchol Producing Plant

Analyses of *SlCYP722C* knockout tomato (*SlCYP722C*-KO) plants established the involvement of the CYP722C subfamily in the direct conversion of CLA to orobanchol. The root exudates of *SlCYP722C*-KO plants, wherein the CRISPR/Cas9 system was employed to disrupt the gene by genome editing, orobanchol and solanacol (a possible derivative of orobanchol) were demonstrated to be below-detection level using LC-MS/MS analysis, and instead, CLA accumulation was observed. The modified profiles of the lacking canonical SLs were also reflected in their germination stimulation activities in the seeds of root parasitic weeds. In other words, the root exudates of *SlCYP722C*-KO induced significantly less germination in *S. hermonthica*, *O. crenata*, and *Phelipanche aegyptiaca* seeds than those of wild-type. Interestingly, the *SlCYP722C*-KO plants appeared similar to the wild-type plants and they did not show the prominent phenotypes of an SL-deficient mutant, such as increased shoot branching and reduced stem length (Wakabayashi et al., 2019). These observations depicted that canonical SLs were not essential for regulating shoot branching in tomato plants and further suggested that the branching inhibiting hormone was a non-canonical SL lacking the ABC ring structure derived from CLA, as *MAX1*/*CYP711A* mutation induces increased shoot branching (Zhang et al., 2018; Wakabayashi et al., 2019). Accordingly, canonical SLs could be more important as rhizosphere signaling molecules than shoot branching inhibitors, and preferentially secreted into the soil and facilitate plant–microbe and plant-plant communications.

DISCUSSION

The determination of the genuine structures of orobanchol (**1**) and its acetate, orobanchyl acetate (alectrol) (**4**), has put an end to the long controversy regarding these structures (Ueno et al., 2011b). Orobanchol is also converted to its didehydro derivatives, didehydro-orobanchol isomers, although

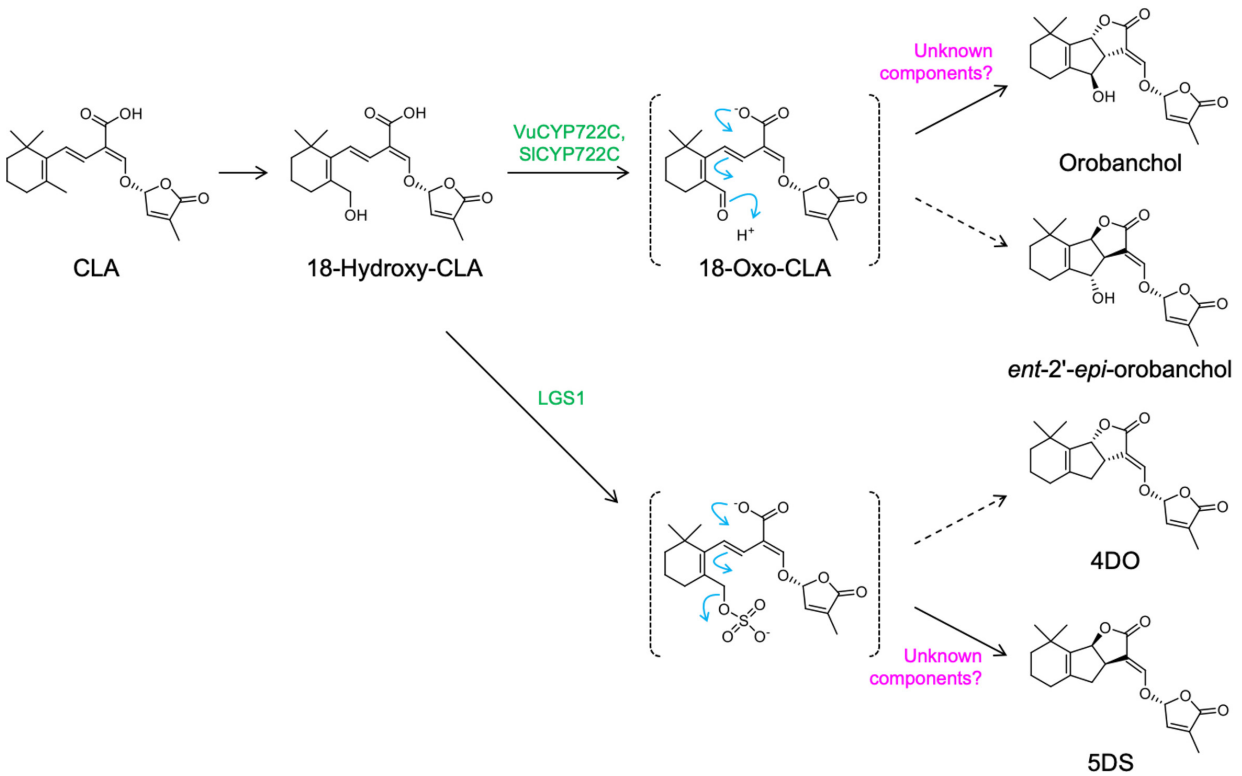

FIGURE 2 | Proposed mechanisms for generating canonical strigolactones with BC ring formation. Additional components may be necessary for the stereospecific conversion of 18-oxo-CLA to orobanchol and the sulfate ester of 18-hydroxy-CLA to 5DS (CLA, carlactonoic acid).

their structures and enzymes responsible for the conversion remain elusive (Zhang et al., 2018). Identification of CYP722C provided additional information on the biosynthesis pathway of orobanchol from β-carotene at a molecular level. The *in vitro* enzymatic reactions of VuCYP722C and SlCYP722C with CLA as a substrate yielded orobanchol and its diastereomer, *ent*-2'-*epi*-orobanchol, as products (Wakabayashi et al., 2019). These reactions further suggested that the members of the CYP722C subfamily catalyzed the two-step oxidization at the C-18 position in CLA, producing 18-oxo-CLA through 18-hydroxy-CLA. The 18-oxo-CLA then undergoes the BC ring closure reaction, without stereoselective control, to yield orobanchol isomers (**Figure 2**). Recently, it was reported that in a co-culture system of *Escherichia coli* and *Saccharomyces cerevisiae* co-expressing SL biosynthesis genes, orobanchol is generated by the co-expression of *VuCYP722C* with the upstream SL biosynthesis genes. However, the production of its diastereomer has not been described (Wu et al., 2021). Therefore, a more detailed functional analysis of the CYP722C subfamily is necessary. The formation of the BC ring without the stereoselective control of the C-ring configuration is also found in 5DS biosynthesis involving the LOW GERMINATION STIMULANT 1 (LGS1) of sorghum. It is strongly suggested that LGS1, encoding for the sulfotransferase protein, catalyzes the sulfonation of 18-hydroxy-CLA and provides an easier leaving group to afford a spontaneous non-selective BC ring formation, resulting in simultaneous production of 5DS and 4DO (Yoda et al., 2021; **Figure 2**). Altogether, there is likely an involvement of unknown components in the stereoselective control of the C-ring in the conversion of 18-oxo-CLA to orobanchol and the sulfate ester of 18-hydroxy-CLA to 5DS.

The CYP722C subfamily is widely conserved in dicot plants, regardless of the type of SL produced (orobanchol- or strigol-type). GaCYP722C of cotton (*G. arboreum*), which generates 5DS as a strigol-type SL, catalyzes the conversion of CLA to 5DS, but it is not involved in the conversion to 4DO (Wakabayashi et al., 2020). Alternatively, GaCYP722C catalyzes stereoselective BC ring formation, unlike VuCYP722C and SlCYP722C. In addition, it has been reported that the CYP722Cs of birdsfoot trefoil (*Lotus japonicus*) and woodland strawberry (*Fragaria vesca*) are involved in the conversion of CLA to 5DS (Mori et al., 2020; Wu et al., 2021). The CYP722C subfamily members are the key enzymes involved in the biosynthesis of canonical SLs, regardless of their C-ring configuration. The differences in their catalytic activity may be due to the differences in the amino acid residues at the catalytic site and conformation of the protein structure domains. Structural biological approaches may clarify the mechanisms regulating the C-ring configuration in canonical SL biosynthesis.

Although much progress has been made in understanding the diverse structures of SLs and their biosynthetic mechanisms,

the physiological significance of SL stereochemistry remains largely unexplored. If the mechanism by which plants control the stereochemistry of the C-ring to produce both types of SLs could be elucidated, it would then become possible to artificially control their structures through genetic engineering. The knowledge obtained from this approach will greatly contribute in comprehending the role of SLs. Additionally, the precise control of SL functions is predicted to have agricultural applications, such as management of root parasitic weeds and promotion of mycorrhizal symbiosis.

AUTHOR CONTRIBUTIONS

TW, KU, and YS wrote the review. All authors contributed to the article and approved the submitted version.

FUNDING

This work was supported in part, by the JST/JICA SATREPS (JPMJSA1607 to YS), JST ACT-X (JPMJAX20BM to TW), and JSPS KAKENHI (25292065 to YS and 20K15459 to TW).

REFERENCES

Abe, S., Sado, A., Tanaka, K., Kisugi, T., Asami, K., Ota, S., et al. (2014). Carlactone is converted to carlactonoic acid by MAX1 in *Arabidopsis* and its methyl ester can directly interact with AtD14 in vitro. *Proc. Natl. Acad. Sci. U S A.* 111, 18084–18089. doi: 10.1073/pnas.1410801111

Akiyama, K., Matsuzaki, K., and Hayashi, H. (2005). Plant sesquiterpenes induce hyphal branching in arbuscular mycorrhizal fungi. *Nature* 435, 824–827. doi: 10.1038/nature03608

Alder, A., Jamil, M., Marzorati, M., Bruno, M., Vermathen, M., Bigler, P., et al. (2012). The path from β-carotene to carlactone, a strigolactone-like plant hormone. *Science* 335, 1348–1351. doi: 10.1126/science.1218094

Brooks, D. W., Bevinakatti, H. S., and Powell, D. R. (1985). The absolute structure of (+)-strigol. *J. Org. Chem.* 50, 3779–3781. doi: 10.1021/jo00220a020

Cook, C. E., Whichard, L. P., Turner, B., Wall, M. E., and Egley, G. H. (1966). Germination of witchweed (*Striga lutea* Lour.): Isolation and properties of a potent stimulant. *Science* 154, 1189–1190. doi: 10.1126/science.154.3753.1189

Cook, C. E., Whichard, L. P., Wall, M., Egley, G. H., Coggon, P., Luhan, P. A., et al. (1972). Germination stimulants. II. Structure of strigol, a potent seed germination stimulant for witchweed (*Striga lutea*). *J. Am. Chem. Soc.* 94, 6198–6199. doi: 10.1021/ja00772a048

Gomez-Roldan, V., Fermas, S., Brewer, P. B., Puech-Pagès, V., Dun, E. A., Pillot, J. P., et al. (2008). Strigolactone inhibition of shoot branching. *Nature* 455, 189–194. doi: 10.1038/nature07271

Hauck, C., Müller, S., and Schildknecht, H. (1992). A germination stimulant for parasitic flowering plants from *Sorghum bicolor*, a genuine host plant. *J. Plant Physiol.* 139, 474–478. doi: 10.1016/S0176-1617(11)80497-9

Iseki, M., Shida, K., Kuwabara, K., Wakabayashi, T., Mizutani, M., Takikawa, H., et al. (2018). Evidence for species-dependent biosynthetic pathways for converting carlactone to strigolactones in plants. *J. Exp. Bot.* 69, 2305–2318. doi: 10.1093/jxb/erx428

Jamil, M., Charnikhova, T., Cardoso, C., Jamil, T., Ueno, K., Verstappen, F., et al. (2011). Quantification of the relationship between strigolactones and *Striga hermonthica* infection in rice under varying levels of nitrogen and phosphorus. *Weed Res.* 51, 373–385. doi: 10.1111/j.1365-3180.2011.00847.x

Matsui, J., Bando, M., Kido, M., Takeuchi, Y., and Mori, K. (1999a). Synthetic disproof of the structure proposed for alectrol, the germination stimulant from *Vigna unguiculata*. *Eur. J. Org. Chem.* 1999, 2195–2199. doi: 10.1002/(SICI)1099-0690(199909)1999:9<2195::AID-EJOC2195<3.0.CO;2-R

Matsui, J., Yokota, T., Bando, M., Takeuchi, Y., and Mori, K. (1999b). Synthesis and structure of orobanchol, the germination stimulant for *Orobanche minor*. *Eur. J. Org. Chem.* 1999, 2201–2210. doi: 10.1002/(SICI)1099-0690(199909)1999:9<2201::AID-EJOC2201<3.0.CO;2-Q

Matsuura, H., Ohashi, K., Sasako, H., Tagawa, N., Takano, Y., Ioka, Y., et al. (2008). Germination stimulant from root exudates of *Vigna unguiculata*. *Plant Growth Regul.* 54, 31–36. doi: 10.1007/s10725-007-9224-9

Mori, N., Nomura, T., and Akiyama, K. (2020). Identification of two oxygenase genes involved in the respective biosynthetic pathways of canonical and non-canonical strigolactones in *Lotus japonicus*. *Planta* 251:40. doi: 10.1007/s00425-019-03332-x

Müller, S., Hauck, C., and Schildknecht, H. (1992). Germination stimulants produced by *Vigna unguiculata* Walp cv Saunders Upright. *J. Plant Growth Regul.* 11, 77–84. doi: 10.1007/BF00198018

Nomura, S., Nakashima, H., Mizutani, M., Takikawa, H., and Sugimoto, Y. (2013). Structural requirements of strigolactones for germination induction and inhibition of *Striga gesnerioides* seeds. *Plant Cell Rep.* 32, 829–838. doi: 10.1007/s00299-013-1429-y

Parker, C. (2009). Observations on the current status of Orobanche and Striga problems worldwide. *Pest. Manag. Sci.* 65, 453–459. doi: 10.1002/ps.1713

Seto, Y., Sado, A., Asami, K., Hanada, A., Umehara, M., Akiyama, K., et al. (2014). Carlactone is an endogenous biosynthetic precursor for strigolactones. *Proc. Natl. Acad. Sci. U S A.* 111, 1640–1645. doi: 10.1073/pnas.1314805111

Sugimoto, Y., Wigchert, S. C. M., Thuring, J. W. J. F., and Zwanenburg, B. (1998). Synthesis of all eight stereoisomers of the germination stimulant sorgolactone. *J. Org. Chem.* 63, 1259–1267. doi: 10.1021/jo9718408

Ueno, K., Fujiwara, M., Nomura, S., Mizutani, M., Sasaki, M., Takikawa, H., et al. (2011a). Structural requirements of strigolactones for germination induction of *Striga gesnerioides* seeds. *J. Agric. Food Chem.* 59, 9226–9231. doi: 10.1021/jf202418a

Ueno, K., Nakashima, H., Mizutani, M., Takikawa, H., and Sugimoto, Y. (2018). Bioconversion of 5-deoxystrigol stereoisomers to monohydroxylated strigolactones by plants. *J. Pestic. Sci.* 43, 198–206. doi: 10.1584/jpestics.D18-021

Ueno, K., Nomura, S., Muranaka, S., Mizutani, M., Takikawa, H., and Sugimoto, Y. (2011b). *Ent*-2′-*epi*-orobanchol and its acetate, as germination stimulants for *Striga gesnerioides* seeds isolated from cowpea and red clover. *J. Agric. Food Chem.* 59, 10485–10490. doi: 10.1021/jf2024193

Ueno, K., Sugimoto, Y., and Zwanenburg, B. (2015). The genuine structure of alectrol: end of a long controversy. *Phytochem. Rev.* 14, 835–847. doi: 10.1007/s11101-014-9380-2

Umehara, M., Cao, M., Akiyama, K., Akatsu, T., Seto, Y., Hanada, A., et al. (2015). Structural requirements of strigolactones for shoot branching inhibition in rice and Arabidopsis. *Plant Cell Physiol.* 56, 1059–1072. doi: 10.1093/pcp/pcv028

Umehara, M., Hanada, A., Yoshida, S., Akiyama, K., Arite, T., Takeda-Kamiya, N., et al. (2008). Inhibition of shoot branching by new terpenoid plant hormones. *Nature* 455, 195–200. doi: 10.1038/nature07272

Wakabayashi, T., Hamana, M., Mori, A., Akiyama, R., Ueno, K., Osakabe, K., et al. (2019). Direct conversion of carlactonoic acid to orobanchol by cytochrome P450 CYP722C in strigolactone biosynthesis. *Sci. Adv.* 5:eaax9067. doi: 10.1126/sciadv.aax9067

Wakabayashi, T., Shida, K., Kitano, Y., Takikawa, H., Mizutani, M., and Sugimoto, Y. (2020). CYP722C from *Gossypium arboreum* catalyzes the conversion of carlactonoic acid to 5-deoxystrigol. *Planta* 251:97. doi: 10.1007/s00425-020-03390-6

Wang, Y., and Bouwmeester, H. J. (2018). Structural diversity in the strigolactones. *J. Exp. Bot.* 69, 2219–2230. doi: 10.1093/jxb/ery091

Wu, S., Ma, X., Zhou, A., Valenzuela, A., Zhou, K., and Li, Y. (2021). Establishment of strigolactone-producing bacterium-yeast consortium. *Sci. Adv.* 7, 1–14. doi: 10.1126/sciadv.abh4048

Xie, X. (2016). Structural diversity of strigolactones and their distribution in the plant kingdom. *J. Pestic. Sci.* 41, 175–180. doi: 10.1584/jpestics.J16-02

Xie, X., Kusumoto, D., Takeuchi, Y., Yoneyama, K., Yamada, Y., and Yoneyama, K. (2007). 2′-*Epi*-orobanchol and solanacol, two unique strigolactones, germination stimulants for root parasitic weeds, produced by tobacco. *J. Agric. Food Chem.* 55, 8067–8072. doi: 10.1021/jf0715121

Xie, X., Yoneyama, K., Harada, Y., Fusegi, N., Yamada, Y., Ito, S., et al. (2009). Fabacyl acetate, a germination stimulant for root parasitic plants from *Pisum sativum*. *Phytochemistry* 70, 211–215. doi: 10.1016/j.phytochem.2008.12.013

Xie, X., Yoneyama, K., Kusumoto, D., Yamada, Y., Yokota, T., Takeuchi, Y., et al. (2008). Isolation and identification of alectrol as (+)-orobanchyl acetate, a germination stimulant for root parasitic plants. *Phytochemistry* 69, 427–431. doi: 10.1016/j.phytochem.2007.07.017

Yoda, A., Mori, N., Akiyama, K., Kikuchi, M., Xie, X., Miura, K., et al. (2021). Strigolactone biosynthesis catalyzed by cytochrome P450 and sulfotransferase in sorghum. *New Phytol.* 232, 1999–2010. doi: 10.1111/nph.17737

Yokota, T., Sakai, H., Okuno, K., Yoneyama, K., and Takeuchi, Y. (1998). Alectrol and orobanchol, germination stimulants for *Orobanche minor*, from its host red clover. *Phytochemistry* 49, 1967–1973. doi: 10.1016/S0031-9422(98)00419-1

Yoneyama, K., Mori, N., Sato, T., Yoda, A., Xie, X., Okamoto, M., et al. (2018). Conversion of carlactone to carlactonoic acid is a conserved function of MAX1 homologs in strigolactone biosynthesis. *New Phytol.* 218, 1522–1533. doi: 10.1111/nph.15055

Zhang, Y., Cheng, X., Wang, Y., Díez-Simón, C., Flokova, K., Bimbo, A., et al. (2018). The tomato *MAX1* homolog, *SlMAX1*, is involved in the biosynthesis of tomato strigolactones from carlactone. *New Phytol.* 219, 297–309. doi: 10.1111/nph.15131

Zhang, Y., van Dijk, A. D. J., Scaffidi, A., Flematti, G. R., Hofmann, M., Charnikhova, T., et al. (2014). Rice cytochrome P450 MAX1 homologs catalyze distinct steps in strigolactone biosynthesis. *Nat. Chem. Biol.* 10, 1028–1033. doi: 10.1038/nchembio.1660

Conflict of Interest: The authors declare that the research was conducted in the absence of any commercial or financial relationships that could be construed as a potential conflict of interest.

Publisher's Note: All claims expressed in this article are solely those of the authors and do not necessarily represent those of their affiliated organizations, or those of the publisher, the editors and the reviewers. Any product that may be evaluated in this article, or claim that may be made by its manufacturer, is not guaranteed or endorsed by the publisher.

frontiers in Plant Science

REVIEW
published: 24 February 2022
doi: 10.3389/fpls.2022.821563

Biological Functions of Strigolactones and Their Crosstalk With Other Phytohormones

Fenghui Wu†, Yinping Gao†, Wenjing Yang, Na Sui and Jianping Zhu**

Shandong Provincial Key Laboratory of Plant Stress, College of Life Sciences, Shandong Normal University, Jinan, China

Phytohormones are small chemicals critical for plant development and adaptation to a changing environment. Strigolactones (SLs), carotenoid-derived small signalling molecules and a class of phytohormones, regulate multiple developmental processes and respond to diverse environmental signals. SLs also coordinate adjustments in the balance of resource distribution by strategic modification of the plant development, allowing plants to adapt to nutrient deficiency. Instead of operating independently, SL interplays with abscisic acid, cytokinin, auxin, ethylene, and some other plant phytohormones, forming elaborate signalling networks. Hormone signalling crosstalk in plant development and environmental response may occur in a fully concerted manner or as a cascade of sequential events. In many cases, the exact underlying mechanism is unclear because of the different effects of phytohormones and the varying backgrounds of their actions. In this review, we systematically summarise the synthesis, signal transduction, and biological functions of SLs and further highlight the significance of crosstalk between SLs and other phytohormones during plant development and resistance to ever-changing environments.

Keywords: strigolactones, development, phytohormones, crosstalk, signalling pathway

OPEN ACCESS

Edited by:
Ruifeng Yao,
Hunan University, China

Reviewed by:
Kunpeng Jia,
Henan University, China
Francois Fabien Barbier,
The University of Queensland, Australia

****Correspondence:***
Na Sui
suina@sdnu.edu.cn
Jianping Zhu
zjp@sdnu.edu.cn

† These authors have contributed equally to this work

Specialty section:
This article was submitted to Plant Physiology, a section of the journal Frontiers in Plant Science

Received: *24 November 2021*
Accepted: *24 January 2022*
Published: *24 February 2022*

Citation:
Wu F, Gao Y, Yang W, Sui N and Zhu J (2022) Biological Functions of Strigolactones and Their Crosstalk With Other Phytohormones. Front. Plant Sci. 13:821563. doi: 10.3389/fpls.2022.821563

INTRODUCTION

Plants are frequently exposed to diverse unfavourable environmental conditions that lead to abiotic stresses and reduce productivity. Phytohormones are crucial for regulating various physiological processes of plants and assisting them to communicate with the external environment (Ciura and Kruk, 2018; Xin et al., 2019; Li et al., 2020). Strigolactones (SLs) were discovered when analysing the ability of a signalling substance secreted by cotton roots to stimulate the seed germination of parasitic weeds (Cook et al., 1966). Approximately 25 types of naturally occurring SLs have been discovered in different plant species, and based on their chemical structures, they are classified into two groups, namely, canonical and non-canonical SLs (Wang and Bouwmeester, 2018). Canonical SLs consist of a butenolide ring (D ring) connected by an enol ether bridge to a tricyclic lactone (ABC rings) (Butler, 1995). In non-canonical SLs, the ABC ring is replaced with an irregular ring structure (Yoneyama et al., 2018). Different forms of SL molecules may exhibit different biological activities (Umehara et al., 2015; Xie et al., 2020). The complex structure and stereochemistry of natural SLs limit their chemical synthesis. GR24, a synthetic SL analogue widely used in SL studies, is a racemic mixture of two 5-deoxystrigol (5DS)-configured enantiomers, namely, $GR24^{5DS}$ and $GR24^{ent-5DS}$ (Yao et al., 2021).

Nitrogen (N) and phosphorus (P) are essential macronutrients for plants. As signalling mediators, SLs regulate the coordinated development of roots and shoots, particularly under N- and P-deficient conditions (Sun et al., 2014; Ito et al., 2015; Xi et al., 2015). Accordingly, SLs regulate above- and belowground plant morphogenesis, including shoot branching, leaf senescence, reproductive development, adventitious root (AR) formation, and root hair (RH) density (Kretzschmar et al., 2012; Yamada et al., 2014; Sun J. et al., 2015; Tan et al., 2019; Mitra et al., 2021). Moreover, a continuously increasing number of studies have suggested that SLs confer tolerance to different suboptimal growth conditions, especially drought and salinity (Saeed et al., 2017; Zhang X. et al., 2020). All these functions require coordinated changes at the molecular level in a complex plant growth network, necessitating the communication and cooperation of two or more hormone signals. The crosstalk between SL and other signalling pathways regulated by phytohormones, such as auxin, cytokinin (CK), ethylene (ET), and abscisic acid (ABA), has attracted extensive attention. This review verifies the latest information concerning the biological functions of SLs and further broadens and clarifies SL-associated hormonal networks in plant development and responses to several environmental challenges.

Strigolactones: Biosynthesis and Signalling Transduction

Given the benefits of SLs in plant biology, SLs exhibit the potential to improve crop genotypes with enhanced abiotic stress resilience and crop productivity. Understanding and exploiting SL biosynthesis are critical for effectively translating this potential into the modern agriculture industry. Although the SL biosynthesis pathway has not been fully elucidated, most enzymes involved in this pathway have been identified (**Figure 1**). SLs are plant secondary metabolites synthesised from carotenoids, which are converted to the SL precursor carlactone (CL) by the carotenoid isomerase DWARF27 (D27) and two carotenoid cleavage dioxygenase genes, namely, CCD7 and CCD8 (Lin et al., 2009; Alder et al., 2012). In *Arabidopsis*, MORE AXILLARY GROWTH1 (MAX1) encodes a cytochrome P450 monooxygenase (CYP711A1) that catalyses the conversion of CL to produce carlactonoic acid (CLA), which is then methylated to methyl carlactonoate (MeCLA) by an unknown methyltransferase (Abe et al., 2014; Seto et al., 2014). Lateral branching oxidoreductase is responsible for the oxidation of MeCLA into the SL-like compound (Brewer et al., 2016). In contrast to *Arabidopsis*, the rice MAX1 homologue Os900 (CYP711A2) converts CL into 4-deoxyorobanchol (4DO), and finally another homologue, Os1400 (CYP711A3), further catalyses the 4DO to form orobanchol (Zhang et al., 2014).

Strigolactone signalling transduction mechanisms are similar to those of other plant phytohormones. These mechanisms involve hormone-activated targetting of transcriptional regulators for degradation, likely involving α/β-fold hydrolases DWARF14 (D14 in rice) and F-box component (MAX2 in *Arabidopsis*) (Hamiaux et al., 2012; Nakamura et al., 2013). The D14 has a conserved catalytic triad (Ser-His-Asp) with hydrolase activity for recognising and deactivating SL (Yao et al., 2016). KARRIKIN INSENSITIVE2 (KAI2) is structurally closely related to D14 that perceives smoke-derived karrikin (KAR) and non-naturally derived SL enantiomers such as GR24$^{ent-5DS}$ (Waters et al., 2012). SL molecules bind to D14, resulting in the conformational change of D14, thereby facilitating D14 interaction with F-box proteins MAX2 (Zhao et al., 2015). This complex triggers the ubiquitination of transcriptional repressor D53 (homologous SMXL6, SMXL7, or SMXL8 in *Arabidopsis*), resulting in the 26S proteasomal degradation of this repressor and thus the transcription of SL responsive genes (Jiang et al., 2013; Wang et al., 2015; Yao et al., 2018). D53 is a key target in controlling axillary bud outgrowth in rice (Jiang et al., 2013; Fang et al., 2020). The SPL family transcription factor Ideal Plant Architecture1 in rice and D53 together mediates the transcriptional activation of genes in the SL regulatory process (Song et al., 2017). Numerous studies using various SL biosynthesis and signalling lines have demonstrated that SLs can positively modulate RH elongation, primary root (PR) growth, and secondary shoot growth, but repress AR development and axillary bud outgrowth (Agusti et al., 2011; Koltai, 2011; Rasmussen et al., 2012).

BIOLOGICAL FUNCTIONS OF STRIGOLACTONES

Effect of Strigolactones on Shoot Architecture and Root Development

Strigolactones are a class of phytohormones shaping the overall plant structure. For example, they control shoot branching, secondary growth, and root morphology. Shoot branching patterns result from the regulation of axillary bud growth. Many endogenous and external signals determine the growth or dormancy of each axillary bud (Qiu et al., 2019; Xie et al., 2020). Apical dominance is a phenomenon in which bud outgrowth is inhibited by the apex of the main shoot. Part of the inhibitory effect of apical dominance on bud outgrowth is due to the production of auxin by the apical young leaves (Domagalska and Leyser, 2011). However, auxin does not enter the buds and acts interdependently, partly by inducing strigolactone synthesis (Rameau et al., 2015; Wang H. W. et al., 2018; Barbier et al., 2019). Both SL biosynthesis and signalling-deficient mutants are semi-dwarf and exhibit increased branching, which gives the mutants a bushy appearance in *Arabidopsis* (**Figure 2**). SL mediates axillary bud outgrowth. This process involves SL-induced upregulation of the TCP transcription factor BRANCHED1 (BRC1) that suppresses bud activity (Braun et al., 2012; Dun et al., 2013). In addition, auxin flow out of axillary buds is contributing to bud outgrowth, and SL inhibition of the auxin efflux carrier PIN1 localisation to the plasma membrane and/or the effect of SL on auxin feedback on PIN1 internalisation reduce auxin efflux from lateral buds, thus enhancing competition among buds in the stem (Crawford et al., 2010; Waldie et al., 2014; Brewer et al., 2015; Zhang J. et al., 2020). Developmental processes contributing to the establishment of shoot architecture, such as tillering,

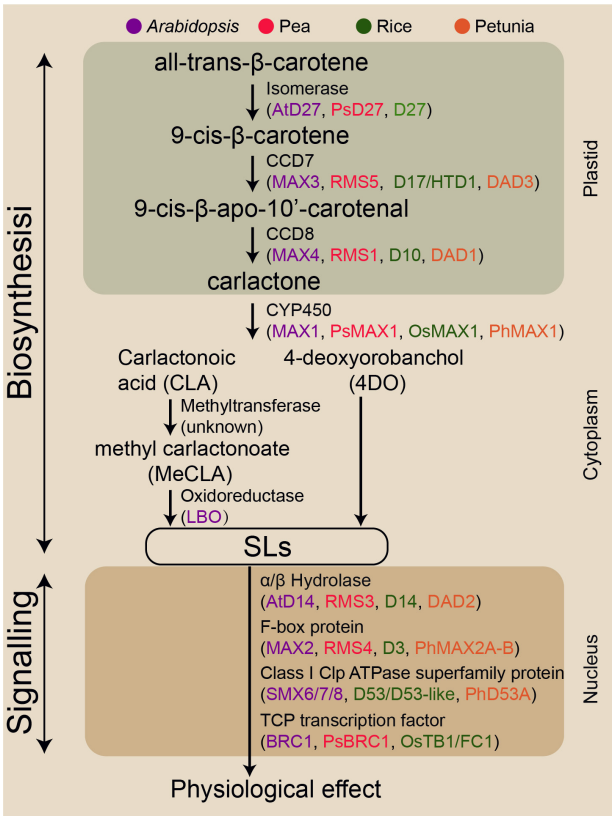

FIGURE 1 | Genes encoding the enzymes involved in SL biosynthesis and signalling pathway identified in the four model species.

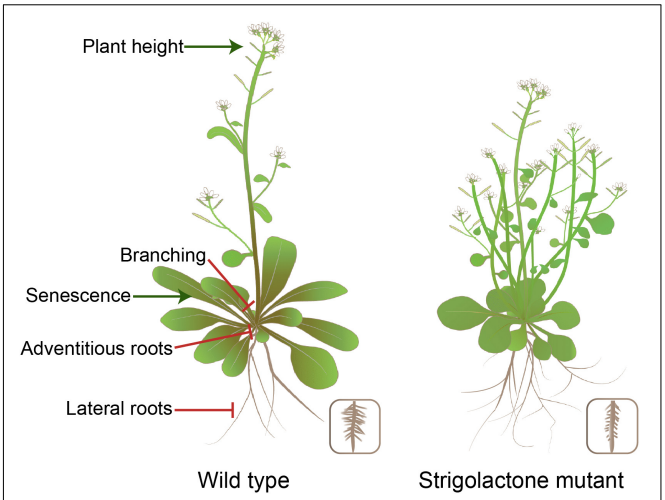

FIGURE 2 | Impact of SL production levels on plant morphology in *Arabidopsis*. SLs are involved in various developmental processes, including plant height, shoot branching, and root system architecture.

vegetative vigour, and dwarfing, are crucial agronomic traits affecting crop yield and can be manipulated by the application of SLs. For rice and wheat, the proper number of tillers is one of the significant factors that improves the grain yield, which may be related to SL exudation (Song et al., 2017; Zhao et al., 2019). In the case of *Brassica napus*, biomass increased the following spray with GR24 in growth chambers (Ma et al., 2017). Stem thickness was reduced in the SL signalling-deficient mutants of *Arabidopsis* and pea (Agusti et al., 2011). The specific features of SL action in the stem and root thickening can be exploited to reduce lodging susceptibility in cereal crops and increase timber production in silviculture. Newer opportunities for SL applications are likely to arise based on the studied examples described earlier.

The root system architecture plays a key role in optimising nutrient use efficiency and water acquisition, thereby enabling plant growth in nutrient-poorer soils. SLs regulate plant root development, although the specific effects vary across species and growth conditions. SL biosynthesis-deficient mutant in *Arabidopsis* developed more lateral roots (LRs) under optimal growth conditions, whereas an opposite effect was observed under the P-deficient conditions (Ruyter-Spira et al., 2011). ET blocks auxin-driven LR formation (Lewis et al., 2011). SLs translate P starvation signals into growth cues in the roots and interact with ET and auxin to exert their impact. In *Arabidopsis* and *pea*, SL signalling-deficient mutant exhibited more ARs, indicating that SLs suppress AR number (Rasmussen et al., 2012). Indeed, GR24 restored AR formation in the SL biosynthesis-deficient mutant *D10* but not in the SL signalling-deficient mutant *D3* of rice (Sun H. et al., 2015). The exact mechanism underlying the involvement of SLs in root development remains unclear because of conflicting data for different species. The highly complex hormonal interactions between SLs and other classes of phytohormones may all contribute to eventual root architectural modifications. Thus, plants can benefit from these interactions during development and adaptation to a changing environment (refer to the "Crosstalk between strigolactones and other hormones in plant growth and development, and in response to environmental changes" section for details).

Improvement of Nutrient Acquisition

Nutrient availability, particularly P deficiency, in agricultural soils affects SL exudation and distribution (Yoneyama et al., 2012). The increase in SL content is consistent with the expression of SL biosynthesis genes in rice roots, and this expression is elevated under N- or P-limiting conditions compared with that under controlled normal development conditions (Sun et al., 2014). Additionally, the ABC transporter Pleiotropic Drug Resistance1 (PDR1) translocated synthesised SLs from the root to shoot, and its transcription level increased in the roots of N- or P-deficient petunia and *Lotus japonicus* (Kretzschmar et al., 2012; Liu et al., 2015; Shiratake et al., 2019). The key genes, triad *IPS1*-miR399-*PHO2* and the high-affinity P transporter *LePT2*, were involved in the response of tomato plants to low P availability (Gamir et al., 2020). No matter growing with P or not, SL biosynthesis-deficient tomato mutant could not efficiently activate most mechanisms associated with the P starvation response compared with wild-type plants (Santoro et al., 2021).

SLs also act as molecular cues favouring arbuscular mycorrhizal (AM) symbiosis establishment in the rhizosphere, particularly increasing their access to nourishment and moisture from the nutrient-limited soil (Kapulnik and Koltai, 2014; Sun J. et al., 2015; Waters et al., 2017).

Strigolactones facilitate plants in responding to N and P starvation by shaping the above-and belowground architecture. Shoot growth and tiller production in rice were inhibited under the suboptimal P concentration, whereas SL signalling-deficient mutant (*D3*) and SL biosynthesis-deficient mutant (*D10*) showed no adverse effects (Luo et al., 2018). SLs positively regulated in stimulating PR length in rice, wheat, and tomato under limited P resources (Jamil et al., 2011; Yoneyama et al., 2012; Santoro et al., 2020). A similar effect was observed for root elongation in rice (Arite et al., 2012). SLs are vital for nitric oxide-regulated rice seminal root elongation during P and N starvation (Sun et al., 2016). The seminal root length of SL biosynthesis-deficient mutant (*D10* and *D27*) and SL signalling-deficient mutant (*D3*) in rice decreased under low-P conditions. By contrast, all these SL-related mutants presented increased LR density during P starvation compared with wild-type plants (Sun et al., 2014). This negative effect on LR growth is attributable to the SL-mediated inhibition of polar auxin transport from shoots to roots and alteration of auxin distribution in roots (Sun et al., 2014). The potential of SLs in nutrient starvation response is valuable in developing strategies to improve nutrient use efficiency and productivity in low-fertility soils.

Mediation of Plant Tolerance to Drought and Salinity

Climatic changes increase drought and soil salinity, reducing crop yield in the affected areas. SLs participate directly in plant tolerance to abiotic stresses. During the analysis of the promoter sequences of SL biosynthesis genes in *Arabidopsis*, *cis*-acting sequences that specifically bind to drought and salt-responsive transcription factors were identified (Marzec and Muszynska, 2015). Under drought conditions, the SL analogue AB01 improved the grain yield and kernel weight of maize and sunflower (Chesterfield et al., 2020). SL biosynthesis- or signalling-deficient mutants are hypersensitive to unfavourable environmental conditions such as drought, salt, and osmotic stress (Zhang et al., 2018; Qiao et al., 2020; Zheng et al., 2021). The expression levels of SL biosynthesis genes (*SlCCD7* and *SlCCD8*) and SL content decreased in tomato roots under drought stress (Visentin et al., 2016). By contrast, SL levels were elevated in rice roots in response to water withholding-induced dehydration (Haider et al., 2018). Monocots and dicots may adopt different survival strategies to cope with the water deficit.

The abundance of AM fungi in the rhizosphere of lettuce plants increased in response to salinity-induced SL secretion from roots (Aroca et al., 2013). However, SL biosynthesis-deficient mutant of rice exhibited lower AM colonisation than wild-type plants (Kobae et al., 2018). Drought stress-induced SL production in lettuce and tomato further triggered the growth of AM fungi, thus improving drought resistance (Ruiz-Lozano et al., 2016). SLs promote communication between the host and beneficial soil microorganisms, an eco-friendly strategy, and allow plants to better withstand environmental changes.

CROSSTALK BETWEEN STRIGOLACTONES AND OTHER HORMONES IN PLANT GROWTH AND DEVELOPMENT, AND IN RESPONSE TO ENVIRONMENTAL CHANGES

Strigolactones and Abscisic Acid

The correlation between ABA and SLs is critical for regulating multiple physiological mechanisms and adaptation to environmental changes in plants. The ABA importer genes *ABCG22/AT5G06530* and *ABCG40/AT1G15520* were downregulated in the SL signalling-deficient mutant *max2* of *Arabidopsis* under well-watered and dehydrated conditions (Ha et al., 2014; Ruiz-Lozano et al., 2016). SLs induce tolerance to drought and salt stress largely by activating ABA signalling. Resistance to drought associated with slower stomatal closure, which was attributed to ABA insensitivity, was impaired in the SL biosynthesis-deficient mutant of *L. japonicus* (Liu et al., 2015). Similar ABA-SL crosstalk was demonstrated in which GR24 pre-treatment alleviated the adverse effects of salt stress in rice and grapevine seedlings and better induced stomatal closure (Min et al., 2019; Ling et al., 2020). The effect of SLs on stomatal closure depends on ABA synthesis, transport, and sensitivity (Visentin et al., 2020). Another recent study found that the SL biosynthesis-deficient mutant *D10* and *D17* and the SL signalling-deficient mutant *D13* of rice had higher ABA accumulation than wild-type plants, resulting in induced drought tolerance (Haider et al., 2018). By contrast, the low-ABA-producing line D27 was susceptible to drought implying that D27 participates in the ABA signalling pathway (Haider et al., 2018). However, the mechanism by which D27 links ABA to SL has not been elucidated. Apart from their role in drought resistance, the positive role of SLs in the cold and heat stress response is associated with ABA biosynthesis. $GR24^{5DS}$ application enhanced heat and cold tolerance in tomato, whereas the ABA-deficient mutant compromised the $GR24^{5DS}$ effects, implying that SL, at least partially in an ABA-dependent manner, allows plants to flexibly acclimate to and overcome these stress conditions (Chi et al., 2021).

Strigolactones and ABA both participate in the regulation of branching or tillering, and ABA acts as downstream of SLs and BRC1 in *Arabidopsis* (González-Grandío et al., 2017; Wang B. et al., 2018; Wang and Bouwmeester, 2018; Wang et al., 2020). SLs mediating axillary bud outgrowth are involved in degrading SMXL6 and releasing BRC1 transcriptional repression, thereby inducing *HB40*/*OsHOX12* expression, activating *AtNCED3*/*OsNCED1* expression, and promoting ABA accumulation in the lateral buds of *Arabidopsis* or shoot bases of rice (Liu et al., 2020; Wang et al., 2020). Indeed, ABA supply inhibits tiller bud growth and suppresses the formation of unproductive upper tillers in rice, but its contribution is less than that of SLs (Liu et al., 2020).

During abiotic stress, ABA levels increase rapidly, but SL content may vary in different species. ABA positively regulated SL levels and the expression of signalling genes to improve salt stress acclimatisation and resistance in *Sesbania cannabina* (Ren et al., 2018). Similarly, plant resilience to water deprivation is promoted through the upregulation of the transcript levels of SL biosynthesis genes in rice root extracts (Haider et al., 2018). However, both the SL level and the SL gene expression in tomato and *L. japonicus* decreased under osmotic stress (Liu et al., 2015; Visentin et al., 2016). Breeding for potentially drought-tolerant crop varieties by SL signal upregulation requires further exploration.

Strigolactones and Cytokinin

As physiological processes vary, so do the interactions between SLs and CK. CK and SLs regulate separate processes and function independently in adventitious rooting, synergistically controlling LR development, but antagonistically regulating axillary bud outgrowth (Dun et al., 2013; Hu et al., 2014; Manandhar et al., 2018; Faizan et al., 2020).

Strigolactones and CK interact directly in buds, and they integratively promote the transcriptional regulation of *BRC1* in *Arabidopsis* and pea or *FINE CULM 1*, an orthologous gene of *BRC1*, in rice (Braun et al., 2012; Dun et al., 2013; Xu et al., 2015). BRC1 is known to modulate the bud activation potential in several species by acting as an important hub of regulatory signals controlling bud outgrowth (Martin-Trillo et al., 2011; Nicolas et al., 2015; Shen et al., 2019). The antagonistic action of CK and SL mediates the inhibitory effect of auxin on bud outgrowth (Rameau et al., 2015; Barbier et al., 2019). In rice, SLs activate CK catabolism to alter the shoot architecture *via* cytokinin oxidase/dehydrogenase 9 (OsCKX9) activity (Duan et al., 2019). Therefore, along with induced activation of OsCKX9, SLs may affect the CK content through crosstalk with auxin. In addition, high sugar levels were found to inhibit SL perception, notably by directly targetting SL signalling (Dierck et al., 2016; Bertheloot et al., 2020; Patil et al., 2021). Sugars were also found to upregulate the levels of CK, which acts antagonistically with SLs (Barbier et al., 2015; Kiba et al., 2019; Salam et al., 2021). However, the exact role of CK in the sugar response remains undetermined.

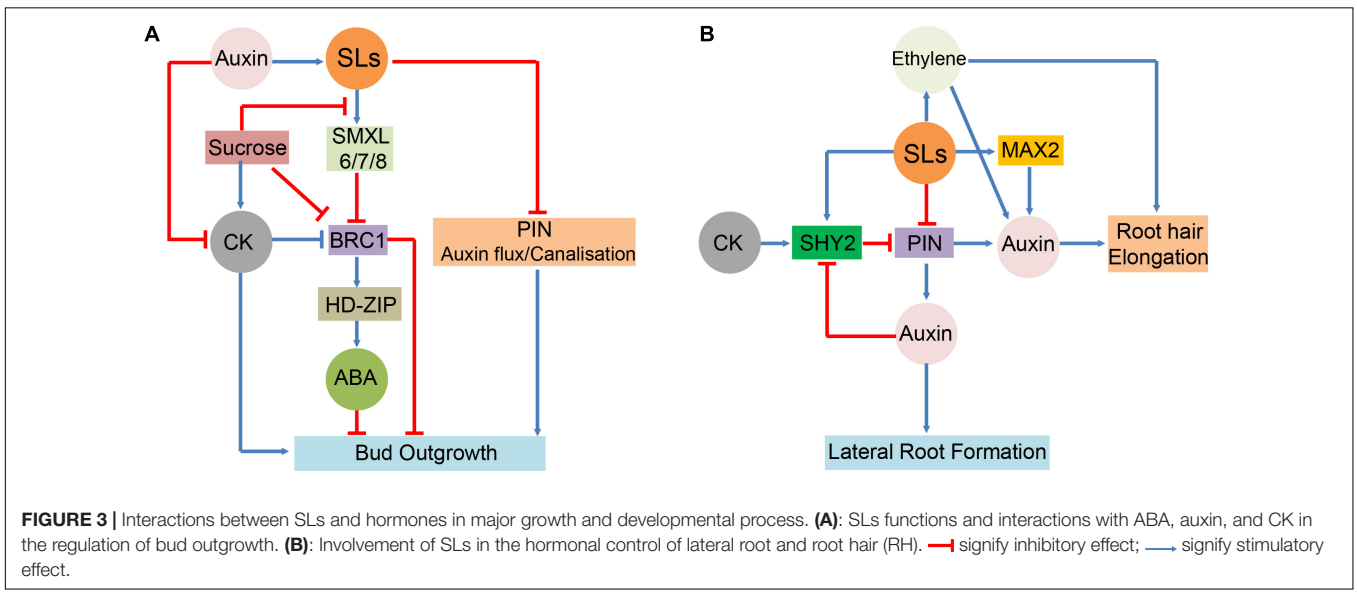

FIGURE 3 | Interactions between SLs and hormones in major growth and developmental process. **(A)**: SLs functions and interactions with ABA, auxin, and CK in the regulation of bud outgrowth. **(B)**: Involvement of SLs in the hormonal control of lateral root and root hair (RH). ⊣ signify inhibitory effect; → signify stimulatory effect.

TABLE 1 | Effects of strigolactones and hormones crosstalk on various plant species.

Plant hormones	Investigated Species	Type of experiment	SL effect	Antagonism or synergism	References
ABA	*Arabidopsis thaliana*	SLs-response max2 mutant	Effect ABA import	Synergism	Ha et al., 2014; Ruiz-Lozano et al., 2016
	L. japonicus	SL-biosynthesis mutant	Slow stomatal closure	Synergism	Liu et al., 2015
	Rice and grapevine seedlings	synthetic GR24	Induces stomatal closure	Synergism	Min et al., 2019; Ling et al., 2020
	Rice	SL-deficient mutants D10 and D17 SL-perception mutant D13	Induce drought tolerance	Synergism	Haider et al., 2018
CK	*Arabidopsis thaliana*	GR24	Inhibits the elongation of the primary root	Synergism	Jiang et al., 2016
	Rice	SLs-insensitive tiller dwarfing mutants	Increase auxin level	Synergism	Sun et al., 2019
IAA	Rice	GR24	Reduced IAA distribution and modulated AR formation	Antagonis	Sun H. et al., 2015
ET	*Arabidopsis thaliana*	ET signalling deficient *ein2* and *etr1* mutants	Eliminate the influence of SLs on the Root morphogenesis	Synergism	Kapulnik et al., 2011

During branching, HEXOKINASE1 mediates the sugar signalling pathway, allowing plants to fine-tune the shoot architecture, and interacts with CK and SLs (Barbier et al., 2021).

GR24 inhibits PR elongation by altering *PIN* gene transcription, which is mediated by Short Hypocotyl2 (SHY2) through CK signalling components (Jiang et al., 2016). The CK response transcription factor (ARR1) directly binds to specific promoter sequences of the protein SHY2 and activates its expression, which in turn represses the *PIN* genes, while auxin stalls LR formation by SHY2-mediated repression of PIN activity (Sengupta and Reddy, 2018). SHY2 acts as a node-linking hormone that regulates root meristem development. SLs may affect the endogenous levels and distribution of each hormone, coordinately controlling the root (meristem) size.

Cytokinins and SLs play opposite regulatory roles in plant adaptation to drought. In CK-depleted and CK-signalling mutants of *Arabidopsis*, CKs and CK-signalling components were found to negatively regulate plant drought acclimation (Nishiyama et al., 2013; Nguyen et al., 2016). Conversely, SLs positively regulate drought resistance-related physiological traits by altering stomatal density and stomatal conductance (Ha et al., 2014; Zhang et al., 2018). In addition, downregulation of CK catabolism genes (*CKX1*, *CKX2*, *CKX3*, and *CKX5*) following dehydration was observed in the SL signalling-deficient mutant *MAX2* compared with wild-type plants (Ha et al., 2014). This indicates that the SL signal might have an antagonistic effect on the CK content, which can be confirmed by detailed studies on SL biosynthesis and signalling mutants under drought stress because MAX2 appears to be shared by both SL signalling and karrikin signalling pathways (Soundappan et al., 2015).

Strigolactones and Auxin

Strigolactones and auxin synergistically regulate shoot branching and root development (Crawford et al., 2010; Ma et al., 2020; Zhang J. et al., 2020). SL-mediated regulation of shoot branching is tightly linked to PIN-dependent auxin transport, specifically its canalisation (Crawford et al., 2010; Shinohara et al., 2013). This is supported by the fact that SL biosynthesis-deficient mutants *MAX4-5* and *D27-1* exhibit enhanced accumulation of the PIN1 auxin efflux carrier on the basal plasma membrane (Bennett et al., 2016) and that GR24 treatment can induce PIN1 endocytosis and reduce auxin transport during SL biosynthesis in *Arabidopsis* but not in response mutants (Shinohara et al., 2013). SLs inhibit auxin feedback on PIN polarity and clathrin-mediated endocytosis of PIN proteins through D14- and MAX2-mediated signalling pathways (Zhang J. et al., 2020). However, exogenous SLs can still suppress bud outgrowth in auxin transport inhibitor 1-N57 naphthylphthalamic acid-treated shoots, suggesting the existence of another mechanism of bud growth inhibition by SLs. This also suggests that SL acts directly on bud outgrowth independent of polar auxin transport (Chabikwa et al., 2019). Many questions about the exact mechanism of SL action and perception may be answered by examining some promising candidates as downstream mediators of SL signalling (Brewer et al., 2015).

During root development, SLs regulate LR and RH development by changing auxin distribution (Haq et al., 2017; Sun et al., 2019). Polar auxin transport mainly depends on the auxin efflux protein PINs. This protein creates local auxin maxima to form the basis for root initiation and elongation (Zhang Y. et al., 2020). GR24 reduced IAA distribution and modulated AR formation by downregulating the levels of PIN family genes in rice (Sun H. et al., 2015). However, in the presence of exogenous auxin, the PIN gene expression level in the PR tip of *Arabidopsis* was not affected by GR24 treatment (Ruyter-Spira et al., 2011). A similar crosstalk between SLs and auxin occurs in the regulation of RH development where SL-mediated reduction of auxin accumulation within root cells results in high RH length and density (Koltai et al., 2010). These root responses are typical to P-deficient conditions (Santoro et al., 2020). The auxin-responsive element of the bHLH transcription factor ROOT HAIR DEFECTIVE SIX-LIKE 4 positively regulates genes involved in cell processes key to RH growth under the P-deficient condition (Bhosale et al., 2018; Zhu et al., 2020). These backgrounds clarify that RSL4 may function as a common integrator for the crosstalk between SLs and auxin in modulating RH elongation (Marzol et al., 2017). RH morphogenesis is driven by interacting processes controlled by complex hormone signalling. How these signalling components induce SL biosynthesis and signalling according to the P status at the molecular level remains unclear. Further studies should focus on cloning genes involved in RH mutants and undertaking reverse genetics and mutant complementation experiments to gain extended knowledge on signalling networks.

Strigolactones and Ethylene

Strigolactones have also been demonstrated to interact with ET signalling and control RH elongation. ET signalling-deficient *ein2* and *etr1* mutants exhibited no influence of SLs on RH morphogenesis (Kapulnik et al., 2011). In *Arabidopsis*, RH elongation was enhanced by GR24 treatment alone but not by treatment with the ET biosynthesis inhibitor aminoethoxyvinylglycine, even in the presence of GR24 (Lee and Yoon, 2020). This indicates that ET is necessary for promoting SL-mediated RH elongation. SLs adjust the balance between auxin and ET signalling pathways to activate different developmental programmes in response to soil nutrient limitations, thereby controlling their own biosynthesis in roots under these conditions. Under P-sufficient conditions, SLs interact with ET and promote auxin signalling transduction (Koltai, 2013). ET forms a crosstalk junction between SLs and auxin pathways in modulating RH formation. Together, these hormones probably create a deliberately coordinated network for regulating plant growth and its response to adverse growth conditions (**Figure 3**).

Strigolactones Application Challenges and Future Directions

With the recent discovery of a hormonal function for SLs, SL-mediated regulation of plant development has been explored extensively. Phenotypic plasticity is crucial for plants adapting to changing or extreme abiotic environments. Modification of SL signalling pathways to create an optimal crop architecture is a pivotal physiological strategy in improving nutrient uptake

and utilisation, crop productivity, and resilience. As novel molecular technologies have increased the feasibility of genetic improvement of crops, variants with modified SL profiles, for example, transgenic rice (OsMADS57 and OsTB1), have led to increased grain yield with upregulated SL response pathways modulating tillering. Furthermore, ontogenetic modification of the SL transport signal, such as overexpression of the SL transporter PDR1, might be useful for obtaining a potential breeding stock. Applying SL analogues for shaping the plant architecture, improving their performance and resistance, and enhancing AM colonisation are of high potential value. Cheaper sources of SLs analogues are required for large-scale agricultural applications.

Similar to other phytohormones, SL biosynthesis and activity are regulated by multiple levels of crosstalk in hormonal networks under suboptimal environmental conditions (**Table 1**). As the interface between the plant and soil, roots are more exposed to adverse soil conditions than the aerial parts of the plant. The roots' perception of the environment influences plant morphology. Progress has been made in understanding how different phytohormones facilitate root growth plasticity. More components involved in these processes and spatial temporal relationships between these components need to be identified. Additional experimental and theoretical studies are warranted to carefully understand the different contributions of SLs and these hormones to the whole plant level of organisation. The endogenous levels of phytohormones need to be optimised to maximise stress-responsive crosstalk between multiple hormones.

AUTHOR CONTRIBUTIONS

FW, YG, and WY wrote the manuscript. NS and JZ edited the manuscript. All the authors discussed and created the review's outline.

FUNDING

This research was supported by the Shandong Province Key Research and Development Programme (2019GSF107079), the Development Plan for Youth Innovation Team of Shandong Provincial (2019KJE012), and the Science and Technology Demonstration Project of "Bohai Granary" of Shandong Province (2019BHLC002).

REFERENCES

Abe, S., Sado, A., Tanaka, K., Kisugi, T., Asami, K., Ota, S., et al. (2014). Carlactone is converted to carlactonoic acid by MAX1 in Arabidopsis and its methyl ester can directly interact with AtD14 *in vitro*. *Proc. Natl. Acad. Sci. U.S.A.* 111, 18084–18089. doi: 10.1073/pnas.1410801111

Agusti, J., Herold, S., Schwarz, M., Sanchez, P., Ljung, K., Dun, E. A., et al. (2011). Strigolactone signaling is required for auxin-dependent stimulation of secondary growth in plants. *Proc. Natl. Acad. Sci. U.S.A.* 108, 20242–20247. doi: 10.1073/pnas.1111902108

Alder, A., Jamil, M., Marzorati, M., Bruno, M., Vermathen, M., Bigler, P., et al. (2012). The path from β-carotene to carlactone, a strigolactone-like plant hormone. *Science* 335, 1348–1351. doi: 10.1126/science.1218094

Arite, T., Kameoka, H., and Kyozuka, J. (2012). Strigolactone positively controls crown root elongation in rice. *J. Plant Growth Regul.* 31, 165–172. doi: 10.1007/s00344-011-9228-6

Aroca, R., Ruiz-Lozano, J. M., Zamarreño, A. M., Paz, J. A., García-Mina, J. M., Pozo, M. J., et al. (2013). Arbuscular mycorrhizal symbiosis influences strigolactone production under salinity and alleviates salt stress in lettuce plants. *J. Plant Physiol.* 170, 47–55. doi: 10.1016/j.jplph.2012.08.020

Barbier, F. F., Cao, D., Fichtner, F., Weiste, C., Perez-Garcia, M., Caradeuc, M., et al. (2021). HEXOKINASE1 signalling promotes shoot branching and interacts with cytokinin and strigolactone pathways. *New Phytol.* 231, 1088–1104. doi: 10.1111/nph.17427

Barbier, F. F., Dun, E. A., Kerr, S. C., Chabikwa, T. G., and Beveridge, C. A. (2019). An update on the signals controlling shoot branching. *Trends Plant Sci.* 24, 220–236. doi: 10.1016/j.tplants.2018.12.001

Barbier, F., Peron, T., Lecerf, M., Perez-Garcia, M. D., Barriere, Q., Rolcik, J., et al. (2015). Sucrose is an early modulator of the key hormonal mechanisms controlling bud outgrowth in Rosa hybrida. *J. Exp. Bot.* 66, 2569–2582. doi: 10.1093/jxb/erv047

Bennett, T., Liang, Y., Seale, M., Ward, S., Müller, D., and Leyser, O. (2016). Strigolactone regulates shoot development through a core signalling pathway. *Biol. Open* 5, 1806–1820.

Bertheloot, J., Barbier, F., Boudon, F., Perez-Garcia, M. D., Péron, T., Citerne, S., et al. (2020). Sugar availability suppresses the auxin-induced strigolactone pathway to promote bud outgrowth. *New Phytol.* 225, 866–879. doi: 10.1242/bio.021402

Bhosale, R., Giri, J., Pandey, B. K., Giehl, R. F., Hartmann, A., Traini, R., et al. (2018). A mechanistic framework for auxin dependent Arabidopsis root hair elongation to low external phosphate. *Nat. Commun.* 9, 1–9. doi: 10.1038/s41467-018-03851-3

Braun, N., de Saint Germain, A., Pillot, J. P., Boutet-Mercey, S., Dalmais, M., Antoniadi, I., et al. (2012). The pea TCP transcription factor PsBRC1 acts downstream of strigolactones to control shoot branching. *Plant Physiol.* 158, 225–238. doi: 10.1104/pp.111.182725

Brewer, P. B., Dun, E. A., Gui, R., Mason, M. G., and Beveridge, C. A. (2015). Strigolactone inhibition of branching independent of polar auxin transport. *Plant Physiol.* 168, 1820–1829. doi: 10.1104/pp.15.00014

Brewer, P. B., Yoneyama, K., Filardo, F., Meyers, E., Scaffidi, A., Frickey, T., et al. (2016). LATERAL BRANCHING OXIDOREDUCTASE acts in the final stages of strigolactone biosynthesis in *Arabidopsis*. *Proc. Natl. Acad. Sci. U.S.A.* 113, 6301–6306. doi: 10.1073/pnas.1601729113

Butler, L. G. (1995). Chemical communication between the parasitic weed Striga and its crop host: a new dimension in allelochemistry. *ACS Symp. Ser.* 582, 158–168. doi: 10.1021/bk-1995-0582.ch012

Chabikwa, T. G., Brewer, P. B., and Beveridge, C. A. (2019). Initial bud outgrowth occurs independent of auxin flow from out of buds. *Plant Physiol.* 179, 55–65. doi: 10.1104/pp.18.00519

Chesterfield, R. J., Vickers, C. E., and Beveridge, C. A. (2020). Translation of strigolactones from plant hormone to agriculture: achievements, future perspectives, and challenges. *Trends Plant Sci.* 25, 1087–1106. doi: 10.1016/j.tplants.2020.06.005

Chi, C., Xu, X., Wang, M., Zhang, H., Fang, P., Zhou, J., et al. (2021). Strigolactones positively regulate abscisic acid-dependent heat and cold tolerance in tomato. *Hortic. Res.* 8:237. doi: 10.1038/s41438-021-00668-y

Ciura, J., and Kruk, J. (2018). Phytohormones as targets for improving plant productivity and stress tolerance. *J. Plant Physiol.* 229, 32–40. doi: 10.1016/j.jplph.2018.06.013

Cook, C. E., Whichard, L. P., Turner, B., Wall, M. E., and Egley, G. H. (1966). Germination of witchweed (*Striga lutea* Lour.): isolation and properties of a potent stimulant. *Science* 154, 1189–1190. doi: 10.1126/science.154.3753.1189

Crawford, S., Shinohara, N., Sieberer, T., Williamson, L., George, G., Hepworth, J., et al. (2010). Strigolactones enhance competition between shoot branches by dampening auxin transport. *Development* 137, 2905–2913. doi: 10.1242/dev.051987

Dierck, R., Dhooghe, E., Van Huylenbroeck, J., De Riek, J., De Keyser, E., and Van Der Straeten, D. (2016). Response to strigolactone treatment in chrysanthemum axillary buds is influenced by auxin transport inhibition and sucrose availability. *Acta Physiol. Plant* 38:271. doi: 10.1007/s11738-016-2292-6

Domagalska, M., and Leyser, O. (2011). Signal integration in the control of shoot branching. *Nat. Rev. Mol. Cell Biol.* 12, 211–221. doi: 10.1038/nrm3088

Duan, J., Yu, H., Yuan, K., Liao, Z., Meng, X., Jing, Y., et al. (2019). Strigolactone promotes cytokinin degradation through transcriptional activation of CYTOKININ OXIDASE/DEHYDROGENASE 9 in rice. *Proc. Natl. Acad. Sci. U.S.A.* 116:14319. doi: 10.1073/pnas.1810980116

Dun, E. A., de Saint Germain, A., Rameau, C., and Beveridge, C. A. (2013). Antagonistic action of strigolactone and cytokinin in bud outgrowth control. *Plant Physiol.* 158, 487–489. doi: 10.1104/pp.111.186783

Faizan, M., Faraz, A., Sami, F., Siddiqui, H., Yusuf, M., Gruszka, D., et al. (2020). Role of strigolactones: signalling and crosstalk with other phytohormones. *Open Life Sci.* 15, 217–228. doi: 10.1515/biol-2020-0022

Fang, Z., Ji, Y., Hu, J., Guo, R., Sun, S., and Wang, X. (2020). Strigolactones and brassinosteroids antagonistically regulate the stability of the D53–OsBZR1 complex to determine FC1 expression in rice tillering. *Mol. Plant* 13, 586–597. doi: 10.1016/j.molp.2019.12.005

Gamir, J., Torres-Vera, R., Rial, C., Berrio, E., de Souza Campos, P. M., Varela, R. M., et al. (2020). Exogenous strigolactones impact metabolic profiles and phosphate starvation signalling in roots. *Plant Cell. Environ.* 43, 1655–1668. doi: 10.1111/pce.13760

González-Grandío, E., Pajoro, A., Franco-Zorrilla, J. M., Tarancón, C., Immink, R. G., and Cubas, P. (2017). Abscisic acid signaling is controlled by a BRANCHED1/HD-ZIP I cascade in *Arabidopsis* axillary buds. *Proc. Natl. Acad. Sci. U.S.A.* 114, E245–E254. doi: 10.1073/pnas.1613199114

Ha, C. V., Leyva-González, M. A., Osakabe, Y., Tran, U. T., Nishiyama, R., Watanabe, Y., et al. (2014). Positive regulatory role of strigolactone in plant responses to drought and salt stress. *Proc. Natl. Acad. Sci. U.S.A.* 111, 851–856. doi: 10.1073/pnas.1322135111

Haider, I., Andreo-Jimenez, B., Bruno, M., Bimbo, A., Floková, K., Abuauf, H., et al. (2018). The interaction of strigolactones with abscisic acid during the drought response in rice. *J. Exp. Bot.* 69, 2403–2414. doi: 10.1093/jxb/ery089

Hamiaux, C., Drummond, R. S., Janssen, B. J., Ledger, S. E., Cooney, J. M., Newcomb, R. D., et al. (2012). DAD2 is an α/β hydrolase likely to be involved in the perception of the plant branching hormone, strigolactone. *Curr. Biol.* 22, 2032–2036. doi: 10.1016/j.cub.2012.08.007

Haq, B. U., Ahmad, M. Z., Ur Rehman, N., Wang, J., Li, P., Li, D., et al. (2017). Functional characterization of soybean strigolactone biosynthesis and signaling genes in *Arabidopsis* MAX mutants and GmMAX3 in soybean nodulation. *BMC Plant Biol.* 17:259. doi: 10.1186/s12870-017-1182-4

Hu, Z., Yamauchi, T., Yang, J., Jikumaru, Y., Tsuchida-Mayama, T., Ichikawa, H., et al. (2014). Strigolactone and cytokinin act antagonistically in regulating rice mesocotyl elongation in darkness. *Plant Cell Physiol.* 55, 30–41. doi: 10.1093/pcp/pct150

Ito, S., Ito, K., Abeta, N., Takahashi, R., Sasaki, Y., and Yajima, S. (2015). Effects of strigolactone signaling onArabidopsisgrowth under nitrogen deficient stress condition. *Plant Signal Behav.* 11, e1126031. doi: 10.1080/15592324.2015.1126031

Jamil, M., Charnikhova, T., Cardoso, C., Jamil, T., Ueno, K., Verstappen, F., et al. (2011). Quantification of the relationship between strigolactones and Striga hermonthica infection in rice under varying levels of nitrogen and phosphorus. *Weed Res.* 51, 373–385. doi: 10.1111/j.1365-3180.2011.00847.x

Jiang, L., Liu, X., Xiong, G., Liu, H., Chen, F., Wang, L., et al. (2013). DWARF 53 acts as a repressor of strigolactone signalling in rice. *Nature* 504, 401–405. doi: 10.1038/nature12870

Jiang, L., Matthys, C., Marquez-Garcia, B., De Cuyper, C., Smet, L., De Keyser, A., et al. (2016). Strigolactones spatially influence lateral root development through the cytokinin signaling network. *J. Exp. Bot.* 67, 379–389. doi: 10.1093/jxb/erv478

Kapulnik, Y., and Koltai, H. (2014). Strigolactone involvement in root development, response to abiotic stress, and interactions with the biotic soil environment. *Plant Physiol.* 166, 560–569. doi: 10.1104/pp.114.244939

Kapulnik, Y., Delaux, P. M., Resnick, N., Mayzlish-Gati, E., Wininger, S., Bhattacharya, C., et al. (2011). Strigolactones affect lateral root formation and root-hair elongation in Arabidopsis. *Planta* 233, 209–216. doi: 10.1007/s00425-010-1310-y

Kiba, T., Takebayashi, Y., Kojima, M., and Sakakibara, H. (2019). Sugar-induced de novo cytokinin biosynthesis contributes to Arabidopsis growth under elevated CO2. *Sci. Rep.* 9:7765. doi: 10.1038/s41598-019-44185-4

Kobae, Y., Kameoka, H., Sugimura, Y., Saito, K., Ohtomo, R., Fujiwara, T., et al. (2018). Strigolactone biosynthesis genes of rice are required for the punctual entry of arbuscular mycorrhizal fungi into the roots. *Plant Cell Physiol.* 59, 544–553. doi: 10.1093/pcp/pcy001

Koltai, H. (2011). Strigolactones are regulators of root development. *New Phytol.* 190, 545–549. doi: 10.1111/j.1469-8137.2011.03678.x

Koltai, H. (2013). Strigolactones activate different hormonal pathways for regulation of root development in response to phosphate growth conditions. *Ann. Bot.* 112, 409–441. doi: 10.1093/aob/mcs216

Koltai, H., Dor, E., Hershenhorn, J., Joel, D. M., Weininger, S., Lekalla, S., et al. (2010). Strigolactones' effect on root growth and root-hair elongation may be mediated by auxin-efflux carriers. *J. Plant Growth Regul.* 29, 129–136. doi: 10.1007/s00344-009-9122-7

Kretzschmar, T., Kohlen, W., Sasse, J., Borghi, L., Schlegel, M., Bachelier, J. B., et al. (2012). A petunia ABC protein controls strigolactone-dependent symbiotic signalling and branching. *Nature* 483, 341–344. doi: 10.1038/nature10873

Lee, H. Y., and Yoon, G. M. (2020). Strigolactone elevates ethylene biosynthesis in etiolated *Arabidopsis* seedlings. *Plant Signal. Behav.* 15:1805232. doi: 10.1080/15592324.2020.1805232

Lewis, D. R., Ramirez, M. V., Miller, N. D., Vallabhaneni, P., Ray, W. K., Helm, R. F., et al. (2011). Auxin and ethylene induce flavonol accumulation through distinct transcriptional networks. *Plant Physiol.* 156, 144–164. doi: 10.1104/pp.111.172502

Li, G., Zhang, C., Zhang, G., Fu, W., Feng, B., Chen, T., et al. (2020). Abscisic acid negatively modulates heat tolerance in rolled leaf rice by increasing leaf temperature and regulating energy homeostasis. *Rice* 13, 1–16. doi: 10.1186/s12284-020-00379-3

Lin, H., Wang, R., Qian, Q., Yan, M., Meng, X., Fu, Z., et al. (2009). DWARF27, an iron-containing protein required for the biosynthesis of strigolactones, regulates rice tiller bud outgrowth. *Plant Cell* 21, 1512–1525. doi: 10.1105/tpc.109.065987

Ling, F., Su, Q., Jiang, H., Cui, J., He, X., Wu, Z., et al. (2020). Effects of strigolactone on photosynthetic and physiological characteristics in salt-stressed rice seedlings. *Sci. Rep.* 10, 1–8. doi: 10.1038/s41598-020-63352-6

Liu, J., He, H., Vitali, M., Visentin, I., Charnikhova, T., Haider, I., et al. (2015). Osmotic stress represses strigolactone biosynthesis in *Lotus japonicus* roots: exploring the interaction between strigolactones and ABA under abiotic stress. *Planta* 241, 1435–1451. doi: 10.1007/s00425-015-2266-8

Liu, X., Hu, Q., Yan, J., Sun, K., Liang, Y., Jia, M., et al. (2020). ζ-Carotene isomerase suppresses tillering in rice through the coordinated biosynthesis of strigolactone and abscisic acid. *Mol. Plant* 13, 1784–1801. doi: 10.1016/j.molp.2020.10.001

Luo, L., Wang, H., Liu, X., Hu, J., Zhu, X., Pan, S., et al. (2018). Strigolactones affect the translocation of nitrogen in rice. *Plant Sci.* 270, 190–197. doi: 10.1016/j.plantsci.2018.02.020

Ma, N., Hu, C., Wan, L., Hu, Q., Xiong, J., and Zhang, C. (2017). Strigolactones improve plant growth, photosynthesis, and alleviate oxidative stress under salinity in rapeseed (*Brassica napus* L.) by regulating gene expression. *Front. Plant Sci.* 8:1671. doi: 10.3389/fpls.2017.01671

Ma, N., Wan, L., Zhao, W., Liu, H., Li, J., and Zhang, C. (2020). Exogenous strigolactones promote lateral root growth by reducing the endogenous auxin level in rapeseed. *J. Integr. Agric.* 19, 465–482. doi: 10.1016/S2095-3119(19)62810-8

Manandhar, S., Funnell, K. A., Woolley, D. J., and Cooney, J. M. (2018). Interaction between strigolactone and cytokinin on axillary and adventitious bud development in *Zantedeschia*. *J. Plant Physiol. Pathol.* 6:1. doi: 10.4172/2329-955X.1000172

Martin-Trillo, M., Grandio, E. G., Serra, F., Marcel, F., Rodriguez-Buey, M. L., Schmitz, G., et al. (2011). Role of tomato BRANCHED1-like genes in the control of shoot branching. *Plant J.* 67, 701–714. doi: 10.1111/j.1365-313X.2011.04629.x

Marzec, M., and Muszynska, A. (2015). In silico analysis of the genes encoding proteins that are involved in the biosynthesis of the RMS/MAX/D pathway revealed new roles of strigolactones in plants. *Int. J. Mol. Sci.* 16, 6757–6782. doi: 10.3390/ijms16046757

Marzol, E., Borassi, C., Denita Juárez, S. P., Mangano, S., and Estevez, J. M. (2017). RSL4 takes control: multiple signals, one transcription factor. *Trends Plant Sci.* 22, 553–555. doi: 10.1016/j.tplants.2017.04.007

Min, Z., Li, R., Chen, L., Zhang, Y., Li, Z., Liu, M., et al. (2019). Alleviation of drought stress in grapevine by foliar-applied strigolactones. *Plant Physiol. Biochem.* 135, 99–110. doi: 10.1016/j.plaphy.2018.11.037

Mitra, D., Rad, K. V., Chaudhary, P., Ruparelia, J., SmruthiSagarika, M., Boutaj, H., et al. (2021). Involvement of strigolactone hormone in root development, influence and interaction with mycorrhizal fungi in plant: mini-review. *Curr. Res. Microb. Sci.* 2:100026. doi: 10.1016/j.crmicr.2021.100026

Nakamura, H., Xue, Y. L., Miyakawa, T., Hou, F., Qin, H. M., Fukui, K., et al. (2013). Molecular mechanism of strigolactone perception by DWARF14. *Nat. Commun.* 4:2613. doi: 10.1038/ncomms3613

Nguyen, K. H., Van Ha, C., Nishiyama, R., Watanabe, Y., Leyva-González, M. A., Fujita, Y., et al. (2016). Arabidopsis type B cytokinin response regulators ARR1, ARR10, and ARR12 negatively regulate plant responses to drought. *Proc. Natl. Acad. Sci. U.S.A.* 113, 3090–3095. doi: 10.1073/pnas.1600399113

Nicolas, M., Rodriguez-Buey, M. L., Franco-Zorilla, J. M., and Cubas, P. (2015). A recently evolved alternative splice site in the BRANCHED1 a gene controls potato plant architecture. *Curr. Biol.* 25, 1799–1809. doi: 10.1016/j.cub.2015.05.053

Nishiyama, R., Watanabe, Y., Leyva-Gonzalez, M. A., Ha, C. V., Fujita, Y., Tanaka, M., et al. (2013). Arabidopsis AHP2, AHP3, and AHP5 histidine phosphotransfer proteins function as redundant negative regulators of drought stress response. *Proc. Natl. Acad. Sci. U.S.A.* 110, 4840–4845. doi: 10.1073/pnas.1302265110

Patil, S. B., Barbier, F. F., Zhao, J., Zafar, S. A., Uzair, M., Sun, Y., et al. (2021). Sucrose promotes D53 accumulation and tillering in rice. *New Phytol.* doi: 10.1111/nph.17834 [Epub ahead of print].

Qiao, Y., Lu, W., Wang, R., Nisa, Z. U., Yu, Y., Jin, X., et al. (2020). Identification and expression analysis of strigolactone biosynthetic and signaling genes in response to salt and alkaline stresses in soybean (Glycine max). *DNA Cell Biol.* 39, 1850–1861. doi: 10.1089/dna.2020.5637

Qiu, Y., Guan, S. C., Wen, C., Li, P., Gao, Z., and Chen, X. (2019). Auxin and cytokinin coordinate the dormancy and outgrowth of axillary bud in strawberry runner. *BMC Plant Biol.* 19:528. doi: 10.1186/s12870-019-2151-x

Rameau, C., Bertheloot, J., Leduc, N., Andrieu, B., Foucher, F., and Sakr, S. (2015). Multiple pathways regulate shoot branching. *Front. Plant Sci.* 5:741. doi: 10.3389/fpls.2014.00741

Rasmussen, A., Mason, M. G., De Cuyper, C., Brewer, P. B., Herold, S., Agusti, J., et al. (2012). Strigolactones suppress adventitious rooting in *Arabidopsis* and pea. *Plant Physiol.* 158, 1976–1987. doi: 10.1104/pp.111.187104

Ren, C. G., Kong, C. C., and Xie, Z. H. (2018). Role of abscisic acid in strigolactone-induced salt stress tolerance in arbuscular mycorrhizal Sesbania cannabina seedlings. *BMC Plant Biol.* 18:74. doi: 10.1186/s12870-018-1292-7

Ruiz-Lozano, J. M., Aroca, R., Zamarreño, ÁM., Molina, S., Andreo-Jiménez, B., Porcel, R., et al. (2016). Arbuscular mycorrhizal symbiosis induces strigolactone biosynthesis under drought and improves drought tolerance in lettuce and tomato. *Plant Cell Environ.* 39, 441–452. doi: 10.1111/pce.12631

Ruyter-Spira, C., Kohlen, W., Charnikhova, T., van Zeijl, A., van Bezouwen, L., de Ruijter, N., et al. (2011). Physiological effects of the synthetic strigolactone analog GR24 on root system architecture in *Arabidopsis*: another belowground role for strigolactones? *Plant Physiol.* 155, 721–734. doi: 10.1104/pp.110.166645

Saeed, W., Naseem, S., and Ali, Z. (2017). Strigolactones biosynthesis and their role in abiotic stress resilience in plants: a critical review. *Front. Plant Sci.* 8:1487. doi: 10.3389/fpls.2017.01487

Salam, B. B., Barbier, F., Danieli, R., Teper-Bamnolker, P., Ziv, C., Spíchal, L., et al. (2021). Sucrose promotes stem branching through cytokinin. *Plant Physiol.* 185, 1708–1721. doi: 10.1093/plphys/kiab003

Santoro, V., Schiavon, M., Gresta, F., Ertani, A., Cardinale, F., Sturrock, C. J., et al. (2020). Strigolactones control root system architecture and tip anatomy in *Solanum lycopersicum* L. plants under P starvation. *Plants* 9:612. doi: 10.3390/plants9050612

Santoro, V., Schiavon, M., Visentin, I., Constán-Aguilar, C., Cardinale, F., and Celi, L. (2021). Strigolactones affect phosphorus acquisition strategies in tomato plants. *Plant Cell Environ.* 44, 3628–3642. doi: 10.1111/pce.14169

Sengupta, D., and Reddy, A. R. (2018). Simplifying the root dynamics: from complex hormone–environment interactions to specific root architectural modulation. *Plant Growth Regul.* 85, 337–349. doi: 10.1007/s10725-018-0397-1

Seto, Y., Sado, A., Asami, K., Hanada, A., Umehara, M., Akiyama, K., et al. (2014). Carlactone is an endogenous biosynthetic precursor for strigolactones. *Proc. Natl. Acad. Sci. U.S.A.* 111, 1640–1645. doi: 10.1073/pnas.1314805111

Shen, J., Zhang, Y., Ge, D., Wang, Z., Song, W., Gu, R., et al. (2019). CsBRC1 inhibits axillary bud outgrowth by directly repressing the auxin efflux carrier CsPIN3 in cucumber. *Proc. Natl. Acad. Sci. U.S.A.* 116, 17105–17114. doi: 10.1073/pnas.1907968116

Shinohara, N., Taylor, C., and Leyser, O. (2013). Strigolactone can promote or inhibit shoot branching by triggering rapid depletion of the auxin efflux protein PIN1 from the plasma membrane. *PLoS Biol.* 11:e1001474. doi: 10.1371/journal.pbio.1001474

Shiratake, K., Notaguchi, M., Makino, H., Sawai, Y., and Borghi, L. (2019). Petunia PLEIOTROPIC DRUG RESISTANCE 1 is a strigolactone short-distance transporter with long-distance outcomes. *Plant Cell Physiol.* 60, 1722–1733. doi: 10.1093/pcp/pcz081

Song, X., Lu, Z., Yu, H., Shao, G., Xiong, J., and Meng, X. (2017). IPA1 functions as a downstream transcription factor repressed by D53 in strigolactone signaling in rice. *Cell Res.* 27, 1128–1141. doi: 10.1038/cr.2017.102

Soundappan, I., Bennett, T., Morffy, N., Liang, Y., Stanga, J. P., Abbas, A., et al. (2015). SMAX1-LIKE/D53 family members enable distinct MAX2-dependent responses to strigolactones and karrikins in *Arabidopsis*. *Plant Cell* 27, 3143–3159. doi: 10.1105/tpc.15.00562

Sun, H., Bi, Y., Tao, J., Huang, S., Hou, M., Xue, R., et al. (2016). Strigolactones are required for nitric oxide to induce root elongation in response to nitrogen and phosphate deficiencies in rice. *Plant Cell Environ.* 39, 1473–1484. doi: 10.1111/pce.12709

Sun, H., Tao, J., Hou, M., Huang, S., Chen, S., Liang, Z., et al. (2015). A strigolactone signal is required for adventitious root formation in rice. *Ann. Bot.* 115, 1155–1162. doi: 10.1093/aob/mcv052

Sun, H., Tao, J., Liu, S., Huang, S., Chen, S., Xie, X., et al. (2014). Strigolactones are involved in phosphate-and nitrate-deficiency-induced root development and auxin transport in rice. *J. Exp. Bot.* 65, 6735–6746. doi: 10.1093/jxb/eru029

Sun, H., Xu, F., Guo, X., Wu, D., Zhang, X., Lou, M., et al. (2019). A Strigolactone signal inhibits secondary lateral root development in rice. *Front. Plant Sci.* 10:1527. doi: 10.3389/fpls.2019.01527

Sun, J., Miller, J. B., Granqvist, E., Wiley-Kalil, A., Gobbato, E., Maillet, F., et al. (2015). Activation of symbiosis signaling by arbuscular mycorrhizal fungi in legumes and rice. *Plant Cell.* 27, 823–838. doi: 10.1105/tpc.114.131326

Tan, M., Li, G., Chen, X., Xing, L., Ma, J., Zhang, D., et al. (2019). Role of cytokinin, strigolactone, and auxin export on outgrowth of axillary buds in apple. *Front. Plant Sci.* 10:616. doi: 10.3389/fpls.2019.00616

Umehara, M., Cao, M., Akiyama, K., Akatsu, T., Seto, Y., Hanada, A., et al. (2015). Structural requirements of strigolactones for shoot branching inhibition in rice and *Arabidopsis*. *Plant Cell Physiol.* 56, 1059–1072. doi: 10.1093/pcp/pcv028

Visentin, I., Pagliarani, C., Deva, E., Caracci, A., Turečková, V., Novák, O., et al. (2020). A novel strigolactone-miR156 module controls stomatal behaviour during drought recovery. *Plant Cell Environ.* 43, 1613–1624. doi: 10.1111/pce.13758

Visentin, I., Vitali, M., Ferrero, M., Zhang, Y., Ruyter-Spira, C., Novák, O., et al. (2016). Low levels of strigolactones in roots as a component of the systemic signal of drought stress in tomato. *New Phytol.* 212, 954–963. doi: 10.1111/nph.14190

Waldie, T., McCulloch, H., and Leyser, O. (2014). Strigolactones and the control of plant development: lessons from shoot branching. *Plant J.* 79, 607–622. doi: 10.1111/tpj.12488

Wang, B., Smith, S. M., and Li, J. (2018). Genetic regulation of shoot architecture. *Annu. Rev. Plant Biol.* 69, 437–468. doi: 10.1146/annurev-arplant-042817-040422

Wang, H. W., Chen, W. X., Eggert, K., Charnikhova, T., Bouwmeester, H., Schweizer, P., et al. (2018). Abscisic acid influences tillering by modulation of strigolactones in barley. *J. Exp. Bot.* 69, 3883–3898. doi: 10.1093/jxb/ery200

Wang, L., Wang, B., Jiang, L., Liu, X., Li, X., Lu, Z., et al. (2015). Strigolactone signaling in *Arabidopsis* regulates shoot development by targeting D53-like SMXL repressor proteins for ubiquitination and degradation. *Plant Cell* 27, 3128–3142. doi: 10.1105/tpc.15.00605

Wang, L., Wang, B., Yu, H., Guo, H., Lin, T., Kou, L., et al. (2020). Transcriptional regulation of strigolactone signalling in *Arabidopsis*. *Nature* 583, 277–281. doi: 10.1038/s41586-020-2382-x

Wang, Y., and Bouwmeester, H. J. (2018). Structural diversity in the strigolactones. *J. Exp. Bot.* 69, 2219–2230. doi: 10.1093/jxb/ery091

Waters, M. T., Brewer, P. B., Bussell, J. D., Smith, S. M., and Beveridge, C. A. (2012). The Arabidopsis ortholog of rice DWARF27 acts upstream of MAX1 in the control of plant development by strigolactones. *Plant Physiol.* 159, 1073–1085. doi: 10.1104/pp.112.196253

Waters, M. T., Gutjahr, C., Bennett, T., and Nelson, D. (2017). Strigolactone signaling and evolution. *Annu. Rev. Plant Biol.* 68, 291–322. doi: 10.1146/annurev-arplant-042916-040925

Xi, L., Wen, C., Fang, S., Chen, X., Nie, J., Chu, J., et al. (2015). Impacts of strigolactone on shoot branching under phosphate starvation in chrysanthemum (Dendranthema grandiflorum cv. Jinba). *Front. Plant Sci.* 6:694. doi: 10.3389/fpls.2015.00694

Xie, Y., Liu, Y., Ma, M., Zhou, Q., Zhao, Y., Zhao, B., et al. (2020). Arabidopsis FHY3 and FAR1 integrate light and strigolactone signaling to regulate branching. *Nat. Commun.* 11:1955. doi: 10.1038/s41467-020-15893-7

Xin, T., Zhang, Z., Li, S., Zhang, S., Li, Q., Zhang, Z. H., et al. (2019). Genetic regulation of ethylene dosage for cucumber fruit elongation. *Plant Cell* 31, 1063–1076. doi: 10.1105/tpc.18.00957

Xu, J., Zha, M., Li, Y., Ding, Y., Chen, L., Ding, C., et al. (2015). The interaction between nitrogen availability and auxin, cytokinin, and strigolactone in the control of shoot branching in rice (*Oryza sativa* L.). *Plant Cell Rep.* 34, 1647–1662. doi: 10.1007/s00299-015-1815-8

Yamada, Y., Furusawa, S., Nagasaka, S., Shimomura, K., Yamaguchi, S., and Umehara, M. (2014). Strigolactone signaling regulates rice leaf senescence in response to a phosphate deficiency. *Planta* 240, 399–408. doi: 10.1007/s00425-014-2096-0

Yao, J., Scaffidi, A., Meng, Y., Melville, K. T., Komatsu, A., Khosla, A., et al. (2021). Desmethyl butenolides are optimal ligands for karrikin receptor proteins. *New Phytol.* 230, 1003–1016. doi: 10.1111/nph.17224

Yao, R., Ming, Z., Yan, L., Li, S., Wang, F., Ma, S., et al. (2016). DWARF14 is a non-canonical hormone receptor for strigolactone. *Nature* 536, 469–473. doi: 10.1038/nature19073

Yao, R., Wang, L., Li, Y., Chen, L., Li, S., Du, X., et al. (2018). Rice DWARF14 acts as an unconventional hormone receptor for strigolactone. *J. Exp. Bot.* 69, 2355–2365. doi: 10.1093/jxb/ery014

Yoneyama, K., Xie, X., Kim, H. I., Kisugi, T., Nomura, T., Sekimoto, H., et al. (2012). How do nitrogen and phosphorus deficiencies affect strigolactone production and exudation? *Planta* 235, 1197–1207. doi: 10.1007/s00425-011-1568-8

Yoneyama, K., Xie, X., Yoneyama, K., Kisugi, T., Nomura, T., Nakatani, Y., et al. (2018). Which are the major players, canonical or non-canonical strigolactones? *J. Exp. Bot.* 69, 2231–2239. doi: 10.1093/jxb/ery090

Zhang, J., Mazur, E., Balla, J., Gallei, M., Kalousek, P., Medveïová, Z., et al. (2020). Strigolactones inhibit auxin feedback on PIN-dependent auxin transport canalization. *Nat. Commun.* 11, 1–10. doi: 10.1038/s41467-020-17252-y

Zhang, X., Zhang, L., Sun, Y., Zheng, S., Wang, J., and Zhang, T. (2020). Hydrogen peroxide is involved in strigolactone induced low temperature stress tolerance in rape seedlings (*Brassica rapa* L.). *Plant Physiol. Biochem.* 157, 402–415. doi: 10.1016/j.plaphy.2020.11.006

Zhang, Y., Hartinger, C., Wang, X., and Friml, J. (2020). Directional auxin fluxes in plants by intramolecular domain-domain coevolution of PIN auxin transporters. *New Phytol.* 227, 1406–1416. doi: 10.1111/nph.16629

Zhang, Y., Lv, S., and Wang, G. (2018). Strigolactones are common regulators in induction of stomatal closure in planta. *Plant Signal. Behav.* 13:e1444322. doi: 10.1080/15592324.2018.1444322

Zhang, Y., Van Dijk, A. D., Scaffidi, A., Flematti, G. R., Hofmann, M., Charnikhova, T., et al. (2014). Rice cytochrome P450 MAX1 homologs catalyze distinct steps in strigolactone biosynthesis. *Nat. Chem. Biol.* 10, 1028–1033. doi: 10.1038/nchembio.1660

Zhao, B., Wu, T. T., Ma, S. S., Jiang, D. J., Bie, X. M., Sui, N., et al. (2019). TaD27-B gene controls the tiller number in hexaploid wheat. *Plant Biotechnol. J.* 18, 513–525. doi: 10.1111/pbi.13220

Zhao, L. H., Zhao, L. H., Zhou, X. E., Yi, W., Wu, Z., Liu, Y., et al. (2015). Destabilization of strigolactone receptor DWARF14 by binding of ligand and E3-ligase signaling effector DWARF3. *Cell Res.* 25, 1219–1236. doi: 10.1038/cr.2015.122

Zheng, X., Li, Y., Xi, X., Ma, C., Sun, Z., Yang, X., et al. (2021). Exogenous Strigolactones alleviate KCl stress by regulating photosynthesis, ROS migration and ion transport in Malus hupehensis Rehd. *Plant Physiol. Biochem.* 159, 113–122. doi: 10.1016/j.plaphy.2020.12.015

Zhu, S., Martínez Pacheco, J., Estevez, J. M., and Yu, F. (2020). Autocrine regulation of root hair size by the RALF-FERONIA-RSL4 signaling pathway. *New Phytol.* 227, 45–49. doi: 10.1111/nph.16497

Conflict of Interest: The authors declare that the research was conducted in the absence of any commercial or financial relationships that could be construed as a potential conflict of interest.

Publisher's Note: All claims expressed in this article are solely those of the authors and do not necessarily represent those of their affiliated organizations, or those of the publisher, the editors and the reviewers. Any product that may be evaluated in this article, or claim that may be made by its manufacturer, is not guaranteed or endorsed by the publisher.

frontiers in Plant Science

ORIGINAL RESEARCH
published: 29 March 2022
doi: 10.3389/fpls.2022.843362

A New Series of Strigolactone Analogs Derived From Cinnamic Acids as Germination Inducers for Root Parasitic Plants

*Taiki Suzuki, Michio Kuruma and Yoshiya Seto**

Laboratory of Plant Chemical Regulation, School of Agriculture, Meiji University, Kawasaki, Japan

Root parasitic plants such as *Striga* and *Orobanche* cause significant damage on crop production, particularly in sub-Saharan Africa. Their seeds germinate by sensing host root-derived signaling molecules called strigolactones (SLs). SL mimics can be used as suicidal germination inducers for root parasitic plants. Previous attempts to develop such chemicals have revealed that the methylbutenolide ring (D-ring), a common substructure in all the naturally occurring SLs, is critical for SL agonistic activity, suggesting that it should be possible to generate new SL mimics simply by coupling a D-ring with another molecule. Because structural information regarding SLs and their receptor interaction is still limited, such an approach might be an effective strategy to develop new potent SL agonists. Here, we report development of a series of new SL analogs derived from cinnamic acid (CA), the basis of a class of phenylpropanoid natural products that occur widely in plants. CA has an aromatic ring and a double-bond side-chain structure, which are advantageous for preparing structurally diverse derivatives. We prepared SL analogs from *cis* and *trans* configuration CA, and found that all the *cis*-CA-derived SL analogs had stronger activities as seed germination inducers for the root parasitic plants, *Orobanche minor* and *Striga hermonthica*, compared with the corresponding *trans*-CA-derived analogs. Moreover, introduction of a substitution at the C-4 position increased the germination-stimulating activity. We also found that the SL analogs derived from *cis*-CA were able to interact directly with SL receptor proteins more effectively than the analogs derived from *trans*-CA. The *cis* isomer of CA was previously reported to have a growth promoting effect on non-parasitic plants such as *Arabidopsis*. We found that SL analogs derived from *cis*-CA also showed growth promoting activity toward *Arabidopsis*, suggesting that these new SL agonists might be useful not only as suicidal germination inducers for root parasitic weeds, but also as plant growth promoters for the host plants.

Keywords: strigolactone, *cis*-cinnamic acid, root parasitic plant, germination, *Orobanche*, *Striga*

OPEN ACCESS

Edited by:
Ruifeng Yao,
Hunan University, China

Reviewed by:
Steven Maina Runo,
Kenyatta University, Kenya
Mikihisa Umehara,
Toyo University, Japan

****Correspondence:***
Yoshiya Seto
yoshiya@meiji.ac.jp

Specialty section:
This article was submitted to Plant Physiology, a section of the journal Frontiers in Plant Science

Received: *25 December 2021*
Accepted: *07 March 2022*
Published: *29 March 2022*

Citation:
Suzuki T, Kuruma M and Seto Y (2022) A New Series of Strigolactone Analogs Derived From Cinnamic Acids as Germination Inducers for Root Parasitic Plants. Front. Plant Sci. 13:843362. doi: 10.3389/fpls.2022.843362

INTRODUCTION

Root parasitic plants such as *Striga* and *Orobanche* parasitize the root of their host plants, which include some important crops such as rice, sorghum, and maize. After invasion into the host, parasitic plants connect their xylem tissue to the vascular tissue of the host plant, and obtain water and nutrients from the host plant *via* this xylem bridge. They produce numerous tiny seeds, which are spread onto the field. The seeds can stay dormant for decades, but once the host plant is planted nearby, they germinate by sensing strigolactone (SL) molecules that are released from the host root (Cook et al., 1966). If the germinated seeds cannot attach to the host, they die within 4–5 days. On the basis of this germination process, suicidal germination induction has been proposed as an effective way to eliminate parasitic plant seeds from infested fields. However, because quantitative production of the SL molecules has become a bottleneck, this method has not been put into practical use.

After the initial discovery of SLs as germination inducers for root parasitic plants, SLs were further shown to be the symbiotic signals for arbuscular mycorrhizal fungi (Akiyama et al., 2005). Moreover, SLs were identified as a new class of plant hormones that regulate shoot branching (Gomez-Roldan et al., 2008; Umehara et al., 2008). After the discovery of SLs as plant hormones, progress in this research field has included uncovering the SL signaling mechanism mediated by an α/β-hydrolase type receptor. In non-parasitic plants, DWARF14 (D14), a member of this protein family, was identified as the SL receptor (Arite et al., 2009; Hamiaux et al., 2012; de Saint Germain et al., 2016; Yao et al., 2016; Seto et al., 2019; Mashiguchi et al., 2021). In addition, a paralogous family of D14, which is called HYPOSENSITIVE TO LIGHT/KARRIKIN INSENSITIVE2 (hereafter denoted HTL), was characterized as a receptor for the smoke-derived germination inducer, karrikin (KAR; Waters et al., 2012). In a root parasitic plant, *Striga hermonthica*, 11 *HTL* genes were found, some of which were characterized as receptors for SL molecules, but KAR was not (Conn et al., 2015; Toh et al., 2015; Tsuchiya et al., 2015). Moreover, one of those HTLs, ShHTL7, was identified as an extremely sensitive receptor for SLs with pM sensitivity when expressed in *Arabidopsis* (Toh et al., 2015).

Many synthetic SL agonists have been reported, among which GR24 is now commonly used in basic research as a positive control (**Figure 1**). Such attempts have revealed that the methylbutenolide (D-ring) part, a common component in all the reported naturally occurring SLs, has a critical role for SL agonistic activity. Although the enol ether bridge connecting the ABC tricyclic ring, a typical part in the canonical SL molecules, and the D-ring has been proposed to be an essential structural feature for SL analogs, debranones, in which the D-ring is connected to a phenolic group *via* a simple ether bridge, have been also reported as SL agonists (**Figure 1**; Fukui et al., 2011). Moreover, yoshimulactone green (YLG), in which the ABC-ring part is replaced with fluorescein, was reported to be a pro-fluorescence SL agonist (**Figure 1**). YLG retains SL agonistic activity both for shoot branching inhibition and

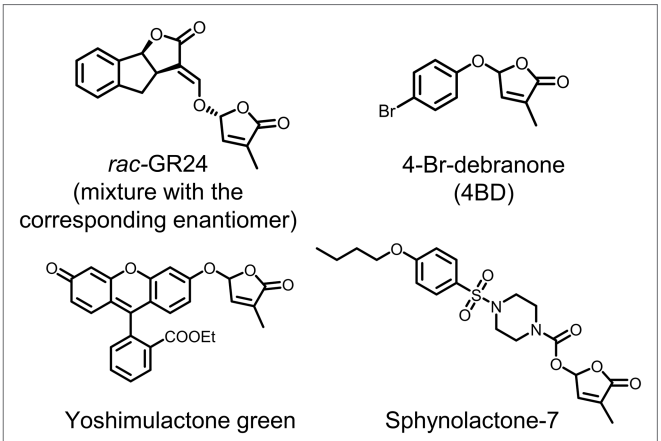

FIGURE 1 | Chemical structures of the synthetic strigolactone (SL) analogs.

for inducing germination in parasitic plants, and it can be hydrolytically cleaved by the D14 and the *Striga* HTL receptors (Tsuchiya et al., 2015). YLG hydrolysis emits fluorescence and it enables high-throughput detection of the receptor function. The discovery of the above-mentioned *Striga* receptors was accomplished using this unique analog (Tsuchiya et al., 2015). Moreover, the receptor identification, combined with YLG, enabled a rapid screening of chemicals that can directly interact with HTL7. By this approach, sphynolactone-7 (SPL7) was discovered as an extremely strong SL agonist that can induce *S. hermonthica* germination at fM concentrations (Uraguchi et al., 2018).

Because the detailed mechanism of receptor-ligand interactions in SL perception has not yet been uncovered, an effective strategy to obtain new potential agonist molecules would be to screen chemicals containing the D-ring structure. Using this approach, here we report development of a new type of SL analog, in which a cinnamic acid (CA) moiety is simply coupled with the D-ring through the carboxylic acid part *via* an ester bond. CA is widely distributed in plant species, and is a precursor of many important plant molecules such as lignin, flavonoids, isoflavonoids, and coumarins. CA exists as both *trans* and *cis* isomers, of which the former is more stable and common in nature. This structural feature enabled us to prepare two types of conformationally distinct analogs. In addition, many different analogs with substitutions on the benzene ring are commercially available. Thus, we were able to prepare a variety of structurally diverse analogs with a common core skeleton. A further feature of interest was that the *cis* isomer of CA was recently reported to act as an auxin efflux inhibitor, which leads to growth-promoting activity at low concentration (Steenackers et al., 2017, 2019). However, at a high concentration, *cis*-CA showed growth-inhibiting activity, and *cis*-CA was identified as an allelopathic compound that suppresses the growth of neighboring plants (Hiradate et al., 2005). Building on these observations, we chose CA as the starting material for synthesizing new SL analogs. These new synthetic analogs showed germination-inducing activity towards two root parasitic plants, *Orobanche minor* and *Striga hermonthica*, at moderately low concentration.

Moreover, the *cis*-CA-derived SL analog showed a growth promoting effect on *Arabidopsis*, possibly as a result of degradation to *cis*-CA in the growth medium and in planta. Thus, we expect that these new SL agonists might provide lead chemicals for developing a new type of suicidal germination inducers with an additional function as growth promoters in the host plant.

MATERIALS AND METHODS

Preparation of *cis*-Isomers of CA

cis-isomers of CA derivatives were individually prepared by isomerization from the corresponding *trans*-isomer. Each *trans*-CA (300–500 mg) was dissolved in MeOH or CH_3CN (50 ml). The solution was placed under UV lamp (254 nm). After the irradiation for 16 h, the solvent was evaporated *in vacuo*, and the mixture of *trans*/*cis* CA was suspended with 5–10 ml of distilled water. The sample was sonicated for 5 min and then centrifuged with 18,000 *g* for 30 min. The supernatant was filtered and diluted with distilled water up to 30 ml. The pH was adjusted to 1 using 1 N HCl and the sample was extracted with ethyl acetate (3 × 30 ml). The organic layer was dried over Na_2SO_4 and concentrated *in vacuo*, and the obtained each *cis*-CA was further subjected to the D-ring coupling reaction.

Chemical Synthesis of CASLs

5-Bromo-3-methyl-2(5H)-franone; 3-methyl-2(5H)-furanone (5 g, 51 mmol) was added to the solution of *N*-bromosuccinimide (9.05 g, 51 mmol) and azobis(isobutyronitrile) (170 mg, 1.02 mmol) in CCl_4 (51 ml). The mixture was refluxed at 90°C for 4 h. After the reaction, the mixture was cooled to room temperature and filtered. The filtrate was concentrated *in vacuo* and purified by silica gel column chromatography (*n*-hexane/EtOAc:8/2) to afford 5-bromo-3-methyl-2(5H)-franone (8.6 g, 95%). ^{1}H-NMR (300 MHz, $CDCl_3$) δ 7.24 (t, J = 1.8, 1 H), 6.85 (q, J = 1.5 Hz, 1 H), 2.07 (m, 3 H).

t-CASL (*t*-CASL1); K_2CO_3 (1.0 mmol) was added to the solution of *trans*-CA (0.50 mmol) in *N*-methyl-2-pyrrolidone (5 ml). 5-Bromo-3-methyl-2(5H)-franone (0.98 mmol) diluted in *N*-methyl-2-pyrrolidone (5 ml) was added to the mixture, and the mixture was stirred for 12 h at room temperature. The reaction was quenched by adding 1 N HCl, and the solution was diluted to 50 ml with water. The sample was extracted with EtOAc (3 × 50 ml). The organic layer was washed with distilled water (3 × 150 ml), dried over Na_2SO_4, and concentrated *in vacuo*. The crude sample was purified by silica gel column chromatography (*n*-hexane/EtOAc:8/2) to afford *t*-CASL (99.8 mg, 0.41 mmol, 82%). ^{1}H-NMR (300 MHz, $CDCl_3$) δ 7.79 (d, J = 16 Hz, 1 H), 7.56–7.52 (m, 2 H), 7.43–7.39 (m, 2 H), 7.03 (t, J = 1.5 Hz, 1 H), 6.99 (t, J = 1.5 Hz, 1 H), 6.43 (d, J = 16 Hz, 1 H), 2.02 (t, J = 1.5 Hz, 3 H); ^{13}C-NMR (75 MHz, $CDCl_3$), δ 10.54, 92.52, 115.82, 128.26, 128.91, 130.92, 133.64, 134.27, 142.19, 147.42, 164.76, 171.12; HRMS [ESI+ (*m*/*z*)] calculated for $(C_{14}H_{12}O_4 + H)^+$ 245.0808, found 245.0818.

c-CASL (*c*-CASL1); K_2CO_3 (1.34 mmol) was added to the solution of *cis*-CA (0.67 mmol) in *N*-methyl-2-pyrrolidone (6.7 ml). 5-Bromo-3-methyl-2(5H)-franone (1.31 mmol) diluted in *N*-methyl-2-pyrrolidone (6.7 ml) was added to the mixture, and the mixture was stirred for 12 h at room temperature. The reaction was quenched by adding 1 N HCl, and the solution was diluted to 50 ml with water, extracted with EtOAc (3 × 50 ml). The organic layer was washed with distilled water (3 × 150 ml) and dried over Na_2SO_4 and concentrated *in vacuo*. The crude sample was purified by silica gel column chromatography (*n*-hexane/EtOAc:8/2) to afford *c*-CASL (96.0 mg, 0.39 mmol, 59%). ^{1}H-NMR (300 MHz, $CDCl_3$) δ 7.64–7.61 (m, 2 H), 7.38–7.36 (m, 3 H), 7.12 (d, J = 13 Hz, 1 H), 6.92 (t, J = 1.2 Hz, 1 H), 6.86 (t, J = 1.8 Hz, 1 H), 5.94 (d, J = 13 Hz, 1 H), 1.97 (t, J = 1.2 Hz, 3 H); ^{13}C-NMR (75 MHz, $CDCl_3$), δ 10.55, 92.26, 117.11, 128.00, 128.92, 129.63, 129.96, 134.16, 142.18, 146.99, 163.68, 171.09; HRMS [ESI+ (*m*/*z*)] calculated for $(C_{14}H_{12}O_4 + H)^+$ 245.0808, found 245.0815.

PPASL; K_2CO_3 (1.0 mmol) was added to the solution of PPA (0.5 mmol) in *N*-methyl-2-pyrrolidone (5 ml). 5-Bromo-3-methyl-2(5H)-franone (0.98 mmol) diluted in *N*-methyl-2-pyrrolidone (5 ml) was added to the mixture, and the mixture was stirred for 12 h at room temperature. The reaction was quenched by adding 1 N HCl, and the solution was diluted to 50 ml with water, extracted with EtOAc (3 × 50 ml). The organic layer was washed with distilled water (3 × 150 ml) and dried over Na_2SO_4 and concentrated *in vacuo*. The crude sample was purified by silica gel column chromatography (*n*-hexane/EtOAc:7/3) to afford PPASL (113.0 mg, 0.46 mmol, 92%). ^{1}H-NMR (300 MHz, $CDCl_3$) δ 7.33–7.18 (m, 5 H), 6.87–6.83 (m, 2 H), 2.98 (t, J = 1.8 Hz, 2 H), 2.74–2.68 (m, 2 H), 1.98 (t, J = 1.5 Hz, 3 H); ^{13}C-NMR (75 MHz, $CDCl_3$), δ 10.50, 30.36, 35.41, 92.24, 126.38, 128.18, 128.48, 134.21, 139.67, 141.95, 170.96, 170.99; HRMS [ESI+ (*m*/*z*)] calculated for $(C_{14}H_{14}O_4 + H)^+$ 247.0965, found 247.0965.

trans-Me-CASL (*t*-CASL2); K_2CO_3 (1.0 mmol) was added to the solution of *trans*-Me-CA (0.5 mmol) in *N*-methyl-2-pyrrolidone (5 ml). 5-Bromo-3-methyl-2(5H)-franone (0.98 mmol) diluted in *N*-methyl-2-pyrrolidone (5 ml) was added to the mixture, and the mixture was stirred for 12 h at room temperature. The reaction was quenched by adding 1 N HCl, and the solution was diluted to 50 ml with water, extracted with EtOAc (3 × 50 ml). The organic layer was washed with distilled water (3 × 150 ml) and dried over Na_2SO_4 and concentrated *in vacuo*. The crude sample was purified by silica gel column chromatography (*n*-hexane/EtOAc:7/3) to afford *trans*-Me-CASL (50.8 mg, 0.20 mmol, 39%). ^{1}H-NMR (300 MHz, $CDCl_3$) δ 7.76 (d, J = 17 Hz, 1 H), 7.43 (d, J = 8.1 Hz, 2 H), 7.20 (d, J = 8.1 Hz, 2 H), 7.02 (t, J = 1.5 Hz, 1 H), 6.98 (t, J = 1.5 Hz, 1 H), 6.37 (d, J = 16 Hz, 1 H), 2.38 (s, 3 H), 2.01 (t, J = 1.5 Hz, 3 H); ^{13}C-NMR (75 MHz, $CDCl_3$), δ 10.51, 21.39, 92.47, 114.64, 128.12, 128.26, 128.31, 129.62, 130.94, 134.18, 141.50, 142.23, 147.42, 164.90, 171.11; HRMS [ESI+ (*m*/*z*)] calculated for $(C_{15}H_{14}O_4 + H)^+$ 259.0965, found 259.0978.

cis-Me-CASL (*c*-CASL2); K_2CO_3 (1.2 mmol) was added to the solution of *cis*-Me-CA (0.6 mmol) in *N*-methyl-2-pyrrolidone (6 ml). 5-Bromo-3-methyl-2(5H)-franone (1.18 mmol) diluted in *N*-methyl-2-pyrrolidone (6 ml) was added to the mixture, and the mixture was stirred for 12 h at room temperature. The reaction was quenched by adding 1 N HCl, and the solution

was diluted to 50 ml with water, extracted with EtOAc (3 × 50 ml). The organic layer was washed with distilled water (3 × 150 ml) and dried over Na_2SO_4 and concentrated *in vacuo*. The crude sample was purified by silica gel column chromatography (*n*-hexane/EtOAc:8/2) to afford *cis*-Me-CASL (70.4 mg, 0.27 mmol, 45%). ^{1}H-NMR (300 MHz, $CDCl_3$) δ 7.58 (d, J = 8.1 Hz, 2 H), 7.18 (d, J = 8.1 Hz, 7.08–7.04 (m, 1H), 6.93 (t, J = 1.5 Hz, 1 H), 6.89 (t, J = 1.5 Hz, 1 H), 5.87 (d, J = 12 Hz, 1 H), 2.37 (d, 3.9 Hz, 3 H), 1.97 (t, J = 1.5 Hz, 3 H); ^{13}C-NMR (75 MHz, $CDCl_3$), δ 10.52, 21.37, 92.25, 115.92, 128.76, 128.79, 130.29, 130.34, 131.20, 134.15, 140.20, 142.11, 147.28, 163.79, 171.12; HRMS [ESI+ (*m*/*z*)] calculated for $(C_{15}H_{14}O_4 + H)^+$ 259.0965, found 259.0976.

trans-OH-CASL (*t*-CASL3); K_2CO_3 (1.0 mmol) was added to the solution of *trans*-OH-CA (0.5 mmol) in *N*-methyl-2-pyrrolidone (5 ml). 5-Bromo-3-methyl-2(5H)-franone (0.98 mmol) diluted in *N*-methyl-2-pyrrolidone (5 ml) was added to the mixture, and the mixture was stirred for 12 h at room temperature. The reaction was quenched by adding 1 N HCl, and the solution was diluted to 50 ml with water, extracted with EtOAc (3 × 50 ml). The organic layer was washed with distilled water (3 × 150 ml) and dried over Na_2SO_4 and concentrated *in vacuo*. The crude sample was purified by a silica gel column chromatography (*n*-hexane/EtOAc:6/4) to afford *trans*-OH-CASL (41.8 mg, 0.16 mmol, 32%). ^{1}H-NMR (300 MHz, $CDCl_3$) δ 7.72 (d, J = 16 Hz, 1 H), 7.43 (d, J = 8.4 Hz, 2 H), 7.03–6.99 (m, 2 H), 6.87 (d, J = 8.7 Hz, 2 H), 6.26 (d, J = 16 Hz, 1 H), 6.16 (brs, 1 H), 2.02 (d, J = 1.2 Hz, 3 H); ^{13}C-NMR (75 MHz, $CDCl_3$), δ 10.49, 93.34, 113.41, 116.75, 126.50, 131.42, 134.28, 144.22, 147.97, 161.13, 165.72, 171.91; HRMS [ESI+ (*m*/*z*)] calculated for $(C_{14}H_{12}O_5 + H)^+$ 261.0757, found 261.0771.

cis-OH-CASL (*c*-CASL3); K_2CO_3 (0.89 mmol) was added to the solution of *cis*-OH-CA (0.44 mmol) in *N*-methyl-2-pyrrolidone (4.5 ml). 5-Bromo-3-methyl-2(5H)-franone (0.87 mmol) diluted in *N*-methyl-2-pyrrolidone (4.5 ml) was added to the mixture, and the mixture was stirred for 3.5 h at room temperature. The reaction was quenched by adding 1 N HCl, and the solution was diluted to 50 ml with water, extracted with EtOAc (3 × 50 ml). The organic layer was washed with distilled water (3 × 150 ml) and dried over Na_2SO_4 and concentrated *in vacuo*. The crude sample was purified by silica gel column chromatography (*n*-hexane/EtOAc:6/4) and reverse phase HPLC (ODS SP-100, CH_3CN/H_2O:4/6). The HPLC purification was conducted for a part of the sample to afford *c*-CASL3 (5.2 mg, 0.02 mmol, 5%). ^{1}H-NMR (300 MHz, acetone-D_6) δ 9.02 (s, 1 H), 7.82 (d, J = 9 Hz, 2 H), 7.23 (s, 1 H), 7.07 (d, J = 13 Hz, 1 H), 7.00 (s, 1 H), 6.87 (d, J = 8.4 Hz, 2 H), 5.81 (d, J = 13 Hz, 1 H), 1.94 (s, 3 H); ^{13}C-NMR (75 MHz, acetone-D_6), δ 10.48, 93.28, 114.10, 115.81, 126.85, 134.17, 134.28, 144.14, 147.76, 160.29, 164.92, 171.90; HRMS [ESI+ (*m*/*z*)] calculated for $(C_{14}H_{12}O_5 + H)^+$ 261.0757, found 261.0772.

trans-OMe-CASL (*t*-CASL4); K_2CO_3 (1.0 mmol) was added to the solution of *trans*-OMe-CA (0.5 mmol) in *N*-methyl-2-pyrrolidone (5 ml). 5-Bromo-3-methyl-2(5H)-franone (0.98 mmol) diluted in *N*-methyl-2-pyrrolidone (5 ml) was added to the mixture, and the mixture was stirred for 12 h at room temperature. The reaction was quenched by adding 1 N HCl, and the solution was diluted to 50 ml with water, extracted with EtOAc (3 × 50 ml). The organic layer was washed with distilled water (3 × 150 ml) and dried over Na_2SO_4 and concentrated *in vacuo*. The crude sample was purified by a silica gel column chromatography (*n*-hexane/EtOAc:7/3) to afford *trans*-OMe-CASL (83.9 mg, 0.31 mmol, 61%). ^{1}H-NMR (300 MHz, $CDCl_3$) δ 7.73 (d, J = 16 Hz, 1 H), 7.49 (d, J = 8.7 Hz, 2 H), 7.02 (t, J = 1.5 Hz, 1 H), 6.98 (d, J = 1.5 Hz, 1 H), 6.92 (d, J = 9.0 Hz, 2 H), 6.28 (m, 1 H), 3.84 (s, 3 H), 2.02 (d, J = 1.5 Hz, 3 H); ^{13}C-NMR (75 MHz, $CDCl_3$), δ 10.59, 55.36, 92.51, 113.15, 114.40, 126.46, 130.11, 134.24, 142.31, 147.18, 161.92, 165.11, 171.20; HRMS [ESI+ (*m*/*z*)] calculated for $(C_{15}H_{14}O_5 + H)^+$ 275.0914, found 275.0927.

cis-OMe-CASL (*c*-CASL4); K_2CO_3 (1.9 mmol) was added to the solution of *cis*-OMe-CA (0.94 mmol) in *N*-methyl-2-pyrrolidone (9.4 ml). 5-Bromo-3-methyl-2(5H)-franone (1.84 mmol) diluted in *N*-methyl-2-pyrrolidone (9.4 ml) was added to the mixture, and the mixture was stirred for 12 h at room temperature. The reaction was quenched by adding 1 N HCl, and the solution was diluted to 50 ml with water, extracted with EtOAc (3 × 50 ml). The organic layer was washed with distilled water (3 × 150 ml) and dried over Na_2SO_4 and concentrated *in vacuo*. The crude sample was purified by silica gel column chromatography (*n*-hexane/EtOAc:7/3) to afford *cis*-OMe-CASL (154.5 mg, 0.56 mmol, 60%). ^{1}H-NMR (300 MHz, $CDCl_3$) δ 7.76 (d, J = 8.7 Hz, 2 H), 7.00 (d, J = 13 Hz, 1 H), 6.95–6.86 (m, 4 H), 5.80 (d, J = 13 Hz, 1 H), 3.84 (d, J = 6.0 Hz, 3 H), 1.98 (t, J = 1.2 Hz, 3 H); ^{13}C-NMR (75 MHz, $CDCl_3$), δ 10.54, 55.25, 92.26, 113.44, 114.08, 126.63, 132.73, 134.15, 142.20, 147.21, 160.99, 163.97, 171.17; HRMS [ESI+ (*m*/*z*)] calculated for $(C_{15}H_{14}O_5 + H)^+$ 275.0914, found 275.0926.

trans-OEt-CASL (*t*-CASL5); K_2CO_3 (1.0 mmol) was added to the solution of *trans*-OEt-CA (0.5 mmol) in *N*-methyl-2-pyrrolidone (5 ml). 5-Bromo-3-methyl-2(5H)-franone (0.98 mmol) diluted in *N*-methyl-2-pyrrolidone (5 ml) was added to the mixture, and the mixture was stirred for 12 h at room temperature. The reaction was quenched by adding 1 N HCl, and the solution was diluted to 50 ml with water, extracted with EtOAc (3 × 50 ml). The organic layer was washed with distilled water (3 × 150 ml) and dried over Na_2SO_4 and concentrated *in vacuo*. The crude sample was purified by silica gel column chromatography (*n*-hexane/EtOAc:7/3) to afford *trans*-OEt-CASL (83.9 mg, 0.29 mmol, 58%). ^{1}H-NMR (300 MHz, $CDCl_3$) δ 7.73 (d, J = 16 Hz, 1 H), 7.47 (d, J = 8.7 Hz, 2 H), 7.02 (d, J = 1.5 Hz, 1 H), 6.98 (t, J = 1.5 Hz, 1 H), 6.90 (d, J = 8.7 Hz, 2 H), 6.27 (m, 1 H), 4.07 (q, J = 6.9 Hz, 2 H), 2.01 (t, J = 1.4 Hz, 3 H), 1.45–1.41 (m, 3 H); ^{13}C-NMR (75 MHz, $CDCl_3$), δ 10.60, 14.63, 63.63, 92.52, 112.98, 114.56, 126.28, 130.12, 134.24, 142.31, 147.28, 161.35, 165.15, 171.21; HRMS [ESI+ (*m*/*z*)] calculated for $(C_{16}H_{16}O_5 + H)^+$ 289.1071, found 289.1082.

cis-OEt-CASL (*c*-CASL5); K_2CO_3 (0.76 mmol) was added to the solution of *cis*-OEt-CA (0.38 mmol) in *N*-methyl-2-pyrrolidone (3.8 ml). 5-Bromo-3-methyl-2(5H)-franone (0.75 mmol) diluted in *N*-methyl-2-pyrrolidone (3.8 ml) was added to the mixture, and the mixture was stirred for 12 h

at room temperature. The reaction was quenched by adding 1 N HCl, and the solution was diluted to 50 ml with water, extracted with EtOAc (3 × 50 ml). The organic layer was washed with distilled water (3 × 150 ml) and dried over Na_2SO_4 and concentrated *in vacuo*. The crude sample was purified by a silica gel column chromatography (*n*-hexane/EtOAc:7/3) to afford *cis*-OEt-CASL (74.5 mg, 0.26 mmol, 68%). ^{1}H-NMR (300 MHz, $CDCl_3$) δ 7.77–7.74 (m, 2 H), 7.08–6.87 (m, 5 H), 5.78 (d, J = 13 Hz, 1 H), 4.07 (q, J = 6.9 Hz, 2 H), 1.99 (t, J = 1.4 Hz, 3 H), 1.45–1.41 (m, 3 H); ^{13}C-NMR (75 MHz, $CDCl_3$), δ 10.59, 14.67, 63.51, 92.29, 113.91, 113.97, 126.50, 132.83, 134.22, 142.21, 147.34, 160.47, 164.04, 171.20; HRMS [ESI+ (*m*/*z*)] calculated for $(C_{16}H_{16}O_5 + H)^+$ 289.1071, found 289.1083.

trans-NO_2-CASL (*t*-CASL6); K_2CO_3 (1.0 mmol) was added to the solution of *trans*-NO_2-CA (0.5 mmol) in *N*-methyl-2-pyrrolidone (5 ml). 5-Bromo-3-methyl-2(5H)-franone (0.98 mmol) diluted in *N*-methyl-2-pyrrolidone (5 ml) was added to the mixture, and the mixture was stirred for 12 h at room temperature. The reaction was quenched by adding 1 N HCl, and the solution was diluted to 50 ml with water, extracted with EtOAc (3 × 50 ml). The organic layer was washed with distilled water (3 × 150 ml) and dried over Na_2SO_4 and concentrated *in vacuo*. The crude sample was purified by silica gel column chromatography (*n*-hexane/EtOAc:7/3) to afford *trans*-NO_2-CASL (72.6 mg, 0.25 mmol, 50%). ^{1}H-NMR (300 MHz, $CDCl_3$) δ 8.27 (d, J = 8.7 Hz, 2 H), 7.81 (d, J = 16 Hz, 1 H), 7.70 (d, J = 8.7 Hz, 2 H), 7.03 (t, J = 1.5 Hz, 1 H), 6.99 (t, J = 1.5 Hz, 1 H), 6.55 (d, J = 16 Hz, 1 H), 2.03 (t, J = 1.2 Hz, 3 H); ^{13}C-NMR (75 MHz, $CDCl_3$), δ 10.73, 92.79, 120.32, 124.30, 128.97, 134.75, 139.74, 141.82, 144.39, 148.89, 164.04, 170.97; HRMS [ESI+ (*m*/*z*)] calculated for $(C_{14}H_{11}NO_6 + H)^+$ 290.0659, found 290.0671.

cis-NO_2-CASL (*c*-CASL6); K_2CO_3 (0.58 mmol) was added to the solution of *cis*-NO_2-CA (0.29 mmol) in *N*-methyl-2-pyrrolidone (2.9 ml). 5-Bromo-3-methyl-2(5H)-franone (0.57 mmol) diluted in *N*-methyl-2-pyrrolidone (2.9 ml) was added to the mixture, and the mixture was stirred for 12 h at room temperature. The reaction was quenched by adding 1 N HCl, and the solution was diluted to 50 ml with water, extracted with EtOAc (3 × 50 ml). The organic layer was washed with distilled water (3 × 150 ml) and dried over Na_2SO_4 and concentrated *in vacuo*. The crude sample was purified by silica gel column chromatography (*n*-hexane/EtOAc:6/4) to afford *cis*-NO_2-CASL (20.7 mg, 0.07 mol, 25%). ^{1}H-NMR (300 MHz, $CDCl_3$) δ 8.23 (d, J = 8.7 Hz, 2 H), 7.71 (d, J = 8.7 Hz, 2 H), 7.18 (d, J = 12 Hz, 1 H), 6.89–6.88 (m, 2 H), 6.13 (d, J = 12 Hz, 1 H), 1.98 (s, 3 H); ^{13}C-NMR (75 MHz, $CDCl_3$), δ 10.66, 92.42, 120.84, 123.29, 130.45, 134.70, 140.52, 141.63, 144.39, 147.93, 163.09, 170.89; HRMS [ESI+ (*m*/*z*)] calculated for $(C_{14}H_{11}NO_6 + H)^+$ 290.0659, found 290.0671.

trans-F-CASL (*t*-CASL7); K_2CO_3 (1.1 mmol) was added to the solution of *trans*-F-CA (0.57 mmol) in *N*-methyl-2-pyrrolidone (5.7 ml). 5-Bromo-3-methyl-2(5H)-franone (1.12 mmol) diluted in *N*-methyl-2-pyrrolidone (5.7 ml) was added to the mixture, and the mixture was stirred for 12 h at room temperature. The reaction was quenched by adding 1 N HCl, and the solution was diluted to 50 ml with water, extracted with EtOAc (3 × 50 ml). The organic layer was washed with distilled water (3 × 150 ml) and dried over Na_2SO_4 and concentrated *in vacuo*. The crude sample was purified by silica gel column chromatography (*n*-hexane/EtOAc:7/3) to afford *trans*-F-CASL (39.0 mg, 0.15 mol, 26%). ^{1}H-NMR (300 MHz, $CDCl_3$) δ 7.75 (d, J = 16 Hz, 1 H), 7.56–7.51 (m, 2 H), 7.13–7.07 (m, 2 H), 7.02–6.98 (m, 2 H), 6.35 (d, J = 16 Hz, 1 H), 2.02 (t, J = 1.5 Hz, 3 H); ^{13}C-NMR (75 MHz, $CDCl_3$), δ 10.59, 92.58, 115.65 (d, $J_{C\text{-}F}$ = 2.5 Hz), 116.15 (d, $J_{C\text{-}F}$ = 22 Hz), 129.99, 130.29 (d, $J_{C\text{-}F}$ = 8.6 Hz), 134.39, 142.12, 146.11, 164.23 (d, $J_{C\text{-}F}$ = 251 Hz), 164.69, 171.09; HRMS [ESI+ (*m*/*z*)] calculated for $(C_{14}H_{11}FO_4 + H)^+$ 263.0714, found 263.0744.

cis-F-CASL (*c*-CASL7); K_2CO_3 (1.26 mmol) was added to the solution of *cis*-F-CA (0.63 mmol) in *N*-methyl-2-pyrrolidone (6.3 ml). 5-Bromo-3-methyl-2(5H)-franone (1.23 mmol) diluted in *N*-methyl-2-pyrrolidone (6.3 ml) was added to the mixture, and the mixture was stirred for 12 h at room temperature. The reaction was quenched by adding 1 N HCl, and the solution was diluted to 50 ml with water, extracted with EtOAc (3 × 50 ml). The organic layer was washed with distilled water (3 × 150 ml) and dried over Na_2SO_4 and concentrated *in vacuo*. The crude sample was purified by silica gel column chromatography (*n*-hexane/EtOAc:7/3) to afford *cis*-F-CASL (94.2 mg, 0.36 mmol, 57%). ^{1}H-NMR (300 MHz, $CDCl_3$) δ 7.72–7.67 (m, 2 H), 7.10–7.03 (m, 3 H), 6.92 (t, J = 1.5 Hz, 1 H), 6.89 (t, J = 1.5 Hz, 1H), 5.91 (d, J = 13 Hz, 1 H), 1.98 (t, J = 1.8 Hz, 3 H); ^{13}C-NMR (75 MHz, $CDCl_3$), δ 10.56, 92.27, 115.14 (d, $J_{C\text{-}F}$ = 22 Hz), 116.73 (d, $J_{C\text{-}F}$ = 2.2 Hz), 130.11, 132.45 (d, $J_{C\text{-}F}$ = 8.7 Hz), 134.34, 141.97, 146.07, 163.34 (d, $J_{C\text{-}F}$ = 249 Hz), 163.65, 171.06; HRMS [ESI+ (*m*/*z*)] calculated for $(C_{14}H_{11}FO_4 + H)^+$ 263.0714, found 263.0734.

trans-Cl-CASL (*t*-CASL8); K_2CO_3 (1.0 mmol) was added to the solution of *trans*-Cl-CA (0.5 mmol) in *N*-methyl-2-pyrrolidone (5 ml). 5-Bromo-3-methyl-2(5H)-franone (0.98 mmol) diluted in *N*-methyl-2-pyrrolidone (5 ml) was added to the mixture, and the mixture was stirred for 12 h at room temperature. The reaction was quenched by adding 1 N HCl, and the solution was diluted to 50 ml with water, extracted with EtOAc (3 × 50 ml). The organic layer was washed with distilled water (3 × 150 ml) and dried over Na_2SO_4 and concentrated *in vacuo*. The crude sample was purified by silica gel column chromatography (*n*-hexane/EtOAc:7/3) to afford *trans*-Cl-CASL (128 mg, 0.46 mmol, 92%). ^{1}H-NMR (300 MHz, $CDCl_3$) δ 7.73 (d, J = 16 Hz, 1 H), 7.48–7.27 (m, 4 H), 7.02 (t, J = 1.5 Hz, 1 H), 6.99 (t, J = 1.5 Hz, 1 H), 6.40 (d, J = 16 Hz, 1H), 2.02 (t, J = 1.5 Hz, 3 H); ^{13}C-NMR (75 MHz, $CDCl_3$), δ 10.55, 92.55, 116.21, 129.42, 132.15, 134.34, 136.85, 142.08, 145.89, 164.53, 171.06; HRMS [ESI+ (*m*/*z*)] calculated for $(C_{14}H_{11}ClO_4 + H)^+$ 279.0419, found 279.0433.

cis-Cl-CASL (*c*-CASL8); K_2CO_3 (1.0 mmol) was added to the solution of *trans*-Cl-CA (0.52 mmol) in *N*-methyl-2-pyrrolidone (5 ml). 5-Bromo-3-methyl-2(5H)-franone (0.98 mmol) diluted in *N*-methyl-2-pyrrolidone (5 ml) was added to the mixture, and the mixture was stirred for 12 h at room temperature. The reaction was quenched by adding 1 N HCl, and the solution was diluted to 50 ml with water, extracted with EtOAc (3 × 50 ml). The organic layer was washed with distilled water (3 × 150 ml) and dried over Na_2SO_4 and concentrated *in vacuo*. The crude sample was purified by silica

gel column chromatography (*n*-hexane/EtOAc:7/3) to afford *cis*-Cl-CASL (80.6 mg, 0.29 mmol, 56%). ^{1}H-NMR (300 MHz, $CDCl_3$) δ 7.60 (d, J = 8.4 Hz, 2 H), 7.37–7.33 (m, 2 H), 7.05 (d, J = 13 Hz, 1 H), 6.92–6.88 (m, 2 H), 5.95 (d, J = 13 Hz, 1 H), 1.98 (t, J = 1.5 Hz, 3 H); ^{13}C-NMR (75 MHz, $CDCl_3$), δ 10.55, 92.27, 117.64, 128.27, 131.45, 132.42, 134.34, 135.66, 141.91, 145.82, 163.52, 171.04; HRMS [ESI+ (*m*/*z*)] calculated for $(C_{14}H_{11}ClO_4 + H)^+$ 279.0419, found 279.0440.

trans-Br-CASL (*t*-CASL9); K_2CO_3 (1.0 mmol) was added to the solution of *trans*-Br-CA (0.5 mmol) in *N*-methyl-2-pyrrolidone (5 ml). 5-Bromo-3-methyl-2(5H)-franone (0.98 mmol) diluted in *N*-methyl-2-pyrrolidone (5 ml) was added to the mixture, and the mixture was stirred for 12 h at room temperature. The reaction was quenched by adding 1 N HCl, and the solution was diluted to 50 ml with water, extracted with EtOAc (3 × 50 ml). The organic layer was washed with distilled water (3 × 150 ml) and dried over Na_2SO_4 and concentrated *in vacuo*. The crude sample was purified by silica gel column chromatography (*n*-hexane/EtOAc:7/3) to afford *trans*-Br-CASL (157 mg, 0.49 mmol, 98%). ^{1}H-NMR (300 MHz, $CDCl_3$) δ 7.71 (d, J = 16 Hz, 1 H), 7.54 (d, J = 8.4 Hz, 2 H), 7.39 (d, J = 8.4 Hz, 2 H), 7.01 (t, J = 1.5 Hz, 1 H), 6.98 (t, J = 1.5 Hz, 1H), 6.41 (d, J = 16 Hz, 1 H), 2.02 (t, J = 1.5 Hz, 3 H); ^{13}C-NMR (75 MHz, $CDCl_3$), δ 10.59, 92.60, 116.59, 125.32, 129.63, 132.22, 132.61, 134.41, 142.05, 146.00, 164.55, 171.04; HRMS [ESI+ (*m*/*z*)] calculated for $(C_{14}H_{11}BrO_4 + H)^+$ 322.9913, found 322.9930.

cis-Br-CASL (*c*-CASL9); K_2CO_3 (0.56 mmol) was added to the solution of *cis*-Br-CA (0.28 mmol) in *N*-methyl-2-pyrrolidone (2.8 ml). 5-Bromo-3-methyl-2(5H)-franone (0.27 mmol) diluted in *N*-methyl-2-pyrrolidone (2.8 ml) was added to the mixture, and the mixture was stirred for 12 h at room temperature. The reaction was quenched by adding 1 N HCl, and the solution was diluted to 50 ml with water, extracted with EtOAc (3 × 50 ml). The organic layer was washed with distilled water (3 × 150 ml) and dried over Na_2SO_4 and concentrated *in vacuo*. The crude sample was purified by silica gel column chromatography (*n*-hexane/EtOAc:7/3) to afford *cis*-Br-CASL (34.8 mg, 0.11 mmol, 39%). ^{1}H-NMR (300 MHz, $CDCl_3$) δ 7.56–7.48 (m, 4 H), 7.03 (d, J = 13 Hz, 1 H), 6.91 (t, J = 1.5 Hz, 1H), 6.88 (t, J = 1.5 Hz, 1 H), 5.96 (d, J = 13 Hz, 1 H), 1.98 (m, 3 H); ^{13}C-NMR (75 MHz, $CDCl_3$), δ 10.60, 92.31, 117.86, 124.10, 131.30, 131.61, 132.93, 134.22, 141.87, 145.87, 163.53, 171.01; HRMS [ESI+ (*m*/*z*)] calculated for $(C_{14}H_{11}BrO_4 + H)^+$ 322.9913, found 322.9935.

trans-CF_3-CASL (*t*-CASL10); K_2CO_3 (1.1 mmol) was added to the solution of *trans*-CF_3-CA (0.56 mmol) in *N*-methyl-2-pyrrolidone (5.6 ml). 5-Bromo-3-methyl-2(5H)-franone (1.10 mmol) diluted in *N*-methyl-2-pyrrolidone (5.6 ml) was added to the mixture, and the mixture was stirred for 12 h at room temperature. The reaction was quenched by adding 1 N HCl, and the solution was diluted to 50 ml with water, extracted with EtOAc (3 × 50 ml). The organic layer was washed with distilled water (3 × 150 ml) and dried over Na_2SO_4 and concentrated *in vacuo*. The crude sample was purified by silica gel column chromatography (*n*-hexane/EtOAc:7/3) to afford *trans*-CF_3-CASL (164 mg, 0.53 mmol, 94%). ^{1}H-NMR (300 MHz, $CDCl_3$) δ 7.80 (d, J = 16 Hz, 1 H), 7.69–7.62 (m, 4 H), 7.03 (t, J = 1.5 Hz, 1 H), 6.99 (t, J = 1.5 Hz, 1 H), 6.50 (d, J = 16 Hz, 1 H), 2.03 (t, J = 1.5 Hz, 3 H); ^{13}C-NMR (75 MHz, $CDCl_3$), δ 10.57, 92.65, 118.56, 123.63 (q, $J_{C\text{-}F}$ = 271 Hz), 125.90 (q, $J_{C\text{-}F}$ = 3.8 Hz), 128.41, 132.26 (q, $J_{C\text{-}F}$ = 33 Hz), 134.50, 137.05 (d, $J_{C\text{-}F}$ = 1.2 Hz), 141.96, 145.42, 164.28, 170.10; HRMS [ESI+ (*m*/*z*)] calculated for $(C_{15}H_{12}F_3O_4 + H)^+$ 313.0682, found 313.0698.

cis-CF_3-CASL (*c*-CASL10); K_2CO_3 (1.1 mmol) was added to the solution of *cis*-CF_3-CA (0.54 mmol) in *N*-methyl-2-pyrrolidone (5.4 ml). 5-Bromo-3-methyl-2(5H)-franone (1.06 mmol) diluted in *N*-methyl-2-pyrrolidone 5.4 ml) was added to the mixture, and the mixture was stirred for 12 h at room temperature. The reaction was quenched by adding 1 N HCl, and the solution was diluted to 50 ml with water, extracted with EtOAc (3 × 50 ml). The organic layer was washed with distilled water (3 × 150 ml) and dried over Na_2SO_4 and concentrated *in vacuo*. The crude sample was purified by silica gel column chromatography (*n*-hexane/EtOAc:7/3) to afford *cis*-CF_3-CASL (45.7 mg, 0.15 mmol, 27%). ^{1}H-NMR (300 MHz, $CDCl_3$) δ 7.68–7.26 (m, 4 H), 8.16 (d, J = 12 Hz, 1 H), 6.89 (t, J = 1.4 Hz, 1 H), 6.85 (t, J = 1.4 Hz, 1 H), 6.06 (d, J = 13 Hz, 1 H), 1.97 (t, J = 1.4 Hz, 3 H); ^{13}C-NMR (75 MHz, $CDCl_3$), δ 10.51, 92.28, 119.62, 123.83 (q, $J_{C\text{-}F}$ = 271 Hz) 124.95 (q, $J_{C\text{-}F}$ = 3.7 Hz), 129.84, 130.99 (q, $J_{C\text{-}F}$ = 32 Hz), 134.45, 137.69 (d, $J_{C\text{-}F}$ = 1.2 Hz), 141.73, 145.27, 163.29, 170.94; HRMS [ESI+ (*m*/*z*)] calculated for $(C_{15}H_{12}F_3O_4 + H)^+$ 313.0682, found 313.0697.

cis and *trans* isomer mixture of the ethyl ester of indanone derived-CA analogs; Ethyl 2-(diethoxyphosphoryl) acetate (12.1 mmol) was added to a solution of NaH (60% oil, 15.2 mmol) in dry THF (12 ml) at −78°C under Ar. The mixture was stirred for 15 min, and then 1-indanone (10.1 mmol) in THF (6 ml) was added. After the stirring for 30 min, the mixture was placed on ice for 2 h and then stirred for 20 h at room temperature. The reaction was quenched with saturated aqueous NH_4Cl and diluted with distilled water up to 100 ml. The mixture was extracted with ethyl acetate (3 × 100 ml) and the organic layer was washed with distilled water (2 × 300 ml). The organic layer was dried with Na_2SO_4, filtered, and concentrated *in vacuo*. The crude product was purified by silica gel column chromatography (*n*-hexane/EtOAc:9.5/0.5) to afford the ethyl ester of *trans*-indanone-CA (154.8 mg, 0.78 mmol, 8%) and *cis*-indanone-CA (58.4 mg, 0.29 mmol, 3%). ethyl ester of *trans*-indanone-CA: ^{1}H-NMR (300 MHz, $CDCl_3$) δ 7.60 (d, J = 7.5 Hz, 1 H), 7.35 (d, J = 3.9 Hz, 2 H), (d, J = 7.8, 1 H), 7.23–7.28 (m, 1 H), 6.31 (t, J = 2.6 Hz, 1H), 4.23 (q, J = 7.2, 2 H), 3.28–3.33 (m, 2 H), 3.08 (t, J = 7.7 Hz, 1 H), 1.33 (t, J = 7.1 Hz, 3 H); ethyl ester of *cis*-indanone-CA: ^{1}H-NMR (300 MHz, $CDCl_3$) δ 8.82 (d, J = 7.8 Hz, 1 H), 7.25–7.37 (m, 3 H), 5.97 (d, J = 2.0 Hz, 1 H), 4.22 (q, J = 7.2 Hz, 2 H), 2.97–3.01 (m, 2H), 2.89–2.94 (m, 2 H), 1.32 (t, J = 7.1 Hz, 2 H).

trans-indanone-CA; Ethanol (1.91 ml) and 5 M NaOHaq (1.93 ml) was added to the round flask containing *trans*-indanone-CA ethyl ester (0.77 mmol). The mixture was stirred for 15 h at room temperature. Distilled water was added to the solution up to 30 ml and extracted with ethyl acetate (3 × 30 ml). The pH of the water layer was adjusted to 1 using 6 N-HCl and, then extracted with ethyl acetate (3 × 30 ml). The organic layer was dried with Na_2SO_4, filtered, and concentrated

in vacuo. The hydrolysis product was checked by TLC and used for the next coupling reaction without purification.

trans-indanone-CASL (*t*-indCASL); K_2CO_3 (0.91 mmol) was added to the crude *trans*-indanone-CA (0.45 mmol) in *N*-methyl-2-pyrrolidone (4.6 ml). 5-Bromo-3-methyl-2(5H)-franone (0.89 mmol) diluted in *N*-methyl-2-pyrrolidone (4.6 ml) was added to the mixture, and the mixture was stirred for 12 h at room temperature. The reaction was quenched by adding 1 N-HCl, and the solution was diluted to 50 ml with water, extracted with EtOAc (3 × 50 ml). The organic layer was washed with distilled water (3 × 150 ml) and dried over Na_2SO_4 and concentrated *in vacuo*. The crude sample was purified by a silica gel column chromatography (*n*-hexane/EtOAc:8/2) and PTLC (*n*-hexane/EtOAc:7/3) to afford *trans*-indanone-CASL (21.4 mg, 0.08 mmol, 18%). ^{1}H-NMR (300 MHz, $CDCl_3$) δ 7.60 (d, J = 7.8 Hz, 1 H), 7.38–7.43 (m, 2 H), 7.25–7.30 (m, 1 H), 7.01 (quin, J = 1.5 Hz, 1 H), 6.97 (quin, J = 1.5 Hz, 2 H), 6.29 (t, J = 2.4 Hz, 1 H), 3.30–3.35 (m, 2 H), 3.11 (t, J = 5.9 Hz, 2 H), 2.01 (t, J = 1.5 Hz, 3 H); ^{13}C-NMR (75 MHz, $CDCl_3$), δ 10.65, 30.57, 31.65, 92.24, 105.16, 121.90, 125.77, 126.93, 131.68, 134.18, 139.39, 142.49, 150.28, 165.12, 167.34, 171.36; HRMS [ESI+ (*m*/*z*)] calculated for $(C_{16}H_{14}O_4 + H)^+$ 271.0965, found 271.0978.

cis-indanone-CA; Ethanol (0.73 ml) and 5 M NaOHaq (0.73 ml) was added to the round flask containing *cis*-indanone-CA-Et (0.29 mmol). The mixture was stirred for 15 h at room temperature. Distilled water was added to the solution up to 30 ml and extracted with ethyl acetate (3 × 30 ml). The pH of the water layer was adjusted to 1 using 6 N-HCl and, then extracted with ethyl acetate (3 × 30 ml). The organic layer was dried with Na_2SO_4, filtered, and concentrated *in vacuo*. The hydrolysis product was checked by TLC and used for the next coupling reaction without purification.

cis-indanone-CASL (*c*-indCASL); K_2CO_3 (0.22 mmol) was added to the crude *cis*-indanone-CA (0.11 mmol) in *N*-methyl-2-pyrrolidone (1.1 ml). 5-Bromo-3-methyl-2(5H)-franone (0.22 mmol) diluted in *N*-methyl-2-pyrrolidone (1.1 ml) was added to the mixture, and the mixture was stirred for 12 h at room temperature. The reaction was quenched by adding 1 N-HCl, and the solution was diluted to 30 ml with water, extracted with EtOAc (3 × 30 ml). The organic layer was washed with distilled water (3 × 90 ml) and dried over Na_2SO_4 and concentrated *in vacuo*. The crude sample was purified by silica gel column chromatography (*n*-hexane/EtOAc:8/2) to afford *cis*-indanone-CASL (17.7 mg, 0.07 mmol, 60%). ^{1}H-NMR (300 MHz, $CDCl_3$) δ 8.86 (d, J = 7.8 Hz, 1 H), 7.29–7.43 (m, 3 H), 6.98–6.99 (m, 1 H), 6.95 (quin, J = 1.7 Hz, 1 H), 5.94 (t, J = 1.8 Hz, 1 H), 6.29 (t, J = 2.4 Hz, 1 H), 2.93–3.0 (m, 4 H), 3.11 (t, J = 5.9 Hz, 2 H), 2.00 (t, J = 1.5 Hz, 3 H); ^{13}C-NMR (75 MHz, $CDCl_3$), δ 10.68, 29.57, 36.03, 92.35, 108.14, 125.17, 126.79, 129.05, 131.65, 134.20, 137.15, 142.49, 151.78, 163.75, 165.45, 171.39; HRMS [ESI+ (*m*/*z*)] calculated for $(C_{16}H_{14}O_4 + H)^+$ 271.0965, found 271.097.

cis and *trans* isomer mixture of the ethyl ester of tetralone derived-CA analogs; Ethyl 2-(diethoxyphosphoryl) acetate (12.08 mmol) was added to a solution of NaH (60% oil, 15.15 mmol) in dry THF (12 ml) at −78°C under Ar. The mixture was stirred for 15 min, and then 1-tetralone (10 mmol) in THF (6 ml) was added. After the stirring for 30 min, the mixture was placed on ice for 16 h and then stirred for 2 h at room temperature. The reaction was quenched with saturated aqueous NH_4Cl and diluted with distilled water up to 50 ml. The mixture was extracted with dichloromethane (3 × 50 ml). The Organic layer was dried with Na_2SO_4, filtered, and concentrated *in vacuo*. The crude product was purified by silica gel column chromatography (*n*-hexane/EtOAc:9/1) to afford the mixture of *trans*-tetralone-CA-Et and *cis*-tetralone-CA-Et. The mixture was used for the next hydrolysis reaction without purification.

cis and *trans* isomer mixture of tetralone derived-CA analogs; Ethanol (0.74 ml) and 5 M NaOHaq (0.75 ml) was added to the round flask containing the mixture of *trans*-tetralone-CA-Et and *cis*-tetralone-CA-Et (0.30 mmol). The mixture was stirred for 17 h at room temperature. Distilled water was added to the solution up to 30 ml and extracted with ethyl acetate (3 × 30 ml). Water phase pH was adjusted to 1 using 6 N-HCl and then extracted with ethyl acetate (3 × 30 ml). The organic layer was dried with Na_2SO_4, filtered, and concentrated *in vacuo*. These hydrolysis products were checked by TLC and used for the next coupling reaction without purification.

trans-tetralone-CASL (*t*-tetCASL) and *cis*-tetralone-CASL (*c*-tetCASL); K_2CO_3 (0.39 mmol) was added to the mixture of *trans*-tetralone-CA and *cis*-tetralone-CA (0.19 mmol) in *N*-methyl-2-pyrrolidone (1.9 ml). 5-Bromo-3-methyl-2(5H)-franone (0.38 mmol) diluted in *N*-methyl-2-pyrrolidone (1.9 ml) was added to the mixture, and the mixture was stirred for 12 h at room temperature. The reaction was quenched by adding 1 N-HCl, and the solution was diluted to 30 ml with water, extracted with EtOAc (3 × 30 ml). The organic layer was washed with distilled water (3 × 90 ml) and dried over Na_2SO_4 and concentrated *in vacuo*. The crude sample was purified by silica gel column chromatography (*n*-hexane/EtOAc:8/2) to afford *trans*-tetralone-CASL (21.4 mg, 0.08 mmol, 40%) and *cis*-tetralone-CASL. *cis*-tetralone-CASL was purified again by reverse phase HPLC (ODS-SP100, CH_3CN/H_2O:7/3; 8.6 mg, 0.03 mmol, 16%). *trans*-tetralone-CASL: ^{1}H-NMR (300 MHz, $CDCl_3$) δ 7.64 (d, J = 7.8 Hz, 1 H), 7.16–7.34 (m, 3 H), 6.99 (s, 1 H), 6.96 (s, 1 H), 6.31 (s, 1 H), 3.20–3.22 (m, 2 H), 2.81 (t, J = 6.0 Hz, 2 H), 2.01 (t, J = 1.5 Hz, 3 H), 1.87 (t, J = 6.0 Hz, 3 H); ^{13}C-NMR (75 MHz, $CDCl_3$), δ 10.69, 22.47, 28.57, 30.10, 92.18, 109.52, 124.93, 126.51, 129.29, 130.56, 133.59, 134.24, 140.85, 142.48, 159.19, 164.53, 171.37; HRMS [ESI+ (m/z)] calculated for $(C_{17}H_{16}O_4 + H)^+$ 285.1121, found 285.1134; *cis*-tetralone-CASL: ^{1}H-NMR (300 MHz, $CDCl_3$) δ 7.65 (d, J = 7.8 Hz, 1 H), 7.27–7.32 (m, 1 H), 7.13–7.18 (m, 2 H), 6.93 (t, J = 1.5 Hz, 1 H), 6.89 (t, J = 1.5 Hz, 1 H), 5.78 (s, 1 H), 2.87 (t, J = 6.6 Hz, 2 H), 2.52–2.56 (m, 2 H), 1.96–2.02 (m, 5 H); ^{13}C-NMR (75 MHz, $CDCl_3$), δ 10.66, 22.99, 29.09, 35.42, 92.29, 111.88, 124.85, 128.42, 129.75, 130.21, 132.61, 134.20, 139.42, 142.28, 158.45, 164.41, 171.34; HRMS [ESI+ (*m*/*z*)] calculated for $(C_{17}H_{16}O_4 + H)^+$ 285.1121, found 285.1132.

GR5; γ-butyrolactone (2.0 mmol) and methyl formate (10 mmol) was added to the solution of potassium *tert* -butoxide in dry tetrahydrofuran at 4°C under Ar. The mixture was

transferred to the room temperature and stirred for 6 h. 5-Bromo-3-methyl-2(5H)-franone (2.0 mmol) was added and stirred for 15 h at room temperature. The reaction was quenched by adding 1 N HCl, and the solution was diluted to 100 ml with distilled water, extracted with EtOAc (3 × 100 ml). The organic layer was dried over Na_2SO_4 and concentrated *in vacuo*. The crude sample was purified by silica gel column chromatography (*n*-hexane/EtOAc:5/5). Fractions containing the GR5 were purified again by silica gel column chromatography (Toluene/EtOAc:6/4; 46.2 mg, 0.22 mmol, 11%). ^{1}H-NMR (300 MHz, $CDCl_3$) δ 7.48 (t, J = 2.7 Hz, 1 H), 6.94 (quin, J = 1.5 Hz, 1 H), 6.17(t, J = 1.5 Hz, 1 H), 4.39 (t, J = 7.2 Hz, 2 H), 2.93–2.87 (m, 2 H), 2.03 (t, J = 1.5 Hz, 3 H).

Germination Assay (*Orobanche minor* and *Striga hermonthica*)

Orobanche minor seeds were washed with 70% EtOH, and then sonicated for 4 min in 1% sodium hypochlorite solution containing 0.2% Tween-20. The seeds were then washed 10 times with sterile water and suspended in 0.1% agar solution. The seeds were loaded onto 5-mm glass fiber filter disks (20–70 seeds/disk) and were conditioned at 23°C for 15 days. Each disk was transferred into a 96-well plate. A 30 µl aliquot of test chemical solution was added to the well. For the germination assay, the chemical solutions were prepared by 1,000 times dilution from each acetone stock solution with water (final acetone concentration was 0.1%). GR24 solution (0.1% acetone) and sterile water (0.1% acetone) was used as positive and negative control, respectively. The 96 well plates were incubated for 5 days at 23°C and the number of total seeds and germinated seeds was counted.

Striga hermonthica seeds were washed with 70% EtOH, and then sonicated for 4 min in 1% sodium hypochlorite solution containing 0.2% Tween-20. The seeds were then washed 10 times with sterile water and suspended in 0.1% agar solution. The seeds were loaded onto 5-mm glass fiber filter disks (20–70 seeds/disk) and were conditioned at 30°C for 7 days. Each disk was transferred into a 96-well plate. A 30 µl aliquot of test chemical solution was added to the well. For the germination assay, the chemical solutions were prepared by 1,000 times dilution from each acetone stock solution with water (final acetone concentration was 0.1%). GR24 solution (0.1% acetone) and sterile water (0.1% acetone) was used as positive and negative control, respectively. The 96 well plates were incubated for 1 day at 30°C and total seeds and germinated seeds were counted.

Protein Expression (ShHTL6, ShHTL7, and AtD14)

The ORF fragment of ShHTL6 and ShHTL7 was synthesized using IDT gBlock service. The PCR amplified ShHTL6 and ShHTL7 fragment was digested with Nco I and EcoR I, and the digested product was introduced into a modified pET28 vector with an N-terminal His8 tag. *Escherichia coli* BL21(DE3) was used for protein expression. The overnight culture (12 ml) was added to a fresh LB medium (1.2 L) containing kanamycin (50 mg/L) at 37°C. After OD_{600} reached 0.8, 0.1 mM IPTG was added and the cell was further incubated at 16°C for 21 h. The culture medium was centrifuged at 3700 *g* and the pellet was stored at −20°C until use. The pellet was resuspended and sonicated in a lysis buffer (50 mM Tris buffer (pH 8.0) containing 500 mM NaCl, 10 mM 2-mercaptoethanol, and 10% glycerol). The supernatant was purified by Ni Sepharose TM 6 Fast Flow (500 µl, Cytiva). After washing with the washing buffer (50 mM Tris buffer (pH 8.0) containing 500 mM NaCl and 20 mM imidazole), The bound protein was eluted with elution buffer (50 mM Tris buffer (pH 8.0) containing 500 mM NaCl and 200 mM imidazole). The eluate was concentrated using VIVASPIN Turbo 15 (Sartorius), and the concentration was adjusted to 5 mg/ml. The purified protein was aliquoted to the appropriate volume, immediately frozen in liquid nitrogen, and stored at −80°C until use.

The cDNA of AtD14 was introduced into pMALHis vector that has both MBP-tag and His6-tag. The vector was transformed in to *E. coli* BL21 (DE3) and the cell was precultured in LB medium containing 50 µg/ml ampicillin. Overnight cultures (10 ml) were added to fresh LB medium (1 L) containing 50 µg/ml ampicillin and it was cultured at 37°C. After OD_{600} reached to 0.8, the cultures were cooled at 16°C for 1 h, and then 0.1 mM IPTG was added. The culture was further incubated at 16°C for 20 h. The culture medium was centrifuged at 3,700 *g* and the pellet was stored at −20°C until use. The pellet was resuspended and sonicated in lysis buffer (50 mM Tris buffer (pH 8.0) containing 500 mM NaCl, 10 mM 2-mercaptoethanol, and 10% glycerol). The supernatant was purified by Ni Sepharose TM 6 Fast Flow (500 µl, Cytiva) After washing with the washing buffer (50 mM Tris buffer (pH 8.0) containing 500 mM NaCl and 20 mM imidazole), The bound protein was eluted with elution buffer (50 mM Tris buffer (pH 8.0) containing 500 mM NaCl and 200 mM imidazole). The eluate was concentrated using VIVASPIN Turbo 15 (Sartorius), and the concentration was adjusted to 5 mg/ml. The purified protein was aliquoted to the appropriate volume, immediately frozen in liquid nitrogen, and stored at −80°C until use.

YLG Assay

In vitro YLG assays were conducted using 1 µg of recombinant ShHTL6 or ShHTL7 in 100 µl of reaction buffer (100 mM HEPES, 150 mM NaCl, pH 7.0) with 0.2% DMSO on a 96-well black plate (Greiner). After YLG was incubated with recombinant ShHTL6 or ShHTL7 for 1 h, the fluorescence was measured by spectraMax i5 (Molecular Devices) at excitation by 480 nm and detection by 520 nm. IC_{50} values were calculated using the online tool Quest GraphTM IC_{50} Calculator (AAT Bioquest, Inc., United States; https://www.aatbio.com/tools/ ic50-calculator).

Branching Assay

Sterilized seeds of the Arabidopsis *max4-8* mutant were put on the rockwool which was soaked in Noren's hydroponic solution (Noren et al., 2004) and cultured at 22°C for 14 days under LED light (105 µmol/m^2/s) with a 16 h light/8 h dark

photoperiod. Seedlings were transferred to a plastic pot containing 800 ml of hydroponic culture and grown under the same conditions for additional 15 or 16 days. Test compounds were dissolved in acetone and added to hydroponic culture. The final concentration of test compounds was 1 or 5 μM and acetone was adjusted to 0.01% (v/v). The hydroponic culture was renewed after 7 days. The number of rosette branches (>5 mm) was counted. In the experience at 5 μM concentration, fresh weight of shoot was also measured to evaluate the side effects of tested compounds.

Differential Scanning Fluorometry Experiments

DSF was conducted using 10 μg of the recombinant AtD14 protein in 20 μl of PBS buffer containing the 0.02 μl of Sypro Orange (Ex/Em: 490/610 nm; Invitrogen) and each compound with 5% (v/v) acetone on 96-well plate. These mixtures were heated from 20°C to 95°C, and the fluorescence (Ex/Em; 483/568) was constantly scanned by using LightCycler480 (Roche). The denaturation curve was calculated by using the LightCycler480 Software.

Hydrolysis Assay

Hydrolysis assays were carried out at 30°C for 60 min in 100 μl of a reaction buffer containing 0.13 pmol recombinant ShHTL7 or AtD14, 10 μM of substrate in 50 mM Phosphate-Na buffer (pH 7.0) containing 2% acetone. The enzyme reaction was stopped by addition of 100 μl of acetonitrile containing 1-naphtaleneacetic acid (NAA; 0.5 ng/μl) as an internal standard. After centrifuged at 13,000 rpm for 5 min, each sample was subjected to LC–MS/MS analysis equipped with reverse-phase column (CORTECS UPLC Phenyl 1.6 μm, ϕ2.1 × 75 mm; Waters). The concentration of remaining substrate and reaction product was calculated by using NAA as an internal standard. Detailed information about the analytical condition is described in **Supplementary Table 1**.

Time Course Monitoring of CASLs Degradation in Hydroponic Culture

t-CASL1, *c*-CASL1, PPASL, and GR5 were separately added to 15 ml tubes containing hydroponic culture. The final concentration of the test compounds is 1 μM and acetone was adjusted to 0.01% (v/v). These solutions were incubated under the same conditions as branching assay. After incubation for 0, 5, 24 72, or 168 h, 495 μl of hydroponic culture containing test compounds was collected and 5 μl of NAA solution (10 μM) was added as an internal standard. The solution was extracted with ethyl acetate. The ethyl acetate phase was dried up under the nitrogen gas and dissolved in acetonitrile. These samples were subjected to LC–MS/MS analysis equipped with reverse-phase column (CORTECS UPLC Phenyl 1.6 μm, ϕ2.1 × 75 mm; Waters). Each peak area of test chemicals and internal standard was calculated, and the remaining percentage of teste chemicals was calculated. At the same time, the degradation products of test compounds (CA or PPA) were also analyzed. Detailed information about the analytical condition was described in **Supplementary Table 1**.

Growth Promoting Assay and Root Phenotypic Analysis

Sterilized seeds of the *Arabidopsis* wild type Col-0 were put on the plate containing 1% (w/v) agar-solidified 0.5× Murashige and Skoog (MS) medium, 1% sucrose. Test compounds were dissolved in the medium at 1 μM by 10,000 times dilution from each acetone stock (final concentration of acetone was 0.01% (v/v)). To evaluate the growth promoting effect, these seedlings were cultured horizontally at 22°C for 20 days under LED light (105 μmol/m^2/s) with a 16 h light/8 h dark photoperiod. After the cultivation, flesh weight of shoot was measured. For root phenotypic analysis, these seedlings were cultured verticaly at 22°C for 11 days under LED light (105 μmol/m^2/s) with a 16 h light/8 h dark photoperiod. After the cultivation, root length was measured by using ImageJ software and number of lateral roots was counted by using a microscope.

RESULTS

Synthesis of SL Analogs Derived From CAs

To develop new SL analogs derived from cinnamic acid, we simply coupled the methylbutenolide (D-ring) to the carboxylic acid part of CA. To obtain structurally diverse analogs, we used as the starting materials both *trans* and *cis* CA isomers, and also 3-phenylpropionic acid (3-PPA), in which the double bond in the side chain is reduced to a single bond (**Figure 2**). It was previously reported that the isomerization of *trans*-CA to *cis*-CA is promoted by UV irradiation (254 nm; Yang et al., 1999). Accordingly, we prepared *cis*-CA according to this reported method. UV irradiation of the commercial *trans*-CA in MeOH solution promoted isomerization to the *cis*-isomer. Only the *cis*-isomer could be dissolved with water. Therefore, we could easily collect the *cis*-isomer after the isomerization, and it was then subjected to the D-ring coupling reaction. Hereafter, these new SL analogs derived from the isomers pair are referred to as *c*-CASL for *cis* isomer and *t*-CASL for *trans* isomer, respectively. The 3-PPA-derived SL analog is referred to as PPASL (**Figure 2**). Using these three analogs (*c*-CASL1, *t*-CASL1, and PPASL), we tested their germination-inducing activity for seeds of a root parasitic plant, *Orobanche minor*. We found that *c*-CASL1 showed approximately 10 times stronger germination-inducing activity than *t*-CASL1. Moreover, PPASL showed much weaker activity compared with *c*-CASL1 or *t*-CASL1, suggesting that the presence of the double bond in the side-chain structure has an important role for the biological activity as germination inducer for *O. minor*.

Synthesis of C-4 Substituted CASLs and Conformationally Fixed Analogs

To obtain more potent analogs derived from CA, we further synthesized structurally diverse CASLs using 4-substituted CA derivatives as the starting materials. Each *cis*-isomer of CA

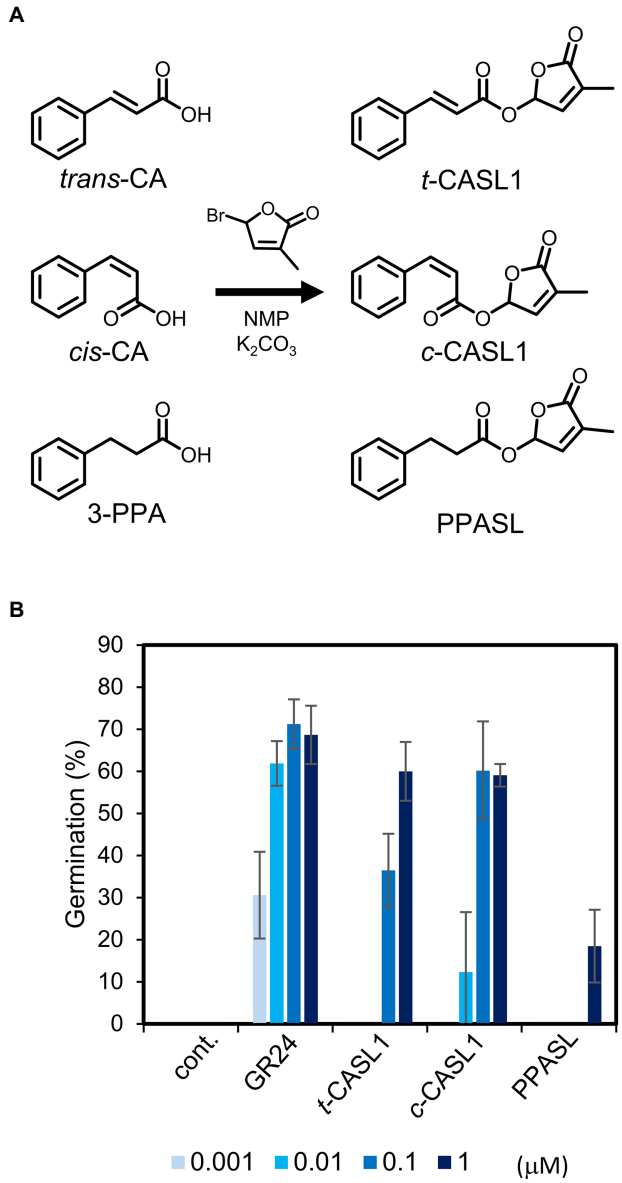

FIGURE 2 | *Orobanche minor* germination inducing activity of cinnamic acid (CA) derived SL analogs. **(A)** Synthetic scheme for the CA derived SL analogs. **(B)** Germination inducing activity of CASLs toward *O. minor* seeds. Data are the means ± SD ($n = 3$). cont. means control with only acetone at 0.1%.

was obtained by the above-mentioned method, and in total we synthesized 18 analogs (*c*-CASL2 to *c*-CASL10, *t*-CASL2 to *t*-CASL10, **Figure 3A**). Among these SL analogs, interestingly, *c*-CASL type isomers showed stronger activity compared with the corresponding *trans* isomer, with the approximately 10 times activity difference. Moreover, we found that introduction of an electron withdrawing group, such as NO_2, CF_3, Br, Cl, increased the germination-inducing activity with almost 10 times strength compared with the non-substituted compounds. These compounds induced *O. minor* germination at 1 nM concentration, which was almost equal activity to the positive control, GR24 (**Figure 3B**).

We found that *c*-CASLs showed stronger activity for inducing *O. minor* germination than *t*-CASLs. In these synthetic analogs, the side-chain structure has flexible conformation because of its free rotation. In a previous study, this rotation of the CA side-chain was fixed by introducing a ring structure to connect the benzene ring to the side-chain double bond. Such conformationally restricted *cis*-CA analogs were found to have stronger activity as allelochemicals than non-fixed analogs (Nishikawa et al., 2013). Thus, we also prepared conformationally-fixed CASL analogs. Starting from indanone or tetralone, we introduced an olefin part by the Horner–Wadsworth–Emmons reaction, which produced a mixture of both *cis* and *trans* isomers of conformationally-fixed CA analogs. After hydrolysis of the ethyl ester, they were further subjected to the D-ring coupling reaction, which yielded conformationally restricted *c*-CASL and *t*-CASL (**Figure 4A**; indCASL or tetCASL). We found that both *c*-indCASL and *c*-tetCASL showed slightly stronger activity for inducing *O. minor* germination, compared with the corresponding unfixed analog (**Figure 4B**). In contrast, both *t*-indCASL and *t*-tetCASL showed much stronger activity, compared with the non-fixed analog, *t*-CASL1 (**Figure 4B**). These *trans* analogs showed activity almost equal to the corresponding *cis* isomer, showing that the activity difference between *cis* and *trans* isomer decreased by fixing the side chain rotation.

Interaction of CA-Derived SLs and the SL Receptor Protein

As mentioned above, we found that *cis*-CA-derived SL analogs showed stronger activity for inducing *O. minor* germination. To understand the molecular basis of the difference in activity between *cis* and *trans* isomers, we examined the interaction of each analog with the SL receptor protein. Because the SL receptors in *O. minor* have not yet been identified, we used the *S. hermonthica* sensitive receptor, HTL7 (Toh et al., 2015). We tested the interaction between HTL7 and each SL analog using yoshimulactone green (YLG), a pro-fluorescence-type SL analog. As mentioned earlier, HTL7 is a member of α/β-fold hydrolase family, and it was reported that YLG is hydrolysable by HTL7. YLG hydrolysis releases the fluorescein molecule, which can be easily monitored by fluorescence detector (Tsuchiya et al., 2018). As was reported previously, the SL analog, GR24, effectively inhibited the fluorescence emission with IC_{50} value 0.17 μM (**Table 1**; **Supplementary Figure 1**). Similarly, we found that the CASLs also inhibited YLG hydrolysis by HTL7 with moderately low IC_{50} values. Interestingly, *c*-CASLs showed lower IC_{50} values, compared with the corresponding *t*-CASLs (**Table 1**; **Supplementary Figure 1**). We also tested the interaction of these analogs with another SL receptor, HTL6, which is close to HTL7 but is not so sensitive compared with HTL7. Even in the case of HTL6, *c*-CASL showed lower IC_{50} value compared with *t*-CASL or PPASL

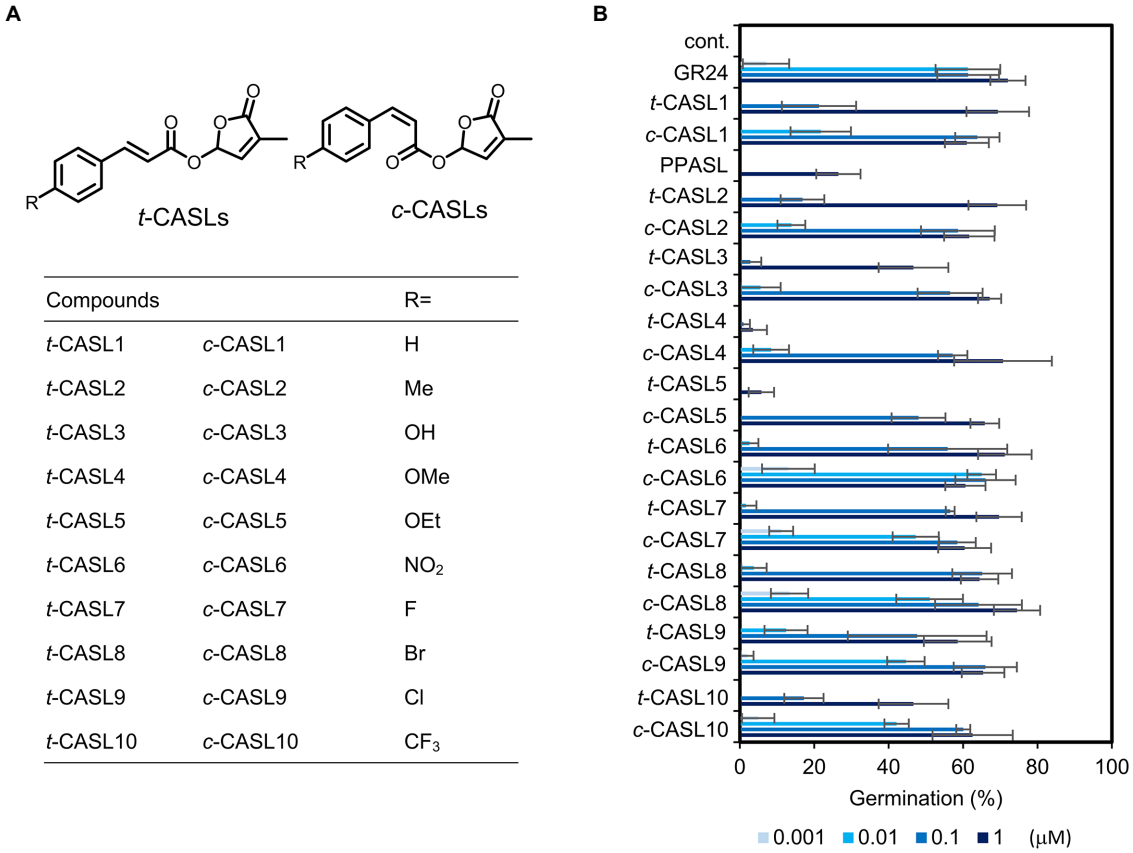

Compounds		R=
t-CASL1	*c*-CASL1	H
t-CASL2	*c*-CASL2	Me
t-CASL3	*c*-CASL3	OH
t-CASL4	*c*-CASL4	OMe
t-CASL5	*c*-CASL5	OEt
t-CASL6	*c*-CASL6	NO_2
t-CASL7	*c*-CASL7	F
t-CASL8	*c*-CASL8	Br
t-CASL9	*c*-CASL9	Cl
t-CASL10	*c*-CASL10	CF_3

FIGURE 3 | *Orobanche minor* germination inducing activity of C-4 substituted CA derived SL analogs. **(A)** Chemical structures of C-4 substituted type CASLs. **(B)** Germination inducing activity of tested compounds toward *O. minor* seeds. Data are the means ± SD ($n = 3$). cont. means control with only acetone at 0.1%.

(**Supplementary Figure 2**). These results strongly suggested that the activity difference between the *cis* and *trans* isomers of CASLs was because of the affinity difference for the receptor protein. As mentioned above, PPASL showed weaker activity for inducing *O. minor* germination, but this analog also inhibited YLG hydrolysis by HTL7 or HTL6, with a moderate IC_{50} value. Because we were able to detect the direct interaction of CASLs with the *Striga* SL receptor, we tested the germination-inducing activity of these compounds toward *S. hermonthica* seeds. We found that CASLs induced the germination of *S. hermonthica* seeds at moderately low concentration, and the activity of *c*-CASLs was stronger than that of the corresponding *t*-CASL, as was the case with *O. minor* (**Figure 5**).

Shoot-Branching Inhibition Activity by CASLs

We next evaluated the activity of CASLs as plant hormones using a shoot-branching inhibition assay. The *Arabidopsis* SL biosynthetic mutant, *max4*, was hydroponically grown in the presence of each synthetic CASL analog. As was reported previously, 1 μM GR5, a simplified SL analog, clearly inhibited shoot branching of the *max4* mutant (Umehara et al., 2015), but we did not see shoot-branching inhibition by any of these CASLs at the same concentration (**Figure 6**). At a higher concentration, 5 μM, we found slight decrease of the branching number by treatment with some of synthetic analogs. However, we also found that such chemicals also showed growth inhibiting activity with significant decrease of shoot weight, which might be the reason for the branching reduction (**Supplementary Figure 3**). Next, we examined the direct interaction of the *Arabidopsis* SL receptor, AtD14, with CASLs, using differential scanning fluorimetry (DSF), which is widely used for SL receptor biochemical analyses (Hamiaux et al., 2012; Seto et al., 2019). This method can evaluate the receptor–ligand interaction by measuring the ligand-inducible melting temperature shift of the receptor protein. Using this method, we found that both *cis*- and *trans*-CASLs induced a melting temperature shift of AtD14, suggesting that these CASLs were able to interact directly with the *Arabidopsis* SL receptor protein, at least *in vitro* (**Supplementary Figure 4**). To further address the weak activity of CASLs in the shoot branching inhibition assay, we examined the chemical stability of CASLs in the hydroponic culture conditions. We speculated that these analogs might be unstable because the D-ring is connected to the CA part by an ester bond. We simply incubated *c*-CASL1, *t*-CASL1, or PPASL in the hydroponic culture medium, which was used

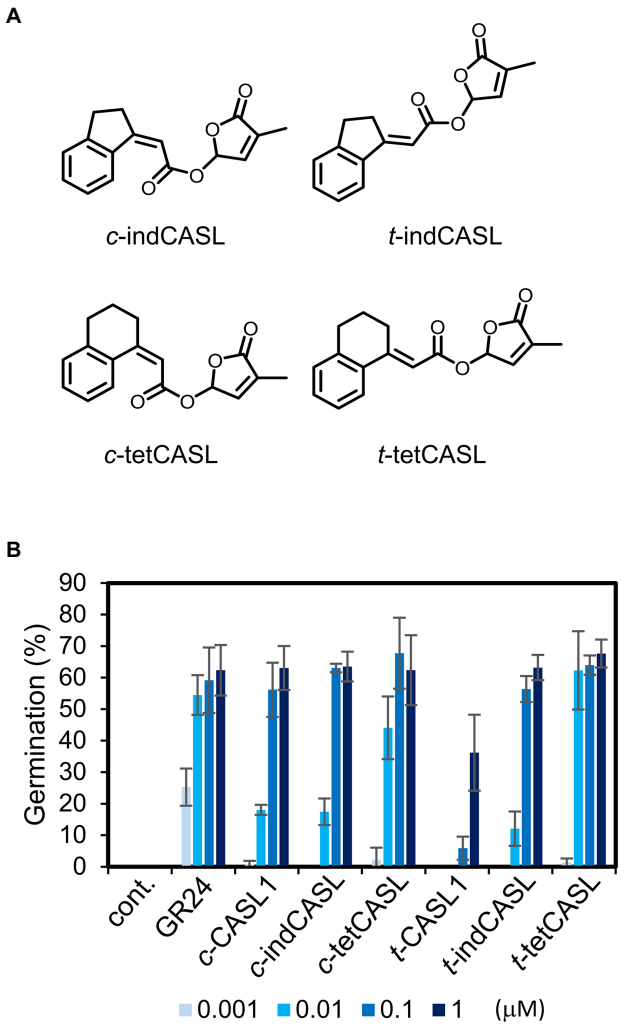

FIGURE 4 | *Orobanche minor* germination inducing activity of conformationally fixed CA derived SL analogs. **(A)** Chemical structures of the conformationally fixed CASLs. **(B)** Germination inducing activity of tested compounds toward *O. minor* seeds. Data are means ± SD ($n = 3$). cont. means control with only acetone at 0.1%.

TABLE 1 | Evaluation of me direct interaction between ShHTL7 and CASLs.

Compounds	IC_{50} (μM)	Compounds	IC_{50} (μM)
GR24	0.17	PPASL	1.46
t-CASL1	2.05	*c*-CASL1	0.59
t-CASL2	1.41	*c*-CASL2	0.68
t-CASL3	>10	*c*-CASL3	3.43
t-CASL4	2.21	*c*-CASL4	0.66
t-CASLS	3.97	*c*-CASLS	0.31
t-CASL6	0.71	*c*-CASL6	0.25
t-CASL7	1.55	*c*-CASL7	1.14
t-CASL8	0.70	*c*-CASL8	0.36
t-CASL9	0.83	*c*-CASL9	0.34
t-CASL10	0.34	*c*-CASL10	0.22
t-indCASL	3.07	*c*-indCASL	2.01
t-tetCASL	3.85	*c*-tetCASL	4.61

IC_{50} values for the tested compounds in YLG assay were calculated using the online tool Quest GraphTM IC_{50} Calculator (AAT Bioquest, Inc., United States).

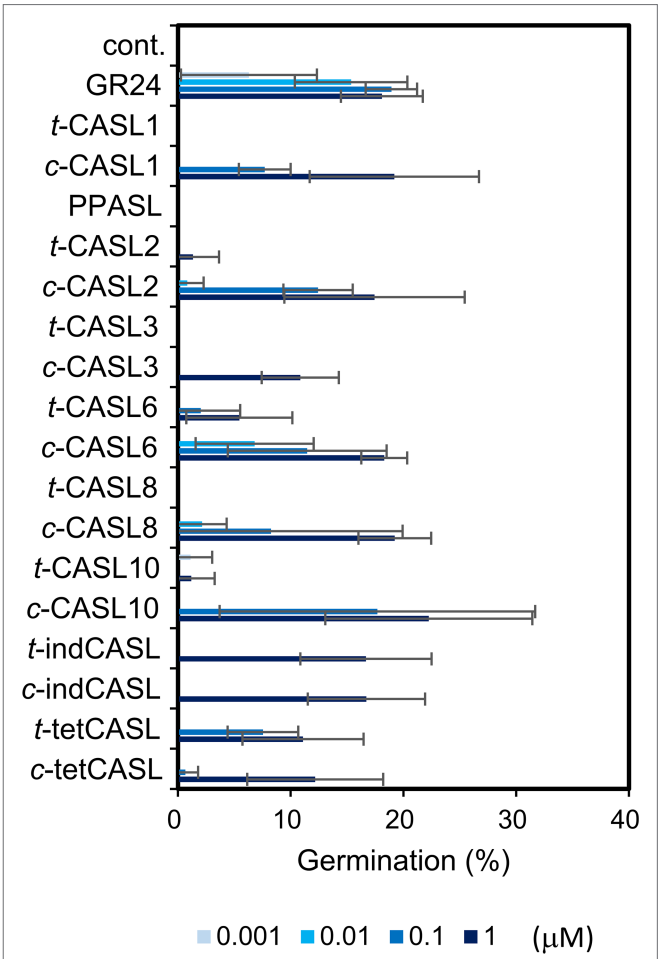

FIGURE 5 | Germination inducing activity of CASLs toward *Striga hermonthica* seeds. Data are the means ± SD ($n = 3$). cont. means control with only acetone at 0.01%.

for the shoot-branching inhibition assay, and the non-enzymatic degradation of each chemical was monitored by LC–MS/MS analysis. As we expected, both *c*-CASL1 and *t*-CASL1 degraded more rapidly than did GR5, with almost 40% loss within 1 week (**Supplementary Figure 5A**). In addition, we detected the release of the CA part, which gradually increased over time (**Supplementary Figure 5B**). Thus, instability of these analogs could be one reason for the inactivity of CASLs in the shoot-branching inhibition assay. We also found that SL receptors, AtD14 and HTL7, can hydrolyze *c*-CASL, *t*-CASL, or PPASL (**Supplementary Figure 6**). Thus, receptor-dependent degradation of these compounds might be also the reason for weak activity in shoot branching inhibition. However, we cannot rule out some other possibilities, for instance that the uptake of these analogs by *Arabidopsis* might be quite poor for some reason, or that CASLs might be metabolized rapidly *in planta*. Moreover, as mentioned above, CASLs exhibited growth inhibiting activity toward Arabidopsis at a high concentration. Thus, this would be another possible reason for apparent weak activity of CASLs as plant hormones.

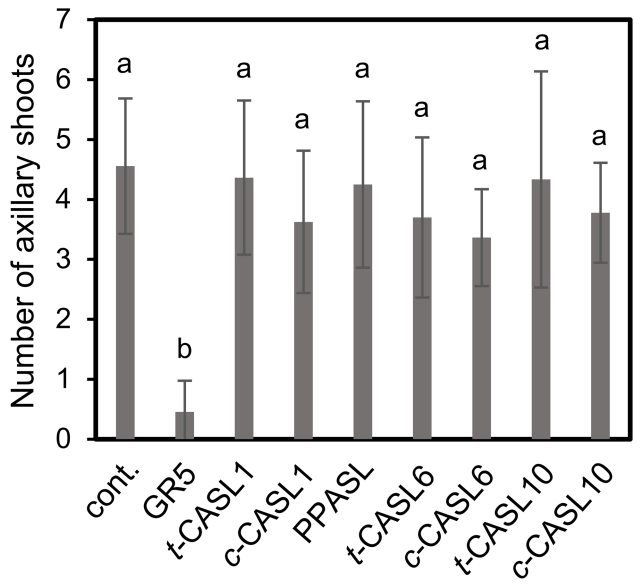

FIGURE 6 | Shoot branching inhibiting activity of CASLs using the Arabidosis *max4* mutant. Number of axillary shoots (Over 5 mm) of *max4* which were grown in hydroponic culture containing test compounds at 1 μM concentration was counted. Data are means ± SD ($n = 8$–11). Different letters indicate significant differences at $p < 0.05$ with Tukey multiple comparison test. cont. means control with only acetone at 0.1%.

Plant Growth Promoting Activity of CASLs

As mentioned earlier, *cis*-CA, but not *trans*-CA, was reported to have plant growth-promoting activity at relatively low concentration by inhibiting the auxin efflux (Steenackers et al., 2017, 2019). Because *c*-CASL1 was found to be non-enzymatically degraded to some extent, we expected that *c*-CASL1 treatment might bring the same effect as treatment with *cis*-CA alone. To test this hypothesis, we grew *Arabidopsis* WT plants on the agar plates containing *c*-CASL1, *t*-CASL1, *cis*-CA, or *trans*-CA. *cis*-CA was reported to promote lateral root growth and thus to increase leaf size. We found that root growth phenotype was affected by not only *cis*-CA but also *c*-CASL1 (**Supplementary Figure 7A**). These two compounds almost equally inhibited the primary root length as well as increased the lateral root density (**Supplementary Figure 7B**). The root growth direction was also affected by *c*-CASL as was the case with *cis*-CA (**Supplementary Figure 7A**). Moreover, we observed an increase in shoot fresh weight after treatment with *cis*-CA or *c*-CASL (**Figure 7**). Thus, we conclude that *c*-CASL1 treatment produced the same effect as *cis*-CA treatment with growth promotion in *Arabidopsis*.

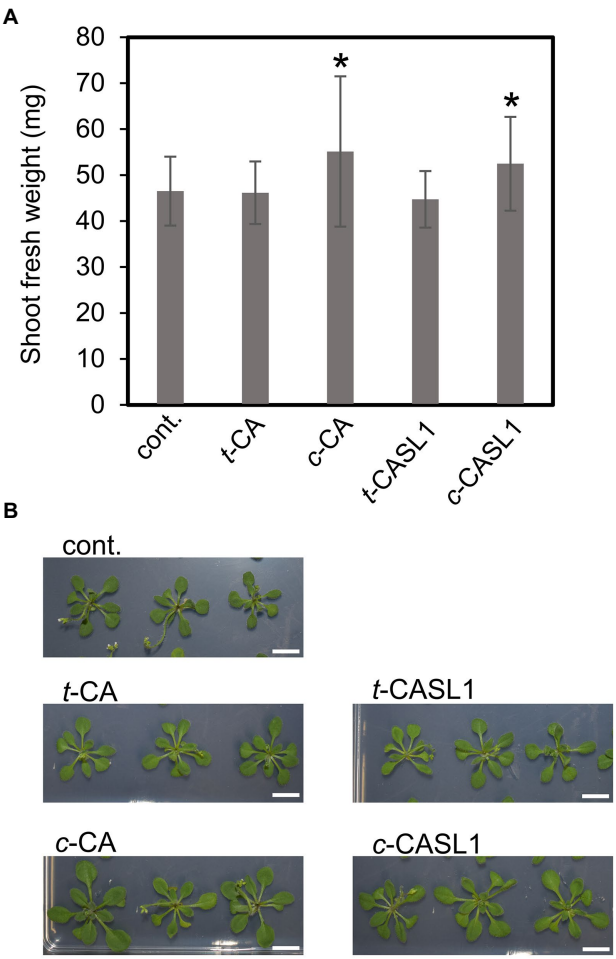

FIGURE 7 | Effects of the CAs and CASLs on the *Arabidosis* seedling growth. **(A)** Fresh weight of the shoot parts after growing for 20 days on agar plate containing 1 μM test compounds. Data are the means ± SD ($n = 13$–25). Asterisk indicate the significant differences between the control using *t*-test (*$p < 0.05$). **(B)** Shoot phenotype of 20-days old seedling which were grown on the agar medium containing the indicated compounds (Scale bar = 1 cm). cont. means control with only acetone at 0.1%.

DISCUSSION

In this paper, we report successful development of a series of new SL analogs derived from CA, which is the basis of a class of phenylpropanoid compounds widely distributed in the plant kingdom. We synthesized 25 analogs, all of which showed moderate activity as suicidal germination inducers for the root parasitic plants, *O. minor* and *S. hermonthica*. The most active compounds, in which an electron withdrawing group was introduced at the C-4 position, showed almost equal activity to GR24. Interestingly, *cis*-CA-derived SL analogs showed stronger activity than the corresponding *trans* isomer-derived analogs. We also found that *cis*-CASLs interacted with the *S. hermonthica* receptor, HTL7 or HTL6, more strongly than the corresponding *trans*-CASLs. We also synthesized an analog from 3-PPA (denoted PPASL), in which the side-chain double bond was reduced to a single bond, and this analog showed very weak activity compared with the CA-derived analogs. However, *in vitro* YLG assay results showed that PPASL interacted directly with HTL7 with a relatively low IC_{50} value, as did other analogs. We still do not know the reason for the weak activity of this analog, but it might be possible that the uptake of this analog by the parasitic plant seeds is less effective than the CA derivatives,

for some reason, or that this analog might be quickly metabolized *in planta*.

Because *cis*-CASL showed stronger activity inducing germination of the parasitic plants, we synthesized conformationally-fixed analogs by introducing a 5-member or 6-member ring structure. However, the activity of the conformationally-fixed *cis* isomer analogs (*c*-indCASL, or *c*-tetCASL) was not increased compared with the non-fixed analog, *c*-CASL1. In contrast, in the case of the *trans* isomer analogs, the fixed conformation analogs (*t*-indCASL, or *t*-tetCASL) showed much stronger activity compared with the non-fixed analog, *t*-CASL1. Therefore, introducing a fixed conformation decreased the activity difference between *cis* and *trans* isomers; however, this strategy would not be suitable as a method to obtain more potent analogs.

We also found that CA-derived SL analogs did not inhibit shoot branching in *Arabidopsis* when applied to the SL biosynthetic mutant, *max4*, at 1 μM. At a high concentration, 5 μM, some of these analogs slightly inhibited shoot branching. However, it was likely that the branching reduction was due to the growth inhibiting activity by a side effect of the tested compounds. If considering that these analogs were active as the germination inducers for root parasitic plants at concentrations well below 1 μM, these new analogs might provide new lead chemicals as suicidal germination inducers that do not affect the host plant architecture. Because *cis*-CA was reported to promote plant growth at relatively low concentration, we evaluated *c*-CASL1 for such activity. As a result, we found that not only *cis*-CA but also *c*-CASL1 showed growth-promoting activity toward the *Arabidopsis* WT plant. As CA-derived SLs were found to be degraded to some extent in the hydroponic culture medium, it is likely that the growth-promoting activity of *c*-CASL1 was simply a result of its degradation in the culture medium, leading to release of free *c*-CA. It would be also possible that CASLs are hydrolyzed to *cis*-CA in a manner dependent on the SL receptor, D14. In fact, CASLs were hydrolyzed by AtD14 or HTL7. Although we have not tested for activity toward other plants, including crop species, these new SL analogs might provide lead chemicals with two activities, as suicidal germination inducers for root parasitic plants as well as plant growth-promoting reagents for the host plants. This feature could be one of advantages compared with the previously reported SL analogs.

In conclusion, we successfully prepared new SL analogs derived from CA with useful biological activities. Many structural analogs of CA are commercially available, therefore it would be possible to prepare more diverse analogs to obtain further potent agonists.

DATA AVAILABILITY STATEMENT

The original contributions presented in the study are included in the article/**Supplementary Material**; further inquiries can be directed to the corresponding author.

AUTHOR CONTRIBUTIONS

TS performed the majority of the experiments. MK performed a part of the YLG assay experiment. YS designed the research. TS, MK, and YS wrote the manuscript. All authors contributed to the article and approved the submitted version.

FUNDING

This work was supported by MEXT KAKENHI grant number 19K05852, Mitsubishi Foundation, and Kato Memorial Bioscience Foundation.

ACKNOWLEDGMENTS

We thank Xie Xiaonan and Steven Runo for kindly providing seeds of *Orobanche minor* and *Striga hermonthica*, respectively. We thank Huw Tyson, from Edanz (https://jp.edanz.com/ac) for editing a draft of this manuscript.

SUPPLEMENTARY MATERIAL

The Supplementary Material for this article can be found online at: https://www.frontiersin.org/articles/10.3389/fpls.2022.843362/full#supplementary-material

REFERENCES

Akiyama, K., Matsuzaki, K., and Hayashi, H. (2005). Plant sesquiterpenes induce hyphal branching in arbuscular mycorrhizal fungi. *Nature* 435, 824–827. doi: 10.1038/nature03608

Arite, T., Umehara, M., Ishikawa, S., Hanada, A., Maekawa, M., Yamaguchi, S., et al. (2009). d14, a strigolactone-insensitive mutant of rice, shows an accelerated outgrowth of tillers. *Plant Cell Physiol.* 50, 1416–1424. doi: 10.1093/pcp/pcp091

Conn, C. E., Bythell-Douglas, R., Neumann, D., Yoshida, S., Whittington, B., Westwood, J. H., et al. (2015). Plant evolution. Convergent evolution of strigolactone perception enabled host detection in parasitic plants. *Science* 349, 540–543. doi: 10.1126/science.aab1140

Cook, C. E., Whichard, L. P., Turner, B., Wall, M. E., and Egley, G. H. (1966). Germination of Witchweed (Striga lutea Lour.): isolation and properties of a potent stimulant. *Science* 154, 1189–1190. doi: 10.1126/science.154.3753.1189

de Saint Germain, A., Clave, G., Badet-Denisot, M. A., Pillot, J. P., Cornu, D., Le Caer, J. P., et al. (2016). An histidine covalent receptor and butenolide complex mediates strigolactone perception. *Nat. Chem. Biol.* 12, 787–794. doi: 10.1038/nchembio.2147

Fukui, K., Ito, S., Ueno, K., Yamaguchi, S., Kyozuka, J., and Asami, T. (2011). New branching inhibitors and their potential as strigolactone mimics in rice. *Bioorg. Med. Chem. Lett.* 21, 4905–4908. doi: 10.1016/j.bmcl.2011.06.019

Gomez-Roldan, V., Fermas, S., Brewer, P. B., Puech-Pages, V., Dun, E. A., Pillot, J. P., et al. (2008). Strigolactone inhibition of shoot branching. *Nature* 455, 189–194. doi: 10.1038/nature07271

Hamiaux, C., Drummond, R. S., Janssen, B. J., Ledger, S. E., Cooney, J. M., Newcomb, R. D., et al. (2012). DAD2 is an alpha/beta hydrolase likely to be involved in the perception of the plant branching hormone, strigolactone. *Curr. Biol.* 22, 2032–2036. doi: 10.1016/j.cub.2012.08.007

Hiradate, S., Morita, S., Furubayashi, A., Fujii, Y., and Harada, J. (2005). Plant growth inhibition by cis-cinnamoyl glucosides and cis-cinnamic acid. *J. Chem. Ecol.* 31, 591–601. doi: 10.1007/s10886-005-2047-0

Mashiguchi, K., Seto, Y., and Yamaguchi, S. (2021). Strigolactone biosynthesis, transport and perception. *Plant J.* 105, 335–350. doi: 10.1111/tpj.15059

Nishikawa, K., Fukuda, H., Abe, M., Nakanishi, K., Tazawa, Y., Yamaguchi, C., et al. (2013). Design and synthesis of conformationally constrained analogues of cis-cinnamic acid and evaluation of their plant growth inhibitory activity. *Phytochemistry* 96, 223–234. doi: 10.1016/j.phytochem.2013.10.001

Noren, H., Svensson, P., and Andersson, B. (2004). A convenient and versatile hydroponic cultivation system for *Arabidopsis thaliana*. *Physiol. Plant.* 121, 343–348. doi: 10.1111/j.0031-9317.2004.00350.x

Seto, Y., Yasui, R., Kameoka, H., Tamiru, M., Cao, M., Terauchi, R., et al. (2019). Strigolactone perception and deactivation by a hydrolase receptor DWARF14. *Nat. Commun.* 10:191. doi: 10.1038/s41467-018-08124-7

Steenackers, W., El Houari, I., Baekelandt, A., Witvrouw, K., Dhondt, S., Leroux, O., et al. (2019). cis-Cinnamic acid is a natural plant growth-promoting compound. *J. Exp. Bot.* 70, 6293–6304. doi: 10.1093/jxb/erz392

Steenackers, W., Klima, P., Quareshy, M., Cesarino, I., Kumpf, R. P., Corneillie, S., et al. (2017). cis-Cinnamic acid is a novel, natural auxin efflux inhibitor that promotes lateral root formation. *Plant Physiol.* 173, 552–565. doi: 10.1104/pp.16.00943

Toh, S., Holbrook-Smith, D., Stogios, P. J., Onopriyenko, O., Lumba, S., Tsuchiya, Y., et al. (2015). Structure-function analysis identifies highly sensitive strigolactone receptors in Striga. *Science* 350, 203–207. doi: 10.1126/science.aac9476

Tsuchiya, Y., Yoshimura, M., and Hagihara, S. (2018). The dynamics of strigolactone perception in *Striga hermonthica*: a working hypothesis. *J. Exp. Bot.* 69, 2281–2290. doi: 10.1093/jxb/ery061

Tsuchiya, Y., Yoshimura, M., Sato, Y., Kuwata, K., Toh, S., Holbrook-Smith, D., et al. (2015). Parasitic plants. Probing strigolactone receptors in *Striga hermonthica* with fluorescence. *Science* 349, 864–868. doi: 10.1126/science.aab3831

Umehara, M., Cao, M., Akiyama, K., Akatsu, T., Seto, Y., Hanada, A., et al. (2015). Structural requirements of strigolactones for shoot branching inhibition in rice and *Arabidopsis*. *Plant Cell Physiol.* 56, 1059–1072. doi: 10.1093/pcp/pcv028

Umehara, M., Hanada, A., Yoshida, S., Akiyama, K., Arite, T., Takeda-Kamiya, N., et al. (2008). Inhibition of shoot branching by new terpenoid plant hormones. *Nature* 455, 195–200. doi: 10.1038/nature07272

Uraguchi, D., Kuwata, K., Hijikata, Y., Yamaguchi, R., Imaizumi, H., Am, S., et al. (2018). A femtomolar-range suicide germination stimulant for the parasitic plant *Striga hermonthica*. *Science* 362, 1301–1305. doi: 10.1126/science.aau5445

Waters, M. T., Nelson, D. C., Scaffidi, A., Flematti, G. R., Sun, Y. K., Dixon, K. W., et al. (2012). Specialisation within the DWARF14 protein family confers distinct responses to karrikins and strigolactones in *Arabidopsis*. *Development* 139, 1285–1295. doi: 10.1242/dev.074567

Yang, X. X., Choi, H. W., Yang, S. F., and Li, N. (1999). A UV-light activated cinnamic acid isomer regulates plant growth and gravitropism via an ethylene receptor-independent pathway. *Aust. J. Plant Physiol.* 26, 325–335. doi: 10.1071/PP99007

Yao, R., Ming, Z., Yan, L., Li, S., Wang, F., Ma, S., et al. (2016). DWARF14 is a non-canonical hormone receptor for strigolactone. *Nature* 536, 469–473. doi: 10.1038/nature19073

Conflict of Interest: The authors declare that they have no known competing financial interests or personal relationships that could have appeared to influence the work reported in this paper.

Publisher's Note: All claims expressed in this article are solely those of the authors and do not necessarily represent those of their affiliated organizations, or those of the publisher, the editors and the reviewers. Any product that may be evaluated in this article, or claim that may be made by its manufacturer, is not guaranteed or endorsed by the publisher.

frontiers | Frontiers in Plant Science

REVIEW
published: 12 May 2022
doi: 10.3389/fpls.2022.887232

Masks Start to Drop: Suppressor of MAX2 1-Like Proteins Reveal Their Many Faces

*Arne Temmerman[1,2], Ambre Guillory[3,4], Sandrine Bonhomme[3], Sofie Goormachtig[1,2] and Sylwia Struk[1,2]**

[1]*Department of Plant Biotechnology and Bioinformatics, Ghent University, Ghent, Belgium,* [2]*VIB-Center for Plant Systems Biology, Ghent, Belgium,* [3]*Université Paris-Saclay, INRAE, AgroParisTech, Institut Jean-Pierre Bourgin (IJPB), Versailles, France,* [4]*LIPME, Université de Toulouse, INRAE, CNRS, Castanet-Tolosan, France*

Although the main players of the strigolactone (SL) signaling pathway have been characterized genetically, how they regulate plant development is still poorly understood. Of central importance are the SUPPRESSOR OF MAX2 1-LIKE (SMXL) proteins that belong to a family of eight members in *Arabidopsis thaliana*, of which one subclade is involved in SL signaling and another one in the pathway of the chemically related karrikins. Through proteasomal degradation of these SMXLs, triggered by either DWARF14 (D14) or KARRIKIN INSENSITIVE2 (KAI2), several physiological processes are controlled, such as, among others, shoot and root architecture, seed germination, and seedling photomorphogenesis. Yet another clade has been shown to be involved in vascular development, independently of the D14 and KAI2 actions and not relying on proteasomal degradation. Despite their role in several aspects of plant development, the exact molecular mechanisms by which SMXLs regulate them are not completely unraveled. To fill the major knowledge gap in understanding D14 and KAI2 signaling, SMXLs are intensively studied, making it challenging to combine all the insights into a coherent characterization of these important proteins. To this end, this review provides an in-depth exploration of the recent data regarding their physiological function, evolution, structure, and molecular mechanism. In addition, we propose a selection of future perspectives, focusing on the apparent localization of SMXLs in subnuclear speckles, as observed in transient expression assays, which we couple to recent advances in the field of biomolecular condensates and liquid–liquid phase separation.

Keywords: SMXL, strigolactones, karrikins, phylogenetics, biomolecular condensates

OPEN ACCESS

Edited by:
Tadao Asami,
The University of Tokyo, Japan

Reviewed by:
Thomas Greb,
Heidelberg University, Germany
David Nelson,
University of California, Riverside, United States

****Correspondence:***
Sylwia Struk
sylwia.struk@psb.vib-ugent.be

Specialty section:
This article was submitted to Plant Physiology, a section of the journal Frontiers in Plant Science

Received: *01 March 2022*
Accepted: *25 April 2022*
Published: *12 May 2022*

Citation:
Temmerman A, Guillory A, Bonhomme S, Goormachtig S and Struk S (2022) Masks Start to Drop: Suppressor of MAX2 1-Like Proteins Reveal Their Many Faces. Front. Plant Sci. 13:887232. doi: 10.3389/fpls.2022.887232

INTRODUCTION

Strigolactones Signal Through D14 and MAX2

Plants continuously tailor their growth to a vast array of external and internal stimuli, which are integrated and translated into a developmental output by the interplay of several endogenous signaling molecules. Numerous aspects of plant development are modulated by one of the most recently characterized class of phytohormones, strigolactones (SLs; reviewed in

Aquino et al., 2021). However, SLs had originally been discovered as rhizosphere signals that enable the interaction between the plant host and symbiotic organisms, both parasitic, i.e., root-parasitic plants from the Orobanchaceae family (reviewed in Bouwmeester et al., 2021), and mutualistic, i.e., arbuscular mycorrhizal fungi (reviewed in Lanfranco et al., 2018). Thus far, more than 30 different SLs have been identified in a multitude of plant species (Yoneyama et al., 2018; Xie et al., 2019). Initially, only compounds, now referred to as canonical SLs, consisting of a tricyclic ABC scaffold connected through an enol ether bridge to a butenolide D-ring, were considered as SLs. Based on the configuration of the stereocenter between the B- and C-rings, canonical SLs can be subdivided in strigol-like and orobanchol-like molecules (Wang and Bouwmeester, 2018). More recent discoveries revealed the existence of noncanonical SLs, in which the D-ring is attached to a chemical structure different from the canonical ABC scaffold (Yoneyama et al., 2018). All natural SLs contain a stereocenter at the 2′ position of the D-ring, which is set in an R configuration (Flematti et al., 2016). In contrast, the most extensively used SL analog, *rac*-GR24, is synthesized as a racemic mixture consisting of both the 2'R and 2'S enantiomers, each with a distinct functionality in plant growth. The current nomenclature of GR24 isomers refers to a stereotypic strigol-like (5-deoxystrigol; 5DS) or orobanchol-like (4-deoxyorobanchol; 4DO) compound, thus specifying the configuration of the ABC rings.

In angiosperms, SLs are perceived by the dual function receptor/enzyme DWARF14 (D14), a member of the α/β-fold hydrolase superfamily (**Figure 1**; Hamiaux et al., 2012; Zhao et al., 2013; de Saint Germain et al., 2016; Yao et al., 2016). A characterizing feature of α/β hydrolases is the presence of a conserved catalytic serine-histidine-aspartic acid (Ser-His-Asp) triad. Based on the crystal structures of the *Arabidopsis thaliana* and *Oryza sativa* (rice) D14 homologs, a mode of action had been suggested, in which D14 hydrolyzes the SL molecule, opening the D-ring and detaching it from the ABC scaffold that subsequently leaves the catalytic site. The open D-ring is covalently bound to the catalytic Ser residue and finally transferred to the catalytic His, through the formation of a 'covalently linked intermediate molecule' (CLIM; Nakamura et al., 2013; Zhao et al., 2013, 2015; Yao et al., 2016; Shabek et al., 2018). Although hydrolysis of SLs had initially been hypothesized as essential to convert D14 into an active state, later evidence resulted in the competing hypothesis that D14 becomes active upon binding of SL, whereas hydrolysis merely deactivates the bioactive molecule (Seto et al., 2019). To date, the precise function of SL hydrolysis and the nature and role of the covalent modifications of D14 remain open questions (Bürger and Chory, 2020).

After perception of its ligand, further signal transduction relies on the D14-mediated recruitment of the F-box protein MORE AXILLARY GROWTH 2 (MAX2; **Figure 1**; Stirnberg et al., 2007; Waters et al., 2012). As a part of an SKP-CULLIN-F-box (SCF) complex, MAX2 is responsible for the polyubiquitination of certain target proteins from the SUPPRESSOR OF MAX2 (SMAX)1-LIKE (SMXL) family, which are consequently degraded by the 26S proteasome, resulting in downstream signaling (Stirnberg et al., 2007; Jiang et al., 2013; Stanga et al., 2013; Zhou et al., 2013; Soundappan et al., 2015). Interaction between MAX2 and D14 involves a cycle of concerted conformational changes of both proteins, partly determining whether D14 continues to activate signaling or is degraded in a MAX2-dependent manner (Chevalier et al., 2014; Hu et al., 2017; Shabek et al., 2018). Crystal structure studies in rice revealed that this balance depends on DWARF3 (D3) and DWARF53 (D53), the rice homologs of MAX2 and SMXL6/7/8, respectively. Indeed, D3 switches between two functional conformations, characterized by different positions of its C-terminal α-helix (CTH) that can either be engaged with or dislodged from the remainder of the protein (Shabek et al., 2018). When D14 binds bioactive SLs, D3 with a dislodged CTH will interact with and hold D14 in an open and enzymatically inactive conformation, until D53, cooperatively bound by D14 and the D3-CTH, is recruited to the signaling complex (Shabek et al., 2018). This tripartite interaction will trigger the D14 enzymatic activity. Hence, D14 will hydrolyze SLs and switch to a closed conformation, in turn converting D3 to its CTH-engaged form. In this form, the signaling complex will ubiquitinate D53, resulting in its degradation and removal from the complex (Jiang et al., 2013; Zhou et al., 2013; Shabek et al., 2018). Finally, D14 itself is also polyubiquitinated and proteasomally degraded. The current knowledge on D14 ligand perception and hydrolysis, as well as the formation of the D14-MAX2-SMXL complex and activation of SL signaling, have been recently reviewed in detail (Bürger and Chory, 2020). Nevertheless, the exact stoichiometry of the process remains unclear: how many SL molecules can D14 hydrolyze before it gets degraded? How many SMXL proteins can be marked for degradation for each hydrolyzed SL molecule (Shabek et al., 2018)?

The D14 Homolog KAI2 Induces a Parallel Signaling Pathway

MAX2 is important not only for SL signaling but also for the response to a class of exogenous compounds, karrikins (KARs), produced from burned plant material (Flematti et al., 2004; Nelson et al., 2009, 2011). This observation was followed by the discovery of another α/β hydrolase and D14 paralog, KARRIKIN INSENSITIVE 2 (KAI2) or HYPOSENSITIVE TO LIGHT (HTL), that acts as a KAR receptor (Sun and Ni, 2011; Waters et al., 2012). In a pathway similar to that of D14-MAX2, perception of KARs by KAI2 results in the recruitment of the SCF^{MAX2} complex and marking for proteasomal degradation of SMXL proteins (**Figure 1**; Nelson et al., 2011; Stanga et al., 2013, 2016; Khosla et al., 2020; Wang et al., 2020b). Despite the use of highly related components, D14- and KAI2 signaling regulate distinct, but overlapping sets of developmental outputs (see below; De Cuyper et al., 2017; Machin et al., 2020). As already established, both pathways also have distinct inputs; considering exogenous compounds, D14 is generally responsive to 2'R-configured SLs and the SL analogs $GR24^{5DS}$ and $GR24^{4DO}$, whereas KAI2 responds to KARs and the 2'S-configured $GR24^{ent\text{-}5DS}$ (Scaffidi et al., 2014; Waters

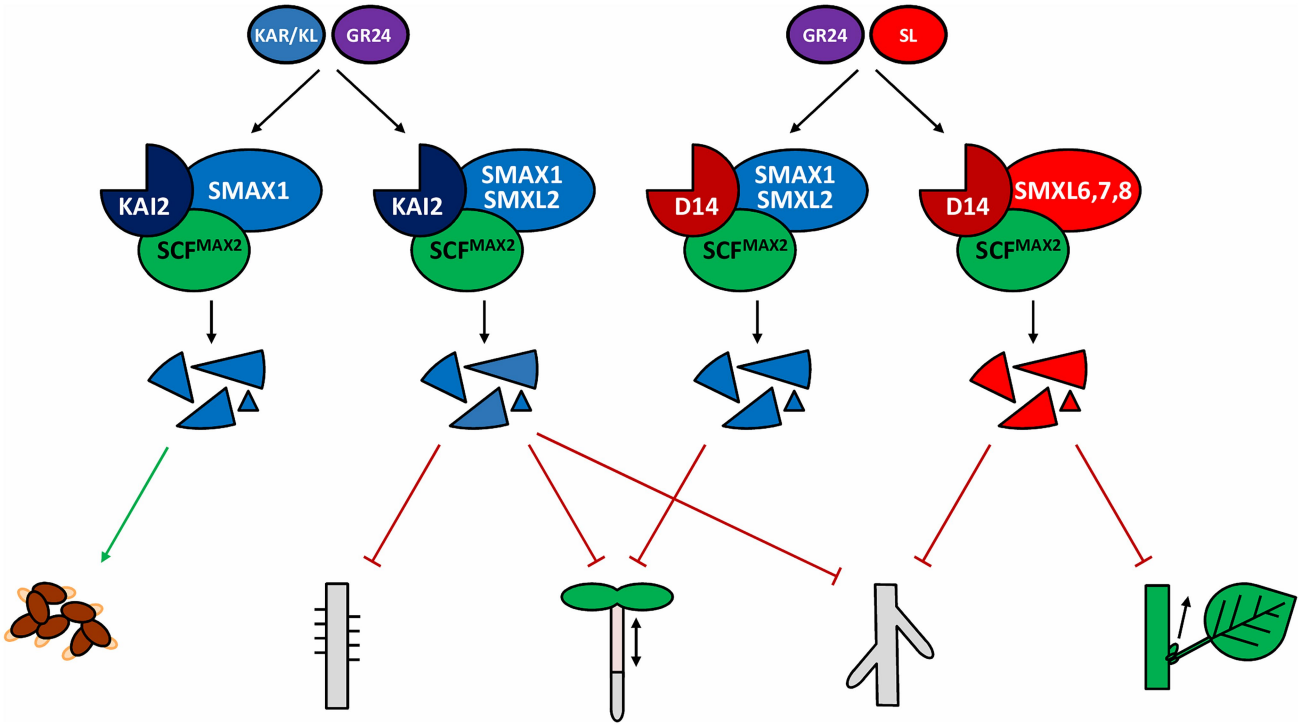

FIGURE 1 | Core D14 and KAI2 signaling pathways. The signaling complexes formed after the perception of their respective ligands as well as a selection of phenotypes affected by the SMXL protein degradation are shown, induction of seed germination induction, inhibition of root hair development, hypocotyl elongation, lateral root formation, and shoot branching. A more extensive list of processes regulated by these pathways can be found in **Table 1**. GR24, *rac*-GR24; KL, KAI2 ligand; SL, strigolactone.

et al., 2015b; Flematti et al., 2016). In contrast to D14, KAI2 is found in all sequenced land plant genomes and in some charophyte algae, suggesting that KAI2-MAX2-dependent signaling is ancestral and that D14 probably evolved through duplication and neofunctionalization of KAI2 (Delaux et al., 2012; Bythell-Douglas et al., 2017). Interestingly, the ability to perceive SLs has been proposed to have arisen at least additionally twice in the evolution of land plants, because both the moss *Physcomitrium patens* and the parasitic plant species from the Orobanchaceae family possess KAI2-like SL-sensitive receptors (Conn et al., 2015; Xu et al., 2018; Lopez-Obando et al., 2021).

Despite its ubiquity in land plant species, ligand perception by KAI2 is much less understood than that of D14. Although the Ser-His-Asp triad of KAI2 was found necessary for signaling and KAI2 displays hydrolytic activity toward GR24$^{ent\text{-}5DS}$, KARs are not susceptible to such hydrolysis (Scaffidi et al., 2012; Waters et al., 2015b; Yao et al., 2018). Additionally, the precise orientation in which KAR molecules bind in the catalytic pocket is inconsistent in crystal structures of different KAI2 homologs (Guo et al., 2013; Xu et al., 2016). As KARs also generally appeared unable to activate KAI2 in assays outside the plant cell, they have been suggested to require some unknown *in planta* metabolic steps to turn them into suitable KAI2 ligands (Guo et al., 2013; Nakamura et al., 2013; Waters et al., 2015a; Xu et al., 2016, 2018; Yao et al., 2018; Khosla et al., 2020; Wang et al., 2020b). Moreover, the currently reigning hypothesis states that both KARs and GR24$^{ent\text{-}5DS}$ are merely substitutes for endogenous KAI2 ligands (KLs; Waters et al., 2012; Conn and Nelson, 2016). Despite many independent lines of evidence supporting their existence, KLs have not been detected yet, and their nature is still unknown (Nelson et al., 2011; Conn et al., 2015; Waters et al., 2015b; Sun et al., 2016). Similar to D14, KAI2 is also subjected to ligand-induced degradation, but its degradation has been shown to be independent of MAX2 and the 26S proteasome (Chevalier et al., 2014; Waters et al., 2015a; Hu et al., 2017; Yao et al., 2018). For both receptors, the role this degradation plays in signaling is still unclear.

SMXL Proteins Regulate a Wide Variety of Physiological Processes

In *Arabidopsis*, the family of SMXLs consists of eight members, classified into four phylogenetic subclades, SMAX1/SMXL2, SMXL3, SMXL4/5, and SMXL6/7/8, which also largely correspond to their functions (Stanga et al., 2013; Moturu et al., 2018; Walker et al., 2019). SMXL6/7/8 are the target proteins first described as being ubiquitinated and degraded upon SL-activated D14-MAX2 signaling. This pathway regulates several physiological processes, including inhibition of shoot branching (Soundappan et al., 2015; Wang et al., 2015), cotyledon expansion (Soundappan et al., 2015) and lateral root outgrowth (Soundappan et al.,

TABLE 1 | Physiological functions of SMXL proteins with the corresponding core signaling pathways and the manner (positive or negative), in which the phenotype is regulated by the SMXLs.

General process	Phenotype	Pathway	Regulation	Species	References
Seed germination	Seed germination	KAI2; MAX2; SMAX1	–	Arabidopsis	Shen et al., 2007; Waters et al., 2012; Stanga et al., 2013
Seedling establishment	Hypocotyl elongation	D14; MAX2; SMAX1/SMXL2	+	Arabidopsis	Waters et al., 2012; Wang et al., 2020b; Li et al., 2022
	Hypocotyl elongation	KAI2; MAX2; SMAX1/SMXL2	+	Arabidopsis	Shen et al., 2007; Sun and Ni, 2011; Waters et al., 2012; Stanga et al., 2013
	Mesocotyl elongation	D14; MAX2; SMXL6/7/8	+	Rice	Kameoka and Kyozuka, 2015; Zheng et al., 2020
	Mesocotyl elongation	KAI2; MAX2; SMAX1	+	Rice	Kameoka and Kyozuka, 2015; Choi et al., 2020a; Zheng et al., 2020
	Cotyledon expansion	KAI2; MAX2; SMAX1/SMXL2	+/–[a]	Arabidopsis	Sun and Ni, 2011; Stanga et al., 2013, 2016
	Cotyledon expansion	D14; MAX2; SMXL6/7/(8)	+/–[a]	Arabidopsis	Waters et al., 2012; Soundappan et al.,2015
Shoot development	Shoot branching	D14; MAX2; SMXL6/7/8	+	Arabidopsis	Gomez-Roldan et al., 2008; Umehara et al., 2008; Waters et al., 2012; Soundappan et al., 2015; Wang et al., 2015
	Shoot branching	D14; MAX2; SMXL7	+	Pea	Gomez-Roldan et al., 2008; de Saint Germain et al., 2016; Kerr et al., 2021
	Shoot branching	SMAX1	–[b]	Arabidopsis	Zheng et al., 2021
	Tillering	D14; MAX2; SMXL6/7/8	+	Rice	Umehara et al., 2008; Arite et al., 2009; Jiang et al., 2013; Zhou et al., 2013
	Tillering	SMXL6/7/8	+[c]		Liu et al., 2017
	Branch angle	D14; MAX2; SMXL6/7/8	–	Arabidopsis	Liang et al., 2016
	Shoot elongation	D14; MAX2; SMXL6/7/8	–	Arabidopsis	Soundappan et al., 2015; Liang et al., 2016
	Secondary growth	D14; MAX2; SMXL(6)/7/(8)	-[b]	Arabidopsis	Agusti et al., 2011; Bennett et al., 2016; Liang et al., 2016
Leaf development	Leaf length	D14; MAX2; SMXL6/7/8	–	Arabidopsis	Scaffidi et al., 2013; Soundappan et al., 2015
	Leaf length	KAI2; MAX2; SMAX1	+	Arabidopsis	Soundappan et al., 2015
	Petiole length	D14; MAX2; SMXL6/7/8	+	Arabidopsis	Scaffidi et al., 2013; Soundappan et al., 2015
	Leaf width	KAI2; MAX2; SMAX1	+	Arabidopsis	Soundappan et al., 2015
	Leaf senescence	D14; MAX2; SMXL6/7/(8)	–	Arabidopsis	Woo et al., 2001; Ueda and Kusaba, 2015; Bennett et al., 2016
Root development	Lateral root formation	MAX2; SMXL6/7/8	+	Arabidopsis	Kapulnik et al., 2011; Ruyter-Spira et al., 2011; Soundappan et al.,2015; Villaécija-Aguilar et al.,2019
	Lateral root formation	KAI2; MAX2; SMAX1/SMXL2	+	Arabidopsis	Villaécija-Aguilar et al., 2019
	Root skewing angle	KAI2; MAX2; SMAX1/SMXL2 and SMXL6/7/8	+[d]	Arabidopsis	Swarbreck et al., 2019; Villaécija-Aguilar et al., 2019
	Root straightness	KAI2; MAX2; SMAX1/SMXL2	–	Arabidopsis	Swarbreck et al., 2019; Villaécija-Aguilar et al.,2019
	Root diameter	KAI2; MAX2; SMAX1	–	Arabidopsis	Swarbreck et al., 2019; Villaécija-Aguilar et al.,2019
	Root hair formation and elongation	KAI2; MAX2; SMAX1/SMXL2	–	Arabidopsis	Villaécija-Aguilar et al., 2019
	Root hair elongation	KAI2; MAX2; SMAX1	–	Lotus	Carbonnel et al., 2020
	Primary root elongation	KAI2; MAX2; SMAX1	+	Lotus	Carbonnel et al., 2020
Drought tolerance	Stomatal closure	D14; MAX2; SMXL6/7/8	–	Arabidopsis	Bu et al., 2014; Van Ha et al., 2014; Lv et al., 2017; Kalliola et al., 2020; Yang et al., 2020a

(Continued)

TABLE 1 | Continued

General process	Phenotype	Pathway	Regulation	Species	References
	Anthocyanin/flavonoid production	D14; MAX2; SMXL6/7/8	–	Arabidopsis	Brewer et al., 2009; Ito et al., 2015; Walton et al., 2016; Li et al., 2020; Struk et al., 2021
	Anthocyanin/flavonoid production	KAI2; MAX2; SMAX1/SMXL2	–	Arabidopsis	Li et al., 2017; Bursch et al., 2021
	Cuticle formation	MAX2; SMXL6/7/8	–	Arabidopsis	Bu et al., 2014; Li et al., 2020
Osmotic stress tolerance	Osmotic stress tolerance	KAI2; MAX2; SMAX1/SMXL2	–	Arabidopsis	Li et al., 2022
	Osmotic stress tolerance	D14; MAX2; SMAX1/SMXL2	-[e]	Arabidopsis	Li et al., 2022
Symbiosis	AM fungi colonization	KAI2; MAX2; SMAX1	–	Rice	Yoshida et al., 2012; Gutjahr et al., 2015; Choi et al., 2020a

[a]*Indications that different SMXLs regulate this phenotype oppositely.*
[b]*Phenotype only found when SMXL is overexpressed.*
[c]*No mutant phenotype, only protein interaction data and effect on SPL expression.*
[d]*Involvement of SMXL6/7/8 not consistent.*
[e]*Unexplained opposite phenotype of smax1/smxl2 and smxl6/7/8 mutants.*

2015; Villaécija-Aguilar et al., 2019); increase of branch angle (Liang et al., 2016) and leaf and petiole length (Soundappan et al., 2015); promotion of stem elongation (Soundappan et al., 2015; Liang et al., 2016), leaf senescence (Bennett et al., 2016) and secondary growth (Liang et al., 2016); and protection against drought stress through stomatal closure (Yang et al., 2020a), thickening of the cuticle and production of anthocyanins (**Figure 1**; **Table 1**; Li et al., 2020). The role for SMXL6/7/8 in shoot branching or tillering in monocotylednous plants, has been studied in several additional species, including rice, wheat (*Triticum aestivum*), and pea (*Pisum sativum*), suggesting that this role for SL signaling is conserved at least across angiosperms (Jiang et al., 2013; Zhou et al., 2013; Liu et al., 2017; Kerr et al., 2021). In apple (*Malus domestica*) and woodland strawberry (*Fragaria vesca*), SMXL6/7/8 has been inferred to play a role in abiotic stress and flower development respectively, although not yet confirmed by functional characterization (Li et al., 2018; Wu et al., 2019).

The KAI2-MAX2 signaling pathway has been proposed to only target SMAX1/SMXL2 for proteasomal degradation (Khosla et al., 2020; Wang et al., 2020b; Zheng et al., 2020). SMAX1 is directly involved in the regulation of seed germination (Stanga et al., 2013) and leaf development (Soundappan et al., 2015) and, together with SMXL2, in hypocotyl elongation (Stanga et al., 2013, 2016), lateral root density and root hair growth (Villaécija-Aguilar et al., 2019), and anthocyanin production (**Figure 1**; **Table 1**; Bursch et al., 2021). In lotus (*Lotus japonicus*), besides its role in KAI2-MAX2-SMAX1 signaling in root hair elongation, SMAX1 also seemingly regulates primary root length (Carbonnel et al., 2020). A new function for D14Like(OsKAI2)-D3(OsMAX2)-OsSMAX1 signaling was reported in rice, namely regulation of the arbuscular mycorrhizal fungi symbiosis establishment (Gutjahr et al., 2015; Choi et al., 2020a). Additionally, mesocotyl elongation in rice seedlings is also controlled by OsSMAX1, reminiscent of its influence on hypocotyl growth in *Arabidopsis* (Choi et al., 2020a; Zheng et al., 2020).

SMXL3/4/5 Function Independently From KAI2 and D14 Signaling

The third and fourth SMXL clade, containing SMXL3 and SMXL4/5, respectively, in *Arabidopsis*, is the least studied, and its involvement in primary phloem formation was discovered relatively recently (Wallner et al., 2017; Wu et al., 2017). In addition, SMXL4/5, but not SMXL3, regulate secondary phloem development during radial growth, pointing to a possible functional distinction between the SMXL3 and SMXL4/5 clade (Shi et al., 2019; Wallner et al., 2020). SMXL4 also plays additional roles in gibberellic acid- and light-dependent regulation of flowering and seed setting, as well as in drought stress tolerance (Yang et al., 2015, 2016, 2020b). Contrary to other SMXL family members in *Arabidopsis*, SMXL3/4/5 are not involved in either KL or SL signaling and are not subjected to MAX2-dependent degradation (Wallner et al., 2017). Even though members of this clade are found throughout seed plants, their physiological roles in species other than *Arabidopsis* remain to be discovered (Walker et al., 2019).

Functional Overlap Between SMXL Clades

Noteworthy, some phenotypes, such as leaf shape and lateral root density in *Arabidopsis*, and mesocotyl elongation in rice, are apparently under the control of both D14- and KAI2-dependent signaling, possibly to be interpreted as common outputs of the canonical D14-MAX2-SMXL6/7/8 and KAI2-MAX2-SMAX1/SMXL2 signaling complexes (Soundappan et al., 2015; Villaécija-Aguilar et al., 2019; Zheng et al., 2020). However, the attribution of a given SMXL subclade to either D14-MAX2 or KAI2-MAX2 partners might not be as clear-cut as initially thought. Indeed, the effect of KAI2 on root skewing depended on both SMAX1/SMXL2 and SMXL6/7/8, although these results were not consistent between different laboratories (Swarbreck et al., 2019; Villaécija-Aguilar et al., 2019). Also, D14-dependent inhibition of hypocotyl elongation was found to require SMAX1/SMXL2, rather than SMXL6/7/8 (**Figure 1**; **Table 1**; Wang

et al., 2020b; Li et al., 2022). This finding is important, but must nonetheless be taken with caution, because this conclusion was based on the use of a synthetic SL analog ($GR24^{4DO}$), and D14 signaling triggered by endogenous SLs is not involved in hypocotyl elongation (Nelson et al., 2011; Waters et al., 2012). However, recently, it was suggested that endogenous SLs might also employ D14-SMAX1/SMXL2 in another physiological context, namely the response to osmotic stress (Li et al., 2022).

Interestingly, in *Arabidopsis*, overaccumulation of SMAX1 could partly complement the increased shoot branching phenotype of *max2*, contrasting with the absence of a shoot branching phenotype in *smax1* (Zheng et al., 2021), but whether SMAX1 is involved in shoot branching regulation under physiological conditions remains to be seen. Along with the observation that AtSMAX1 is able to complement a *smxl45* double mutant, when expressed under the SMXL5 promoter, SMXL proteins from different subclades might possibly operate through a partially conserved mechanism/interaction network (Wallner et al., 2017).

Although knowledge on SMXL proteins is gradually increasing, several open questions on the activity and regulation of SMXLs still remain. The fact that SMXL3/4/5 are not subjected to MAX2-dependent degradation hints at the regulation of SMXL activity through another mechanism. Indeed, SMXL5 activity in sieve elements has been reported to be regulated at a translational level, through JULGI dependent formation of G-quadruplexes in *SMXL5* mRNA (Cho et al., 2018). However, it is not clear whether SMXL5 activity is controlled only in this manner and whether it is unique to SMXL3/4/5 or a general characteristic throughout the SMXL family. Additionally, novel insights on the physiological function of D14 and KAI2 signaling and their target SMXLs point toward an overlap and interaction between different SMXL clades, not yet recognized previously. Finally, the molecular mechanism by which SMXLs regulate physiological processes is still not completely uncovered. Through a compilation of recent findings on the phylogeny, activity, and regulation of SMXLs, we provide future cues to address the questions still surrounding these enigmatic proteins.

EVOLUTION AND PHYLOGENY OF SMXLs

Since the discovery of D53/SMXL proteins in rice (Jiang et al., 2013; Zhou et al., 2013; Zheng et al., 2020) and *Arabidopsis* (Stanga et al., 2013; Soundappan et al., 2015), SMXL family members have gradually been characterized in additional plant species, including wheat (Liu et al., 2017), apple (Li et al., 2018), woodland strawberry (Wu et al., 2019), lotus (Carbonnel et al., 2020), and pea (Kerr et al., 2021). Recent efforts to unravel the evolutionary history of this gene family have shown that SMXLs are both unique to and ubiquitously present in all land plants (**Figure 2A**; Walker et al., 2019). In angiosperms (a), SMXLs are grouped in four distinct clades, designated aSMAX1, aSMXL3/9, aSMXL4, and aSMXL7/8, which presumably arose from a single ancestral SMXL clade through two whole-genome duplication events, respectively at the origin of the seed plants and angiosperms (Moturu et al., 2018; Walker et al., 2019).

Based on genomic and *de novo* transcriptome assembly data from several species belonging to the bryophytes, lycophytes, and monilophytes, nonseed plants were concluded to generally possess only one ancestral SMXL clade, and most often a single *SMXL* copy (Walker et al., 2019). This ancestral SMXL is the most similar to the aSMAX1 clade and thought to be involved in the ancient KAI2-MAX2-dependent responses to KL (Bythell-Douglas et al., 2017; Walker et al., 2019). Recently, this hypothesis was supported by the discovery that in the liverwort *Marchantia polymorpha*, KAI2 and MAX2 homologs regulate thallus growth and gemma elongation through the degradation of the only SMXL homolog found in this species (Mizuno et al., 2021).

Despite the presence of the SL biosynthesis enzymes D27, CAROTENOID CLEAVAGE DIOXYGENASE (CCD) 7, CCD8, and MAX1 in most nonseed plants, the canonical SL receptor D14 is only found in seed plants (Bythell-Douglas et al., 2017; Walker et al., 2019), leading to the assumption that SLs first acted as symbiotic signals in the rhizosphere, rather than as plant development-regulating phytohormones (Kodama et al., 2021). Interestingly, most nonvascular land plants possess additional KAI2-like receptors, whereas in the moss *P. patens*, they appear to have evolved independently from D14 to act as SL receptors (Bythell-Douglas et al., 2017; Lopez-Obando et al., 2021). This SL sensitivity emergence in mosses is correlated with the acquisition of a second clade of SMXLs (Walker et al., 2019), allowing us to speculate that these additional SMXLs have been recruited as SL signaling targets (**Figure 2A**). Independently, a similar event has seemingly occurred at the origin of the angiosperms, when the SMAX1 lineage split into aSMAX1 and aSMXL7/8 (Walker et al., 2019). However, SL signaling in *P. patens* does not depend on MAX2, suggesting that this comparison is not entirely reliable and that functional examination of SMXL homologs in mosses is still needed to uncover their precise role (Lopez-Obando et al., 2021).

The currently designated canonical (i.e., D14- and MAX2-dependent) SL signaling has seemingly evolved at the source of the seed plants. Gymnosperms (g) only possess one gSMAX1 and one gSMXL4 clade, both originating from and very similar to the ancestral SMXL (Moturu et al., 2018; Walker et al., 2019). Based on data in angiosperms, the SMXL4 clade is not assumed to be involved in either KL or SL signaling, leading to the hypothesis that both pathways could target members of the gSMAX1 clade in gymnosperms (Wallner et al., 2017; Walker et al., 2019). This duplication of a single ancestral SMXL into a SMAX1 and SMXL4 correlates with the acquisition of two important traits, namely the formation of seeds and secondary growth (Linkies et al., 2010; Spicer and Groover, 2010; Walker et al., 2019). Especially interesting is that in *Arabidopsis* members of the SMAX1 clade are important for seed germination and seedling establishment, whereas the SMXL4 clade is involved in secondary phloem formation (Stanga et al., 2013; Shi et al., 2019; Wallner et al.,

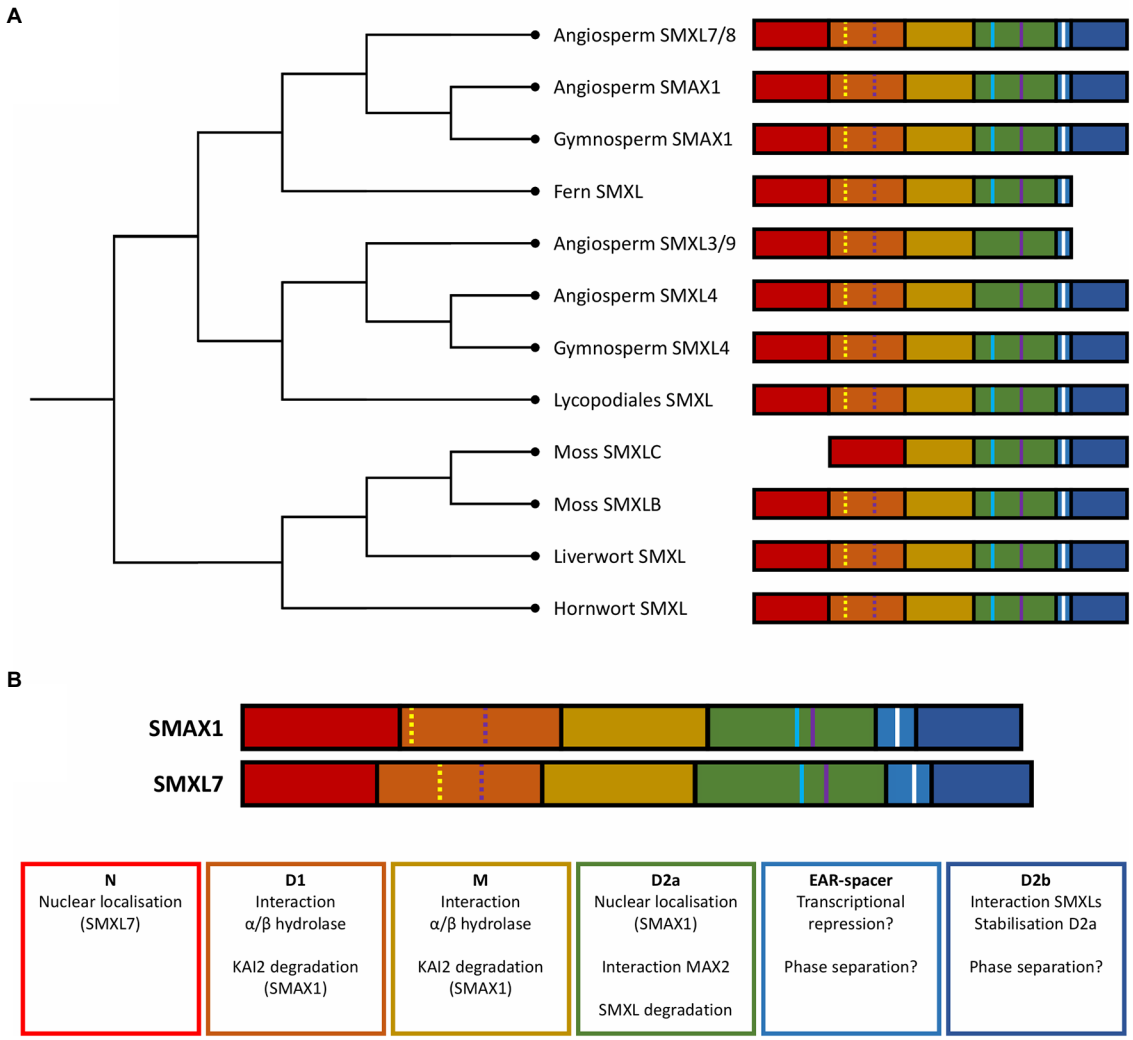

FIGURE 2 | Evolution and structure of SMXL proteins. **(A)** Dendrogram showing the phylogenetic relationships between the major SMXL clades in different land plants. **(B)** Function of the structural domains of *Arabidopsis* SMAX1 and SMXL7. Colored blocks represent structural domains: N domain (red), D1 domain (orange), M domain (yellow), D2 domain NTPase 1 (D2a; green), a spacer containing the EAR-motif (light blue), and D2 domain NTPase 2 (D2b; dark blue). Colored lines represent short amino acid motifs: Walker A motif (yellow line), Walker B motif (purple line), EAR motif (white), and RGKT motif (blue).

2020; Wang et al., 2020b). Hence, duplication and neofunctionalization of SMXLs might possibly have played a part in the development of these traits. Alternatively, because the main role of SMXL4 clade members apparently lies in vascular tissue formation (Wallner et al., 2017, 2020), we might consider that the SMXL4 clade possibly originated from subfunctionalization, rather than from neofunctionalization, and that the ancestral SMXL clade had already acquired a role in vascular development in Tracheophyta. To determine whether the SMXL4 clade or the other divisions of SMXLs in subclades originated through subfunctionalization or neofunctionalization, the recent, but still scarce, data on the SMXL phylogeny should be supplemented with functional insights into the roles of SMXLs in non-angiosperms.

A second whole-genome duplication at the origin of the angiosperms resulted in the further subdivision of the SMXL4 clade into aSMXL4 and aSMXL3/9. On the contrary, the SMAX1 clade diverged into aSMAX1, preserving its putative function in KL signaling, and aSMXL7/8, mainly functioning as targets for D14-dependent SL signaling. Further duplications of aSMXL7/8 and aSMXL3/9 in dicotyledonous plants resulted in SMXL7 and SMXL8, and SMXL3 and SMXL9, respectively. Finally, presumably at the origin of the Brassicaceae, SMXL2, SMXL6, and SMXL5 emerged from the dicot SMAX1, SMXL7, and SMXL4, respectively, together with the loss of SMXL9 leading to the SMXL diversity, as observed nowadays in *Arabidopsis* (Walker et al., 2019). Based on amino acid sequence identity, most of the divergence between different SMXL clades has been assumed to have happened during the evolution of angiosperms, possibly hinting at a need for neofunctionalization of these regulatory proteins (Walker et al., 2019).

SMXL ARE PLANT-SPECIFIC ATYPICAL Clp-ATPases

Early reports on SMXL proteins have highlighted that their domain organization and certain key motifs resembled that of members of the caseinolytic peptidase B (ClpB) ATPase family (Zhou et al., 2013). Clp proteins are present in all three domains of life: Bacteria, Archaea, and Eukaryotes. In bacteria, they are known to assemble in ATPase complexes that unfold proteins by using energy from ATP hydrolysis, functioning either as "proto-proteasomes" or chaperones in the removal of protein aggregates (Singh and Grover, 2010). Indeed, depending on the addition of an unrelated ClpP serine protease to the ATPase complex, unfolded proteins can subsequently be either degraded or refolded correctly (Kim et al., 2001).

Based on the presence of certain domains, Clp ATPase proteins can be divided in two distinct classes, but both classes contain a Clp-N domain at the N-terminus, apparently mainly involved in substrate recognition, often through the association with adaptor proteins, such as ClpS (Wojtyra et al., 2003; Mizuno et al., 2012; Zhang et al., 2012; Nishimura et al., 2013, 2015; Mishra and Grover, 2016). In class I Clp ATPases, the N-terminal domain is followed by two nucleotide-binding domains (NBDs), which are separated by a variable M domain. In contrast, class II Clp ATPases lack the M domain and contain only the C-terminal NBD2 (Kress et al., 2009). The NBDs are necessary for ATP hydrolysis and oligomerization in a hexameric pore complex and require two conserved motifs for their function, Walker A and Walker B (Gottesman et al., 1990; Schirmer et al., 1996). In addition, the NBD2 domain can also contain an IGF/L motif, the presence of which will grant the Clp ATPase the ability to interact with a ClpP protease, and thus to degrade the unfolded protein (Kim et al., 2001; Singh et al., 2001).

Besides SMXLs, plants possess three class I (ClpB, ClpC, and ClpD) and one class II (ClpX) Clp ATPase subtypes, as well as ClpP proteases and ClpS adaptors (Peltier et al., 2004). As previously shown for bacteria and yeast ClpB, plant ClpB proteins cannot interact with ClpP and are hence presumed to act exclusively as chaperones (Kim et al., 2001; Peltier et al., 2004). Indeed, in bacteria and eukaryotes, ClpB homologs are transcriptionally induced under heat shock conditions and they protect the cells against heat stress (Squires et al., 1991; Sanchez et al., 1992; Schirmer et al., 1994). Moreover, plant ClpB proteins can be cytosolic (Agarwal et al., 2002; Singh and Grover, 2010), whereas other Clp subtypes are generally localized to the chloroplasts or the mitochondria and contain a ClpP interaction motif (Nishimura and van Wijk, 2015). In these organelles, the ClpP complexes mainly perform a housekeeping function similar to that of the nuclear and cytoplasmic 26S proteasomes, i.e., the degradation of incorrectly neosynthesized proteins (Ali and Baek, 2020).

In SMXLs, the N-terminal domain containing a double Clp-N motif is globally conserved (**Figure 2B**; Jiang et al., 2013; Stanga et al., 2013; Zhou et al., 2013; Moturu et al., 2018; Walker et al., 2019). This is also true for NBD1 and NBD2 (D1 and D2), that also contain the Walker A and B motifs and are separated by an M domain (Soundappan et al., 2015; Moturu et al., 2018; Walker et al., 2019). The D2 domain, in turn, consists of two nucleoside-triphosphatase (NTPase) subdomains, with one most closely resembling the NBD of Clp ATPases. Characteristics that differentiate SMXL proteins from other Clp ATPases are the presence of an ETHYLENE-RESPONSE FACTOR Amphiphilic Repression (EAR) motif between the two NTPase subdomains in D2, as well as an elongated M domain (Jiang et al., 2013; Zhou et al., 2013; Soundappan et al., 2015).

SMXL proteins retain a domain organization and certain key motifs similar to ClpB proteins and also lack the IGF/L motif (Moturu et al., 2018). As such, SMXLs resemble more closely the ClpB ATPases, which act as chaperones rather than participating in proteolytic complexes, and, therefore, might potentially share the same molecular function. However, Clp ATPases have been shown to control a wide variety of processes, based on their diverging expression patterns and substrates (Frees et al., 2007; Nishimura and van Wijk, 2015). In general, chaperones can regulate transcription by influencing the late maturation steps of transcriptional regulators, effectively regulating their chromatin-binding ability (Morimoto, 2002; Cha et al., 2017; Roncarati and Scarlato, 2017; Gvozdenov et al., 2019). For instance, in rice, ClpB has been proposed to modulate gene expression through interaction with heat stress transcription factors (Singh et al., 2012). Similarly, SMXL proteins might be assumed to influence a transcriptional output through the stabilization of certain transcriptional regulators in an active conformation. Finally, like other Clp ATPases, SMXL proteins could function as hexameric chaperone complexes, as it was shown they can interact with each other (Liang et al., 2016; Khosla et al., 2020). The existence of such complexes has been suggested for SMXLs in rice, but further validation is still required (Ma et al., 2017).

At first sight, SMXLs seem to have diverged from their supposed ancestral role as ClpB chaperones. A possible chaperone activity for SMXLs has not yet been studied in detail, even though it could, for instance, account for the transcriptional regulation of target genes, as described above. As the molecular mechanism by which SMXLs function is still not completely resolved, research on the similarities and differences with Clp proteins might lead to new insights to address this question.

SMXL PROTEINS ARE COMPOSED OF STRUCTURAL AND FUNCTIONAL DOMAINS

As Clp proteins have been shown to be modular, with different structural domains responsible for diverse functional aspects of the proteins as a whole, it is interesting to examine the SMXL domains from the same perspective. Recently, different functional characteristics of AtSMAX1 have been attributed to certain parts of the protein (**Figure 2B**; Khosla et al., 2020). In short, the D1-M domain appears to be important for binding with D14 or KAI2 receptors, whereas the D2 domain is essential for KAR-induced degradation. In addition, the D2 domain can be divided into two functional subdomains that loosely correspond

to the two NTPase domains discussed above: D2a, which mainly determines the nuclear localization of SMAX1, and D2b, which is seemingly involved in the interaction between SMXL proteins and in the stabilization of D2a (Khosla et al., 2020).

The Function of a Conserved ClpN Domain Is Uncertain

Initially, the N domain of SMXLs was thought to enable nuclear localization, because nuclear localization signals (NLSs) are present in AtSMXL7 and OsSMAX1 (Liang et al., 2016; Choi et al., 2020a). Since SMXLs so far appear universally localized to the nucleus, this would fit the conservation of the N domain in these proteins (Zhou et al., 2013; Soundappan et al., 2015; Liang et al., 2016; Wallner et al., 2017; Khosla et al., 2020; Zheng et al., 2020; Mizuno et al., 2021). However, whereas the N domain has been demonstrated to be indeed responsible for the nuclear localization of AtSMXL7, the D2a domain seems to be necessary for the nuclear localization of AtSMAX1 (Liang et al., 2016; Khosla et al., 2020). Additionally, the N domain is broadly conserved among Clp ATPases as a whole, further hinting at additional roles, besides nuclear localization (Moturu et al., 2018).

The D1 and M Domains Interact With the Receptors

In general, the D1, and even more so the M domains are less conserved among the SMXL clades and, in AtSMAX1 and AtSMXL7, they were shown to be critical for the binding with KAI2 and D14, respectively (Walker et al., 2019; Khosla et al., 2020). Possibly, the variation in the clade-specific D1-M region arose either from the required interaction with the respective receptor, or from the putative absence of interaction with either, as can be hypothesized for AtSMXL3/4/5 due to their independence from both SL and KAR signaling (Wallner et al., 2017). The presence of intact AtSMAX1 proteins is needed for the MAX2-dependent degradation of the isolated $SMAX1_{D2}$ domain, suggesting that SMXL degradation only occurs when SMXLs can directly bind the KAI2 receptor *via* D1-M (Khosla et al., 2020). Additionally, the KAR-induced MAX2-independent degradation of KAI2 seems to require the presence of both SMAX1 and SMXL2, implying that the interaction between KAI2 and these SMXLs has an additional function in this process (Waters et al., 2015a; Khosla et al., 2020). A similar suggestion has been made after the discovery of a $KAI2^{D184N}$ mutant (*kai2-10*) in *Arabidopsis*, which is unable to induce downstream signaling and hypersensitive to the aforementioned MAX2-independent degradation (Yao et al., 2018). As D184 lies next to the D14-MAX2-binding interface in AtD14, *kai2-10* might also be defective in its ability to interact with MAX2. Moreover, it cannot be excluded that this mutation affects the presumed interaction between KAI2 and SMAX1 or SMXL2, leading to rapid degradation of $KAI2^{D184N}$ (Yao et al., 2018).

The D2a Domain Regulates SMXL Stability and Interaction With MAX2

The involvement of the D2 domain in the MAX2-dependent degradation of SMXLs can be attributed to the presence of the Walker A motif. D2-Walker A is required in several species for the degradation of SMAX1 (Khosla et al., 2020; Wang et al., 2020b; Zheng et al., 2020; Mizuno et al., 2021) and SMXL6/7/8 (Jiang et al., 2013; Zhou et al., 2013; Soundappan et al., 2015; Wang et al., 2015; Liang et al., 2016; Struk et al., 2018; Kerr et al., 2021). Several publications term this motif P-loop or (F)RGKT, according to its structure or its amino-acid sequence, respectively (Zhou et al., 2013; Soundappan et al., 2015; Wang et al., 2015; Liang et al., 2016; Struk et al., 2018). Interestingly, for rice D53, affinity pull-down and size exclusion chromatography revealed that the D2 domain can interact with the D14 receptor, but only in a complex with D3 (OsMAX2) and with an intact RGKT motif (Shabek et al., 2018), implying that the D2 domain contains the interaction interface between D53 and D3 and that the RGKT motif is part of this interface.

Interestingly, the importance of the RGKT-dependent interaction between SMXL and MAX2 mainly lies in the stabilization of the ternary complex, whereas the main driving interactions of the signaling complex formation occur between activated D14 and the other signaling components. Indeed, for D53 and D3, a *rac*-GR24-independent interaction was only demonstrated by *in vitro* studies (Jiang et al., 2013; Wang et al., 2015). Moreover, no direct *rac*-GR24 dependent interaction was shown between MAX2 and SMXL7 through FRET-FLIM, as was demonstrated for D14-MAX2 and D14-SMXL7 (Liang et al., 2016).

Additionally, the RGKT motif was proposed to destabilize AtSMAX1 in a MAX2-independent manner, by conferring an inherent instability to the protein or by subjecting it to an additional degradation pathway (Khosla et al., 2020). Other SMXL members are probably also degraded in a MAX2-independent manner, but the biological significance remains tentative and challenging to elucidate. We can speculate that the MAX2-independent control of the level of SMXLs in plant cells might possibly trigger the sensitivity for their further degradation in response to MAX2-dependent signaling.

SMXLs Act as Transcriptional Regulators Through an EAR Motif

Besides the RGKT motif, the D2 domain also contains the EAR motif that is conserved throughout all the SMXL clades (Moturu et al., 2018; Walker et al., 2019). The demonstrated purpose of this EAR motif is to enable interaction with proteins containing a C-terminal to Lissencephaly Homology (CTLH) domain (Szemenyei et al., 2008). In plants, CTLH domains are found in transcriptional corepressors, called TOPLESS (TPL)/TPL-Related (TPR), which associate with multiple transcription factors to regulate developmental processes, such as meristem maintenance, leaf growth and development, regulation of the circadian clock, seed germination, and stress response (reviewed in Plant et al., 2021). In hormone signaling pathways, at least for brassinosteroids, gibberellic acid, auxin, and jasmonate, recruitment of TPL/TPR has been shown to be a mechanism for repression of target genes (Szemenyei et al., 2008; Pauwels et al., 2010; Oh et al., 2014; Ryu et al., 2014; Fukazawa et al., 2015). TPL/TPR corepressors are proposed

to inhibit gene expression through association with histone deacetylase proteins, which induce compaction of chromatin and gene silencing (Krogan et al., 2012; Wang et al., 2013; Ryu et al., 2014).

Interaction with TPL/TPR proteins has been confirmed for rice D53 and *Arabidopsis* SMAX1 and SMXL6/7/8 (Causier et al., 2012; Jiang et al., 2013; Soundappan et al., 2015; Wang et al., 2015; Struk et al., 2018). Additionally, transcriptional activity assays in *Arabidopsis* protoplasts revealed that SMXL6/7/8 were able to repress gene expression in an EAR-dependent manner (Wang et al., 2015). This observation sparked the first hypotheses on the molecular mechanism by which SMXLs might regulate downstream effects, namely repression of gene expression by interaction with a transcription factor and recruitment of TPL/TPR corepressors to the promoter region of target genes. Later research confirmed the role of SMXLs as transcriptional regulators by indicating that SMXL6 can repress transcription factors that control the expression of *BRANCHED 1* (*BRC1*), *TCP DOMAIN PROTEIN 1*, and *PRODUCTION OF ANTHOCYANIN PIGMENT 1* genes, regulating shoot branching, leaf shape, and anthocyanin production (Wang et al., 2020a). SQUAMOSA PROMOTER BINDING PROTEIN-LIKE (SPL) 9 and SPL15 were identified as the transcription factors interacting with SMXL6/7/8 in the regulation of *BRC1* expression, mirroring the interaction of D53 with IDEAL PLANT ARCHITECTURE 1 (IPA1), also an SPL transcription factor, in rice (Song et al., 2017; Xie et al., 2020). In turn, because IPA1 induces the expression of *TEOSINTE BRANCHED 1* (*TB1*; *OsBRC1*), this pathway has been assumed to be conserved between rice and *Arabidopsis* (Lu et al., 2013). However, whereas interaction with IPA1 is also necessary for D53 to repress its own transcription, presumably through TPL/TPR as a feedback mechanism, AtSMXL6 was shown to bind directly to the promoters of *AtSMXL6/7/8* (Song et al., 2017; Wang et al., 2020a). A key difference between members of the monocotyledonous and dicotyledonous D53/SMXL6/7/8 clade is the presence of two predicted, monocotyledonous-specific EAR motifs, of which one interacts with TPL and TPR proteins (Jiang et al., 2013; Zhou et al., 2013; Ma et al., 2017; Moturu et al., 2018). The function of this second monocot-specific EAR motif, or its relation to differences in the SMXL mechanism in monocots and dicots has not been uncovered yet.

Besides a clear role for SMXLs as transcriptional repressors, SMXLs have also been suggested to function through other mechanisms. Indeed, not all the SMXL6/7/8 responses require the presence of an intact EAR motif (Liang et al., 2016). Additionally, SL-dependent inhibition of shoot branching has been suggested to be partly regulated by the localization of PINFORMED (PIN) proteins to the plasma membrane (Shinohara et al., 2013; Liang et al., 2016). As the effect on the PIN localization is not sensitive to treatment with cycloheximide treatment, it had initially been proposed to be a non-transcriptional output (Shinohara et al., 2013). However, more recent results hint at a more indirect regulation of the PIN localization by D14 and KAI2 signaling, thereby not ruling out that the direct output of the pathways is transcriptional (Zhang et al., 2020; Hamon-Josse et al., 2022). As such, whether SMXLs also regulate the signaling output in a nontranscriptional manner is not entirely clear. Interesting perspectives could be provided by unraveling the way in which SMXLs regulate EAR-independent phenotypes, such as shoot angle, petiole, and leaf blade length (Liang et al., 2016) or conversely whether nontranscriptional output requires the EAR motif or not. SMXLs have also been proposed to possibly regulate the PIN localization through their EAR motif-driven interaction with other CTLH-containing proteins that are involved in endocytosis (Kobayashi et al., 2007; Tomaštíková et al., 2012; Waldie et al., 2014). Additionally, we could hypothesize that SMXLs might influence events outside of the nucleus by targeting proteins that shuttle between the nucleus and the cytosol. Further exploration of SMXL protein interaction networks might help to assess this assumption.

The D2b Domain Confers Protein Stability and the Ability to Oligomerize

Finally, the C-terminal part of the D2 domain, termed as D2b, seemed important for the interaction between SMXLs in *Arabidopsis*, both for SMAX1, SMXL2, and SMXL7 (Khosla et al., 2020). SMXLs have been found to form homo-, heterodimers and possibly even hexamers (Liang et al., 2016; Ma et al., 2017). AtSMAX1 constructs containing D2a without D2b were apparently severely destabilized, even in the absence of exogenous treatment (Khosla et al., 2020). This observation implies that D2b-mediated oligomerization improves SMXL stability (Khosla et al., 2020).

The Functional Implications of Absent Domains or Motifs

Different aspects of SMXLs can be loosely attributed to the different recognized structural domains. In general, most SMXLs possess the same structural domains that differ in degree of conservation between different clades (Walker et al., 2019). However, some exceptions provide unique opportunities to enhance our understanding of the function of these separate domains (**Figure 2A**). Members of the aSMXL3/9 and aSMXL4 clade, for instance, lost their RGKT-motif (Moturu et al., 2018; Walker et al., 2019). In *Arabidopsis*, SMXL3/4/5 are indeed not degraded by addition of *rac*-GR24 and the process they regulate is unaffected in the *max2* mutant, demonstrating they are neither targets of SL/KL signaling nor of MAX2-dependent degradation (Wallner et al., 2017). Although the absence of the RGKT-motif seemingly abolishes the interaction between SMXLs and MAX2, the interaction between SMXLs and their respective α/β-hydrolase can presumably still occur when the D1-M domain is present, as demonstrated for $SMAX1^{D1\text{-}M}$ (Khosla et al., 2020). Noteworthy, α/β hydrolases belonging to the DLK23 clade, which are closely related to D14 and KAI2, are missing a canonical MAX2 interaction interface, and diverged from D14 at the origin of the seed plants, when also SMAX1 and SMXL4/5 diverged into separate clades (Bythell-Douglas et al., 2017; Végh et al., 2017; Walker et al., 2019). This lead to the hypothesis that the SMXL4 clade evolved as targets for these DLK23 receptors (Machin et al., 2020). In addition to

the absence of the RGKT motif, members of the aSMXL3/9 clade also appear to have lost their C-terminal domain. Based on the role of $SMAX1^{D2b}$, we can speculate that the loss of the D2b domain would render these SMXLs unable to oligomerize (Khosla et al., 2020). The D2b domain would also confer protein stability, but because of the RGKT motif absence, members of the aSMXL3/9 clade are presumably stabilized and protected from MAX2-independent degradation. In correlation with the missing D2b domain, AtSMXL3 is not completely functionally redundant to AtSMXL4 and AtSMXL5, and functions at different, though overlapping, stages in vascular development (Miyashima et al., 2019; Shi et al., 2019; Wallner et al., 2020).

Interestingly, SMXLs from ferns also lack a D2b domain but retain the RGKT motif (Walker et al., 2019). We could speculate that fern SMXLs are somehow stabilized, either through inherent, clade-specific features of the proteins, or by a difference in cellular context. Besides the presence of KAI2-MAX2 signaling components and SL biosynthesis genes, no information is available on the role and mechanism of SMXL proteins in ferns (Bythell-Douglas et al., 2017; Walker et al., 2019).

Finally, members of one of the SMXL clades in moss, dubbed SMXLC, lack the D1 domain (Walker et al., 2019), which might potentially correlate with a loss or change of their ability to interact with an α/β-hydrolase. Although KAI2-like receptors independently acquired SL sensitivity in *P. patens*, this SL perception and signaling occurs independently of PpMAX2 (Lopez-Obando et al., 2018, 2021). Although SMXLs would need their D1 domain in canonical SL signaling, the independently evolved SL signaling pathway in moss might also differ in this regard. Future research will teach us which specific role the different SMXLs play in KL and SL signaling pathways of these organisms and how the putative role of SMXLs in moss SL signaling differs from that in seed plants.

SMXLs MIGHT BE REGULATED THROUGH THEIR ABILITY TO ENTER BIOMOLECULAR CONDENSATES

SMXLs Participate in Subnuclear Condensates

Lately, the function and formation of cellular membraneless compartments has gained attention (Choi et al., 2020b). These compartments are commonly referred to as biomolecular condensates, because they represent a region of the nucleoplasm or cytosol, in which biomolecules, usually proteins and RNA, are spatially concentrated (Banani et al., 2017). Many types of condensates form through a physical process, called liquid–liquid phase separation (LLPS), in which a solution spontaneously demixes into two phases (Hyman et al., 2014; Choi et al., 2020b). Whether a protein can or will demix into a condensate is highly dependent on its properties and its concentration, as well as on the surrounding conditions, such as temperature and pH (Ruff et al., 2018). One of the general functions of condensate formation is to act as an integration point for environmental signals (Yoo et al., 2019). Additionally, these compartments sequester specific biomolecules, buffer biomolecule concentration, or concentrate components involved in a specific process (Cao et al., 2020; Pavlovic et al., 2020). Some condensates are commonly found in eukaryotic organisms, such as the nucleolus, nuclear speckles, Cajal bodies, and stress granules (Collier et al., 2006; Boisvert et al., 2007; Reddy et al., 2012; Cao et al., 2020). Plants additionally display specific condensates, including nuclear photobodies, AUXIN RESPONSE FACTOR 19/7 condensates in the cytosol of upper root cells, and condensates of FLOWERING LOCUS A in the nucleus (Van Buskirk et al., 2012; Fang et al., 2019; Powers et al., 2019).

Shortly after their discovery, some SMXL proteins were also found to be confined to distinct subnuclear condensates when transiently expressed in tobacco (*Nicotiana benthamiana*) leaves (Soundappan et al., 2015; Liang et al., 2016). To date, it is unclear whether this observation is an artifact due to protein tagging or overexpression, or also occurs in a physiological context. Either way, this aspect of SMXLs remains seriously understudied. Demonstration of a functional role for this subnuclear localization would open new interesting perspectives on the molecular mechanism by which SMXL proteins operate. Most importantly, it is still unknown whether SMXLs have the intrinsic ability to participate in LLPS, or whether SMXLs need to be localized in condensates to be functional, although their nuclear localization has been shown to be functionally relevant (Liang et al., 2016). Interestingly, AtSMAX1, AtSMXL7, and AtSMXL5 were shown to localize in nuclear condensates, suggesting that this characteristic is conserved across different SMXL clades, at least in angiosperms (Soundappan et al., 2015; Liang et al., 2016; Wallner et al., 2021). Whether this is true for all land plant species remains to be investigated, but the subnuclear localization of SMXLs might be an ancestral property. The remainder of this review will allude to speculative mechanisms by which SMXLs might form nuclear condensates and to some of possible functional implications.

Multivalent SMXL-TPL/TPR Complexes Might Drive Phase Separation

Interaction studies in tobacco leaves showed that AtSMXL7 is able to direct D14 to subnuclear condensates in a *rac*-GR24-dependent manner, implying this is where downstream SL signaling takes place (Liang et al., 2016). Additionally, the interaction of TPR2 with AtSMAX1 or AtSMXL7 also localizes to subnuclear condensates (Soundappan et al., 2015). Interestingly, a second EAR motif in rice D53 is able to simultaneously bind two TPR2 tetramers, of which each can interact with four EAR motifs (Ke et al., 2015; Ma et al., 2017). Multivalency is currently regarded as one of the main determining factors for biomolecules to phase-separate into condensates (Choi et al., 2020b). As D53 and TPR2 tetramers each have multiple interacting domains, they could potentially form multivalent units together, possibly forming higher-order aggregates (**Figure 3A**). Although the C-terminal EAR motif cannot bridge two TPR2 tetramers like the monocot-specific EAR motif, SMXLs have been proposed to be capable of interacting with each other as well and to form

dimers or even hexamers (Ma et al., 2017; Khosla et al., 2020). Hypothetically, as such, the lack of a second EAR motif would be complemented, still providing the SMXL-TPR2 complex with multivalent interaction interfaces (**Figure 3B**). We hypothesize that the transcriptional control exerted by SMXL through association with TPL proteins might involve SMXL and TPL acting in a condensate. Such a mechanism is not unprecedented, because the transcription factor TERMINATING FLOWER (TMF) has recently been discovered to require redox-regulated reversible phase separation to repress gene expression as a so-called transcriptional condensate (Huang et al., 2021). If transcriptional repression by SMXL also depends on their ability to group in condensates, this could represent an additional level of SMXL activity control, besides their degradation. Moreover, as SMXL7 exerts EAR-dependent and EAR-independent functions (Liang et al., 2016), it is tempting to hypothesize that these functions correspond, respectively, to SMXL7 acting in a condensate or as "free" SMXL7. Indeed, it was noted that shoot phenotypes sensitive to SMXL7 overexpression depended on an intact EAR motif (Liang et al., 2016). According to our hypothesis, these phenotypes might be induced by SMXL7 entering condensates, which under the conditions tested might require higher SMXL7 levels than those in the wild type, as well as an EAR motif. SMXL levels lower than those in the wild type would not further inhibit their ability to form a condensate nor cause a phenotype. Conversely, phenotypes only associated with reduced SMXL6/7/8 levels could be complemented by SMXL7, regardless of the presence of the EAR motif and these phenotypes were not as strongly affected by SMXL7 overexpression (Liang et al., 2016). As a possible explanation, we might presume that once condensation starts, levels of "free" SMXL7 are buffered by condensation, because all excess SMXL7 would enter the condensate.

Another property of SMXL proteins that could account for their presence in subnuclear condensates, is the occurrence of intrinsically disordered regions (IDRs). Intrinsically disordered proteins are characterized by their lack of a fixed three-dimensional structure and instead adopt a collection of different, dynamic conformations (Dunker et al., 2013). Noteworthy, protein disorder exists as a continuum and most proteins contain both folded domains and IDRs (Oates et al., 2013; van der Lee et al., 2014). Accordingly, IDR predictions extracted from the D^2P^2 database (discussed in Oates et al., 2013) reveal that in AtSMXLs and D53 the ordered D1, D2a, and D2b domains are generally separated by three IDRs corresponding to the M domain and a spacer between N and D1, and D2a and D2b, respectively, (**Figure 4**). Whereas protein disorder is not an absolute requirement for a protein to be part of a condensate, intrinsically disordered proteins are often driving LLPS (Posey et al., 2018; Martin and Holehouse, 2020). In proteins containing both ordered and disordered regions, the IDRs often confer the flexibility to a protein that is needed to engage in multiple dynamic interactions, using interaction interfaces that often reside in the folded domains (Choi et al., 2020b). Interestingly, the EAR motif is seemingly localized in the disordered spacer between D2a and D2b. As the EAR motif and the D2b domain are in close proximity, this flexible spacer might be essential to allow both interaction interfaces of SMXLs to aid in the formation of multivalent complexes with TPL/TPR.

SMXL Condensates Could Act as Signaling Hubs

As biomolecular condensates often exist as a collection of hundreds of different biomolecules, SMXLs, D14, and TPL/TPR might not be the only components of the observed subnuclear condensates (Saitoh et al., 2004; Hubstenberger et al., 2017; Kosmacz et al., 2019). This implies that SMXLs could rely on other, possibly still unknown, interactors to enter condensates and are not necessarily the driving force behind the formation of the condensates. The scaffold and client hypothesis describes that biomolecules that are not essentially multivalent and not driving LLPS, i.e., the client, can be recruited to biomolecular condensates through an interaction with multivalent LLPS-driving scaffold molecules (Banani et al., 2016). Regardless of whether SMXLs direct LLPS through interaction with TPL or other biomolecules, we could speculate that the recruitment to or expulsion from the observed subnuclear condensates could act as an independent mechanism to modulate the SMXL activity in addition to proteasomal degradation. As addition of *rac*-GR24 does not seem to affect the SMXL7 localization into nuclear condensates (Liang et al., 2016), this added level of control might be employed by other signaling pathways, i.e., SMXLs might function as hubs for additional developmental environmental cues. SMXLs could thus perform a similar function as DELLA proteins, the primary repressors in the gibberellic acid signaling pathway, which had been shown to act as an integration point for almost all plant hormones (reviewed in Davière and Achard, 2016). Moreover, whereas the canonical gibberellic acid signaling pathway mainly regulates DELLA activity through proteasomal degradation, certain posttranslational modifications (PTMs), such as phosphorylation, sumoylation, and glycosylation, can also modulate DELLA functions, for example, in the drought stress response (reviewed in Blanco-Touriñán et al., 2020). For SMXLs, the functional importance of PTMs, other than ubiquitination, has not been investigated in detail, although proteomics experiments have revealed that several SMXLs in *Arabidopsis*, as well as rice D53, contain phosphorylated and sumoylated sites (**Figure 4**; Roitinger et al., 2015; Hou et al., 2017; Rytz et al., 2018; Mergner et al., 2020). Interestingly, the phosphorylation sites of SMXLs appear to be mainly localized in regions predicted to be IDRs, indicating that these IDRs, besides or instead of a potential role in LLPS, could also facilitate access to phosphorylation sites (van der Lee et al., 2014).

PERSPECTIVES AND CONCLUDING REMARKS

To start comprehending the understudied role of SMXLs in condensates and to test the proposed hypotheses, it is essential to first study the nature of these SMXL condensates. Most importantly, evidence that naturally expressed SMXLs enter subnuclear speckles in a physiological context is still missing. Importantly, whether SMXL-containing compartments overlap with known nuclear condensates is still unknown but could be investigated by means of colocalization with proteins known to localize to specific types of condensates. Additionally, assays

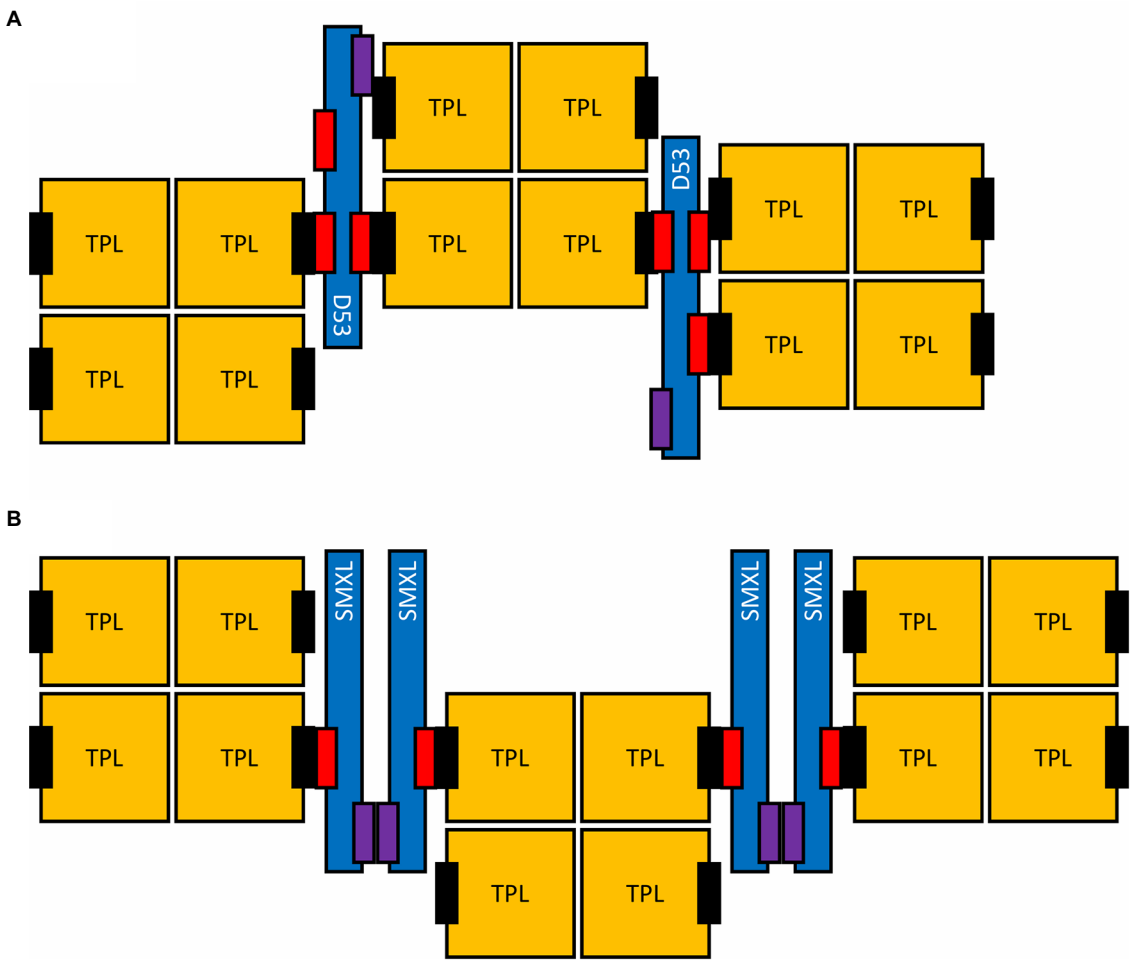

FIGURE 3 | Possible higher-order assembly of SMXL proteins and TPL tetramers. Two alternative assemblies are shown, either specific for monocotyledous D53 **(A)** or for SMXLs in general **(B)**. The EAR motifs (red) and the putative oligomerization interface on SMXL proteins (purple), as well as the CTLH domain of TPL proteins (black) are indicated.

have been developed to demonstrate whether a protein displays LLPS *in vitro*, which could help to detect whether SMXLs also drive LLPS, possibly in the presence of additional biomolecules or compounds, or under specific conditions. Additionally, interactomics experiments could help functionally to characterize SMXL condensates, hence uncovering possible interactions with proteins identified to localize to condensates and to drive LLPS. Finally, detailed localization studies could discover the specific circumstances in which SMXLs adopt this localization and the necessary protein domains or motifs. An interesting aspect of SMXLs to assess is their PTM landscape, both in relation to their subnuclear localization and their general function. Despite the identification of PTMs for some *Arabidopsis* SMXLs, very little is known on their impact on the SMXL function. This interesting, but understudied aspect of SMXLs, might very well provide the perspectives necessary to fill some holes in our knowledge of these puzzling proteins.

In conclusion, the rapid accumulation of insights on SMXL proteins opens a lot of interesting avenues to be studied. The characterization of functional domains in AtSMAX1 and AtSMXL7, as well as in SMXL homologs in other plant species that apparently lack one of these domains, could allow us to separately study the functional aspects of SMXLs that correspond to these distinct domains. Additionally, although functional insights on SMXLs in several angiosperm species are uncovered, they are still lacking in non-angiosperms, leaving an unexplored source of knowledge on these perplexing proteins. Research on the similarities and differences between SMXLs across land plants might ultimately help us to understand their array of physiological roles and molecular mechanisms.

Two understudied aspects of SMXLs remain their similarity to Clp ATPases and their localization to subnuclear condensates, which might be more relevant than has been appreciated thus far. As chaperones, SMXLs could regulate responses of the plant cell through the modulation of a wide array of target proteins, including transcriptional regulators. As members of biomolecular condensates, SMXLs could come in contact with multiple other factors, possibly functioning as integration points

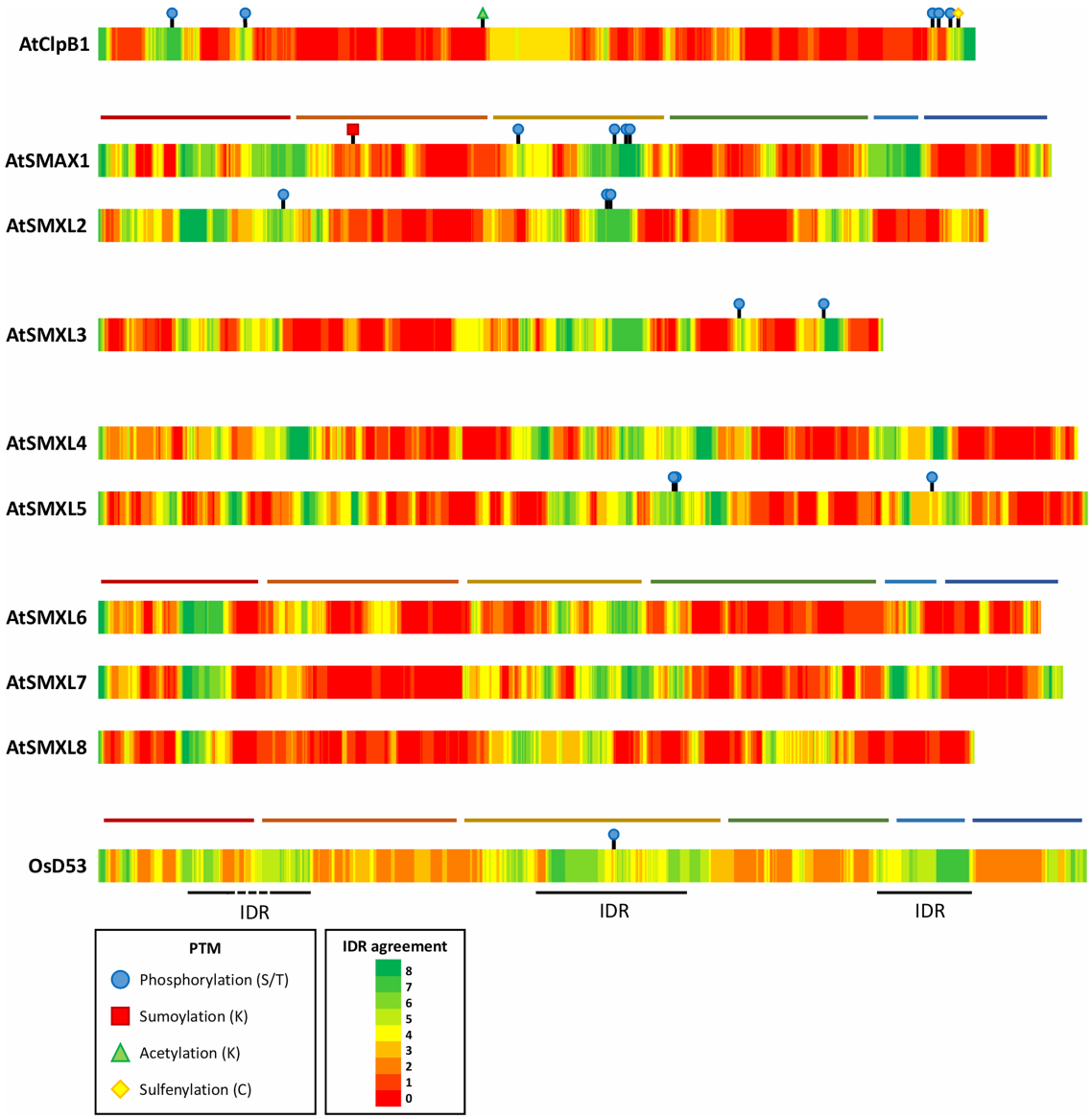

FIGURE 4 | Posttranslational modifications and predicted disordered regions in *Arabidopsis* SMXLs, ClpB1, and rice D53. Predicted intrinsically disordered regions (IDRs) were acquired from different prediction tools collected by the D^2P^2 database (Oates et al., 2013). Per amino acid, how many prediction tools agree on the disorder are color indicated. When available, experimentally verified PTMs were obtained from the PTM viewer and displayed on the corresponding locations on the proteins (Willems et al., 2019). The domain structure of AtSMAX1, AtSMXL7 and OsD53 was added represented by horizontal, colored lines: N domain (red), D1 domain (orange), M domain (yellow), D2 domain NTPase 1 (D2a; green), a spacer containing the EAR-motif (light blue), and D2 domain NTPase 2 (D2b; dark blue).

for more than one signaling pathway. Moreover, switching between the context of the nucleoplasm and a condensate might be an additional mechanism by which the SMXL function is regulated. The overview we provided might provide new avenues for the next steps in SMXL research.

AUTHOR CONTRIBUTIONS

AT was the main author of the manuscript. AG made significant contributions, especially to the second part of the review (SMXL Are Plant-Specific Atypical Clp-ATPases). AT, AG, SB, SG, and SS conceived and initiated the review and were involved in drafting and critically revising the manuscript. All authors contributed to the article and approved the submitted version.

FUNDING

AT is indebted to the Research Foundation-Flanders for a predoctoral fellowship (3S015819). AG, SG, and SB acknowledge the support of Tournesol (Communauté Flandres-France) program N° 40660PF. The IJPB benefits from the support of Saclay Plant Sciences-SPS (ANR-17-EUR-0007).

REFERENCES

Agarwal, M., Katiyar-Agarwal, S., and Grover, A. (2002). Plant Hsp100 proteins: structure, function and regulation. *Plant Sci.* 163, 397–405. doi: 10.1016/S0168-9452(02)00209-1

Ali, M. S., and Baek, K.-H. (2020). Protective roles of cytosolic and plastidal proteasomes on abiotic stress and pathogen invasion. *Plan. Theory* 9:832. doi: 10.3390/plants9070832

Aquino, B., Bradley, J. M., and Lumba, S. (2021). On the outside looking in: roles of endogenous and exogenous strigolactones. *Plant J.* 105, 322–334. doi: 10.1111/tpj.15087

Arite, T., Umehara, M., Ishikawa, S., Hanada, A., Maekawa, M., Yamaguchi, S., et al. (2009). *d14*, a Strigolactone-Insensitive Mutant of Rice, Shows an Accelerated Outgrowth of Tillers. *Plant Cell Physiol.* 50, 1416–1424. doi: 10.1093/pcp/pcp091

Agusti, J., Herold, S., Schwarz, M., Sanchez, P., Ljung, K., Dun, E. A., et al. (2011). Strigolactone signaling is required for auxin-dependent stimulation of secondary growth in plants. *Proc. Natl. Acad. Sci. USA* 108, 20242–20247. doi: 10.1073/pnas.1111902108

Banani, S. F., Lee, H. O., Hyman, A. A., and Rosen, M. K. (2017). Biomolecular condensates: organizers of cellular biochemistry. *Nat. Rev. Mol. Cell Biol.* 18, 285–298. doi: 10.1038/nrm.2017.7

Banani, S. F., Rice, A. M., Peeples, W. B., Lin, Y., Jain, S., Parker, R., et al. (2016). Compositional control of phase-separated cellular bodies. *Cell* 166, 651–663. doi: 10.1016/j.cell.2016.06.010

Bennett, T., Liang, Y., Seale, M., Ward, S., Müller, D., and Leyser, O. (2016). Strigolactone regulates shoot development through a core signalling pathway. *Biol. Open* 5, 1806–1820. doi: 10.1242/bio.021402

Blanco-Touriñán, N., Serrano-Mislata, A., and Alabadí, D. (2020). Regulation of DELLA proteins by post-translational modifications. *Plant Cell Physiol.* 61, 1891–1901. doi: 10.1093/pcp/pcaa113

Boisvert, F.-M., van Koningsbruggen, S., Navascués, J., and Lamond, A. I. (2007). The multifunctional nucleolus. *Nat. Rev. Mol. Cell Biol.* 8, 574–585. doi: 10.1038/nrm2184

Bouwmeester, H., Li, C., Thiombiano, B., Rahimi, M., and Dong, L. (2021). Adaptation of the parasitic plant lifecycle: germination is controlled by essential host signaling molecules. *Plant Physiol.* 185, 1292–1308. doi: 10.1093/plphys/kiaa066

Brewer, P. B., Dun, E. A., Ferguson, B. J., Rameau, C., and Beveridge, C. A. (2009). Strigolactone acts downstream of auxin to regulate bud outgrowth in pea and Arabidopsis. *Plant Physiol.* 150, 482–493. doi: 10.1104/pp.108.134783

Bu, Q., Lv, T., Shen, H., Luong, P., Wang, J., Wang, Z., et al. (2014). Regulation of drought tolerance by the F-box protein MAX2 in Arabidopsis. *Plant Physiol.* 164, 424–439. doi: 10.1104/pp.113.226837

Bürger, M., and Chory, J. (2020). The many models of strigolactone signaling. *Trends Plant Sci.* 25, 395–405. doi: 10.1016/j.tplants.2019.12.009

Bursch, K., Niemann, E. T., Nelson, D. C., and Johansson, H. (2021). Karrikins control seedling photomorphogenesis and anthocyanin biosynthesis through a HY5-BBX transcriptional module. *Plant J.* 107, 1346–1362. doi: 10.1111/tpj.15383

Bythell-Douglas, R., Rothfels, C. J., Stevenson, D. W. D., Graham, S. W., Wong, G. K.-S., Nelson, D. C., et al. (2017). Evolution of strigolactone receptors by gradual neo-functionalization of KAI2 paralogues. *BMC Biol.* 15:52. doi: 10.1186/s12915-017-0397-z

Cao, X., Jin, X., and Liu, B. (2020). The involvement of stress granules in aging and aging-associated diseases. *Aging Cell* 19:e13136. doi: 10.1111/acel.13136

Carbonnel, S., Das, D., Varshney, K., Kolodziej, M. C., Villaécija-Aguilar, J. A., and Gutjahr, C. (2020). The karrikin signaling regulator SMAX1 controls *Lotus japonicus* root and root hair development by suppressing ethylene biosynthesis. *Proc. Natl. Acad. Sci. U. S. A.* 117:21757–21765. doi: 10.1073/pnas.2006111117

Causier, B., Ashworth, M., Guo, W., and Davies, B. (2012). The TOPLESS interactome: a framework for gene repression in Arabidopsis. *Plant Physiol.* 158, 423–438. doi: 10.1104/pp.111.186999

Cha, J.-Y., Kim, J., Kim, T.-S., Zeng, Q., Wang, L., Lee, S. Y., et al. (2017). GIGANTEA is a co-chaperone which facilitates maturation of ZEITLUPE in the *Arabidopsis* circadian clock. *Nat. Commun.* 8:3. doi: 10.1038/s41467-016-0014-9

Chevalier, F., Nieminen, K., Sánchez-Ferrero, J. C., Rodríguez, M. L., Chagoyen, M., Hardtke, C. S., et al. (2014). Strigolactone promotes degradation of DWARF14, an α/β hydrolase essential for strigolactone signaling in *Arabidopsis*. *Plant Cell* 26, 1134–1150. doi: 10.1105/tpc.114.122903

Cho, H., Cho, H. S., Nam, H., Jo, H., Yoon, J., Park, C., et al. (2018). Translational control of phloem development by RNA G-quadruplex–JULGI determines plant sink strength. *Nat. Plants* 4, 376–390. doi: 10.1038/s41477-018-0157-2

Choi, J.-M., Holehouse, A. S., and Pappu, R. V. (2020b). Physical principles underlying the complex biology of intracellular phase transitions. *Annu. Rev. Biophys.* 49, 107–133. doi: 10.1146/annurev-biophys-121219-081629

Choi, J., Lee, T., Cho, J., Servante, E. K., Pucker, B., Summers, W., et al. (2020a). The negative regulator SMAX1 controls mycorrhizal symbiosis and strigolactone biosynthesis in rice. *Nat. Commun.* 11:2114. doi: 10.1038/s41467-020-16021-1

Collier, S., Pendle, A., Boudonck, K., van Rij, T., Dolan, L., and Shaw, P. (2006). A distant coilin homologue is required for the formation of Cajal bodies in *Arabidopsis*. *Mol. Biol. Cell* 17, 2942–2951. doi: 10.1091/mbc.e05-12-1157

Conn, C. E., Bythell-Douglas, R., Neumann, D., Yoshida, S., Whittington, B., Westwood, J. H., et al. (2015). Convergent evolution of strigolactone perception enabled host detection in parasitic plants. *Science* 349, 540–543. doi: 10.1126/science.aab1140

Conn, C. E., and Nelson, D. C. (2016). Evidence that KARRIKIN-INSENSITIVE2 (KAI2) receptors may perceive an unknown signal that is not karrikin or strigolactone. *Front. Plant Sci.* 6:1219. doi: 10.3389/fpls.2015.01219

Davière, J.-M., and Achard, P. (2016). A pivotal role of DELLAs in regulating multiple hormone signals. *Mol. Plant* 9, 10–20. doi: 10.1016/j.molp.2015.09.011

De Cuyper, C., Struk, S., Braem, L., Gevaert, K., De Jaeger, G., and Goormachtig, S. (2017). Strigolactones, karrikins and beyond. *Plant Cell Environ.* 40, 1691–1703. doi: 10.1111/pce.12996

de Saint Germain, A., Clavé, G., Badet-Denisot, M.-A., Pillot, J.-P., Cornu, D., Le Caer, J.-P., et al. (2016). An histidine covalent receptor and butenolide complex mediates strigolactone perception. *Nat. Chem. Biol.* 12, 787–794. doi: 10.1038/nchembio.2147

Delaux, P.-M., Xie, X., Timme, R. E., Puech-Pages, V., Dunand, C., Lecompte, E., et al. (2012). Origin of strigolactones in the green lineage. *New Phytol.* 195, 857–871. doi: 10.1111/j.1469-8137.2012.04209.x

Dunker, A. K., Babu, M. M., Barbar, E., Blackledge, M., Bondos, S. E., Dosztányi, Z., et al. (2013). What's in a name? Why these proteins are intrinsically disordered. *Intrinsically Disord. Proteins* 1:e24157. doi: 10.4161/idp.24157

Fang, X., Wang, L., Ishikawa, R., Li, Y., Fiedler, M., Liu, F., et al. (2019). *Arabidopsis* FLL2 promotes liquid–liquid phase separation of polyadenylation complexes. *Nature* 569, 265–269. doi: 10.1038/s41586-019-1165-8

Flematti, G. R., Ghisalberti, E. L., Dixon, K. W., and Trengove, R. D. (2004). A compound from smoke that promotes seed germination. *Science* 305:977. doi: 10.1126/science.1099944

Flematti, G. R., Scaffidi, A., Waters, M. T., and Smith, S. M. (2016). Stereospecificity in strigolactone biosynthesis and perception. *Planta* 243, 1361–1373. doi: 10.1007/s00425-016-2523-5

Frees, D., Savijoki, K., Varmanen, P., and Ingmer, H. (2007). Clp ATPases and ClpP proteolytic complexes regulate vital biological processes in low GC, gram-positive bacteria. *Mol. Microbiol.* 63, 1285–1295. doi: 10.1111/j.1365-2958.2007.05598.x

Fukazawa, J., Ito, T., Kamiya, Y., Yamaguchi, S., and Takahashi, Y. (2015). Binding of GID1 to DELLAs promotes dissociation of GAF1 from DELLA in GA dependent manner. *Plant Signal. Behav.* 10:e1052923. doi: 10.1080/15592324.2015.1052923

Gomez-Roldan, V., Fermas, S., Brewer, P., Virginie Puech-Pagès, V., Dun, E. A., Pillot, J.-P., et al. (2008). Strigolactone inhibition of shoot branching. *Nature* 455, 189–194. doi: 10.1038/nature07271

Gottesman, S., Clark, W. P., and Maurizi, M. R. (1990). The ATP-dependent Clp protease of *Escherichia coli*. Sequence of *clpA* and identification of a Clp-specific substrate. *J. Biol. Chem.* 265, 7886–7893. doi: 10.1016/S0021-9258(19)39014-3

Guo, Y., Zheng, Z., La Clair, J. J., Chory, J., and Noel, J. P. (2013). Smoke-derived karrikin perception by the α/β-hydrolase KAI2 from *Arabidopsis*. *Proc. Natl. Acad. Sci. U. S. A.* 110, 8284–8289. doi: 10.1073/pnas.1306265110

Gutjahr, C., Gobbato, E., Choi, J., Riemann, M., Johnston, M. G., Summers, W., et al. (2015). Rice perception of symbiotic arbuscular mycorrhizal fungi requires the karrikin receptor complex. *Science* 350, 1521–1524. doi: 10.1126/science.aac9715

Gvozdenov, Z., Bendix, L. D., Kolhe, J., and Freeman, B. C. (2019). The Hsp90 molecular chaperone regulates the transcription factor network controlling chromatin accessibility. *J. Mol. Biol.* 431, 4993–5003. doi: 10.1016/j.jmb.2019.09.007

Ha, C. V., Leyva-González, M. A., Osakabe, Y., Tran, U. T., Nishiyama, R., Watanabe, Y., et al. (2014). Positive regulatory role of strigolactone in plant responses to drought and salt stress. *Proc. Natl. Acad. Sci. U. S. A.* 111, 851–856. doi: 10.1073/pnas.1322135111

Hamiaux, C., Drummond, R. S. M., Janssen, B. J., Ledger, S. E., Cooney, J. M., Newcomb, R. D., et al. (2012). DAD2 is an α/β hydrolase likely to be involved in the perception of the plant branching hormone, strigolactone. *Curr. Biol.* 22, 2032–2036. doi: 10.1016/j.cub.2012.08.007

Hamon-Josse, M., Villaécija-Aguilar, J. A., Ljung, K., Leyser, O., Gutjahr, C., and Bennett, T. (2022). KAI2 regulates seedling development by mediating light-induced remodelling of auxin transport. *New Phytol.* 234. doi: 10.1111/nph.18110 (in press).

Hou, Y., Qiu, J., Wang, Y., Li, Z., Zhao, J., Tong, X., et al. (2017). A quantitative proteomic analysis of brassinosteroid-induced protein phosphorylation in rice (*Oryza sativa* L.). *Front. Plant Sci.* 8:514. doi: 10.3389/fpls.2017.00514

Hu, Q., He, Y., Wang, L., Liu, S., Meng, X., Liu, G., et al. (2017). DWARF14, a receptor covalently linked with the active form of strigolactones, undergoes strigolactone-dependent degradation in rice. *Front. Plant Sci.* 8:1935. doi: 10.3389/fpls.2017.01935

Huang, X., Chen, S., Li, W., Tang, L., Zhang, Y., Yang, N., et al. (2021). ROS regulated reversible protein phase separation synchronizes plant flowering. *Nat. Chem. Biol.* 17, 549–557. doi: 10.1038/s41589-021-00739-0

Hubstenberger, A., Courel, M., Bénard, M., Souquere, S., Ernoult-Lange, M., Chouaib, R., et al. (2017). P-body purification reveals the condensation of repressed mRNA regulons. *Mol. Cell* 68, 144–157. doi: 10.1016/j.molcel.2017.09.003

Hyman, A. A., Weber, C. A., and Jülicher, F. (2014). Liquid-liquid phase separation in biology. *Annu. Rev. Cell Dev. Biol.* 30, 39–58. doi: 10.1146/annurev-cellbio-100913-013325

Ito, S., Nozoye, T., Sasaki, E., Imai, M., Shiwa, Y., Shibata-Hatta, M., et al. (2015). Strigolactone regulates anthocyanin accumulation, acid phosphatases production and plant growth under low phosphate condition in *Arabidopsis*. *PLoS One* 10:e0119724. doi: 10.1371/journal.pone.0119724

Jiang, L., Liu, X., Xiong, G., Liu, H., Chen, F., Wang, L., et al. (2013). DWARF 53 acts as a repressor of strigolactone signalling in rice. *Nature* 504, 401–405. doi: 10.1038/nature12870

Kalliola, M., Jakobson, L., Davidsson, P., Pennanen, V., Waszczak, C., Yarmolinsky, D., et al. (2020). Differential role of MAX2 and strigolactones in pathogen, ozone, and stomatal responses. *Plant Direct* 4:e00206. doi: 10.1002/pld3.206

Kameoka, H., and Kyozuka, J. (2015). Downregulation of Rice DWARF 14 LIKE Suppress Mesocotyl Elongation via a Strigolactone Independent Pathway in the Dark. *J Genet. Genomics* 42, 119–124. doi: 10.1016/j.jgg.2014.12.003

Kapulnik, Y., Delaux, P.-M., Resnick, N., Mayzlish-Gati, E., Wininger, S., Bhattacharya, C., et al. (2011). Strigolactones affect lateral root formation and root-hair elongation in *Arabidopsis*. *Planta* 233, 209–216. doi: 10.1007/s00425-010-1310-y

Ke, J., Ma, H., Gu, X., Thelen, A., Brunzelle, J. S., Li, J., et al. (2015). Structural basis for recognition of diverse transcriptional repressors by the TOPLESS family of corepressors. *Sci. Adv.* 1:e1500107. doi: 10.1126/sciadv.1500107

Kerr, S. C., Patil, S. B., de Saint Germain, A., Pillot, J.-P., Saffar, J., Ligerot, Y., et al. (2021). Integration of the SMXL/D53 strigolactone signalling repressors in the model of shoot branching regulation in *Pisum sativum*. *Plant J.* 107, 1756–1770. doi: 10.1111/tpj.15415

Khosla, A., Morffy, N., Li, Q., Faure, L., Chang, S. H., Yao, J., et al. (2020). Structure–function analysis of SMAX1 reveals domains that mediate its karrikin-induced proteolysis and interaction with the receptor KAI2. *Plant Cell* 32, 2639–2659. doi: 10.1105/tpc.19.00752

Kim, Y.-I., Levchenko, I., Fraczkowska, K., Woodruff, R. V., Sauer, R. T., and Baker, T. A. (2001). Molecular determinants of complex formation between Clp/Hsp100 ATPases and the ClpP peptidase. *Nat. Struct. Biol.* 8, 230–233. doi: 10.1038/84967

Kobayashi, N., Yang, J., Ueda, A., Suzuki, T., Tomaru, K., Takeno, M., et al. (2007). RanBPM, Muskelin, p48EMLP, p44CTLH, and the armadillo-repeat proteins ARMC8α and ARMC8β are components of the CTLH complex. *Gene* 396, 236–247. doi: 10.1016/j.gene.2007.02.032

Kodama, K., Rich, M. K., Yoda, A., Shimazaki, S., Xie, X., Akiyama, K., et al. (2021). An ancestral function of strigolactones as symbiotic rhizosphere signals. bioRxiv [Preprint]. 2021, 2021.2008.2020.457034. doi: 10.1101/2021.08.20.457034

Kosmacz, M., Gorka, M., Schmidt, S., Luzarowski, M., Moreno, J. C., Szlachetko, J., et al. (2019). Protein and metabolite composition of Arabidopsis stress granules. *New Phytol.* 222, 1420–1433. doi: 10.1111/nph.15690

Kress, W., Maglica, Ž., and Weber-Ban, E. (2009). Clp chaperone–proteases: structure and function. *Res. Microbiol.* 160, 618–628. doi: 10.1016/j.resmic.2009.08.006

Krogan, N. T., Hogan, K., and Long, J. A. (2012). APETALA2 negatively regulates multiple floral organ identity genes in *Arabidopsis* by recruiting the co-repressor TOPLESS and the histone deacetylase HDA19. *Development* 139, 4180–4190. doi: 10.1242/dev.085407

Lanfranco, L., Fiorilli, V., Venice, F., and Bonfante, P. (2018). Strigolactones cross the kingdoms: plants, fungi, and bacteria in the arbuscular mycorrhizal symbiosis. *J. Exp. Bot.* 69, 2175–2188. doi: 10.1093/jxb/erx432

Li, R., An, J.-P., You, C.-X., Wang, X.-F., and Hao, Y.-J. (2018). Genome-wide analysis and identification of the *SMXL* gene family in apple (*Malus* × *domestica*). *Tree Genet. Genomes* 14:61. doi: 10.1007/s11295-018-1275-8

Li, W., Nguyen, K. H., Chu, H. D., Ha, C. V., Watanabe, Y., Osakabe, Y., et al. (2017). The karrikin receptor KAI2 promotes drought resistance in *Arabidopsis thaliana*. *PLoS Genet.* 13:e1007076. doi: 10.1371/journal.pgen.1007076

Li, W., Nguyen, K. H., Tran, C. D., Watanabe, Y., Tian, C., Yin, X., et al. (2020). Negative roles of strigolactone-related SMXL6, 7 and 8 proteins in drought resistance in *Arabidopsis*. *Biomol. Ther.* 10:607. doi: 10.3390/biom10040607

Li, Q., Sánchez Martín-Fontecha, E., Khosla, A., White, A. R. F., Chang, S., Cubas, P., et al. (2022). The strigolactone receptor D14 targets SMAX1 for degradation in response to GR24 treatment and osmotic stress. *Plant Commun.* doi: 10.1016/j.xplc.2022.100303 (in press).

Liang, Y., Ward, S., Li, P., Bennett, T., and Leyser, O. (2016). SMAX1-LIKE7 signals from the nucleus to regulate shoot development in Arabidopsis via partially EAR motif-independent mechanisms. *Plant Cell* 28, 1581–1601. doi: 10.1105/tpc.16.00286

Linkies, A., Graeber, K., Knight, C., and Leubner-Metzger, G. (2010). The evolution of seeds. *New Phytol.* 186, 817–831. doi: 10.1111/j.1469-8137.2010.03249.x

Liu, J., Cheng, X., Liu, P., and Sun, J. (2017). miR156-targeted SBP-box transcription factors interact with DWARF53 to regulate *TEOSINTE BRANCHED1* and *BARREN STALK1* expression in bread wheat. *Plant Physiol.* 174, 1931–1948. doi: 10.1104/pp.17.00445

Lopez-Obando, M., de Villiers, R., Hoffmann, B., Ma, L., de Saint Germain, A., Kossmann, J., et al. (2018). *Physcomitrella patens* MAX2 characterization suggests an ancient role for this F-box protein in photomorphogenesis rather than strigolactone signalling. *New Phytol.* 219, 743–756. doi: 10.1111/nph.15214

Lopez-Obando, M., Guillory, A., Boyer, F.-D., Cornu, D., Hoffmann, B., Le Bris, P., et al. (2021). The *Physcomitrium* (*Physcomitrella*) *patens* PpKAI2L receptors for strigolactones and related compounds function via MAX2-dependent and -independent pathways. *Plant Cell* 33, 3487–3512. doi: 10.1093/plcell/koab217

Lu, Z., Yu, H., Xiong, G., Wang, J., Jiao, Y., Liu, G., et al. (2013). Genome-wide binding analysis of the transcription activator IDEAL PLANT ARCHITECTURE1 reveals a complex network regulating rice plant ARCHITECTURE. *Plant Cell* 25, 3743–3759. doi: 10.1105/tpc.113.113639

Lv, S., Zhang, Y., Li, C., Liu, Z., Yang, N., Pan, L., et al. (2017). Strigolactone-triggered stomatal closure requires hydrogen peroxide synthesis and nitric oxide production in an abscisic acid-independent manner. *New Phytol.* 217, 290–304. doi: 10.1111/nph.14813

Ma, H., Duan, J., Ke, J., He, Y., Gu, X., Xu, T.-H., et al. (2017). A D53 repression motif induces oligomerization of TOPLESS corepressors and promotes assembly of a corepressor-nucleosome complex. *Sci. Adv.* 3:e1601217. doi: 10.1126/sciadv.1601217

Machin, D. C., Hamon-Josse, M., and Bennett, T. (2020). Fellowship of the rings: a saga of strigolactones and other small signals. *New Phytol.* 225, 621–636. doi: 10.1111/nph.16135

Martin, E. W., and Holehouse, A. S. (2020). Intrinsically disordered protein regions and phase separation: sequence determinants of assembly or lack thereof. *Emerg. Top. Life Sci.* 4, 307–329. doi: 10.1042/ETLS20190164

Mergner, J., Frejno, M., List, M., Papacek, M., Chen, X., Chaudhary, A., et al. (2020). Mass-spectrometry-based draft of the *Arabidopsis* proteome. *Nature* 579, 409–414. doi: 10.1038/s41586-020-2094-2

Mishra, R. C., and Grover, A. (2016). ClpB/Hsp100 proteins and heat stress tolerance in plants. *Crit. Rev. Biotechnol.* 36, 862–874. doi: 10.3109/07388551.2015.1051942

Miyashima, S., Roszak, P., Sevilem, I., Toyokura, K., Blob, B., Heo, J.-O., et al. (2019). Mobile PEAR transcription factors integrate positional cues to prime cambial growth. *Nature* 565, 490–494. doi: 10.1038/s41586-018-0839-y

Mizuno, Y., Komatsu, A., Shimazaki, S., Naramoto, S., Inoue, K., Xie, X., et al. (2021). Major components of the KARRIKIN INSENSITIVE2-dependent signaling pathway are conserved in the liverwort *Marchantia polymorpha*. *Plant Cell* 33, 2395–2411. doi: 10.1093/plcell/koab106

Mizuno, S., Nakazaki, Y., Yoshida, M., and Watanabe, Y.-H. (2012). Orientation of the amino-terminal domain of ClpB affects the disaggregation of the protein. *FEBS J.* 279, 1474–1484. doi: 10.1111/j.1742-4658.2012.08540.x

Morimoto, R. I. (2002). Dynamic remodeling of transcription complexes by molecular chaperones. *Cell* 110, 281–284. doi: 10.1016/S0092-8674(02)00860-7

Moturu, T. R., Thula, S., Singh, R. K., Nodzyński, T., Vařeková, R. S., Friml, J., et al. (2018). Molecular evolution and diversification of the SMXL gene family. *J. Exp. Bot.* 69, 2367–2378. doi: 10.1093/jxb/ery097

Nakamura, H., Xue, Y.-L., Miyakawa, T., Hou, F., Qin, H.-M., Fukui, K., et al. (2013). Molecular mechanism of strigolactone perception by DWARF14. *Nat. Commun.* 4:2613. doi: 10.1038/ncomms3613

Nelson, D. C., Riseborough, J.-A., Flematti, G. R., Stevens, J., Ghisalberti, E. L., Dixon, K. W., et al. (2009). Karrikins discovered in smoke trigger Arabidopsis seed germination by a mechanism requiring gibberellic acid synthesis and light. *Plant Physiol.* 149, 863–873. doi: 10.1104/pp.108.131516

Nelson, D. C., Scaffidi, A., Dun, E. A., Waters, M. T., Flematti, G. R., Dixon, K. W., et al. (2011). F-box protein MAX2 has dual roles in karrikin and strigolactone signaling in *Arabidopsis thaliana*. *Proc. Natl. Acad. Sci. U. S. A.* 108, 8897–8902. doi: 10.1073/pnas.1100987108

Nishimura, K., Apitz, J., Friso, G., Kim, J., Ponnala, L., Grimm, B., et al. (2015). Discovery of a unique Clp component, ClpF, in chloroplasts: a proposed binary ClpF-ClpS1 adaptor complex functions in substrate recognition and delivery. *Plant Cell* 27, 2677–2691. doi: 10.1105/tpc.15.00574

Nishimura, K., Asakura, Y., Friso, G., Kim, J., Oh, S.-H., Rutschow, H., et al. (2013). ClpS1 is a conserved substrate selector for the chloroplast Clp protease system in *Arabidopsis*. *Plant Cell* 25, 2276–2301. doi: 10.1105/tpc.113.112557

Nishimura, K., and van Wijk, K. J. (2015). Organization, function and substrates of the essential Clp protease system in plastids. *Biochim. Biophys. Acta* 1847, 915–930. doi: 10.1016/j.bbabio.2014.11.012

Oates, M. E., Romero, P., Ishida, T., Ghalwash, M., Mizianty, M. J., Xue, B., et al. (2013). D^2P^2: database of disordered protein predictions. *Nucleic Acids Res.* 41, D508–D516. doi: 10.1093/nar/gks1226

Oh, E., Zhu, J.-Y., Ryu, H., Hwang, I., and Wang, Z.-Y. (2014). TOPLESS mediates brassinosteroid-induced transcriptional repression through interaction with BZR1. *Nat. Commun.* 5:4140. doi: 10.1038/ncomms5140

Pauwels, L., Fernández Barbero, G., Geerinck, J., Tilleman, S., Grunewald, W., Cuéllar Pérez, A., et al. (2010). NINJA connects the co-repressor TOPLESS to jasmonate signalling. *Nature* 464, 788–791. doi: 10.1038/nature08854

Pavlovic, M., Plucinski, A., Zhang, J., Antonietti, M., Zeininger, L., and Schmidt, B. V. K. J. (2020). Cascade kinetics in an enzyme-loaded aqueous two-phase system. *Langmuir* 36, 1401–1408. doi: 10.1021/acs.langmuir.0c00186

Peltier, J.-B., Ripoll, D. R., Friso, G., Rudella, A., Cai, Y., Ytterberg, J., et al. (2004). Clp protease complexes from photosynthetic and non-photosynthetic plastids and mitochondria of plants, their predicted three-dimensional structures, and functional implications. *J. Biol. Chem.* 279, 4768–4781. doi: 10.1074/jbc.M309212200

Plant, A. R., Larrieu, A., and Causier, B. (2021). Repressor for hire! The vital roles of TOPLESS-mediated transcriptional repression in plants. *New Phytol.* 231, 963–973. doi: 10.1111/nph.17428

Posey, A. E., Holehouse, A. S., and Pappu, R. V. (2018). Phase separation of intrinsically disordered proteins. *Methods Enzymol.* 611, 1–30. doi: 10.1016/bs.mie.2018.09.035

Powers, S. K., Holehouse, A. S., Korasick, D. A., Schreiber, K. H., Clark, N. M., Jing, H., et al. (2019). Nucleo-cytoplasmic partitioning of ARF proteins controls auxin responses in *Arabidopsis thaliana*. *Mol. Cell* 76, 177–190. doi: 10.1016/j.molcel.2019.06.044

Reddy, A. S. N., Day, I. S., Göhring, J., and Barta, A. (2012). Localization and dynamics of nuclear speckles in plants. *Plant Physiol.* 158, 67–77. doi: 10.1104/pp.111.186700

Roitinger, E., Hofer, M., Köcher, T., Pichler, P., Novatchkova, M., Yang, J., et al. (2015). Quantitative phosphoproteomics of the ataxia telangiectasia-mutated (ATM) and ataxia telangiectasia-mutated and Rad3-related (ATR) dependent DNA damage response in *Arabidopsis thaliana*. *Mol. Cell. Proteomics* 14, 556–571. doi: 10.1074/mcp.M114.040352

Roncarati, D., and Scarlato, V. (2017). Regulation of heat-shock genes in bacteria: from signal sensing to gene expression output. *FEMS Microbiol. Rev.* 41, 549–574. doi: 10.1093/femsre/fux015

Ruff, K. M., Roberts, S., Chilkoti, A., and Pappu, R. V. (2018). Advances in understanding stimulus-responsive phase behavior of intrinsically disordered protein polymers. *J. Mol. Biol.* 430, 4619–4635. doi: 10.1016/j.jmb.2018.06.031

Ruyter-Spira, C., Kohlen, W., Charnikhova, T., van Zeijl, A., van Bezouwen, L., de Ruijter, N., et al. (2011). Physiological effects of the synthetic strigolactone analog GR24 on root system architecture in Arabidopsis: another belowground role for strigolactones? *Plant Physiol.* 155, 721–734. doi: 10.1104/pp.110.166645

Rytz, T. C., Miller, M. J., McLoughlin, F., Augustine, R. C., Marshall, R. S., Juan, Y.-T., et al. (2018). SUMOylome profiling reveals a diverse array of nuclear targets modified by the SUMO ligase SIZ1 during heat stress. *Plant Cell* 30, 1077–1099. doi: 10.1105/tpc.17.00993

Ryu, H., Cho, H., Bae, W., and Hwang, I. (2014). Control of early seedling development by BES1/TPL/HDA19-mediated epigenetic regulation of *ABI3*. *Nat. Commun.* 5:4138. doi: 10.1038/ncomms5138

Saitoh, N., Spahr, C. S., Patterson, S. D., Bubulya, P., Neuwald, A. F., and Spector, D. L. (2004). Proteomic analysis of interchromatin granule clusters. *Mol. Biol. Cell* 15, 3876–3890. doi: 10.1091/mbc.e04-03-0253

Sanchez, Y., Taulien, J., Borkovich, K. A., and Lindquist, S. (1992). Hsp104 is required for tolerance to many forms of stress. *EMBO J.* 11, 2357–2364. doi: 10.1002/j.1460-2075.1992.tb05295.x

Scaffidi, A., Waters, M. T., Bond, C. S., Dixon, K. W., Smith, S. M., Ghisalberti, E. L., et al. (2012). Exploring the molecular mechanism of karrikins and strigolactones. *Bioorg. Med. Chem. Lett.* 22, 3743–3746. doi: 10.1016/j.bmcl.2012.04.016

Scaffidi, A., Waters, M. T., Ghisalberti, E. L., Dixon, K. W., Flematti, G. R., and Smith, S. M. (2013). Carlactone-independent seedling morphogenesis in Arabidopsis. *Plant J.* 76, 1–9. doi: 10.1111/tpj.12265

Scaffidi, A., Waters, M. T., Sun, Y. K., Skelton, B. W., Dixon, K. W., Ghisalberti, E. L., et al. (2014). Strigolactone hormones and their stereoisomers signal through two related receptor proteins to induce different physiological responses in Arabidopsis. *Plant Physiol.* 165, 1221–1232. doi: 10.1104/pp.114.240036

Schirmer, E. C., Glover, J. R., Singer, M. A., and Lindquist, S. (1996). Hsp100/Clp proteins: a common mechanism explains diverse functions. *Trends Biochem. Sci.* 21, 289–296. doi: 10.1016/S0968-0004(96)10038-4

Schirmer, E. C., Lindquist, S., and Vierling, E. (1994). An Arabidopsis heat shock protein complements a thermotolerance defect in yeast. *Plant Cell* 6, 1899–1909. doi: 10.1105/tpc.6.12.1899

Seto, Y., Yasui, R., Kameoka, H., Tamiru, M., Cao, M., Terauchi, R., et al. (2019). Strigolactone perception and deactivation by a hydrolase receptor DWARF14. *Nat. Commun.* 10:191. doi: 10.1038/s41467-018-08124-7

Shabek, N., Ticchiarelli, F., Mao, H., Hinds, T. R., Leyser, O., and Zheng, N. (2018). Structural plasticity of D3–D14 ubiquitin ligase in strigolactone signalling. *Nature* 563, 652–656. doi: 10.1038/s41586-018-0743-5

Shen, H., Luong, P., and Huq, E. (2007). The F-Box Protein MAX2 Functions as a Positive Regulator of Photomorphogenesis in Arabidopsis. *Plant Physiol.* 45, 1471–1483. doi: 10.1104/pp.107.107227

Shi, D., Lebovka, I., López-Salmerón, V., Sanchez, P., and Greb, T. (2019). Bifacial cambium stem cells generate xylem and phloem during radial plant growth. *Development* 146:dev.171355. doi: 10.1242/dev.171355

Shinohara, N., Taylor, C., and Leyser, O. (2013). Strigolactone can promote or inhibit shoot branching by triggering rapid depletion of the auxin efflux protein PIN1 from the plasma membrane. *PLoS Biol.* 11:e1001474. doi: 10.1371/journal.pbio.1001474

Singh, A., and Grover, A. (2010). Plant Hsp100/ClpB-like proteins: poorly-analyzed cousins of yeast ClpB machine. *Plant Mol. Biol.* 74, 395–404. doi: 10.1007/s11103-010-9682-8

Singh, A., Mittal, D., Lavania, D., Agarwal, M., Mishra, R. C., and Grover, A. (2012). OsHsfA2c and OsHsfB4b are involved in the transcriptional regulation of cytoplasmic *OsClpB* (*Hsp100*) gene in rice (*Oryza sativa* L.). *Cell Stress Chaperones* 17, 243–254. doi: 10.1007/s12192-011-0303-5

Singh, S. K., Rozycki, J., Ortega, J., Ishikawa, T., Lo, J., Steven, A. C., et al. (2001). Functional domains of the ClpA and ClpX molecular chaperones identified by limited proteolysis and deletion analysis. *J. Biol. Chem.* 276, 29420–29429. doi: 10.1074/jbc.M103489200

Song, X., Lu, Z., Yu, H., Shao, G., Xiong, J., Meng, X., et al. (2017). IPA1 functions as a downstream transcription factor repressed by D53 in strigolactone signaling in rice. *Cell Res.* 27, 1128–1141. doi: 10.1038/cr.2017.102

Soundappan, I., Bennett, T., Morffy, N., Liang, Y., Stanga, J. P., Abbas, A., et al. (2015). SMAX1-LIKE/D53 family members enable distinct MAX2-dependent responses to strigolactones and karrikins in Arabidopsis. *Plant Cell* 27, 3143–3159. doi: 10.1105/tpc.15.00562

Spicer, R., and Groover, A. (2010). Evolution of development of vascular cambia and secondary growth. *New Phytol.* 186, 577–592. doi: 10.1111/j.1469-8137.2010.03236.x

Squires, C. L., Pedersen, S., Ross, B. M., and Squires, C. (1991). ClpB is the *Escherichia coli* heat shock protein F84.1. *J. Bacteriol.* 173, 4254–4262. doi: 10.1128/jb.173.14.4254-4262.1991

Stanga, J. P., Morffy, N., and Nelson, D. C. (2016). Functional redundancy in the control of seedling growth by the karrikin signaling pathway. *Planta* 243, 1397–1406. doi: 10.1007/s00425-015-2458-2

Stanga, J. P., Smith, S. M., Briggs, W. R., and Nelson, D. C. (2013). *SUPPRESSOR OF MORE AXILLARY GROWTH2 1* controls seed germination and seedling development in Arabidopsis. *Plant Physiol.* 163, 318–330. doi: 10.1104/pp.113.221259

Stirnberg, P., Furner, I. J., and Leyser, H. M. O. (2007). MAX2 participates in an SCF complex which acts locally at the node to suppress shoot branching. *Plant J.* 50, 80–94. doi: 10.1111/j.1365-313X.2007.03032.x

Struk, S., Braem, L., Walton, A., De Keyser, A., Boyer, F.-D., Persiau, G., et al. (2018). Quantitative tandem affinity purification, an effective tool to investigate protein complex composition in plant hormone signaling: strigolactones in the spotlight. *Front. Plant Sci.* 9:528. doi: 10.3389/fpls.2018.00528

Struk, S., De Cuyper, C., Jacobs, A., Braem, L., Walton, A., De Keyser, A., et al. (2021). Unraveling the MAX2 protein network in arabidopsis thaliana: identification of the protein phosphatase PAPP5 as a novel MAX2 interactor. *Mol. Cell. Proteomics* 20:100040. doi: 10.1074/mcp.RA119.001766

Sun, Y. K., Flematti, G. R., Smith, S. M., and Waters, M. T. (2016). Reporter gene-facilitated detection of compounds in *Arabidopsis* leaf extracts that activate the karrikin signaling pathway. *Front. Plant Sci.* 7:1799. doi: 10.3389/fpls.2016.01799

Sun, X.-D., and Ni, M. (2011). HYPOSENSITIVE TO LIGHT, an alpha/beta fold protein, acts downstream of ELONGATED HYPOCOTYL 5 to regulate seedling de-etiolation. *Mol. Plant* 4, 116–126. doi: 10.1093/mp/ssq055

Swarbreck, S. M., Guerringue, Y., Matthus, E., Jamieson, F. J. C., and Davies, J. M. (2019). Impairment in karrikin but not strigolactone sensing enhances root skewing in *Arabidopsis thaliana*. *Plant J.* 98, 607–621. doi: 10.1111/tpj.14233

Szemenyei, H., Hannon, M., and Long, J. A. (2008). TOPLESS mediates auxin-dependent transcriptional repression during *Arabidopsis* embryogenesis. *Science* 319, 1384–1386. doi: 10.1126/science.1151461

Tomaštíková, E., Cenklová, V., Kohoutová, L., Petrovská, B., Váchová, L., Halada, P., et al. (2012). Interactions of an *Arabidopsis* RanBPM homologue with LisH-CTLH domain proteins revealed high conservation of CTLH complexes in eukaryotes. *BMC Plant Biol.* 12:83. doi: 10.1186/1471-2229-12-83

Ueda, H., and Kusaba, M. (2015). Strigolactone regulates leaf senescence in concert with ethylene in Arabidopsis. *Plant Physiol.* 169, 138–147. doi: 10.1104/pp.15.00325

Umehara, M., Hanada, A., Yoshida, S., Akiyama, K., Arite, T., Takeda-Kamiya, N., et al. (2008). Inhibition of shoot branching by new terpenoid plant hormones. *Nature* 455, 195–200. doi: 10.1038/nature07272

Van Buskirk, E. K., Decker, P. V., and Chen, M. (2012). Photobodies in light signaling. *Plant Physiol.* 158, 52–60. doi: 10.1104/pp.111.186411

van der Lee, R., Buljan, M., Lang, B., Weatheritt, R. J., Daughdrill, G. W., Dunker, A. K., et al. (2014). Classification of intrinsically disordered regions and proteins. *Chem. Rev.* 114, 6589–6631. doi: 10.1021/cr400525m

Végh, A., Incze, N., Fábián, A., Huo, H., Bradford, K., Balázs, E., et al. (2017). Comprehensive analysis of DWARF14-LIKE2 (DLK2) reveals its functional divergence from strigolactone-related paralogs. *Front. Plant Sci.* 8:1641. doi: 10.3389/fpls.2017.01641

Villaécija-Aguilar, J. A., Hamon-Josse, M., Carbonnel, S., Kretschmar, A., Schmidt, C., Dawid, C., et al. (2019). SMAX1/SMXL2 regulate root and root hair development downstream of KAI2-mediated signalling in Arabidopsis. *PLoS Genet.* 15:e1008327. doi: 10.1371/journal.pgen.1008327

Waldie, T., McCulloch, H., and Leyser, O. (2014). Strigolactones and the control of plant development: lessons from shoot branching. *Plant J.* 79, 607–622. doi: 10.1111/tpj.12488

Walker, C. H., Siu-Ting, K., Taylor, A., O'Connell, M. J., and Bennett, T. (2019). Strigolactone synthesis is ancestral in land plants, but canonical strigolactone signalling is a flowering plant innovation. *BMC Biol.* 17:70. doi: 10.1186/s12915-019-0689-6

Wallner, E.-S., López-Salmerón, V., Belevich, I., Poschet, G., Jung, I., Grünwald, K., et al. (2017). Strigolactone- and karrikin-independent SMXL proteins are central regulators of phloem formation. *Curr. Biol.* 27, 1241–1247. doi: 10.1016/j.cub.2017.03.014

Wallner, E.-S., Tonn, N., Shi, D., Jouannet, V., and Greb, T. (2020). *SUPPRESSOR OF MAX2 1-LIKE 5* promotes secondary phloem formation during radial stem growth. *Plant J.* 102, 903–915. doi: 10.1111/tpj.14670

Wallner, E.-S., Tonn, N., Shi, D., Luzzietti, L., Wanke, F., Hunziker, P., et al. (2021). OBERON3 and SUPPRESSOR OF MAX2 1-LIKE proteins form a regulatory module specifying phloem identity. bioRxiv [Preprint]. 2021, 2019.2012.2021.885863. doi: 10.1101/2019.12.21.885863

Walton, A., Stes, E., Goeminne, G., Braem, L., Vuylsteke, M., Matthys, C., et al. (2016). The response of the root proteome to the synthetic strigolactone GR24 in *Arabidopsis*. *Mol. Cell. Proteomics* 15, 2744–2755. doi: 10.1074/mcp.M115.050062

Wang, Y., and Bouwmeester, H. J. (2018). Structural diversity in the strigolactones. *J. Exp. Bot.* 69, 2219–2230. doi: 10.1093/jxb/ery091

Wang, L., Kim, J., and Somers, D. E. (2013). Transcriptional corepressor TOPLESS complexes with pseudoresponse regulator proteins and histone deacetylases to regulate circadian transcription. *Proc. Natl. Acad. Sci. U. S. A.* 110, 761–766. doi: 10.1073/pnas.1215010110

Wang, L., Wang, B., Jiang, L., Liu, X., Li, X., Lu, Z., et al. (2015). Strigolactone signaling in Arabidopsis regulates shoot development by targeting D53-like SMXL repressor proteins for ubiquitination and degradation. *Plant Cell* 27, 3128–3142. doi: 10.1105/tpc.15.00605

Wang, L., Wang, B., Yu, H., Guo, H., Lin, T., Kou, L., et al. (2020a). Transcriptional regulation of strigolactone signalling in *Arabidopsis*. *Nature* 583, 277–281. doi: 10.1038/s41586-020-2382-x

Wang, L., Xu, Q., Yu, H., Ma, H., Li, X., Yang, J., et al. (2020b). Strigolactone and karrikin signaling pathways elicit ubiquitination and proteolysis of SMXL2 to regulate hypocotyl elongation in Arabidopsis. *Plant Cell* 32, 2251–2270. doi: 10.1105/tpc.20.00140

Waters, M. T., Nelson, D. C., Scaffidi, A., Flematti, G. R., Sun, Y. K., Dixon, K. W., et al. (2012). Specialisation within the DWARF14 protein family confers distinct responses to karrikins and strigolactones in *Arabidopsis*. *Development* 139, 1285–1295. doi: 10.1242/dev.074567

Waters, M. T., Scaffidi, A., Flematti, G., and Smith, S. M. (2015a). Substrate-induced degradation of the α/β-fold hydrolase KARRIKIN INSENSITIVE2 requires a functional catalytic triad but is independent of MAX2. *Mol. Plant* 8, 814–817. doi: 10.1016/j.molp.2014.12.020

Waters, M. T., Scaffidi, A., Moulin, S. L. Y., Sun, Y. K., Flematti, G. R., and Smith, S. M. (2015b). A *Selaginella moellendorffii* ortholog of KARRIKIN INSENSITIVE2 functions in Arabidopsis development but cannot mediate

responses to karrikins or strigolactones. *Plant Cell* 27, 1925–1944. doi: 10.1105/tpc.15.00146

Willems, P., Horne, A., Van Parys, T., Goormachtig, S., De Smet, I., Botzki, A., et al. (2019). The Plant PTM viewer, a central resource for exploring plant protein modifications. *Plant J.* 99, 752–762. doi: 10.1111/tpj.14345

Wojtyra, U. A., Thibault, G., Tuite, A., and Houry, W. A. (2003). The N-terminal zinc binding domain of ClpX is a dimerization domain that modulates the chaperone function. *J. Biol. Chem.* 278, 48981–48990. doi: 10.1074/jbc.M307825200

Woo, H. R., Chung, K. M., Park, J.-H., Oh, S. A., Ahn, T., Hong, S. H., et al. (2001). ORE9, an F-box protein that regulates leaf senescence in Arabidopsis. *Plant Cell* 13, 1779–1790. doi: 10.1105/TPC.010061

Wu, Y.-Y., Hou, B.-H., Lee, W.-C., Lu, S.-H., Yang, C.-J., Vaucheret, H., et al. (2017). DCL2- and RDR6-dependent transitive silencing of *SMXL4* and *SMXL5* in Arabidopsis *dcl4* mutants causes defective phloem transport and carbohydrate over-accumulation. *Plant J.* 90, 1064–1078. doi: 10.1111/tpj.13528

Wu, H., Li, H., Chen, H., Qi, Q., Ding, Q., Xue, J., et al. (2019). Identification and expression analysis of strigolactone biosynthetic and signaling genes reveal strigolactones are involved in fruit development of the woodland strawberry (*Fragaria vesca*). *BMC Plant Biol.* 19:73. doi: 10.1186/s12870-019-1673-6

Xie, Y., Liu, Y., Ma, M., Zhou, Q., Zhao, Y., Zhao, B., et al. (2020). *Arabidopsis* FHY3 and FAR1 integrate light and strigolactone signaling to regulate branching. *Nat. Commun.* 11:1955. doi: 10.1038/s41467-020-15893-7

Xie, X., Mori, N., Yoneyama, K., Nomura, T., Uchida, K., Yoneyama, K., et al. (2019). Lotuslactone, a non-canonical strigolactone from *Lotus japonicus*. *Phytochemistry* 157, 200–205. doi: 10.1016/j.phytochem.2018.10.034

Xu, Y., Miyakawa, T., Nakamura, H., Nakamura, A., Imamura, Y., Asami, T., et al. (2016). Structural basis of unique ligand specificity of KAI2-like protein from parasitic weed *Striga hermonthica*. *Sci. Rep.* 6:31386. doi: 10.1038/srep31386

Xu, Y., Miyakawa, T., Nosaki, S., Nakamura, A., Lyu, Y., Nakamura, H., et al. (2018). Structural analysis of HTL and D14 proteins reveals the basis for ligand selectivity in *Striga*. *Nat. Commun.* 9:3947. doi: 10.1038/s41467-018-06452-2

Yang, T., Lian, Y., Kang, J., Bian, Z., Xuan, L., Gao, Z., et al. (2020a). The SUPPRESSOR of MAX2 1 (SMAX1)-like SMXL6, SMXL7 and SMXL8 act as negative regulators in response to drought stress in Arabidopsis. *Plant Cell Physiol.* 61, 1477–1492. doi: 10.1093/pcp/pcaa066

Yang, T., Sun, Y., Wang, Y., Zhou, L., Chen, M., Bian, Z., et al. (2020b). *AtHSPR* is involved in GA- and light intensity-mediated control of flowering time and seed set in Arabidopsis. *J. Exp. Bot.* 71, 3543–3559. doi: 10.1093/jxb/eraa128

Yang, T., Zhang, L., Hao, H., Zhang, P., Zhu, H., Cheng, W., et al. (2015). Nuclear-localized AtHSPR links abscisic acid-dependent salt tolerance and antioxidant defense in Arabidopsis. *Plant J.* 84, 1274–1294. doi: 10.1111/tpj.13080

Yang, T., Zhang, P., and Wang, C. (2016). AtHSPR may function in salt-induced cell death and ER stress in Arabidopsis. *Plant Signal. Behav.* 11:e1197462. doi: 10.1080/15592324.2016.1197462

Yao, J., Mashiguchi, K., Scaffidi, A., Akatsu, T., Melville, K. T., Morita, R., et al. (2018). An allelic series at the *KARRIKIN INSENSITIVE 2* locus of *Arabidopsis thaliana* decouples ligand hydrolysis and receptor degradation from downstream signalling. *Plant J.* 96, 75–89. doi: 10.1111/tpj.14017

Yao, R., Ming, Z., Yan, L., Li, S., Wang, F., Ma, S., et al. (2016). DWARF14 is a non-canonical hormone receptor for strigolactone. *Nature* 536, 469–473. doi: 10.1038/nature19073

Yoneyama, K., Xie, X., Yoneyama, K., Kisugi, T., Nomura, T., Nakatani, Y., et al. (2018). Which are the major players, canonical or non-canonical strigolactones? *J. Exp. Bot.* 69, 2231–2239. doi: 10.1093/jxb/ery090

Yoo, H., Triandafillou, C., and Drummond, D. A. (2019). Cellular sensing by phase separation: using the process, not just the products. *J. Biol. Chem.* 294, 7151–7159. doi: 10.1074/jbc.TM118.001191

Yoshida, S., Kameoka, H., Tempo, M., Akiyama, K., Umehara, M., Yamaguchi, S., et al. (2012). The D3 F-box protein is a key component in host strigolactone responses essential for arbuscular mycorrhizal symbiosis. *New Phytol.* 196, 1208–1216. doi: 10.1111/j.1469-8137.2012.04339.x

Zhang, J., Mazur, E., Balla, J., Gallei, M., Kalousek, P., Medveďová, Z., et al. (2020). Strigolactones inhibit auxin feedback on PIN-dependent auxin transport canalization. *Nat. Commun.* 11:3508. doi: 10.1038/s41467-020-17252-y

Zhang, T., Ploetz, E. A., Nagy, M., Doyle, S. M., Wickner, S., Smith, P. E., et al. (2012). Flexible connection of the N-terminal domain in ClpB modulates substrate binding and the aggregate reactivation efficiency. *Proteins* 80, 2758–2768. doi: 10.1002/prot.24159

Zhao, L.-H., Zhou, X. E., Wu, Z.-S., Yi, W., Xu, Y., Li, S., et al. (2013). Crystal structures of two phytohormone signal-transducing α/β hydrolases: karrikin-signaling KAI2 and strigolactone-signaling DWARF14. *Cell Res.* 23, 436–439. doi: 10.1038/cr.2013.19

Zhao, L.-H., Zhou, X. E., Yi, W., Wu, Z., Liu, Y., Kang, Y., et al. (2015). Destabilization of strigolactone receptor DWARF14 by binding of ligand and E3-ligase signaling effector DWARF3. *Cell Res.* 25, 1219–1236. doi: 10.1038/cr.2015.122

Zheng, J., Hong, K., Zeng, L., Wang, L., Kang, S., Qu, M., et al. (2020). Karrikin signaling acts parallel to and additively with strigolactone signaling to regulate rice mesocotyl elongation in darkness. *Plant Cell* 32, 2780–2805. doi: 10.1105/tpc.20.00123

Zheng, X., Yang, X., Chen, Z., Xie, W., Yue, X., Zhu, H., et al. (2021). *Arabidopsis* SMAX1 overaccumulation suppresses rosette shoot branching and promotes leaf and petiole elongation. *Biochem. Biophys. Res. Commun.* 553, 44–50. doi: 10.1016/j.bbrc.2021.03.006

Zhou, F., Lin, Q., Zhu, L., Ren, Y., Zhou, K., Shabek, N., et al. (2013). D14–SCF^{D3}-dependent degradation of D53 regulates strigolactone signalling. *Nature* 504, 406–410. doi: 10.1038/nature12878

Conflict of Interest: The authors declare that the research was conducted in the absence of any commercial or financial relationships that could be construed as a potential conflict of interest.

Publisher's Note: All claims expressed in this article are solely those of the authors and do not necessarily represent those of their affiliated organizations, or those of the publisher, the editors and the reviewers. Any product that may be evaluated in this article, or claim that may be made by its manufacturer, is not guaranteed or endorsed by the publisher.

frontiers | Frontiers in Plant Science

ORIGINAL RESEARCH
published: 02 June 2022
doi: 10.3389/fpls.2022.887347

Expansion of the Strigolactone Profluorescent Probes Repertory: The Right Probe for the Right Application

*Alexandre de Saint Germain[1], Guillaume Clavé[2], Paul Schouveiler[1], Jean-Paul Pillot[1], Abhay-Veer Singh[1], Arnaud Chevalier[2], Suzanne Daignan Fornier[2], Ambre Guillory[1], Sandrine Bonhomme[1], Catherine Rameau[1] and François-Didier Boyer[2]**

[1] Université Paris-Saclay, INRAE, AgroParisTech, Institut Jean-Pierre Bourgin (IJPB), Versailles, France, [2] Université Paris-Saclay, CNRS, Institut de Chimie des Substances Naturelles, Gif-sur-Yvette, France

Strigolactones (SLs) are intriguing phytohormones that not only regulate plant development and architecture but also interact with other organisms in the rhizosphere as root parasitic plants (*Striga*, *Orobanche,* and *Phelipanche*) and arbuscular mycorrhizal fungi. Starting with a pioneering work in 2003 for the isolation and identification of the SL receptor in parasitic weeds, fluorescence labeling of analogs has proven a major strategy to gain knowledge in SL perception and signaling. Here, we present novel chemical tools for understanding the SL perception based on the enzymatic properties of SL receptors. We designed different profluorescent SL Guillaume Clavé (GC) probes and performed structure-activity relationship studies on pea, *Arabidopsis thaliana*, and *Physcomitrium* (formerly *Physcomitrella*) *patens*. The binding of the GC probes to PsD14/RMS3, AtD14, and OsD14 proteins was tested. We demonstrated that coumarin-based profluorescent probes were highly bioactive and well-adapted to dissect the enzymatic properties of SL receptors in pea and a resorufin profluorescent probe in moss, contrary to the commercially available fluorescein profluorescent probe, Yoshimulactone Green (YLG). These probes offer novel opportunities for the studies of SL in various plants.

Keywords: strigolactone, profluorescent probes, pea, *Arabidopsis thaliana*, *Physcomitrium patens*, α/β-hydrolases, plant hormone, structure-activity relationship

OPEN ACCESS

Edited by:
Tadao Asami,
The University of Tokyo, Japan

Reviewed by:
Yuichiro Tsuchiya,
Nagoya University, Japan
Kosuke Fukui,
Okayama University of Science, Japan

***Correspondence:**
François-Didier Boyer
francois-didier.boyer@cnrs.fr

Specialty section:
This article was submitted to Plant Physiology, a section of the journal Frontiers in Plant Science

Received: *01 March 2022*
Accepted: *02 May 2022*
Published: *02 June 2022*

Citation:
de Saint Germain A, Clavé G, Schouveiler P, Pillot J-P, Singh A-V, Chevalier A, Daignan Fornier S, Guillory A, Bonhomme S, Rameau C and Boyer F-D (2022) Expansion of the Strigolactone Profluorescent Probes Repertory: The Right Probe for the Right Application. Front. Plant Sci. 13:887347. doi: 10.3389/fpls.2022.887347

INTRODUCTION

Bioactive fluorescent-labeled plant hormones are highly valuable tools in hormone research either to address the mechanism of hormone transport and to obtain quantitative data on the dynamic of hormone levels or in the search for novel agonists or antagonists *via* the screening of chemical libraries (Lace and Prandi, 2016; Geisler, 2018; Balcerowicz et al., 2021). These probes are generally designed to retain the original hormonal activity and to activate signaling by binding to hormone receptors. For *in planta* imaging, the fluorophores should possess the best molecular brightness (Grimm and Lavis, 2022) and the detection of their fluorescence should not be affected by tissue autofluorescence (García-Plazaola et al., 2015). Indeed, the high abundance of endogenous fluorescent molecules (e.g., not only chlorophyll but also lignin, carotenes, xanthophylls, flavonoids, anthocyanins, alkaloids, etc.) is a real challenge for *in vivo* imaging in plants (Donaldson, 2020). For this purpose, the best spectral suitable window is reported to be between 550 and 650 nm for excitation and emission wavelengths of fluorophores. Due to these specific properties demanded in plant research, the available fluorophores are limited in this context (Grimm and Lavis, 2022).

Strigolactones are the last discovered class of phytohormones, controlling shoot branching, and many other aspects of plant development in vascular and non-vascular plants (Gomez-Roldan et al., 2008; Umehara et al., 2008; Proust et al., 2011; Lopez-Obando et al., 2015). They were first discovered as key signals in the rhizosphere as signaling the presence of a host root for parasitic plants and for arbuscular mycorrhizal fungi (AMF; Cook et al., 1966; Akiyama et al., 2005; Xie et al., 2010).

Strigolactones are a large family of specialized metabolite and to date, more than 30 natural SLs have been identified in root exudates of various plants (Yoneyama, 2020). SLs are derived from all-*trans*-β-carotene and are characterized by two specific chemical groups: an invariant butenolide D-ring bearing a 4′-methyl group and a structurally variable cargo group, linked by an enol ether bridge (**Figure 1A**). This connection has a 2'*R* configuration that is highly conserved in natural SLs (de Saint Germain et al., 2013; Yoneyama, 2020). SLs are classified into two distinct types: canonical SLs which have the cargo group containing an ABC tricycle and non-canonical SLs with the absence of the ABC tricycle (**Figure 1A**; Yoneyama et al., 2018). Based on the structure–activity relationship studies, it has been demonstrated that the D-ring is absolutely required for the SL bioactivity and can be qualified as an active group, whereas the cargo group can be drastically modified or even replaced by another hydrophobic group (i.e., in Debranone or Nijmegen; Takahashi and Asami, 2018).

In seed plants, SL perception as phytohormone involves a receptor called, DWARF14 (D14), [OsD14 in rice, AtD14 in Arabidopsis, RAMOSUS3 (RMS3) in pea, DECREASED APICAL DOMINANCE2 (DAD2) in petunia] which belongs to the α/β hydrolase family with a conserved catalytic triad (Ser, His, Asp; Arite et al., 2009; Hamiaux et al., 2012; Waters et al., 2012; de Saint Germain et al., 2016; Yao et al., 2016). In *Physcomitrium patens* and in obligate root parasitic plants, SLs are perceived by their ancestral paralogs, HYPOSENSITIVE TO LIGHT/KARRIKIN INSENSITIVE2 (HTL/KAI2) (Conn et al., 2015; Toh et al., 2015; de Saint Germain et al., 2021b; Lopez-Obando et al., 2021; Mizuno et al., 2021), referred hereinafter as KAI2s.

Interestingly, the D14 and KAI2 proteins can interact and cleave SLs, releasing the cargo group, which can therefore be called leaving group. To decipher the SL perception mechanism, bioactive fluorescent SL mimics were designed by different groups to investigate and characterize the mechanism of SL perception in multiple organisms (non-vascular and seed plants, including root parasitic plants and fungi). SL fluorescent probes have been developed since 2003 as tracers to investigate the spatiotemporal distribution of SLs in plants and fungi (Reizelman et al., 2003; Prandi et al., 2014; Lace and Prandi, 2016; Van Overtveldt et al., 2019). However, these fluorescence-based approaches allow no distinction between intact and hydrolyzed SL analogs, which may be an important drawback for data analyses.

Thanks to the structure–activity relationship (SAR) studies, fluorescent-labeled SLs have been designed by replacing the editable SL cargo group with a fluorophore, which becomes fluorescent only after perception and cleavage of the D-ring

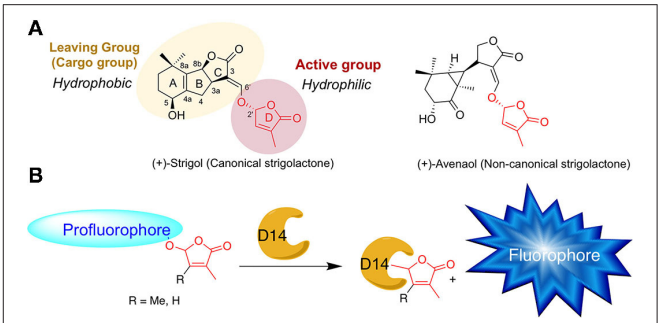

FIGURE 1 | (A) Chemical structures of natural strigolactones. **(B)** Principle of SL profluorescent probes. D14 = SL receptor.

(**Figure 1B**). These so-called profluorescent probes allow the dynamic/temporal monitoring of the enzymatic activity of SL receptors *in vitro* (Tsuchiya et al., 2015; de Saint Germain et al., 2016; Wang et al., 2021) and *in planta* (Tsuchiya et al., 2015, 2018; Wang et al., 2021).

The profluorescent probes include the Guillaume Clavé (GC) series, made of molecules bearing the 6,8-difluoro-7-hydroxy-4-methyl-2*H*-chromen-2-one (DiFMU) profluorescent moiety, either connected to a non-methylated [(±)-GC486] group, a mono-methylated [(±)-GC240] group, or a dimethylated [(±)-GC242] D-ring (de Saint Germain et al., 2016; **Figures 1B**, **2**). *In vitro* enzymatic assays carried out with these probes revealed two-phase cleavage kinetics. The presence of a second phase with a plateau or a curve with a low slope suggests the formation of a relatively stable covalent adduct to the protein.

In the hypothetical model, the cleavage activity of SL receptors could be a way to stabilize the interaction between D14 and SL by a covalent link. From this model, an unusual hormonal perception mechanism has been proposed in which SLs are cleaved by the D14 receptor and form a covalent adduct linked to the histidine residue of the catalytic triad. Upon SL cleavage and perception, the D14 interacts with signaling partners to transduce the hormonal signal (de Saint Germain et al., 2016; Yao et al., 2016; Shabek et al., 2018). More recently, another SL perception mechanism independent of the enzymatic activity has been proposed (Seto et al., 2019). It highlights the necessity to develop innovative tools to better characterize the kinetics of SL perception (Bürger and Chory, 2020).

The GC series of profluorescent probes has also been recently used to characterize enzymatic properties of other putative SL receptors, such as PrKAI2d3 from *Phelipanche ramosa* root parasitic plant (de Saint Germain et al., 2021b) and PpKAI2L proteins from *Physcomitrium patens* (Lopez-Obando et al., 2021). Desmethyl profluorescent probes are particularly relevant for investigating the KAI2 pathway as the preference of this ancient pathway for desmethyl butenolides was recently demonstrated, and the role of (−)-desmethyl GR24 as an agonist of KAI2 protein was highlighted (Yao et al., 2021).

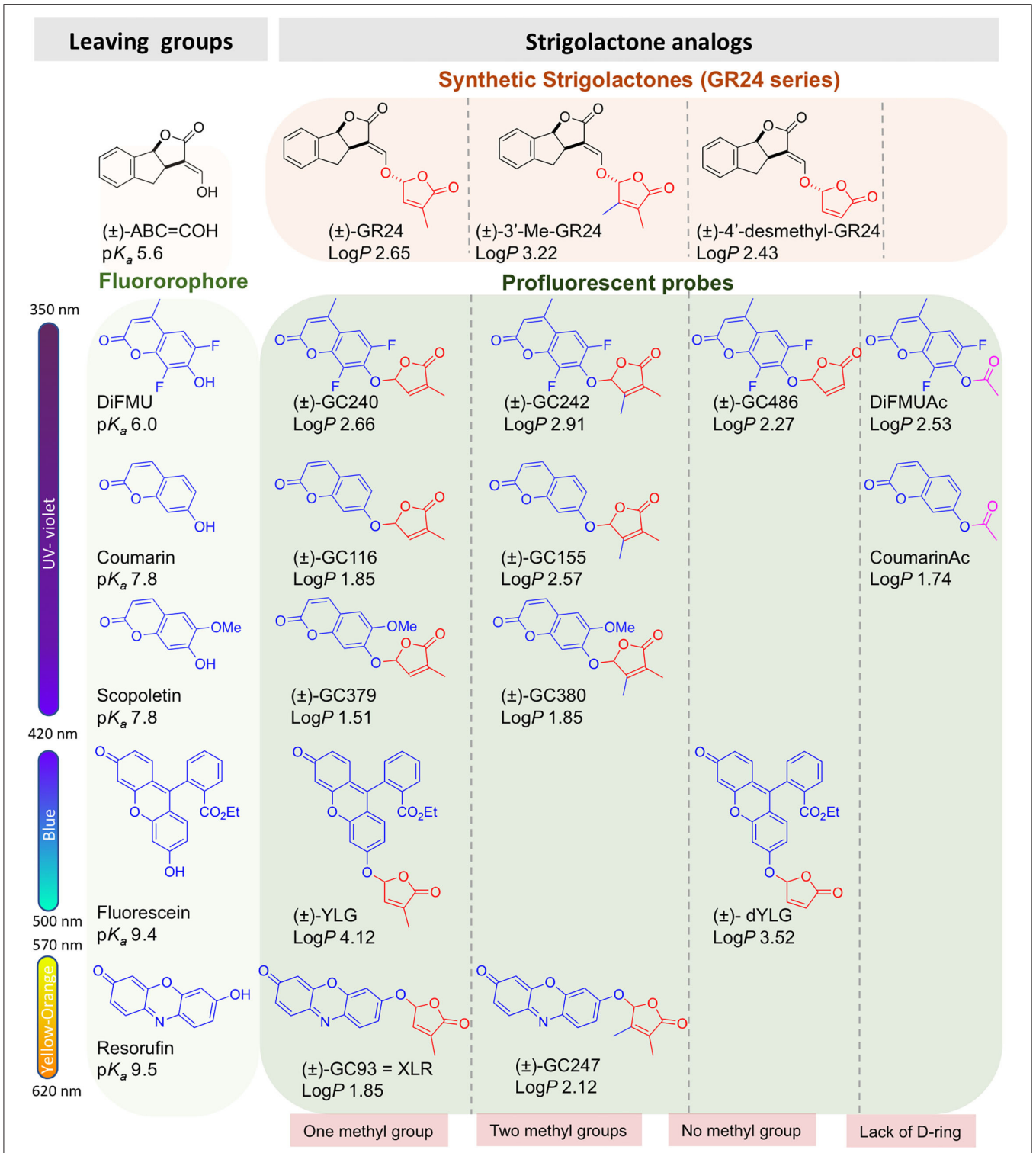

FIGURE 2 | Chemical probes discussed in this study. Log*P* and pK_a are calculated by the ACD program.

Yoshimulactone Green (YLG) is another profluorescent probe based on a fluorescein moiety linked to the D-ring by an ether bond (**Figure 2**; Tsuchiya et al., 2015). It has been developed for the characterization of SL receptors from *Striga* root parasitic plants, especially ShHTL7. The mechanism of SL perception by ShHTL7 was demonstrated to be similar to that of the

D14 protein (Yao et al., 2017). The development of a variant of YLG (YLGW) allowed for the visualization of SL receptor activity in germinating *Striga hermonthica* seeds (Tsuchiya et al., 2018). The YLG is commercially available and has been used thereafter to identify SL receptor antagonists as tolfenamic acid (Hamiaux et al., 2018), KK094, and DL1b (Nakamura et al., 2019; Yoshimura et al., 2020) toward DAD2 and AtD14 proteins, respectively, highlighting the usefulness of this probe. Very recently, a novel resorufin-based SL profluorescent probe, Xilatone Red (XLR) based on a resorufin moiety has been developed (Wang et al., 2021).

Due to the structural diversities of SL receptors from different organisms, as well as the different functions of SL as a plant hormone and/or as a rhizospheric signal, the search for novel profluorescent probes is still necessary. For example, ShD14 is not able to cleave YLG whereas it could cleave (±)-GR24 (Xu et al., 2018). Here, we designed and characterized other different profluorescent SL mimic series with three different fluorophores (coumarin, scopoletin, and resorufin). These mimics have various physicochemical (Log*P*, pK_a) and optical properties and bear a different number of methyl groups on the D-ring, aimed at meeting specific requirements for SL research. Their bioactivity for the control of shoot branching in pea, Arabidopsis, and for controlling moss development was evaluated. Their biochemical characterization was also performed with all four characterized SL receptors from flowering plants: AtD14, OsD14, DAD2, and RMS3.

MATERIALS AND METHODS

Chemistry, General Experimental Procedure

All non-aqueous reactions were run under an inert atmosphere (argon), by using standard techniques for manipulating air-sensitive compounds. All glassware were stored in the oven and/or were flame-dried prior to use. Anhydrous solvents were obtained by filtration through drying columns. Analytical thin-layer chromatography (TLC) was performed on plates precoated with silica gel layers. Compounds were visualized by one or more of the following methods: (1) illumination with a short wavelength UV lamp (i.e., $\lambda = 254$ nm) and (2) spraying with a 3.5% (w/v) phosphomolybdic acid solution in absolute ethanol. Flash column chromatography was performed using 40–63 mesh silica. Nuclear magnetic resonance spectra (^{1}H; ^{13}C NMR) were recorded at [300; 75] MHz on a Bruker DPX 300 spectrometer. For the ^{1}H spectra, data are reported as follows: chemical shift, multiplicity (s = singlet, d = doublet, t = triplet, q = quartet, m = multiplet, bs = broad singlet, coupling constant in Hz and integration). Infrared (IR) spectra are reported in reciprocal centimeters (cm^{-1}). Buffers and aqueous mobile-phases for high-performance liquid chromatography (HPLC) were prepared using water purified with a Milli-Q system (purified to 18.2 MΩcm). Analytical ultra-performance liquid chromatography (UPLC) was performed on an Acquity Waters UPLC system equipped with a PDA and a mass spectrometer detector. Semi-preparative HPLC was performed on a Waters system equipped with 600 E pump system, a Waters 2,767 sample manager, injector and collector, and a waters PDA 2,996 UV-vis detector. Mass spectra (MS) and high-resolution mass spectra (HRMS) were determined by electrospray ionization (ESI) coupled to a time-of-flight analyzer (Waters LCT Premier XE). 7-Hydroxycoumarin (Coumarin) was synthesized according to the procedure of Timonen et al. (2011) in one step. 7-Acetoxycoumarin (CoumarinAc) was prepared according to the method of Confalone and Confalone (1980), and DiFMUAc was performed according to the method of Bürger et al. (2012). (±)-GC240, (±)-GC242, and (±)-GC486 were prepared according to the method of de Saint Germain et al. (2016); 5-bromo-4-methylfuran-2(5*H*)-one and 5-chloro-3,4-dimethylfuran-2(5H)-one were synthetized according to the procedure of Wolff and Hoffmann (1988) and Canévet and Graff (1978). (±)-GR24, (±)-ABC=CHOH tricycle [3-(hydroxymethylene)-3,3a,4,8b-tetrahydro-2*H*-indeno[1,2-*b*]furan-2-one] were prepared according to the method of Mangnus et al. (1992). (+)-GR24 was obtained as described by Lopez-Obando et al. (2021). DiFMU and (±)-YLG were purchased from Carbosynth™ and TCI™, respectively. All structures of GC probes were confirmed by NMR, IR, and HRMS analyses.

7-[(4-Methyl-5-Oxo-2,5-Dihydrofuran-2-yl)Oxy]-4-Methyl-2H-1-Benzopyran-2-One [(±)-GC116]

To a solution of 5-bromo-3-methylfuran-2(5*H*)-one (448 mg, 3.10 mmol), 7-hydroxycoumarin (400 mg, 2.46 mmol), and *N*, *N*-diisopropylethylamine (DIEA; 1.05 mL, 6.00 mmol) were sequentially added to MeCN (10.0 ml). The resulting mixture was stirred at room temperature and after 10 min, a white solid precipitated. The reaction was allowed to proceed for 14 h, and then checked for completion by TLC (heptane/EtOAc 3:2 v/v). A large part of the product was recovered by filtration and the remaining part was purified on a silica gel column (heptane/EtOAc 3:2 v/v) giving (±)-GC116 as a white solid (446 mg, 1.73 mmol, 70%). Mp 216°C. ^{1}H-NMR (300 MHz, $CDCl_3$) δ: 2.04 (s, 3H), 6.33–6.36 (m, 2H), 7.02–7.09 (m, 3H), 7.44–7.46 (d, $J = 8.6$ Hz, 1H), 7.65–7.67 (d, $J = 9.8$ Hz, 1H). ^{13}C-NMR (125 MHz, $CDCl_3$) δ: 10.5, 98.1, 104.7, 113.5, 114.6, 114.7, 129.2, 134.8, 141.8, 143.0, 155.3, 159.0, 160.6, 170.8. IR ν_{max} (film): 680, 746, 794, 841, 879, 956, 1,018, 1,092, 1,138, 1,165, 1,208, 1,283, 1,363, 1,508, 1,562, 1,622, 1,664, 1,730, 1,778, 3,078 cm^{-1}. HRMS (ESI): *m/z* calc. for $C_{14}H_{11}O_5$ $[M + H]^+$: 259.0606, found: 259.0605.

7-[(3,4-Dimethyl-5-Oxo-2,5-Dihydrofuran-2-yl)Oxy]-4-Methyl-2H-1-Benzopyran-2-One [(±)-GC155]

To a solution of 5-chloro-3,4-dimethylfuran-2(5*H*)-one (352 mg, 2.00 mmol; Canévet and Graff, 1978), 7-hydroxycoumarin (300 mg, 1.85 mmol), and DIEA (697 μL, 4.00 mmol) were sequentially added to MeCN (10 ml). The resulting mixture was stirred at room temperature for 14 h and then checked for completion by TLC (heptane/EtOAc 1:1 v/v). The crude was evaporated to dryness and then purified on a silica gel column (heptane/EtOAc 6:4 v/v) giving (±)-GC155 as a white solid (423 mg, 1.55 mmol, 84%). Mp 176°C. ^{1}H-NMR (300 MHz,

$CDCl_3$) δ: 1.85 (t, $J = 1.2$ Hz, 3H), 2.04 (t, $J = 0.9$ Hz, 3H), 6.08 (s, 1H), 6.24–6.27 (d, $J = 9.5$ Hz, 1H), 6.98–7.01 (m, 2H), 7.37–7.39 (d, $J = 8.1$ Hz, 1H), 7.58–7.61 (d, $J = 9.6$ Hz, 1H). ^{13}C-NMR (75 MHz, $CDCl_3$) δ: 8.7, 11.7, 99.9, 104.6, 113.5, 114.8, 114.9, 127.5, 129.3, 143.1, 153.3, 155.5, 159.5, 160.7, 171.4. IR ν_{max} (film): 674, 661, 750, 834, 886, 975, 1,052, 1,088, 1,131, 1,162, 1,195, 1,236, 1,285, 1,318, 1,361, 1,387, 1,505, 1,565, 1,615, 1,624, 1,689, 1,745, 1,781, 3,081 cm^{-1}. HRMS (ESI): *m/z* calc. for $C_{15}H_{13}O_5$ $[M + H]^+$: 273.0718, found: 273.0753.

7-[(4-Methyl-5-Oxo-2,5-Dihydrofuran-2-yl)Oxy]-6-Methoxy-4-Methyl-2H-1-Benzopyran-2-One [(±)-GC379]

To a solution of 5-bromo-3-methylfuran-2(5*H*)-one (53.0 mg, 300 μmol), scopoletin (30.0 mg, 156 μmol) and DIEA (156 μmol, 900 μmol) were sequentially added to MeCN (4 mL) The resulting mixture was stirred at room temperature for 14 h, and then checked for completion by TLC (heptane/EtOAc 1:1 v/v). The crude was evaporated to dryness and then purified on a silica gel column (heptane/EtOAc 1:1 v/v) giving (±)-GC379 as a white solid (43.0 mg, 149 μmol, 96%). Mp 164°C. ^{1}H-NMR (300 MHz, $CDCl_3$) δ: 2.01 (s, 3H), 3.90 (s, 3H), 6.33-6.36 (m, 2H), 6.92 (s, 1H), 7.06–7.07 (t, $J = 1.6$ Hz, 1H), 7.21 (s, 1H), 7.61–7.63 (d, $J = 9.5$ Hz, 1H). ^{13}C-NMR (125 MHz, $CDCl_3$) δ: 10.8, 56.5, 98.8, 106.1, 109.2, 114.4, 115.4, 135.2, 141.9, 142.9, 147.0, 148.6, 149.1, 160.9, 170.9. IR ν_{max} (film): 820, 869, 928, 954, 1,014, 1,072, 1,099, 1,147, 1,173, 1,196, 1,214, 1,250, 1,278, 1,376, 1,390, 1,423, 1,459, 1,512, 1,568, 1,616, 1,721, 1,776 cm^{-1}. HRMS (ESI): *m/z* calc. for $C_{15}H_{13}O_6$ $[M + H]^+$: 289.0712, found: 289.0714.

7-[(3,4-Dimethyl-5-Oxo-2,5-Dihydrofuran-2-yl)Oxy]-6-Methoxy-4-Methyl-2H-1-Benzopyran-2-One [(±)-GC380]

To a solution of 5-chloro-3,4-dimethylfuran-2(5*H*)-one (43.0 mg, 300 μmol), scopoletin (30.0 mg, 156 μmol) and DIEA (156 μmol, 900 μmol) were sequentially to MeCN (4 mL) added. The resulting mixture was stirred at room temperature for 14 h, and then checked for completion by TLC (heptane/EtOAc 1:1 v/v). The crude was evaporated to dryness and then purified on a silica gel column (heptane/EtOAc 1:1 v/v) giving (±)-GC380 as a white solid (32.0 mg, 106 μmol, 68%). Mp 172°C. ^{1}H-NMR (300 MHz, $CDCl_3$) δ: 1.88–1.89 (t, $J = 1.5$ Hz, 3H), 2.12–0.13 (t, $J = 0.9$ Hz, 3H), 3.89 (s, 3H), 6.12 (s, 1H), 6.31–6.34 (d, $J = 9.5$ Hz, 2H), 6.92 (s, 1H), 7.20 (s, 1H), 7.61–7.64 (d, $J = 9.6$ Hz, 1H). ^{13}C-NMR (75 MHz, $CDCl_3$) δ: 8.7, 11.8, 56.5, 100.8, 106.4, 109.3, 114.4, 115.4, 127.5, 143.0, 147.2, 149.0, 149.1, 153.4, 160.9, 171.5. IR ν_{max} (film): 750, 817, 850, 860, 922, 972, 1,016, 1,053, 1,096, 1,143, 1,172, 1,194, 1,246, 1,276, 1,369, 1,387, 1,423, 1,513, 1,568, 1,615, 1,720, 1,776, 2,851, 2,924, 3,065 cm^{-1}. HRMS (ESI): *m/z* calc. for $C_{16}H_{15}O_6$ $[M + H]^+$: 303.0869, found: 303.0872.

7-[(4-Methyl-5-Oxo-2,5-Dihydrofuran-2-yl)Oxy]-3H-Phenoxazin-3-One [(±)-GC93]

To a solution of 5-bromo-3-methylfuran-2(5*H*)-one (51.0 mg, 290 μmol), resorufin sodium salt (65.0 mg, 277 μmol) and DIEA (1.05 ml, 6.00 mmol) were sequentially added to DMF (4 ml). The resulting mixture was stirred at room temperature for 14 h and then checked for completion by TLC (CH_2Cl_2/EtOAc 8:2 v/v). The crude was diluted with EtOAc, successively washed with 10% aqueous citric acid, brine, dried over Na_2SO_4, and evaporated to dryness. The resulting residue was purified by chromatography on a silica gel column with a step gradient of EtOAc (0-10% v/v) in CH_2Cl_2 as the mobile phase, giving (±)-GC93 as yellow solid (53.0 mg, 172 μmol, 62%). Mp decomposition at 244°C. ^{1}H-NMR (300 MHz, $CDCl_3$) δ: 2.06–2.07 (t, $J = 1.6$ Hz, 3H), 6.33–6.34 (d, $J = 2.1$ Hz, 1H), 6.38–6.39 (t, $J = 1.6$ Hz, 1H), 7.44–7.46 (dd, $J_1 = 9.9$ Hz, $J_2 = 2.0$ Hz, 1H), 7.04–7.05 (t, $J = 1.7$ Hz, 1H), 7.10–7.14 (m, 2H), 7.41–7.44 (d, $J = 9.9$ Hz, 1H), 7.75–7.78 (d, $J = 8.3$ Hz, 1H). RMN ^{13}C (75 MHz, $CDCl_3$) δ: 10.9, 98.1, 103.8, 107.3, 114.7, 129.9, 131.9, 134.9, 135.2, 141.6, 145.3, 145.4, 147.3, 149.6, 159.6, 170.3, 186.5. IR ν_{max} (film): 711, 742, 758, 782, 799, 817, 831, 862, 907, 950, 976, 994, 1,016, 1,036, 1,078, 1,096, 1,159, 1,210, 1,251, 1,319, 1,336, 1,366, 1,448, 1,480, 1,505, 1,561, 1,590, 1,642, 1,775, 2,926, 3,043, 3,094 cm^{-1}. HRMS (ESI): *m/z* calc. for $C_{17}H_{12}NO_5$ $[M + H]^+$: 310.0715, found: 310.0766.

7-[(3,4-Dimethyl-5-Oxo-2,5-Dihydrofuran-2-yl)Oxy]-3H-Phenoxazin-3-One [(±)-GC247]

To a solution of 5-chloro-3,4-dimethylfuran-2(5*H*)-one (35.0 mg, 240 μmol), resorufin sodium salt (28.2 mg, 120 μmol) and DIEA [84.0 μL, 480 μmol were sequentially added to DMF (2 ml)]. The resulting mixture was stirred at 64°C for 14 h. and then checked for completion by TLC (CH_2Cl_2/EtOAc 8:2). The crude mixture was diluted with EtOAc, successively washed with 10% aqueous citric acid, brine, dried over Na_2SO_4, and evaporated to dryness. The resulting residue was purified by chromatography on a silica gel column with a step gradient of EtOAc (0–20% v/v) in CH_2Cl_2 as the mobile phase, giving (±)-GC247 as yellow solid (25.0 mg, 77.0 μmol, 64%). Mp decomposition at 246°C. ^{1}H-NMR (300 MHz, $CDCl_3$) δ: 1.92–1.93 (t, $J = 1.5$ Hz, 3H), 2.11–2.12 (t, $J = 1.6$ Hz, 3H), 6.18 (bs, 1H), 6.32–6.33 (d, $J = 2$ Hz, 1H), 6.82–6.86 (dd, $J_1 = 9.8$ Hz, $J_2 = 2.1$ Hz, 1H), 7.04–7.05 (t, $J = 1.7$ Hz, 1H), 7.10–7.15 (m, 1H), 7.40–7.44 (d, $J = 9.9$ Hz, 1H), 7.74–7.77 (dd, $J_1 = 9.8$ Hz, $J_2 = 0.6$ Hz, 1H). ^{13}C-NMR (75 MHz, $CDCl_3$) δ: 8.7, 11.8, 99.7, 103.7, 107.2, 114.7, 127.6, 129.8, 131.8, 134.8, 134.9, 145.3, 147.1, 149.6, 153.1, 159.9, 171.3, 186.4. IR ν_{max} (film): 711, 742, 758, 782, 799, 817, 831, 862, 907, 950, 976, 994, 1,016, 1,036, 1,078, 1,096, 1,159, 1,210, 1,251, 1,319, 1,336, 1,366, 1,448, 1,480, 1,505, 1,561, 1,590, 1,642, 1,775, 2,926, 3,043, 3,094 cm^{-1}. HRMS (ESI): *m/z* calc. for $C_{18}H_{14}NO_5$ $[M + H]^+$: 324.0872, found: 324.0857.

Stability of CoumarinAc and DiFMUAc in Dimethyl Sulfoxide

Dimethyl sulfoxide (DMSO) solution of the compound to be tested (1 mM) was incubated at 20°C in the HPLC vials. (±)-1-Indanol [Alfa Aesar, purity >97.5% (GC); 10 mM] was used as the internal standard. The samples were subjected to reverse-phase-ultra-performance liquid chromatography (RP-UPLC)-MS analyses by means of UPLC system equipped with a photo diode array (PDA) and a triple quadrupole detector (TQD) mass spectrometer (Acquity UPLC-TQD, Waters). RP-UPLC (HSS C_{18}

column, 1.8 μm, 2.1 × 50 mm) with 0.1% (v/v) of formic acid in CH_3CN and 0.1% (v/v) of formic acid in water (aq. FA, 0.1%, v/v, pH 2.8) were used as eluents [10% CH_3CN, followed by linear gradient from 10 to 100% of CH_3CN (4 min)] at a flow rate of 0.6 ml min^{-1}. The detection was done by PDA and with the TQD mass spectrometer operated in electrospray ionization-positive mode at 3.2 kV capillary voltage. To maximize the signal, the cone voltage and collision energy were optimized to 20 V and 12 eV, respectively. The collision gas used was argon at a pressure maintained near 4.5 10^{-3} mBar. The relative quantity of the remaining (non-degraded) product was determined by integration comparison with the internal standard.

Expression and Purification of Proteins

Expression and purification of RMS3, AtD14, DAD2, and OsD14 proteins with cleavable GST tag were performed in accordance with the study by de Saint Germain et al. (2016) and de Saint Germain et al. (2021b). For DAD2 protein expression, the full-length coding sequences from *Petunia hybrida* were amplified by PCR using cDNA as template and specific primers (DAD2_attb1_HRV3C (5′-ggggacaagtttgtacaaaaaagcaggctccctg gaagtgctgtttcagggcccg**ATG**GGACAGACCCTTTTAGA-3′) and DAD2_attb2 (5′-ggggaccactttgtacaagaaagct gggtc**tcaTCA**CCTATGTGAAAGAGCTCTTC-3′) containing a protease cleavage site for tag removal, and subsequently cloned into the pGEXT-4T-3 expression vector. Similarly, for OsD14 protein expression, the coding sequences from *Ozyza sativa* were deleted from 153 nucleotides (51 amino acid) amplified by PCR using cDNA as template and specific primers (OsD14Δ51_attb1_HRV3C (5′-ggggacaagtttgtacaaaaaagcag gctccctggaagtgctgtttcagggcccg **ATG**CCGAGCGGGGCGAAGCTGCTGC-3′) and OsD14Δ51_attb2 (5′-ggggaccact ttgtacaagaaagctgggtc**tcaTTA**GTACCGGGCGAGAGCGCGGCGGAG-3′).

Method for Log*P* and pK_a Calculation

Relative hydrophobicity (log*P*) and pK_a values of SL probes and fluorophores were calculated using the ACD program (Advanced Chemistry Development, Inc.: https://ilab.acdlabs.com/ilab2/).

Pea Shoot Branching Assay

Pea (*Pisum sativum*) branching mutant plants used in this study were described previously (Rameau et al., 1997). The SL biosynthesis *rms1-10* (M3T-884) and SL response *rms3-4* (M2T-30) mutants were obtained from the dwarf cv. Térèse. Plants were grown in a greenhouse under long days as described by Braun et al. (2012).

Pea Shoot-Branching Assay by Direct Application on the Bud

The compounds to be tested were applied directly to the axillary bud with a micropipette as 10 μL of a solution containing 0.1% of acetone with 2% of polyethylene glycol 1,450, 50% of ethanol, and 0.4% of DMSO. The control 0 is the treatment with 0.1% of DMSO without compound. A total of 24 plants were sown per treatment in trays (2 repetitions of 12 plants). The treatment was done 8 days after sowing, on the axillary bud at node 3. The branches at nodes 1–2 were removed to encourage the outgrowth of axillary buds at nodes above. Nodes were numbered acropetally from the first scale leaf as node 1 and cotyledonary node as node 0. Bud growth at node 3 was measured 10 days after treatment. Plants with damaged main shoot apex or showing a dead white treated bud were discarded from the analysis. The SL-deficient *rms1-10* pea mutant was used for all experiments and WT Térèse as control. SL-perceived *rms3-4* pea mutant was used to test that when bioactive, the analog acts *via* RMS3, and it was also used to check the putative toxicity of probes.

Pea Shoot-Branching Assay by Vascular Supply

The compounds to be tested were applied by vascular supply (Muñoz et al., 2021). The control was the treatment with 0.1% of DMSO in water. A total of 12 plants were sown per treatment in trays and were treated with probes under node 3 bud generally 10 days after sowing. Compounds in DMSO solution were diluted with water to 3,000 nM for a treatment with 0.1% (v/v) DMSO. The branches at nodes 1 and 2 were removed to encourage the outgrowth of axillary buds at the nodes above. Nodes were numbered acropetally from the first scale leaf as node 1 and cotyledonary node as node 0. Bud growth at nodes 3 and 4 was measured with digital calipers 8–10 days after treatment. Plants with damaged main shoot apex or with a dead white treated-bud were discarded from the analysis. The SL-deficient *rms1-10* pea mutant was used for all experiments.

Hydroponic Assay on Arabidopsis

The hydroponic assay was adapted from the study by Cornet et al. (2021). Seeds were surface-sterilized for 8 min in a solution of ethanol (95%) and hypochlorite solution (10%; Bayrol, Mundolsheim, France) and were rinsed two times with ethanol (100%). Each seed was sown on top of a cut 0.5 ml Eppendorf tube filled with agar medium containing 0.65% of agar and 10% of nutritive solution of 5 mM NO_3. Tubes were soaked in water and stored in the dark at 4°C for 2 days. Twelve plants per pipette tip box (13 × 9 × 7 cm) were grown and supplied with nutrient solution as in the study by Boyer et al. (2014) at a concentration of 5 ml/L (750 ml of solution per box). Every week, the nutrient solution was renewed and every 10 days one time, a fresh batch of treatment was added to the solution. The first treatment occurred at day 27 after sowing when plants started to bolt. The number of rosette branches was counted at day 42.

Physcomitrium patens Bioassay

Assays on *Physcomitrium patens* were performed on plants grown in 24-well plates, starting from very small pieces of moss tissues as described by Guillory and Bonhomme (2021). As for pea *rms1*, the *Ppccd8* SL synthesis mutant was used for assays, since the effect of the compounds was better seen in this mutant vs. wild type (WT; Lopez-Obando et al., 2021). For each treatment, 24 plants were grown in $PpNO_3$ medium [minimal medium described by Ashton et al., 1979], dispatched in three different plates. Plants were grown for 2 weeks under control conditions, then treated with fluorophores or probes (all compounds used at 1 μM), before being placed vertically in the

dark for 10 days. A single picture of each well was taken under an Axio Zoom microscope (Zeiss) with a dedicated program. Filaments were counted using ImageJ software (http://imagej.nih.gov/ij/) as described by Guillory and Bonhomme (2021). Twenty-four plants were tested in each treatment.

Enzymatic Assays With Profluorescent Probes

The enzyme activity was determined by measuring the release of the fluorescent intensities of each fluorophores resulting from the cleavage of profluorescent probes by RMS3, AtD14, OsD14, and DAD2 proteins in a SPARK M10 in a 96-well format (de Saint Germain et al., 2021a). In the assay, using an Integra Viaflo 96 robot, 50 μL of a solution of protein at 0.33 μM in same buffer was added simultaneously in all 96 wells to 50 μL of profluorescent substrate solution (at varying concentrations, prepared from a 10 mM stock solution in 100% of DMSO) in PBS (100 mM of phosphate, pH 6.8, 150 mM of NaCl). After a lag time of 15 s, the formation of fluorophores was recorded over 3 h at 15 s intervals at 25°C. Each fluorophore was analyzed with the following excitation (ex) and emission (em) wavelengths: DiFMU λ_{ex} 360 nm/λ_{em} 450 nm, coumarin λ_{ex} 360 nm/λ_{em} 450 nm, resorufin λ_{em} 540/λ_{ex} 590 nm, and fluorescein λ_{em} 475 nm/λ_{ex} 520 nm. All experiments were repeated with three technical replicates. The fluorescence of each fluorophore was also determined for each measurement at the same time frame but in the absence of enzyme in order to determine the standard curves. For rapid enzymatic assays (**Figure 8A**, small panel), the solution of protein was added by the injector of the plate reader and then, the well was immediately read over 5 min with 1 s intervals. Same parameters were used to determine the fluorophore concentration.

Statistical Analysis

Since deviations from normality were observed for axillary bud length after SL treatment in pea bioassay, the Kruskal–Wallis test was used to assess the significance of one treatment with one compound in comparison to treatment with another using R Commander version 1.7–3 (Fox, 2005). For the bioassay in moss, ANOVA and Tukey's test as *post-hoc* test was used.

RESULTS

Design and Synthesis of SL Profluorescent Probes

SL Profluorescent Probes With Various Optical/Spectra Properties

We previously developed bioactive fluorogenic SL mimics, the racemic GC series, with commercially available coumarin moiety: 6,8-difluoro-7-hydroxy-4-methyl-2*H*-chromen-2-one (DiFMU) (±)-GC486, (±)-GC240, and (±)-GC242, respectively, with no, one, or two methyl groups on the bioactive group (de Saint Germain et al., 2016; **Figure 2**). For biochemical applications, the ideal fluorophore should exhibit a high molecular brightness ($\varepsilon \times \Phi_f$, with ε as the extinction coefficient and Φ_f as the quantum yield), which considers the efficiencies of fluorescence and light absorption. The ideal fluorophore should possess a large difference between λ_{ex} and λ_{em} (called Stokes shift), no toxicity, a good aqueous solubility, good cell permeability, high stability, and a resistance to photobleaching. Among the fluorophores compatible with the definition of SL mimics, the DiFMU showed all these requirements, especially the better spectral properties: Stokes shift 97 nm and $\varepsilon \times \Phi_f$ 17,800 $M^{-1}cm^{-1}$ (**Figure 3**, **Supplementary Figure 1**). Moreover, DiFMU was compatible with differential scanning fluorimetry (DSF) and intrinsic fluorescence assays since its emission spectrum does not overlap with those of protein dyed with SYPRO^{TM} orange and the intrinsic protein fluorescence (**Figure 3**).

To expand the repertory of SL profluorescent probes, new mimics have been designed with other fluorophores, such as coumarin [(±)-GC116, (±)-GC155] and scopoletin [(±)-GC379, (±)-GC380], bearing a methoxy group at the C-6 position and connected to D-ring butenolide with one or two methyl groups (**Figure 2**). These molecules could be valuable tools to study the effect of substitutions on the coumarin moiety, especially to evaluate the influence of the molecule reactivity (pK_a of the leaving group) and hydrophobicity (log*P*) on both biological and biochemical activity toward the various SL receptors, in order to perform SAR studies (**Figure 2**). A resorufin moiety was also targeted [(±)-GC93 = XLR (Wang et al., 2021), (±)-GC247 (**Figure 2**)], which has optical properties compatible for *in planta* imaging, contrary to coumarins. The excitation and emission maxima of resorufin (568 and 581 nm) and fluorescein (475 and 520 nm) made it suitable for use in plant tissue imaging compared to the other fluorophores (coumarin and DiFMU, 350–360 and 450–460 nm; **Figure 3**, **Supplementary Figure 1**). Likewise, resorufin allows for competitive enzymatic assay with UV fluorescent molecules like karrikins, for which intrinsic fluorescence assays are not possible.

SL Profluorescent Probes With Substitute D-Ring

To characterize the enzymatic properties of α/β hydrolase proteins like SL receptors, *para*-nitrophenyl acetate (*p*-NPA) is commonly used. Quantification of *p*-NPA hydrolysis is based on the measurement of absorbance, which has the disadvantage of requiring a large amount of protein in comparison to fluorescence-based detection. To overcome this drawback, we designed two fluorescent acetate probes (DiFMUAc and CoumarinAc) by acetylation of their phenolic moieties (**Figure 2**). These compounds could allow for the comparison of the enzymatic profile between probes and *per se* reveal the biological role of the D-ring.

Synthesis of SL Profluorescent Probes

GC probes have been prepared by the reaction of coumarins and resorufin with 5-bromo-3-methylfuran-2(5*H*)-one and 5-chloro-3,4-dimethylfuran-2(5*H*)-one and *N*, *N*-diisopropylethylamine as a base, in acetonitrile in yield up to 96% (**Figure 4**).

Biological Activity of the Profluorescent Probes

Various Coumarin SL Profluorescent Probes Are Bioactive in Pea

In order to check whether the designed probes were biologically active on shoot branching inhibition, we performed branching assay with the SL-deficient *rms1-10* mutant of pea. If the probe

A

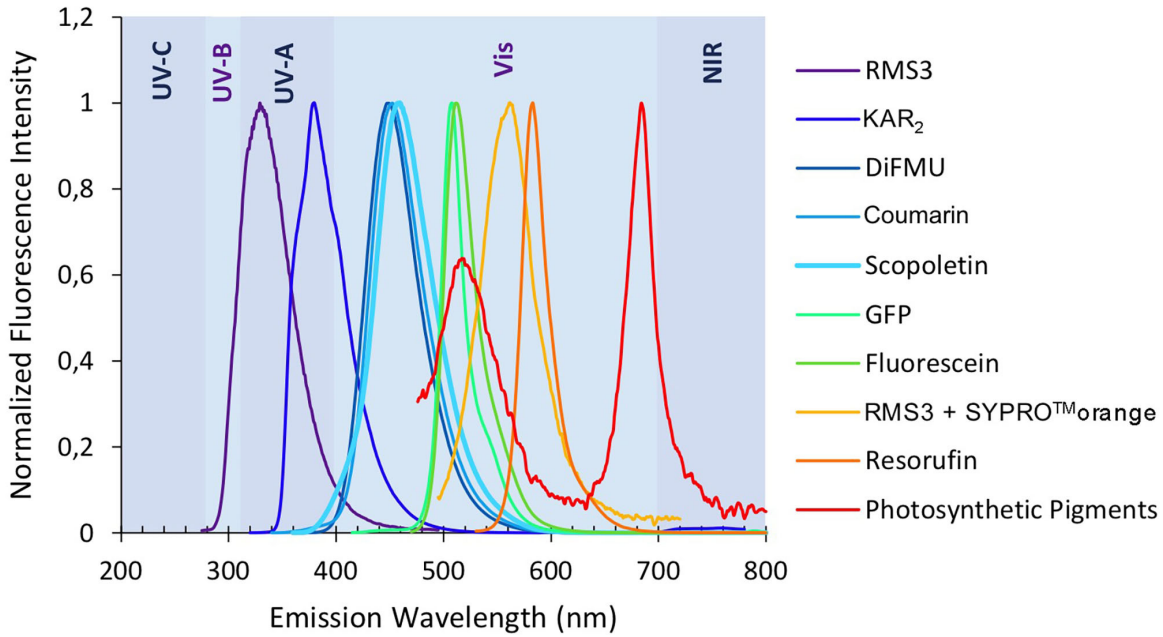

B

	λ_{abs} (nm)	λ_{ex} (nm)	λ_{em} (nm)	Stokes shift (nm)	Φ_f	ε ($M^{-1}cm^{-1}$)	Φ_f X ε ($M^{-1}cm^{-1}$)	Log*P*[8]
RMS3	278	279	329	50	/	/	/	/
KAR_2	332	331	379	48	n.a.	n.a.	n.a.	0.40
DiFMU	359	358	449	91	0.64[1]	17,800[1]	11,392	2.34
Coumarin	327	326	452	126	0.76[2]	13,000[2]	9,880	1.58
Scopoletin	359	363	459	96	0.56[3]	12,810[4]	7,173	1.48
GFP	/	392	508	116	/	/	/	/
Fluorescein	490	489	512	23	0.95[7]	80,000[7]	76,000	4.07
RMS3 + SYPRO™ orange	/	474	562	88	/	/	/	/
Resorufin	570	569	583	14	0.74[5,6]	56,000[5]	41,440	1.81
Photosynthetic Pigments	/	/	517/684	/	/	/	/	/

FIGURE 3 | Optical properties of fluorophores. Normalized fluorescence emission spectra of the fluorophores and some chemical compounds **(A)** (mentioned in this study). Chemical and spectral data for each molecule as λ_{abs} (nm) λ_{ex} (nm) λ_{em} (nm) ε ($M^{-1}cm^{-1}$) Φ_f Φ_f X ε ("molecular brightness") ($M^{-1}cm^{-1}$) Log*P* **(B)** [1]pH 10 (Sun et al., 1998). [2]pH 7.4 (Setsukinai et al., 2000). [3]pH 6.8 (Pham et al., 2019). [4]In EtOH (Abu-Eittah and El-Tawil, 1985). [5]pH 9.5 (Tan et al., 2021). [6](Bueno et al., 2002). [7]In 0.1 N NaOH, https://www.aatbio.com. [8]Log*P* are calculated by the ACD program. n.a. not available.

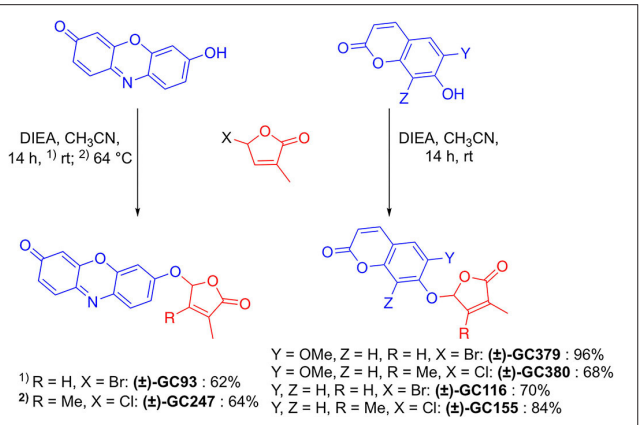

FIGURE 4 | Synthesis of novel profluorescent SL probes.

is biologically active, it should inhibit branch development. To evaluate this inhibition, we compared our results with *rms1-10* mutants treated with a control solution, and with non-treated (NT) Térèse plants, for which bud development was inhibited by endogenous natural SLs. Globally, the acetate probes (DiFMUAc and CoumarinAc) showed no effect on *rms1-10* mutant plants, confirming that the D-ring group is essential for a significant biological effect (**Figure 5A**, **Supplementary Table 1**). The significant effect observed for DiFMUAc at 100 nM could be due to the slight toxicity of DIFMUAc on axillary bud; however, it is not detected at higher concentration.

Both (±)-GC242 and (±)-GC155 probes with two methyl groups on their D-ring appeared to be among the most bioactive molecules. We also observed an inhibition of bud development for the probes with one methyl group [(±)-GC240, (±)-GC116 and (±)-YLG] though the (±)-GC240 and (±)-YLG probes were less efficient than (±)-GR24 and probes with two methyl groups. This suggests that a two-methyl D-ring group improves the biological activity in pea as observed for SL analogs (Boyer et al., 2012, 2014). Surprisingly, when comparing the probes with one methyl group on the D-ring [(±)-GR24, (±)-GC116 and (±)-GC240], we observed the strongest inhibition of bud development, at 10 nM for (±)-GC116, suggesting that the coumarin moiety improved biological efficiency. Bearing scopoletin moiety (±)-GC379 and (±)-GC380 were bioactive for the three tested concentrations (**Figure 5B**). In contrast, the probes of the resorufin series [(±)-GC93 and (±)-GC247] showed an inhibitory effect with statistical significance only at 10 μM (**Figure 5C**). The (±)-YLG probe was less bioactive than (±)-GC240 and (±)-GC116 probes suggesting that the fluorescein group affected probe activity. We confirmed that (±)-GC486, without methyl on the D-ring, showed no biological activity on branching inhibition (de Saint Germain et al., 2016; **Figure 5A**) similar to (±)-dYLG (Yao et al., 2021). GC analogs could not repress branching of the pea *rms3-4* perception mutant (**Supplementary Table 2**). These results suggest that GC probes, such as (±)-GR24, are bioactive SL analogs and inhibit bud outgrowth in pea *via* the RMS3 receptor, and not because of toxicity.

In order to explain the lower bioactivity of resorufin probes [(±)-GC93, (±)-GC247] and fluorescein (±)-YLG (**Figures 5A,C**), we fed the SL analogs to the vascular stream of pea shoots as previously described (de Saint Germain et al., 2021b; Muñoz et al., 2021). This feeding method allowed to circumvent a putative problem of tissue penetration due to compound hydrophobicity; however, this is not highlighted by Log*P* modeling (partition coefficient; **Figure 2**). Again, we found lower bioactivity for (±)-YLG and (±)-GC93 compared to the coumarin derivatives series, ruling out the role of tissue penetration on the weak bioactivity (**Supplementary Figure 2**, **Supplementary Table 3**). If not hydrophobicity, the most plausible explanation could be relatively the bigger size of fluorescein and resorufin compared to coumarin moiety.

Bioactivity of GC Probes in Arabidopsis

To compare the bioactivity of our probes between species, we performed a hydroponic bioassay with the Arabidopsis SL-deficient mutant *max3-11*. Since (±)-GC242 was previously found bioactive (de Saint Germain et al., 2016), we only tested the probes with one methyl group on the D-ring [(±)-GC240, (±)-GC116, (±)-GC93, and (±)-YLG] at two concentrations (0.5, 3 μM). The (±)-GR24 control treatment was bioactive at both concentrations whereas only the (±)-GC116 probe was found bioactive at 3 μM (**Figure 6**). This probe was also the most bioactive probe on pea for the control of shoot branching. In our conditions (±)-YLG and (±)-GC93 compounds were not bioactive contrary to previous studies (Tsuchiya et al., 2015; Wang et al., 2021). This result highlights the efficiency of our GC coumarin series on Arabidopsis and its appropriateness for *in vivo* investigations.

Coumarin and Resorufin Profluorescent Probes Are Bioactive in *P. patens*

In the moss *P. patens*, the biological activity of SL analogs was previously assayed by counting the number of filaments per plant, grown for 2 weeks in the dark following compound application (Guillory and Bonhomme, 2021). Both (±)-GR24 and (+)-GR24 enantiomer led to a decrease in filament number, in WT plants and in the *Ppccd8* mutant, where the activity was more pronounced (Hoffmann et al., 2014; Lopez-Obando et al., 2021). Using the two methyl profluorescent probe (±)-GC242 (**Figure 2**), a dose-dependent decrease in the filament number was observed in the *Ppccd8* mutant. However, the (±)-GC242 was found less active than (±)-GR24 (Lopez-Obando et al., 2021). We tested the activity of the GC series with only one methyl group and various fluorophores and compared it to that of (±)-GR24 and (±)-GC242. We also tested a profluorescent probe without a methyl group [(±)-GC486] since desmethyl GR24 was described as a better ligand for KAI2 in *Marchantia polymorpha*, which is another bryophyte (Yao et al., 2021; **Figure 7**). In the *Ppccd8* mutant, we first observed that none of the fluorophores had an effect on the filament number, and we confirmed the previous activity reported for (±)-GR24 and (±)-GC242. (±)-GC240 (one methyl group) had similar

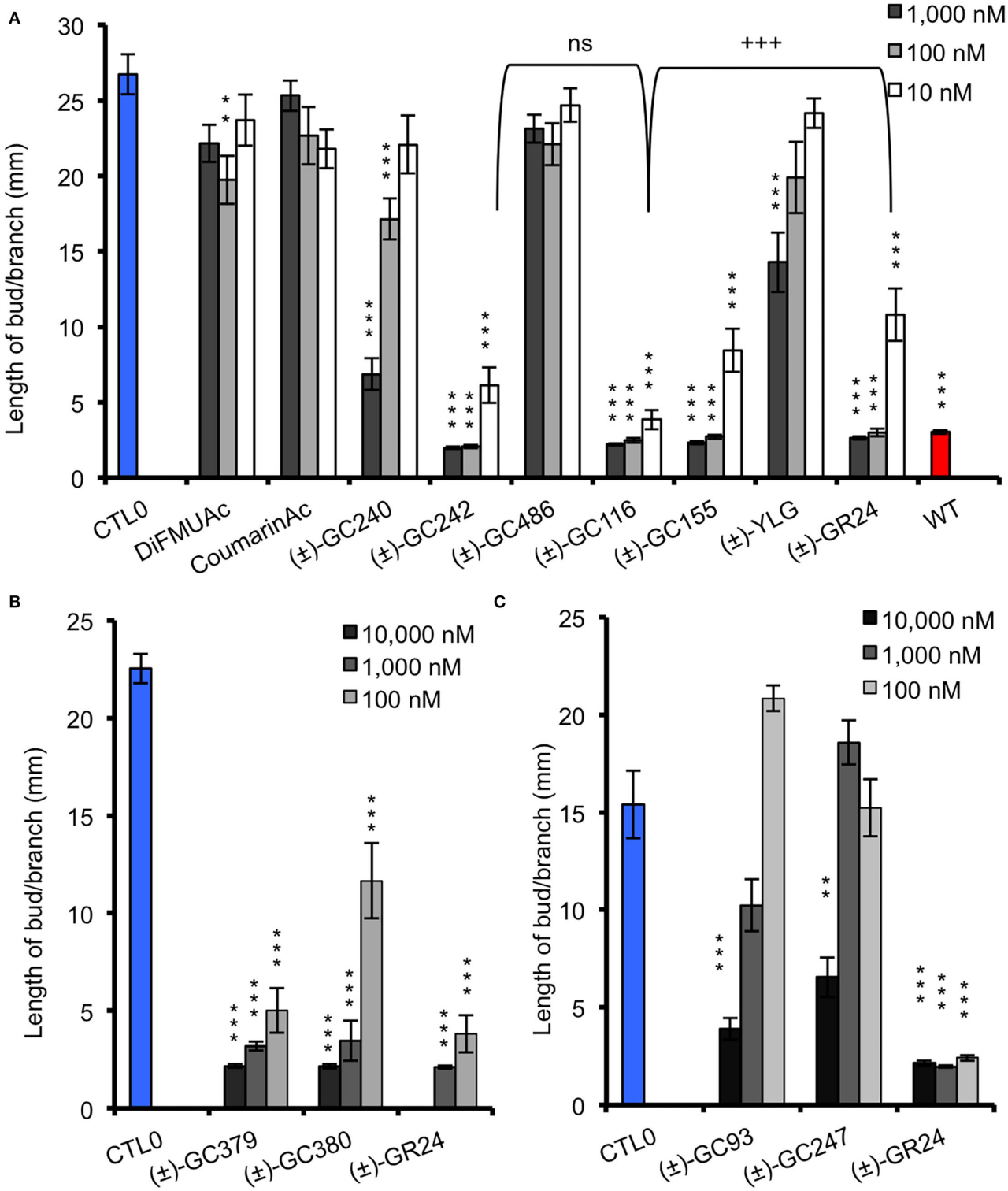

FIGURE 5 | Bioactivity in pea of probes vs. (±)-GR24 (*rms1-10*), coumarin and fluorescein probes **(A)**, scopoletin probes **(B)**, and resorufin derivative probes **(C)**. Length of the axillary buds of *rms1-10* plants, 8 days after direct application of probes and of (±)-GR24. All replicates are presented in **Supplementary Table 1** with control 0. These data were obtained from means ± SE ($n \geq 20$ plants). $^{**}P < 0.01$, $^{***}P < 0.001$ indicate significant differences with the control treatment (0 nM) (CTL0) (Kruskal–Wallis rank sum test). CTL0, control 0. All the replicates are presented in **Supplementary Table 1**. $^{+++}P < 0.001$ indicates significant differences with the (±)-GR24 treatment (10 nM) (Kruskal–Wallis rank sum test). ns, not significant.

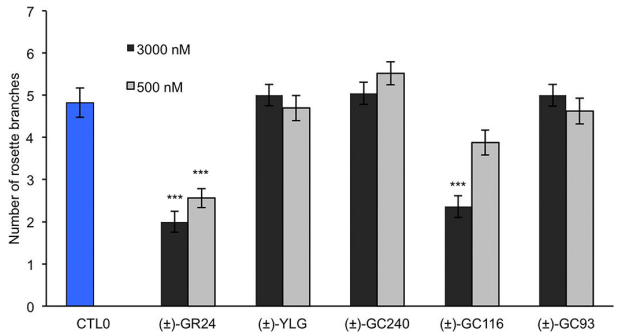

FIGURE 6 | Bioactivity in Arabidopsis of probes vs. (±)-GR24 (*max3-11*). Number of rosette branches of mutant plants *max3-11* grown in long-day conditions. These data were obtained from means ± SE ($n = 12$ plants). ***$P < 0.001$ indicate significant differences with the control treatment (0 nM) (CTL0) (Kruskal–Wallis rank sum test). CTL0, control 0.

activity as (±)-GC242 (two methyl groups), while (±)-GC486 had a slight opposite effect on the number of filaments in one bioassay replication (**Supplementary Figure 3**). Thus, the presence/absence of a methyl group on the D-ring has a strong influence, but not the number of groups. All profluorescent probes with one methyl group but various fluorophores had a significant effect on the filament number. However, the strongest activity was observed with resorufin derivative (±)-GC93, while both coumarin probes [(±)-GC240 and (±)-GC116] showed similar moderate activities, and fluorescein probe (±)-YLG was found to be less active. In one bioassay replication, no significant bioactivity was detected for (±)-YLG and (±)-GC116 (**Supplementary Figure 3**). These data suggest that, in addition to the presence of methyl on the D-ring, the nature of fluorophore has an effect on the profluorescent probe activity in *P. patens*.

Enzymatic Assays With the Profluorescent Probes

As previously described, after cleavage by the D14 proteins, these probes emit light when excited by a specific wavelength (**Figure 3**, **Supplementary Figure 1**). They allow us to have a quantitative follow-up of the reaction.

Two-phase cleavage kinetics was obtained with both (±)-GC242 and (±)-GC240: (1) an initial phase or burst phase corresponding to the fluorophore release during the first turnover (pre-steady state) and after a delay (few minutes or hours, depending on the ligand and the receptor); (2) a slow phase or a plateau (depending on the number of methyl on the D-ring) which can lead to return to the initial situation of a free D14 protein without ligand (steady state) for the probes bearing one methyl group. With two methyl group probes, a plateau was observed which does not allow for a second cleavage run for the protein, making this receptor unable to interact with other SLs (single turnover; de Saint Germain et al., 2016). We proposed that the different probes newly described, could be used to determine the parameters influencing the kinetic process and better understand the perception mechanism.

The Hydrolysis Kinetics by RMS3/PsD14 Are Different According to the GC Series Depending on the Number of Methyl Groups on the D-Ring

We performed enzymatic assays to study the effect of the D-ring structure on the kinetic cleavage. We used DiFMU probes harboring one [(±)-GC240], two [(±)-GC242], or no methyl group [(±)-GC486] on the D-ring, along with a molecule where the D-ring was replaced by an acetate group (DiFMU acetate, DiFMUAc; **Figure 8A**). We observed that the acetate probe kinetic differed from the other ones, with a higher extent of reaction but a slower reaction rate than those with one or two methyl groups. Moreover, the reaction seemed to be blocked at very low concentration for (±)-GC242 and (±)-GC240, in accordance with previous results (de Saint Germain et al., 2016). The (±)-GC486 kinetic differed from that of the other probes with a D-ring, with a high reaction rate, but the low slope of the cleavage kinetic curves during the initial phase in comparison to (±)-GC242 and (±)-GC240, suggests an initial slower cleavage velocity. We observed the same pattern with Coumarin acetate (CoumarinAc) vs. (±)-GC116 and (±)-GC155 (**Figure 8B**). However, CoumarinAc showed a slower velocity than DiFMUAc. The RMS3 showed Michaelian kinetics toward the acetate probes and (±)-GC486. Indeed, the hydrolysis of these probes was not blocked at a very low level, unlike for (±)-GC240 or (±)-GC242 (respectively due to the lack of D-ring or the absence of methyl group on the D-ring). This could be linked to the lack of bioactivity of these molecules on pea branching. Despite a higher velocity of DiFMUAc cleavage by RMS3, this probe shows the drawback to be poorly stable in PBS even in DMSO, in comparison to CoumarinAc (**Supplementary Figure 4**).

To study the effect of the cargo group on the SL cleavage kinetics, we compared (±)-GC242, (±)-GC155, and (±)-GC247 probes, harboring two methyl groups on the D-ring but having three different fluorophores (**Figure 9**) and for which a single turnover mechanism was proposed (de Saint Germain et al., 2016). By recording the fluorescence, we observed a two-phase kinetic for all three probes (**Figure 9B**), with a burst phase, or a presteady phase, followed by a steady phase where the product concentration reached a plateau as previously described with (±)-GC242. Looking at the slope of the presteady state for all the four probes [(±)-GC240, (±)-GC116, (±)-GC93 and (±)-YLG], we estimated that the enzymatic activity depended on the probe, and thus on the fluorophore molecule replacing the ABC-tricycle (**Figure 9A**). We speculated that the fluorophore group may mimic a cargo group that interacts with the binding pocket of RMS3 and may therefore, influence the affinity. On the contrary, the heights of the plateau values were all in the same range and did not seem to depend on the probe. These results support the hypothesis of a single turnover enzymatic mechanism for the probes with two methyl groups.

We performed similar assays for the probes with one methyl group on the D-ring and noticed a different kinetic mechanism (**Figure 9A**). We observed two steps:

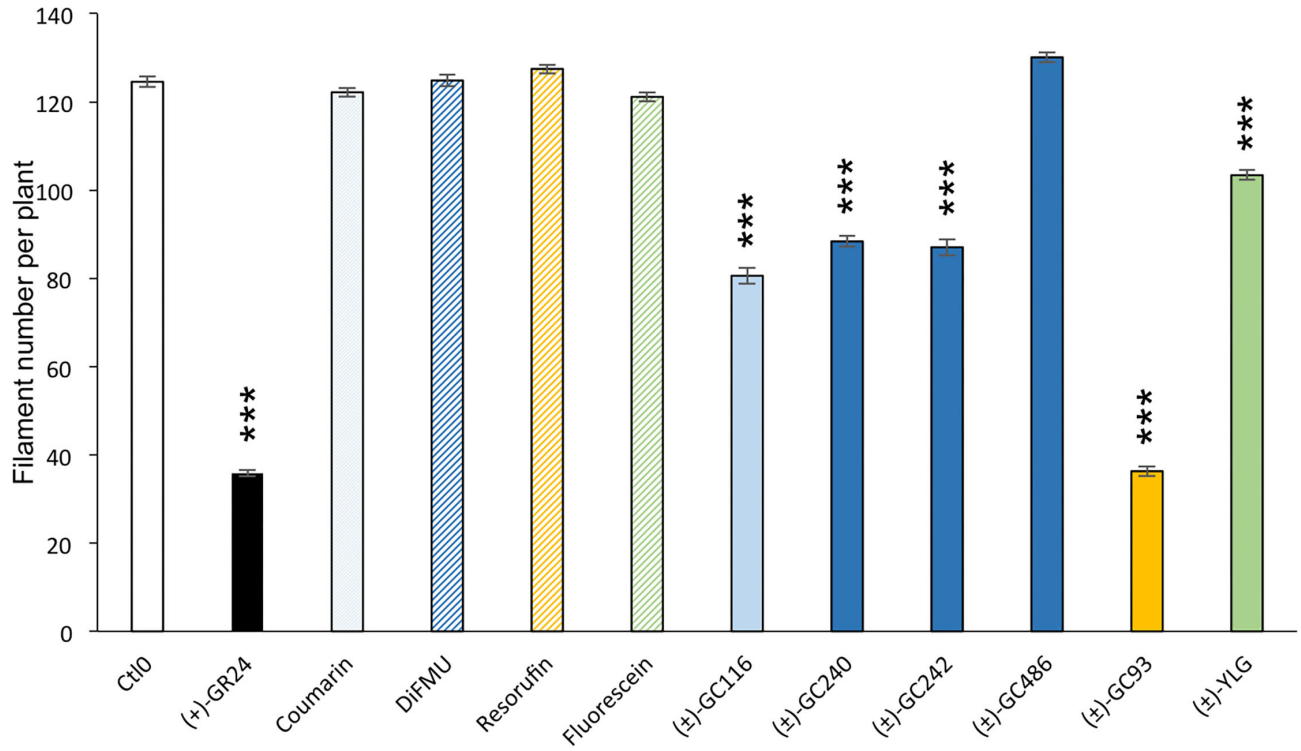

FIGURE 7 | Probe bioactivity tested on the moss *P. patens*. Bioactivity of fluorophores and profluorescent probes was assayed by counting the number of filaments in the dark following application and was compared to that of DMSO (control 0, white), and (+)-GR24 (in black). Each compound was used at 1 μM. Fluorophore bars appear hatched, while the profluorescent probe bars appear plain. Data are mean ± SE of 24 *Ppccd8* mutant plants ($n = 24$) grown in three different 24-well plates. Significant differences between the control treatment (0 nM) and treated plants are based on ANOVA and Tukey's test as a *post-hoc* test; ***$P < 0.001$. CTL0, control 0.

a very fast burst phase (<30 s), difficult to highlight in our conditions, followed by a slow phase (steady state) with no plateau, contrary to two methyl D-ring probes (**Figure 9B**). Indeed, in this second phase, the reaction did not seem to be blocked, but the velocity was very low, meaning that the reaction did not perfectly follow a single turnover mechanism. Presumably, some RMS3 protein might catalyze more than one probe molecule. We also observed differences between the progress curves of the different probes, meaning that the cargo group still had an influence on the enzymatic mechanism.

To search for a destabilization effect, which characterizes bioactive SL analogs with SL receptors, we performed DSF binding assay with our novel probes on RMS3 protein. We confirmed that the (±)-GC116, (±)-GC155, and (±)-GC379 probes were able to destabilize RMS3 (**Supplementary Figure 5**). Similar investigations were not possible with resorufin and fluorescein probes [(±)-GC93, (±)-GC247, (±)-YLG] due to the overlap of their emission spectra with that of SYPRO^{TM} orange and RMS3 (**Figure 3**). We noticed three different behaviors for the probes with a D-ring according to their number of methyl groups. The (±)-GC486, with no methyl group on the D-ring, did not show a single turnover kinetic, but more likely a curve that resembled that of the acetate probes. The probes with two methyl groups showed a rapid and blocked enzymatic reaction that fits with the hypothesis of a single turnover mechanism. Finally, the probes with one methyl group had a particular kinetic that could be partly linked to a single turnover mechanism. These assays suggest that the number of methyl groups is important for covalent adduct stability.

Comparison of the Hydrolysis Kinetics Between SL Receptor From Different Species

Finally, the GC probes were used to compare the enzymatic activity of RMS3, AtD14, DAD2, and OsD14 proteins. We compared the enzymatic kinetics of these proteins at a concentration of 0.33 μM toward three different probes at 10 μM [(±)-GC240, (±)-GC242, and (±)-YLG, **Figure 10**]. All tested proteins were able to cleave the (±)-GC240 and (±)-GC242 probes but differences in the reaction kinetics were observed. With (±)-GC240 cleavage, it was highly difficult to highlight the rapid phase of the kinetic (due to the low time resolution), except for OsD14 suggesting a lower affinity of the rice SL receptor toward (±)-GC240 (**Figure 10A**), confirmed by the cleavage profile of (±)-GC242 (**Figure 10B**). Surprisingly, we observed that OsD14 was unable to cleave (±)-YLG, in contrast to the three other proteins (**Figure 10C**).

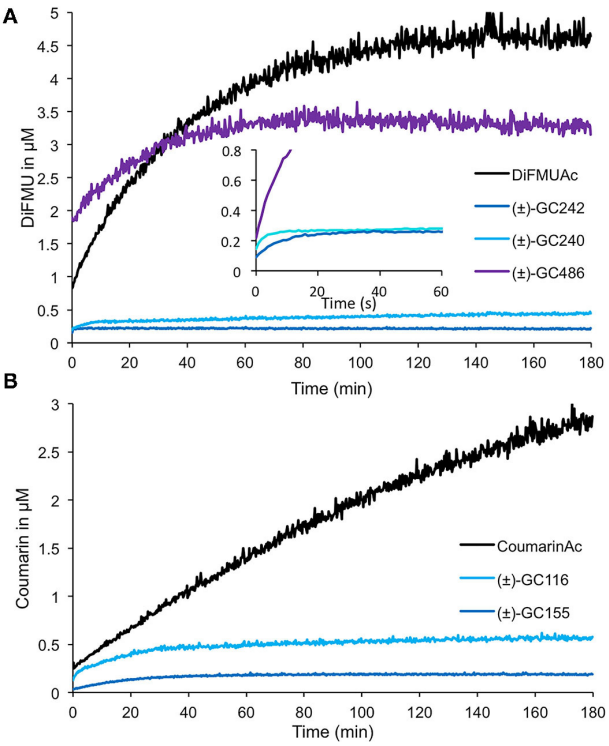

FIGURE 8 | Enzymatic assays with profluorescent probes harboring various D-ring moieties or acetate groups. Progress curves during DiFMU **(A)** and Coumarin **(B)** profluorescent probes at 10 µM cleavage with RMS3 protein at 400 nM monitored (λ_{em}: 460 nm) at 25°C. These traces represent one of the three replicates, and the experiments were repeated at least two times.

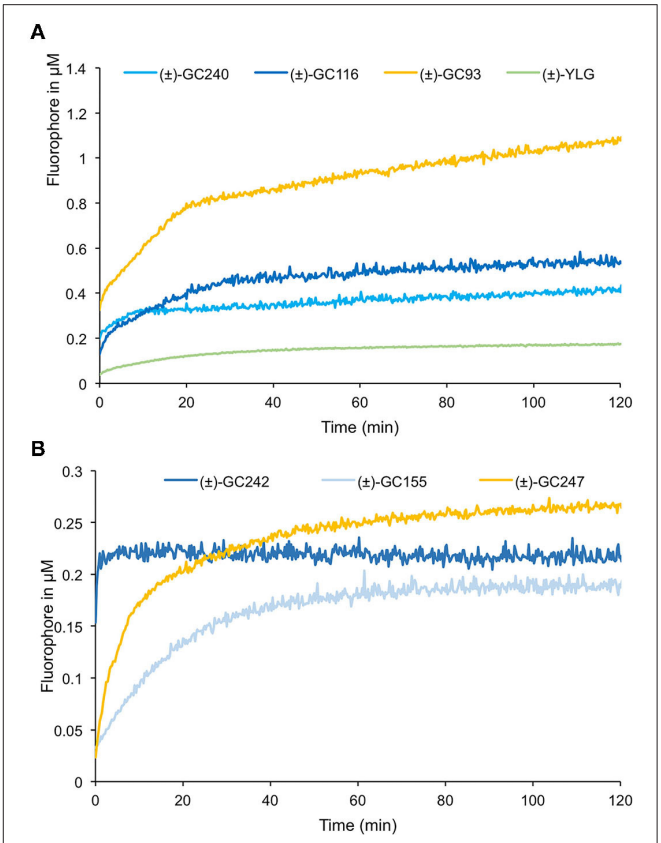

FIGURE 9 | Enzymatic assays with profluorescent probes harboring various fluorophores. Progress curves profluorescent probes at 10 µM cleavage harboring D-ring with one methyl **(A)** or two methyl groups **(B)**, with RMS3 protein at 400 nM monitored (λ_{em}: 460 nm) at 25°C. These traces represent one of the three replicates, and the experiments were repeated at least two times.

DISCUSSION

Importance of Having Probes With Different Spectral Properties

The design of profluorescent SL probes was focused on obtaining bioactive molecules with spectral properties compatible with biochemistry approaches, such as enzymatic kinetics and fluorescence-based binding assays (DSF, nanoDSF, or intrinsic fluorescence assays). Probes should present a high molecular brightness and a large Stokes shift to easily record the fluorescence emission with classical equipment. Probes also need to be highly stable to perform kinetic measurements. Unfortunately, none of the molecules tested here could combine all these properties, for example, resorufin. Resorufin is a common fluorophore used in profluorescent probes (Gao et al., 2003; Zhang et al., 2015; Yan et al., 2016; Biswas et al., 2017; Wu et al., 2017; Tian et al., 2021). It showed a high brightness, a broad spectrum, and longer analytical wavelength than the fluorescein moiety present in YLG, efficient for *in planta* imaging and has been claimed (Wang et al., 2021) to outperform YLG series, for its optical properties more adapted to *in planta* imaging. However, resorufin probes present small Stokes shifts, which are the major limitations of resorufin series, and are not suitable for DSF assays. An opportunity in the development of efficient SL profluorescent probes focussed not only on the modulations of resorufin unit to improve the pK_a, solubility and the membrane permeability but also on expanding the Stokes shifts as recently reported (Tan et al., 2021). Thus, the development of novel profluorescent SL should offer tools for dedicated applications.

Important Effect of Chemical Structures of Profluorescent Probes for Bioactivity

In comparison to (±)-YLG, the GC probes showed lower brightness, which is a drawback of fluorescent detection, but with the leaving group, the GC probes showed a hindrance more similar to that of natural SLs. Accordingly, we found out that GC probes were biologically active in pea, with a better bioactivity for coumarin-based probes. Only the most active probes in pea [(±)-GC242 and (±)-GC116] were significantly bioactive in Arabidopsis. We demonstrated that the coumarin profluorescent probes were highly bioactive and well-adapted to dissect the enzymatic properties of SL receptors. The high bioactivity of GC coumarin probes is linked not only to their hydrophobicity (Log*P*) close to that of (±)-GR24 but also to the good cleavability of the leaving groups in relation to their

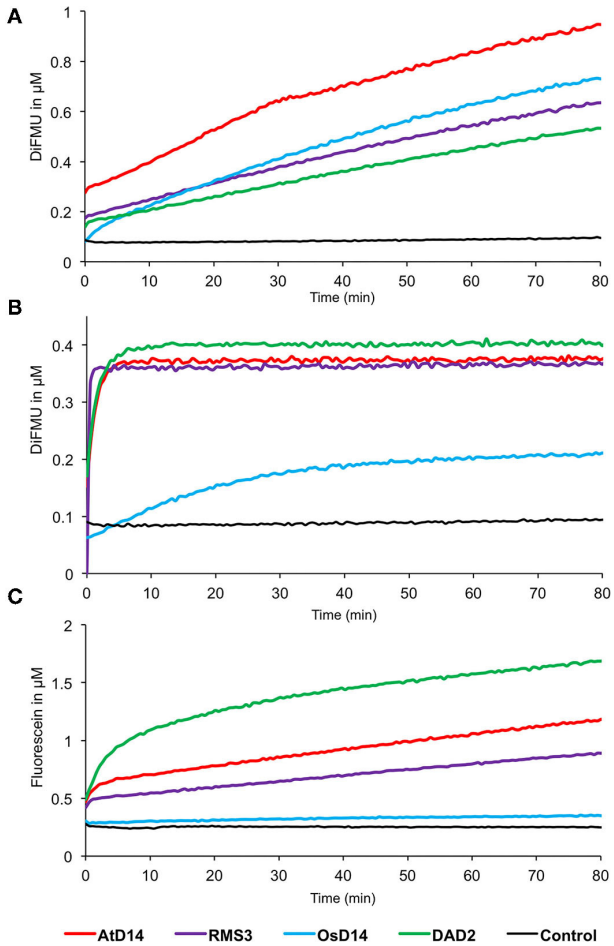

FIGURE 10 | Enzymatic kinetics for AtD14, RMS3, OsD14, and DAD2 proteins incubated with (±)-GC240 **(A)**, (±)-GC242 **(B)**, or (±)-YLG **(C)**. Progress curves during probes cleavage, monitored (λ_{em} 460 nm for (±)-GC240 and (±)-GC242 and λ_{em} 510 nm for (±)-YLG) at 25°C. Protein catalyzed cleavage with 400 nM of protein and 20 µM of probes. These traces represent one of the three replicates, and the experiments were repeated at least two times.

low pK_a values (**Figure 2**) as noticed for debranones (Fukui et al., 2017). This high bioactivity could also be attributed to their binding affinity to SL receptors, mainly based on the cargo group (i.e., fluorescent part). Our experimental data are consistent with a recent molecular simulation study (Wang et al., 2021). Based on the demonstrated high bioactivity of different SL coumarin profluorescent probes in vascular plants, we can assert that this chemical backbone constitutes a relevant working basis for developing new probes with refined properties. Coumarin is a fluorophore that has been repeatedly used to design sensors aiming at the detection of biological elements and phenomena of many different origins (Cao et al., 2019). It is reported in several studies that can easily inspire us in this quest. Further design on the fluorophore backbone itself, in order to adjust its optical properties (brightness, absorption, and emission wavelengths) and/or physicochemical properties (solubility, pK_a, log$P$) may also allow us to develop new molecules that are more relevant for use in biological environments (Roubinet et al., 2015).

Profluorescent Probes: Clues for Knowledge in SL Perception in Pea and Arabidopsis

Enzymatic competition assay with YLG and GC probes have been used to characterize the perception mechanism of newly identified D14 ligand. However, the interpretation of these results and the determination of kinetic constant like K_i (inhibition constant) remains challenging because D14 does not behave like a Michaelian enzyme toward these probes. To overcome this difficulty, it is possible to use the acetate probes to perform enzymatic competition assay and characterize more easily the type of competition mechanism and compare different ligand binding properties.

We observed that some of these probes are not only hydrolyzed by D14 proteins but are also not biologically active on pea [i.e., DiFMUAc, coumarinAc, and (±)-GC486]. This means that the bioactivity does not depend on the cleavage of the molecules, but more probably on the formation of a particular intermediate. The biological activity is also dependent on the presence of D-ring with one or two methyl groups, which suggests that this part of the molecule participates in the perception mechanism. Different parameters influence the affinity and kinetics of plant SL receptors in the presence of SLs: they depend both on the D-ring and on the cargo group. The cargo group, which corresponds to ABC-tricycle in canonical SLs, is partially responsible for the interaction with D14. Thus, it could influence the reaction rate and the apparent affinity because this part of the molecule acts in the first contact with D14. Moreover, the structure of the D-ring part also influences the enzymatic mechanism as it was observed with the variation of the number of methyl groups. Indeed, the probes with two methyl groups seemed to undergo a strict single turnover mechanism while those with one methyl group showed a burst phase followed by a slow phase. The covalent adduct created with the D-ring with two methyl groups could be more stable due to steric interactions and/or electronic effects in contrast to the D-ring with one methyl group and even with no methyl group for which no covalent adduct was detected with RMS3 (de Saint Germain et al., 2016). To precisely compare the enzymatic activity of the different receptors toward each probe, and to provide a better understanding of SL perception mechanism, it is necessary to determine kinetic constants like K_M, V_{max}, and k_{cat}. Since it is clear that this mechanism depends on the structure of the SL molecule, it could be interesting to modulate pK_a, hindrance, and hydrophobicity of the probes to link cleavage kinetics, bioactivity, and perception mechanism.

Profluorescent Probes: Tools to Perform SAR Study and Compare Bioactivity Between Species

We have shown that the hydrolysis profile of profluorescent probes is not only dependent on the probes but also on the

SL receptors. There is generally a correlation between a fast cleavage of the probe and a good biological activity on pea and Arabidopsis. This should be verified not only for petunia but also for rice for which OsD14 protein is not able to cleave (±)-YLG.

Furthermore, the hydrolysis activity is proposed to be determinant to have a highly sensitive SL receptor as in *Striga, Orobanche*, and *Phelipanche* (de Saint Germain et al., 2021b; Chen et al., 2022). GC and (±)-YLG probes showed germination activity in these parasitic plant seeds but much weaker than SLs and without selectivity (de Saint Germain et al., 2021b; Wang et al., 2021). SL profluorescent probes with better efficiency would be worth being developed for the study of SL receptors in these plants.

In *P. patens* where there is no D14 ortholog, 13 *PpKAI2Like* genes have been reported as encoding candidate receptors for SL and for the so far unknown KAI2-Ligand (KL). Strikingly, the SL and the KL pathways have opposite effects on the filament number and the phenotype assayed in the present study. The (+)-GR24 is a good mimic for SL in moss, decreasing the number of filaments, and is likely to be perceived by the PpKAI2L (GJM) clade (Lopez-Obando et al., 2021). Here, we show that (±)-GC93 has the best bioactivity as SL mimics in *P. patens,* being even more potent than (±)-GC242. This profluorescent probe could thus be used to further analyze SL perception mechanism in moss, when PpKAI2L-G,J recombinant proteins will be available (Lopez-Obando et al., 2021). Besides, the (−)-GR24 has proven as a poor mimic for studying the KL pathway by the PpKAI2L (A-E) clade. Although the natural SLs have only one methyl group on the D-ring (Yoneyama, 2020), recent results demonstrated that (−)-desmethyl GR24 was a better mimic of KAI2-ligands (KL) than (−)-GR24 (Yao et al., 2021). In one assay reported above, the (±)-GC486 (no methyl on the D-ring) showed an opposite effect to that of other probes, increasing the number of filaments (**Supplementary Figure 3**). The (±)-GC486 thus needs to be tested as a potential KL agonist on moss WT and *Ppkai2La-e* mutants (Lopez-Obando et al., 2021).

Tools for new Investigation/Applications

Research of Agonists and Antagonists With Profluorescent Probes

Synthetic inhibitors KK094 (Nakamura et al., 2019), TFA (Hamiaux et al., 2018), and DL1b (Yoshimura et al., 2020) of D14 SL receptors have been described in Arabidopsis and petunia. Their discovery was based especially on their aptitude to inhibit the hydrolysis of (±)-YLG in competition assays with SL receptors. However, no bioactivity of these molecules (KK094, TFA, DL1b) was detected in pea. A screen of chemical libraries for potential SL agonists and antagonists could thus be undertaken using our GC coumarin tools [e.g., (±)-GC242 or (±)-GC116] highly bioactive in pea for bud outgrowth inhibition *via* RMS3, to discover novel hits. With the GC probes, it would be also possible to characterize OsD14 enzymatic properties and screen for compounds interacting with the SL rice receptor, that is not possible with (±)-YLG. The use of different fluorophores could facilitate high throughput screening for active molecules and inhibitor, especially to detect molecules with fluorescence property that perturb the signal detection and are therefore used to be eliminated from the screen.

The (±)-YLG has also been used to validate SL receptor agonists (Uraguchi et al., 2018) or antagonists (Holbrook-Smith et al., 2016; Arellano-Saab et al., 2022; Zarban et al., 2022) for *Striga*. Again, the discovery of a profluorescent probe, which is as active as SLs, remains to be discovered to obtain a more relevant screening tool for the discovery of efficient inhibitors for SL receptors or SL mimics.

Characterization of Other Enzymes

Very recently, a degradation pathway for SLs has been discovered in *Arabidopsis thaliana* (Xu et al., 2021). It involves a carboxylesterase (AtCXE15), with no SL reception function, which was demonstrated to be able to break SL molecules and thereby modulate shoot branching. The SL profluorescent probes are also very promising tools to characterize this type of enzyme or any protein that is able to cleave SLs.

For in Planta Imaging

Fluorogenic SL probes are essential tools for *in planta* imaging, but tissue autofluorescence is a major problem in plants, due to the high content of photosynthetic pigments. With the expansion of profluorescent probes repertory, it would be possible to develop microscopy imaging specifically to localize SL perception. Co-localization with GFP-tagged proteins would also be easier with GC probes, while fluorescein spectra overlapping with GFP prevents such studies (**Figure 3**).

CONCLUSION

To conclude, our experiments partially unveiled the complexity and the diversity of SL perception by the D14 family of receptors. We emphasized that no profluorescent SL probe was universal and that these probes should be used with caution depending on their designated purpose. Our molecular tools described could help to discover novel useful agonists/antagonists of SL receptors for applications and fundamental knowledge.

DATA AVAILABILITY STATEMENT

The raw data supporting the conclusions of this article will be made available by the authors, without undue reservation.

AUTHOR CONTRIBUTIONS

F-DB, AdSG, SB, and CR designed the research. GC and SDF designed and synthesized the probes. F-DB performed the HPLC analyses. F-DB, J-PP, AG, A-VS, and SB performed the biological experiments. AdSG and PS performed the biochemical experiments. AC recorded the fluorescent spectra. AdSG, SB, CR, and F-DB wrote the paper. All authors analyzed the data. All authors critically revised the manuscript. All authors contributed to the article and approved the submitted version.

FUNDING

We are grateful to the Agence Nationale de la Recherche (contracts ANR-12-BSV6-0004-01 and ANR-21-CE20-0026-04) for financial support. The IJPB benefits from the support of Saclay Plant Sciences-SPS (ANR-17-EUR-0007). This work has benefited from the support of IJPB's Plant Observatory technological platforms. AdSG has received the support of the EU in the framework of the Marie-Curie FP7 COFUND People Programme, through the award of an AgreenSkills/AgreenSkills+ fellowship and the support of Saclay Plant Sciences-SPS (ANR-17-EUR-0007) through the award of a fellowship. The CHARM3AT LabEx program (ANR-11-LABX-39) is also acknowledged for its support.

ACKNOWLEDGMENTS

CNRS-ICSN and the STREAM COST Action FA1206 are acknowledged for their support. We are grateful to Hemp *it adn* for financial support. The authors thank Sébastien Vidal for his comments on the manuscript.

SUPPLEMENTARY MATERIAL

The Supplementary Material for this article can be found online at: https://www.frontiersin.org/articles/10.3389/fpls.2022.887347/full#supplementary-material

REFERENCES

Abu-Eittah, R. H., and El-Tawil, B. A. H. (1985). The electronic absorption spectra of some coumarins. A molecular orbital treatment. *Can. J. Chem*. 63, 1173–1179. doi: 10.1139/v85-200

Akiyama, K., Matsuzaki, K., and Hayashi, H. (2005). Plant sesquiterpenes induce hyphal branching in arbuscular mycorrhizal fungi. *Nature* 435, 824–827. doi: 10.1038/nature03608

Arellano-Saab, A., McErlean, C. S. P., Lumba, S., Savchenko, A., Stogios, P. J., and McCourt, P. (2022). A novel strigolactone receptor antagonist provides insights into the structural inhibition, conditioning, and germination of the crop parasite Striga. *J. Biol. Chem*. 2022:101734. doi: 10.1016/j.jbc.2022.101734

Arite, T., Umehara, M., Ishikawa, S., Hanada, A., Maekawa, M., Yamaguchi, S., et al. (2009). d14, a strigolactone-insensitive mutant of rice, shows an accelerated outgrowth of tillers. *Plant Cell Physiol*. 50, 1416–1424. doi: 10.1093/pcp/pcp091

Ashton, N. W., Grimsley, N. H., and Cove, D. J. (1979). Analysis of gametophytic development in the moss, *Physcomitrella patens*, using auxin and cytokinin resistant mutants. *Planta* 144, 427–435. doi: 10.1007/BF00380118

Balcerowicz, M., Shetty, K. N., and Jones, A. M. (2021). Fluorescent biosensors illuminating plant hormone research. *Plant Physiol*. 187, 590–602. doi: 10.1093/plphys/kiab278

Biswas, S., McCullough, B. S., Ma, E. S., LaJoie, D., Russell, C. W., Garrett Brown, D., et al. (2017). Dual colorimetric and fluorogenic probes for visualizing tyrosine phosphatase activity. *Chem. Commun*. 53, 2233–2236. doi: 10.1039/C6CC09204G

Boyer, F.-D., de Saint Germain, A., Pillot, J.-P., Pouvreau, J.-B., Chen, V. X., Ramos, S., et al. (2012). Structure-activity relationship studies of strigolactone-related molecules for branching inhibition in garden pea: molecule design for shoot branching. *Plant Physiol*. 159, 1524–1544. doi: 10.1104/pp.112.195826

Boyer, F.-D., de Saint Germain, A., Pouvreau, J.-B., Clavé, G., Pillot, J.-P., Roux, A., et al. (2014). New strigolactone analogs as plant hormones with low activities in the rhizosphere. *Mol. Plant*. 7, 675–690. doi: 10.1093/mp/sst163

Braun, N., de Saint Germain, A., Pillot, J. P., Boutet-Mercey, S., Dalmais, M., Antoniadi, I., et al. (2012). The pea TCP transcription factor PsBRC1 acts downstream of Strigolactones to control shoot branching. *Plant Physiol*. 158, 225–238. doi: 10.1104/pp.111.182725

Bueno, C., Villegas, M. L., Bertolotti, S. G., Previtali, C. M., Neumann, M. G., and Encinas, M. V. (2002). The excited-state interaction of resazurin and resorufin with aminesin aqueous solutions. Photophysics and photochemical reaction. *Photochem. Photobiol*. 76, 385–390. doi: 10.1562/0031-8655(2002)0760385TESIOR2.0.CO2

Bürger, M., and Chory, J. (2020). The many models of strigolactone signaling. *Trends Plant Sci*. 25, 395–405. doi: 10.1016/j.tplants.2019.12.009

Bürger, M., Zimmermann, T. J., Kondoh, Y., Stege, P., Watanabe, N., Osada, H., et al. (2012). Crystal structure of the predicted phospholipase LYPLAL1 reveals unexpected functional plasticity despite close relationship to acyl protein thioesterases. *J. Lipid Res*. 53, 43–50. doi: 10.1194/jlr.M019851

Canévet, J. C., and Graff, Y. (1978). Réactions de Friedel-Crafts de dérivés aromatiques sur des composés dicarbonylés-1,4éthyléniques-2,3.II Alkylations par quelques hydroxy-5 ou chloro-5 dihydro-2,5 furannones-2. Nouvelle méthode de synthèse des acides 1H-indènecarboxyliques-1. *Tetrahedron* 34, 1935–1942. doi: 10.1016/0040-4020(78)80100-8

Cao, D., Liu, Z., Verwilst, P., Koo, S., Jangjili, P., Kim, J. S., et al. (2019). Coumarin-based small-molecule fluorescent chemosensors. *Chem. Rev*. 119, 10403–10519. doi: 10.1021/acs.chemrev.9b00145

Chen, J., Nelson, D. C., and Shukla, D. (2022). Activation mechanism of strigolactone receptors and its impact on ligand selectivity between host and parasitic plants. *J. Chem. Inf. Model*. 62, 1712–1722. doi: 10.1021/acs.jcim.1c01258

Confalone, P. N., and Confalone, D. L. (1980). Total synthesis of the major metabolite of methoxsalen. *J. Org. Chem*. 45, 1470–1473. doi: 10.1021/jo01296a024

Conn, C. E., Bythell-Douglas, R., Neumann, D., Yoshida, S., Whittington, B., Westwood, J. H., et al. (2015). Convergent evolution of strigolactone perception enabled host detection in parasitic plants. *Science* 349, 540–543. doi: 10.1126/science.aab1140

Cook, C. E., Whichard, L. P., Turner, B., and Wall, M. E. (1966). Germination of witchweed (striga lutea lour) - isolation and properties of a potent stimulant. *Science* 154, 1189–1190. doi: 10.1126/science.154.3753.1189

Cornet, F., Pillot, J.-P., Le Bris, P., Pouvreau, J.-B., Arnaud, N., de Saint Germain, A., et al. (2021). Strigolactones (SLs) modulate the plastochron by regulating KLUH (KLU) transcript abundance in Arabidopsis. *New Phytol*. 232, 1909–1916. doi: 10.1111/nph.17725

de Saint Germain, A., Bonhomme, S., Boyer, F.-D., and Rameau, C. (2013). Novel insights into strigolactone distribution and signalling. *Curr. Opin. Plant Biol*. 16, 583–589. doi: 10.1016/j.pbi.2013.06.007

de Saint Germain, A., Clavé, G., Badet-Denisot, M.-A., Pillot, J.-P., Cornu, D., Le Caer, J.-P., et al. (2016). An histidine covalent receptor and butenolide complex mediates strigolactone perception. *Nat Chem Biol*. 12, 787–794. doi: 10.1038/nchembio.2147

de Saint Germain, A., Clavé, G., and Boyer, F.-D. (2021a). Synthesis of profluorescent strigolactone probes for biochemical studies. *Methods Mol. Biol*. 2309, 219–231. doi: 10.1007/978-1-0716-1429-7_17

de Saint Germain, A., Jacobs, A., Brun, G., Pouvreau, J.-B., Braem, L., Cornu, D., et al. (2021b). A Phelipanche ramosa KAI2 protein perceives strigolactones and isothiocyanates enzymatically. *Plant Commun*. 2:100166. doi: 10.1016/j.xplc.2021.100166

Donaldson, L. (2020). Autofluorescence in plants. *Molecules* 25:2393. doi: 10.3390/molecules25102393

Fox, J. (2005). The R commander: a basic-statistics graphical user interface to R. *J. Stat. Softw*. 14, 1–42. doi: 10.18637/jss.v014.i09

Fukui, K., Yamagami, D., Ito, S., and Asami, T. (2017). A taylor-made design of phenoxyfuranone-type strigolactone mimic. *Front Plant Sci*. 8:936. doi: 10.3389/fpls.2017.00936

Gao, W., Xing, B., Tsien, R. Y., and Rao, J. (2003). Novel fluorogenic substrates for imaging β-lactamase gene expression. *J. Am. Chem. Soc*. 125, 11146–11147. doi: 10.1021/ja036126o

García-Plazaola, J. I., Fernández-Marín, B., Duke, S. O., Hernández, A., López-Arbeloa, F., and Becerril, J. M. (2015). Autofluorescence: biological functions and technical applications. *Plant Sci*. 236, 136–145. doi: 10.1016/j.plantsci.2015.03.010

Geisler, M. (2018). Seeing is better than believing: visualization of membrane transport in plants. *Curr. Opin. Plant Biol*. 46, 104–112. doi: 10.1016/j.pbi.2018.09.005

Gomez-Roldan, V., Fermas, S., Brewer, P. B., Puech-Pages, V., Dun, E. A., Pillot, J.-P., et al. (2008). Strigolactone inhibition of shoot branching. *Nature* 455, 189–194. doi: 10.1038/nature07271

Grimm, J. B., and Lavis, L. D. (2022). Caveat fluorophore: an insiders' guide to small-molecule fluorescent labels. *Nat Methods* 19, 149–158. doi: 10.1038/s41592-021-01338-6

Guillory, A., and Bonhomme, S. (2021). "Methods for medium-scale study of biological effects of strigolactone-like molecules on the moss *Physcomitrium (Physcomitrella) patens*," in *Strigolactones. Methods in Molecular Biology*, Vol. 2309, eds C. Prandi and F. Cardinale (New York, NY: Humana). doi: 10.1007/978-1-0716-1429-7_12

Hamiaux, C., Drummond, R. S. M., Janssen, B. J., Ledger, S. E., Cooney, J. M., Newcomb, R. D., et al. (2012). DAD2 Is an α/β hydrolase likely to be involved in the perception of the plant branching hormone, strigolactone. *Curr. Biol*. 22, 2032–2036. doi: 10.1016/j.cub.2012.08.007

Hamiaux, C., Drummond, R. S. M., Luo, Z. W., Lee, H. W., Sharma, P., Janssen, B. J., et al. (2018). Inhibition of strigolactone receptors by N-phenylanthranilic acid derivatives: structural and functional insights. *J. Biol. Chem*. 293, 6530–6543. doi: 10.1074/jbc.RA117.001154

Hoffmann, B., Proust, H., Belcram, K., Labrune, C., Boyer, F. D., Rameau, C., et al. (2014). Strigolactones inhibit caulonema elongation and cell division in the moss *Physcomitrella patens*. *PLoS ONE* 9:e99206. doi: 10.1371/journal.pone.0099206

Holbrook-Smith, D., Toh, S., Tsuchiya, Y., and McCourt, P. (2016). Small-molecule antagonists of germination of the parasitic plant *Striga hermonthica*. *Nat. Chem. Biol*. 12, 724–729. doi: 10.1038/nchembio.2129

Lace, B., and Prandi, C. (2016). Shaping small bioactive molecules to untangle their biological function: a focus on fluorescent plant hormones. *Mol. Plant* 9, 1099–1118. doi: 10.1016/j.molp.2016.06.011

Lopez-Obando, M., Guillory, A., Boyer, F.-D., Cornu, D., Hoffmann, B., Le Bris, P., et al. (2021). The *Physcomitrium (Physcomitrella) patens* PpKAI2L receptors for strigolactones and related compounds function *via* MAX2-dependent and -independent pathways. *Plant Cell* 33, 3487–3512. doi: 10.1093/plcell/koab217

Lopez-Obando, M., Ligerot, Y., Bonhomme, S., Boyer, F.-D., and Rameau, C. (2015). Strigolactone biosynthesis and signaling in plant development. *Development* 142, 3615–3619. doi: 10.1242/dev.120006

Mangnus, E. M., Dommerholt, F. J., Dejong, R. L. P., and Zwanenburg, B. (1992). Improved synthesis of strigol analog GR24 and evaluation of the biological-activity of its diastereomers. *J. Agric. Food Chem*. 40, 1230–1235. doi: 10.1021/jf00019a031

Mizuno, Y., Komatsu, A., Shimazaki, S., Naramoto, S., Inoue, K., Xie, X., et al. (2021). Major components of the KARRIKIN INSENSITIVE2-dependent signaling pathway are conserved in the liverwort *Marchantia polymorpha*. *Plant Cell* 33, 2395–2411. doi: 10.1093/plcell/koab106

Muñoz, A., Pillot, J.-P., Cubas, P., and Rameau, C. (2021). "Methods for phenotyping shoot branching and testing strigolactone bioactivity for shoot branching in Arabidopsis and Pea," in *Strigolactones. Methods in Molecular Biology*, Vol. 2309, eds C. Prandi and F. Cardinale (New York, NY: Humana). doi: 10.1007/978-1-0716-1429-7_10

Nakamura, H., Hirabayashi, K., Miyakawa, T., Kikuzato, K., Hu, W., Xu, Y., et al. (2019). Triazole ureas covalently bind to strigolactone receptor and antagonize strigolactone responses. *Mol. Plant* 12, 44–58. doi: 10.1016/j.molp.2018.10.006

Pham, H. T., Yoo, J., VandenBerg, M., and Muyskens, M. A. (2019). Fluorescence of scopoletin including its photoacidity and large stokes shift. *J. Fluoresc*. 30, 71–80. doi: 10.1007/s10895-019-02471-4

Prandi, C., Ghigo, G., Occhiato, E. G., Scarpi, D., Begliomini, S., Lace, B., et al. (2014). Tailoring fluorescent strigolactones for *in vivo* investigations: a computational and experimental study. *Org. Biomol. Chem*. 12, 2960–2968. doi: 10.1039/C3OB42592D

Proust, H., Hoffmann, B., Xie, X., Yoneyama, K., Schaefer, D. G., Yoneyama, K., et al. (2011). Strigolactones regulate protonema branching and act as a quorum sensing-like signal in the moss *Physcomitrella patens*. *Development*. 138, 1531–1539. doi: 10.1242/dev.058495

Rameau, C., Bodelin, C., Cadier, D., Grandjean, O., Miard, F., and Murfet, I. C. (1997). New ramosus mutants at loci Rms1, Rms3 and Rms4 resulting from the mutation breeding program at Versailles. *Pisum Genet*. 29, 7–12.

Reizelman, A., Wigchert, S. C. M., del-Bianco, C., and Zwanenburg, B. (2003). Synthesis and bioactivity of labelled germination stimulants for the isolation and identification of the strigolactone receptor. *Org. Biomol. Chem*. 1, 950–959. doi: 10.1039/b210678g

Roubinet, B., Chevalier, A., Renard, P.-Y., and Romieu, A. (2015). A synthetic route to 3-(heteroaryl)-7-hydroxycoumarins designed for biosensing applications. *Eur. J. Org. Chem*. 2015, 166–182. doi: 10.1002/ejoc.201403215

Seto, Y., Yasui, R., Kameoka, H., Tamiru, M., Cao, M., Terauchi, R., et al. (2019). Strigolactone perception and deactivation by a hydrolase receptor DWARF14. *Nat. Commun*. 10:191. doi: 10.1038/s41467-018-08124-7

Setsukinai, K.-i., Urano, Y., Kikuchi, K., Higuchi, T., and Nagano, T. (2000). Fluorescence switching by O-dearylation of 7-aryloxycoumarins. Development of novel fluorescence probes to detect reactive oxygen species with high selectivity. *J. Chem. Soc.* 2, 2453–2457. doi: 10.1039/b006449l

Shabek, N., Ticchiarelli, F., Mao, H., Hinds, T. R., Leyser, O., and Zheng, N. (2018). Structural plasticity of D3-D14 ubiquitin ligase in strigolactone signalling. *Nature* 563, 652–656. doi: 10.1038/s41586-018-0743-5

Sun, W. C., Gee, K. R., and Haugland, R. P. (1998). Synthesis of novel fluorinated coumarins: excellent UV-light excitable fluorescent dyes. *Bioorg. Med. Chem. Lett*. 8, 3107–3110. doi: 10.1016/S0960-894X(98)00578-2

Takahashi, I., and Asami, T. (2018). Target-based selectivity of strigolactone agonists and antagonists in plants and their potential use in agriculture. *J. Exp. Bot*. 69, 2241–2254. doi: 10.1093/jxb/ery126

Tan, Q., Zhao, S., Li, Y., Jiang, J., Tang, H., Chen, Y., et al. (2021). Regioselective difluoromethane sulfonylation and triflylation of resorufin derivatives. *Org. Lett*. 23, 8477–8481. doi: 10.1021/acs.orglett.1c03192

Tian, L., Feng, H., Dai, Z., and Zhang, R. (2021). Resorufin-based responsive probes for fluorescence and colorimetric analysis. *J. Mater. Chem. B* 9, 53–79. doi: 10.1039/D0TB01628D

Timonen, J. M., Nieminen, R. M., Sareila, O., Goulas, A., Moilanen, L. J., Haukka, M., et al. (2011). Synthesis and anti-inflammatory effects of a series of novel 7-hydroxycoumarin derivatives. *Eur. J. Med. Chem*. 46, 3845–3850. doi: 10.1016/j.ejmech.2011.05.052

Toh, S., Holbrook-Smith, D., Stogios, P. J., Onopriyenko, O., Lumba, S., Tsuchiya, Y., et al. (2015). Structure-function analysis identifies highly sensitive strigolactone receptors in *Striga*. *Science* 350, 203–207. doi: 10.1126/science.aac9476

Tsuchiya, Y., Yoshimura, M., and Hagihara, S. (2018). The dynamics of strigolactone perception in *Striga hermonthica*: a working hypothesis. *J. Exp. Bot*. 69, 2281–2290. doi: 10.1093/jxb/ery061

Tsuchiya, Y., Yoshimura, M., Sato, Y., Kuwata, K., Toh, S., Holbrook-Smith, D., et al. (2015). Probing strigolactone receptors in *Striga hermonthica* with fluorescence. *Science* 349, 864–868. doi: 10.1126/science.aab3831

Umehara, M., Hanada, A., Yoshida, S., Akiyama, K., Arite, T., Takeda-Kamiya, N., et al. (2008). Inhibition of shoot branching by new terpenoid plant hormones. *Nature* 455, 195–200. doi: 10.1038/nature07272

Uraguchi, D., Kuwata, K., Hijikata, Y., Yamaguchi, R., Imaizumi, H., Sathiyanarayanan, A. M., et al. (2018). A femtomolar-range suicide germination stimulant for the parasitic plant *Striga hermonthica*. *Science* 362, 1301–1305. doi: 10.1126/science.aau5445

Van Overtveldt, M., Braem, L., Struk, S., Kaczmarek, A. M., Boyer, F.-D., Van Deun, R., et al. (2019). Design and visualization of second-generation cyanoisoindole-based fluorescent strigolactone analogs. *Plant J*. 98, 165–180. doi: 10.1111/tpj.14197

Wang, D.-W., Yu, S.-Y., Pang, Z.-L., Ma, D.-J., Liang, L., Wang, X., et al. (2021). Discovery of a broad-spectrum fluorogenic agonist for strigolactone receptors through a computational approach. *J. Agric. Food Chem*. 69, 10486–10495. doi: 10.1021/acs.jafc.1c03471

Waters, M. T., Nelson, D. C., Scaffidi, A., Flematti, G. R., Sun, Y. K., Dixon, K. W., et al. (2012). Specialisation within the DWARF14 protein family confers distinct responses to karrikins and strigolactones in Arabidopsis. *Development* 139, 1285–1295. doi: 10.1242/dev.074567

Wolff, S., and Hoffmann, H. M. R. (1988). Aflatoxins revisited - convergent synthesis of the ABC-moiety. *Synthesis* 1988, 760–763. doi: 10.1055/s-1988-27700

Wu, X., Li, X., Li, H., Shi, W., and Ma, H. (2017). A highly sensitive and selective fluorescence off-on probe for the detection of intracellular endogenous tyrosinase activity. *Chem. Commun*. 53, 2443–2446. doi: 10.1039/C6CC09679D

Xie, X., Yoneyama, K., and Yoneyama, K. (2010). The strigolactone story. *Annu. Rev. Phytopathol*. 48, 93–117. doi: 10.1146/annurev-phyto-073009-114453

Xu, E., Chai, L., Zhang, S., Yu, R., Zhang, X., Xu, C., et al. (2021). Catabolism of strigolactones by a carboxylesterase. *Nat. Plants* 7, 1495–1504. doi: 10.1038/s41477-021-01011-y

Xu, Y., Miyakawa, T., Nosaki, S., Nakamura, A., Lyu, Y., Nakamura, H., et al. (2018). Structural analysis of HTL and D14 proteins reveals the basis for ligand selectivity in Striga. *Nat Commun*. 9.

Yan, J.-W., Wang, X. L., Tan, Q.-F., Yao, P.-F., Tan J.-H., and Zhang, L. (2016). A colorimetric and fluorescent dual probe for palladium in aqueous medium and live cell imaging. *Analyst*. 141, 2376–2379. doi: 10.1039/C6AN00204H

Yao, J., Scaffidi, A., Meng, Y., Melville, K. T., Komatsu, A., Khosla, A., et al. (2021). Desmethyl butenolides are optimal ligands for karrikin receptor proteins. *New Phytol*. 230, 1003–1016. doi: 10.1111/nph.17224

Yao, R., Ming, Z., Yan, L., Li, S., Wang, F., Ma, S., et al. (2016). DWARF14 is a non-canonical hormone receptor for strigolactone. *Nature* 536, 469–473. doi: 10.1038/nature19073

Yao, R., Wang, F., Ming, Z., Du, X., Chen, L., Wang, Y., et al. (2017). ShHTL7 is a non-canonical receptor for strigolactones in root parasitic weeds. *Cell Res*. 27, 838–841. doi: 10.1038/cr.2017.3

Yoneyama, K. (2020). Recent progress in the chemistry and biochemistry of strigolactones. *J. Pestic Sci*. 45, 45–53. doi: 10.1584/jpestics.D19-084

Yoneyama, K., Xie, X., Yoneyama, K., Kisugi, T., Nomura, T., Nakatani, Y., et al. (2018). Which are the major players, canonical or non-canonical strigolactones? *J. Exp. Bot*. 69, 2231–2239. doi: 10.1093/jxb/ery090

Yoshimura, M., Kim, S. F., Takise, R., Kusano, S., Nakamura, S., Izumi, M., et al. (2020). Development of potent inhibitors for strigolactone receptor DWARF 14. *Chem. Commun*. 56, 14917–14919. doi: 10.1039/D0CC01989E

Zarban, R. A., Hameed, U. F. S., Jamil, M., Ota, T., Wang, J. Y., Arold, S. T., et al. (2022). Rational design of *Striga hermonthica*-specific seed germination inhibitors. *Plant Physiol*. 188, 1369–1384. doi: 10.1093/plphys/kiab547

Zhang, H., Xu, C., Liu, J., Li, X., Guo, L., and Li, X. (2015). An enzyme-activatable probe with a self-immolative linker for rapid and sensitive alkaline phosphatase detection and cell imaging through a cascade reaction. *Chem. Commun*. 51, 7031–7034. doi: 10.1039/C5CC01005E

Conflict of Interest: The authors declare that the research was conducted in the absence of any commercial or financial relationships that could be construed as a potential conflict of interest.

Publisher's Note: All claims expressed in this article are solely those of the authors and do not necessarily represent those of their affiliated organizations, or those of the publisher, the editors and the reviewers. Any product that may be evaluated in this article, or claim that may be made by its manufacturer, is not guaranteed or endorsed by the publisher.

frontiers | Frontiers in Plant Science

ORIGINAL RESEARCH
published: 01 July 2022
doi: 10.3389/fpls.2022.837136

Strigolactones and Cytokinin Interaction in Buds in the Control of Rice Tillering

Manrong Zha[1,2], Yanhui Zhao[1,2], Yan Wang[1,2], Bingxian Chen[3] and Zecheng Tan[1,2]*

[1] College of Biology Resources and Environmental Sciences, Jishou University, Jishou, China, [2] Key Laboratory of Plant Resources Conservation and Utilization, College of Hunan Province, Jishou, China, [3] Guangdong Key Lab for Crop Germplasm Resources Preservation and Utilization, Guangzhou, China

Shoot branching is among the most crucial morphological traits in rice (*Oryza sativa* L.) and is physiologically modulated by auxins, cytokinins (CKs), and strigolactones (SLs) cumulatively in rice. A number of studies focused on the interplay of these three hormones in regulating rice tiller extension. The present study primarily aimed at determining the impact of different treatments, which were used to regulate rice tiller and axillary bud development on node 2 at the tillering stage and full heading stage, respectively. Transcription levels of several genes were quantified through qRT-PCR analysis, and an endogenous auxin and four types of CKs were determined through LC-MS/MS. Both nutrient deficiency and exogenous SL supply were found to inhibit rice tiller outgrowth by reducing the CK content in the tiller buds. Furthermore, supplying the inhibitor of both exogenous SLs and endogenous SL synthesis could also affect the expression level of *OsCKX* genes but not the *OsIPT* genes. Comparison of *OsCKX* gene expression pattern under exogenous SL and CK supply suggested that the induction of *OsCKX* expression was most likely via a CK-induced independent pathway. These results combined with the expression of CK type-A *RR* genes in bud support a role for SLs in regulating bud outgrowth through the regulation of local CK levels. SL functioned antagonistically with CK in regulating the outgrowth of buds on node 2, by promoting the *OsCKX* gene expression in buds.

Keywords: rice, tiller bud, strigolactones, cytokinin, *OsCKXs*

OPEN ACCESS

Edited by:
Ruifeng Yao,
Hunan University, China

Reviewed by:
Kai Jiang,
Southern University of Science and Technology, China
Kosuke Fukui,
Okayama University of Science, Japan

****Correspondence:***
Yan Wang
wy90408@163.com

Specialty section:
This article was submitted to Plant Physiology, a section of the journal Frontiers in Plant Science

Received: *16 December 2021*
Accepted: *27 May 2022*
Published: *01 July 2022*

Citation:
Zha M, Zhao Y, Wang Y, Chen B and Tan Z (2022) Strigolactones and Cytokinin Interaction in Buds in the Control of Rice Tillering. Front. Plant Sci. 13:837136. doi: 10.3389/fpls.2022.837136

KEY MESSAGES

Strigolactones and cytokinins play antagonistically in the control of shoot branching in rice. The transcription level of *OsCKXs* was highly induced by SLs, suggesting an insight into the role of SLs in inhibiting the development of axillary buds.

INTRODUCTION

Shoot architecture is a crucial morphological feature for plant survival and competition. It is among the key agronomic and major contributing factors to the yield and overall performance of rice (*Oryza Sativa* L.). As a major determinant of plant architecture, shoot branching involves the formation of axillary buds in the axils of leaves and subsequent outgrowth of buds. It is a well-known fact that shoot branching is strikingly affected by various environmental factors like drought and soil nutrient deficiencies (Horvath et al., 2003; Umehara et al., 2010; Sun et al., 2014;

Luo et al., 2018). The initiation of axillary branching and development is a complex phenomenon and is found to be implicated with plant hormones like auxins, CKs, and SLs. Auxins and SLs are involved in inhibiting the bud outgrowth, while CK promotes it (Dun et al., 2009; Leyser, 2009; Beveridge and Kyozuka, 2010).

Rice tillering is strongly affected by nutrient availability, such as nitrogen (N) and phosphorus (P). N and P deficiency has been evidenced to increase SL content in roots and root exudates (Yoneyama et al., 2007; Xie et al., 2010; Brewer et al., 2013; Sun et al., 2014). The suppression of tiller bud outgrowth under P deficiency in wild-type plants will not happen in SL-deficient and signal mutants (Umehara et al., 2010). Based on previous studies, SLs were proved to be involved in the inhibition of rice tillering in response to N and P deficiency (Umehara et al., 2010; Xu et al., 2015). N deficiency inhibits the cell division-determined elongation (Luo et al., 2017), thus affecting the development of rice tiller buds. Meanwhile, N-controlled branching was proved partially by SLs, by using SL biosynthesis mutant in Arabidopsis (de Jong et al., 2014).

Strigolactones are a class of carotenoid-derived hormones that have been found in the root exudates of most plant species (Cook et al., 1966; Akiyama et al., 2005). Studies regarding SL biosynthesis and signaling mutants have indicated that SLs perform various roles in regulating plant development (Zou et al., 2006; Arite et al., 2007, 2009). The most featured role of SLs is in the regulation of axillary shoot branching in many plant species. Grafting studies demonstrated the synthesis of branch-inhibiting signals in the root or shoot tissues, and their subsequent movement in the upward direction (Domagalska and Leyser, 2011). This could result in inhibiting the bud outgrowth through branch-inhibiting signals or translocation of its precursors over long distances and may act locally in or near the axillary buds (Beveridge et al., 1996, 1997; Napoli, 1996; Morris et al., 2001; Turnbull et al., 2002; Booker et al., 2005; Simons et al., 2007). It is well-documented that the SMXL/D53 acts as a target for SL-induced D14-SCF-dependent protein degradation (Zhou et al., 2013; Jiang et al., 2013; Soundappan et al., 2015; Wang et al., 2015). In a broader sense, the second-messenger and canalization can be considered as two main models to study shoot branching regulation via SLs. As per the second-messenger model, root synthesized SLs and CKs are transported to shoot and directly affect branching in buds (Dun et al., 2012; Brewer et al., 2015). Auxin from apices acts indirectly to inhibit the release of dormant buds by regulating the synthesis of SLs and CKs in nearby tissues (Domagalska and Leyser, 2011). Both SLs and CKs affect branching by regulating *BRANCHED1* (*BRC1*, a major regulatory nexus for shoot branching) expression in buds. The *BRC1* expression is significantly reduced in the *max2* mutant and remarkably enhanced in *smxl6 smxl7 smxl8 max2* multiple mutants (Seale et al., 2017). In addition, exogenous SLs *rac*-GR24 supply can upregulate the *BRC1* expression rapidly, independent of any new protein synthesis, suggesting that *BRC1* is the most direct target of SL signaling (Dun et al., 2012).

Cytokinin is the only hormone that has been shown to promote axillary shoot branching. CK levels in the axillary bud can be affected by local auxin contents by regulating the expression of *adenosine phosphate-isopentenyl transferase* (*IPT*) genes (Turnbull et al., 1997; Shimizu-Sato et al., 2009). In addition, likely a trigger for bud release, CK was reported to promote auxin production and basipetal auxin transport out of the growing buds, consequently repressing the production of CK in the stem and limiting its availability for other buds (Bangerth et al., 2000; Tanaka et al., 2006; Shimizu-Sato et al., 2009).

Regarding the contrary roles of CKs and SLs in axillary bud outgrowth (Braun et al., 2012; Dun et al., 2012), the mechanism of their antagonistic functions on branching regulation is seldom studied. In pea and Arabidopsis, the CKs in the xylem sap of SL-deficient mutants were lower relative to wild-type plants due to feedback regulation operating in the SL branching pathways (Beveridge et al., 1997; Morris et al., 2001; Foo et al., 2007). The promotion of CK on axillary bud outgrowth can be reduced by exogenous SLs without affecting the CK biosynthesis genes in pea (Dun et al., 2012). Also, SL biosynthesis might be affected by CK, and the auxin induced the upregulation of *More Axillary Growth 4* (*MAX4*, SL biosynthesis gene), which can be prevented by CKs (Bainbridge et al., 2005). CKs and SLs may converge at a common point in the bud outgrowth regulation pathway in pea (Dun et al., 2012). In rice, CK levels in nodal tissues were found to be higher in D10-RNAi plants (presumed SL deficient) when compared to the wild-type plants (Zhang et al., 2010). Transcriptome analysis revealed that four *CKX* genes of Arabidopsis were downregulated in the *max2* mutant (SL mutant) (Ha et al., 2014). Recently, one of the *CKX* genes (*CKX9)* was promoted by SL signaling, thus leading to CK degradation in rice plants (Duan et al., 2019). On the other hand, CKs suppress biosynthesis in roots (Yoneyama et al., 2020), thus SLs and CKs could supress each other systemically.

In the current study, two different bud types of rice, tiller bud (located at fifth leaf axils) and node bud (located at the second nodes from the top), were investigated. Different treatments were applied to shift buds between the dormant stage and the transition stage. Auxin and CK content in both nodes and buds were measured using HPLC (LC-MS/MS). Also, hormone-related gene expression patterns, in response to each treatment, were also examined in this study. Our results gave an insight into how SLs integrate with CK to regulate bud outgrowth in rice tiller buds.

MATERIALS AND METHODS

Plant Growth

The experiment was divided into two sessions according to different stages of treatment. Both sessions were conducted in the net house of Nanjing Agriculture University (Jiangsu Province, China) during the rice-growing season. An indicator cultivar, Yangdao 6, was used as a test crop in this study.

In the first group, 20-day-old rice seedlings (planted in a seedbed) were transplanted to 20 L plastic pots containing

Abbreviations: SLs, strigolactones; BA 6, benzyladenine; CK, cytokinin; CKX, cytokinin oxidase/dehydrogenase; HPLC, high-performance liquid chromatography; iP, isopentenyladenine; iPR, isopentenyladenine riboside; tZ, *trans*-zeatin; tZR, *trans*-zeatin riboside; ARR, type-A Arabidopsis response regulators.

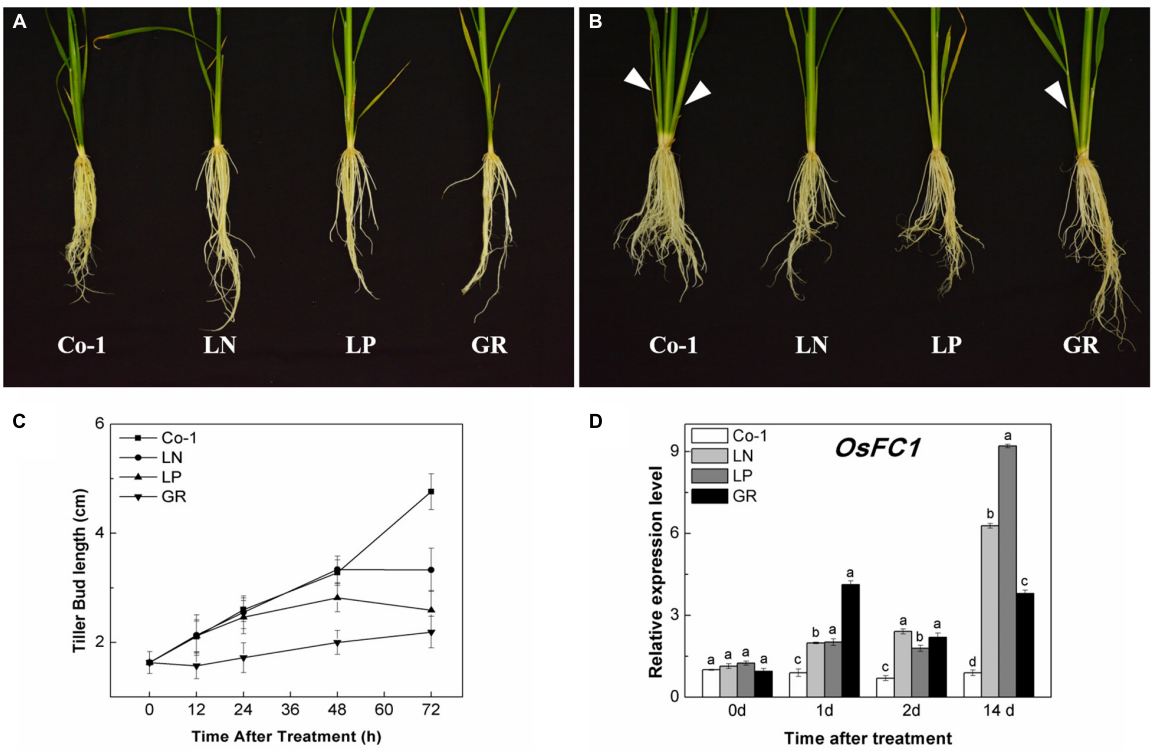

FIGURE 1 | Effects of LN, LP, and GR treatments on the growth of rice tiller and OsFC1 expression in tiller bud. **(A)** Rice plant before treatment; **(B)** rice plants after 2 weeks of treatment; **(C)** outgrowth of rice tiller buds at the fifth leaf axils; and **(D)** OsFC1 expression in tiller buds at the fifth leaf axils. The arrows in **(A)** and **(B)** refer to the growth of new tillers within 2 weeks. Co-1 contains 2.5 mM N and 300 μM P in a nutrient solution, LN contains 0.02 mM N and 300 μM P in a nutrient solution, LP contains 2.5 mM N and 2 μM P in a nutrient solution, GR contains 2.5 mM N, 300 μM P, and 2 μM rac-GR24 in a nutrient solution. The expression of *OsFC1* in the tiller buds at 0, 1, 2, and 14 days after each treatment is represented relative to the Co-1 at 0 day. Vertical bars **(C)** represent mean ± standard error (n = 60). The value **(D)** obtained from the control treatment at 0 h after treatment was arbitrarily set at 1.0. Quantitative real-time PCR was performed in triplicate (three biological replicates), and mean values with SD are shown.

full nutrient solution with composition as described by Yoshida (1975). The nutrient solution contained 40 mg·L^{-1} $CaCl_2$, 40 mg·L^{-1} K_2SO_4, 40 mg·L^{-1} $MgSO_4{\cdot}7H_2O$, 0.5 mg·L^{-1} $MnCl_2{\cdot}4H_2O$, 10 mg·L^{-1}, $NaH_2PO_4{\cdot}2H_2O$, 0.05 mg·L^{-1} $(NH_4)_6{\cdot}Mo_7O_{24}{\cdot}2H_2O$, 0.01 mg·$L^{-1}$ $ZnSO_4{\cdot}7H_2O$, 0.2 mg·L^{-1} H_3BO_3, 2.0 mg·L^{-1} $FeCl_2{\cdot}6H_2O$, and 0.01 mg·L^{-1} $CuSO_4{\cdot}5H_2O$. The N and P concentrations varied in the treatments depending upon the amounts of NH_4NO_3 and $NaH_2PO_4{\cdot}2H_2O$. The nutrient solutions of all treatments were treated with 0.1 M HCl to maintain a PH value of 5.5. In the second group, the rice seedlings of the same age were transplanted into plastic pots having diameter and height of 30 cm. Each pot, where four seedlings were transplanted, contained 15 kg of sieved soil. N (1.6 g $plot^{-1}$ as urea), P (0.8 g $plot^{-1}$ as single superphosphate), and potassium (1.2 g $plot^{-1}$ as KCl) were applied at the time of seedling transplantation. Surface water was applied to irrigate these pots over the entire growing season of the plants.

Plant Materials and Treatment

Tillering Stage

The rice plants were grown in a sufficient N (2.5 mM) and P (300 μM) concentration for sustainable growth. When these rice seedlings developed up to seven leaves on their main stems, they were divided into four treatment groups. One was treated with 2.5 mM N and 300 μM P (normal nutrient levels, Co-1 treatment), the second with 0.02 mM N and 300 μM P (LN treatment), the third with 2.5 mM N and 2 μM P (LP treatment), and the fourth with 2.5 mM N, 300 μM P, and a final concentration of 2 μM rac-GR24 (synthetic strigolactone, GR treatment).

As a reverse, some rice seedlings were grown under P-deficient conditions (2 μM). When these rice seedlings developed seven leaves on their main stems, they were divided into three treatment groups. One was treated with 2 μM P (Low P levels, Co-2 treatment), the second with 300 μM P (HP treatment), and the third with 2 μM P and a final concentration of 2 μM TIS108 (TIS treatment, as a potent and specific SL biosynthesis inhibitor).

Full Heading Stage

Different concentrations of BA (30 μM) and rac-GR24 (2 μM) were supplied in a volume of 0.5 ml directly to the axillary bud on node 2 as described by Gomez-Roldan et al. (2008) and Dun et al. (2009). Different from other plants, the bud on node 2 in rice is always covered by leaf sheaths. We peeled out the sheaths from the stem to pour the solution into the gap between the stem and

sheaths. The sheath of control treatment (Co-3) was also peeled out as other hormone treatments but treated with solvent.

Measurement of Endogenous Plant Hormones

The measurement of SL in root exudates was performed as described previously (Ishikawa et al., 2005; Umehara et al., 2008). For each sample, 50 ml of hydroponic culture medium loaded into a pre-treated Oasis HLB 3cc cartridge (Waters) was used after adding internal standard (1 ng of d_6-5DS) and washing with de-ionized water. The SLs were determined using a UPLC-MS/MS analysis as described before (Zhou et al., 2013).

The extraction and purification of indole-3-acetic acid (IAA) and four types of CKs (tZ, tZR, iP, and iPR) were carried out using methods described by Dobrev and Kaminek (2002). The determination of IAA, tZ, tZR, iP, and iPR was performed using an LC-MS/MS (Aglient1290 and SCIEX-6500trap) system as previously described by Nakagawa et al. (2005).

Gene Expression Analysis

Bud and node tissues were frozen, and total RNA isolation and cDNA synthesis were carried out as described in our previous work (Xu et al., 2015). Quantitative real-time PCR (qRT-PCR) was performed using the Roche LC 480 (Roche diagnostics, Penzberg, Germany) and SYBR *premix Ex Taq* Kit (TaKaRa). Each reaction contained 10 μL of SYBR *Premix Ex Taq*, 1 μL each of 10 μM gene-specific primer pair, 5 μL of template cDNA, and 4 μL of water. The thermal cycle of qRT-PCR was carried out at 95°C for 3 min, 40 cycles at 95°C for 15 s, and at 60°C for 60 s. Primer sequences used to amplify the transcripts are shown in **Supplementary Table 1**.

Statistical Analysis

ANOVA test was performed using SPSS 17.0. Data from each sampling event were analyzed separately. Mean values were tested with the least significant difference test, and the significance level was set at $p \leq 0.05$.

RESULTS

Tiller Bud Growth Was Suppressed by LN, LP, and GR Treatment at Tillering Stage

The tillers of the Co-1 plants grew naturally during the first 2 weeks of treatments; meanwhile, tillers were significantly reduced in response to nitrate deficiency (LN), phosphorous deficiency (LP), and exogenous rac-GR24 (GR) treatments (**Figures 1A,B**). The color of older leaves turned yellow in LN and LP plants, but remained green in GR plants, as in the case of Co-1 (**Figures 1A,B**). During 72 h of post-treatment, the growth of tiller buds of Co-1 remained active and grew normally. However, the tiller bud length in LN and LP plants was inhibited and found to be significantly shorter than those in the Co-1 plants at just 48 and 72 h of treatment, respectively (**Figure 1C**). Not surprisingly, the tiller buds in GR plants were inhibited significantly and showed growth stagnancy 12 h after treatment (**Figure 1C**). *OsFC1* is known to be a negative regulator of bud growth and works downstream of the SL signaling pathway. Consistent with the outcome, the transcription level of *OsFC1* was highly induced in LN, LP, and GR plants when compared to the Co-1 plants (**Figure 1D**).

Cytokinin Content in Tiller Buds Was Reduced During Bud Inhibition by Strigolactones

Auxins and CKs play a major role in regulating rice tiller outgrowth. To check whether the CK and auxin levels would change in rice tiller buds and nodes with nutrient deficiency and GR treatment, we measured the endogenous concentrations of several natural CKs and auxins in both tiller nodes and buds. In Co-1 control plants, the contents of IAA and CK in tiller buds and nodes changed after 12 h, which may be due to the plant growth during the daytime. The amounts of IAA decreased profoundly in GR and LP plants in both tiller buds and tiller nodes, and only decreased in tiller nodes in LN plants when compared to Co-1 plants (**Figure 2**). All forms of CKs, in reponse to GR treatment, showed decreased concentrations than those observed in Co-1 treatment after 12 h of treatment in tiller buds, indicating that exogenous SLs can reduce the amount of CKs in tiller buds (**Figure 2A**). In response to LN and LP treatments, the CK levels were observed to be lower than in Co-1 plants but not as significant as in GR plants in tiller buds. However, the CK concentration in tiller nodes did not show similar trends as noticed in tiller buds (**Figure 2B**). The tZ, tZR, and iPR contents were induced by GR, but only tZR and iP produced enhanced response to LP in tiller nodes. Interestingly, the iPR treatment was not affected by all the treatments and remained at a stable level with Co-1 in tiller nodes (**Figure 2B**).

The deficiency of both N and P led to an increase in the endogenous SL contents in rice roots (Sun et al., 2014). In our study, LN and LP significantly increased the expression of genes involved in the synthesis of SL in rice roots and tiller buds (**Figure 3**). The relative expression levels of *OsD10*, *OsD17,* and *OsD27* in both tiller nodes and buds were found to be higher in both LN and LP plants when compared to Co-1 plants, although the enhancement in the case of LP was more prominent than in LN (**Figure 3**). Interestingly, the expression levels of *OsD3* and *OsD14* were enhanced in tiller buds under GR compared with Co-1, but decreased in roots. Without a doubt, GR was found to be involved in the expression of SL signaling genes and negatively affected the transcription of SL synthesis genes significantly (**Figure 3**). All these results were consistent with the previous study on SL-related gene response to nutrient deficiency and exogenous SL treatment (Sun et al., 2014). Further, measurement of 2′-epi-5-deoxystrigol (epi-5DS), a native SL of rice, in the root exudates proved that none of the P treatments significantly promoted the endogenous SL biosynthesis, but was inhibited by GR24 supply (**Supplementary Figure 1**). Combining all the above-mentioned findings, we hypothesized that the decreased content of CK in tiller buds under LN, LP, and GR treatments may

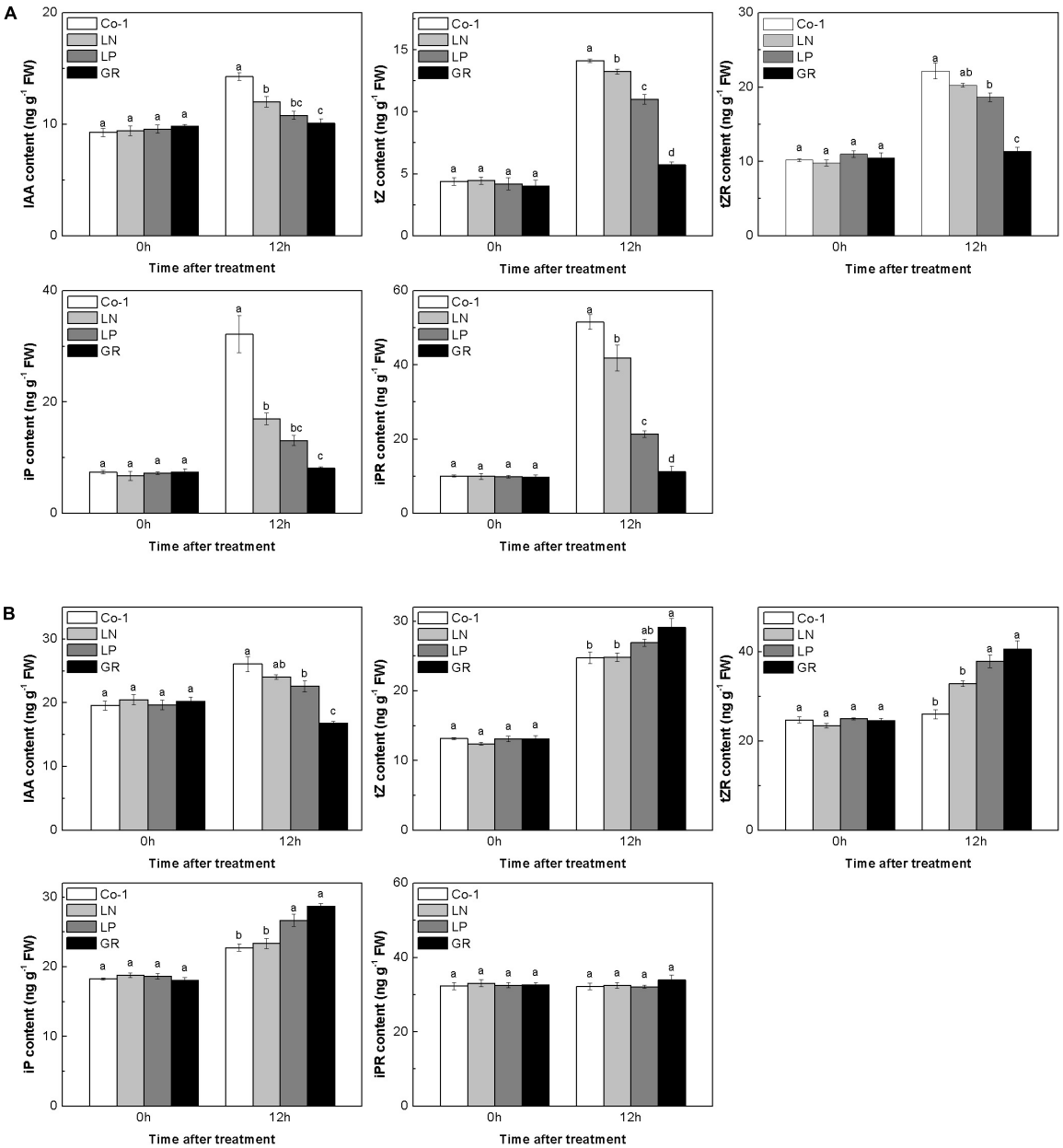

FIGURE 2 | Effect of N, phosphorous, and GR24 on the amounts of CK and indole-3-acetic (IAA) in rice tiller buds **(A)** and nodes **(B)**. At 0 and 12 h after treatment, the amounts of CK and IAA in rice tiller buds located at the fifth leaf axils and nodes were measured (tZ, tZR, iP, iPR). FW, fresh weight. Values in each column at the same amount of hormone followed by different letters were significantly different at $p = 0.05$ ($n = 3$).

be correlated with endogenous and exogenous SLs. Furthermore, SLs may inhibit tiller bud outgrowth partly by reducing the local CK content in the bud.

Strigolactone Promotes Cytokinin Degradation in Rice Tiller Buds at Tillering Stage

The level of CKs is controlled by both CK biosynthesis and degradation in rice. Adenosine phosphate-isopentenyl transferase (IPT) catalyzes the rate-limiting step of CK biosynthesis. In Arabidopsis, *AtIPTs* respond specifically to NO^{3-} and NH^{4+} treatments (Takei et al., 2004; Sakamoto et al., 2006). Auxin moves basipetally and controls local CK biosynthesis by mediating *PsIPT* expression in pea plants (Li et al., 1995; Tanaka et al., 2006). Eight *OsIPT*s genes were revealed by molecular and biochemical studies in the rice genome (Sakamoto et al., 2006). The *CKX* encoding genes control the level of endogenous CKs, which are required for irreversible CK degradation in plants and play an indicating role in detecting CK

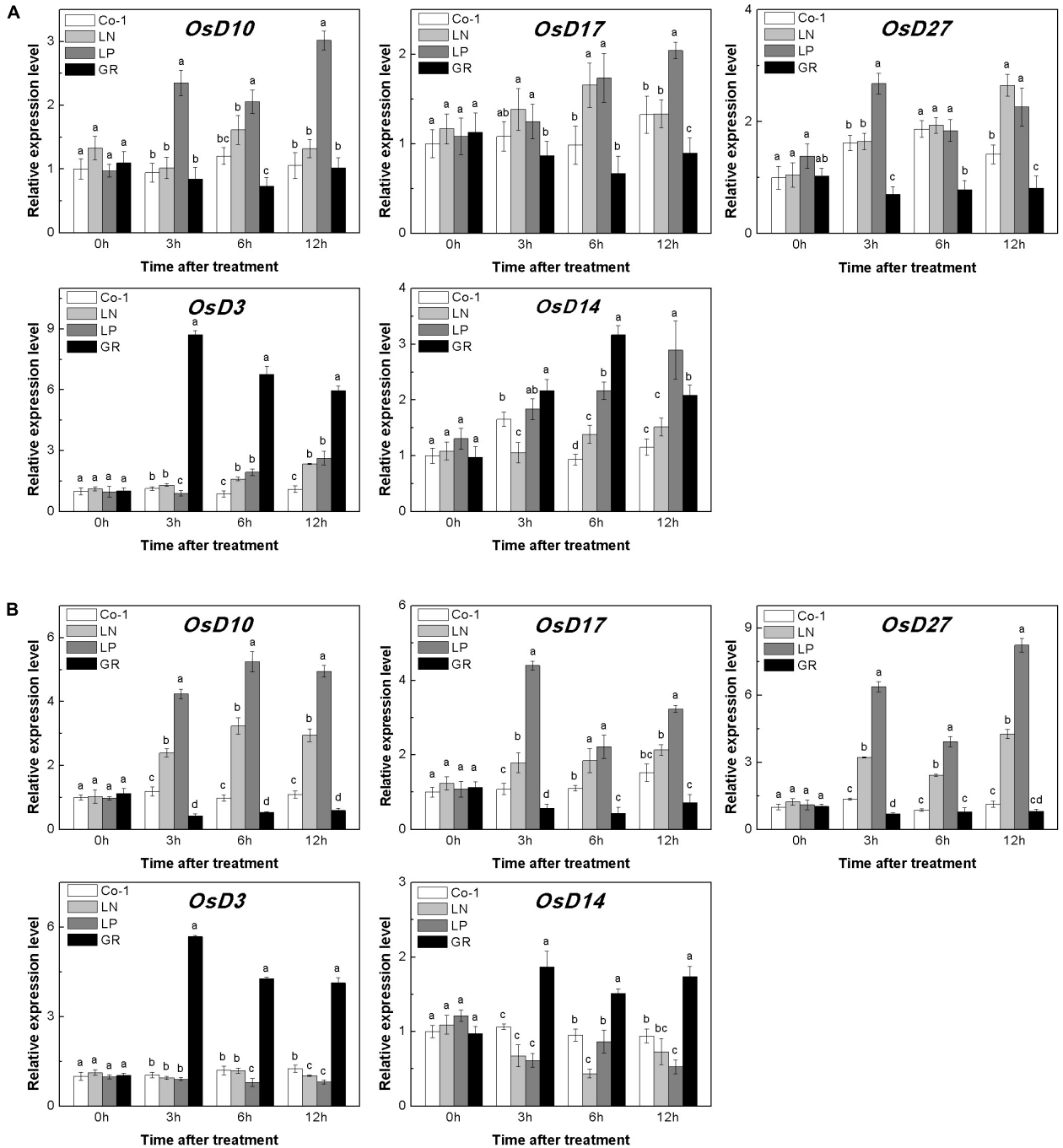

FIGURE 3 | Expression patterns of *OsD10*, *OsD17*, *OsD27*, *OsD3,* and *OsD14* ST biosynthesis and signaling genes in rice tiller buds **(A)** located at the fifth leaf axils and root **(B)** expressed in response to the treatment. Total RNA was isolated from less than 0.1 g of buds and nodes each time. β-Actin was used as a reference gene. The value obtained from the control treatment at 0 h after treatment was arbitrarily set at 1.0. Expression of each gene at 0, 3, and 6 h after treatments is represented relative to the Co-1 treatment at 0 h. Quantitative real-time PCR was performed in triplicate (three biological replicates), and mean values with SD are shown.

levels (Galuszka et al., 2001; Ha et al., 2012). The CKX enzymes, encoded by the multigene family, include 11 *OsCKXs* in rice. We only successfully detected five *OsIPTs* and five *OsCKXs* in our samples. The expression of the most detected *OsIPT* genes was increased by more than 1.5 times in rice tiller buds but decreased quickly in tiller nodes in response to LN and LP (**Figure 4**). However, GR did not change significantly the expression level of five *OsIPT* genes in either tiller nodes or buds (**Figure 4**). All

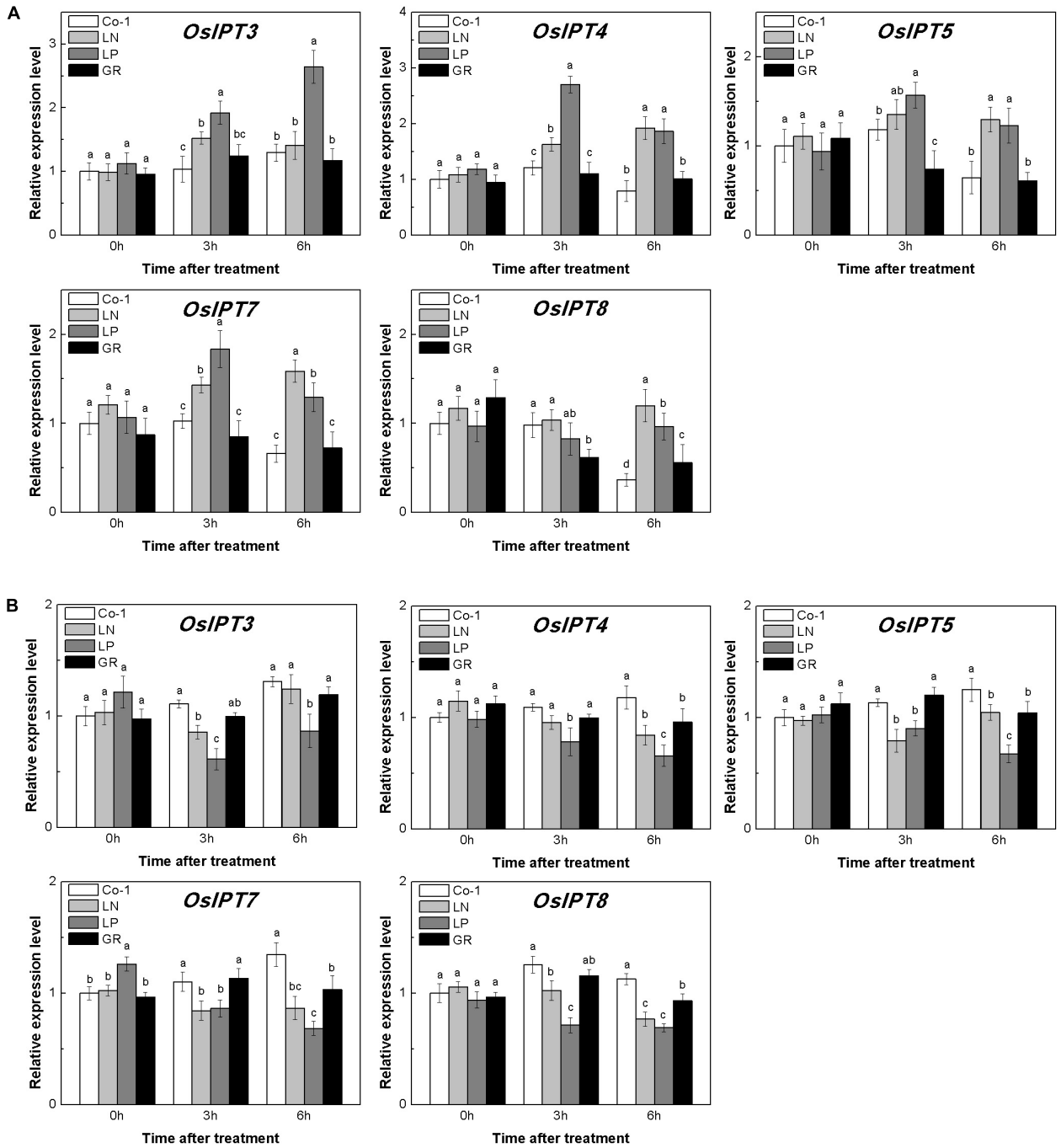

FIGURE 4 | Expression patterns of *OsIPT3*, *OsIPT4*, *OsIPT5*, *OsIPT7,* and *OsIPT8* CK biosynthesis genes in rice tiller buds **(A)** and tiller nodes **(B)** located at the fifth leaf axils expressed in response to the treatment. Total RNA was isolated from less than 0.1 g of buds and nodes each time. β-Actin was used as a reference gene. The value obtained from the control treatment at 0 h after treatment was arbitrarily set at 1.0. Quantitative real-time PCR was performed in triplicate (three biological replicates), and mean values with SD are shown.

the five detected *OsCKX* genes were significantly upregulated by LP, but only *OsCKX2, OsCKX4,* and *OsCKX9* increased by more than two times in the rice tiller buds of LN plants (**Figure 5A**). In tiller nodes, LN and LP did not significantly affect the OsCKX gene expression (**Figure 5B**). Three *OsCKX* genes, except for *OsCKX1* and *OsCKX5,* were enhanced by GR, while only GR prominently induced the expression of five *OsCKX* genes in tiller nodes (**Figure 5B**). These results suggest that SLs can decrease the CK content in buds by increasing CK degradation, whereas only exogenous SLs functioned in tiller nodes.

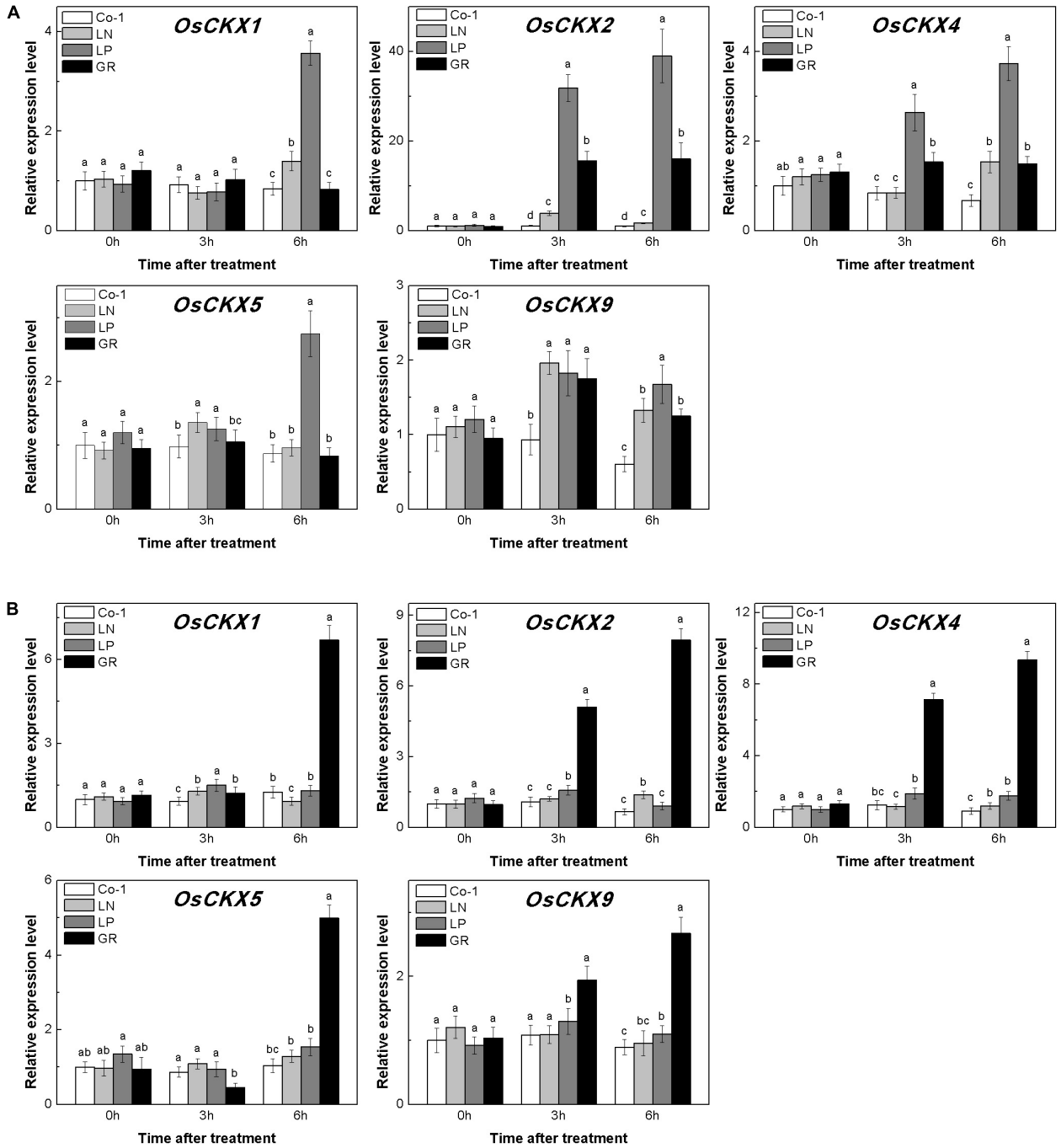

FIGURE 5 | Expression patterns of *OsCKX1*, *OsCKX2*, *OsCKX4*, *OsCKX5,* and *OsCKX9* CK degradation genes in rice tiller buds **(A)** and tiller nodes **(B)** located at the fifth leaf axils expressed in response to the treatment. Total RNA was isolated from less than 0.1 g of buds and nodes each time. β-Actin was used as a reference gene. The value obtained from the control treatment at 0 h after treatment was arbitrarily set at 1.0. Quantitative real-time PCR was performed in triplicate (three biological replicates), and mean values with SD are shown.

To confirm our hypothesis, reverse experiments were designed using high phosphorous (HP) treatment and TIS108 (a neogenesis SL synthesis inhibitor) supply. The TIS108 is a specific SL biosynthesis inhibitor that inhibits SL biosynthesis in both rice and Arabidopsis (Ito et al., 2011, Ito et al., 2013), but its target site is still unknown. HP or TIS108 supply could release the tiller buds from dormancy and reduce endogenous SLs biosynthesis in rice, based on low P growth conditions (**Supplementary Figures 2**, **3**). With these treatments, five *OsCKXs* genes were found to be reduced in different degrees (**Figure 6**). At the same time, the transcription levels of *OsIPT3*, *OsIPT4,* and *OsIPT7* in tiller buds increased more than 1.5 times in response to HP when

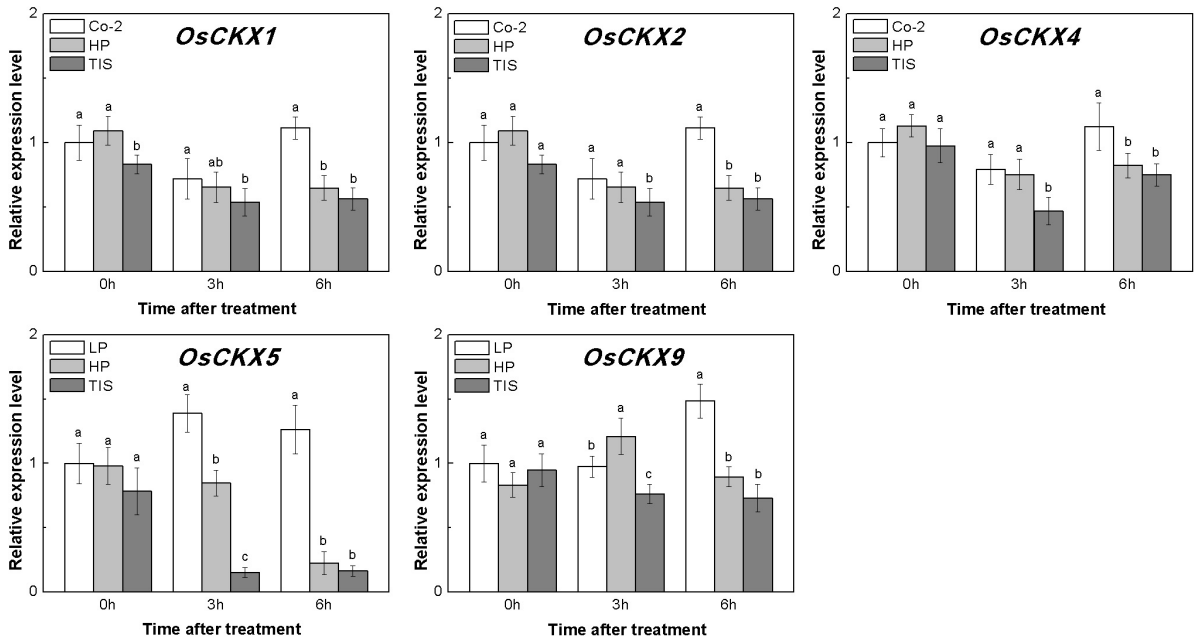

FIGURE 6 | Expression patterns of *OsCKX1*, *OsCKX2*, *OsCKX4*, *OsCKX5,* and *OsCKX9* CK degradation genes in rice tiller buds located at the fifth leaf axils expressed in response to the treatment. Co-2 contains 2 μM P in a nutrient solution, HP contains 300 μM P in a nutrient solution, and TIS contains 2 μM P and 2 μM TIS108 in a nutrient solution. Total RNA was isolated from less than 0.1 g of buds and nodes each time. β-Actin was used as a reference gene. The value obtained from the control treatment at 0 h after treatment was arbitrarily set at 1.0. Quantitative real-time PCR was performed in triplicate (three biological replicates), and mean values with SD are shown.

compared to Co-2 plants (**Supplementary Figure 4**). However, the transcription level of five *OsIPT* genes remained at a relatively stable level in response to TIS in tiller buds (**Supplementary Figure 4**). Under the conditions of nutrient deficiency and GR, it emerged that SLs functioned as regulators of CK degradation in rice tiller bud. In a previous study, exogenous SL supply appeared to be reducing bud growth in response to CK in pea (Dun et al., 2012). Furthermore, impaired SL signaling led to the downregulation of *CKX*-encoding genes (Ha et al., 2014). All these results can support our notion that SL promotes CK degradation in rice buds.

Exogenous Strigolactone Supply Reduces the Cytokinin Promotion of Bud Growth Directly at Full Heading Stage

To further explore the relationship between SLs and CK degradation in rice bud inhibition, we shifted our attention to rice node 2 at the full heading stage, to enable focusing on each specific bud. At full heading stage, all the buds at node 2 no longer outgrew and maintained a dormant state unless stimulated by the environmental conditions, such as decapitated and plant hormone supply. Buds on node 2 were released from the dormant state and grew out with BA supply (**Figure 7**). A direct supply of GR24 to the bud resulted in a reduction of BA-induced bud growth in rice, and the reduction was enhanced with the increase amonts of GR24 (**Figure 7**). This finding demonstrated that SLs and CK played antagonistic roles in the regulation of bud outgrowth in rice.

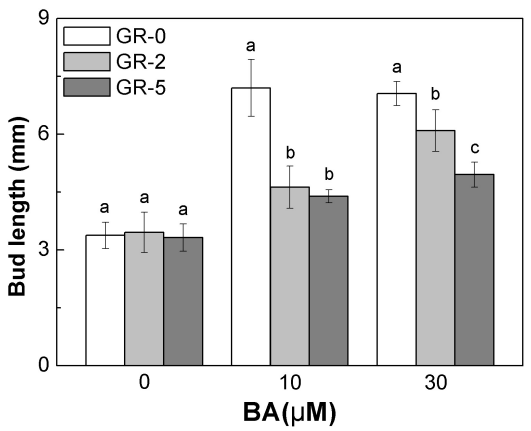

FIGURE 7 | Strigolactone reduces the stimulatory effect of BA-induced bud outgrowth in rice. rac-GR24 and/or BA were supplied to the axillary bud directly on node 2 at the full heading stage. Bud length of 60 buds at node 2 was measured 3 days after treatment. Vertical bars in C represent mean ± standard error values (n = 60).

The outgrowth of axillary bud has been well-confirmed and is correlated with the local CK concentration in rice, where the CK acted independently to regulate the bud growth (Chatfield et al., 2000). The genes *type-A RRs* have been defined as the CK-mediated genes that are required for bud activation in Arabidopsis (Müller et al., 2015). Also, such genes were used

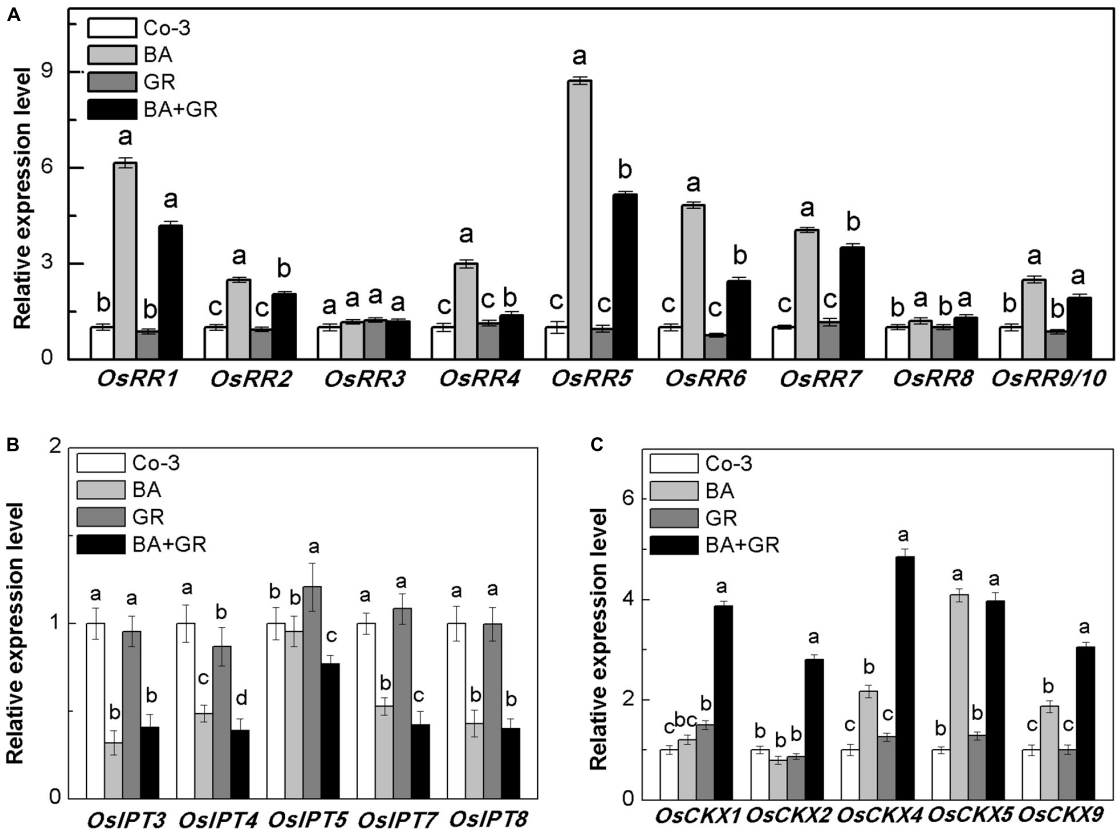

FIGURE 8 | Effect of GR or/and BA treatments on CK-related gene expression in axillary buds at node 2 at full heading stage. **(A)** Cytokinin-type-A RR genes expression, **(B)** five isopentenyl transferase genes expression, and **(C)** five cytokinin oxidase/dehydrogenase genes expression. The axillary bud at node 2 was treated for 12 h with or without BA (40 μM) or/and rac-GR (2 μM). The expression of each gene in the bud at node 2 is represented relative to Co-3. Total RNA was isolated from less than 0.1 g of buds and nodes each time. β-Actin was used as a reference gene. The value obtained from the control treatment at 0 h after treatment was arbitrarily set at 1.0. Quantitative real-time PCR was performed in triplicate (three biological replicates), and mean values with SD are shown.

as marker genes of CK-inducible processes (López-Bucio et al., 2007). To determine whether the exogenous SLs reduced the bud outgrowth via the CK pathway directly, the transcript levels of ten *OsRR* genes were detected with the interaction of BA and GR24. Most of the *OsRR* genes increased on treatment with BA and reduced up to different extents following the application of GR24 (**Figure 8A**), suggesting that the exogenous SL supply may act upon the CK-mediated bud activation pathway.

To determine if the observed reduction of *OsRR* gene expression was directly due to CK biosynthesis or degradation, the expression of *OsIPT* and *OsCKX* genes was also observed in the bud on node 2 (**Figures 8B,C**). There was a significant reduction in the expression of *OsIPT* genes, which may be due to the feedback regulation of exogenous BA supply. With or without BA, the exogenous SLs and GR24 did not affect the expression of *OsIPT* genes. As expected, the transcription level of *OsCKX* genes was highly induced by GR treatment in the presence of BA (**Figure 8C**). The endogenous CK contents in the bud on node 2 were profoundly induced by BA and reversed by GR combined treatment (**Supplementary Figure 5**). Our result, here, supported the hypothesis that SLs inhibit bud growth by inducing CK degradation in rice, and the effectiveness of SL treatment depends on the local content of CK.

DISCUSSION

Nutrient Deficiency and rac-GR24 Supply Inhibited Rice Tiller at Tillering Stage

Our results for rice were consistent with substantial evidence that N and P deficiencies inhibit axillary buds to grow out in many species (**Figure 1**). The long-term inhibition of GR on tillering was not as significant as observed in LN and LP treatments (**Figures 1A,B**), which may be due to the unstable characteristics of rac-GR24 in water (Akiyama et al., 2010; Bromhead et al., 2015). The tiller bud growth had a quicker response to GR than to LN and LP (**Figure 1C**). The inhibited tiller phenotype under LN, LP, and GR conditions might be related to the *OsFC1* increase in tiller buds (**Figure 1D**). The expression level of *OsFC1* appeared to be under hormonal control, thus manipulating shoot branching (Minakuchi et al., 2010; Braun et al., 2012). Nutrient deficiencies elevated SL biosynthesis and exudation in roots, which is suggested to be one of the factors responsible for tiller suppression (Koltai et al., 2010; Kapulnik et al., 2011a,b; Ruyter-Spira et al., 2011). These reports were consistent with our finding that LN and LP can increase endogenous SL biosynthesis and signaling in both nodes and tiller buds. Together, exogenous SL

supply and nutrient deficiency-induced endogenous SLs acted in the same manner in the inhibition of rice tiller bud growth.

Cytokinin Contents Show a Decreasing Response to Both Exogenous and Endogenous Strigolactones in Tiller Buds

Strigolactone exudation was enhanced by low P and low N concentrations (Yoneyama et al., 2007, 2012; Jamil et al., 2011a,b; Sun et al., 2014). By using nutrient deficiency and GR24 treatment, we were able to create increased levels of endogenous SLs and exogenous SLs, respectively (**Figure 3**). Here, we showed that LN, LP, and GR induced a decrease in the contents of all the four endogenous CKs only in the rice tiller buds when compared to that observed in the control treatment (**Figure 2**). CK content in buds can be well correlated with the outgrowth of. A direct application of endogenous CK to buds causes the activation of axillary buds (Pillay and Railton, 1983; Cline et al., 1997). Above all, we hypothesized that the decreased levels of CK concentrations in tiller buds, in case of nutrient deficiencies and GR24 treatment, might be the reason for the inhibition of bud formation.

Plenty of evidence suggested that SLs may affect the levels of CK. CK levels in root xylem sap decreased in both SL-deficient and response mutants in pea and Arabidopsis (Foo et al., 2007; Waldie et al., 2010). In *D10*-RNAi rice plants, the CK level in nodal tissues was increased and led to a longer growth of local buds than observed in the wild type (Zhang et al., 2010). All these findings suggest that the effect of SLs on CK levels is diverse in different tissues. Also, decreased CK content induced by SLs in buds was not caused by the delivery of lower CK amounts from tiller nodes to buds, as reported by Dun et al. (2012). So, it is not surprising that even CK content shows converse results between tiller buds and nodes (**Figure 2**). Based on a previous study, endogenous IAA could decrease the biosynthesis of CK (Nordström et al., 2004; Shimizu-Sato et al., 2009). The reduced level of IAA may likely be the reason that led the CK contents to an increment in roots and then transport to the tiller node after 12 h of treatment.

Endogenous Strigolactone and Exogenous rac-GR24 Promote the Cytokinin Degradation

The CK is recognized as an essential regulator of both the plant root system and shoot branching. Previous work suggested that exogenous GR24 promoted CK degradation in rice (Sun et al., 2014). Also, *OsCKX9* was proved to be activated by SLs signaling, and thus promotes CK degradation in rice. In this study, the expression of *OsIPT* genes showed different transcription patterns in tiller nodes and tiller buds under LN and LP conditions at tillering stage. But GR does not change the biosynthesis pattern in both rice tiller nodes and tiller buds. Consistent with our hypothesis, CK biosynthesis was not affected by GR24 supply in pea plants (Dun et al., 2012). Five *OsCKX* genes were significantly induced by GR24 supply and even by LP in our results. However, GR treatment and nutrient deficiency displayed different effects on the expression levels of *OsIPTs* and *OsCKXs* (**Figures 4**, **5**), suggesting the different modes of action response to these treatments. This is probably because the exogenous SLs may function only through SL signal transduction, but nutrient deficiency is linked to multiple signals including SL signaling.

Furthermore, we examined the effect of reduced endogenous SLs on the expression of *OsCKX* genes. As expected, HP and TIS decreased the expression of *OsCKX* genes in the tiller bud. These reports indicated that both endogenous and exogenous SLs may, somehow, regulate the expression of *OsCKX* genes in rice. Above all, these five increased/reduced *OsCKX* genes corresponded to local CK levels in rice tiller buds.

Strigolactones and Cytokinin Act Antagonistically on the Rice Buds Outgrowth

The supply of exogenous SLs and CK to the buds on node 2 at the full heading stage (**Figure 7**) showed that SLs and CK acted antagonistically on bud outgrowth. This was also confirmed in other species like pea and Arabidopsis (Braun et al., 2012; Dun et al., 2012), but never in rice. GR24 supply can suppress the increment of *OsRR* gene expression induced by BA. The *type-A RR* genes are the targets of CK signaling for primary transcription and rapid response (Brandstatter and Kieber, 1998; Imamura et al., 1998; D'Agostino et al., 2000; Jennifer et al., 2007). These findings suggested that the inhibition function of GR24 may be partly attributed to the impairment of CK downstream reaction.

We further explored the CK biosynthesis and degradation mechanisms with the BA and GR24 treatment (**Figure 8**). Consistent with the results we got at tillering stage, combined treatment of BA and GR24 induced an intermediate enhancement in the CK degradation, rather than exhibited by the CK biosynthesis change alone in buds on node 2. However, the application of GR24 alone to the buds did not change the expression of *OsCKX* genes in dormant buds, suggesting that local CK was required in the process of GR24 promoted expression of *OsCKX* genes.

Exogenous CK supply on buds directly induced the endogenous CK in buds and subsequently induced a negative feedback loop of CK biosynthesis, resulting in increased CK degradation. The combined GR24 supply showed an enhancement of CK degradation, but no changes were observed in CK biosynthesis. The expression pattern of *OsCKX* genes was partly different in response to BA and GR treatment. Together with the expression of the *OsRR* genes, we hypothesized that exogenous GR24 supply promoted the CK degradation partly by an independent pathway, and not just by promoting CK-induced CK degradation.

Interaction Between Strigolactones, Cytokinin, and Auxins in the Control of Shoot Branching

Tiller outgrowth in rice is the combined function of a number of contributing factors, including varying levels of different plant hormones in the growing buds. SLs and CKs were implicated in

the regulation of bud outgrowth. In this paper, we hypothesized that the SLs act directly in bud to inhibit the axillary bud outgrowth by promoting the local CK degradation. However, CK can also act independently of *PsBRC1*, as in pea, CK can still promote branching even in *psbrc1* mutants (Braun et al., 2012). The rice *OsFC1* transcription factor, which was implicated in bud outgrowth, was upregulated by rac-GR24 and downregulated by BA in rice axillary buds in our previous work (Xu et al., 2015). As described in the second-messenger model, SLs can regulate the expression level of *OsFC1* directly via the SL signaling pathway. Alternatively, SLs could also affect the *OsFC1* transcription level through CK signaling pathway by promoting the degradation of CK in the bud. Besides, CK can also act independently of *PsBRC1* (*OsFC1* in rice), as in pea, CK can still promote bud outgrowth even in *brc1* mutants (Braun et al., 2012). It was reported that the change in the local CK level in the bud always preceded the auxin efflux from the bud (Shimizu-Sato et al., 2008), which supports the notion that auxin transport is important for continued bud growth after bud release (Hayward et al., 2009; Prusinkiewicz et al., 2009; Crawford et al., 2010).

DATA AVAILABILITY STATEMENT

The original contributions presented in this study are included in the article/**Supplementary Material**, further inquiries can be directed to the corresponding author/s.

AUTHOR CONTRIBUTIONS

MZ designed the research and YW improved it. MZ performed research. MZ and ZT analyzed the data. MZ and YZ wrote the manuscript. YW and BC gave useful suggestions. All authors contributed to the article and approved the submitted version.

FUNDING

This study was supported by the National Natural Science Foundation of China (Project No. 32060432), the Natural Science Foundation of Hunan Province (Project No. 2021JJ40438), the Natural Science Foundation of Hunan Province (Project No. 2021JJ40440), and the Foundation of Guangdong Key Lab for Crop Germplasm Resources Preservation and Utilization (Project No. 2020B121201008).

SUPPLEMENTARY MATERIAL

The Supplementary Material for this article can be found online at: https://www.frontiersin.org/articles/10.3389/fpls.2022.837136/full#supplementary-material

REFERENCES

Akiyama, K., Matsuzaki, K., and Hayashi, H. (2005). Plant sesquiterpenes induce hyphal branching in arbuscular mycorrhizal fungi. *Nature* 435, 824–827. doi: 10.1038/nature03608

Akiyama, K., Ogasawara, S., Ito, S., and Hayashi, H. (2010). Structural requirements of strigolactones for hyphal branching in AM fungi. *Plant Cell Physiol.* 51, 1104–1117. doi: 10.1093/pcp/pcq058

Arite, T., Iwata, H., Ohshima, K., Maekawa, M., Nakajima, M., Kojima, M., et al., (2007). DWARF10, an RMS1/MAX4/DAD1 ortholog, controls lateral bud outgrowth in rice. *Plant J.* 51, 1019–1029. doi: 10.1111/j.1365-313X.2007.03210.x

Arite, T., Umehara, M., Ishikawa, S., Hanada, A., Maekawa, M., Yamaguchi, S., et al., (2009). d14, a strigolactone-insensitive mutant of rice, shows an accelerated outgrowth of tillers. *Plant Cell Physiol.* 50, 1416–1424. doi: 10.1093/pcp/pcp091

Bainbridge, K., Sorefan, K., Ward, S., and Leyser, O. (2005). Hormonally controlled expression of the *Arabidopsis* MAX4 shoot branching regulatory gene. *Plant J.* 44, 569–580. doi: 10.1111/j.1365-313X.2005.02548.x

Bangerth, F., Li, C.-J., and Gruber, J. (2000). Mutual interaction of auxin and cytokinins in regulating correlative dominance. *Plant Growth Regul.* 32, 205–217.

Beveridge, C. A., and Kyozuka, J. (2010). New genes in the strigolactone-related shoot branching pathway. *Curr. Opin. Plant Biol.* 13, 34–39. doi: 10.1016/j.pbi.2009.10.003

Beveridge, C. A., Ross, J. J., and Murfet, I. C. (1996). Branching in pea (action of genes Rms3 and Rms4). *Plant Physiol.* 110, 859–865. doi: 10.1104/pp.110.3.859

Beveridge, C. A., Symons, G. M., Murfet, I. C., Ross, J. J., and Rameau, C. (1997). The rms1 mutant of pea has elevated indole-3-acetic acid levels and reduced root-sap zeatin riboside content but increased branching controlled by graft-transmissible signal(s). *Plant Physiol.* 115, 1251–1258.

Booker, J., Sieberer, T., Wright, W., Williamson, L., Willett, B., Stirnberg, P., et al., (2005). MAX1 encodes a cytochrome P450 family member that acts downstream of MAX3/4 to produce a carotenoid-derived branch-inhibiting hormone. *Dev. Cell* 8, 443–449. doi: 10.1016/j.devcel.2005.01.009

Brandstatter, I., and Kieber, J. J. (1998). Two genes with similarity to bacterial response regulators are rapidly and specifically induced by cytokinin in *Arabidopsis*. *Plant cell* 10, 1009–1019. doi: 10.1105/tpc.10.6.1009

Braun, N., de Saint Germain, A., Pillot, J. P., Boutet-Mercey, S., Dalmais, M., Antoniadi, I., et al., (2012). The pea TCP transcription factor PsBRC1 acts downstream of Strigolactones to control shoot branching. *Plant Physiol.* 158, 225–238. doi: 10.1104/pp.111.182725

Brewer, P. B., Dun, E. A., Gui, R., Mason, M. G., and Beveridge, C. A. (2015). Strigolactone inhibition of branching independent of polar auxin transport. *Plant Physiol.* 168, 1820–1829. doi: 10.1104/pp.15.00014

Brewer, P. B., Koltai, H., and Beveridge, C. A. (2013). Diverse roles of strigolactones in plant development. *Mol. Plant* 6, 18–28. doi: 10.1093/mp/sss130

Bromhead, L. J., Smith, J., and McErlean, C. S. P. (2015). Chemistry of the synthetic strigolactone mimic GR24. *Australian J. Chem.* 68, 1221–1227.

Chatfield, S. P., Stirnberg, P., Forde, B. G., and Leyse, O. (2000). The hormonal regulation of axillary bud growth in *Arabidopsis*. *Plant J.* 24, 159–169. doi: 10.1046/j.1365-313x.2000.00862.x

Cline, M., Wesse, T., and Iwamura, H. (1997). Cytokinin/auxin control of apical dominance in *Ipomoea nil*. *Plant Cell Physiol.* 38, 659–667.

Cook, C. E., Whichard, L. P., Turner, B., Wall, M. E., and Egley, G. H. (1966). Germination of witchweed (*Striga lutea* Lour.): isolation and properties of a potent stimulant. *Science* 154, 1189–1190. doi: 10.1126/science.154.3753.1189

Crawford, S., Shinohara, N., Sieberer, T., Williamson, L., George, G., Hepworth, J., et al., (2010). Strigolactones enhance competition between shoot branches by dampening auxin transport. *Development* 137, 2905–2913. doi: 10.1242/dev.051987

D'Agostino, I. B., Deruere, J., and Kieber, J. J. (2000). Characterization of the response of the *Arabidopsis* ARR gene family to cytokinin. *Plant Physiol.* 124, 1706–1717.

de Jong, M., George, G., Ongaro, V., Williamson, L., Willetts, B., Ljung, K., et al., (2014). Auxin and strigolactone signaling are required for modulation

of *Arabidopsis* shoot branching by nitrogen supply. *Plant Physiol.* 166, 384–395. doi: 10.1104/pp.114.242388

Dobrev, P. I., and Kaminek, M. (2002). Fast and efficient separation of cytokinins from auxin and abscisic acid and their purification using mixed mode solid-phase extraction. *J. Chromatogr.* 950, 21–29. doi: 10.1016/s0021-9673(02)00024-9

Domagalska, M. A., and Leyser, O. (2011). Signal integration in the control of shoot branching. *Nat. Rev. Mol. Cell Biol.* 12, 211–221. doi: 10.1038/nrm3088

Duan, J., Yu, H., Yuan, K., Liao, Z., Meng, X., Jing, Y., et al., (2019). Strigolactone promotes cytokinin degradation through transcriptional activation of CYTOKININ OXIDASE/DEHYDROGENASE 9 in rice. *Proc. Natl. Acad. Sci. U.S.A.* 166, 14319–14324. doi: 10.1073/pnas.1810980116

Dun, E. A., Brewer, P. B., and Beveridge, C. A. (2009). Strigolactones: discovery of the elusive shoot branching hormone. *Trends Plant Sci.* 14, 364–372. doi: 10.1016/j.tplants.2009.04.003

Dun, E. A., de Saint Germain, A., Rameau, C., and Beveridge, C. A. (2012). Antagonistic action of strigolactone and cytokinin in bud outgrowth control. *Plant Physiol.* 158, 487–498. doi: 10.1104/pp.111.186783

Foo, E., Morris, S. E., Parmenter, K., Young, N., Wang, H., Jones, A., et al., (2007). Feedback regulation of xylem cytokinin content is conserved in pea and *Arabidopsis*. *Plant Physiol.* 143, 1418–1428. doi: 10.1104/pp.106.093708

Galuszka, P., Frébort, I., Sebela, M., Sauer, P., Jacobsen, S, and Pec, P. (2001). Cytokinin oxidase or dehydrogenase? *Eur. J. Biochem.* 268, 450–461. doi: 10.1046/j.1432-1033.2001.01910.x

Gomez-Roldan, V., Fermas, S., Brewer, P. B., Puech-Pages, V., Dun, E. A., Pillot, J. P., et al., (2008). Strigolactone inhibition of shoot branching. *Nature* 455, 189–194.

Ha, C. V., Leyva-Gonzalez, M. A., Osakabe, Y., Tran, U. T., Nishiyama, R., Watanabe, Y., et al., (2014). Positive regulatory role of strigolactone in plant responses to drought and salt stress. *Proc. Natl. Acad. Sci. U.S.A.* 111, 851–856. doi: 10.1073/pnas.1322135111

Ha, C. V., Vankova, R., Yamaguchi-Shinozaki, K., Shinozaki, K., and Tran, L. S. P. (2012). Cytokinins: metabolism and function in plant adaptation to environmental stresses. *Trends Plant Sci.* 17, 172–179. doi: 10.1016/j.tplants.2011.12.005

Hayward, A., Stirnberg, P., Beveridge, C., and Leyser, O. (2009). Interactions between auxin and strigolactone in shoot branching control. *Plant Physiol.* 151, 400–412. doi: 10.1104/pp.109.137646

Horvath, D., Anderson, J., Chao, W., and Foley, M. (2003). Knowing when to grow: signals regulating bud dormancy. *Trends Plant Sci.* 8, 534–540. doi: 10.1016/j.tplants.2003.09.013

Imamura, A., Hanaki, N., Umeda, H., Nakamura, A., Suzuki, T., Ueguchi, C., et al., (1998). Response regulators implicated in His-to-Asp phosphotransfer signaling in *Arabidopsis*. *Proc. Natl. Acad. Sci. U.S.A.* 95, 2691–2696. doi: 10.1073/pnas.95.5.2691

Ishikawa, S., Maekawa, M., Arite, T., Onishi, K., Takamure, I., and Kyozuka, J. (2005). Suppression of tiller bud activity in tillering dwarf mutants of rice. *Plant Cell Physiol.* 46, 79–86. doi: 10.1093/pcp/pci022

Ito, S., Umehara, M., Hanada, A., Kitahata, N., Hayase, H., Yamaguchi, S., et al., (2011). Effects of triazole derivatives on strigolactone levels and growth retardation in rice. *PLoS One* 6:e21723. doi: 10.1371/journal.pone.0021723

Ito, S., Umehara, M., Hanada, A., Yamaguchi, S., and Asami, T. (2013). Effects of strigolactone-biosynthesis inhibitor TIS108 on *Arabidopsis*. *Plant Signal. Behav.* 8:e24193. doi: 10.4161/psb.24193

Jamil, M., Charnikhova, T., Cardoso, C., Jamil, T., Ueno, K., Verstappen, F., et al., (2011a). Quantification of the relationship between strigolactones and *Striga hermonthica* infection in rice under varying levels of nitrogen and phosphorus. *Weed Res.* 51, 373–385.

Jamil, M., Rodenburg, J., Charnikhova, T., and Bouwmeester, H. J. (2011b). Pre-attachment Striga hermonthica resistance of new rice for africa (NERICA) cultivars based on low strigolactone production. *New Phytol.* 192, 964–975. doi: 10.1111/j.1469-8137.2011.03850.x

Jennifer, J. P., Deruere, J., Maxwell, B. B., Morris, V. F., Hutchison, C. E., Ferreira, F. J., et al., (2007). Cytokinin regulates type-A *Arabidopsis* response regulator activity and protein stability via two-component phosphorelay. *Plant Cell* 19, 3901–3914. doi: 10.1105/tpc.107.052662

Jiang, L., Liu, X., Xiong, G., Liu, H., Chen, F., Wang, L., et al., (2013). DWARF 53 acts as a repressor of strigolactone signalling in rice. *Nature* 504, 401–405. doi: 10.1038/nature12870

Kapulnik, Y., Delaux, P. M., Resnick, N., Mayzlish-Gati, E., Wininger, S., Bhattacharya, C., et al., (2011a). Strigolactones affect lateral root formation and root-hair elongation in *Arabidopsis*. *Planta* 233, 209–216. doi: 10.1007/s00425-010-1310-y

Kapulnik, Y., Resnick, N., Mayzlish-Gati, E., Kaplan, Y., Wininger, S., Hershenhorn, J., et al., (2011b). Strigolactones interact with ethylene and auxin in regulating root-hair elongation in *Arabidopsis*. *J. Exp. Bot.* 62, 2915–2924. doi: 10.1093/jxb/erq464

Koltai, H., LekKala, S. P., Bhattacharya, C., Mayzlish-Gati, E., Resnick, N., Wininger, S., et al., (2010). A tomato strigolactone-impaired mutant displays aberrant shoot morphology and plant interactions. *J. Exp. Bot.* 61, 1739–1749. doi: 10.1093/jxb/erq041

Leyser, O. (2009). The control of shoot branching: an example of plant information processing. *Plant Cell Environ.* 32, 694–703. doi: 10.1111/j.1365-3040.2009.01930.x

Li, C.-J., Guevara, E., Herrera, J., and Bangerth, F. (1995). Effect of apex excision and replacement by 1-naphthylacetic acid on cytokinin concentration and apical dominance in pea plants. *Physiol. Plant.* 94, 465–469.

López-Bucio, J., Millán-Godínez, M., Méndez-Bravo, A., Morquecho-Contreras, A., Ramírez-Chávez, E., Molina-Torres, J., et al., (2007). Cytokinin receptors are involved in alkamide regulation of root and shoot development in *Arabidopsis*. *Plant Physiol.* 145, 1703–1713. doi: 10.1104/pp.107.107953

Luo, L., Pan, S., Liu, X., Wang, H., and Xu, G. (2017). Nitrogen deficiency inhibits cell division-determined elongation, but not initiation, of rice tiller buds. *Israel J. Plant Sci.* 64, 32–40.

Luo, L., Wang, H., Liu, X., Hu, J., Zhu, X., Pan, S., et al., (2018). Strigolactones affect the translocation of nitrogen in rice. *Plant Sci.* 270, 190–197. doi: 10.1016/j.plantsci.2018.02.020

Minakuchi, K., Kameoka, H., Yasuno, N., Umehara, M., Luo, L., Kobayashi, K., et al., (2010). FINE CULM1 (FC1) works downstream of strigolactones to inhibit the outgrowth of axillary buds in rice. *Plant Cell Physiol.* 51, 1127–1135. doi: 10.1093/pcp/pcq083

Morris, S. E., Turnbull, C. G. N., Murfet, I. C., and Beveridge, C. A. (2001). Mutational analysis of branching in pea evidence that Rms1 and Rms5 regulate the same novel signal. *Plant Physiol.* 126, 1205–1213. doi: 10.1104/pp.126.3.1205

Müller, D., Waldie, T., Miyawaki, K., To, J. P., Melnyk, C. W., Kieber, J. J., et al., (2015). Cytokinin is required for escape but not release from auxin mediated apical dominance. *Plant J.* 82, 874–886. doi: 10.1111/tpj.12862

Nakagawa, H., Jiang, C. J., Sakakibara, H., Kojima, M., Honda, I., Ajisaka, H., et al., (2005). Overexpression of a petunia zinc-finger gene alters cytokinin metabolism and plant forms. *Plant J.* 41, 512–523. doi: 10.1111/j.1365-313X.2004.02316.x

Napoli, C. (1996). Highly branched phenotype of the petunia dad1-1 mutant is reversed by grafting. *Plant Physiol.* 111, 27–37. doi: 10.1104/pp.111.1.27

Nordström, A., Tarkowski, P., Tarkowska, D., Norbaek, R., Åstot, C., Dolezal, K., et al., (2004). Auxin regulation of cytokinin biosynthesis in *Arabidopsis thaliana*: a factor of potential importance for auxin–cytokinin-regulated development. *Proc. Natl. Acad. Sci. U.S.A.* 101, 8039–8044. doi: 10.1073/pnas.0402504101

Pillay, I., and Railton, I. D. (1983). Complete release of axillary buds from apical dominance in intact, light-grown seedlings of *Pisum sativum* L. following a single application of cytokinin. *Plant Physiol.* 71, 972–974. doi: 10.1104/pp.71.4.972

Prusinkiewicz, P., Crawford, S., Richard, S. S., Ljung, K., Bennett, T., Ongaro, V., et al., (2009). Control of bud activation by an auxin transport switch. *Proc. Natl. Acad. Sci. U.S.A.* 106, 17431–17436. doi: 10.1073/pnas.0906696106

Ruyter-Spira, C., Kohlen, W., Charnikhova, T., van Zeijl, A., van Bezouwen, L., de Ruijter, N., et al., (2011). Physiological effects of the synthetic strigolactone analog GR24 on root system architecture in *Arabidopsis*: another belowground role for strigolactones? *Plant Physiol.* 155, 721–734. doi: 10.1104/pp.110.166645

Sakamoto, T., Sakakibara, H., Kojima, M., Yamamoto, Y., Nagasaki, H., Inukai, Y., et al., (2006). Ectopic expression of KNOTTED1-like homeobox protein induces expression of cytokinin biosynthesis genes in rice. *Plant Physiol.* 142, 54–62. doi: 10.1104/pp.106.085811

Seale, M., Bennett, T., and Leyser, O. (2017). BRC1 expression regulates bud activation potential but is not necessary or sufficient for bud growth inhibition in *Arabidopsis*. *Development* 144, 1661–1673. doi: 10.1111/nph.16470

Shimizu-Sato, S., Ike, Y., and Mori, H. (2008). PsRBR1 encodes a pea retinoblastoma-related protein that is phosphorylated in axillary buds during dormancy-to-growth transition. *Plant Mol. Biol.* 66, 125–135. doi: 10.1007/s11103-007-9257-5

Shimizu-Sato, S., Tanaka, M., and Mori, H. (2009). Auxin-cytokinin interactions in the control of shoot branching. *Plant Mol. Biol.* 69, 429–435. doi: 10.1007/s11103-008-9416-3

Simons, J. L., Napoli, C. A., Janssen, B. J., Plummer, K. M., and Snowden, K. C. (2007). Analysis of the decreased apical dominance genes of petunia in the control of axillary branching. *Plant Physiol.* 143, 697–706. doi: 10.1104/pp.106.087957

Soundappan, I., Bennett, T., Morffy, N., Liang, Y., Stanga, J. P., Abbas, A., et al., (2015). SMAX1-LIKE/D53 family members enable distinct MAX2-dependent responses to strigolactones and karrikins in *Arabidopsis*. *Plant Cell* 27, 3143–3159. doi: 10.1105/tpc.15.00562

Sun, H., Tao, J., Liu, S., Huang, S., Chen, S., Xie, X., et al., (2014). Strigolactones are involved in phosphate- and nitrate-deficiency-induced root development and auxin transport in rice. *J. Exp. Bot.* 65, 6735–6746. doi: 10.1093/jxb/eru029

Takei, K., Ueda, N., Aoki, K., Kuromori, T., Hirayama, T., Shinozaki, K., et al., (2004). AtIPT3 is a key determinant of nitrate-dependent cytokinin biosynthesis in *Arabidopsis*. *Plant Cell Physiol.* 45, 1053–1062. doi: 10.1093/pcp/pch119

Tanaka, M., Takei, K., Kojima, M., Sakakibara, H., and Mori, H. (2006). Auxin controls local cytokinin biosynthesis in the nodal stem in apical dominance. *Plant J.* 45, 1028–1036. doi: 10.1111/j.1365-313X.2006.02656.x

Turnbull, C. G. N., Booker, J. P., and Leyser, H. M. O. (2002). Micrografting techniques for testing long-distance signalling in *Arabidopsis*. *Plant J.* 32:255. doi: 10.1046/j.1365-313x.2002.01419.x

Turnbull, C. G. N., Raymond, M. A. A., Dodd, I. C., and Morris, S. E. (1997). Rapid increases in cytokinin concentration in lateral buds of chickpea (*Cicer arietinum* L.) during release of apical dominance. *Planta* 202, 271–276.

Umehara, M., Hanada, A., Magome, H., Takeda-Kamiya, N., and Yamaguchi, S. (2010). Contribution of strigolactones to the inhibition of tiller bud outgrowth under phosphate deficiency in rice. *Plant Cell Physiol.* 51, 1118–1126. doi: 10.1093/pcp/pcq084

Umehara, M., Hanada, A., Yoshida, S., Akiyama, K., Arite, T., Takeda-Kamiya, N., et al., (2008). Inhibition of shoot branching by new terpenoid plant hormones. *Nature* 455, 195–200. doi: 10.1038/nature07272

Waldie, T., Hayward, A., and Beveridge, C. A. (2010). Axillary bud outgrowth in herbaceous shoots: how do strigolactones fit into the picture? *Plant Mol. Biol.* 73, 27–36. doi: 10.1007/s11103-010-9599-2

Wang, L., Wang, B., Jiang, L., Liu, X., Li, X., Lu, Z., et al., (2015). Strigolactone signaling in *Arabidopsis* regulates shoot development by targeting D53-Like SMXL repressor proteins for ubiquitination and degradation. *Plant Cell* 27, 3128–3142. doi: 10.1105/tpc.15.00605

Xie, X., Yoneyama, K., and Yoneyama, K. (2010). The strigolactone story. *Annu. Rev. Phytopathol.* 48, 93–117.

Xu, J., Zha, M., Li, Y., Ding, Y., Chen, L., Ding, C., et al., (2015). The interaction between nitrogen availability and auxin, cytokinin, and strigolactone in the control of shoot branching in rice (*Oryza sativa* L.). *Plant Cell Rep.* 34, 1647–1662. doi: 10.1007/s00299-015-1815-8

Yoneyama, K., Takeuchi, Y., and Sekimoto, H. (2007). Phosphorus deficiency in red clover promotes exudation of orobanchol, the signal for mycorrhizal symbionts and germination stimulant for root parasites. *Planta* 225, 1031–1038. doi: 10.1007/s00425-006-0410-1

Yoneyama, K., Xie, X., Kim, H. I., Kisugi, T., Nomura, T., Sekimoto, H., et al., (2012). How do nitrogen and phosphorus deficiencies affect strigolactone production and exudation? *Planta* 235, 1197–1207. doi: 10.1007/s00425-011-1568-8

Yoneyama, K., Xie, X., Nomura, T., and Yoneyama, K. (2020). Do phosphate and cytokinin interact to regulate strigolactone biosynthesis or act independently? *Front. Plant Sci.* 11:438. doi: 10.3389/fpls.2020.00438

Yoshida, S. (1975). *Laboratory Manual for Physiological Studies of Rice*. Beijing: Science Press, 57–64.

Zhang, S., Li, G., Fang, J., Chen, W., Jiang, H., Zou, J., et al., (2010). The interactions among DWARF10, auxin and cytokinin underlie lateral bud outgrowth in rice. *J. Integr. Plant Biol.* 52, 626–638. doi: 10.1111/j.1744-7909.2010.00960.x

Zhou, F., Lin, Q., Zhu, L., Ren, Y., Zhou, K., Shabek, N., et al., (2013). D14-SCF(D3)-dependent degradation of D53 regulates strigolactone signalling. *Nature* 504, 406–410.

Zou, J., Zhang, S., Zhang, W., Li, G., Chen, Z., Zhai, W., et al., (2006). The rice HIGH-TILLERING DWARF1 encoding an ortholog of *Arabidopsis* MAX3 is required for negative regulation of the outgrowth of axillary buds. *Plant J.* 48, 687–698. doi: 10.1111/j.1365-313X.2006.02916.x

Conflict of Interest: The authors declare that the research was conducted in the absence of any commercial or financial relationships that could be construed as a potential conflict of interest.

Publisher's Note: All claims expressed in this article are solely those of the authors and do not necessarily represent those of their affiliated organizations, or those of the publisher, the editors and the reviewers. Any product that may be evaluated in this article, or claim that may be made by its manufacturer, is not guaranteed or endorsed by the publisher.

frontiers | Frontiers in Plant Science

REVIEW
published: 12 July 2022
doi: 10.3389/fpls.2022.889045

How Strigolactone Shapes Shoot Architecture

*Khopeno Khuvung, Federico A. O. Silva Gutierrez and Didier Reinhardt**

Department of Biology, University of Fribourg, Fribourg, Switzerland

Despite its central role in the control of plant architecture, strigolactone has been recognized as a phytohormone only 15 years ago. Together with auxin, it regulates shoot branching in response to genetically encoded programs, as well as environmental cues. A central determinant of shoot architecture is apical dominance, i.e., the tendency of the main shoot apex to inhibit the outgrowth of axillary buds. Hence, the execution of apical dominance requires long-distance communication between the shoot apex and all axillary meristems. While the role of strigolactone and auxin in apical dominance appears to be conserved among flowering plants, the mechanisms involved in bud activation may be more divergent, and include not only hormonal pathways but also sugar signaling. Here, we discuss how spatial aspects of SL biosynthesis, transport, and sensing may relate to apical dominance, and we consider the mechanisms acting locally in axillary buds during dormancy and bud activation.

Keywords: strigolactone, auxin, cytokinin, abscisic acid, branching, apical dominance, dormancy, BRANCHED1

OPEN ACCESS

Edited by:
Catherine Rameau, INRA UMR1318 Institut Jean Pierre Bourgin, France

Reviewed by:
Francois Fabien Barbier, The University of Queensland, Australia
Catalina Iulia Pislariu, Texas Woman's University, United States
Philip B. Brewer, University of Adelaide, Australia

****Correspondence:***
Didier Reinhardt
didier.reinhardt@unifr.ch

Specialty section:
This article was submitted to Plant Physiology, a section of the journal Frontiers in Plant Science

Received: *03 March 2022*
Accepted: *10 June 2022*
Published: *12 July 2022*

Citation:
Khuvung K, Silva Gutierrez FAO and Reinhardt D (2022) How Strigolactone Shapes Shoot Architecture. Front. Plant Sci. 13:889045. doi: 10.3389/fpls.2022.889045

INTRODUCTION

Its central role in the regulation of shoot architecture is arguably the most conspicuous function of the phytohormone strigolactone (SL; Domagalska and Leyser, 2011; Barbier et al., 2019). Indeed, most of the information about SL biosynthesis and SL sensing comes from bushy mutants identified in forward genetic screens in thale cress (*Arabidopsis thaliana*), rice (*Oryza sativa*), petunia (*Petunia hybrida*), and pea (*Pisum sativum*) (reviewed in Al-Babili and Bouwmeester, 2015; Yoneyama and Brewer, 2021). Plant architecture is to a large degree defined by branching patterns, that is the number, position, and size of lateral branches. The extent of branching is controlled by the activity of the main shoot apex, which inhibits the outgrowth of axillary buds along the stem. Axillary meristems are initiated in all leaf axils (Wang et al., 2016b); however, they usually only initiate a few leaf primordia and then become dormant, until they are activated to grow out either in response to endogenous/exogenous developmental signals, or as a consequence of removal (or inactivation) of the main shoot apex. This phenomenon is known as apical dominance (AD; Phillips, 1975).

The central feature of AD is systemic correlative inhibition of bud outgrowth, which is under the control of auxin and SL, involving a mechanism known as auxin canalization (Crawford et al., 2010; Shinohara et al., 2013; Zhang et al., 2020). On the other hand, inducing signals such as cytokinin and sugars are involved in the activation of axillary buds (Domagalska and Leyser, 2011; Rameau et al., 2015; Barbier et al., 2019). While several excellent reviews discuss the function of SL in AD (Domagalska and Leyser, 2011; Rameau et al., 2015; Barbier et al., 2019), we focus here more on spatial aspects of SL biosynthesis and sensing, and on local

downstream events in the buds required to inhibit bud outgrowth, and to trigger bud activation, respectively. Furthermore, we discuss parallels in meristem dormancy in annual versus perennial plants.

SELECTIVE ADVANTAGE OF BRANCHING AND APICAL DOMINANCE

Plants with just a single shoot meristem suffer extinction if the meristem is damaged. For example, a palm tree infested with the red palm weevil (*Rhynchophorus ferrugineus*) cannot recover after its meristem has been consumed by the larvae (Al-Dosary et al., 2016). This can result in serious damage in infested date palm plantations (El-Sabea et al., 2009). Hence, having extra axillary meristems and multiple branches, as in most dicots, is an important selective advantage. However, shoot branching has to be kept in check to avoid shoot overgrowth and a relative depletion of root biomass (low root:shoot ratio), which would interfere with overall plant fitness. Plants have characteristic root:shoot ratios that are species-specific and genetically determined (Wilson, 1988), but root:shoot ratio can also change in response to environmental factors, such as light, nutrient status, and altitude (Körner and Renhardt, 1987; Shipley and Meziane, 2002).

These considerations highlight the importance of regulation of axillary bud outgrowth. AD contributes to focus the resources of the plant to one (or few) growth points, and eventually, to a limited number of fruits and seeds. Hence, plant fitness and reproductive success are tightly linked with the degree of AD (Aarssen, 1995; Lennartsson et al., 2018). However, the relationship is not simple, since removal of apical buds (experimental or by animal grazing) can either reduce reproductive success, because less fruits can be produced, or it leads to increased reproductive success due to the release of multiple axillary branches with inflorescences, which over-compensate the loss of flowers at the original apex (Aarssen, 1995). These findings raise interesting questions concerning the adaptive mechanisms that may have shaped the evolution of AD and the control of bud outgrowth, in particular in the context of its plasticity towards environmental and developmental factors (e.g., light, mineral nutrients, damage, developmental stage, etc.; Aarssen, 1995). In this context, it is interesting to note that some taxa have integrated the loss-of-apical meristem activity in their developmental programs during the evolution of sympodial branching patterns (Danert, 1958; Schmitz and Theres, 1999; Reinhardt and Kuhlemeier, 2002). Sympodial branching involves the programmed arrest of the apical meristem (often with the production of a terminal flower) and the outgrowth of axillary (lateral) meristems which have a defined life-span before they terminate themselves in a reiterative "stop-and-go" fashion. This sympodial branching pattern is characteristic for the inflorescences of the Solanaceae (Danert, 1958; Schmitz and Theres, 1999; Reinhardt and Kuhlemeier, 2002).

As a general rule, high AD is advantageous in densely populated environments, in which plants compete for nutrients and/or light, whereas harsh conditions (e.g., cold, heat, UV radiation, and strong wind) with scarce vegetation favor bushy shoots with low AD, as for example in alpine environments (Körner, 2003). Considering agricultural crops, strong AD is a favored trait in panicoid cereal crops (e.g., maize and millet), since it tends to increase yield per surface area of cultivated soil, and because simpler shoot architecture facilitates harvest (Doust, 2007). Maize is a prominent example which has been bred from bushy ancestors (the Mexican wild maize teosinte) to plants with a single main shoot axis (Yang et al., 2019). In some high-value vegetable and ornamental crops, e.g., tomato, cucumber, and Chrysanthemum, breeding for desired strong AD has not been achieved yet. Hence, their axillary branches have to be manually pruned (Navarrete and Jeannequin, 2000; Xi et al., 2015; Shen et al., 2019), because they would represent sinks that consume resources and cause yield losses. In contrast, low apical dominance (i.e., high branching) is a favored trait in pooid cereal crops, such as wheat, barley, and oat, in which intense tillering increases yield (Doust, 2007). In addition, crops that were bred for simultaneous fruit ripening, e.g., soybean (Tian et al., 2010) and cotton (McGarry et al., 2016), show decreased indeterminacy of the main shoot, usually associated with increased branching.

In many plant species, AD is more pronounced during vegetative development, while the onset of flowering coincides with a stimulation of bud outgrowth and increased branching (Hempel and Feldman, 1994; Beveridge et al., 2003; McSteen and Leyser, 2005; Rameau et al., 2015). An example for such a strategy is Arabidopsis, which does not branch during vegetative development, and which initiates a single main inflorescence at the time of bolting (**Figure 1A**). During the generative phase, several axillary/caulinary branches grow out (Hempel and Feldman, 1994; McSteen and Leyser, 2005), but always much fewer than there are axillary buds. An example of a plant with low AD is the alpine species *Silene acaulis*, which is adapted to harsh climate with strong winds and abundant snow fall (**Figure 1B**). Mutants with defective AD are highly branched and dwarfed (Beveridge et al., 2003; Snowden and Napoli, 2003; Domagalska and Leyser, 2011; Rameau et al., 2015), in case of petunia to the extent that flowering is delayed (Napoli, 1996; **Figures 1C,D**), conceivably as a result of resource diversion from the apical inflorescence meristem to the actively growing lateral branches.

A CENTRAL ROLE FOR SL IN APICAL DOMINANCE

A wealth of classical literature documents a central role for polar auxin transport (PAT) in AD and in the regulation of axillary bud outgrowth (Cline, 1991; Leyser, 2005; McSteen and Leyser, 2005). Auxin from apical tissues (in particular young leaves) is transported downward (basipetally) *via* PAT in xylem parenchyma cells, inhibiting bud outgrowth on the way through the stem, however, without entering the buds (Domagalska and Leyser, 2011). A well-founded theory of AD posits that PAT in the stem promotes AD by interfering with

Abbreviations: SL, Strigolactone; AD, Apical dominance; ABA, Abscisic acid; BRC1, BRANCHED1; CK, Cytokinin; P, Phosphorus; N, Nitrogen; GA, Gibberellic acid.

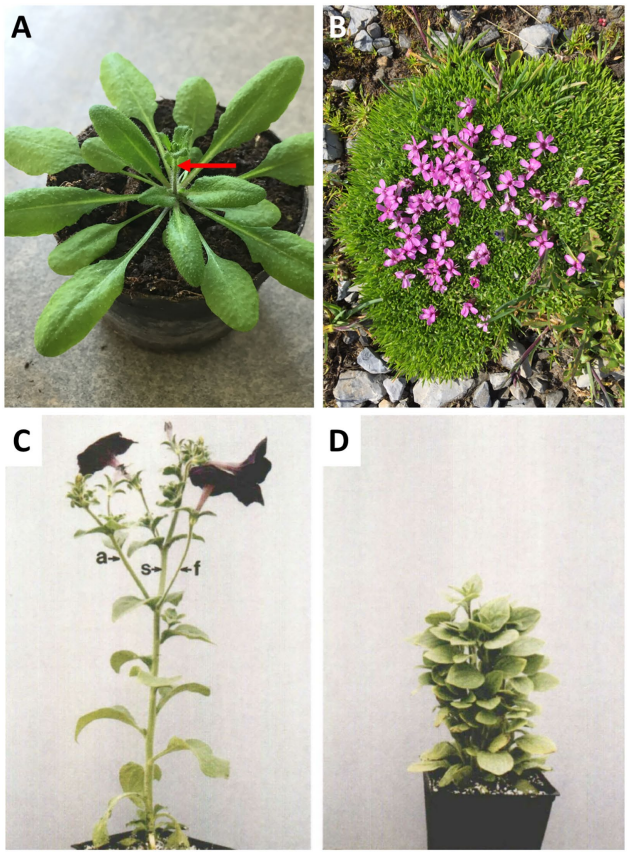

FIGURE 1 | Apical dominance. **(A)** Apical dominance in the pioneer plant *Arabidopsis thaliana* at the onset of flowering. **(B)** The alpine plant *Silene acaulis* exhibits very low apical dominance. It exhibits a profusely branched shoot, in which no main shoot can be distinguished. **(C,D)** The model plant for apical dominance *Petunia hybrida* V26, and the isogenic mutant *decreased apical dominance1* (*dad1*). The pleiotropic phenotype includes short stature, high branching, and late flowering (**C,D**, with permission from Napoli, 1996).

auxin canalization and export from the buds (Domagalska and Leyser, 2011). How the lack of auxin canalization is mechanistically related to growth arrest in the bud is not clear, but it may have to do with limited supply of signals and/or resources that would promote meristem activity in the bud. Alternatively, it may impinge on the cell cycle in order to attenuate meristem activity in the bud (Müller and Leyser, 2011). The identification of SL as a second inhibitory element in AD (Gomez-Roldan et al., 2008; Umehara et al., 2008) has raised the question how SL is linked with auxin action. The fact that mutants in either auxin or SL biology have strong defects in AD shows that the effects of the two phytohormones are not redundant. The currently available hypotheses for the action of SL are that it either inhibits auxin canalization from axillary buds to the main stem (by interfering with PAT), or that it directly inhibits bud outgrowth (Domagalska and Leyser, 2011). These hypotheses are not mutually exclusive, and several lines of evidence suggest that they are both valid (see below). Forward genetic screens in Arabidopsis, rice, pea, and petunia for mutants affected in shoot branching have led to the discovery of numerous genes encoding components of SL biosynthesis and signaling (reviewed in Al-Babili and Bouwmeester, 2015; Yoneyama and Brewer, 2021), and missing links in SL biosynthesis and sensing continue to be discovered (Wakabayashi et al., 2021). Taken together, these efforts document the prominent role of SL in apical dominance. The parallel work in these four model species showed how conserved SL biosynthesis and signaling is among flowering plants, and, on the other hand, revealed subtle species-specific differences. Importantly, the parallel approaches allowed to identify signaling elements that are genetically redundant in some of the species, and, therefore, evaded identification in forward mutant screens, as for example the duplicated *MAX2* gene in petunia (Drummond et al., 2012), or the redundant *SMAXL6*, *SMAXL7,* and *SMAXL8* in Arabidopsis (Soundappan et al., 2015). Additional evidence for the role of SL in branching came from crop species such as tomato and potato (Vogel et al., 2010; Pasare et al., 2013). Taken together, these findings substantiate the central and conserved role of SL in the regulation of shoot branching.

SL TRANSPORT WITHIN THE PLANT: IDENTIFYING SOURCES AND TARGETS OF SL BY GRAFTING

The action of auxin in AD is non-cell autonomous, since it is transported throughout the plant and acts on the buds indirectly (Domagalska and Leyser, 2011). Similarly, SL acts in a systemic fashion and can be transported over long distances in the plant (Mashiguchi et al., 2021). Compelling evidence for spatially separated sites of SL biosynthesis and action comes from grafting experiments with mutants that are defective in SL biosynthesis or sensing (**Figure 2**). Shoot-to-root grafting in Arabidopsis, petunia, and pea revealed that a wild-type root stock can establish normal AD in an SL-deficient mutant scion, indicative of acropetal SL transport from the root to the shoot (Beveridge, 2000; Booker et al., 2005; Dun et al., 2009; Waldie et al., 2014). Even a relatively small inter-graft between a mutant stock and a mutant scion was sufficient to restore AD to the mutant scion (Napoli, 1996; Simons et al., 2007; Hepworth, 2012) but not to the mutant stock, showing that SL transport is strictly unidirectional (**Figures 2A,B**; Foo et al., 2001; Simons et al., 2007). Although SL can be transported over long distances (from the root to the shoot), it is not clear whether this transport is required for AD. Wild-type scions grafted on SL-defective mutant stocks grow normally, showing that for AD, SL production in the shoot can be sufficient, at least in such grafts, implying that SL transport from the root may not be necessary for normal AD.

The fact that SL can be transported acropetally raises the question concerning the transport route. Root-to-shoot transport could proceed by mass flow with the transpiration stream in the xylem, or by cellular transport, as in the case of PAT (Petrasek and Friml, 2009; but in the reverse direction). Support for a xylem route of SL transport came from the detection

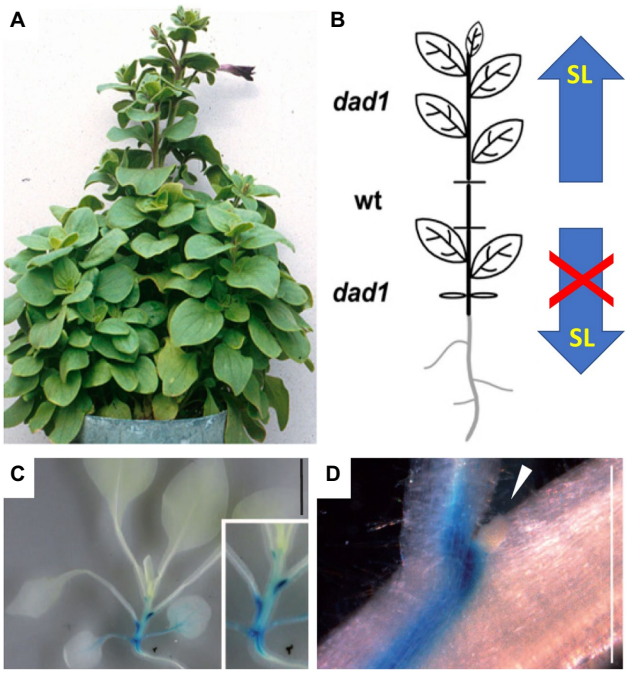

FIGURE 2 | SL transport in the plant. **(A,B)** Grafting experiments have proven acropetal SL transport in the shoot. A small wild-type stem segment (wt) complements the *dad1* phenotype in the scion (top), while the *dad1* stock exhibits the non-complemented high branching phenotype (bottom); thus, only upward SL transport occurred. The scheme in **(B)** represents the organization of the grafted plant in **(A)**. **(C,D)** Expression pattern of the cellular SL transporter *pPhPDR1::GUS* in the shoot of *P. hybrida*. Note highest expression just below the axillary buds, while the buds themselves [arrowhead in **(D)**] show no expression [modified with permission from Simons et al., 2007 **(A,B)** and Kretzschmar et al., 2012 **(C,D)**].

of SL in xylem sap of Arabidopsis and tomato (Kohlen et al., 2011); however, these findings were not confirmed by subsequent work on various plant species, including Arabidopsis and tomato (Xie et al., 2015; see also below).

An alternative route of SL translocation is cell-to-cell transport in a way analogous to PAT (Borghi et al., 2016). Indeed, the first cellular SL transporter identified in *P. hybrida* (PDR1), an ABC transporter of the G-type subfamily, was shown to functionally contribute both to mycorrhizal symbiosis (by targeted secretion from the root), and to AD in the shoot (Kretzschmar et al., 2012). *PDR1* is expressed in root and stem tissues (Kretzschmar et al., 2012), with highest levels at the nodes, next to the axillary buds (**Figures 2C,D**). PDR1 protein is localized to the plasma membrane, and, based on its expression pattern and loss-of-function mutant phenotype, is likely to function as an SL exporter (Kretzschmar et al., 2012). *Pdr1* mutants exhibit premature bud outgrowth (Kretzschmar et al., 2012), indicating that SL transport to the buds contributes significantly to AD. However, long-distance transport of SL appears to be independent of PDR1 (Shiratake et al., 2019); thus, the mechanism of SL translocation from the root to the shoot remains unclear (Wheeldon and Bennett, 2021).

SPATIAL REGULATION OF SL-BIOSYNTHETIC GENES

Powerful tools to identify the sites of action of genes are promoter::reporter constructs (Jefferson et al., 1987; Chalfie et al., 1994) that show gene expression patterns with great spatial resolution. While fluorescent proteins are often the marker of choice because they allow identification in undisturbed live tissues with cellular resolution, they have the disadvantage that the optical permeability of live plant tissues is often limited, and, in addition, autofluorescence of many plant components (cell walls, secondary metabolites in vacuoles, etc.) considerably hampers their analysis. A widely used alternative is the use of enzymatic reporters such as the beta-glucuronidase gene (UidA), also known as the GUS gene, which generates (from the substrate X-gluc) a blue insoluble deposit (5,5′-dibrom-4,4′-dichlor-indigo), which is stable enough to allow for complete tissue clearing and embedding in paraffin or resin for sectioning. Importantly, cleared plant tissues have no blue background color, thus eliminating problems with endogenous background staining (**Figures 2C,D**).

Promoter::GUS analysis with the major SL-biosynthetic genes in Arabidopsis revealed that several of them are active in the vasculature (besides other sites of expression), and some of them (*MAX3*, *MAX1*; *LBO*) are expressed almost exclusively along vascular strands (**Figure 3**; Booker et al., 2005; Liang et al., 2011; Brewer et al., 2016). The expression of SL-biosynthetic genes along the vasculature was also found in rice for D27 (Lin et al., 2009) and CCD7 (Zou et al., 2006). Hence, it can be assumed that SL, or an SL precursor such as carlactone (Alder et al., 2012), is produced along the vascular system. Although all SL-biosynthetic genes are expressed mainly in the root, they also show expression in aerials tissues, in particular the stem, in Arabidopsis (**Figure 3**), as well as in other species (Zou et al., 2006; Drummond et al., 2009; Dun et al., 2009; Lin et al., 2009; Vogel et al., 2010; Pasare et al., 2013). This provides a plausible explanation for the fact that in Arabidopsis, petunia, and pea, wild-type scions grafted onto SL-defective mutant stocks are self-sufficient for SL production (Beveridge et al., 1994, 1996, 1997; Napoli, 1996; Morris et al., 2001; Turnbull et al., 2002; Sorefan et al., 2003; Booker et al., 2005; Simons et al., 2007; Drummond et al., 2009).

The vicinity of SL-biosynthetic gene expression to the xylem strands could explain why SL can be detected in the transpiration stream (Kohlen et al., 2011). SL produced along the vasculature could be loaded to the xylem by cellular transporters or by diffusive release from biosynthetic cells. It would then be continuously translocated to the shoot with the transpiration stream, even at low concentrations. While acropetal SL transport may not be essential for AD (see grafting experiments discussed above), SL transport through the xylem could represent a significant contribution to SL function in other aspects of shoot development, e.g., for the regulation of leaf senescence (Ueda and Kusaba, 2015).

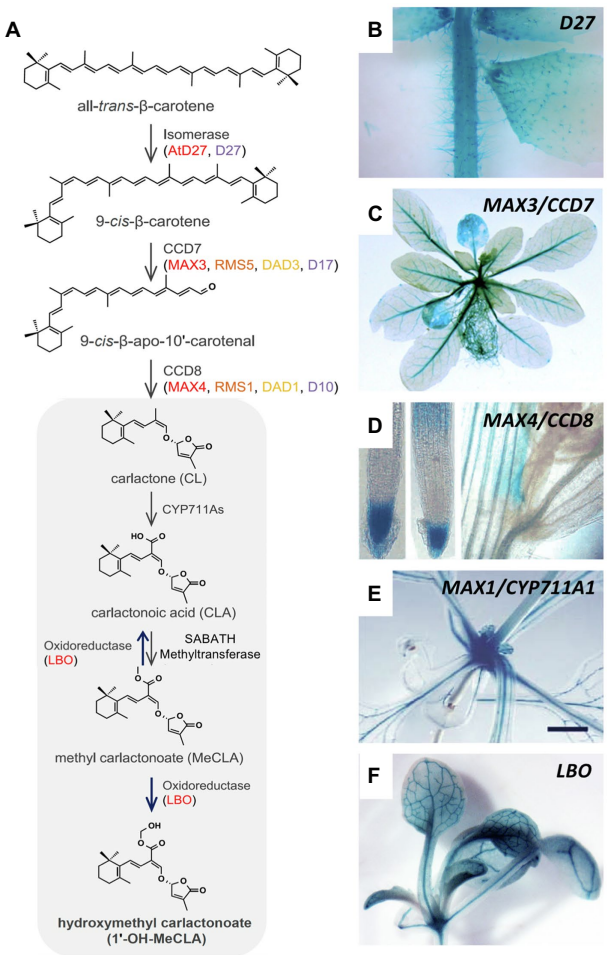

FIGURE 3 | Expression pattern of SL-biosynthetic genes in Arabidopsis. **(A)** Biosynthetic pathway of strigolactone comprising the activity of the isomerase D27, the carotenoid cleavage dioxygenases CCD7 and CCD8, CYP711A, the oxidoreductase LBO, and the SABATH methyltransferase. **(B–F)** Expression pattern of Arabidopsis SL-biosynthetic genes such as *D27* **(B)**, *CCD7/MAX3* **(C)**, *CCD8/MAX4* **(D)**, *CYP711A1/MAX1* **(E)**, and *LBO* **(F)**, as indicated, revealed by promoter::GUS analysis. Note prominent expression in the vasculature of *MAX3*, *MAX1*, and *LBO* [**C,E,F**; modified with permission from Yoneyama and Brewer, 2021 **(A)**; Abuauf et al., 2018 **(B)**; Liang et al., 2011 **(C)**; Sorefan et al., 2003 **(D)**; Booker et al., 2005 **(E)**, and Brewer et al., 2016 **(F)**].

NUTRITIONAL CONTROL OF SHOOT BRANCHING IMPINGES ON THE SL PATHWAY

In addition to the above-mentioned factors that influence AD, nutrients influence shoot architecture, since well-fertilized plants tend to branch more than nutritionally starved plants (Cline, 1991; Czarnecki et al., 2013; Wang et al., 2019; Hou et al., 2021). This effect can be explained, at least partially, by the fact that nutrients, in particular nitrogen (N) and phosphorus (P), impinge on the auxin- and SL-related mechanisms involved in AD (Sakakibara et al., 2006; Yoneyama and Brewer, 2021; Marro et al., 2022). High N status not only promotes branching, an effect that requires auxin and SL signaling (De Jong et al., 2014), but also involves the activation of cytokinin biosynthesis (Takei et al., 2002; Sakakibara et al., 2006; Xu et al., 2015). High P status represses SL-biosynthetic genes, consistent with the observation that SL secretion from the root system is repressed by P fertilization (Yoneyama et al., 2007a,b; Kohlen et al., 2011). P-replenished plants exhibit increased branching (Czarnecki et al., 2013; Wang et al., 2019), conceivably as a result of reduced SL biosynthesis (Umehara et al., 2010; Abuauf et al., 2018; Yoneyama and Brewer, 2021). In P-starved plants, SL biosynthesis is induced (Yoneyama and Brewer, 2021), presumably resulting in acropetal SL transport into the buds. Under these conditions, xylem transport of SL could become relevant (Kohlen et al., 2011), in particular since SL-biosynthetic genes are expressed along the vasculature (**Figure 3**). However, the role of the xylem in acropetal SL transport is a matter of debate (Xie et al., 2015), and the broad expression pattern of SL-biosynthetic genes throughout the shoot suggests that acropetal SL transport may not be necessary for apical dominance (see above).

SITES OF SL SENSING AND CONSEQUENCES FOR AD

Interestingly, several SL-sensing genes (*D14*, *MAX2*, *SMAXL6*, *SMAXL7*, and *SMAXL8*) share the expression pattern along the vascular strands with SL-biosynthetic genes (**Figure 4**; Gao et al., 2004; Shen et al., 2007; Stirnberg et al., 2007; Chevalier et al., 2014; Soundappan et al., 2015; Song et al., 2022). In general, the identity of the cells that express SL-sensing genes along the vasculature is uncertain; however, for the SL receptor D14, expression was attributed to the phloem in Arabidopsis roots (Chevalier et al., 2014), and in the axillary buds of rice (Kameoka et al., 2016), suggesting that SL perception may be possible in these tissues. An association of SL-sensing genes with the vasculature is striking given the function of SL as inhibitor of PAT, which is located to the xylem parenchyma cells (Petrasek and Friml, 2009). Hence, SL perception in these cells would allow for a direct regulation of PAT in these cells. It will be important to identify the sites of SL sensing in more detail, with refined promoter::reporter studies, and with complementation experiments, in which SL-sensing genes are expressed in the respective mutant background under the control of cell-specific promoters. Further insight into SL sensing will come from fluorescent SL reporters, which allow to identify sites of high SL levels in living plant tissues with cellular resolution (Song et al., 2022).

A powerful tool to assign biological function to precisely defined cell populations is clonal analysis, in which the fate of genetically distinct cell lineages is followed in chimeras (Buckingham and Meilhac, 2011), a technique that has been pioneered in plants (Poethig, 1987). Clonal analysis has shown that SL perception in axillary buds acts locally (Stirnberg et al., 2007). Introduction of a mutation in the *MAX2* gene encoding the F-BOX protein component of the SL-sensing machinery,

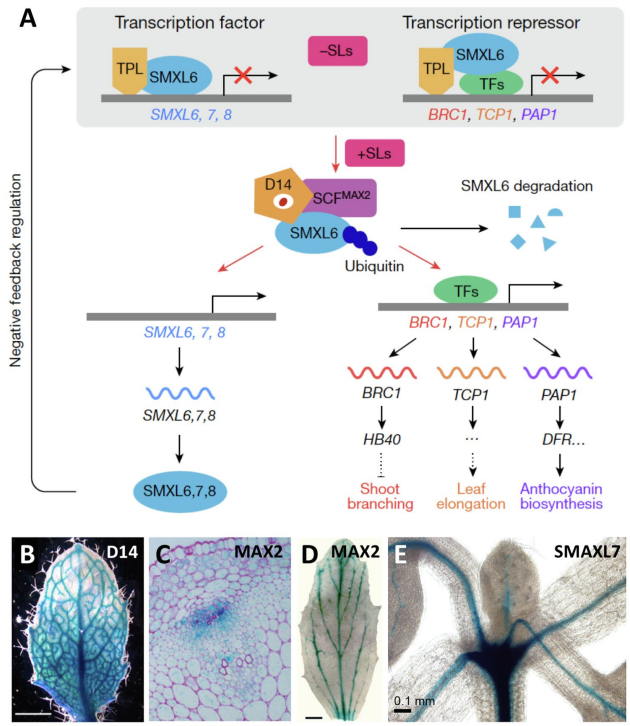

FIGURE 4 | Expression pattern of SL-sensing genes in Arabidopsis. **(A)** Schematic representation of the elements involved in SL perception and signal transduction, including the SL receptor D14, the ubiquitin conjugating enzyme complex SCF^{MAX2} containing the F-box protein MAX2, and the redundantly acting transcriptional repressors SMAXL6, SMAXL7, and SMAXL8, which regulate the expression of target genes such as *BRC1*. **(B–E)** Expression pattern of the SL perception and signaling genes *D14* **(B)**, *MAX2* **(C,D)**, and *D53/SMAXL7* **(E)**, as indicated, revealed by promoter::GUS analysis. Note highest expression in vascular strands as revealed in whole-mount preparations **(B,D,E)**, and in a transverse section of the stem [**C**; modified with permission from Wang et al., 2020 **(A)**; Chevalier et al., 2014 **(B)**; Stirnberg et al., 2007 **(C)**; Shen et al., 2007 **(D)**; and Soundappan et al., 2015 **(E)**].

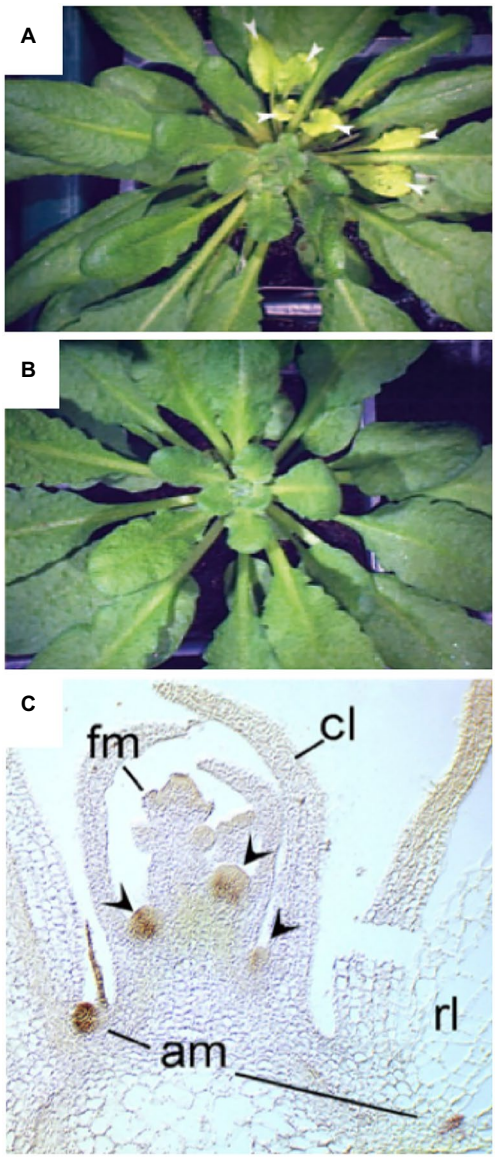

FIGURE 5 | Local action of SL through *MAX2* and *BRC1* in leaf axillary meristems. **(A,B)** Clonal analysis with *max2* mutant sectors reveals local function of *MAX2* in axillary buds. A sector marked by chlorophyll deficiency (yellowish leaves) comprised a single axillary bud that grew out to produce numerous leaves (arrowheads), that are identified as a *max2* mutant sector by the cosegregating genetic defect in chlorophyll biosynthesis **(A)**. A wild-type control plant of the same age does not show bud outgrowth, nor yellowish leaves **(B)**. **(C)** Expression analysis of *BRC1* by *in situ* hybridization reveals expression in axillary meristems (am), but not in floral meristems (fm) at the shoot apex, cl, cauline leaf; rl, rosette leaf. Modified with permission from Stirnberg et al., 2007 **(A,B)**, and Aguilar-Martinez et al., 2007 **(C)**.

comprising a sector with a single axillary bud, is sufficient to release its meristem from AD (**Figures 5A,B**). The fact that the surrounding wild-type tissues were not able to functionally complement the *max2* defect in the axillary bud (Stirnberg et al., 2007) shows that SL perception acts locally to inhibit bud outgrowth. However, SL perception and sensing may not be entirely cell autonomous, since D14 was shown to be mobile over several cell diameters from the meristem base to the stem cells of axillary buds in rice (Kameoka et al., 2016), and was even graft-transmissible in pea (Beveridge et al., 1996). Furthermore, D14 protein was detected in phloem sap by proteomic analysis (Aki et al., 2008; Batailler et al., 2012), and by microscopic analysis of GFP-tagged D14 protein (Kameoka et al., 2016). Taken together, these results indicate that D14 protein is transported from cell to cell and by phloem transport (Chevalier et al., 2014; Kameoka et al., 2016; Barbier et al., 2019). This may allow D14 to function in the meristem proper of the axillary buds, in which the *D14* promoter is not expressed (Kameoka et al., 2016).

WHICH PATHWAYS ACT DOWNSTREAM OF SL TO PREVENT BUD OUTGROWTH?

While it is clear that auxin and SL impose dormancy on axillary buds, it is less clear how exactly growth and organogenesis is inhibited in the axillary meristems. Is the cell cycle attenuated?

Are the meristems metabolically starved? Or is there an additional inhibitory principle involved? The auxin canalization model, including SL as a major player, can explain many aspects of correlative inhibition between the shoot tip and axillary buds, but how does it interfere––locally––with growth of the buds? On the other hand, the direct signaling model posits that SL prevents axillary growth through the inhibitory transcription factor BRANCHED1 (BRC1) in Arabidopsis (Aguilar-Martinez et al., 2007). BRC1 is functionally conserved in monocots and dicots (Aguilar-Martinez et al., 2007; Brewer et al., 2009; Finlayson et al., 2010). Interestingly, gain-of-function alleles of the *BRC1* orthologue in maize, *Teosinte branched1* (*Tb1*), have been selected for during domestication of modern maize for low branching (Dong et al., 2019a).

BRC1 is expressed at high levels in dormant buds (**Figure 5C**), and *brc1* mutants exhibit excessive branching, consistent with a role of *BRC1* in AD (Aguilar-Martinez et al., 2007). SL can activate *BRC1* expression (Wang et al., 2019, 2020; Kerr et al., 2020, 2021), indicating that SL could act directly in the buds to inhibit bud outgrowth. Although BRC1 is probably not the only inhibitor of bud outgrowth (Seale et al., 2017), it is a conserved central player in Arabidopsis, pea, tomato, and maize (Martin-Trillo et al., 2011; Braun et al., 2012). Interestingly, TB1 homologues in cereals have functionally diversified to control ear architecture in crop-specific ways (Dong et al., 2019a). This is likely to reflect the particular development of reproductive structures in cereals (ears, tassels; Dong et al., 2019a), which represent highly branched generative shoot axes (Wang et al., 2021).

As a TCP-type transcription factor, BRC1 can be expected to act through activation (or repression) of downstream genes, which could provide a hint regarding the action mechanisms in AD. *BRC1* itself is under transcriptional control by SL through the action of the transcription factors SMAXL6, SMAXL7, and SMAXL8, which promote bud outgrowth through inhibition of *BRC1* expression (**Figure 4A**; Soundappan et al., 2015; Wang et al., 2020). BRC1 directly activates several homeobox proteins to mediate bud dormancy in Arabidopsis (Gonzalez-Grandio et al., 2017), and an orthologous transcriptional mechanism involving TB1 and GT1 controls branching in maize (Dong et al., 2019a). Hence, genetic evidence indicates that the molecular mechanism controlling bud dormancy may be conserved between monocots and dicots. How does the BRC1/TB1 nexus regulate branching? RNAseq and CHIPseq analysis in Arabidopsis showed that BRC1, in concert with several homeobox proteins, activates abscisic acid (ABA) biosynthesis by NCED3 in axillary buds (Gonzalez-Grandio et al., 2017). Similarly, TB1 acts through ABA to inhibit axillary buds in maize (Dong et al., 2019b). This includes activation of ABA biosynthetic genes in axillary buds during dormancy (Luo et al., 2019).

Interestingly, bud dormancy during the resting period (e.g., winter) in perennial plants such as poplar also involves ABA (Pan et al., 2021). The finding that BRC1 acts through ABA in axillary buds may explain the overlap between *max2* phenotypes and ABA signaling in drought resistance (Bu et al., 2014) and in the resistance against bacterial pathogens (Piisilä et al., 2015). On the other hand, it is consistent with reports that have shown a role for ABA in the inhibition of axillary branching in Arabidopsis and maize (Cline and Oh, 2006; Yao and Finlayson, 2015; Cao et al., 2020). One might ask why then no ABA-related mutants were identified in screens for increased branching? ABA has numerous roles in plant development from seed dormancy to regulation of leaf transpiration and stress responses; therefore, ABA-deficient and ABA-insensitive mutants have rather pleiotropic phenotypes (Nambara and Marion-Poll, 2005; Cutler et al., 2010), which could potentially mask quantitative branching phenotypes. Nevertheless, ABA biosynthetic mutants such as *nced3* and *aba2* showed branching phenotypes in the context of phytochrome-dependent regulation of shoot branching (Reddy et al., 2013), a phenomenon that involves the canonical BRC1-dependent pathway (Gonzalez-Grandio et al., 2013).

HOW ARE BUDS TRIGGERED TO GROW OUT WHEN THEY ARE RELEASED FROM DORMANCY?

Given the fact that bud dormancy is mediated by auxin and SL, it could be assumed that the activation of bud outgrowth (in response to environmental cues or after decapitation) may require simply the release from this inhibitory mechanism. Indeed, the highly branched mutant phenotypes of auxin-insensitive (Stirnberg et al., 1999) and SL-deficient (Beveridge et al., 2003; Domagalska and Leyser, 2011; Rameau et al., 2015) mutants show that the inactivation of auxin- and SL-mediated AD is sufficient to promote bud outgrowth. However, does this also apply to the rapid events triggered by decapitation? Several lines of evidence suggest that activation of dormant buds involves additional mechanisms independent of auxin and SL.

Cytokinin has long been known to promote growth of axillary branches in various plant species (Sachs and Thimann, 1967; Chatfield et al., 2000; Tanaka et al., 2006; Ferguson and Beveridge, 2009; Dun et al., 2012; Chen et al., 2013; Young et al., 2014), suggesting that it may contribute to bud activation following decapitation (Shimizu-Sato et al., 2009), or in response to favorable light conditions (Roman et al., 2016). Cytokinin biosynthesis is inhibited by auxin (Tanaka et al., 2006), while SL induces a CK-degrading oxidase (Duan et al., 2019), conversely, decapitation leads to the induction of CK biosynthetic genes and increased CK levels in the vicinity of the buds (Tanaka et al., 2006), consistent with a role of CK in bud activation (Shimizu-Sato et al., 2009; Müller et al., 2015).

However, CK may not be the first, and not the only element in bud activation. In pea, one of the first signs of bud activation can be observed after just a few hours from decapitation, long before changes in auxin transport and canalization can

be expected to result in the release of buds, and before CK can have accumulated to induce bud outgrowth (Mason et al., 2014). This argues for the involvement of a rapid activating principle in bud activation. This signal has been assigned to sucrose and trehalose-6-phosphate (T6P), whose levels increase rapidly after decapitation (Fichtner et al., 2017, 2021; Barbier et al., 2019). In agreement with such a scenario, elegant recent work with cell-specific genetic manipulation of phloem transport (Paterlini et al., 2021) and sugar supply (Fichtner et al., 2021) indicated that sugars may indeed contribute to axillary bud activation in Arabidopsis. Since *BRC1* expression is repressed by sugars (Mason et al., 2014; Barbier et al., 2015; Otori et al., 2019; Patil et al., 2022), a plausible model is that sugars contribute to bud outgrowth by attenuating BRC1-dependent dormancy (Wang et al., 2019). The role of sugars in bud activation is likely to represent a signaling function, since non-metabolizable sugars can mimic the effects of sucrose and T6P (Rabot et al., 2012; Barbier et al., 2015, 2021).

A connection between sugar activation and SL signaling has been revealed in rice, where sucrose interferes with SL signaling by repressing a component in SL perception (D3) and destabilizing the SL receptor D14, whereas their target D53, a promoter of bud outgrowth, is stabilized by sucrose, ultimately resulting in reduced expression of BRC1/TB1 (Patil et al., 2022). Similar effects were found in pea (Bertheloot et al., 2020; Patil et al., 2022), suggesting that the antagonistic action of sugars against SL signaling may be conserved in angiosperms. Ultimately, the release from BRC1/TB1, together with the induction of cytokinin levels (Müller and Leyser, 2011), results in the activation of the cell cycle and of basic cell metabolism (incl. protein synthesis and primary metabolism; Devitt and Stafstrom, 1995; Gonzalez-Grandio et al., 2013; Luo et al., 2019; Dong et al., 2019b), which are required to promote outgrowth and organogenesis in the axillary meristems (Müller and Leyser, 2011).

Is there a conflict between the models of bud inhibition (auxin canalization vs. direct SL-dependent inhibition), or between the mechanisms assumed to mediate bud activation (onset of local auxin canalization in the bud vs. sugar activation)? These alternative mechanisms are not necessarily mutually exclusive. The collective evidence shows that SL can promote AD both, locally in the buds (through BRC1), and systemically, by modulating auxin canalization (**Figure 6**). Similarly, bud activation could independently involve both sugar activation and the onset of auxin canalization and cytokinin accumulation in the bud (**Figure 6**). The relative importance, and the dynamics, of these processes may differ between plant species, to the extent that one or the other could become the dominating mechanism. It is plausible that in the rapidly responsive buds of decapitated pea, the first events are changes in sugar levels, while in Arabidopsis, this effect is less obvious. It is also possible that the sequence of events triggered by decapitation differs from the mechanisms involved in the slower bud activation conditions associated with developmental or nutritional changes (e.g., flowering or high P status).

COMPETITION AMONG BUDS KICKS IN *VIA* AUXIN- AND SL-MEDIATED CORRELATIVE INHIBITION

Once a shoot is decapitated, numerous axillary meristems could potentially grow out. Even if not all of them are activated at the same time and with the same dynamics (depending, e.g., on their distance from the shoot tip), still several axillary buds may simultaneously be activated to grow. Hence, decapitation could potentially lead to bushy shoot phenotypes as in mutants with decreased AD (*max*, *dad*, *rms,* and *dwarf*). However, this is normally not the case, because the remaining buds are in mutual competition (Crawford et al., 2010; Shinohara et al., 2013; Balla et al., 2016; Paterlini et al., 2021), and often, one bud rapidly outcompetes all the others. Therefore, soon after decapitation, AD is reestablished resulting in a single new main shoot. It is plausible that this phenomenon is due to the rapid re-activation of correlative inhibition among the buds as a result of dominating auxin canalization in the new main shoot (Crawford et al., 2010; Shinohara et al., 2013; Balla et al., 2016; Paterlini et al., 2021). Hence, the SL-modulated auxin-based competition mechanism in AD is not only required to maintain axillary meristems in a silent state during normal development but also to quickly re-establish branching hierarchy after a disturbance (Domagalska and Leyser, 2011).

ACTIVATION OF THE CELL CYCLE AND ESTABLISHMENT OF A SYMPLASTIC CONDUIT FOR RESOURCE SUPPLY: A PARADIGM FOR THE EVOLUTIONARY ORIGIN OF BUD ACTIVATION MECHANISMS?

Bud dormancy is a common phenomenon in perennial plants that have to cope with periods of harsh environmental conditions (e.g., cold winters; Rohde and Bhalerao, 2007). Dormancy and bud induction have been studied particularly well in birch, hybrid aspen, and various fruit trees (Arora et al., 2003). The notion that, in annual plants, the activation of axillary buds upon decapitation involves inductive signals in addition to the release from AD, is paralleled by studies on bud activation in perennials (Rohde and Bhalerao, 2007). After a dormant phase during winter, such plants activate their meristems (including the most apical dormant buds) in spring (Arora et al., 2003). Although not directly comparable, the hypothesis that bud activation in annual plants, and the induction of the winter buds in perennials, may share common elements of regulation, has received substantial support (Rohde and Bhalerao, 2007).

The meristems of perennials in an inactive state during the winter period are comparable to silent axillary buds of annuals with strong AD. In both cases, the cell cycle is nearly arrested, and symplastic connectivity appears to be reduced, involving the accumulation of callose in the phloem and in plasmodesmata (Tylewicz et al., 2018). Notably,

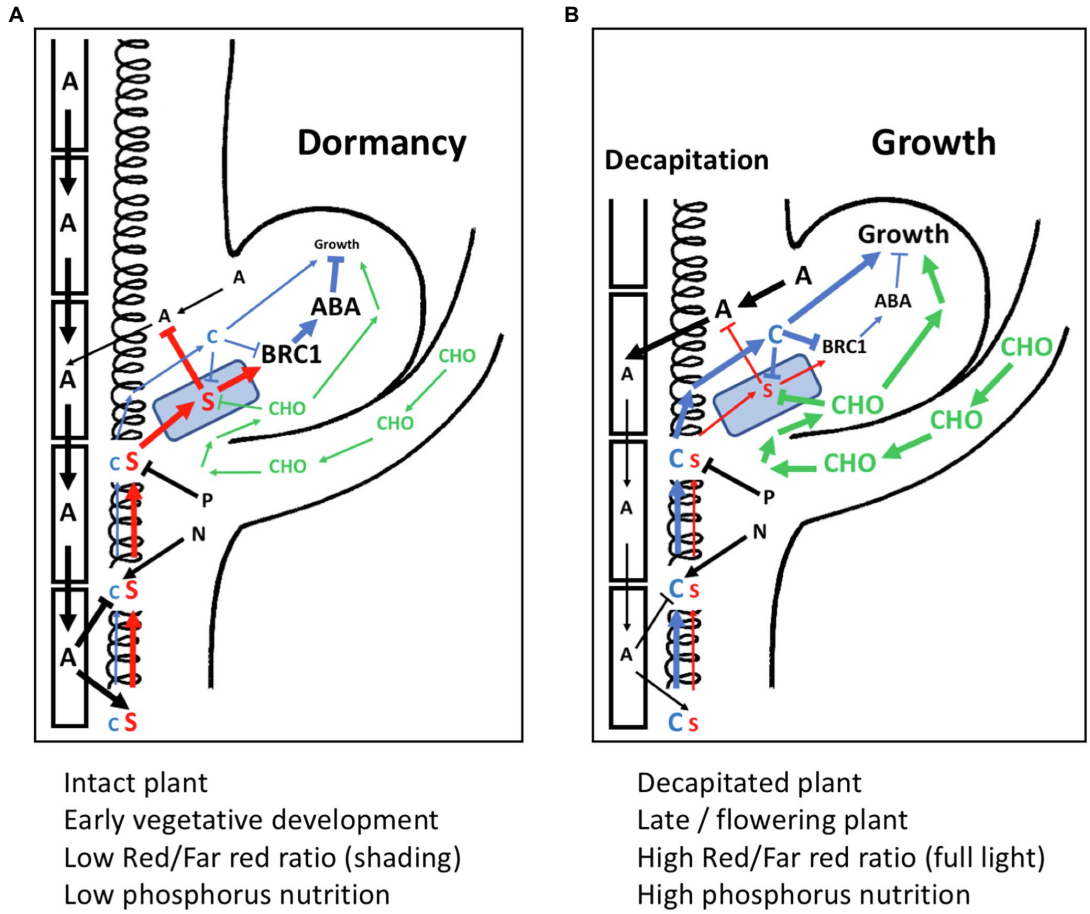

FIGURE 6 | Model for the interactions of SL with other components in apical dominance. **(A)** An axillary bud under the influence of apical dominance with active polar auxin transport stream in the stem, which inhibits cytokinin (C) biosynthesis, and stimulates strigolactone (S) production. Strigolactone enters the buds *via* PDR1 transport (represented by a blue PDR1-expressing square). Strigolactone inhibits auxin canalization from the bud, and stimulates *BRC1* gene expression. BRC1 activates the ABA dormancy program, resulting in growth arrest. The stimulatory effect of nitrogen (N) on cytokinin biosynthesis and the inhibition of strigolactone biosynthetic genes by phosphorus (P) are indicated, although they are at a steady-state intermediate level and do not influence bud activity. Relative signaling strength is represented by font size and thickness of the arrows. **(B)** Situation as in **(A)** depicting changes upon decapitation of the main shoot apex. Sugars (CHO) rapidly enter the bud, where they interfere with strigolactone sensing, and rapidly stimulate growth. Polar auxin transport in the stem is weak, reducing strigolactone biosynthesis and releasing the inhibition of cytokinin biosynthesis in the stem. Lower strigolactone levels allow canalization of auxin from the bud, while increased cytokinin levels further stimulate bud outgrowth by reducing BRC expression. Relative signaling strength is represented by font size and thickness of the arrows.

similar regulatory circuits are involved in bud dormancy of annuals and perennials, including ABA and BRC1 (Liu and Sherif, 2019; Maurya et al., 2020; Azeez et al., 2021; Pan et al., 2021). In addition, bud dormancy and sprouting of potato tubers appears to involve mechanisms related to AD in annuals (Sonnewald and Sonnewald, 2014). Hence, the regulation of bud dormancy and bud activation in annuals and perennials may involve a shared mechanism with a common evolutionary origin.

Interestingly, ABA is also a central element in seed dormancy (Finkelstein et al., 2008), indicating that seed dormancy and bud dormancy could be regulated by similar hormonal pathways (Ruttink et al., 2007; Wang et al., 2016a). This analogy extends to the notion that, as in seed dormancy (Skubacz and Daszkowska-Golec, 2017; Tuan et al., 2018), bud outgrowth in perennials involves antagonistic interactions of ABA and gibberellic acid (GA; Pan et al., 2021). However, the role of GA is complex and context-dependent (Katyayini et al., 2020; Pan et al., 2021). Indeed, GA can promote (Rinne et al., 2011, 2016; Ni et al., 2015; Katyayini et al., 2020) or inhibit (Scott et al., 1967; Zheng et al., 2018; Katyayini et al., 2020) bud outgrowth, depending on the plant species, and on the developmental and environmental conditions, but in most cases, GA contributes to bud activation (Liu and Sherif, 2019; Pan et al., 2021).

CONCLUSION

SL is produced in most parts of the plant, presumably along the vasculature, and it is mobile in an acropetal fashion by

a mechanism that may involve the transpiration stream. The function of SL in AD acts at different levels of the plant. Attenuation of auxin transport capacity mediates bud dormancy by interfering with auxin canalization from the buds. In addition, SL can directly exert bud dormancy by inducing *BRC1*/*TB1*, and through the induction of ABA signaling. Bud release involves both inductive signals such as sucrose, T6P, and cytokinin, as well as the release from the inhibitory BRC1/TB1 and ABA. Ultimately, this results in the activation of the cell cycle and metabolism in the buds. Common patterns in the regulation of dormancy in axillary buds of annual plants, and in bud dormancy in perennials, suggest that the phenomena may be related.

AUTHOR CONTRIBUTIONS

DR, KK, and FS discussed and wrote the manuscript. All authors contributed to the article and approved the submitted version.

FUNDING

The work has been funded by two grants from the Swiss National Science Foundation to DR (IZCSZ0 174608, 310030_200367), the COST action FA1206 (STREAM), and the "National Overseas Scholarship" to KK from the Indian Government.

REFERENCES

Aarssen, L. W. (1995). Hypotheses for the evolution of apical dominance in plants—implications for the interpretation of overcompensation. *Oikos* 74, 149–156. doi: 10.2307/3545684

Abuauf, H., Haider, I., Jia, K. P., Ablazov, A., Mi, J. N., Blilou, I., et al. (2018). The Arabidopsis *DWARF27* gene encodes an all-trans-/9-cis-beta-carotene isomerase and is induced by auxin, abscisic acid and phosphate deficiency. *Plant Sci.* 277, 33–42. doi: 10.1016/j.plantsci.2018.06.024

Aguilar-Martinez, J. A., Poza-Carrion, C., and Cubas, P. (2007). Arabidopsis *BRANCHED1* acts as an integrator of branching signals within axillary buds. *Plant Cell* 19, 458–472. doi: 10.1105/tpc.106.048934

Aki, T., Shigyo, M., Nakano, R., Yoneyama, T., and Yanagisawa, S. (2008). Nano scale proteomics revealed the presence of regulatory proteins including three FT-like proteins in phloem and xylem saps from rice. *Plant Cell Physiol.* 49, 767–790. doi: 10.1093/pcp/pcn049

Al-Babili, S., and Bouwmeester, H. J. (2015). Strigolactones, a novel carotenoid-derived plant hormone. *Annu. Rev. Plant Biol.* 66, 161–186. doi: 10.1146/annurev-arplant-043014-114759

Alder, A., Jamil, M., Marzorati, M., Bruno, M., Vermathen, M., Bigler, P., et al. (2012). The path from beta-carotene to carlactone, a strigolactone-like plant hormone. *Science* 335, 1348–1351. doi: 10.1126/science.1218094

Al-Dosary, N. M. N., Al-Dobai, S., and Faleiro, J. R. (2016). Review on the management of red palm weevil *Rhynchophorus ferrugineus* olivier in date palm *Phoenix dactylifera* L. *Emir. J. Food Agric.* 28, 34–44. doi: 10.9755/ejfa.2015-10-897

Arora, R., Rowland, L. J., and Tanino, K. (2003). Induction and release of bud dormancy in woody perennials: a science comes of age. *Hortscience* 38, 911–921. doi: 10.21273/HORTSCI.38.5.911

Azeez, A., Zhao, Y. C., Singh, R. K., Yordanov, Y. S., Dash, M., Miskolczi, P., et al. (2021). EARLY BUD-BREAK 1 and EARLY BUD-BREAK 3 control resumption of poplar growth after winter dormancy. *Nat. Commun.* 12:1123. doi: 10.1038/s41467-021-21449-0

Balla, J., Medveďova, Z., Kalousek, P., Matijescukova, N., Friml, J., Reinohl, V., et al. (2016). Auxin flow-mediated competition between axillary buds to restore apical dominance. *Sci. Rep.* 6:35955. doi: 10.1038/srep35955

Barbier, F. F., Cao, D., Fichtner, F., Weiste, C., Perez-Garcia, M. D., Caradeuc, M., et al. (2021). HEXOKINASE1 signalling promotes shoot branching and interacts with cytokinin and strigolactone pathways. *New Phytol.* 231, 1088–1104. doi: 10.1111/nph.17427

Barbier, F. F., Dun, E. A., Kerr, S. C., Chabikwa, T. G., and Beveridge, C. A. (2019). An update on the signals controlling shoot branching. *Trends Plant Sci.* 24, 220–236. doi: 10.1016/j.tplants.2018.12.001

Barbier, F., Peron, T., Lecerf, M., Perez-Garcia, M. D., Barriere, Q., Rolcik, J., et al. (2015). Sucrose is an early modulator of the key hormonal mechanisms controlling bud outgrowth in *Rosa hybrida*. *J. Exp. Bot.* 66, 2569–2582. doi: 10.1093/jxb/erv047

Batailler, B., Lemaitre, T., Vilaine, F., Sanchez, C., Renard, D., Cayla, T., et al. (2012). Soluble and filamentous proteins in Arabidopsis sieve elements. *Plant Cell Environ.* 35, 1258–1273. doi: 10.1111/j.1365-3040.2012.02487.x

Bertheloot, J., Barbier, F., Boudon, F., Perez-Garcia, M. D., Peron, T., Citerne, S., et al. (2020). Sugar availability suppresses the auxin-induced strigolactone pathway to promote bud outgrowth. *New Phytol.* 225, 866–879. doi: 10.1111/nph.16201

Beveridge, C. A. (2000). Long-distance signalling and a mutational analysis of branching in pea. *Plant Growth Regul.* 32, 193–203. doi: 10.1023/A:1010718020095

Beveridge, C. A., Ross, J. J., and Murfet, I. C. (1994). Branching mutant *rms-2* in *Pisum sativum*—grafting studies and endogenous indole-3-acetic-acid levels. *Plant Physiol.* 104, 953–959. doi: 10.1104/pp.104.3.953

Beveridge, C. A., Ross, J. J., and Murfet, I. C. (1996). Branching in pea—action of genes *rms3* and *rms4*. *Plant Physiol.* 110, 859–865. doi: 10.1104/pp.110.3.859

Beveridge, C. A., Symons, G. M., Murfet, I. C., Ross, J. J., and Rameau, C. (1997). The *rms1* mutant of pea has elevated indole-3-acetic acid levels and reduced root-sap zeatin riboside content but increased branching controlled by graft-transmissible signal(s). *Plant Physiol.* 115, 1251–1258. doi: 10.1104/pp.115.3.1251

Beveridge, C. A., Weller, J. L., Singer, S. R., and Hofer, J. M. I. (2003). Axillary meristem development. Budding relationships between networks controlling flowering, branching, and photoperiod responsiveness. *Plant Physiol.* 131, 927–934. doi: 10.1104/pp.102.017525

Booker, J., Sieberer, T., Wright, W., Williamson, L., Willett, B., Stirnberg, P., et al. (2005). *MAX1* encodes a cytochrome P450 family member that acts downstream of *MAX3/4* to produce a carotenoid-derived branch-inhibiting hormone. *Dev. Cell* 8, 443–449. doi: 10.1016/j.devcel.2005.01.009

Borghi, L., Liu, G. W., Emonet, A., Kretzschmar, T., and Martinoia, E. (2016). The importance of strigolactone transport regulation for symbiotic signaling and shoot branching. *Planta* 243, 1351–1360. doi: 10.1007/s00425-016-2503-9

Braun, N., De Saint Germain, A., Pillot, J. P., Boutet-Mercey, S., Dalmais, M., Antoniadi, I., et al. (2012). The pea TCP transcription factor PsBRC1 acts downstream of strigolactones to control shoot branching. *Plant Physiol.* 158, 225–238. doi: 10.1104/pp.111.182725

Brewer, P. B., Dun, E. A., Ferguson, B. J., Rameau, C., and Beveridge, C. A. (2009). Strigolactone acts downstream of auxin to regulate bud outgrowth in pea and Arabidopsis. *Plant Physiol.* 150, 482–493. doi: 10.1104/pp.108.134783

Brewer, P. B., Yoneyama, K., Filardo, F., Meyers, E., Scaffidi, A., Frickey, T., et al. (2016). *LATERAL BRANCHING OXIDOREDUCTASE* acts in the final stages of strigolactone biosynthesis in Arabidopsis. *Proc. Natl. Acad. Sci. U. S. A.* 113, 6301–6306. doi: 10.1073/pnas.1601729113

Bu, Q. Y., Lv, T. X., Shen, H., Luong, P., Wang, J., Wang, Z. Y., et al. (2014). Regulation of drought tolerance by the F-Box protein MAX2 in Arabidopsis. *Plant Physiol.* 164, 424–439. doi: 10.1104/pp.113.226837

Buckingham, M. E., and Meilhac, S. M. (2011). Tracing cells for tracking cell lineage and clonal behavior. *Dev. Cell* 21, 394–409. doi: 10.1016/j.devcel.2011.07.019

Cao, D., Barbier, F., Yoneyama, K., and Beveridge, C. A. (2020). A rapid method for quantifying RNA and phytohormones from a small amount of plant tissue. *Front. Plant Sci.* 11:605069. doi: 10.3389/fpls.2020.605069

Chalfie, M., Tu, Y., Euskirchen, G., Ward, W. W., and Prasher, D. C. (1994). Green fluorescent protein as a marker for gene expression. *Science* 263, 802–805. doi: 10.1126/science.8303295

Chatfield, S. P., Stirnberg, P., Forde, B. G., and Leyser, O. (2000). The hormonal regulation of axillary bud growth in Arabidopsis. *Plant J.* 24, 159–169. doi: 10.1046/j.1365-313x.2000.00862.x

Chen, X. L., Zhou, X. Y., Xi, L., Li, J. X., Zhao, R. Y., Ma, N., et al. (2013). Roles of *DgBRC1* in regulation of lateral branching in chrysanthemum (*Dendranthema grandiflora* cv. Jinba). *Plos One* 8:e61717. doi: 10.1371/journal.pone.0084522

Chevalier, F., Nieminen, K., Sanchez-Ferrero, J. C., Rodriguez, M. L., Chagoyen, M., Hardtke, C. S., et al. (2014). Strigolactone promotes degradation of DWARF14, an alpha/beta hydrolase essential for strigolactone signaling in Arabidopsis. *Plant Cell* 26, 1134–1150. doi: 10.1105/tpc.114.122903

Cline, M. G. (1991). Apical dominance. *Bot. Rev.* 57, 318–358. doi: 10.1007/BF02858771

Cline, M. G., and Oh, C. (2006). A reappraisal of the role of abscisic acid and its interaction with auxin in apical dominance. *Ann. Bot.* 98, 891–897. doi: 10.1093/aob/mcl173

Crawford, S., Shinohara, N., Sieberer, T., Williamson, L., George, G., Hepworth, J., et al. (2010). Strigolactones enhance competition between shoot branches by dampening auxin transport. *Development* 137, 2905–2913. doi: 10.1242/dev.051987

Cutler, S. R., Rodriguez, P. L., Finkelstein, R. R., and Abrams, S. R. (2010). "Abscisic acid: emergence of a core signaling network," in *Annual Review of Plant Biology*. eds. S. Merchant, W. R. Briggs and D. Ort, 651–679.

Czarnecki, O., Yang, J., Weston, D. J., Tuskan, G. A., and Chen, J. G. (2013). A dual role of strigolactones in phosphate acquisition and utilization in plants. *Int. J. Mol. Sci.* 14, 7681–7701. doi: 10.3390/ijms14047681

Danert, S. (1958). Die Verzweigung der Solanaceen im reproduktiven Bereich. *Abh. Deutsch. Akad. Wiss. Berlin, Math.-Naturwiss. Kl. 1957* 6, 1–184.

De Jong, M., George, G., Ongaro, V., Williamson, L., Willetts, B., Ljung, K., et al. (2014). Auxin and strigolactone signaling are required for modulation of Arabidopsis shoot branching by nitrogen supply. *Plant Physiol.* 166, 384–395. doi: 10.1104/pp.114.242388

Devitt, M. L., and Stafstrom, J. P. (1995). Cell-cycle regulation during growth-dormancy cycles in pea axillary buds. *Plant Mol. Biol.* 29, 255–265. doi: 10.1007/BF00043650

Domagalska, M. A., and Leyser, O. (2011). Signal integration in the control of shoot branching. *Nat. Rev. Mol. Cell Biol.* 12, 211–221. doi: 10.1038/nrm3088

Dong, Z. B., Alexander, M., and Chuck, G. (2019a). Understanding grass domestication through maize mutants. *Trends Genet.* 35, 118–128. doi: 10.1016/j.tig.2018.10.007

Dong, Z. B., Xiao, Y. G., Govindarajulu, R., Feil, R., Siddoway, M. L., Nielsen, T., et al. (2019b). The regulatory landscape of a core maize domestication module controlling bud dormancy and growth repression. *Nat. Commun.* 10:3810. doi: 10.1038/s41467-019-11774-w

Doust, A. N. (2007). Grass architecture: genetic and environmental control of branching. *Curr. Opin. Plant Biol.* 10, 21–25. doi: 10.1016/j.pbi.2006.11.015

Drummond, R. S. M., Martinez-Sanchez, N. M., Janssen, B. J., Templeton, K. R., Simons, J. L., Quinn, B. D., et al. (2009). *Petunia hybrida CAROTENOID CLEAVAGE DIOXYGENASE7* is involved in the production of negative and positive branching signals in petunia. *Plant Physiol.* 151, 1867–1877. doi: 10.1104/pp.109.146720

Drummond, R. S. M., Sheehan, H., Simons, J. L., Martines-Sanchez, N. M., Turner, R. M., Putterill, J., et al. (2012). The expression of petunia strigolactone pathway genes is altered as part of the endogenous developmental program. *Front. Plant Sci.* 2:115. doi: 10.3389/fpls.2011.00115

Duan, J. B., Yu, H., Yuan, K., Liao, Z. G., Meng, X. B., Jing, Y. H., et al. (2019). Strigolactone promotes cytokinin degradation through transcriptional activation of *CYTOKININ OXIDASE/DEHYDROGENASE9* in rice. *Proc. Natl. Acad. Sci. U. S. A.* 116, 14319–14324. doi: 10.1073/pnas.1810980116

Dun, E. A., De Saint Germain, A., Rameau, C., and Beveridge, C. A. (2012). Antagonistic action of strigolactone and cytokinin in bud outgrowth control. *Plant Physiol.* 158, 487–498. doi: 10.1104/pp.111.186783

Dun, E. A., Hanan, J., and Beveridge, C. A. (2009). Computational modeling and molecular physiology experiments reveal new insights into shoot branching in pea. *Plant Cell* 21, 3459–3472. doi: 10.1105/tpc.109.069013

El-Sabea, A. M. R., Faleiro, J. R., and Abo-El-Saad, M. M. (2009). The threat of red palm weevil *Rhynchophorus ferrugineus* to date plantations of the gulf region in the middle-east: an economic perspective. *Outlooks Pest Manag.* 20, 131–134. doi: 10.1564/20jun11

Ferguson, B. J., and Beveridge, C. A. (2009). Roles for auxin, cytokinin, and strigolactone in regulating shoot branching. *Plant Physiol.* 149, 1929–1944. doi: 10.1104/pp.109.135475

Fichtner, F., Barbier, F. F., Annunziata, M. G., Feil, R., Olas, J. J., Mueller-Roeber, B., et al. (2021). Regulation of shoot branching in Arabidopsis by trehalose 6-phosphate. *New Phytol.* 229, 2135–2151. doi: 10.1111/nph.17006

Fichtner, F., Barbier, F. F., Feil, R., Watanabe, M., Annunziata, M. G., Chabikwa, T. G., et al. (2017). Trehalose 6-phosphate is involved in triggering axillary bud outgrowth in garden pea (*Pisum sativum* L.). *Plant J.* 92, 611–623. doi: 10.1111/tpj.13705

Finkelstein, R., Reeves, W., Ariizumi, T., and Steber, C. (2008). Molecular aspects of seed dormancy. *Annu. Rev. Plant Biol.* 59, 387–415. doi: 10.1146/annurev.arplant.59.032607.092740

Finlayson, S. A., Krishnareddy, S. R., Kebrom, T. H., and Casal, J. J. (2010). Phytochrome regulation of branching in Arabidopsis. *Plant Physiol.* 152, 1914–1927. doi: 10.1104/pp.109.148833

Foo, E., Turnbull, C. G. N., and Beveridge, C. A. (2001). Long-distance signaling and the control of branching in the *rms1* mutant of pea. *Plant Physiol.* 126, 203–209. doi: 10.1104/pp.126.1.203

Gao, L. L., Knogge, W., Delp, G., Smith, F. A., and Smith, S. E. (2004). Expression patterns of defense-related genes in different types of arbuscular mycorrhizal development in wild-type and mycorrhiza-defective mutant tomato. *Mol. Plant Microbe Interact.* 17, 1103–1113. doi: 10.1094/MPMI.2004.17.10.1103

Gomez-Roldan, V., Fermas, S., Brewer, P. B., Puech-Pagès, V., Dun, E. A., Pillot, J. P., et al. (2008). Strigolactone inhibition of shoot branching. *Nature* 455, 189–194. doi: 10.1038/nature07271

Gonzalez-Grandio, E., Pajoro, A., Franco-Zorrilla, J. M., Tarancon, C., Immink, R. G. H., and Cubas, P. (2017). Abscisic acid signaling is controlled by a BRANCHED1/HD-ZIP I cascade in Arabidopsis axillary buds. *Proc. Natl. Acad. Sci. U. S. A.* 114, E245–E254. doi: 10.1073/pnas.1613199114

Gonzalez-Grandio, E., Poza-Carrion, C., Sorzano, C. O. S., and Cubas, P. (2013). BRANCHED1 promotes axillary bud dormancy in response to shade in Arabidopsis. *Plant Cell* 25, 834–850. doi: 10.1105/tpc.112.108480

Hempel, F. D., and Feldman, L. J. (1994). Bidirectional inflorescence development in *Arabidopsis thaliana*—Acropetal initiation of flowers and basipetal initiation of paraclades. *Planta* 192, 276–286. doi: 10.1007/BF01089045

Hepworth, J. A. (2012). Comparative analysis of the MAX pathway. PhD thesis. University of York.

Hou, M. M., Wu, D. X., Li, Y., Tao, W. Q., Chao, L., and Zhang, Y. L. (2021). The role of auxin in nitrogen-modulated shoot branching. *Plant Signal. Behav.* 16:e1885888. doi: 10.1080/15592324.2021.1885888

Jefferson, R. A., Kavanagh, T. A., and Bevan, M. W. (1987). GUS fusions: ß-glucuronidase as a sensitive and versatile gene fusion marker in higher plants. *EMBO J.* 6, 3901–3907. doi: 10.1002/j.1460-2075.1987.tb02730.x

Kameoka, H., Dun, E. A., Lopez-Obando, M., Brewer, P. B., De Saint Germain, A., Rameau, C., et al. (2016). Phloem transport of the receptor DWARF14 protein is required for full function of strigolactones. *Plant Physiol.* 172, 1844–1852. doi: 10.1104/pp.16.01212

Katyayini, N. U., Rinne, P. L. H., Tarkowska, D., Strnad, M., and Van Der Schoot, C. (2020). Dual role of gibberellin in perennial shoot branching: inhibition and activation. *Front. Plant Sci.* 11:736 doi: 10.3389/fpls.2020.00736

Kerr, S. C., De Saint Germain, A., Dissanayanke, I. M., Mason, M. G., Dun, E. A., Beveridge, C. A., et al. (2020). Hormonal regulation of the BRC1-dependent strigolactone transcriptome involved in shoot branching responses. bioRxiv [Preprint].

Kerr, S. C., Patil, S. B., Germain, A. D., Pillot, J. P., Saffar, J., Ligerot, Y., et al. (2021). Integration of the SMXL/D53 strigolactone signalling repressors in the model of shoot branching regulation in *Pisum sativum*. *Plant J.* 107, 1756–1770. doi: 10.1111/tpj.15415

Kohlen, W., Charnikhova, T., Liu, Q., Bours, R., Domagalska, M. A., Beguerie, S., et al. (2011). Strigolactones are transported through the xylem and play a key role in shoot architectural response to phosphate deficiency in non-arbuscular mycorrhizal host arabidopsis. *Plant Physiol.* 155, 974–987. doi: 10.1104/pp.110.164640

Körner, C. (2003). *Alpine Plant Life*. Berlin, Heidelberg: Springer.

Körner, C., and Renhardt, U. (1987). Dry-matter partitioning and root length leaf-area ratios in herbaceous perennial plants with diverse altitudinal distribution. *Oecologia* 74, 411–418. doi: 10.1007/BF00378938

Kretzschmar, T., Kohlen, W., Sasse, J., Borghi, L., Schlegel, M., Bachelier, J. B., et al. (2012). A petunia ABC protein controls strigolactone-dependent symbiotic signalling and branching. *Nature* 483, 341–346. doi: 10.1038/nature10873

Lennartsson, T., Ramula, S., and Tuomi, J. (2018). Growing competitive or tolerant? Significance of apical dominance in the overcompensating herb *Gentianella campestris*. *Ecology* 99, 259–269. doi: 10.1002/ecy.2101

Leyser, O. (2005). The fall and rise of apical dominance. *Curr. Opin. Genet. Dev.* 15, 468–471. doi: 10.1016/j.gde.2005.06.010

Liang, Y. S., Jeon, Y. A., Lim, S. H., Kim, J. K., Lee, J. Y., Kim, Y. M., et al. (2011). Vascular-specific activity of the Arabidopsis carotenoid cleavage dioxygenase 7 gene promoter. *Plant Cell Rep.* 30, 973–980. doi: 10.1007/s00299-010-0999-1

Lin, H., Wang, R. X., Qian, Q., Yan, M. X., Meng, X. B., Fu, Z. M., et al. (2009). DWARF27, an iron-containing protein required for the biosynthesis of strigolactones, regulates rice tiller bud outgrowth. *Plant Cell* 21, 1512–1525. doi: 10.1105/tpc.109.065987

Liu, J. Y., and Sherif, S. M. (2019). Hormonal orchestration of bud dormancy cycle in deciduous woody perennials. *Front. Plant Sci.* 10:1136. doi: 10.3389/fpls.2019.01136

Luo, L., Takahashi, M., Kameoka, H., Qin, R. Y., Shiga, T., Kanno, Y., et al. (2019). Developmental analysis of the early steps in strigolactone-mediated axillary bud dormancy in rice. *Plant J.* 97, 1006–1021. doi: 10.1111/tpj.14266

Marro, N., Lidoy, J., Chico, M. A., Rial, C., Garcia, J., Varela, R. M., et al. (2022). Strigolactones: new players in the nitrogen-phosphorus signalling interplay. *Plant Cell Environ.* 45, 512–527. doi: 10.1111/pce.14212

Martin-Trillo, M., Grandio, E. G., Serra, F., Marcel, F., Rodriguez-Buey, M. L., Schmitz, G., et al. (2011). Role of tomato *BRANCHED1*-like genes in the control of shoot branching. *Plant J.* 67, 701–714. doi: 10.1111/j.1365-313X.2011.04629.x

Mashiguchi, K., Seto, Y., and Yamaguchi, S. (2021). Strigolactone biosynthesis, transport and perception. *Plant J.* 105, 335–350. doi: 10.1111/tpj.15059

Mason, M. G., Ross, J. J., Babst, B. A., Wienclaw, B. N., and Beveridge, C. A. (2014). Sugar demand, not auxin, is the initial regulator of apical dominance. *Proc. Natl. Acad. Sci. U. S. A.* 111, 6092–6097. doi: 10.1073/pnas.1322045111

Maurya, J. P., Miskolczi, P. C., Mishra, S., Singh, R. K., and Bhalerao, R. P. (2020). A genetic framework for regulation and seasonal adaptation of shoot architecture in hybrid aspen. *Proc. Natl. Acad. Sci. U. S. A.* 117, 11523–11530. doi: 10.1073/pnas.2004705117

McGarry, R. C., Prewitt, S. F., Culpepper, S., Eshed, Y., Lifschitz, E., and Ayre, B. G. (2016). Monopodial and sympodial branching architecture in cotton is differentially regulated by the *Gossypium hirsutum SINGLE FLOWER TRUSS* and *SELF-PRUNING* orthologs. *New Phytol.* 212, 244–258. doi: 10.1111/nph.14037

McSteen, P., and Leyser, O. (2005). Shoot branching. *Annu. Rev. Plant Biol.* 56, 353–374. doi: 10.1146/annurev.arplant.56.032604.144122

Morris, S. E., Turnbull, C. G. N., Murfet, I. C., and Beveridge, C. A. (2001). Mutational analysis of branching in pea. Evidence that *Rms1* and *Rms5* regulate the same novel signal. *Plant Physiol.* 126, 1205–1213. doi: 10.1104/pp.126.3.1205

Müller, D., and Leyser, O. (2011). Auxin, cytokinin and the control of shoot branching. *Ann. Bot.* 107, 1203–1212. doi: 10.1093/aob/mcr069

Müller, D., Waldie, T., Miyawaki, K., To, J. P. C., Melnyk, C. W., Kieber, J. J., et al. (2015). Cytokinin is required for escape but not release from auxin mediated apical dominance. *Plant J.* 82, 874–886. doi: 10.1111/tpj.12862

Nambara, E., and Marion-Poll, A. (2005). Abscisic acid biosynthesis and catabolism. *Annu. Rev. Plant Biol.* 56, 165–185. doi: 10.1146/annurev.arplant.56.032604.144046

Napoli, C. (1996). Highly branched phenotype of the petunia *dad1-1* mutant is reversed by grafting. *Plant Physiol.* 111, 27–37. doi: 10.1104/pp.111.1.27

Navarrete, M., and Jeannequin, B. (2000). Effect of frequency of axillary bud pruning on vegetative growth and fruit yield in greenhouse tomato crops. *Sci. Hortic.* 86, 197–210. doi: 10.1016/S0304-4238(00)00147-3

Ni, J., Gao, C. C., Chen, M. S., Pan, B. Z., Ye, K. Q., and Xu, Z. F. (2015). Gibberellin promotes shoot branching in the perennial woody plant *Jatropha curcas*. *Plant Cell Physiol.* 56, 1655–1666. doi: 10.1093/pcp/pcv089

Otori, K., Tanabe, N., Tamoi, M., and Shigeoka, S. (2019). Sugar Transporter Protein 1 (STP1) contributes to regulation of the genes involved in shoot branching via carbon partitioning in Arabidopsis. *Biosci. Biotech. Bioch.* 83, 472–481. doi: 10.1080/09168451.2018.1550355

Pan, W. Q., Liang, J. H., Sui, J. J., Li, J. R., Liu, C., Xin, Y., et al. (2021). ABA and bud dormancy in perennials: current knowledge and future perspective. *Genes* 12:1635. doi: 10.3390/genes12101635

Pasare, S. A., Ducreux, L. J. M., Morris, W. L., Campbell, R., Sharma, S. K., Roumeliotis, E., et al. (2013). The role of the potato (*Solanum tuberosum*) *CCD8* gene in stolon and tuber development. *New Phytol.* 198, 1108–1120. doi: 10.1111/nph.12217

Paterlini, A., Dorussen, D., Fichtner, F., Van Rongen, M., Delacruz, R., Vojnovic, A., et al. (2021). Callose accumulation in specific phloem cell types reduces axillary bud growth in *Arabidopsis thaliana*. *New Phytol.* 231, 516–523. doi: 10.1111/nph.17398

Patil, S. B., Barbier, F. F., Zhao, J. F., Zafar, S. A., Uzair, M., Sun, Y. L., et al. (2022). Sucrose promotes D53 accumulation and tillering in rice. *New Phytol.* 234, 122–136. doi: 10.1111/nph.17834

Petrasek, J., and Friml, J. (2009). Auxin transport routes in plant development. *Development* 136, 2675–2688. doi: 10.1242/dev.030353

Phillips, I. D. J. (1975). Apical dominance. *Annu. Rev. Plant. Physiol. Plant. Mol. Biol.* 26, 341–367. doi: 10.1146/annurev.pp.26.060175.002013

Piisilä, M., Keceli, M. A., Brader, G., Jakobson, L., Joesaar, I., Sipari, N., et al. (2015). The F-box protein MAX2 contributes to resistance to bacterial phytopathogens in *Arabidopsis thaliana*. *BMC Plant Biol.* 15:53. doi: 10.1186/s12870-015-0434-4

Poethig, R. S. (1987). Clonal analysis of cell lineage patterns in plant development. *Am. J. Bot.* 74, 581–594. doi: 10.1002/j.1537-2197.1987.tb08679.x

Rabot, A., Henry, C., Ben Baaziz, K., Mortreau, E., Azri, W., Lothier, J., et al. (2012). Insight into the role of sugars in bud burst under light in the rose. *Plant Cell Physiol.* 53, 1068–1082. doi: 10.1093/pcp/pcs051

Rameau, C., Bertheloot, J., Leduc, N., Andrieu, B., Foucher, F., and Sakr, S. (2015). Multiple pathways regulate shoot branching. *Front. Plant Sci.* 5:741. doi: 10.3389/fpls.2014.00741

Reddy, S. K., Holalu, S. V., Casal, J. J., and Finlayson, S. A. (2013). Abscisic acid regulates axillary bud outgrowth responses to the ratio of red to far-red light. *Plant Physiol.* 163, 1047–1058. doi: 10.1104/pp.113.221895

Reinhardt, D., and Kuhlemeier, C. (2002). Plant architecture. *EMBO Rep.* 3, 846–851. doi: 10.1093/embo-reports/kvf177

Rinne, P. L. H., Paul, L. K., Vahala, J., Kangasjarvi, J., and Van Der Schoot, C. (2016). Axillary buds are dwarfed shoots that tightly regulate GA pathway and GA-inducible 1,3-beta-glucanase genes during branching in hybrid aspen. *J. Exp. Bot.* 67, 5975–5991. doi: 10.1093/jxb/erw352

Rinne, P. L. H., Welling, A., Vahala, J., Ripel, L., Ruonala, R., Kangasjarvi, J., et al. (2011). Chilling of dormant buds hyperinduces *FLOWERING LOCUS T* and recruits GA-inducible 1,3-beta-glucanases to reopen signal conduits and release dormancy in populus. *Plant Cell* 23, 130–146. doi: 10.1105/tpc.110.081307

Rohde, A., and Bhalerao, R. P. (2007). Plant dormancy in the perennial context. *Trends Plant Sci.* 12, 217–223. doi: 10.1016/j.tplants.2007.03.012

Roman, H., Girault, T., Barbier, F., Peron, T., Brouard, N., Pencik, A., et al. (2016). Cytokinins are initial targets of light in the control of bud outgrowth. *Plant Physiol.* 172, 489–509. doi: 10.1104/pp.16.00530

Ruttink, T., Arend, M., Morreel, K., Storme, V., Rombauts, S., Fromm, J., et al. (2007). A molecular timetable for apical bud formation and dormancy induction in poplar. *Plant Cell* 19, 2370–2390. doi: 10.1105/tpc.107.052811

Sachs, T., and Thimann, K. V. (1967). The role of auxins and cytokinins in the release of buds from dominance. *Am. J. Bot.* 54, 136–144. doi: 10.1002/j.1537-2197.1967.tb06901.x

Sakakibara, H., Takei, K., and Hirose, N. (2006). Interactions between nitrogen and cytokinin in the regulation of metabolism and development. *Trends Plant Sci.* 11, 440–448. doi: 10.1016/j.tplants.2006.07.004

Schmitz, G., and Theres, K. (1999). Genetic control of branching in *Arabidopsis* and tomato. *Curr. Opin. Plant Biol.* 2, 51–55. doi: 10.1016/S1369-5266(99)80010-7

Scott, T. K., Case, D. B., and Jacobs, W. P. (1967). Auxin-gibberellin interaction in apical dominance. *Plant Physiol.* 42, 1329–1333. doi: 10.1104/pp.42.10.1329

Seale, M., Bennett, T., and Leyser, O. (2017). *BRC1* expression regulates bud activation potential but is not necessary or sufficient for bud growth inhibition in Arabidopsis. *Development* 144, 1661–1673. doi: 10.1242/dev.145649

Shen, H., Luong, P., and Huq, E. (2007). The F-Box protein MAX2 functions as a positive regulator of photomorphogenesis in Arabidopsis. *Plant Physiol.* 145, 1471–1483. doi: 10.1104/pp.107.107227

Shen, J. J., Zhang, Y. Q., Ge, D. F., Wang, Z. Y., Song, W. Y., Gu, R., et al. (2019). CsBRC1 inhibits axillary bud outgrowth by directly repressing the auxin efflux carrier CsPIN3 in cucumber. *Proc. Natl. Acad. Sci. U. S. A.* 116, 17105–17114. doi: 10.1073/pnas.1907968116

Shimizu-Sato, S., Tanaka, M., and Mori, H. (2009). Auxin-cytokinin interactions in the control of shoot branching. *Plant Mol. Biol.* 69, 429–435. doi: 10.1007/s11103-008-9416-3

Shinohara, N., Taylor, C., and Leyser, O. (2013). Strigolactone can promote or inhibit shoot branching by triggering rapid depletion of the auxin efflux protein PIN1 from the plasma membrane. *PLoS Biol.* 11:e1001474. doi: 10.1371/journal.pbio.1001474

Shipley, B., and Meziane, D. (2002). The balanced-growth hypothesis and the allometry of leaf and root biomass allocation. *Funct. Ecol.* 16, 326–331. doi: 10.1046/j.1365-2435.2002.00626.x

Shiratake, K., Notaguchi, M., Makino, H., Sawai, Y., and Borghi, L. (2019). Petunia PLEIOTROPIC DRUG RESISTANCE 1 is a strigolactone short-distance transporter with long-distance outcomes. *Plant Cell Physiol.* 60, 1722–1733. doi: 10.1093/pcp/pcz081

Simons, J. L., Napoli, C. A., Janssen, B. J., Plummer, K. M., and Snowden, K. C. (2007). Analysis of the *DECREASED APICAL DOMINANCE* genes of petunia in the control of axillary branching. *Plant Physiol.* 143, 697–706. doi: 10.1104/pp.106.087957

Skubacz, A., and Daszkowska-Golec, A. (2017). "Seed dormancy: the complex process regulated by abscisic acid, gibberellins, and other phytohormones that makes seed germination work," in *Phytohormones—Signaling Mechanisms and Crosstalk in Plant Development and Stress Responses*. ed. M. A. El-Esawi (London: Intech Open), 77–100.

Snowden, K. C., and Napoli, C. A. (2003). A quantitative study of lateral branching in petunia. *Funct. Plant Biol.* 30, 987–994. doi: 10.1071/FP03081

Song, C. Z., Zhao, J., Guichard, M., Shi, D. B., Grossmann, G., Schmitt, C., et al. (2022). Strigo-D2-a bio-sensor for monitoring spatio-temporal strigolactone signaling patterns in intact plants. *Plant Physiol.* 188, 97–110. doi: 10.1093/plphys/kiab504

Sonnewald, S., and Sonnewald, U. (2014). Regulation of potato tuber sprouting. *Planta* 239, 27–38. doi: 10.1007/s00425-013-1968-z

Sorefan, K., Booker, J., Haurogne, K., Goussot, M., Bainbridge, K., Foo, E., et al. (2003). *MAX4* and *RMS1* are orthologous dioxygenase-like genes that regulate shoot branching in Arabidopsis and pea. *Genes Dev.* 17, 1469–1474. doi: 10.1101/gad.256603

Soundappan, I., Bennett, T., Morffy, N., Liang, Y. Y., Stang, J. P., Abbas, A., et al. (2015). SMAX1-LIKE/D53 family members enable distinct MAX2-dependent responses to strigolactones and karrikins in Arabidopsis. *Plant Cell* 27, 3143–3159. doi: 10.1105/tpc.15.00562

Stirnberg, P., Chatfield, S. P., and Leyser, H. M. O. (1999). AXR1 acts after lateral bud formation to inhibit lateral bud growth in Arabidopsis. *Plant Physiol.* 121, 839–847. doi: 10.1104/pp.121.3.839

Stirnberg, P., Furner, I. J., and Leyser, H. M. O. (2007). MAX2 participates in an SCF complex which acts locally at the node to suppress shoot branching. *Plant J.* 50, 80–94. doi: 10.1111/j.1365-313X.2007.03032.x

Takei, K., Takahashi, T., Sugiyama, T., Yamaya, T., and Sakakibara, H. (2002). Multiple routes communicating nitrogen availability from roots to shoots: a signal transduction pathway mediated by cytokinin. *J. Exp. Bot.* 53, 971–977. doi: 10.1093/jexbot/53.370.971

Tanaka, M., Takei, K., Kojima, M., Sakakibara, H., and Mori, H. (2006). Auxin controls local cytokinin biosynthesis in the nodal stem in apical dominance. *Plant J.* 45, 1028–1036. doi: 10.1111/j.1365-313X.2006.02656.x

Tian, Z. X., Wang, X. B., Lee, R., Li, Y. H., Specht, J. E., Nelson, R. L., et al. (2010). Artificial selection for determinate growth habit in soybean. *Proc. Natl. Acad. Sci. U. S. A.* 107, 8563–8568. doi: 10.1073/pnas.1000088107

Tuan, P. A., Kumar, R., Rehal, P. K., Toora, P. K., and Ayele, B. T. (2018). Molecular mechanisms underlying abscisic acid/gibberellin balance in the control of seed dormancy and germination in cereals. *Front. Plant Sci.* 9:668. doi: 10.3389/fpls.2018.00668

Turnbull, C. G. N., Booker, J. P., and Leyser, H. M. O. (2002). Micrografting techniques for testing long-distance signalling in Arabidopsis. *Plant J.* 32, 255–262. doi: 10.1046/j.1365-313X.2002.01419.x

Tylewicz, S., Petterle, A., Marttila, S., Miskolczi, P., Azeez, A., Singh, R. K., et al. (2018). Photoperiodic control of seasonal growth is mediated by ABA acting on cell-cell communication. *Science* 360, 212–215. doi: 10.1126/science.aan8576

Ueda, H., and Kusaba, M. (2015). Strigolactone regulates leaf senescence in concert with ethylene in Arabidopsis. *Plant Physiol.* 169, 138–147. doi: 10.1104/pp.15.00325

Umehara, M., Hanada, A., Magome, H., Takeda-Kamiya, N., and Yamaguchi, S. (2010). Contribution of strigolactones to the inhibition of tiller bud outgrowth under phosphate deficiency in rice. *Plant Cell Physiol.* 51, 1118–1126. doi: 10.1093/pcp/pcq084

Umehara, M., Hanada, A., Yoshida, S., Akiyama, K., Arite, T., Takeda-Kamiya, N., et al. (2008). Inhibition of shoot branching by new terpenoid plant hormones. *Nature* 455, 195–200. doi: 10.1038/nature07272

Vogel, J. T., Walter, M. H., Giavalisco, P., Lytovchenko, A., Kohlen, W., Charnikhova, T., et al. (2010). SlCCD7 controls strigolactone biosynthesis, shoot branching and mycorrhiza-induced apocarotenoid formation in tomato. *Plant J.* 61, 300–311. doi: 10.1111/j.1365-313X.2009.04056.x

Wakabayashi, T., Yasuhara, R., Miura, K., Takikawa, H., Mizutani, M., and Sugimoto, Y. (2021). Specific methylation of (11R)-carlactonoic acid by an Arabidopsis SABATH methyltransferase. *Planta* 254:88. doi: 10.1007/s00425-021-03738-6

Waldie, T., Mcculloch, H., and Leyser, O. (2014). Strigolactones and the control of plant development: lessons from shoot branching. *Plant J.* 79, 607–622. doi: 10.1111/tpj.12488

Wang, D. L., Gao, Z. Z., Du, P. Y., Xiao, W., Tan, Q. P., Chen, X. D., et al. (2016a). Expression of ABA metabolism-related genes suggests similarities and differences between seed dormancy and bud dormancy of peach (*Prunus persica*). *Front. Plant Sci.* 6:1248. doi: 10.3389/fpls.2015.01248

Wang, Q., Hasson, A., Rossmann, S., and Theres, K. (2016b). Divide et impera: boundaries shape the plant body and initiate new meristems. *New Phytol.* 209, 485–498. doi: 10.1111/nph.13641

Wang, M., Le Moigne, M. A., Bertheloot, J., Crespel, L., Perez-Garcia, M. D., Oge, L., et al. (2019). BRANCHED1: A key hub of shoot branching. *Front. Plant Sci.* 10:1782. doi: 10.3389/fpls.2019.01782

Wang, L., Wang, B., Yu, H., Guo, H. Y., Lin, T., Kou, L. Q., et al. (2020). Transcriptional regulation of strigolactone signalling in Arabidopsis. *Nature* 583, 277–281. doi: 10.1038/s41586-020-2382-x

Wang, C. Y., Yang, X. J., and Li, G. (2021). Molecular insights into inflorescence meristem specification for yield potential in cereal crops. *Int. J. Mol. Sci.* 22:3508. doi: 10.3390/ijms22073508

Wheeldon, C. D., and Bennett, T. (2021). There and back again: An evolutionary perspective on long-distance coordination of plant growth and development. *Semin. Cell Dev. Biol.* 109, 55–67. doi: 10.1016/j.semcdb.2020.06.011

Wilson, J. B. (1988). A review of evidence on the control of shoot:root ratio, in relation to models. *Ann. Bot.* 61, 433–449. doi: 10.1093/oxfordjournals.aob.a087575

Xi, L., Wen, C., Fang, S., Chen, X. L., Nie, J., Chu, J. F., et al. (2015). Impacts of strigolactone on shoot branching under phosphate starvation in chrysanthemum (*Dendranthema grandiflorum* cv. Jinba). *Front. Plant Sci.* 6:694. doi: 10.3389/fpls.2015.00694

Xie, X., Yoneyama, K., Kisugi, T., Nomura, T., Akiyama, K., Asami, T., et al. (2015). Strigolactones are transported from roots to shoots, although not through the xylem. *J. Pestic. Sci.* 40, 214–216. doi: 10.1584/jpestics.D15-045

Xu, J. X., Zha, M. R., Li, Y., Ding, Y. F., Chen, L., Ding, C. Q., et al. (2015). The interaction between nitrogen availability and auxin, cytokinin, and strigolactone in the control of shoot branching in rice (*Oryza sativa* L.). *Plant Cell Rep.* 34, 1647–1662. doi: 10.1007/s00299-015-1815-8

Yang, C. J., Samayoa, L. F., Bradbury, P. J., Olukolu, B. A., Xue, W., York, A. M., et al. (2019). The genetic architecture of teosinte catalyzed and constrained maize domestication. *Proc. Natl. Acad. Sci. U. S. A.* 116, 5643–5652. doi: 10.1073/pnas.1820997116

Yao, C., and Finlayson, S. A. (2015). Abscisic acid is a general negative regulator of Arabidopsis axillary bud growth. *Plant Physiol.* 169, 611–626. doi: 10.1104/pp.15.00682

Yoneyama, K., and Brewer, P. (2021). Strigolactones, how are they synthesized to regulate plant growth and development? *Curr. Opin. Plant Biol.* 63:102072. doi: 10.1016/j.pbi.2021.102072

Yoneyama, K., Xie, X. N., Kusumoto, D., Sekimoto, H., Sugimoto, Y., and Takeuchi, Y. (2007a). Nitrogen deficiency as well as phosphorus deficiency in sorghum promotes the production and exudation of 5-deoxystrigol, the host recognition signal for arbuscular mycorrhizal fungi and root parasites. *Planta* 227, 125–132. doi: 10.1007/s00425-007-0600-5

Yoneyama, K., Yoneyama, K., Takeuchi, Y., and Sekimoto, H. (2007b). Phosphorus deficiency in red clover promotes exudation of orobanchol, the signal for mycorrhizal symbionts and germination stimulant for root parasites. *Planta* 225, 1031–1038. doi: 10.1007/s00425-006-0410-1

Young, N. F., Ferguson, B. J., Antoniadi, I., Bennett, M. H., Beveridge, C. A., and Turnbull, C. G. N. (2014). Conditional auxin response and differential cytokinin profiles in shoot branching mutants. *Plant Physiol.* 165, 1723–1736. doi: 10.1104/pp.114.239996

Zhang, J., Mazur, E., Balla, J., Gallei, M., Kalousek, P., Medvedova, Z., et al. (2020). Strigolactones inhibit auxin feedback on PIN-dependent auxin transport canalization. *Nat. Commun.* 11:3508. doi: 10.1038/s41467-020-17252-y

Zheng, C. L., Acheampong, A. K., Shi, Z. W., Halaly, T., Kamiya, Y., Ophir, R., et al. (2018). Distinct gibberellin functions during and after grapevine bud dormancy release. *J. Exp. Bot.* 69, 1635–1648. doi: 10.1093/jxb/ery022

Zou, J. H., Zhang, S. Y., Zhang, W. P., Li, G., Chen, Z. X., Zhai, W. X., et al. (2006). The rice *HIGH-TILLERING DWARF1* encoding an ortholog of Arabidopsis MAX3 is required for negative regulation of the outgrowth of axillary buds. *Plant J.* 48, 687–698. doi: 10.1111/j.1365-313X.2006.02916.x

Conflict of Interest: The authors declare that the research was conducted in the absence of any commercial or financial relationships that could be construed as a potential conflict of interest.

Publisher's Note: All claims expressed in this article are solely those of the authors and do not necessarily represent those of their affiliated organizations, or those of the publisher, the editors and the reviewers. Any product that may be evaluated in this article, or claim that may be made by its manufacturer, is not guaranteed or endorsed by the publisher.

frontiers | Frontiers in Plant Science

TYPE Original Research
PUBLISHED 12 December 2022
DOI 10.3389/fpls.2022.1019538

OPEN ACCESS

EDITED BY
Ruifeng Yao,
Hunan University, China

REVIEWED BY
Yuzhou Zhang,
Institute of Science and Technology Austria (IST Austria), Austria
Peipei Xu,
Shanghai Institutes for Biological Sciences (CAS), China

*CORRESPONDENCE
Peijian Cao
peijiancao@163.com
Wenxuan Pu
puwx0605@hngytobacco.com

SPECIALTY SECTION
This article was submitted to Plant Physiology, a section of the journal Frontiers in Plant Science

RECEIVED 15 August 2022
ACCEPTED 24 November 2022
PUBLISHED 12 December 2022

CITATION
Wang L, Xie X, Xu Y, Li Z, Xu G, Cheng L, Yang J, Li L, Pu W and Cao P (2022) Comprehensive analysis of the carboxylesterase gene reveals that *NtCXE22* regulates axillary bud growth through strigolactone metabolism in tobacco.
Front. Plant Sci. 13:1019538.
doi: 10.3389/fpls.2022.1019538

Comprehensive analysis of the carboxylesterase gene reveals that *NtCXE22* regulates axillary bud growth through strigolactone metabolism in tobacco

Lin Wang[1,2], Xiaodong Xie[2], Yalong Xu[2], Zefeng Li[2], Guoyun Xu[2], Lingtong Cheng[2], Jun Yang[2], Lei Li[1], Wenxuan Pu[3]* and Peijian Cao[2]*

[1]State Key Laboratory of Protein and Plant Gene Research, School of Life Sciences and School of Advanced Agricultural Sciences, Peking University, Beijing, China, [2]China Tobacco Gene Research Center, Zhengzhou Tobacco Research Institute of China National Tobacco Corporation (CNTC), Zhengzhou, China, [3]Technology Center, China Tobacco Hunan Industrial Co., Ltd., Changsha, China

Carboxylesterases (CXE) are a class of hydrolytic enzymes with α/β-folding domains that play a vital role in plant growth, development, stress response, and activation of herbicide-active substances. In this study, 49 *Nicotiana tabacum* L. *CXE* genes (NtCXEs) were identified using a sequence homology search. The basic characteristics, phylogenetic evolution, gene structure, subcellular location, promoter *cis*-elements, and gene expression patterns of the CXE family were systematically analyzed. RNA-seq data and quantitative real-time PCR showed that the expression level of CXEs was associated with various stressors and hormones; gene expression levels were significantly different among the eight tissues examined and at different developmental periods. As a new class of hormones, strigolactones (SLs) are released from the roots of plants and can control the germination of axillary buds.*NtCXE7*, *NtCXE9*, *NtCXE22*, and *NtCXE24* were homologous to *Arabidopsis* SLs hydrolase *AtCXE15*, and changes in their expression levels were induced by topping and by GR24 (a synthetic analogue of strigolactone). Further examination revealed that *NtCXE22*-mutant (*ntcxe22*) plants generated by CRISPR-Cas9 technology had shorter bud outgrowth with lower SLs content. Validation of *NtCXE22* was also performed in *NtCCD8*-OE plants (with fewer axillary buds) and in *ntccd8* mutant plants (with more axillary buds). The results suggest that *NtCXE22* may act as an efficient SLs hydrolase and affects axillary bud development, thereby providing a feasible method for manipulating endogenous SLs in crops and ornamental plants.

KEYWORDS

carboxylesterase, tobacco, differential expression, axillary bud, strigolactone, NtCXE22

Introduction

Carboxylesterases (CXEs) are a class of hydrolytic enzymes with α/β-folded domains that are found in many animals, plants, and microorganisms, which can influence the hydrolysis of esters and amides (Hatfield et al., 2016). The active sites of CXEs include nucleophilic serine, acidic amino acids (arginine or glutamic acid), and histidine (Marshall et al., 2003). Hydrolysis of natural compounds may cause changes in the biological activity and transport of CXEs, which play important roles in plants. At present, 20 *CXE* genes have been identified in *Arabidopsis thaliana* (Marshall et al., 2003), 16 in *Malus domestica* (Schaffer et al., 2007), 33 in *Prunus persica* (Cao et al., 2019), and 72 in *Gossypium barbadense* (Rui et al., 2022). Plant CXE isoenzymes are found in multiple organs, at various developmental stages, and in various parts of cells (Nomura et al., 2015; Abdel-Daim et al., 2018). The expression of *CXE* genes in plants shows certain tissue specificity (Kamatham et al., 2017). For example, among the 20 *AtCXE* genes identified in *A. thaliana*, *AtCXE13* is only expressed in flowers and fruits, whereas *AtCXE1* is expressed in multiple organs but not in leaves, while other genes are expressed in all plant tissues (Marshall et al., 2003). Furthermore, *CXE* genes are constitutively expressed in plants. The expression of *MdCXE1* is low in the early stages of fruit development but increases sharply after 146 d of flowering (Schaffer et al., 2007). Expression is induced by hormones and pathogens, and in *Vitis flexuosa*, infection with *Botrytis cinerea* upregulates *VfCXE12827*, *VfCXE5585*, and *VfCXE13132* (Islam and Yun, 2016).

Plant CXE proteins have extensive substrate catalytic activities and take part in plant growth and development, secondary metabolism, and biological stress response (Mindrebo et al., 2016). *CXE* genes are also involved in ester metabolism. *MdCXE1* may affect apple flavor by hydrolyzing the 4-methyl umbelliferyl ester substrates in apple fruit at harvest maturity (Souleyre et al., 2011), and Di-n-butyl phthalate (DnBP), commonly used as a plasticizer, is easily absorbed by plants and contributes to the metabolism of rice (Zhu et al., 2019). The expression of *PpCXE1* is related to the catabolic activity of volatile acetate in peach fruits (Cao et al., 2019). CXEs also participate in the regulation of plant tolerance to both biotic and abiotic stresses. For example, *GBCXE49* regulates the tolerance of cotton to alkali stress (Rui et al., 2022); *AtCXE8* enhances plant resistance to gray mold, with the knockout of this gene increasing plant susceptibility (Lee et al., 2013); and *NbCXE* is a novel resistance-related gene that inhibits the accumulation of tobacco mosaic virus (TMV) in tobacco plants (Guo and Wong, 2020). CXEs participate in the activation of plant hormone-signaling substances, regulating IAA metabolism in immature maize endosperm tissues (Kowalczyk et al., 2003). *CXE* genes also regulate strigolactones (SLs) metabolism in *A. thaliana* (Xu et al., 2021) and are involved in herbicide activation. For example, in *A. thaliana*, *AtCXE12* shares the properties of the hydrolytic herbicide precursor methyl-2, 4-dichlorophenoxyacetic acid (Gershater et al., 2007a). Jasmonic acid (JA) seed treatment also influences the expression level of *CXE* genes and promotes the detoxification of mustard seed insecticides (Sharma et al., 2018).

SLs and their derivatives are novel plant hormones derived from β-carotene, which play a crucial role in axillary bud outgrowth (Luo et al., 2019), root elongation (Sun et al., 2021), abiotic stress response (Marzec et al., 2020), and plant-fungi symbiosis (Akiyama et al., 2005). For example, the interference of SLs synthesis gene *CCD8* results in increased branching of potato plants, and its gene editing was found to increase the branching of grapevines (Pasare et al., 2013; Ren et al., 2020). At present, the identified plant endogenous (natural) SLs contain a tricyclic lactone (ABC ring) and monocyclic lactone linked together by an enol ether bond (Yoneyama et al., 2018). The sensory mechanism of SLs is characteristic compared with other phytohormones, as the SLs receptor is an α/β hydrolase folding protein, which is regulated by ligand binding ability and hydrolysability (Toh et al., 2015; Seto et al., 2019). *ShHTL7*, a SLs receptor, enhances binding ability, having a large binding-pocket volume (Chen et al., 2021). Another SLs receptor, *D14*, is a member of the hydrolase family with α/β-folding characteristics, but its binding effect is greater than that of hydrolysis and may not be the key mechanism in SLs hydrolysis (Hamiaux et al., 2012; Zhao et al., 2013). In *A. thaliana*, *AtCXE15* and its homologues have been identified as highly hydrolytic enzymes for SLs; *AtCXE15* catalyzes the hydrolysis of various SLs analogs, and overexpression of *AtCXE15* induces bud branching by SLs (Xu et al., 2021). Ectopic expression of *AtCXE20* in *A. thaliana* and maize also results in increased plant branching and tillering (Roesler et al., 2021).

Tobacco (*Nicotiana tabacum* L.) is an economically important commercial crop and a model plant for genetic studies. Axillary bud germination and lateral branch growth in tobacco plants are also regulated by SLs. However, the *CXE* gene family has not yet been thoroughly evaluated in tobacco. Therefore, in this study, we examine the *CXE* gene family in tobacco and identify those *CXE* genes responsible for environmental stress tolerance and tissue specificity using bioassays. In addition, we verify a *CXE* gene that regulates axillary bud development in tobacco *via* genetic transformation. Our results not only provide a valuable reference for further research into the functional mechanisms of this gene family and the biological functions of CXEs in plant growth and development, but also suggest that CXEs may regulate SLs.

Materials and methods

Acquisition and sequence analysis of *NtCXE* family

Tobacco *CXE* (*NtCXE*) genes were found in the tobacco genome database (unpublished) based on the conserved

domain (accession PF07859) and protein sequences of *A. thaliana* using "HMMER" software. In addition, the gene length, protein molecular weight, and the theoretical potential of the members of the CXE family of tobacco plants were analyzed using the software "ExPASy" (http://www.expasy.org/tools/). The subcellular localization of 49 *NtCXE* gene family members was carried out using the "Genscript" tool (https://www.genscript.com/psort.html) for prediction. To analyze the evolutionary relationships, the amino acid sequences of *CXE* genes in *Arabidopsis*, tomato, peach, apple and tobacco. were aligned using "CLUSTALX" and "MEGA 7.0" (Kumar et al., 2018).

Chromosomal location and gene duplication analyses

All the *NtCXE* genes were mapped onto their corresponding chromosomes. "TBtools" (Chen et al., 2020) was adopted to display the positions of chromosome locations and draw the chromosome distribution map of the *NtCXE* genes family. "KaKs_Calculator" was used to calculate the non-synonymous replacement rate (Ka), synonymous replacement rate (Ks), and their ratio (Ka/Ks) (Zhang et al., 2006).

Gene structure and conserved domain analysis

The "MEME" tool (http://meme.sdsc.edu/meme) was adopted to detect the *NtCXE* conserved motif in members of the gene family. For this, the number of conserved radicals detected was 15, and the length of the motifs was a minimum of six and a maximum of 50 amino acids. The coding sequence (CDS) and genome sequences of the CXE family members were uploaded to the Gene Structure Display Server program (http://gsds.cbi.pku.edu.cn/) to generate an intron-exon structure map.

Cis-acting element analysis and regulatory network prediction

The upstream 3,000-base-pair (bp) sequence of the *CXE* genes were adopted as the promoter region, and the promoter sequence was downloaded from the tobacco genome database. The PlantCare website (http://bioinformatics.psb.ugent.be/webtools/plantcare/html/search_CARE.html) (Lescot et al., 2002) was used to identify *cis*-elements in the promoter regions of the *NtCXE*s. Regulatory elements of promoters were then be classified according to hormones, light, stress, etc. miRNAs downloaded from the miRBase database were used to build the miRNA-*NtCXE* regulatory relationships (http://plantgrn.noble.org/psRNATarget/) (Dai and Zhao, 2011; Kozomara et al., 2019). Transcription factors (TFs) screened from the Plant Transcription Factor Database (PlantTFDB; http://planttfdb.cbi.pku.edu.cn) were used to build the TF-*NtCXE* regulatory relationship network (http://plantgrn.noble.org/psRNATarget/) (Jin et al., 2016), and "Cytoscape" was used to map the regulatory networks (Smoot et al., 2011).

Plant growth conditions

The common tobacco variety K326 was cultured at the Zhengzhou Tobacco Research Institute in April 2022. Seedlings were grown in a greenhouse with a 14-h light at 28° C/10-h dark at 25°C cycle and a relative humidity of 50-60%. Uniformly growing tobacco (four-week-old seedlings) was screened for hormonal treatment.The tobacco seedlings were planted in 1/2 Hoagland nutrient solution with IAA (10 μM), MeJA (50 μM), ABA (10 μM), SA (10 μM), GA (10 μM), 6-BA (10 μM), GR24 (10 μM), and sucrose (10 mM) for 6 h. Uniformly growing tobacco (six-week-old seedlings) was screened for abiotic stress treatment. Tobacco seedlings were exposed to in 1/2 Hoagland nutrient solution at high temperature (35°C), low temperature (4 °C), salty (150 mM NaCl), dark, cadmium (10 μM), and drought (40% polyethylene glycol, PEG) conditions for 3 d. Roots, stems, leaves, axillary buds, and flowers were subsequently collected during the flowering stage. All collected examples were frozen in liquid nitrogen quickly and stored at -80°C in the refrigerator.

NtCXE gene expression in different tissues exposed to different stress treatments

The transcriptome data was adopted to reveal the expression patterns of *CXE* genes in tobacco in various tissue types and under the different stress conditions. Organizational data including leaves, roots, stems, veins, axillary buds, blades, calluses, and seeds were obtained from the tobacco genome database (unpublished). The sampling method is described in detail in Supplementary Table 1. Data on stress, including cold, drought, cadmium (Cd), topping, and CMV and *Phytophthora nicotianae* infection were obtained from the Sequence Read Archive (SRA) (Leinonen et al., 2011; He et al., 2016; Jin et al., 2017; Yang H. et al., 2017; Yang J. K. et al., 2017; Chen et al., 2019). These data were mapped to the tobacco reference genome using "HISAT2.2.1" with default parameters (Kim et al., 2019).

RNA isolation and expression analysis

Total RNA from each sample was extracted using Trizol reagent. RNA quality and purity were determined using 2% agarose gel electrophoresis and ultraviolet spectrophotometry, respectively. The reverse-transcribed cDNA was synthesized using the Prime Script RT Reagent Kit and stored at -20°C. Primers were designed using the Primer 3.0 online program based on the CDS sequence of *NtCXE* genes for quantitative real-time (qRT)-PCR. An Applied Biosystems CFX96 machine was used for the qRT-PCR with the SYBR qPCR kit (TaKaRa). The tobacco ribosomal protein gene, *L25* (GenBank No. L18908), was used as an internal reference, and three biological replicates were performed (Schmidt and Delaney, 2010). The gene primers used in this study are listed in Supplementary Table 2.

Subcellular localization and GUS staining assay

The Open Reading Frame of the target gene was fused downstream of the PC1300s-GFP vector using *Ecro*RI enzyme digestion. The enzymatic digestion product was purified and recombined with the amplified products (ClonExpress-II One Step Cloning Kit). The recombinant plasmid was then transferred into *Agrobacterium tumefaciens* (LBA4404). The monoclonal cells were coated with kanamycin resistant plates and cultured in yeast extract broth liquid medium on a 28 °C shaking table for 2 d. The bacteria were centrifuged at 4,000 rpm/min for 4 min. After supernatant removal, the bacteria were re-suspended in 10 mM $MgCl_2$ (including 120 μM AS) suspension, and the OD600 was adjusted to approximately 0.6. The *Agrobacterium* solution was then injected into the lower epidermis (back side) of the tobacco leaves. The injected tobacco plants were then cultured under low light for 2 d and observed using laser confocal microscopy. The empty vector-transformed *A. tumefaciens* was used as a control. The vector map of PC1300s-NtCEX22-GFP was shown in Supplementary Figure 1.

The plasmid PBI121 was digested with *BamH*I enzyme and *Sac*I enzyme at 37 °C for 3h. The reaction system included 15 μL of PBI121 plasmid, 1μL of BamHI enzyme, and 1 μL of SacI enzyme. The digested product was analyzed by electrophoresis, recovered, and purified. The promoter sequence of *NtCXE22* was subcloned into the vector pBI121 by clonEZ homologous recombination, and 35S in the vector was replaced. The vector map of proCXE22-GUS was shown in Supplementary Figure 2. The proCXE22-GUS vector was then transformed into the tobacco plants (Horsch et al., 1985). The plant materials were placed into β-glucuronidase (GUS) staining solution and then stained for 12 h in the dark at 37°C. After staining, the GUS staining solution was recovered. Plant tissues were immersed in 75% ethanol for decolorization, and after chlorophyll removal, the staining results were photographed for analysis. The gene primers used in this study are listed in Supplementary Table 2.

Gene mutation plasmid construction, plant transformation and mutant analysis

A Cas9/sgRNA vector was constructed as previously described (Gao et al., 2015). According to the mRNA sequence information of *NtCXE22*, two CRISPR target sites of 20 nucleotides were designed to produced small guide RNA (sgRNA). Plasmid Cas9/gRNA was digested by *Bsa*I. enzyme at 37 °C for 4 h. The target site sequence was ligated into pORE-Cas9 binary vector using T4 ligase. The connected carriers were transformed into DH5α competent cells and coated onto lysogeny broth (LB) solid medium. The cells were cultured overnight at 37 °C until positive plaques grew (approximately 16 h). After sequencing, the plasmid was extracted using the OMEGA plasmid extraction kit and transformed into *Agrobacterium tumefaciens* (LBA4404). The vectors were subsequently transformed into tobacco plants using the *A. tumefaciens*-mediated leaf disk method (Horsch et al., 1985). The design method of PCR primers and detection methods of mutation efficiency were carried out accoring to previous literature (Xie et al., 2017).

Plant tissue safranin O-fast green staining and scanning electron microscope

For plant tissue safranin O-fast green staining, axillary buds were selected as samples and fixed in FAA soution. The sections of samples were rehydrated in BioDewax and put into the safranin O staining solution for 3-8s. The sections were then decolorized and put into plant solid green staining solution for 6-20s. The last, the sections was transparent and sealed for microscope observation.

For the scanning electron microscope, samples (axilalry buds) were quickly taken and fixed with SEM fixation solution for 2h. Then the post-fixation was performed (PBS washing; fixed with OsO4 for 2h; PBS washing). The sample was dehydrated in alcohol and isoamyl acetate. The dehydrated samples were dried and treated with conductive metal coating. Finally, the samples were observed and photographed under a scanning electron microscope.

Extraction and detection of strigolactone

SL was determined using a plant SL ELISA kit (RJ21771, Shanghai; China). The chemical formula for SL is $C_{17}H_{14}O_5$, the

molecular weight is 298.29. Samples were collected from the roots of the wild type and *NtCXE22* mutant plants following the manufacturer's instructions.

Statistical analyses

Excel 2016, SPSS 26.0 and GraphPad Prism 9.0 software were used for data analysis and visualization. All treatments and sample assays were performed with at least three replicates, and each biological replicate included at least three uniformly grown plants.

Results

Genome-wide identification of the *NtCXE* family in *N. tabacum*

To identify members of the CXE family in tobacco, gene annotation and the hidden Markov model-based profile of the CXE domain (accession PF07859) were used as query conditions, and 49 *CXE* genes were identified in the *N. tabacum* genome database. To understand the evolutionary relationships of CXEs, a phylogenetic tree was constructed using full-length deduced amino acid sequences from *Arabidopsis*, tobacco, peach, apple and tobacco (Figure 1). The 49 tobacco *CXE* genes were divided into seven subfamilies according to their sequence homology. Group three contains 12 tobacco CXE members, accounting for 24% of the entire gene family, and was the subgroup with the largest number of members. The CDS length of the *NtCXE* genes ranged from 411 to 1,479 bp, and the protein length ranged from 136 to 492 amino acids. The protein molecular weights (MWs) of the NtCXE proteins were between 15.55 and 53.98 kDa, with the isoelectric points of members of the *CXE* gene family ranging from 4.58 to 5.93. The predicted locations of the NtCXE proteins in the cell were mostly in the cytoplasm and mitochondria based on subcellular localization prediction. The CDS sequences, physical and chemical properties of the 49 identified *NtCXE* genes are listed in Supplementary Table 3.

Chromosomal locations, duplication, and multiple sequence alignment

The chromosome analysis of *NtCXE* genes is presented in Figure 2A. We found that 33 *NtCXE* genes were present on the following 14 chromosomes: Chr01, Chr02, Chr03, Chr5, Chr6, Chr8, Chr11, Chr12, Chr13, Chr14, Chr16, Chr17, Chr20, and Chr21. The largest gene cluster (13 members) was observed on

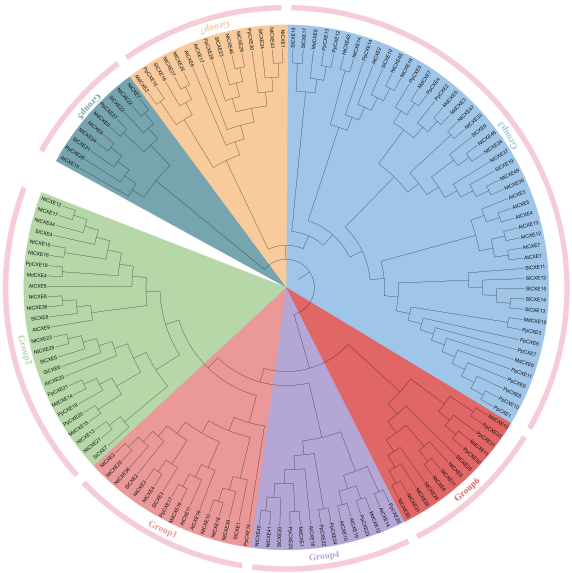

FIGURE 1
Phylogenetic analysis of carboxylesterase (CXE) families. The Neighbour-Joining (NJ) phylogenetic tree was constructed according to amino acid sequences of *CXE* genes in *Arabidopsis*, tomato, peach, apple and tobacco by MEGA 7.0. The CXE proteins were divided into seven groups (marked as groups 1-7), distinguished by different colors. The standard value of nodes was derived using bootstrapping, with 1000 replicates.

Chr6 (Figure 2A). There were five *NtCXE*s on Chr13 (*NtCXE5*, *NtCXE6*, *NtCXE30*, *NtCXE31*, and *NtCXE32*), four on Chr11 (*NtCXE26*, *NtCXE33*, *NtCXE34*, and *NtCXE35*), and three on Chr20 (*NtCXE15*, *NtCXE16*, and *NtCXE45*). Chr01, Chr02, Chr03, Chr5, and Chr8 contained the fewest *NtCXE* genes, with only one each. In addition, 16 *NtCXE* genes were not located on a chromosome but were mapped onto certain scaffolds (Figure 2A). The nucleotide sequences of the *NtCXE* genes were subsequently compared in a gene replication analysis. A total of 27 gene replication events occurred in the *NtCXE* gene family, including two tandem replication events and 25 segmental replication events. The Ka and Ks values of the gene replication pairs were used to evaluate the factors affecting gene evolution in tobacco. The same type of duplicated gene showed different Ka and Ks distributions; whole genome duplication (WGD)-type repeat gene pairs showed a smaller Ka/Ks ratio, revealing slower sequencing or functionalization over a longer period of time (Supplementary Table 4). The CXE family belongs to the α/β sheet hydrolase superfamily, and contain a conserved core-a HGGGF-and-GXSXG-motif-associated with catalysis and degradation (Ueguchi-Tanaka et al., 2005). The *NtCXE* protein sequence alignment showed that this motif was highly conserved (Figure 2B). This warrants further study regarding the degradation of *NtCXE*s.

10.3389/fpls.2022.1019538

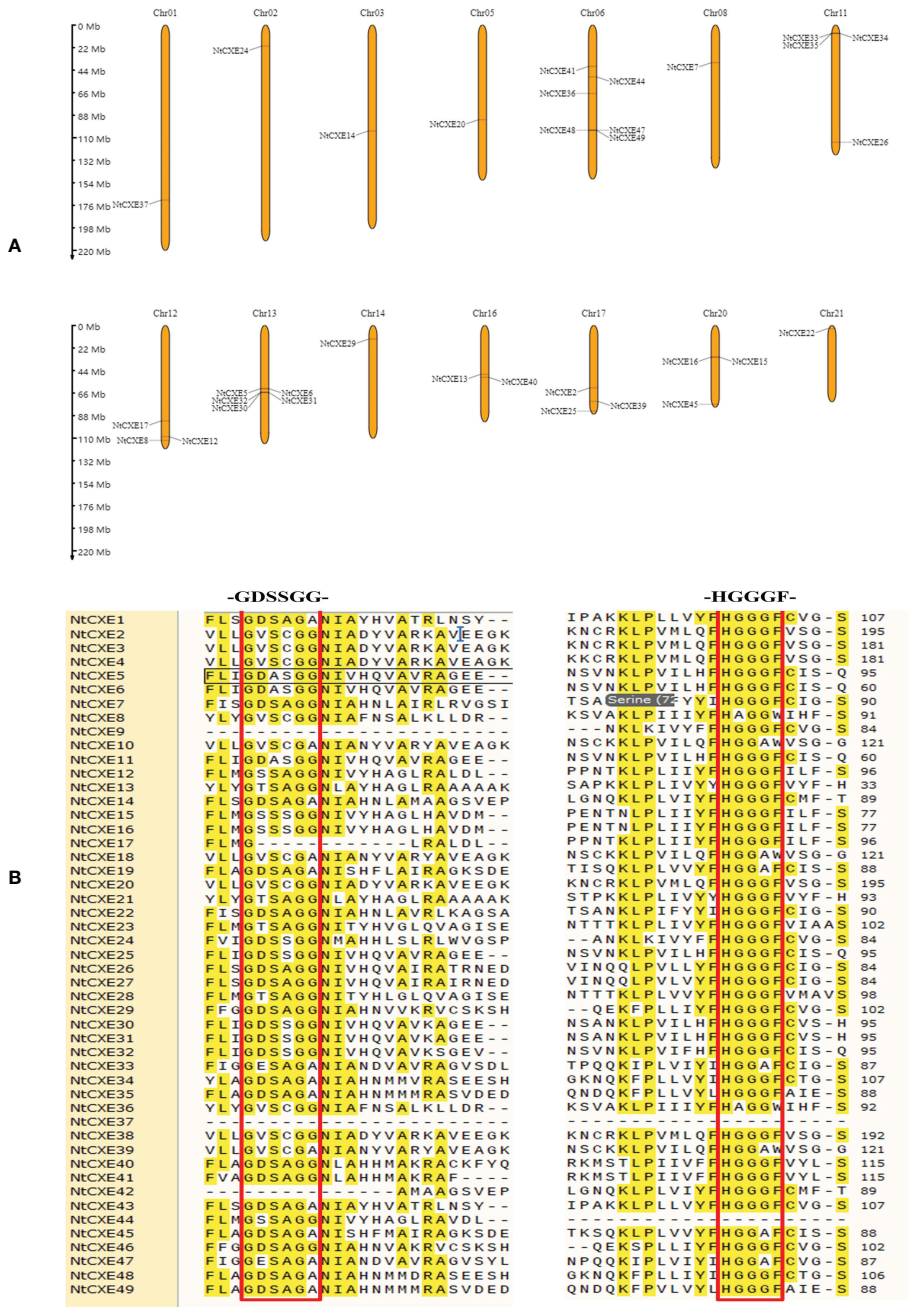

FIGURE 2
Analysis of genomic location, duplicated gene pairs, and sequence comparison of tobacco NtCXE proteins. **(A)** Chromosomal positions of the *CXE* genes. The chromosomal names are in red and are shown at the top, and the gene names are shown on the chromosome. The length of chromosomes is shown to scale. **(B)** Multiple sequence alignment of conserved domain of NtCXE proteins. The amino acid sequences were aligned using ClustalX.

Gene structure and conserved motif analysis

The "MEME" suite tool was chosen to analyze the conserved motifs, 10 of which were identified (Supplementary Table 5; Figure 3A). Analysis of these genes suggested that the motif of the *NtCXE* gene family had a certain conserved type. Introns are an important component of eukaryotic genes that can participate in the post-transcriptional re-splicing of structural genes. Some introns also participate in the regulation of

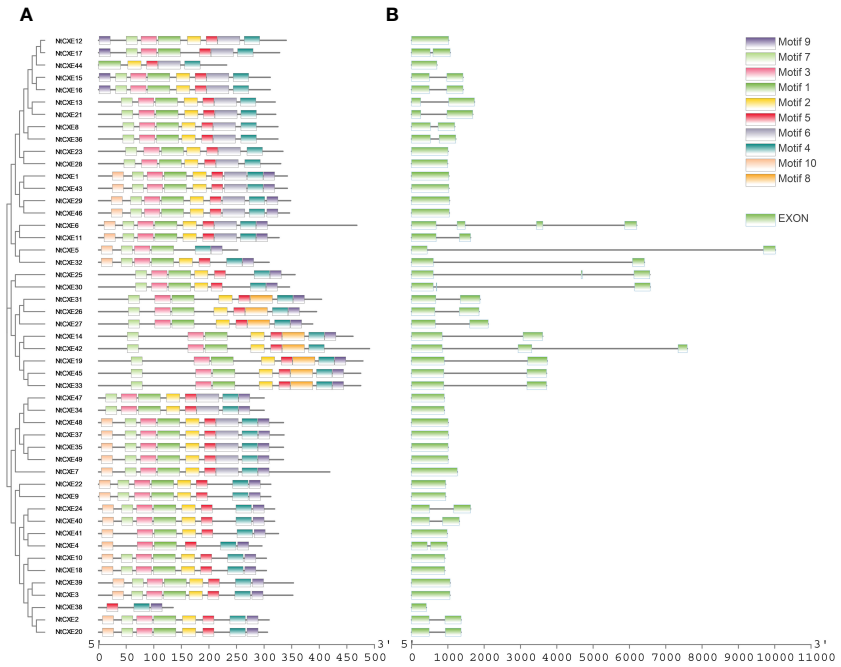

FIGURE 3
Phylogenetic relationship, gene structures, and protein conserved motif of NtCXE genes. **(A)** Analysis of conserved motif in the amino acid sequences of NtCXEs. The differently colored boxes in the upper right corner represent different conserved motifs with the number 1 to 10. The sequence information corresponding to different motifs is provided in Supplementary Table 5. **(B)** Exon-intron structure of NtCXEs in tobacco.

promoter activity and the activity of response elements contained in promoter introns (Hoshida et al., 2017). The CDS of the *NtCXE* genes was more deeply analyzed with the genome sequences; intron and exon analyses were performed using GSDS 2.0 (Figure 3B). The 26 *NtCXE*s were all intron-containing genes, and exons were separated by introns. However, the gene structures were very different, and the number of exons ranged from one to four. Twenty (40.81%) genes had one intron, whereas *NtCXE6* had three introns. Notably, paralogous *NtCXE*s genes shared similar exon/intron distribution rules.

Cis-acting elements and interaction networks of the CXE family

In view of the potential regulatory mechanisms of various *cis*-acting elements in the CXE family, the 3 kb upstream region of the transcription start site was detected, and the putative functions were identified in seven groups. Of these, light-responsive and promoter-related elements were the most abundant (Figure 4A). Elements related to the environment include low temperature, defense and stress responsiveness, and anaerobic induction. The plant hormone-responsive category includes auxin, MeJA, abscisic acid, salicylic acid, zein, and gibberellin (Figure 4B). Notably, the promoter regions of 44 *NtCXE* members (89.8%) included ABA response elements (ABRE), 35 genes (89.8%) with MeJA response elements, 33 genes (89.8%) with gibberellin response elements, and 30 genes (89.8%) with auxin response elements (Figure 4C) (Supplementary Table 6). In addition, the promoter regions of the 25 *NtCXE* genes comprised meristem expression related components. Analysis of promoter elements revealed that *NtCXE* genes may take part in many plant growth and developmental processes.

Promoter *cis*-element-binding transcription factors (TFs) can regulate genetic expression. Here, TFs were predicted using "PlantTFDB" and regulatory relationships were displayed using "Cytoscape" (Jin et al., 2016). We predicted 731 TF members binding to the *NtCXE* promoters, divided into 33 TF families including WRKY, TCP, and NAC. Potential miRNA-binding sites for *NtCXE*s were subsequently identified using "PsRNATarget" (Dai and Zhao, 2011). In total, 138 miRNA members from 23 miRNA families were screened, implying their complex and potentially important roles in the regulation of *NtCXE*s. Some of miRNAs have several *NtCXE* targets; nta-*miR167a*, for example, targeted three *NtCXE* genes. In addition, some *NtCXE*s could be targeted by multiple miRNAs; for instance, *CXE2* could be regulated by 20 miRNAs. The regulatory network of *NtCXE*s with transcription factors and miRNAs is shown in

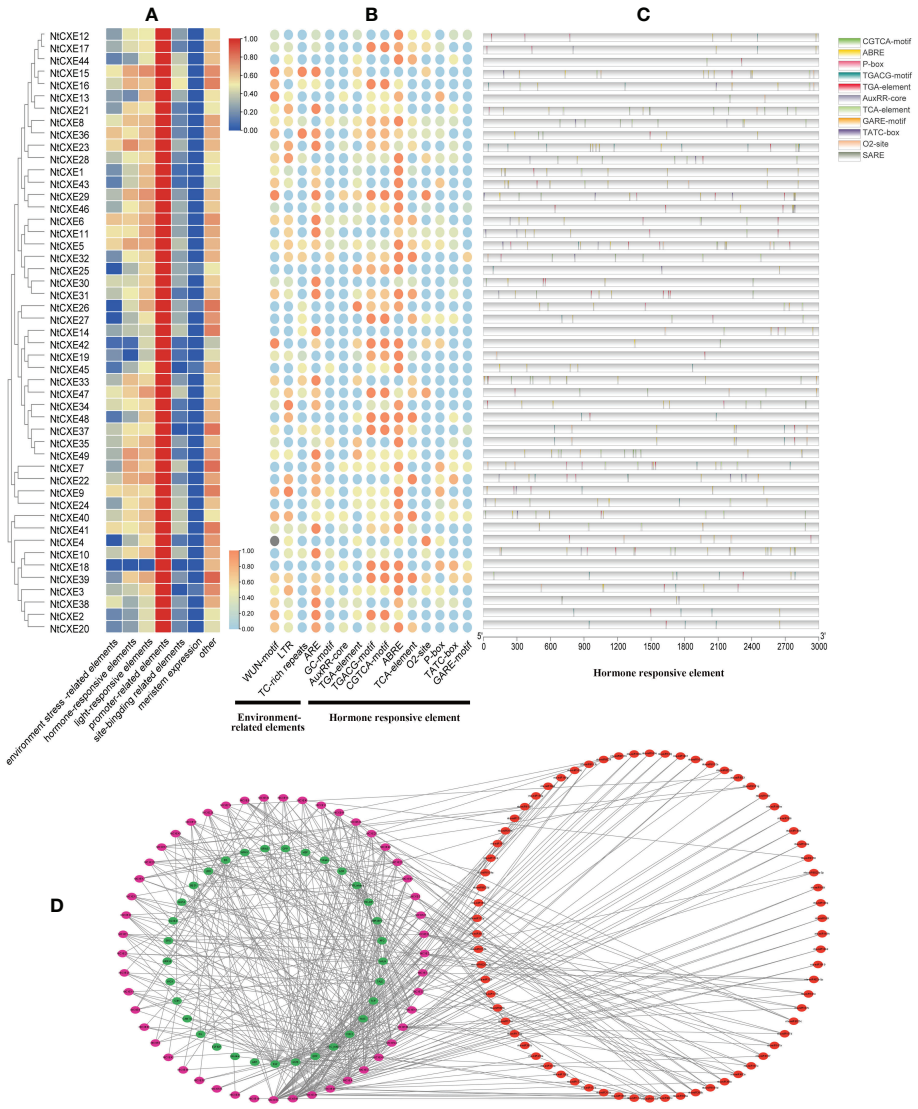

FIGURE 4
Analysis of promoters and interaction network of the tobacco *NtCXE* genes. **(A)** Predicted *cis*-acting elements divided into six types for each *NtCXE* promoter using PlantCARE software. Heat maps were drawn by TBtools using FPKM mean values. Color represents the gene expression levels (red, high expression level; and blue, low expression level). **(B)** Prediction of the magnitude of elements related to hormone and environmental stress in *NtCXE* promoters. The heat map is drawn in the same way as figure A (orange, high expression level; and blue, low expression level). **(C)** Position, type, and number of hormone-related elements in *NtCXE* promoters using "TBtools". **(D)** Regulation network of *NtCXE*s in tobacco plants. The purple, green, and red circles denote *NtCXE* genes, transcription factors (TFs), and miRNAs, respectively.

Figure 4D. Notably, the relationships between *NtCXE*s and TFs/miRNAs require further study. Specific regulatory information is presented in Supplementary Table 7.

Expression patterns of *NtCXE* genes in different tissues

To further explore the possible roles of *NtCXE* genes, their expression in eight different tissues (seeds, veins, axillary buds, blades, calluses, roots, stems, and leaves) were screened and analyzed. Of these genes, six were not expressed, and the remaining genes were expressed in five of the screened tissues (Figure 5A; Supplementary Table 8). *NtCXE35* and *NtCXE49* had higher expression levels in seeds; *NtCXE13* and *NtCXE35* had higher expression levels in seeding roots, *NtCXE21* and *NtCXE35* in seeding leaves, *NtCXE26* and *NtCXE47* in axillary buds, *NtCXE25* and *NtCXE35* in stems, *NtCXE13* and *NtCXE35* in veins, *NtCXE35* and *NtCXE49* in blades, and *NtCXE35* and *NtCXE44* in calluses. Thus, the *NtCXE* genes have distinct

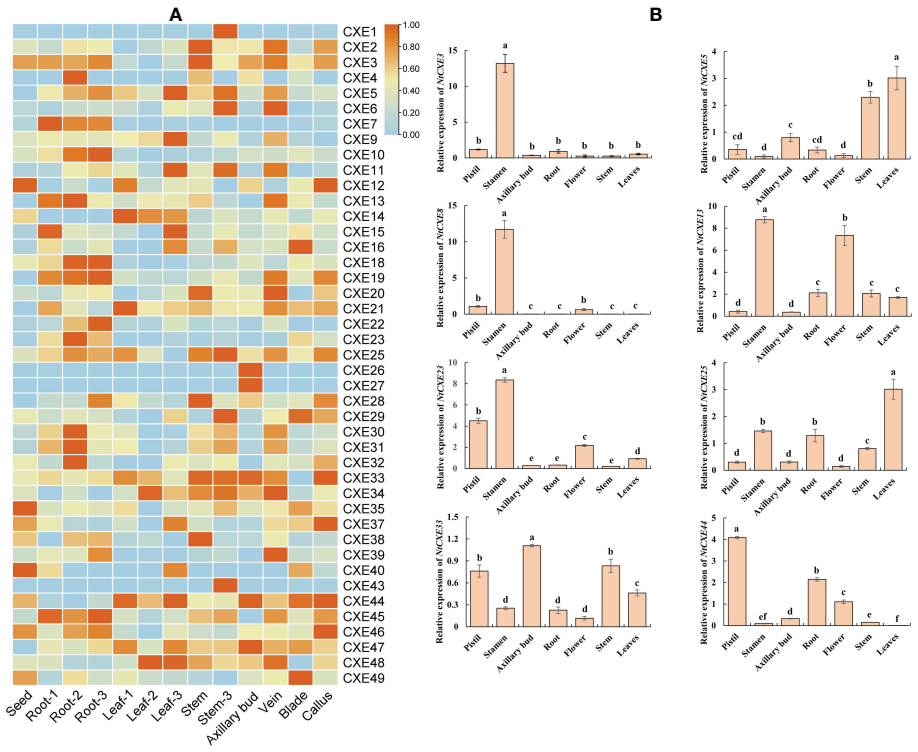

FIGURE 5
Analysis of tobacco *NtCXE* genes in various plant tissues. **(A)** Expression specificity of all *NtCXE* genes in various plant tissues, some with three developmental stages. '1', '2', and '3' represent the seedling stage, mature stage, and 2 d after topping, respectively. Heat maps were drawn by TBtools using FPKM mean values, scaled by rows. Color represents the gene expression levels (orange, high expression level; and blue, low expression level). **(B)** qRT-PCR analysis of *NtCXE3, NtCXE5, NtCXE8, NtCXE13, NtCXE23, NtCXE25, NtCXE33, NtCXE44* in axillary buds, flowers, leaves, roots, terminal buds, and veins. Data are presented as means ± SDs (n = 3). Different letters indicate significant differences between various tissues, based on one-way ANOVA.

expression profiles in different tissues, underlying their potential functions in various physiological processes. In addition, the expression of *NtCXE* genes was significantly affected by the developmental stage (i.e., seedling, maturity, and 2 d after topping). Topping promoted *NtCXE* gene expression in roots but decreased expression in leaves and stems, including *NtCXE5* and *NtCXE28*. Topping increased the expression level of NtCXE7/9/22 in the leaves. *NtCXE* gene expression at maturity was significantly different from that at the seedling stage. For example, *NtCXE38* was not expressed in seedling roots but was expressed in roots at the mature stage, and *NtCXE29* was highly expressed in seeding leaves but was significantly decreased in mature leaves. Eight *NtCXE* genes (*NtCXE 3*, *5*, *8*, *13*, *22*, *25*, *33*, and *44*) were randomly selected to validate the transcriptome results using qRT-PCR analysis, which showed similar expression patterns (Figure 5B).

Expression of *NtCXE* genes under stress

To further analyze the *NtCXE* genes involved in stress response, we used publicly available transcriptome data to assess their expression levels (Supplementary Table 9). As shown in Figure 6A, *NtCXE14* and *NtCXE42* showed a decreasing trend in response to cold stress, while *NtCXE27* showed an increasing trend. *NtCXE7*, *NtCXE47*, and *NtCXE48* were significantly upregulated in response to drought, whereas eight *NtCXE*s were downregulated. *NtCXE5*, *NtCXE25*, and seven other *NtCXE*s were upregulated in response to cadmium, while *NtCXE22*, *NtCXE34*, and seven other *NtCXE*s were downregulated. The expression of *NtCXE6* and *NtCXE7* increased in response to CMV treatment relative to that under normal nutritional conditions, while *NtCXE9*, *NtCXE24*, and *NtCXE28* expression decreased. Sixteen *NtCXE*s showed an increasing trend upon inoculation with *P. nicotianae*, with the expression level of *NtCXE14* increasing by a factor of 5.47 compared to the control. In contrast, the expression levels of six *NtCXE*s decreased upon inoculation with *P. nicotianae*, with *NtCXE9* decreasing by a factor of 6.16 relative to the control. Finally, topping promoted the expression of *NtCXE4* and *NtCXE28* but inhibited the expression of *NtCXE37* and *NtCXE46*. Subsequently, nine *NtCXE* genes (*NtCXE 5*, *10*, *14*, *22*, *27*, *30*, *39*, *42*, and *47*) were randomly selected to validate the

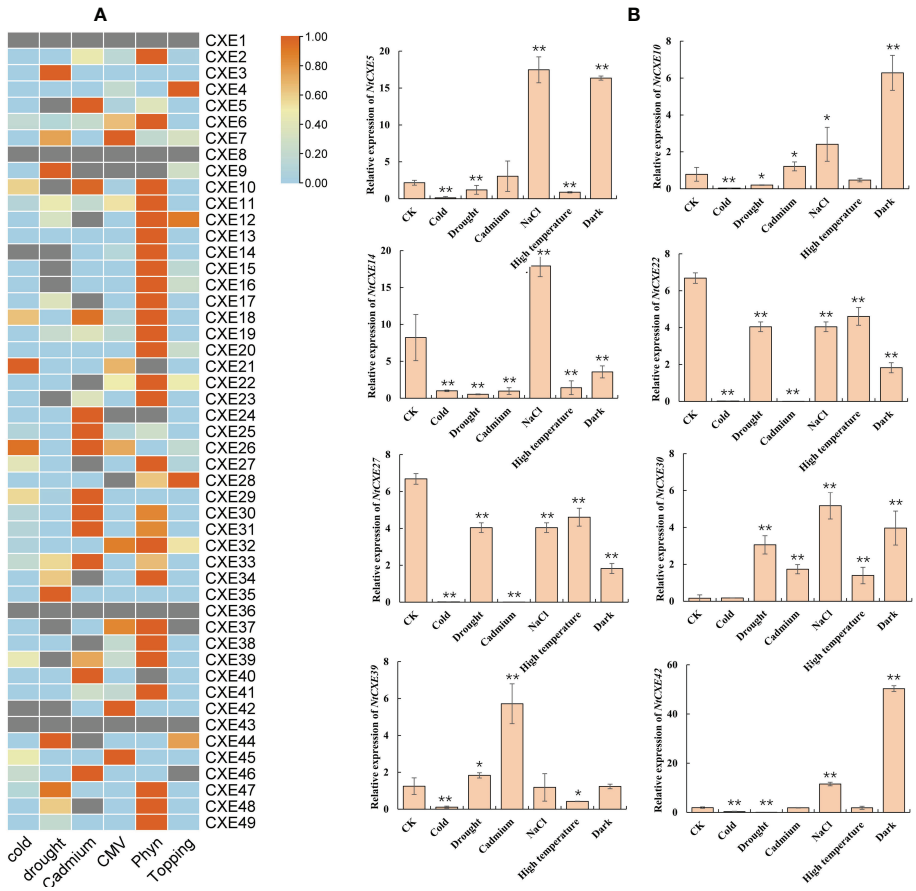

FIGURE 6
Analysis of tobacco *NtCXE* genes under various stress states. **(A)** Expression profiles of all *NtCXE* genes under cold, cadmium, topping, *P. nicotiana* infection, drought, and cucumber mosaic virus stresses, compared to the control treatment. Heat maps were drawn by TBtools using FPKM mean values, scaled by rows. Color represents the gene expression levels (orange, high expression level; and blue, low expression level). **(B)** qRT-PCR quantitative analysis of *NtCXE5*, *NtCXE10*, *NtCXE14*, *NtCXE22*, *NtCXE27*, *NtCXE30*, *NtCXE39*, *NtCXE42* in response to NaCl, cold, cadmium, drought, high temperature, cold, darkness stressors. Data are presented as means ± SDs (n = 3). *P < 0.05, **P < 0.01 (significant difference between the stress treatment and control, based on Student's t-test).

transcriptome results using qRT-PCR analysis, which showed similar expression patterns. *CXE* genes were also found to respond to salt, high temperature, and darkness (Figure 6B).

Expression of *NtCXE* genes under the influence plant hormones

Phytohormones are small-molecule organic substances produced during plant metabolism that move from their production sites to action sites to perform regulatory functions. These hormones play key roles in regulating almost all processes of plant growth and development, and response to environmental stress. To analyze the response of *NtCXE* genes to these hormones, tobacco seedlings were treated with ABA, 6-BA, GA, GR24, IAA, SA, and MeJA, which we found to differentially induce different *CXE* genes. Some genes responded to multiple hormones, such as *NtCXE2*, which responded to ABA, 6-BA, GA, GR24, IAA, SA, and MeJA, while some responded to only one, such as *NtCXE2*, which responded to ABA, and *NtCXE5*, which responded to GA. Notably, for the group-five genes, *NtCXE9/22/24* were all induced by GA, GR24, IAA, SA, and MeJA. *NtCXE7/22/24* were inhibited by ABA and 6-BA(Figure 7).

Identification of the SLs hydrolase genes in tobacco

In *A. thaliana*, *AtCXE15* participates in hydrolysis of SLs and affects axillary bud development. Through homology comparison, we found that in tobacco, *NtCXE7*, *NtCXE9*, *NtCXE22*, and *NtCXE24* are homologous to *AtCXE15*, being significantly

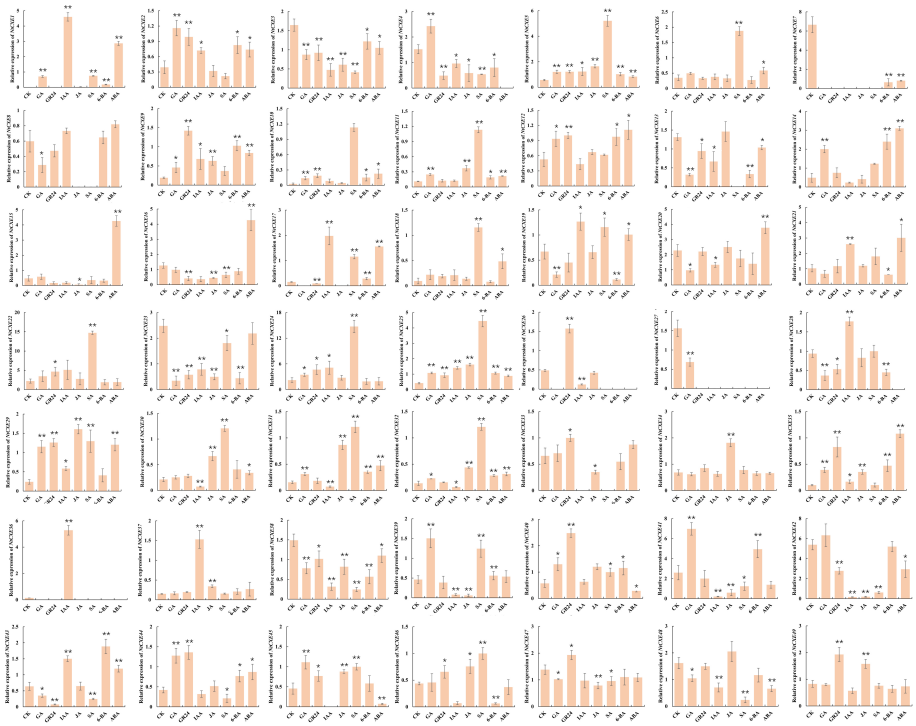

FIGURE 7
Expression profiles of 49 *NtCXE* genes under diverse hormone treatments. The expression patterns of all *NtCXE* genes in response to ABA, 6-BA, GA, GR24, IAA, SA, and JA were analyzed by qRT-PCR. Seedlings grown under normal conditions were used as controls. Data are presented as means ± SDs (n = 3). *P < 0.05, **P < 0.01 (significant difference between the hormone treatment and control, based on Student's t-test).

promoted in the axillary buds at different time points after topping (Figure 8A). Among them, the expression level of *NtCXE7* and *NtCXE22* was also increased in the roots after topping (Figure 6A). According to the induction of GR24 and its highest homology of *AtCXE15*, *NtCXE22* was selected further verify its function in axillary bud development. *NtCXE22* was expressed in different tissues, and its expression level in dormant axillary buds was higher than that in the other two types of axillary bud (Figure 8B). The constructed plant expression vector with GUS gene fusion of the *NtCXE22* promoter was used to infect tobacco seedlings *via Agrobacteria*-mediated transient transformation, and GUS staining was adopted to verify the tissue expression pattern of *NtCXE22*. We found that the GUS gene driven by the *NtCXE22* promoter was expressed in all tissues, which was similar to the qRT-PCR results (Figure 8C). To determine the subcellular localization of *NtCXE22*, a PC1300s-NtCEX22-GFP construct was introduced into the tobacco leaf protoplasts. As shown in Figure 8D, the GFP was predominantly localized in the nucleus and cytoplasm (The original pictures were shown in Supplementary Figure 3-12). These results are consistent with the network predictions and confirm the location of NtCXE22 in the cytoplasm (Figure 8D).

Knockout of *NtCXE22* inhibits tiller bud outgrowth in tobacco plants

To further understand the function of *NtCXE22* in axillary buds, targeted *NtCXE22* mutants were built using the CRISPR/Cas9 technology. The two 20 bp target sequences were introduced into a Cas9 vector and transformed into tobacco using *A. tumefaciens*-mediated transformation. Ten T0 transgenic lines were obtained from the two editing sites, which were evaluated for mutants. Among the ten plants, six mutants were identified in this study with a ratio of 60%. *NtCXE22* mutants (*ntcxe22)* resulted in the smaller axillary buds than in the wild type tobacco plants (Figure 9A). The axillary bud length of wild-type and *ntcxe22* plants were also quantified in the Figure 9B. Sections and electron microscope images of the axillary buds in wild-type and *ntcxe22*-g1 plants are shown in Figures 9C-D (The original pictures were shown in Supplementary Figures 15-18). Cells in the wild type plants divided more rapidly than those in the *NtCXE* plants. The mutation sites of the two mutated materials (*ntcxe22*-g1-2, *ntcxe22*-g2-3*)* are shown in Figure 9E, which were determined to be putative homozygous genotype.

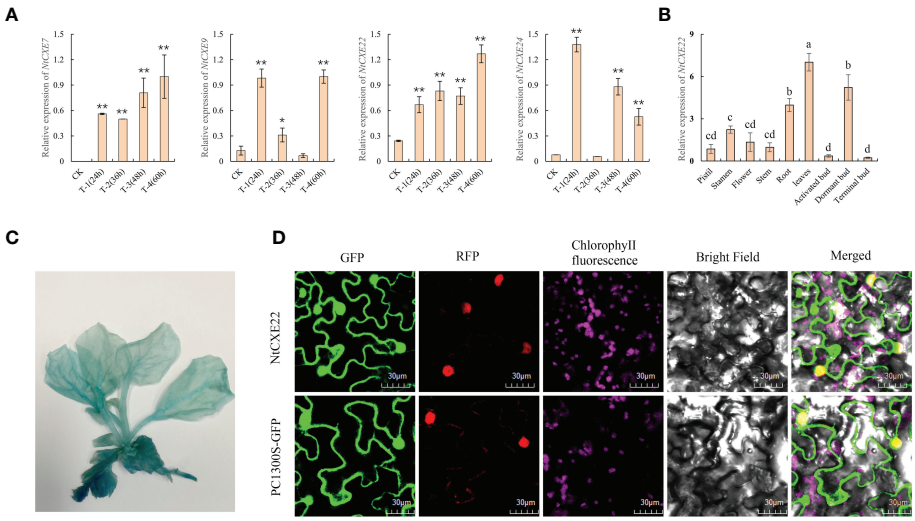

FIGURE 8
Expression patterns of *NtCXE22* and subcellular localization of the NtCXE22 protein. **(A)** qRT-PCR quantitative analysis of *NtCXE7*, *NtCXE9*, *NtCXE22*, and *NtCXE24* genes at different time points after topping, compared with that before topping. Data are presented as means ± SDs (n = 3). *P < 0.05, **P < 0.01 (significant difference between the topping treatment and control, based on Student's t-test). **(B)** qRT-PCR quantitative analysis of *NtCXE22* in different tissues. Data are presented as means ± SDs (n = 3). Different letters indicate significant differences between various tissues, based on one-way ANOVA. **(C)** Histochemical analysis of GUS expression driven by proCXE22. **(D)** Subcellular localization of NtCXE22 protein.

NtCXE22 participates in SLs regulation

The SLs-affected *NtCXE22* plants had axillary bud phenotypes similar to those of plants over-expressing *NtCCD8*, a synthetic gene that inhibits the axillary bud development (Pasare et al., 2013; Ren et al., 2020). Therefore, we hypothesized that *NtCXE22* might affect axillary bud development through SLs signaling. *NtTB1*, a SLs downstream target gene, that inhibits axillary bud outgrowth (Braun et al., 2012; Dun et al., 2013). To investigate further, we first monitored the expression levels of *NtCXE22* and *NtTB1* in the axillary buds of tobacco lines exposed to GR24. The exogenous application of GR24 induced an increase in *NtCXE22* and *NtTB1* expression (Figure 10A). Moreover, in the *ntcxe22* plants, we found the SL content was increased in the roots, and the expression levels of *NtTB1* was increased in the axillary bud relative to that in the wild type, similar to the phenotypic changes in the *NtCCD8*-overexpression (*NtCCD8*-OE) plants (Figure 10B). These results preliminary verify that *NtCXE22* has a regulatory effect on axillary bud development *via* SL catabolism or impaired signaling. Moreover, the expression level of *NtCXE22* was determined in transgenic plants with a distinct axillary bud phenotype. For this, *NtCCD8-OE* plants with smaller axillary buds were cultivated, and CRISPR/Cas9-mediated gene editing of *NtCCD8* (*ccd8*) were cultivated, with more axillary buds than in the wild type plants. The relative expression of *NtCXE22* was increased in the roots of the *NtCCD8*-OE and reduced in the *ntccd8* plants (Figure 10C). The regulatory network between the CXE22, CCD8, SL, and TB1 in the tobacco were shown as follow (Figure 10D). These results strongly suggest that *NtCXE22* regulates axillary bud development not only by mediating SL signaling but also through other pathways, which require further study.

Discussion

Characteristics of the *NtCXE* gene family

CXEs are enzymes with α/β-folding domains that catalyze the hydrolysis of esters and amides and play a role in many physiological reactions in plants (Mindrebo et al., 2016; Lin et al., 2017). The functions of *CXE* genes have been extensively investigated in *Arabidopsis*, cotton, peaches, and other plants, but there are few studies on tobacco, despite it being a model plant (Yang et al., 2008; Cao et al., 2019; Rui et al., 2022). Based on our results, 49 *CXE* genes were identified and characterized in tobacco, which is more than in *Arabidopsis* (20), peach (33), and apple (16) (Schaffer et al., 2007; Mindrebo et al., 2016; Lin et al., 2017). The molecular weight of the *NtCXE* gene family was varied from 15.56 to 53.98 kDa, and most NtCXEs have pI values of <7, which indicates that most NtCXE proteins are acidic. The phylogenetic tree divided *CXE* genes into seven groups, which is similar to other plants. Members of the same subfamily are similar in CDS length, molecular weight, and motifs, suggesting that they may have similar functions.

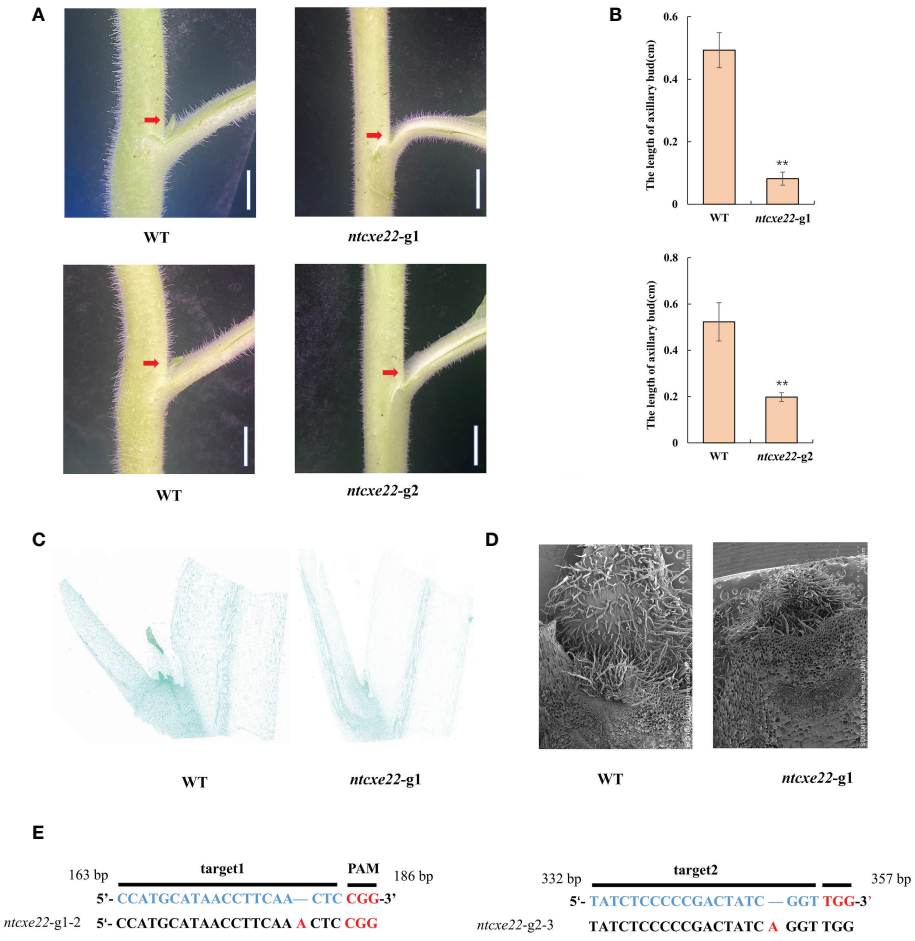

FIGURE 9
CRISPR/Cas9-mediated gene editing of *NtCXE22* in tobacco. **(A)** Appearance of visible axillary buds in the wild type and *NtCXE22* mutant (*ntcxe22*) tobacco seedings. Scale bar = 1 cm. Phenotypes of the whole plants were shown in Supplementary Figures 13, 14. **(B)** Quantitative analysis of axillary bud length in the wild type and *ntcxe22* tobacco seedings. Data are presented as means ± SDs (n = 3). *P < 0.05, **P < 0.01 (significant difference relative to controls based on Student's t-test). **(C)** Paraffin section of axillary bud in the wild type and *ntcxe22* tobacco seedings. **(D)** Scanning electron micrograph of axillary bud in the wild type and *ntcxe22* tobacco seedings. **(E)** Target locations in *NtCXE22* are marked with blue letters, the protospacer adjacent motif (PAM) with red letters, and mutations in *ntcxe22* -g1 and *ntcxe22* -g2 are also shown.

Gene duplication and subsequent functional divergence are important drivers of genome and species evolution. Tandem replication, genome-wide replication, and fragment replication play major roles in the expansion of individual gene families (Panchy et al., 2016; Kong et al., 2019). In our study, 49 tobacco *CXE* genes were found to be distributed on 14 chromosomes, and two replicas containing five gene clusters were distributed across 13 chromosomes. All of these patterns suggest that gene duplication may benefit gene expansion in the tobacco *CXE* gene family. According to the motif and gene structure analyses, the tobacco *CXE* gene family is relatively conserved. Among them, all members contained motif 4, which can be used to explore the putative origin of *CXE*s. Introns are not directly involved in the proteome, but introns usually contain regulatory elements. Thus, the number and length of introns can affect the protein-coding potential of the genome (Jacob and Smith, 2017; Morgan et al., 2019; Parenteau et al., 2019). Based on previous research, we assume that the long intron of *NtCXE11* may be used to further explore the vital regulatory roles of these genes. The introns and exons of the coding regions of eukaryotic genes control gene transcription and can, therefore, be used to further study the evolution of *CXE*s.

The analysis of promoter *cis*-elements can help understand the tissue specificity and regulatory functions of genes. Numerous environmental stress- and hormonal-response elements are widely distributed, which suggests crucial functions in plant bio/abiotic stress resistance (Rui et al., 2022). Furthermore, TFs, miRNAs, and enzymes can form a complex network that influences plant biological processes (Ibraheem et al., 2010; Chen et al., 2018). TFs interact with

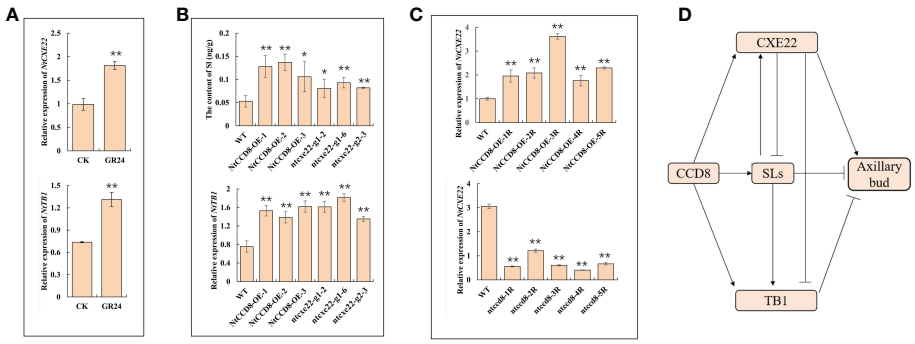

FIGURE 10
The verification of *NtCXE22* involved in regulating SLs. **(A)** Transcriptional response of *NtCXE22* and *NtTB1* to GR24 (strigolactone analog) by qRT-PCR. **(B)** Expression level of *NtTB1* and the content of SL in the axillary buds and roots of the wild type, *NtCCD8*-OE, and *ntcxe22* plants by qRT-PCR. **(C)** Expression level of *NtCXE22* were monitored in the roots of *NtCCD8* mutant (*ntccd8)* and *NtCCD8*-OE plants by qRT-PCR. **(D)** The regulatory network between the CXE22, CCD8, SL, and TB1. Data are presented as means ± SDs (n = 3). *P < 0.05, **P < 0.01 (significant difference relative to controls based on Student's t-test).

cis-acting elements on downstream gene promoters to regulate the expression of target genes and induce a series of responses, thereby enhancing plant growth and development (Priest et al., 2009). In our study, accoring to the *cis*-elements, 731 TFs from 33 TF families may be associated with Nt*CXE* gene regulation. miRNAs regulate various biological functions by controlling the expression of target genes (Begum, 2022; Guo et al., 2022). In our study, 138 miRNA members predicated may have regulatory relationships with *NtCXE* genes. Specifically, we found that three *NtCXE*s (*NtCXE2*, *NtCXE38*, and *NtCXE20*) are targeted by miRNA167, which is involved in the regulation of *Arabidopsis* flowering time (Yao et al. 2019). NAC, a well-known flower-development-related TF (Wang J et al., 2022), may also be involved in regulating *NtCXE38* expression. miR156-*NtCXE45*-ERF was another regulation module, and previous studies indicate that both miR156 and ERF are involved in drought tolerance (González-Villagra et al., 2017; Yu et al., 2022). Our interaction network can further contribute to the functional research of *NtCXE*s. Notably, 36 *NtCXE*s can be targeted by miR169, which is involved in plant disease and abiotic stress regulation (Luan et al., 2015; Hanemian et al., 2016), and *NtCXE22* can be targeted by miR482, a miRNA superfamily that is critical for both disease resistance and plant development (Zhang et al., 2022).

Expression of the *NtCXE* gene family

Plant CXE isoenzymes are found in many plants including in different tissues, organs, and at different developmental stages (Pontier et al., 1998; Ichinose et al., 2001). The *NtCXE* genes are expressed in a wide range of tissues similar to the finding of *AtCXE* genes in *A. thaliana* (Marshall et al., 2003). In apples, *MdCXE1* expression is low during early fruit development and peaks at harvest ripening (Souleyre et al., 2011). In our study, the expression of *NtCXE12* and *NtCXE23* was low in the leaves of seedlings but increased in mature leaves. Topping is an important agronomic procedure in tobacco cultivation, which can promote the development of axillary buds (Wang L et al., 2022) and the accumulation of secondary metabolites in leaves (Zhao et al., 2018). In our results, topping increased the expression of *NtCXE22* in the stems and roots of tobacco and decreased the expression of *NtCXE22* in leaves. We speculate that *NtCXE22* may be involved in the regulation of axillary buds and the secondary metabolism of leaves in tobacco plants. Analysis of *NtCXE* genes expression in different tissues and at different stages should prove helpful in further clarifying the different functions of *NtCXE* genes.

CXEs are highly specific and only act on certain substrates with very high efficiency, whereas other enzymes are able to hydrolyze a wide range of substrates. The functions of *CXE* genes in plants include the activation of plant hormone signaling substances and responses to biotic stresses (Griffiths et al., 2006). The expression of many *CXE* genes is upregulated under abiotic stress, such as alkaline stress (Rui et al., 2022) and *V. flexuosa* infection (Islam and Yun, 2016). In our study, the expression levels of *NtCXE6* and *NtCXE7* were significantly increased after CMV infection, which is consistent with *NbCXE* expression in tobacco infected with TMV (Guo and Wong, 2020). Overexpression of the *AtCXE8* gene in *A. thaliana* enhances resistance to *Botrytis cinerea* (Lee et al., 2013), and in our study, *NtCXE14* expression was significantly increased upon inoculation with *P. nicotianae*. Furthermore, *NtCXE22* was responsive to the cadmium and Phyn infection treatments, and *NtCXE5* was responsive to the

drought treatment. These results suggest that *CXE* genes are responsive to a wide range of biotic and abiotic stresses.

Hormone-signaling molecules may control plant physiological processes through conversion between inactive esters and active molecules, and these signaling molecules are released through the selective hydrolysis of esterases (Westfall et al., 2013; Kamatham et al., 2017). Plant CXEs can demethylate inactive methyl salicylate and methyl jasmonate to produce active salicylate and jasmonate (Kumar and Klessig, 2003; Stuhlfelder et al., 2004). In our study, RT-qPCR experiments were performed using multi-hormone treatments, which showed that the expression levels of many *NtCXE*s were significantly enhanced by MeJA and SA, such as *NtCXE5* and *NtCXE22*. CXEs have been reported to control IAA metabolism in immature maize endosperm tissues, and these genes also regulate GA20 glycogroup metabolism in maize (Schneider et al., 1992; Kowalczyk et al., 2003). Similarly, we found that *CXE* gene expression was also induced by IAA, ABA, 6-BA, GA, and GR24. However, the types of hormone-induced genes were inconsistent, indicating that different *CXE* genes participate in different biological processes in response to different hormones, which requires further exploration.

NtCXE22 is involved in axillary bud development *via* SL

SLs are newly identified hormones with important applications in agriculture, being notably involved in tillering regulation (Wang et al., 2018). SLs biosynthesis and signaling have been extensively studied in the regulation of axillary bud development (Lin et al., 2009; Vogel et al., 2010; Pasare et al., 2013; Wen et al., 2016; Ren et al., 2020). In particular, *CCD8* (a synthetic SLs gene) mutation caused increased branching in tobacco (Gao et al., 2018), and *CpCCD8* overexpression reduces the branching in the *Arabidopsis CCD8* mutant (Wang et al., 2021). On account of low abundance of SLs, little is known about their inactivation at the catabolic level (Snowden et al., 2005; Arite et al., 2007; Simons et al., 2007). In *Arabidopsis*, *AtCXE15* has been identified as a functionally important SLs hydrolase (Xu et al., 2021), and the ectopic expression of *CXE20* effectively reduces the concentration of free SLs and increases the number of branches (Roesler et al., 2021). These studies indicate a new mechanism of SLs degradation regulation in plants. In our study, *NtCXE22* was identified in tobacco and was homologous with *AtCXE15*. *NtCXE22* is located in the cytoplasm and nucleus, which is consistent with observations in peach and cotton (Cao et al., 2019; Rui et al., 2022). SLs are involved in the regulation of apical dominance in plants, and play a direct inhibitory role in branching (Cheng et al., 2013). Our results imply that topping (i.e., removal of apical dominance) increases the expression of the *NtCXE22* gene in roots and leaves, which may be involved in the regulation of SLs degradation. CRISPR/*Cas9*-mediated gene editing of *NtCXE22* (*ntcxe22*) in tobacco also inhibited axillary bud development with increased SLs content, which is consistent with the phenotype of *AtCXE15*. In addition, altered expression levels of *NtCXE22* in *CCD8* (the SLs synthesis gene) overexpression also indirectly confirms its regulatory effect on SLs. CXEs belong to the ABH superfamily, whose members function as carboxylic ester hydrolases of both xenobiotics and endogenous metabolites in plants (Gershater and Edwards, 2007b). We hypothesize that *CXE22* might mediate SLs catabolism and, thereby, affect axillary bud development, which provides the basis for further research into the molecular mechanisms of *CXE* genes in plant growth and development. In addition, as SLs are distributed in both roots and axillary buds (Gomez-Roldan et al., 2008; Xie, 2016), the targeted degradation of SLs content in different tissues by CXE gene can be regarded as a research direction, which can be used to specifically regulate plant architecture or root system.

Conclusion

In summary, we explored the evolutionary relationships, functional information, and regulatory networks of the *CXE* gene family in tobacco plants. We successfully revealed the details of 49 genes, including gene structures, chromosomes, promoter *cis*-elements, associated transcription factors, and miRNAs. In addition, the expression levels of *CXE* genes in various tissues, under various abotic stresses, and in response to a range of plant hormones were determined. We found that *NtCXE7*, *NtCXE9*, *NtCXE22*, and *NtCXE24* are regulated by topping and GR24. Furthermore, knockout of *NtCXE22* inhibited axillary bud development and increased SLs content and the expression level of *NtTB1*, which was consistent with *NtCCD8* (the SLs synthesis gene) overexpression lines. Overall, our work provides a solid foundation for the functional study of CXE genes as well as new understanding of the regulation of plant architecture.

Data availability statement

The datasets presented in this article are not readily available because the China tobacco genome database is not publicly available . Requests to access the datasets should be directed to Peijian Cao, peijiancao@163.com.

Author contributions

LW, WP, and PC conceived the experiments. LW drafted the manuscript. LW and XX conducted the experiments with assistance from JY and GX. YX, ZL, and LC processed and analyzed the data. LL revised the manuscript. All authors contributed to the manuscript and approved the submitted version.

Funding

This work was supported by grants from the CNTC Research Program (No. 110202001020 [JY-03]), the Joint Laboratory of HNTI and ZTRI for Tobacco Gene Research and Utilization, and the Science and Technology Planning Project of Henan Province, China (No. 202102110147, 222102110347).

Acknowledgments

The authors are grateful for the software support provided by OmicShare's work platform. We also thank Editage for their assistance with language editing.

Conflict of interest

Author WP was employed by China Tobacco Hunan Industrial Co., Ltd..The remaining authors declare that the research was conducted in the absence of any commercial or financial relationships that could be construed as a potential conflict of interest.

Publisher's note

All claims expressed in this article are solely those of the authors and do not necessarily represent those of their affiliated organizations, or those of the publisher, the editors and the reviewers. Any product that may be evaluated in this article, or claim that may be made by its manufacturer, is not guaranteed or endorsed by the publisher.

Supplementary material

The Supplementary Material for this article can be found online at: https://www.frontiersin.org/articles/10.3389/fpls.2022.1019538/full#supplementary-material

References

Abdel-Daim, A., Ohura, K., and Imai, T. (2018). A novel quantification method for serine hydrolases in cellular expression system using fluorophosphonate-biotin probe. *Eur. J. Pharm. Sci.* 114, 267–274. doi: 10.1016/j.ejps.2017.12.016

Akiyama, K., Matsuzaki, K., and Hayashi, H. (2005). Plant sesquiterpenes induce hyphal branching in arbuscular mycorrhizal fungi. *Nature* 435, 824–827. doi: 10.1038/nature03608

Arite, T., Iwata, H., Ohshima, K., Maekawa, M., Nakajima, M., Kojima, M., et al. (2007). DWARF10, an RMS1/MAX4/DAD1 ortholog, controls lateral bud outgrowth in rice. *Plant J.* 51 (6), 1019–1029. doi: 10.1111/j.1365-313X.2007.03210.x

Begum, Y. (2022). Regulatory role of microRNAs (miRNAs) in the recent development of abiotic stress tolerance of plants. *Gene* 5 (821), 146283. doi: 10.1016/j.gene.2022.146283

Braun, N., de Saint Germain, A., Pillot, J. P., Boutet-Mercey, S., Dalmais, M., Antoniadi, I., et al. (2012). Te Pea TCP transcription factor PsBRC1 acts downstream of strigolactones to control shoot branching. *Plant Physiol.* 158, 225–238. doi: 10.1104/pp.111.182725

Cao, X., Duan, W., Wei, C., Chen, K., Grierson, D., and Zhang, B. (2019). Prunus persicagenome-wide identification and functional analysis of carboxylesterase and methylesterase gene families in peach (L. batsch). *Front. Plant Sci.* 10, 1511–1523. doi: 10.3389/fpls.2019.01511

Chen, C., Chen, H., Zhang, Y., Thomas, H. R., Frank, M. H., He, Y., et al. (2020). TBtools: an integrative toolkit developed for interactive analyses of big biological data. *Mol. Plant* 13 (8), 1194–1202. doi: 10.1016/j.molp.2020.06.009

Cheng, X., Ruyter-Spira, C., and Bouwmeester, H. (2013). The interaction between strigolactones and other plant hormones in the regulation of plant development. *Front. Plant Sci.* 4, 199. doi: 10.3389/fpls.2013.00199

Chen, X., Sun, S., Liu, F., Shen, E., Liu, L., Ye, C., et al. (2019). A transcriptomic profile of topping responsive non-coding RNAs in tobacco roots (Nicotiana tabacum). *BMC Genomics* 20 (1), 856. doi: 10.1186/s12864-019-6236-6

Chen, J. M., White, A., Nelson, D. C., and Shukla, D. (2021). Role of substrate recognition in modulating strigolactone receptor selectivity in witchweed. *J. Biol. Chem.* 297 (4), 101092. doi: 10.1016/j.jbc.2021.101092

Chen, D., Yan, W., Fu, L. Y., and Kaufmann, K. (2018). Architecture of gene regulatory networks controlling flower development in arabidopsis thaliana. *Nat. Commun.* 9 (1), 4534. doi: 10.1038/s41467-018-06772-3

Dai, X., and Zhao, P. X. (2011). PsRNATarget: a plant small rNA target analysis server. *Nucleic. Acids Res.* 39 (Suppl. l_2), W155–W159. doi: 10.1093/nar/gkr319

Dun, E. A., de Saint Germain, A., Rameau, C., and Beveridge, C. A. (2013). Dynamics of strigolactone function and shoot branching responses in pisum sativum. *Mol. Plant* 6, 128–140. doi: 10.1093/mp/sss131

Gao, J., Wang, G., Ma, S., Xie, X., Wu, X., Zhang, X., et al. (2015). CRISPR/cas9-mediated targeted mutagenesis in Nicotiana tabacum. *Plant Mol. Biol.* 87, 99–110. doi: 10.1007/s11103-014-0263-0

Gao, J., Zhang, T., Xu, B., Jia, L., Xiao, B., Liu, H., et al. (2018). CRISPR/Cas9-mediated mutagenesis of carotenoid cleavage dioxygenase 8 (CCD8) in tobacco affects shoot and root architecture. *Int. J. Mol. Sci.* 19, 1062. doi: 10.3390/ijms19041062

Gershater, M. C., Cummins, I., and Edwards, R. (2007a). Role of a carboxylesterase in herbicide bioactivation in arabidopsis thaliana. *J. Biol. Chem.* 282 (29), 21460–21466. doi: 10.1074/jbc.M701985200

Gershater, M. C., and Edwards, R. (2007b). Regulating biological activity in plants with carboxylesterases. *Plant Sci.* 173 (6), 579–588. doi: 10.1016/j.plantsci.2007.08.008

Gomez-Roldan, V., Fermas, S., Brewer, P., Puech-Pagès, V., Dun, E., Pillot, J. P., et al. (2008). Strigolactone inhibition of shoot branching. *Nature* 455, 189–194. doi: 10.1038/nature07271

González-Villagra, J., Kurepin, L. V., and Reyes-Díaz, M. M. (2017). Evaluating the involvement and interaction of abscisic acid and miRNA156 in the induction of anthocyanin biosynthesis in drought-stressed plants. *Planta* 246, 299–312. doi: 10.1007/s00425-017-2711-y

Griffiths, J., Murase, K., Rieu, I., Zentella, R., Zhang, Z. L., Powers, S. J., et al. (2006). Genetic characterization and functional analysis of the GID1 gibberellin receptors in Arabidopsis. *Plant Cell* 18 (12), 3399–414. doi: 10.1105/tpc.106.047415

Guo, Z., Kuang, Z., Zhao, Y., Deng, Y., He, H., Wan, M., et al. (2022). PmiREN2.0: from data annotation to functional exploration of plant microRNAs. *Nucleic. Acids Res.* 50 (D1), 1475–D1482. doi: 10.1093/nar/gkab811

Guo, S., and Wong, S. M. (2020). A conserved carboxylesterase inhibits tobacco mosaic virus (TMV) accumulation in nicotiana benthamiana plants. *Viruses* 12 (2), 195. doi: 10.3390/v12020195

Hamiaux, C., Drummond, R. S., Janssen, B. J., Ledger, S. E., Cooney, J. M., Newcomb, R. D., et al. (2012). DAD2 is an α/β hydrolase likely to be involved in the perception of the plant branching hormone, strigolactone. *Curr. Biol.* 22 (21), 2032–2036. doi: 10.1016/j.cub.2012.08.007

Hanemian, M., Barlet, X., Sorin, C., Yadeta, K. A., Keller, H., Favery, B., et al. (2016). Arabidopsis CLAVATA1 and CLAVATA2 receptors contribute to

ralstonia solanacearum pathogenicity through a miR169-dependent pathway. *New Phytol.* 211 (2), 502–515. doi: 10.1111/nph.13913

Hatfield, M., Umans, R., Hyatt, J., Edwards, C., Wierdl, M., Tsurkan, L., et al. (2016). Carboxylesterases: general detoxifying enzymes. *Chem. Biol. Interact.* 259, 327–331. doi: 10.1016/j.cbi.2016.02.011

He, X., Zheng, W., Cao, F., and Wu, F. (2016). Identification and comparative analysis of the microRNA transcriptome in roots of two contrasting tobacco genotypes in response to cadmium stress. *Sci. Rep.* 6 (1), 32805–32814. doi: 10.1038/srep32805

Horsch, R. B., Fry, J. E., Hoffmann, N. L., Eichholtz, D., Rogers, S. G., and Fraley, R. T. (1985). A simple and general-method for transferring genes into plants. *Science* 227, 1229–1231. doi: 10.1126/science.227.4691.1229

Hoshida, H., Kondo, M., Kobayashi, T., Yarimizu, T., and Akada, R. (2017). 5′-UTR introns enhance protein expression in the yeast saccharomyces cerevisiae. *Appl. Microbiol. Biotechnol.* 101 (1), 241–251. doi: 10.1007/s00253-016-7891-z

Ibraheem, O., Botha, C. E., and Bradley, G. (2010). In silico analysis of cis-acting regulatory elements in 5′ regulatory regions of sucrose transporter gene families in rice (Oryza sativa japonica) and arabidopsis thaliana. *Comput. Biol. Chem.* 34 (5-6), 268–283. doi: 10.1016/j.compbiolchem.2010.09.003

Ichinose, Y., Hisayasu, Y., Sanematsu, S., Ishiga, Y., Seki, H., Toyoda, K., et al. (2001). Molecular cloning and functional analysis of pea cDNA E86 encoding homologous protein to hypersensitivity-related hsr203J. *Plant Sci.* 160 (5), 997–1006. doi: 10.1016/S0168-9452(01)00343-0

Islam, M. Z., and Yun, H. K. (2016). Identification and expression profiles of six transcripts encoding carboxylesterase protein in vitis flexuosa infected with pathogens. *Plant Pathol. J.* 32 (4), 347–356. doi: 10.5423/PPJ.OA.11.2015.0241

Jacob, A. G., and Smith, C. W. J. (2017). Intron retention as a component of regulated gene expression programs. *Hum. Genet.* 136, 1043–1057. doi: 10.1007/s00439-017-1791-x

Jin, J., Tian, F., Yang, D. C., Meng, Y. Q., Kong, L., Luo, J., et al. (2016). PlantTFDB 4.0: toward a central hub for transcription factors and regulatory interactions in plants. *Nucleic. Acids Res.* 45 (D1), D1040–D1045. doi: 10.1093/nar/gkw982

Jin, J., Zhang, H., Zhang, J., Liu, P., Chen, X., Li, Z., et al. (2017). Integrated transcriptomics and metabolomics analysis to characterize cold stress responses in nicotiana tabacum. *BMC Genomics* 18 (1), 496. doi: 10.1186/s12864-017-3871-7

Kamatham, S., Pallu, R., Pasupulati, A., Singh, S., and Gudipalli, P. (2017). Benzoylsalicylic acid derivatives as defense activators in tobacco and arabidopsis. *Phytochemistry* 143 (1), 160–169. doi: 10.1016/j.phytochem.2017.07.014

Kim, D., Paggi, J. M., Park, C., Bennett, C., and Salzberg, S. L. (2019). Graph-based genome alignment and genotyping with HISAT2 and HISAT-genotype. *Nat. Biotechnol.* 37 (8), 907–915. doi: 10.1038/s41587-019-0201-4

Kong, W. L., An, B. G., Zhang, Y., Yang, J., Li, S. M., Sun, T., et al. (2019). Sugar transporter proteins (STPs) in gramineae crops: comparative analysis, phylogeny, evolution, and ex-pression profiling. *Cells* 8 (6), 560. doi: 10.3390/cells8060560

Kowalczyk, S., Jakubowska, A., Zielinska, E., and Bandurski, R. (2003). Bifunctional indole-3-acetyl transferase catalyses synthesis and hydrolysis of indole-3-acetyl-myo-inositol in immature endosperm of zea mays. *Physiol. Plant* 119 (2), 165–174. doi: 10.1034/j.1399-3054.2003.00158.x

Kozomara, A., Birgaoanu, M., and Griffiths-Jones, S. (2019). MiRBase: from microRNA sequences to function. *Nucleic. Acids Res.* 47 (D1), D155–D162. doi: 10.1093/nar/gky1141

Kumar, D., and Klessig, D. F. (2003). High-affinity salicylic acid-binding protein 2 is required for plant innate immunity and has salicylic acid-stimulated lipase activity. *Proc. Natl. Acad. Sci.* 100 (26), 16101–16106. doi: 10.1073/pnas.0307162100

Kumar, S., Stecher, G., Li, M., Knyaz, C., and Tamura, K. (2018). MEGA X: molecular evolutionary genetics analysis across computing platforms. *Mol. Biol. Evol.* 35 (6), 1547–1549. doi: 10.1093/molbev/msy096

Lee, S., Hwang, S., Seo, Y. W., Jeon, W. B., and Oh, B. J. (2013). Molecular characterization of the AtCXE8 gene, which promotes resistance to botrytis cinerea infection. *Plant Biotechnol. Rep.* 7, 109–119. doi: 10.1007/s11816-012-0253-0

Leinonen, R., Sugawara, H., and Shumway, M. (2011). The international nucleotide sequence database collaboration. the sequence read archive. *Nucleic. Acids Res.* 39 (1), D19–D21. doi: 10.1093/nar/gkr1006

Lescot, M., Dehais, P., Thijs, G., Marchal, K., Moreau, Y., Van de Peer, Y., et al. (2002). PlantCARE, a database of plant cis-acting regulatory elements and a portal to tools for in silico analysis of promoter sequences. *Nucleic. Acids Res.* 30, 325–327. doi: 10.1093/nar/30.1.325

Lin, Q., Chen, S., Chao, Y., Huang, X., Wang, S., and Qiu, R. (2017). Carboxylesterase-involved metabolism of di-n-butyl phthalate in pumpkin (Cucurbita moschata) seedlings. *Environ. pollut.* 220 (Pt A), 421–430. doi: 10.1016/j.envpol.2016.09.084

Lin, H., Wang, R., Qian, Q., Yan, M., Meng, X., Fu, Z., et al. (2009). DWARF27, an iron-containing protein required for the biosynthesis of strigolactones, regulates rice tiller bud outgrowth. *Plant Cell.* 21 (5), 1512–1525. doi: 10.1105/tpc.109.065987

Luan, M., Xu, M., Lu, Y., Zhang, L., Fan, Y., and Wang, L. (2015). Expression of zma-miR169 miRNAs and their target ZmNF-YA genes in response to abiotic stress in maize leaves. *Gene* 555 (2), 178–185. doi: 10.1016/j.gene.2014.11.001

Luo, L., Takahashi, M., Kameoka, H., Qin, R., Shiga, T., Kanno, Y., et al. (2019). Developmental analysis of the early steps in strigolactone-mediated axillary bud dormancy in rice. *Plant J.* 97 (6), 1006–1021. doi: 10.1111/tpj.14266

Marshall, S. D., Putterill, J. J., Plummer, K. M., and Newcomb, R. D. (2003). The carboxylesterase gene family from arabidopsis thaliana. *J. Mol. Evol.* 57, 487–500. doi: 10.1007/s00239-003-2492-8

Marzec, M., Daszkowska-Golec, A., Collin, A., Melzer, M., Eggert, K., and Szarejko, I. (2020). Barley strigolactone signaling mutant hvd14.d reveals the role of strigolactones in abscisic acid-dependent response to drought. *Plant Cell Environ.* 43 (9), 2239–2253. doi: 10.1111/pce.13815

Mindrebo, J., Nartey, C., Seto, Y., Burkart, M., and Noel, J. (2016). Unveiling the functional diversity of the alpha/beta hydrolase superfamily in the plant kingdom. *Curr. Opin. Struct. Biol.* 41 (1), 233–246. doi: 10.1016/j.sbi.2016.08.005

Morgan, J. T., Fink, G. R., and Bartel, D. P. (2019). Excised linear introns regulate growth in yeast. *Nature* 565, 606–611. doi: 10.1038/s41586-018-0828-1

Nomura, T., Murase, T., Ogita, S., and Kato, Y. (2015). Molecular identification of tuliposide b-converting enzyme:a lactone-forming carboxylesterase from the pollen of tulip. *Plant J.* 83 (2), 252–262. doi: 10.1111/tpj.12883

Panchy, N., Lehti-Shiu, M., and Shiu, S. H. (2016). Evolution of gene duplication in plants. *Plant Physiol.* 171 (4), 2294–2316. doi: 10.1104/pp.16.00523

Parenteau, J., Maignon, L., Berthoumieux, M., Catala, M., Gagnon, V., and Abou Elela, S. (2019). Introns are mediators of cell response to starvation. *Nature* 565, 612–617. doi: 10.1038/s41586-018-0859-7

Pasare, S. A., Ducreux, L. J. M., Morris, W. L., Campbell, R., Sharma, S. K., Roumeliotis, E., et al. (2013). The role of the potato (Solanum tuberosum) CCD8 gene in stolon and tuber development. *New Physiol.* 198 (4), 1108–1120. doi: 10.1111/nph.12217

Pontier, D., Tronchet, M., Rogowsky, P., Lam, E., and Roby, D. (1998). Activation of hsr203, a plant gene expressed during incompatible plant-pathogen interactions, is correlated with programmed cell death. *Mol. Plant Microbe Interact.* 11 (6), 544–554. doi: 10.1094/MPMI.1998.11.6.544

Priest, H. D., Filichkin, S. A., and Mockler, T. C. (2009). Cis-regulatory elements in plant cell signaling. *Curr. Opin. Plant Biol.* 12 (5), 643–649. doi: 10.1016/j.pbi.2009.07.016

Ren, C., Guo, Y. C., Kong, J. H., Lecourieux, F., Dai, Z. W., Li, S. H., et al. (2020). Knockout of VvCCD8 gene in grapevine affects shoot branching. *BMC Plant Biol.* 20 (1), 47. doi: 10.1186/s12870-020-2263-3

Roesler, K., Lu, C., Thomas, J., Xu, Q., Vance, P., Hou, Z., et al. (2021). Arabidopsis carboxylesterase 20 binds strigolactone and increases branches and tillers when ectopically expressed in arabidopsis and maize. *Front. Plant Sci.* 12, 639401. doi: 10.3389/fpls.2021.639401

Rui, C., Peng, F., Fan, Y., Zhang, Y., Zhang, Z., Xu, N., et al. (2022). Genome-wide expression analysis of carboxylesterase (CXE) gene family implies GBCXE49 functional responding to alkaline stress in cotton. *BMC Plant Biol.* 22 (1), 194. doi: 10.1186/s12870-022-03579-9

Schaffer, R., Friel, E., Souleyre, E., Bolitho, K., Thodey, K., Ledger, S., et al. (2007). A genomics approach reveals that aroma production in apple is controlled by ethylene predominantly at the final step in each biosynthetic pathway. *Plant Physiol.* 144 (4), 1899–1912. doi: 10.1104/pp.106.093765

Schmidt, G. W., and Delaney, S. K. (2010). Stable internal reference genes for normalization of real-time RT-PCR in tobacco (Nicotiana tabacum) during development and abiotic stress. *Mol. Genet. Genomics* 283, 233–241. doi: 10.1007/s00438-010-0511-1

Schneider, G., Jensen, E., Spray, C. R., and Phinney, B. O. (1992). Hydrolysis and reconjugation of gibberellin A20 glucosyl ester by seedlings of zea mays l. *Proc. Natl. Acad. Sci. U. S. A.* 89 (17), 8045–8048. doi: 10.1073/pnas.89.17.8045

Seto, Y., Yasui, R., Kameoka, H., Tamiru, M., Cao, M., Terauchi, R., et al. (2019). Strigolactone perception and deactivation by a hydrolase receptor DWARF14. *Nat. Commun.* 10 (1), 191. doi: 10.1038/s41467-018-08124-7

Sharma, A., Kumar, V., Yuan, H., Kanwar, M. K., Bhardwaj, R., Thukral, A. K., et al. (2018). Jasmonic acid seed treatment stimulates insecticide detoxification in brassica juncea l. *Front. Plant Sci.* 9, 1609. doi: 10.3389/fpls.2018.01609

Simons, J. L., Napoli, C. A., Janssen, B. J., Plummer, K. M., and Snowden, K. C. (2007). Analysis of the DECREASED APICAL DOMINANCE genes of petunia in the control of axillary branching. *Plant Physiol.* 143, 697–706. doi: 10.1104/pp.106.087957

Smoot, M. E., Ono, K., Ruscheinski, J., Wang, P. L., and Ideker, T. (2011). Cytoscape 2.8: new features for data integration and network visualization. *Bioinformatics* 27 (3), 431–432. doi: 10.1093/bioinformatics/btq675

Snowden, K. C., Simkin, A. J., Janssen, B. J., Templeton, K. R., Loucas, H. M., Simons, J. L., et al. (2005). The decreased apical dominance1/Petunia hybrida CAROTENOID CLEAVAGE DIOXYGENASE8 gene affects branch production and plays a role in leaf senescence, root growth, and flower development. *Plant Cell.* 17 (3), 746–759. doi: 10.1105/tpc.104.027714

Souleyre, E. J., Marshall, S. D., Oakeshott, J. G., Russell, R. J., Plummer, K. M., and Newcomb, R. D. (2011). Biochemical characterisation of MdCXE1, a carboxylesterase from apple that is expressed during fruit ripening. *Phytochemistry* 72 (7), 564–571. doi: 10.1016/j.phytochem.2011.01.020

Stuhlfelder, C., Mueller, M. J., and Warzecha, H. (2004). Cloning and expression of a tomato cDNA encoding a methyl jasmonate cleaving esterase. *Eur. J. Biochem.* 271 (14), 2976–2983. doi: 10.1111/j.1432-1033.2004.04227.x

Sun, H., Guo, X., Qi, X., Feng, F., Xie, X., Zhang, Y., et al. (2021). SPL14/17 act downstream of strigolactone signaling to modulate rice root elongation in response to nitrate supply. *Plant J.* 106 (3), 649–660. doi: 10.1111/tpj.15188

Toh, S., Holbrook-Smith, D., Stogios, P. J., Onopriyenko, O., Lumba, S., Tsuchiya, Y., et al. (2015). Structure-function analysis identifies highly sensitive strigolactone receptors in striga. *Science* 350 (6257), 203–212. doi: 10.1126/science.aac9476

Ueguchi-Tanaka, M., Ashikari, M., Nakajima, M., Itoh, H., Katoh, E., Kobayashi, M., et al. (2005). GIBBERELLIN INSENSITIVE DWARF1 encodes a soluble receptor for gibberellin. *Nature* 437 (7059), 693–698. doi: 10.1038/nature04028

Vogel, J. T., Walter, M. H., Giavalisco, P., Lytovchenko, A., Kohlen, W., Charnikhova, T., et al. (2010). SlCCD7 controls strigolactone biosynthesis, shoot branching and mycorrhiza-induced apocarotenoid formation in tomato. *Plant J.* 61 (2), 300–311. doi: 10.1111/j.1365-313X.2009.04056.x

Wang, L., Gao, J. P., Wang, C., Xu, Y. L., Li, X. X., Yang, J., et al. (2022). Comprehensive analysis of long non-coding RNA modulates axillary bud development in tobacco (Nicotiana tabacum l.). *Front. Plant Sci.* 13. doi: 10.3389/fpls.2022.809435

Wang, X., Liu, D., Lin, J., Zhu, T., Liu, N., Yang, X., et al. (2021). Carotenoid cleavage dioxygenase genes of chimonanthus praecox, CpCCD7 and CpCCD8, regulate shoot branching in arabidopsis. *Int. J. Mol. Sci.* 22, 8750. doi: 10.3390/ijms22168750

Wang, B., Smith, S. M., and Li, J. (2018). Genetic regulation of shoot architecture. *Annu. Rev. Plant Biol.* 69, 437–468. doi: 10.1146/annurev-arplant-042817-040422

Wang, J. L., Wang, H. B., Yang, H. Q., Hu, R. L., Wei, D. Y., Tang, Q. L., et al. (2022). The role of NAC transcription factors in flower development in plants. *Chin. J. Biotechnol.* 38 (8), 2687–2699. doi: 10.13345/j.cjb.210943

Wen, C., Zhao, Q., Nie, J., Liu, G. Q., Shen, L., Cheng, C. X., et al. (2016). Physiological controls of chrysanthemum DgD27 gene expression in regulation of shoot branching. *Plant Cell Rep.* 35, 1053–1070. doi: 10.1007/s00299-016-1938-6

Westfall, C. S., Muehler, A. M., and Jez, J. M. (2013). Enzyme action in the regulation of plant hormone responses. *J. Biol. Chem.* 288 (27), 19304–19311. doi: 10.1074/jbc.R113.475160

Xie, X. (2016). Structural diversity of strigolactones and their distribution in the plant kingdom. *J. Pestic. Sci.* 41, 175–180. doi: 10.1584/jpestics.J16-02

Xie, X., Qin, G., Si, P., Luo, Z., Gao, J., Chen, X., et al. (2017). Analysis of nicotiana tabacum PIN genes identifies NtPIN4 as a key regulator of axillary bud growth. *Physiol. Plant.* 160, 222–239. doi: 10.1111/ppl.12547

Xu, E., Chai, L., Zhang, S., Yu, R., Zhang, X., Xu, C., et al. (2021). Catabolism of strigolactones by a carboxylesterase. *Nat. Plants.* 7 (11), 1495–1504. doi: 10.1038/s41477-021-01011-y

Yang, J. K., Tong, Z. J., Fang, D. H., Chen, X. J., Zhang, K. Q., and Xiao, B. G. (2017). Transcriptomic profile of tobacco in response to phytophthora nicotianae infection. *Sci. Rep.* 7 (1), 401–407. doi: 10.1038/s41598-017-00481-5

Yang, Y., Xu, R., Ma, C. J., Vlot, A. C., Klessig, D. F., and Pichersky, E. (2008). Inactive methyl indole-3-acetic acid ester can be hydrolyzed and activated by several esterases belonging to the AtMES esterase family of arabidopsis. *Plant Physiol.* 147, 1034–1045. doi: 10.1104/pp.108.118224

Yang, H., Zhao, L., Zhao, S., Wang, J., and Shi, H. (2017). Biochemical and transcriptomic analyses of drought stress responses of LY1306 tobacco strain. *Sci. Rep.* 7 (1), 17442. doi: 10.1038/s41598-017-17045-2

Yao, X. Z., Chen, J. L., Zhou, J., Yu, H. C., Ge, C. N., Zhang, M., et al. (2019). An essential role for miRNA167 in maternal control of embryonic and seed development. *Plant Physiol.* 180 (1), 453–464. doi: 10.1104/pp.19.00127

Yoneyama, K., Xie, X., Yoneyama, K., Kisugi, T., Nomura, T., Nakatani, Y., et al. (2018). Which are the major players, canonical or non-canonical strigolactones? *J. Exp. Bot.* 69 (9), 2231–2239. doi: 10.1093/jxb/ery090

Yu, Y., Yu, M., Zhang, S., Song, T., Zhang, M., Zhou, H., et al. (2022). Transcriptomic identification of wheat AP2/ERF transcription factors and functional characterization of TaERF-6-3A in response to drought and salinity stresses. *Int. J. Mol. Sci.* 23, 3272. doi: 10.3390/ijms23063272

Zhang, Z., Li, J., Zhao, X. Q., Wang, J., Wong, G. K., and Yu, J. (2006). KaKs_Calculator: calculating ka and ks through model selection and model averaging. *Genomics Proteomics Bioinf.* 4 (4), 259–263. doi: 10.1016/S1672-0229(07)60007-2

Zhang, Y., Waseem, M., Zeng, Z., Xu, J., Chen, C., Liu, Y., et al. (2022). MicroRNA482/2118, a miRNA superfamily essential for both disease resistance and plant development. *New Phytol.* 233 (5), 2047–2057. doi: 10.1111/nph.17853

Zhao, J., Li, L., Zhao, Y., Zhao, C. X., Chen, X., Liu, P. P., et al. (2018). Metabolic changes in primary, secondary, and lipid metabolism in tobacco leaf in response to topping. *Anal. Bioanal. Chem.* 410, 839–851. doi: 10.1007/s00216-017-0596-z

Zhao, L. H., Zhou, X. E., Wu, Z. S., Yi, W., Xu, Y., Li, S., et al. (2013). Crystal structures of two phytohormone signal-transducing α/β hydrolases: karrikin-signaling KAI2 and strigolactone-signaling DWARF14. *Cell Res.* 23 (3), 436–439. doi: 10.1038/cr.2013.19

Zhu, T. K., Du, P. P., Zeng, L. J., Lü, H., Zhao, H. M., Li, Y. W., et al. (2019). Variation in metabolism and degradation of di-n-butyl phthalate (DBP) by high- and low-DBP accumulating cultivars of rice (Oryza sativa l.) and crude enzyme extracts. *Sci. Total. Environ.* 10 (668), 1117–1127. doi: 10.1016/j.scitotenv.2019.03.047

Frontiers in Plant Science

Cultivates the science of plant biology and its applications

The most cited plant science journal, which advances our understanding of plant biology for sustainable food security, functional ecosystems and human health.

Discover the latest Research Topics

See more →

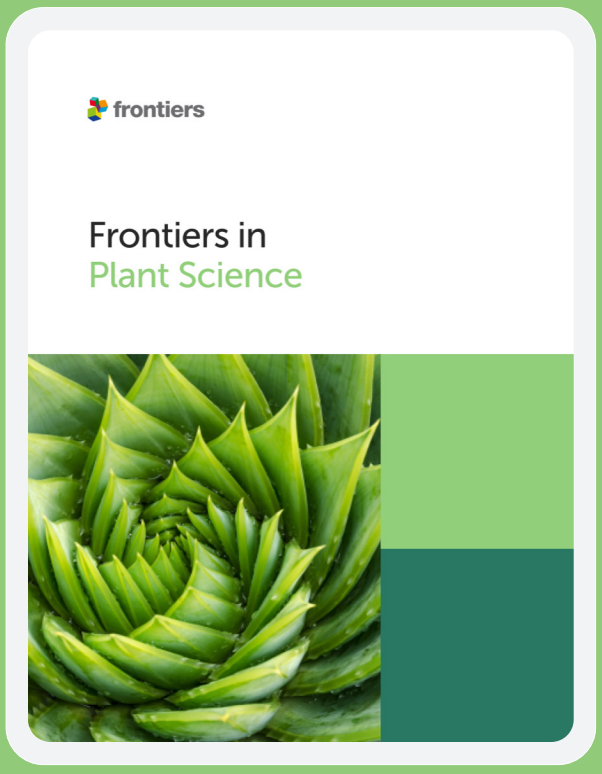

Frontiers

Avenue du Tribunal-Fédéral 34
1005 Lausanne, Switzerland
frontiersin.org

Contact us

+41 (0)21 510 17 00
frontiersin.org/about/contact